MISE EN PLACE DE NOUVELLES STRATEGIES THERAPEUTIQUES POUR CONTOURNER LES RESISTANCES A LA MORT DES CELLULES TUMORALES

Aude Robert

Mémoire présenté pour l'obtention du Diplôme d'habilitation à diriger des recherches

Par

Aude ROBERT

MISE EN PLACE DE NOUVELLES STRATEGIES THERAPEUTIQUES POUR CONTOURNER LES RESISTANCES A LA MORT DES CELLULES TUMORALES

Soutenance le 8 janvier 2019 devant le jury composé de :

Dr. Muriel Priault	CR-CNRS	Rapporteuse
Dr. Ludger Johannes	DR-INSERM	Rapporteur
Dr. Santos Susin	DR-CNRS	Rapporteur
Dr. Martine Amiot	DR-CNRS	Examinatrice
Dr. Olivier Bernard	DR-INSERM	Examinateur
Dr. Jérome Thiery	CR-INSERM	Examinateur

UMR8126
Institut Gustave Roussy
114 rue Edouard Vaillant
94805 Villejuif

Mémoire présenté pour l'obtention du Diplôme d'habilitation à diriger des recherches

Par

Aude ROBERT

MISE EN PLACE DE NOUVELLES STRATEGIES THERAPEUTIQUES POUR CONTOURNER LES RESISTANCES A LA MORT DES CELLULES TUMORALES

UMR8126
Institut Gustave Roussy
114 rue Edouard Vaillant
94805 Villejuif

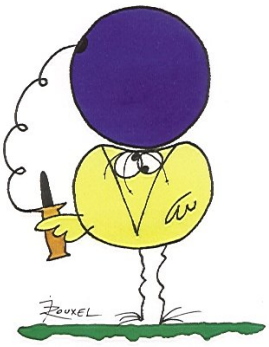

En essayant continuellement on finit par réussir, donc : plus ça rate, plus on a de chances que ça marche.

S'il n'y a pas de solution, c'est qu'il n'y a pas de problème.

Devises Shadoks,

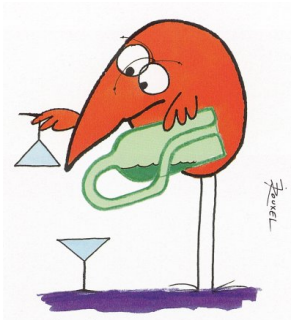

Remerciements

Je tiens à remercier Mesdames Amiot et Priault ainsi que Messieurs Bernard, Johannes, Susin et Thiery d'avoir accepté de faire partie de ce jury d'HDR.

Mes remerciements iront en premier lieu à Joëlle Wiels. Cela fait 11 ans que tu m'as recrutée dans ton équipe et presque autant de temps que tu me fais confiance. Pourtant passer ce concours n'était pas prévu encore moins l'avoir. A mon arrivée, il a fallu s'atteler à la tâche : remplacer l'irremplaçable Cécile Tétaud. J'ai essayé de prendre sa relève, j'espère avoir réussi. Et puis surtout merci pour m'avoir laissé être plus qu'une ITA, de m'avoir laissée recruter Justine et développer mes projets. Si j'en suis là actuellement c'est grâce à toi.

Tout au long de mon parcours scientifique, j'ai eu l'opportunité de côtoyer de nombreuses personnes qui ont contribué de près ou de loin à mon travail et à mon cheminement. Ce manuscrit est l'occasion de pouvoir les remercier.

Dans l'ordre chronologique, et en essayant d'être brève mais exhaustive, cela donne :

Un grand merci à ma directrice de thèse Chantal Desdouets qui m'a quasi-tout appris en science et à Christian Bréchot pour avoir joué le rôle de directeur officiel pendant les 2 premières années de mon doctorat.

Merci à tous les ex-U370 et plus particulièrement à France Demaugre, Florianne Garreau, Olivier Brégerie et à mes co-thésards devenus grands eux aussi : Julie Hervé et Jonathan Pol. Une pensée aussi pour ceux qui ne sont plus là : Maurice et Sokavut.

Merci à tous les Ex-U567 : JEG, Germain, Claudia, Dominique, Hélène et surtout à Séverine (quand tu veux pour la Cantinella).

Merci aux Alsaciens : Jan De Mey pour m'avoir accueilli en post doc et m'avoir laissé partir quand il le fallait. Jan Brants, Julien Bellis et surtout Elyette Martin (loin des yeux mais jamais loin du cœur) pour avoir facilité mon intégration en nouvelle France.

Merci à l'ensemble des membres passé·e·s et actuel·le·s de l'UMR8126 et plus particulièrement :

A Marc Lipinski pour m'avoir accueilli au sein de l'unité

A ceux et celles qui m'ont accueilli dans l'équipe et qui sont parti·e·s : Benjamin Renouf, Sonia Chelouah et surtout Emilie Hollville.

A celles avec qui j'ai partagé le bocal : Anaïs Pujals, Loëtitia Favre et Justine Debernardi, la team des 3 C : Champagne, Chocolat, Chat. Une dédicace spéciale à Justine qui a essuyé les plâtres en tant que première doctorante et qui m'a donné l'envie de continuer l'encadrement.

Et Bien sûr, Merci à tou·te·s mes stagiaires pour leur travail : Mélanie, Pauline, Florian SB, Delphine, Laura, Anaïs M., Ophélie, Sophie, Tiphaine, Benjamin M., avec une mention particulière pour Crystal à qui je souhaite le meilleur. Merci à Florian qui prend la suite dans un contexte un peu spécial.

Merci aux ITA pour les séances de psychanalyse : Aurore, Sonia, Catherine, Chloé, Alexandra, Muriel.

Merci aux étudiant·e·s en thèse présent·e·s ou passé·e·s qui savent toujours rendre l'ambiance de ce laboratoire chaleureuse : Carlita, Clément, Claire, Jeremy, Niki, Valentin...

Enfin, Merci à mes ami·e·s pour le soutien continu (depuis longtemps maintenant) : Lulux Et Gillou, Lolila, Gord, Ced, Mat et les pièces rapportées dans le désordre : Anne, Christine, Cécile, Milan, tous les enfants avec une pensée particulière pour l'enfant terrible (ses parents le reconnaitront).

Merci à Schib d'être toujours là.

Merci à mes parents pour tout.

Résumé

L'altération des mécanismes d'apoptose joue un rôle central dans le développement des cancers et limite l'efficacité des thérapies conventionnelles. Les travaux que je mène ont une triple visée : 1) analyser les mécanismes d'apoptose induits par certains stimuli, 2) essayer de mieux comprendre comment les mécanismes de résistance à l'apoptose se mettent en place, 3) tenter de les contrecarrer et d'induire l'apoptose des cellules tumorales par d'autres voies. Nos modèles d'études sont différents lymphomes B notamment ceux associés au virus d'Epstein-Barr (EBV) comme le lymphome de Burkitt (LB), le syndrome lymphoprolifératif post-transplant (PTLD) et le lymphome diffus à grandes cellules B (DLBCL).

Dans ce cadre, je me suis intéressée au glycolipide Gb3/CD77, qui est fortement exprimé à la surface des cellules de certains lymphomes B comme le LB, et de certaines tumeurs solides résistantes aux chimiothérapies. Nous avons montré que l'induction de l'apoptose par une toxine bactérienne se fixant spécifiquement sur Gb3/CD77 implique plusieurs membres pro-apoptotiques de la famille BCL-2 dans. Par ailleurs, nous avons montré, dans un modèle de carcinome ovarien que l'expression de Gb3/CD77 est directement corrélée à la résistance des cellules aux drogues et à l'expression de MDR1 (Multidrug resistance-1), une protéine impliquée dans ce mécanisme grâce à ses propriétés de pompes membranaires d'efflux des substances cytotoxiques. Enfin, nos travaux récents ont mis en évidence que la fixation d'anticorps spécifiques de Gb3/CD77 à la surface des cellules cancéreuses exprimant ce glycolipide pouvait induire leur mort en utilisant le système de la cascade du complément. Ces résultats font de Gb3/CD77 une cible thérapeutique intéressante. La suite de ce projet consistera à explorer le potentiel thérapeutique d'un anticorps monoclonal dirigé contre l'Ag Gb3/CD77 dans le traitement du LB et de certaines tumeurs chimiorésistantes.

L'inactivation de p53 par la surexpression de protéines régulatrices est aussi un mécanisme permettant aux cellules tumorales d'échapper à l'apoptose. Des travaux précédents ont montré que de nombreuses lignées de LB exprimant une p53 sauvage présentent aussi une forte expression de MDM2. La réactivation de p53 par la nutline 3 (une petite molécule rompant l'interaction entre p53 et MDM2) dans les cellules de LB EBV- et EBV+ en latence I permet leur entrée massive en apoptose, cependant, elle ne suffit pas à induire la mort des cellules EBV+ en latence III. Cette résistance à l'apoptose p53 dépendante induite par EBV repose sur deux mécanismes complémentaires : une autophagie constitutive et la surexpression de la protéine anti-apoptotique BCL-2. Ainsi, nous avons montré qu'ABT-737, un inhibiteur de BCL-2 restaurait la sensibilité des cellules à l'apoptose induite par la nutline 3 *in vitro* et grâce à l'utilisation de modèles murins xénogreffés qu'il représentait une nouvelle approche thérapeutique intéressante dans le cadre du traitement des PTLD que ce soit seul ou en combinaison avec des traitements conventionnels. Néanmoins, l'utilisation d'inhibiteurs de BCL-2 peut induire une résistance des cellules cancéreuses en raison d'une surexpression des protéines non ciblées. Nous cherchons donc à développer en collaboration avec le laboratoire de F. Roussi à ICSN à Gif sur Yvette, d'autres inhibiteurs des membres de la famille BCL-2 pour contrecarrer ces résistances.

Sommaire

Abréviations

AcM	– Anticorps Monoclonal
ADCC	– Antibody dependent cell mediated cytotoxicity
BAK	– Bcl-2 Antagonist Killer
BAX	– Bcl-2 Associated X protein
BCL-2	– B-Cell Lymphoma-2
BCL-6	– B-Cell Lymphoma-6
BCL-xL	– B-Cell Lymphoma-extra Large
BID	– BH3 Interacting-domain Death agonist
BH	– BCL-2 Homology
Caspase	– Cystein aspartic Acid-Specific ProteASE
CD	– Cluster of Differenciation
CDC	– Complement Dependent Cytotoxicity
CDDP	– Cis-DiamineDichloroPlatine (cisplatine)
CG	– Centre Germinatif
DLBCL	– Diffuse Large B Cell Lymphoma
DRAM-1	– DNA Damage-Regulated Autophagy Modulator 1
DXR	– Doxorubicine
EBNA	– Epstein-Barr virus Nuclear Antigen
EBV	– Epstein Barr Virus
FDA	– Food and Drug Administration
IFT	– IntraFlagellar Transport
L_B, L_T	– Lymphocyte B, T
LB	– Lymphome de Burkitt
LCL	– Lymphoblastoïd Cell Line
LMP	– Latent Membrane Protein
LNH	– Lymphome Non Hodgknien
GalCer	– Galactosylceramide
Gb3/CD77	– Globotriaosylceramide
GlcCer	– Glucosylceramide
GR	– Gustave Roussy

GSL – GlycoSphingoLipide

Ig H, L – Immunoglobuline , H Heavy, L Light

IP – Immunoprécipitation

MDR – MultiDrug Resistance

MCL-1 – Myeloid leukemia sequence 1

MTOC – MicroTubule Organizing Center

MUM-1 – Multiple Myeloma Oncogene 1

NEB – Nuclear Envelope Breakdown

NPC – NasoPharynx Carcinoma

NOS – Not Otherwise Specified

OMS – Organisation Mondiale de la Santé

PARP – Poly ADP-Ribose Polymerase

PCM – PeriCentriolar Material

PE – PhycoErythrin

PF – Polarisation de fluorescence

PI – Propidium Iodide, Iodure de Propidium

PS – PhosphatidylSérine

PTLD – Post-transplant Lymphoproliferative Disorder

RE – Reticulum Endoplasmique

SAC – Spindle Assembly Checkpoint

Stx – Shiga toxin

TPR –TetratricoPeptide Repeat

TTLL –Tubulin Tyrosin Ligase Like

VCR – VinCRistine

VDAC – Voltage-Dependent Anion Channel

VIH – Virus de l'Immunodéficience Humaine

VT – VéroToxine

Table des figures

Préambule

Ce document synthétise l'ensemble de mes activités de recherche depuis mon doctorat soit seize années dans quatre laboratoires différents. Il se compose de deux parties : la première est une synthèse de mes travaux depuis 2002, la deuxième une description de mes futurs axes de recherche.

Au cours de ces années, j'ai eu l'occasion d'encadrer ou co-encadrer un certain nombre d'étudiant·e·s de tous niveaux, dans un premier temps essentiellement sur un plan technique puis au fur et à mesure, j'ai élaboré les projets et participé à toutes les facettes de l'encadrement.

Ma « carrière » commence en 2002 avec ma thèse réalisée sous la direction scientifique du Dr. Chantal Desdouets dans un premier temps au sein de l'unité U370 dirigée par le Pr C. Bréchot à l'hôpital Necker-Enfants malades puis à l'institut Cochin dans l'unité U567 dirigée par le Pr. A. Kahn. Soutenu en 2006, mon doctorat avait pour thématique : l'implication du centrosome dans la signalisation et la prolifération cellulaires. Pendant cette période, mes travaux m'ont permis d'acquérir de solides compétences et connaissances en biologie cellulaire et moléculaire ainsi qu'en expérimentation animale.

En 2007, après une courte période comme chercheuse postdoctorale dans mon laboratoire de thèse (deux mois), j'ai rejoint l'équipe du Professeur Jan De Mey au sein de l'UMR7175 à l'université Louis Pasteur de Strasbourg pour un stage post-doctoral de deux ans. Mon choix d'aller dans ce laboratoire a été guidé par l'envie de continuer mes travaux de recherche sur le cycle cellulaire, le cytosquelette et leur lien avec le cancer. Notre équipe était au sein d'un consortium dirigé par le Dr. Bohdan Wasylyk soutenu par l'INCA et ayant pour but l'évaluation du potentiel thérapeutique, pronostique et diagnostique de la protéine TTLL12 (tubulin tyrosine ligase like) impliquée dans les cancers de la prostate et de la région ORL. Ayant finalement obtenu un poste d'ingénieure de recherche au concours de l'université Paris-Sud, je ne suis restée qu'une année à Strasbourg pendant laquelle j'ai pu acquérir une expertise en microscopie photonique et en temps réel.

Au 1er décembre 2007, j'ai donc été affectée dans l'équipe du Dr. Joëlle Wiels au sein de l'UMR8126 à l'institut Gustave Roussy (GR) dont la thématique était la résistance à l'apoptose dans les cellules de lymphomes B. A mon arrivée, j'ai participé aux travaux de thèse d'Anaïs Pujals et de Sonia Chelouah, qui visaient à analyser les mécanismes de résistance à l'apoptose induits par le virus d'Epstein-Barr. Puis, j'ai repris les travaux d'Emilie Hollville, sur les mécanismes d'apoptose induits via le glycolipide Gb3/CD77. Depuis mon recrutement, j'ai eu l'opportunité, en plus des projets déjà en cours auxquels je participe en collaboration avec les autres membres du groupe, de développer ma propre thématique de recherche au sein du laboratoire. Ainsi, mon projet de recherche vise à mettre en place de nouvelles stratégies thérapeutiques pour contourner les résistances à la mort des cellules tumorales et s'articule autour de deux grands axes. Le premier consiste à explorer le potentiel thérapeutique d'un anticorps dirigé contre l'antigène (Ag) Gb3/CD77 dans le traitement de certains lymphomes B et tumeurs chimiorésistantes. Le deuxième vise à développer grâce à une collaboration entre notre équipe et celle de F. Roussi à l'institut de chimie des substances naturelles (ICSN) à Gif sur Yvette, des inhibiteurs des membres de la famille de BCL-2 pour contrecarrer les résistances à l'apoptose dues à la surexpression, dans de nombreux cancers, des membres anti-apoptotiques de cette famille.

S'il m'a semblé au départ difficile d'établir un lien entre mes différentes expériences scientifiques, il s'est avéré que les différentes thématiques de recherche que j'ai abordées : prolifération, instabilité chromosomique, résistance à l'apoptose sont autant de mécanismes permettant l'émergence de cellules tumorale. Ainsi, l'ensemble de mes travaux a pour fil conducteur la recherche en cancérologie.

Chapitre 1. Synthèse des travaux de recherche (2002-2018)

Chaque jour, dans le corps humain, environ 200 milliards de cellules meurent majoritairement par apoptose. Pratiquement tous les organes et tous les tissus sont soumis à ce renouvellement permanent dont la fréquence est plus ou moins élevée. L'équilibre entre prolifération et mort cellulaire est donc capital pour maintenir l'homéostasie. L'altération de l'un de ces deux processus peut conduire à la prolifération cellulaire aberrante qui caractérise le cancer. Dans la première partie de mon parcours, j'ai plutôt abordé le versant prolifération de ce processus en étudiant le cycle cellulaire et ses points de contrôle et l'importance du bon déroulement de la mitose. Actuellement et depuis ma prise de poste, mon travail porte plus sur la thématique de la résistance à l'apoptose des cellules tumorales.

I. Travaux de doctorat (2002-2006) : le centrosome dans la signalisation et la prolifération cellulaires

Pendant mon doctorat sous la direction du Dr. Chantal Desdouets, mes recherches ont porté sur deux sujets : le premier s'inscrivait dans le projet plus vaste du laboratoire sur la polyploïdie hépatocytaire et consistait à caractériser le rôle des centrosomes dans le maintien de ce processus physiologique, le deuxième que je qualifierai de plus personnel a été l'étude du rôle de la protéine Polaris dans la transition G_1/S. En ce qui concerne la formation des étudiant·e·s, j'ai encadré deux stagiaires faisant des stages volontaires (sans rapports finaux) : Mélanie Levasseur pour son stage de M1 en 2003 (deux mois) et Pauline Chang Yane pour son stage de L3 en 2004 (un mois). Toutes deux ont participé à mon projet de thèse sur la protéine IFT88/Polaris. Mélanie est maintenant gestionnaire de sites cliniques chez Parexel et Pauline est cheffe de projet chez FRS consulting.

A. Rôle des centrosomes dans le maintien de la tétraploïdie hépatocytaire

1) Contexte de recherche

Identifiée chez les plantes, il y a plus d'un siècle, la ploïdie d'une cellule est le nombre d'exemplaires de ses chromosomes. Une cellule est haploïde si elle possède n chromosomes c'est à dire une seule copie de chaque chromosome, un jeu complet où n est spécifique de l'espèce. Le nombre total de lots de chromosomes est indiqué par un préfixe.

Chez les mammifères, la majorité des cellules sont diploïdes, elles possèdent 2n chromosomes c'est à dire deux copies de chaque, et un seul centrosome. Un centrosome se compose de 2 centrioles (structures cylindriques creuses composées de microtubules) associés à une matrice protéique appelée matériel péricentriolaire (PCM) (Nigg et al., 2018). En interphase, il sert dans les cellules animales de centre organisateur des microtubules (MTOC) et a un rôle important dans la plupart des processus liés aux microtubules comme la motilité, le transport intracellulaire et la signalisation cellulaire. Dans les cellules quiescentes (G_0), un des deux centrioles a la capacité de s'accrocher à la membrane cellulaire et de commencer la croissance d'un axonème composé de 9 paires de microtubules pour donner un cil primaire (structure non motile se projetant à partir de la membrane cellulaire vers l'espace

extracellulaire). Le centrosome étant à la fois impliqué dans la division cellulaire et dans la ciliogenèse, ces deux processus sont mutuellement exclusifs. La présence du cil primaire est donc corrélée au cycle cellulaire et il disparait la plupart du temps à la transition G_1/S. Parallèlement à la réplication du génome, les cellules assurent donc la duplication de leur centrosome, et ce, une seule fois par cycle pour former deux centrosomes qui permettront l'établissement du fuseau mitotique. A la fin du cycle, chaque cellule fille hérite donc d'un centrosome et d'un lot de chromosomes ce qui nécessite une coordination des mécanismes de duplication des centrosomes avec le cycle cellulaire (Figure 1)

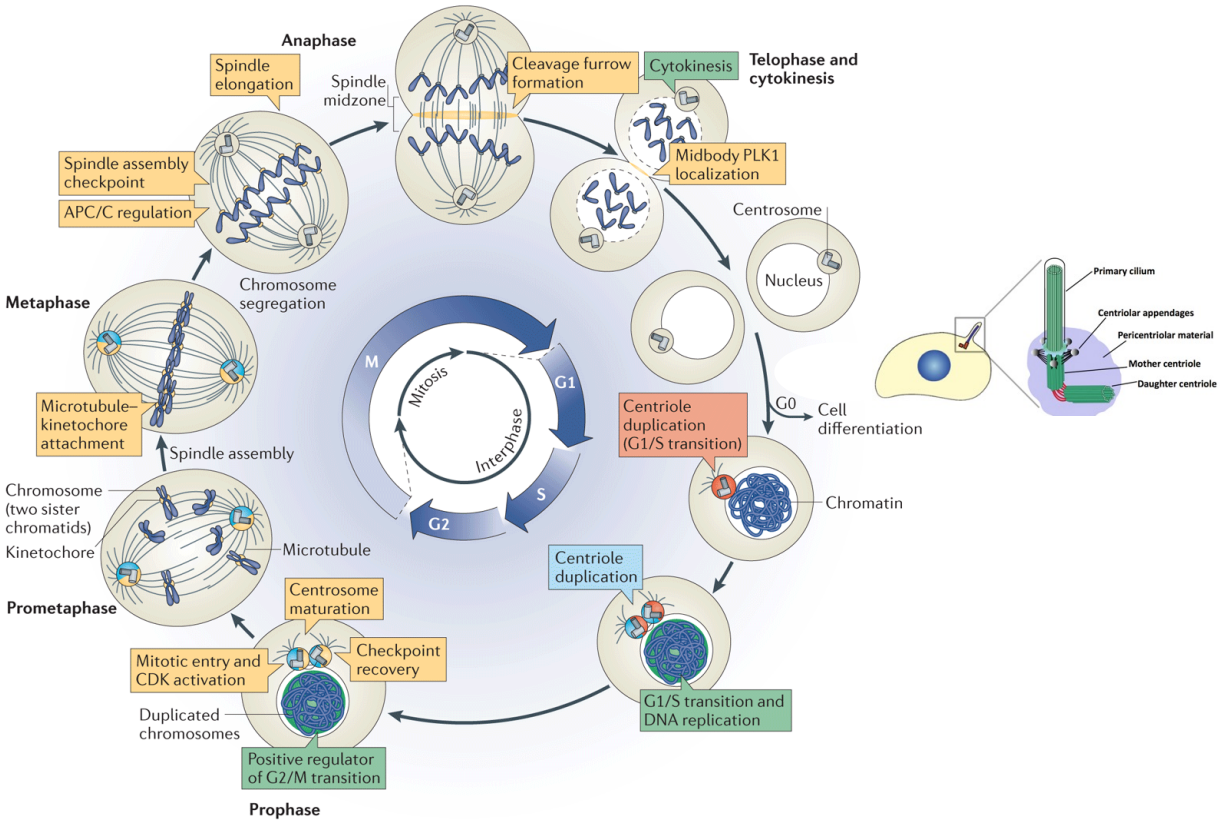

Figure 1 : Coordination du cycle cellulaire et du cycle des centrosomes modifiée à partir de (Zitouni et al., 2014)

Cependant, il existe des cellules dites polyploïdes ayant donc n patrimoine chromosomique au moins égal à 3 lots complets de chromosomes (3n) voire plus. Le terme « aneuploïdie » couvre l'ensemble des situations où le nombre de répétitions n'est pas le même pour les différents chromosomes, en s'opposant à « euploïdie » qui correspond aux degrés réguliers de ploïdie (multiple de n).

La conversion diploïdie vers polyploïdie fait partie des processus normaux de développement et de différentiation dans un contexte physiologique (Storchova et al., 2004). Chez les mammifères, l'apparition de cellules polyploïdes est observée au niveau du tissu myocardique, dans le trophoblaste, dans le tissu nerveux, dans l'épithélium rétinien, dans le rein, la vessie, le pancréas, le foie et la moelle osseuse (Vinogradov et al., 2001). La présence d'une polyploïdie avancée est généralement considérée comme la marque d'une différenciation terminale et de l'acquisition d'un état sénescent (Brodsky et al., 1977; Sigal et al., 1995; Sigal et al., 1999).

Cependant, la tétraploïdie constituerait un intermédiaire entre la diploïdie et l'aneuploïdie. Dans la littérature, nombreux sont les exemples corrélant la polyploïdisation cellulaire à l'apparition de l'instabilité chromosomique et au développement du processus de cancérogenèse. En effet, dans les stades précoces de développement de cancers de l'utérus, du sein ou de l'œsophage, l'apparition d'un contingent cellulaire tétraploïde est fréquemment observée et précède l'apparition de cellules aneuploïdes et le développement de tumeurs (Davoli et al., 2011). Pour empêcher la prolifération ou la survie de ces cellules tétraploïdes, différents mécanismes peuvent se mettre en place. Ainsi, les cellules tétraploïdes nouvellement générées peuvent subir un arrêt du cycle cellulaire dépendant de p38 / p53 lors de la phase G_1 qui conduit soit à la mort apoptotique soit à l'état de sénescence (Ganem et al., 2009). Si les cellules contournent ce point de contrôle et progressent vers la mitose, le point de contrôle de l'assemblage du fuseau mitotique (SAC, Spindle Assembly Checkpoint) peut être activé et exercer un niveau de contrôle supplémentaire pour maintenir l'intégrité de l'ADN. Des défauts de l'expression de certains composants du SAC ont été relevés dans de nombreux cancers. Dans ce contexte, les cellules en prolifération sont exposées lors de l'anaphase à une mauvaise séparation des chromosomes conduisant à un état aneuploïde. En effet, une cellule polyploïdie doit non seulement gérer un contenu en ADN augmenté, mais un nombre de centrosomes plus élevé. Des anomalies du nombre de centrosomes (centrosomes surnuméraires) ont été observées dans de nombreux types de tumeurs comme celles du côlon, du poumon, du cerveau, du sein (Pihan et al., 1998), et de la prostate (Pihan et al., 2001). La présence de ces centrosomes surnuméraires favoriserait la formation d'un fuseau mitotique multipolaire induisant des défauts de ségrégation des chromosomes.

Si la tétraploïdie peut conduire à l'aneuploïdie : quels sont les mécanismes mis en jeu pour assurer le maintien d'une ploïdie hépatocytaire contrôlée au cours du développement post-natal ? Qu'advient-il des cellules tétraploïdes au cycle suivant ? Comment est gérée la présence de centrosomes multiples ?

2) Résultats

Cette étude a permis en premier lieu de caractériser au cours du développement post-natal du foie chez le rat, le lignage existant entre les hépatocytes de ploïdie variable. Ces recherches ont été menées avec Jacques Emmanuel Guidotti alors en stage post-doctoral dans l'équipe et Olivier Brégerie, alors assistant ingénieur.

Le foie est un organe qui remplit de multiples fonctions vitales comme le métabolisme des glucides, des lipides et des protéines. Il produit et sécrète la bile, et participe à l'élimination des déchets toxiques de l'organisme. En condition physiologique, le foie adulte est un organe quiescent et polyploïde (Gupta, 2000). Bien que le foie soit constitué de différents types cellulaires, les hépatocytes comptent pour 78% du volume du foie et représentent 70% des cellules (Si-Tayeb et al., 2010).

Grâce à une technique d'analyse *in vivo* de la ploïdie hépatocytaire, nous avons pu quantifier, *in situ*, le contenu en ADN dans chaque noyau (marquage hoechst, distinction des hépatocytes mononucléés 2n/4n) et définir le nombre de noyaux par cellules (marquage β-

caténine : distinction hépatocytes monucléés/binucléés). Nous avons ainsi déterminé la cinétique d'apparition des hépatocytes polyploïdes au cours du développement. Lors des 22 premiers jours après la naissance, le foie est constitué d'hépatocytes mononucléés 2n. Puis entre 22 et 28 jours, le déclin de cette population est strictement corrélé avec l'apparition d'une population binucléée 2x2n. Enfin, après 30 jours, au moment où la population binucléée 2x2n diminue doucement, apparaît une population mononucléée 4n. Ces observations suggèrent que l'hépatocyte binucléé est une étape intermédiaire pour la genèse de l'hépatocyte mononucléé 4n.

Nous avons démontré pour la première fois, par vidéomicroscopie en temps réel, que des hépatocytes mononucléés 2n en culture primaire peuvent avoir un cycle de division modifié. En effet, après avoir interrompu leur cytocinèse, ces cellules mononucléées 2n donnent naissance à des hépatocytes binucléés 2x2n. Cet hépatocyte 2x2n peut, ensuite, entrer dans un nouveau cycle de division et donner alors naissance à deux hépatocytes mononucléés 4n, suite à une mitose unique de ces deux noyaux. Dans d'autres types cellulaires, la binucléation a été associée à un arrêt de la prolifération. De manière paradoxale, l'hépatocyte binucléé 2x2n est capable de réaliser un cycle de division complet en présence de p53 et de maintenir son état tétraploïde (genèse de deux cellules filles mononucléées 4n) sans dériver vers l'aneuploïdie.

Dans cette étude, j'ai caractérisé les différentes étapes de la mitose d'un hépatocyte binucléé 2x2n afin de comprendre le maintien de l'état tétraploïde. En prophase, il y a une rupture synchrone des membranes des deux noyaux. Puis, en métaphase, les chromosomes s'alignent sur une plaque métaphasique unique résultant de la mise en place d'un fuseau bipolaire unique qui permet à la cellule de maintenir son état tétraploïde. Les centrosomes jouent un rôle capital dans ce processus. En effet, j'ai démontré que l'hépatocyte binucléé 2x2n à l'état quiescent a deux centrosomes. Au cours de la phase S, les centrosomes de cette cellule sont correctement dupliqués. Lors de la mitose, les quatre centrosomes participent, dès la prophase, à la formation du fuseau bipolaire. Ils ont, en effet, la propriété de nucléer les microtubules. Lors de la métaphase, ils co-migrent 2 à 2 aux pôles de la cellule contrôlant ainsi la formation du fuseau mitotique unique, et conduisent donc à la division de la cellule en deux cellules filles mononucléées 4n (Figure 2).

En conclusion, dans cette étude, nous avons montré que la polyploidisation hépatocytaire est un processus physiologique original passant par un stade binucléation (cellules tétraploïdes). Dans ce système, la tétraploïdie n'est jamais associée avec des anomalies de mitoses et ces cellules sont capables d'entrer dans un nouveau cycle de division malgré la présence de p53.

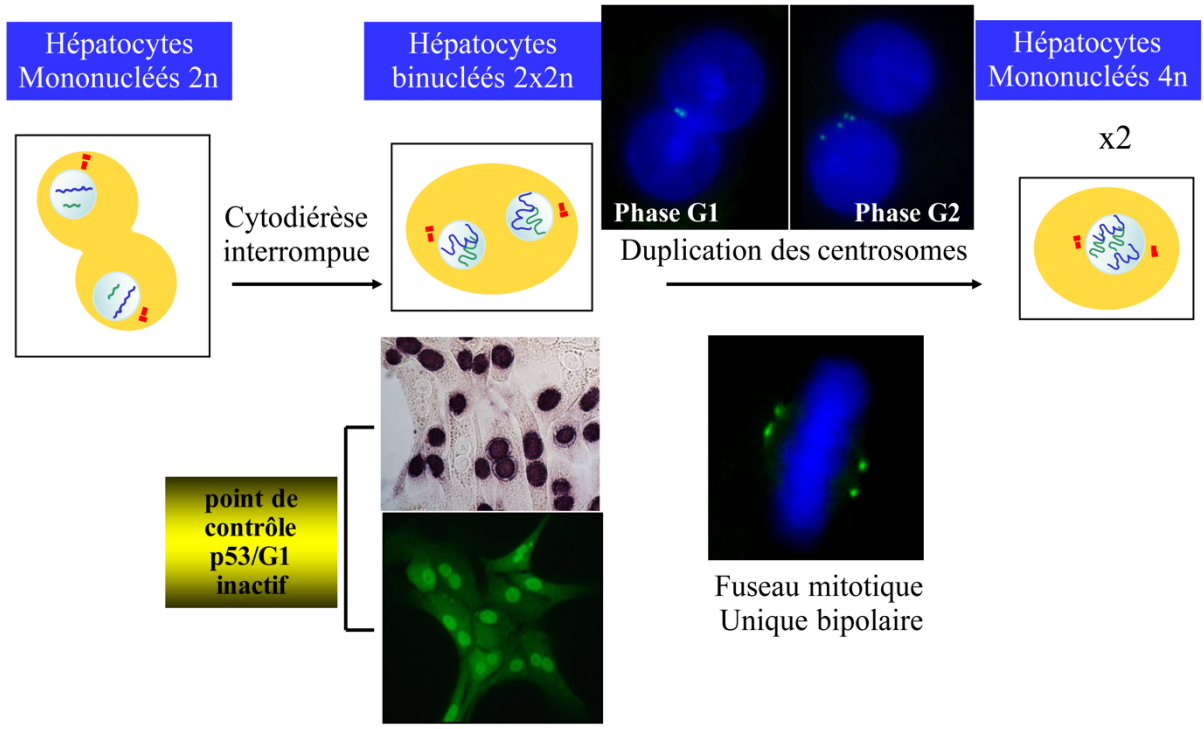

Figure 2: Ploïdisation du foie, un rôle de pivot pour l'hépatocyte binucléé

L'hépatocyte binuclée 2x2n est une étape intermédiaire pour la genèse d'hépatocytes 4n. Lors de la mitose, les centrosomes migrent deux à deux pour former un fuseau bipolaire et conduire à la formation de deux hépatocytes 4n et, ce en présence de p53. Image de mitose : les centrosomes sont en vert (gamma-tubuline) le noyau en bleu (DAPI). Image de phase S : Les cellules ont été incubées en présence de BrdU pendant 48h (image du haut) ou marquées avec un anticorps anti-p53. Aucunes différences de prolifération et d'expression de p53 ne sont observées entre les cellules binucléées et mononucléées.

Publication p.71

Guidotti JE, Bregerie O., **Robert A.,** Debey P., Brechot C., Desdouets C. Liver cell polyploidization : a pivotal role for binuclear hepatocytes. J. Biol. Chem. 2003,

B. Polaris est une protéine centrosomique impliquée dans la transition G_1/S

1) Contexte de Recherche

Dans le cadre de la recherche de protéines candidates induisant la binucléation hépatocytaire, nous nous sommes intéressés à la protéine IFT88/Polaris. Elle est codée par le gène *Tg737*, et comprend 824 aa contenant 10 motifs tetratricopeptides repeat (TPR) organisés en 2 domaines, un en N-terminal (trois motifs), un en C-terminal (sept motifs) (Moyer et al., 1994; Yoder et al., 1994). Des analyses bioinformatiques ont montré que cette protéine possède aussi deux domaines coiled-coil putatifs. Ces différents domaines sont impliqués dans les interactions protéines-protéines et dans l'assemblage de complexes multiprotéiques.

Chez la souris *Tg737*^{orpk} (mutant hypomorphe), il existe, dans le foie, une prolifération sans différenciation de cellules qui morphologiquement et immunologiquement ressemblent à des cellules ovales (Richards et al., 1996). Les cellules ovales sont considérées comme des cellules progénitrices du foie. En effet, elles peuvent donner naissance à toutes les cellules

épithéliales quel que soit leur niveau de différenciation, notamment aux hépatocytes et aux cellules biliaires. La ré-expression ectopique du gène *Tg737*, dans des lignées issues du foie des souris *Tg737*^{orpk}, a pour effet de rétablir la réponse de ces cellules aux facteurs externes de différenciation, de ralentir leur prolifération et conduit à l'apparition de cellules multinucléées (Richards et al., 1997). Ces données suggéraient un rôle éventuel de IFT88/Polaris dans la cytocinèse et par conséquent, un rôle potentiel dans la genèse de l'hépatocyte binucléé.

Par ailleurs, le gène *Tg737* a été trouvé altéré dans 40% des tumeurs du foie induites chimiquement chez le rongeur (Diéthynitrosamine) et dans des lignées cellulaires tumorales hépatiques, rénales, et pancréatiques. Plusieurs études ont montré que l'expression de *Tg737* était réduite chez les patients atteints de carcinomes hépatocellulaires (Chen et al., 2005; Isfort et al., 1997). La polyploïdie du foie étant fortement modifiée en conditions pathologiques, ceci conduit à envisager un rôle de IFT88/Polaris dans le processus de tumorigenèse hépatique.

Si les mutants *Tg737*^{orpk} sont viables, la délétion complète du gène *Tg737* murin (*Tg737*$^{\Delta 2\text{-}3\beta\text{-}gal}$) est létal au stade embryonnaire (Murcia et al., 2000). Les défauts de développement observés chez ces animaux notamment la spécification droite/gauche aléatoire (jusqu'à l'inversion complète de la position des organes) ont conduit à rechercher des défauts des cils. En effet, certains cils et notamment ceux du nœud embryonnaire de Hensen sont nécessaires à la mise en place de la latéralité lors du développement. L'absence et la malformation des cils observées chez les souris mutantes *Tg737*^{orpk} and *Tg737*$^{\Delta 2\text{-}3\beta\text{-}gal}$ (Murcia et al., 2000 ; Pazour et al., 2000) ainsi que l'analyse des homologues de IFT88/Polaris chez *Chlamydomonas et chez C. elegans* ont permis de montrer que IFT88/Polaris est une protéine du transport intraflagellaire (IFT), essentielle pour l'assemblage du cil et du flagelle (Haycraft et al., 2001; Pazour et al., 2000). Durant la croissance du cil ou du flagelle, l'axonème est assemblé par addition de nouvelles sous-unités de tubulines à son bout distal. Le transport des protéines du cytoplasme vers le site d'assemblage et leur recyclage se fait grâce à l'IFT, un processus hautement conservé au cours de l'évolution. Par exemple, IFT88/Polaris est conservée sur plus de $1{,}5.10^9$ années d'évolution allant de *Chlamydomonas* aux vertébrés. La protéine murine présente 45% d'identité avec la protéine OSM-5 de *C. elegans* (Haycraft et al., 2001) et 41% d'identité avec IFT88 de *Chlamydomonas* (Pazour et al., 2000). Le transport intraflagellaire est bi-directionnel : le mouvement antérograde (base vers bout) est médié par des kinésines motrices alors que le mouvement rétrograde est médié par une dyneine. Les mécanismes contrôlant la charge et la décharge de la cargaison, permettant le demi-tour exécuté par les particules de l'IFT à l'extrémité du cil ainsi que les modalités d'échange des moteurs à la base et à l'extrémité de l'axonème sont inconnues (revu dans (Veland et al., 2009)).

Pendant longtemps, la recherche s'est concentrée sur l'étude du cil motile considérant le cil primaire comme un simple vestige de l'évolution. Pourtant les cils primaires sont des organites présents à la surface de presque toutes les cellules des animaux à quelques exceptions près : les hépatocytes, les cellules nucléées du sang et les adipocytes. Depuis une vingtaine d'années, le cil primaire est devenu le centre d'une recherche intense notamment depuis l'association de certains composants du cil avec des maladies humaines (Ciliopathies). En effet, sa perte ou son dysfonctionnement entraîne (comme le montrent les défauts des

souris mutées pour *Tg737*) de nombreux désordres : absence de différentiation des cellules épithéliales, hyperprolifération et formation de kystes, ce qui suggèrent un rôle du cil dans la balance ciliogenèse/prolifération.

2) Résultats

Dans un premier temps, j'ai étudié l'expression d'IFT88/Polaris dans différents tissus chez la souris. Après avoir montré que IFT88/Polaris était exprimée dans le foie et dans les hépatocytes en culture primaire, j'ai cherché à définir si la surexpression de IFT88/Polaris avait un effet sur l'apparition d'hépatocytes binucléés en culture et *in vivo*. N'ayant pas obtenu de différences notables entre la condition normale et la condition de surexpression, nous en avons conclu qu'IFT88/Polaris n'était pas impliquée dans la binucléation hépatocytaire. Cependant, la présence de IFT88/Polaris dans des cellules non ciliées (hépatocytes) et l'émergence de l'idée que certaines protéines impliquées dans la ciliogénèse avait d'autres fonctions lors du cycle cellulaire m'ont incitées à caractériser le rôle de IFT88/Polaris dans les cellules en prolifération ciliées ou non. Nous avons montré que dans les cellules quiescentes, IFT88/Polaris est localisée dans le cil primaire alors qu'elle est localisée au centrosome tout au long du cycle cellulaire. Notre étude montre que IFT88/Polaris peut se relocaliser du cil vers la partie proximale des centrioles en fonction du stade différencié/prolifératif de la cellule ciliée. Différents mutants de délétion nous ont permis d'identifier les deux domaines TPR de IFT88/Polaris comme deux domaines indépendamment impliqués dans le ciblage au centrosome. Le fait que cette localisation au corps basal/centriole existe dans des cellules non ciliées suggérait que IFT88/Polaris soit associée à une autre fonction que celle de l'assemblage du cil dans ces cellules. Effectivement, nous avons montré qu'IFT88/Polaris, une protéine indispensable à l'assemblage du cil, est aussi une protéine centrosomique régulant la transition G_1/S : la surexpression de Polaris induit un arrêt du cycle à la transition G_1/S et une mort par apoptose. A l'inverse, sa déplétion accroît le nombre de cellules en phase S et G_2/M. De plus, nous avons montré que Polaris interagit avec Che1, une protéine liant Rb qui régule l'activité du facteur de transcription E2F essentiel pour la transition G_1/S (Figure 3A). Notre hypothèse est que la surexpression de IFT88/Polaris interfère avec la transition G_1/S en séquestrant Che1, qui est normalement requise à cette étape. Ainsi nous envisageons que durant la progression cellulaire, IFT88/Polaris, en interagissant avec Che1, régule sa localisation et/ou son activité pour contrôler l'entrée en phase G_1/S (Figure 3B).

En conclusion, le centrosome est le siège de mécanismes de surveillance de la progression du cycle cellulaire notamment lors de la transition G_1/S. Il n'est donc pas étonnant que si le cil envoie effectivement des signaux qui contrôlent la progression du cycle cellulaire, ces signaux passent par le centrosome. Ainsi, IFT88/Polaris est sûrement au centre d'un système complexe de régulation impliquant plusieurs voies de signalisation contrôlant la balance prolifération/différentiation cellulaire. Il est intéressant de noter que depuis ce travail, IFT88/Polaris a été impliquée dans l'orientation du fuseau mitotique (Delaval et al., 2011) et dans la migration et l'invasion (You et al., 2017).

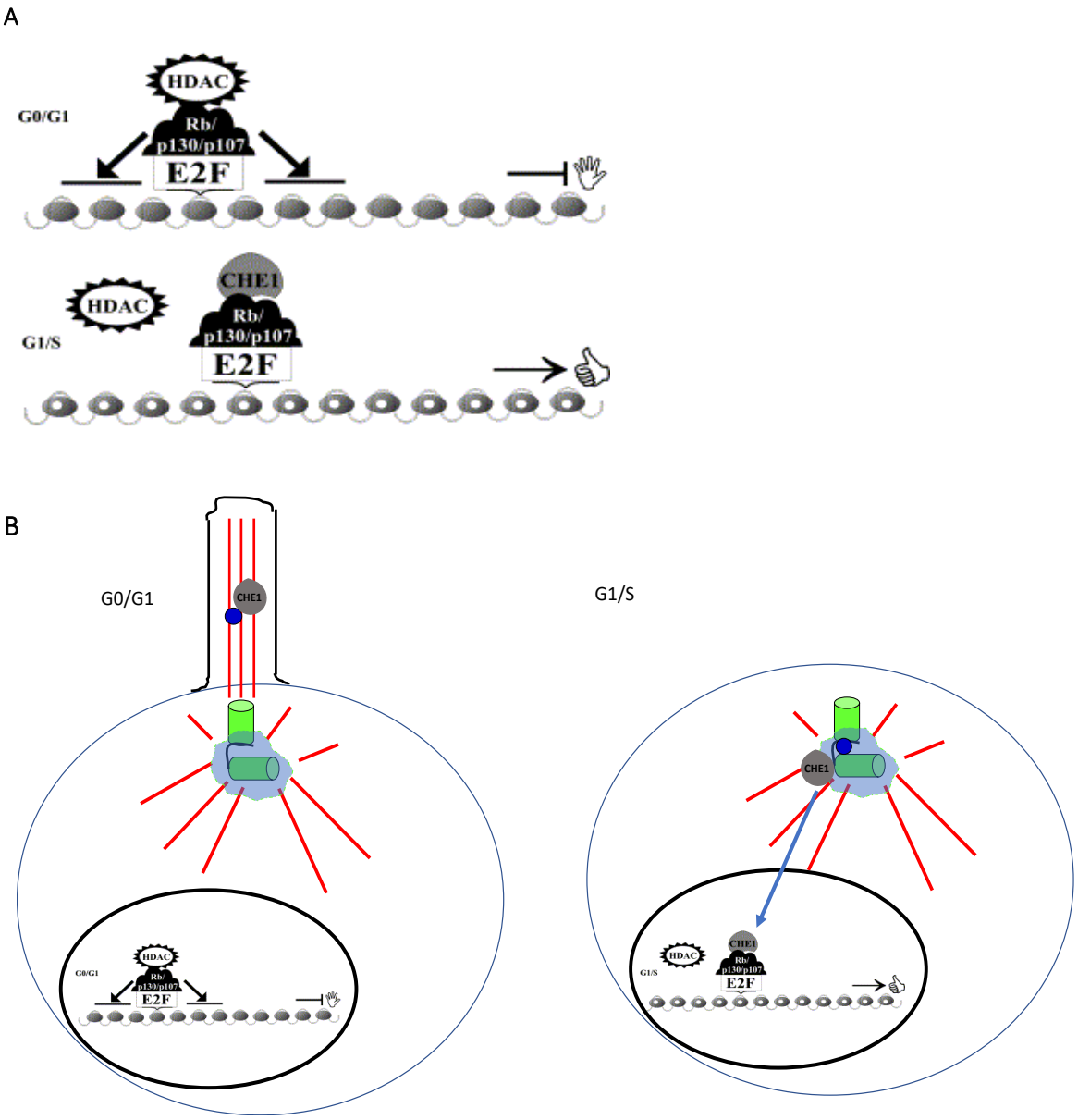

Figure 3 : Polaris et la transition G_1/S

A. En se fixant sur l'ADN, E2F active la plupart des gènes nécessaires à la phase S. En effet, en phase G_0/G_1, Rb interagit sous sa forme active (non phosphorylée) avec l'enzyme HDAC1 (Histone DéAcétylase 1), un complexe bloquant le facteur E2F ce qui empêche la transcription. A la transition $G_{1/S}$, Che1 entre en compétition avec HDAC1 pour la liaison à Rb. Une fois Che1 liée à Rb, il y a initiation de la transcription à bas niveau. Ensuite, quand Rb est inactivée par phosphorylation, elle se détache de E2F et ne verrouille plus du tout le système, c'est l'entrée en phase S. B. Polaris (en bleu) régulerait la localisation et/ou l'activité de Che1 (en gris).

Publication p.73

Robert A., Margall Ducos G., Guidotti J.E., Bregerie O., Celati C., Brechot C, Desdouets C. The Intraflagellar component Polaris is a centrosomal protein regulating G_1/S transition in nonciliated cells. J cell science. 2007, Feb 15;120(Pt 4):628-37.

II. Travaux de post-doctorat (2007) : TTLL12, une tubuline tyrosine ligase like impliquée dans l'instabilité chromosomique.

En 2007, j'ai rejoint l'équipe du Professeur Jan De Mey à l'université Louis Pasteur de Strasbourg pour un stage post-doctoral. Pendant cette période, j'ai pu encadré pendant deux mois, Florian Sirmain-Bousquet pendant son stage de 4ème année à l'ESBS (école supérieure de biotechnologie de Strasbourg). Cet encadrement était aussi bien technique que scientifique. Florian a mis au point la quantification par western blot des effets de la surexpression ou de l'inhibition de TTLL12 sur les modifications post-traductionnelles de la tubuline.

A. Contexte de recherche

Le cancer de la prostate est la 3ème cause de mortalité chez l'homme en France, soit environ 9000 décès par an depuis les années quatre-vingt-dix (source : bulletin épidémiologique du cancer de la prostate, http ://invs.santepubliquefrance.fr/beh/2016/39-40/2016_39-40_1.html). Un criblage des ARNs différentiellement exprimés dans des tumeurs par rapport à des tissus sains issus de patients atteints d'un cancer de la prostate a permis l'identification de potentiels nouveaux marqueurs et nouvelles cibles thérapeutiques.

En raison de ses propriétés enzymatiques, hTTLL12, un membre de la famille des tubulines tyrosines ligases qui est très conservée au cours de l'évolution, a particulièrement retenu notre attention. Chez les mammifères, il existe treize TTLLs : 1, 2, 4 5, 6, 9, 11 et 13 sont des glutamylases alors que 3, 8 et 10 sont des glycylases. En 2007, TTLL12 n'était pas caractérisée mais des analyses du laboratoire montrait qu'elle possédait à la fois des domaines SET-like et TTL-like suggérant qu'elle pourrait avoir des activités de méthylation des histones et de tubuline tyrosine ligase (Wasylyk et al., 2010).

Les modifications de la partie C-terminale de la tubuline sont importantes pour son rôle dans de nombreux processus cellulaires comme l'organisation subcellulaire, le transport intracellulaire, la migration et la mitose. De plus, une polyglutamylation ou une tyrosination altérées des microtubules ont été associées avec la tumorigénèse (Janke et al., 2010; Soucek et al., 2006). De même, les modifications post-traductionnelles de la tubuline peuvent affecter la sensibilité aux chimiothérapies ciblant les microtubules (Taxol, estramustine) (Ohta et al., 1994 ; Sangrajrang et al., 1998).

Ces données faisaient de TTLL12 une cible thérapeutique éventuelle. Le but du projet était donc d'évaluer son potentiel pronostique, diagnostique et thérapeutique.

B. Résultats

Au sein du consortium, chaque laboratoire avait sa spécialité et par conséquent, étudiait une facette des fonctions de TTLL12. Nous avions pour but d'étudier le rôle de TTLL12 pendant la mitose, nous avons donc développé un système d'imagerie en temps réel nous permettant d'analyser un grand nombre de cellules en mitose. La dynamique des chromosomes a été suivie en utilisant le Hoechst, un colorant vital. Pour chaque cellule surexprimant (Figure 4A) ou inhibées (Figure 4B) pour TTLL2, le temps écoulé entre la rupture de l'enveloppe nucléaire ou NEB (Nuclear envelope breakdown, t=0), signe de l'entrée en mitose et le début de l'anaphase (disjonction des chromatides) a été déterminé. Les chromosomes qui ne rejoignaient pas la

plaque métaphasique avant l'anaphase ont été comptabilisés comme non alignés, ceux qui restaient bloqués au niveau de l'équateur du fuseau après l'anaphase ont été comptabilisé comme en retard. La fragmentation de la chromatine et le bourgeonnement de la membrane (marqueurs de mort cellulaire), l'orientation de la plaque métaphasique, la formation de fuseaux multipolaires ont été évalués à partir des images de contraste de phase et de fluorescence (Figure 3C). Ainsi, j'ai pu mettre en évidence que la surexpression et l'inhibition de TTLL12 entrainaient un allongement du temps de mitose. En effet, les modifications d'expression de TTL12 affectent la position du fuseau mitotique ce qui empêche la congression des chromosomes et par conséquent augmente la durée de la prophase et de la pro-métaphase. Le groupe a aussi montré que des niveaux altérés de TTLL12 conduisaient à des changements de la méthylation des histones et des tyrosinations de l'alpha tubuline. De même, son expression modifiée conduit à une augmentation du nombre de chromosomes par cellules. Aussi, nous pouvons penser que TTLL12 a un effet sur la dynamique du cytosquelette. En effet, la tyrosination de la tubuline est un facteur important pour le recrutement des protéines CAP-Gly (CLIP-170, p150glued) aux extrémités des microtubules ce qui permettrait la stabilisation de ces derniers (Peris et al., 2006).

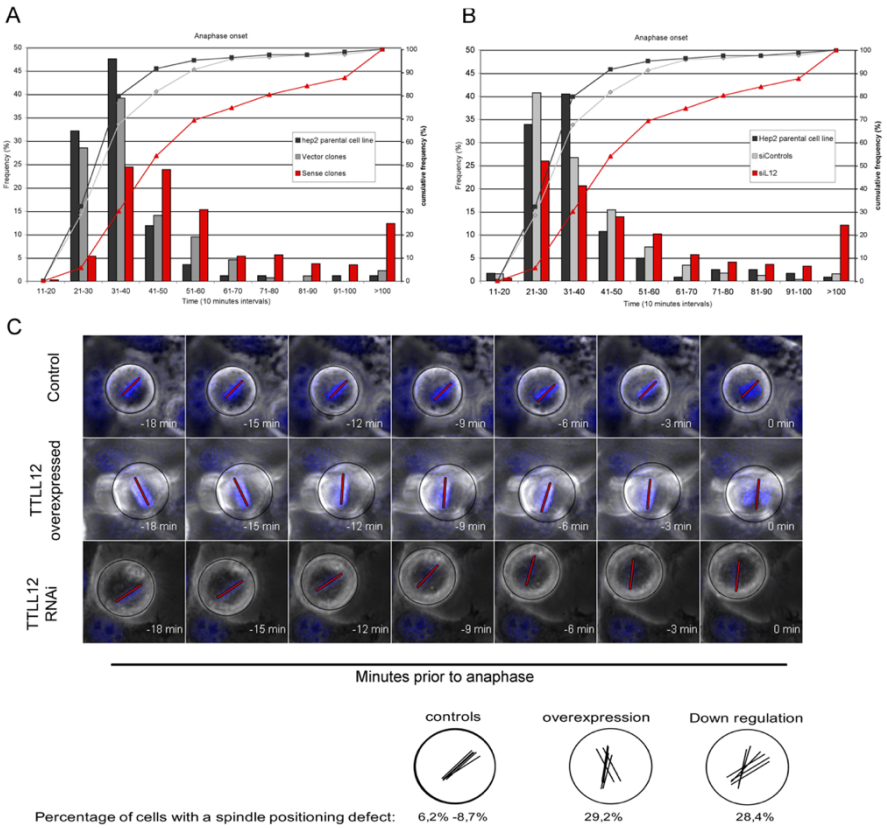

Figure 4 : Les modifications d'expression de TTLL12 interfèrent avec la congression des chromosomes et l'orientation du fuseau mitotique entrainant un allongement du temps de mitose.

A-B. Fréquences cumulatives (courbes, axe de droite) et fréquences de distribution (histogrammes, axe de gauche) de la durée de la mitose pour les clones surexprimant TTLL12 (A) et ceux inhibés (B).
C. Un exemple d'images obtenues montrant l'instabilité de la plaque métaphasique dans les clones où l'expression de TTLL12 est modifiée. 48h (clones surexprimant) ou 72h (clones inhibés) après ensemencement, les cellules sont marquées au Hoechst vital, placées sous le microscope dans une chambre thermostatée régulée en CO2 pendant 4h. Une image est prise toutes les 3 min.

En résumé, nos travaux montrent que la perte de fonction et la surexpression de TTLL12 conduisent au même phénotype suggérant qu'une régulation fine de l'expression de TTLL12 est nécessaire. Quelle peut être la relation entre le phénotype observé lors de la mitose et le rôle de TTLL12 dans le cancer ? Des défauts du contrôle du positionnement du fuseau ont été proposé en tant que facteur favorisant l'invasion tumorale. En effet, un mauvais positionnement du fuseau faciliterait le détachement des cellules filles de l'épithélium et donc leur dissémination dans l'organisme (Vasiliev et al., 2004). De plus, le délai transitoire de l'entrée en mitose suite aux modifications d'expression de TTLL12 n'est peut-être pas suffisant pour assurer la ségrégation correcte et complète des chromosomes. On peut donc penser que ces modifications prédisposent les cellules à des mauvaises ségrégations des chromosomes et donc à l'aneuploïdie.

Publication p.75
Brants J., Semenchenko K., Wasylyk C., **Robert A.**, Carles A., Zambrano A., Pradeau-Aubreton K., Birck C., Schalken J., Poch O., de Mey J., and Wasylyk B. Tubulin Tyrosine Ligase Like 12, a novel TTLL family member with SET- and TTL-like domains and roles in histone and tubulin modifications and mitosis. Plos One décembre 2012; 7(12)

III. Travaux de recherches en tant qu'ingénieure de recherche (2008-2018) : mécanismes d'apoptose dans les cellules de lymphomes B

Au 1er décembre 2007, j'ai rejoint en tant qu'ingénieure de recherche de l'université Paris Sud, l'équipe du Dr. Joëlle Wiels au sein de l'UMR8126 à GR dont la thématique était la résistance à l'apoptose dans les cellules de lymphomes B. Depuis mon arrivée dans l'UMR8126, mon poste me conduit à accompagner techniquement les différents membres de l'équipe, je ne mentionnerai donc au fil de l'eau que les étudiants que j'ai encadré à la fois sur le plan technique et sur le plan scientifique.

Nos modèles d'études sont différents lymphomes B notamment ceux associés au virus d'Epstein-Barr (EBV) comme le lymphome de Burkitt (LB), le lymphome diffus à grandes cellules B (DLBCL) et le syndrome lymphoprolifératif post-transplantation (PTLD).

Le LB est un lymphome non-hodgkinien (LNH) caractérisé par une prolifération monoclonale de lymphocytes B qui fut décrit pour la première fois par Denis Burkitt en 1958 (Burkitt, 1958). L'OMS (Organisation Mondiale de la Santé) distingue à ce jour trois formes cliniques de cette maladie dont la forme majoritaire, dite endémique, touche principalement des enfants d'Afrique équatoriale et de Papouasie-Nouvelle Guinée. Elle se manifeste par des tumeurs de la mâchoire et de la cavité abdominale ; elle est associée à EBV dans 98 % des cas. Une forme sporadique et une forme associée au syndrome d'immunodéficience des patients infectés par le VIH (Virus d'Immunodéficience Humaine) ont aussi été décrites. Elles se traduisent par une atteinte tumorale multiviscérale et sont plus faiblement associées à EBV (10 à 20% et 40 à 50% respectivement). Une caractéristique majeure du LB est la présence d'une translocation chromosomique qui place l'oncogène *c-Myc* au voisinage d'une région

chromosomique codant pour des chaînes lourdes (IgH) ou légères (IgL) des immunoglobulines (revu dans (Shannon-Lowe et al., 2017)).

Les DLBCL appartiennent comme le LB à la catégorie des LNH-B agressifs. Selon la classification de l'OMS de 2017, ils représentent 25 à 30 % des LNH de l'adulte dans les pays occidentaux (le pourcentage est plus élevé dans les pays en voie de développement). Ils sont définis principalement par deux critères histopathologiques : l'architecture diffuse de la population tumorale et la grande taille des cellules tumorales qui sont des cellules lymphoïdes matures de phénotype B. Leur hétérogénéité moléculaire rend leur classification complexe (revu dans (Ott, 2017)). On distingue les DLBCL NOS (Not Otherwise Specified) et les DLBCL, correspondant aux entités suivantes :

- Lymphome à grandes cellules B riche en lymphocytes T
- DLBCL primitif du système nerveux central
- DLBCL cutané primitif, de type jambe (leg-type)
- DLBCL EBV-positif du sujet âgé.

Les DLBCL NOS sont classés en deux sous-groupes moléculaires selon leur profil d'expression génique :

- DLBCL-GCB, de type centro-folliculaire, ayant pour origine les lymphocytes B des centres germinatifs.
- DLBCL-ABC, de type cellules B activées, ayant pour origine des lymphocytes B post-germinatifs.

La majorité des DLBCL survenant dans la population générale ne sont pas associés à l'EBV. Toutefois dans des contextes cliniques particuliers, tels que les sujets âgés ou immunodéprimés, l'EBV est fréquemment retrouvé chez ces patients. De plus, les DLBCL associés à une inflammation chronique ainsi que la granulomatose lymphomatoïde sont également associés au virus d'Epstein-Barr (revu dans (Shannon-Lowe et al., 2017)).

Les PTLD sont des syndromes prolifératifs ayant pour origine des cellules B dans 85% des cas et qui peuvent constituer une complication fatale des transplantations. Survenant précocement suite au traitement immunodépresseur prescrit après toute greffe d'organe, leur incidence est de 1 à 20 % selon l'organe transplanté. La majorité des cas est associée à EBV et qui plus est, la séroconversion du receveur, par infection via l'organe donneur, constitue un facteur de risque (revu dans (Vegso et al., 2011)). Comme les cellules de PTLD présentent peu d'anomalies génétiques et que peu de lignées cellulaires issues de patients ont été établies, les lignées cellulaires lymphoblastoïdes (LCL) obtenues *in vitro* après transformation de lymphocytes B humains normaux par EBV constituent un bon modèle de substitution (Nourse et al., 2011).

Le traitement conventionnel du LB et des DLBCL repose sur une chimiothérapie intensive de quelques mois (régime CHOP : cyclosphamide, hydroxyadriamycine, vincristine, prédnisone). Une prise en charge rapide et un traitement anti-tumoral approprié sont les clés de la guérison dont les taux sont actuellement de l'ordre de 80-90 % chez les enfants atteints de LB, tous stades confondus. En cas de rechute, si le lymphome reste sensible à la chimiothérapie, 10 à 20 % de guérisons sont obtenues grâce à une thérapeutique massive mais,

s'il existe une chimiorésistance, le pronostic est sombre. Chez l'adulte, le pronostic est d'emblée plus mauvais notamment chez les sujets âgés. Toutefois, des approches agressives utilisant des hautes doses de chimiothérapie ont permis pour le BL, d'obtenir un taux de réponses complètes compris entre 60 et 80% avec un taux de guérison variant de 40 à 60% (Thomas et al., 2006). Un essai clinique de phase 3 a récemment montré que l'ajout de Rituximab à la chimiothérapie (R-CHOP) augmente légèrement la survie sans événements des patients à 3 ans (75 *vs* 62%) (Ribrag et al., 2016). Pour les DLBCL, ce traitement a, de même, permis d'améliorer leur pronostic mais nombre de patients ne répondent pas au traitement ou développent des résistances et rechutent**.**

La prise en charge des PTLD, elle, repose sur la levée de l'immunosuppression, pour permettre à l'organisme de lutter contre EBV mais expose le patient à un rejet de la greffe. Le traitement par le Rituximab seul ou combiné à une chimiothérapie conventionnelle à faible dose (R-CHOP) est ensuite envisagé chez les patients réfractaires. En effet, le Rituximab induit la déplétion des L_B matures réduisant ainsi le contingent de cellules infectées par EBV. Cependant, si la fonction des L_T cytotoxiques n'est pas restaurée, cela peut conduire à des rechutes lors de la réapparition des L_B (Vegso et al., 2011).

La résistance des cellules tumorales aux agents cytotoxiques représente aujourd'hui encore un obstacle majeur de la chimiothérapie anticancéreuse. Cette résistance peut être intrinsèque (primaire) ou acquise (secondaire). La résistance intrinsèque survient d'emblée lors de l'administration des premières séances de chimiothérapie, sans phase de sensibilité initiale. De nombreuses tumeurs sont ainsi d'emblée résistantes : c'est le cas du mélanome, de nombreux sarcomes et de tumeurs cérébrales. La chimio-résistance acquise apparaît après une phase initiale de grande chimio-sensibilité, et est corrélée à une progression de la maladie. Elle peut être due à l'hétérogénéité des cellules qui composent une tumeur. En effet, un médicament peut détruire la majorité des cellules tumorales, mais être incapable de s'attaquer à une fraction résiduelle. Le traitement semble alors au départ très efficace : la destruction des cellules majoritaires conduit à une réduction rapide et importante de la tumeur. Mais, les cellules minoritaires résistantes vont se multiplier et conduire à la formation d'une nouvelle tumeur qui sera insensible au traitement. Par ailleurs, les cellules cancéreuses sont capables d'évoluer rapidement et d'acquérir la capacité de se multiplier et de survivre en présence d'une molécule conçue pour les détruire. Cette résistance est donc un processus complexe qui implique divers mécanismes comme l'augmentation de l'efflux des drogues, les mutations touchant la cible, l'activation de voies de signalisation alternatives et l'échappement à la mort cellulaire. Il est donc important, à la fois, de décrypter les voies de signalisation apoptotique « activables » dans les cellules tumorales mais également de comprendre les différents mécanismes qui leur permettent de résister à ce processus de mort cellulaire, et ce afin de pouvoir développer de nouveaux outils thérapeutiques ciblés, en alternative aux traitements conventionnels. Le groupe de Joëlle Wiels travaille depuis plusieurs années sur les mécanismes de résistance à l'apoptose induits par divers stimuli dans les cellules de lymphomes B. Dans la continuité de cette thématique, les travaux que je mène actuellement ont une triple visée : 1)

analyser les mécanismes d'apoptose induits par certains stimuli, 2) essayer de mieux comprendre comment les mécanismes de résistance à l'apoptose se mettent en place, 3) tenter de les contrecarrer et d'induire l'apoptose des cellules tumorales par d'autres voies.

A. Mécanismes de résistances à l'apoptose p53 dépendante induits par le virus d'Epstein-Barr

1) Contexte de recherche

Un des mécanismes qui permet aux cellules cancéreuses d'échapper à l'apoptose est leur infection par des virus dit oncogénique. En effet, certaines protéines virales sont capables d'interagir avec des protéines des voies de signalisation apoptotique et d'abolir leurs activités. Le virus d'Epstein-Barr (EBV) sur lequel nous travaillons, est l'un d'entre eux (Figure 5).

L'EBV est un Herpes virus associé à différentes tumeurs lymphoïdes ou épithéliales dont les principales sont le LB, les PTLD et le carcinome nasopharyngé (NPC) (Young et al., 2004). L'ADN viral est présent dans les cellules sous forme épisomal et les cellules malignes infectées expriment des protéines virales dites « de latence » : six nucléaires (EBNA1, 2, 3A, B, C, LP) et trois membranaires (LMP1, 2A, 2B). En fonction de leur expression, trois grands types de latence ont été décrits :

- La latence I (expression d'EBNA1 uniquement) retrouvée dans la majorité des cellules de LB
- La latence II (expression d'EBNA1 et des LMP) retrouvée dans les cellules de NPC
- La latence III (expression de toutes les protéines virales) retrouvée dans les cellules de PTLD et dans certains cas de LB (Rowe et al., 1987 ; Thompson et al., 2004).

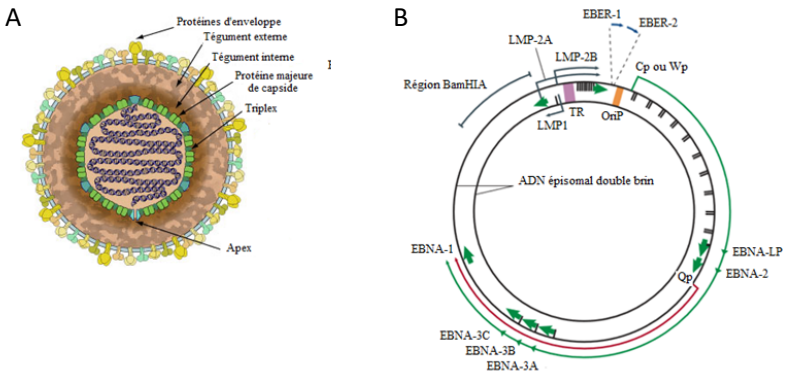

Figure 5 : Structure du virus d'Epstein-Barr, adaptée de (Young and Rickinson, 2004)

(*A) Schéma de la particule virale de l'EBV (adapté de ViralZone, Swiss Institute of Bioinformatics, 2017), le tégument contient des phosphoprotéines et l'enveloppe des glycoprotéines. (B) Diagramme montrant la localisation de la transcription des gènes latents sur l'ADN double brin de l'EBV sous forme épisomale. L'origine de réplication du plasmide est représentée en orange (OriP). Les flèches vertes en gras représentent les exons codant chaque protéine de latence, la flèche indique le sens de transcription du gène. Les protéines de latence correspondent aux 6 protéines nucléaires (EBNA-1, -2, -3A, -3B, -3C et -LP) et aux 3 protéines membranaires (LMP-1, -2A et -2B). EBNA-LP est transcrit à partir d'un nombre variable d'exons répétés. LMP-2A et LMP-2B sont transcrits à partir de multiples exons situés au niveau de la région TR qui se forment lors de la circularisation de l'ADN viral en épisome. Les flèches bleues indiquent les ARNs non codants, les EBER-1 et EBER-2, dont la transcription est caractéristique d'une infection latente. La longue flèche verte externe représente la transcription de l'EBV lors d'un profil de latence III, durant laquelle tous les EBNAs sont transcrits à partir du promoteur Cp ou Wp, les différents EBNAs sont codés par leurs propres ARN messagers qui sont générés par l'épissage alternatif d'un même transcrit primaire. La flèche interne rouge représente le transcrit de EBNA-1 qui prend son origine à partir du promoteur Qp durant les latences I et II. Des transcrits de la région BamHIA peuvent être détectés durant l'infection latente, cependant aucune protéine codée par cette région n'a encore été identifiée. Ces transcrits sont appelés les BARTs (BamHIA rightward transcripts).*

Par ailleurs, il est admis que l'inactivation de la protéine p53 peut se faire soit par la présence de mutations au niveau de son gène ou par la surexpression de son régulateur principal, la protéine MDM2 et qu'elle est impliquée dans le processus de transformation des cellules de LB. Des travaux réalisés au laboratoire ont montré que les lignées de LB exprimant une forme sauvage de p53 présentent aussi une forte expression de MDM2 (Capoulade et al., 1998) et que l'inhibition de MDM2 par des oligonucléotides antisens induit l'apoptose de ces cellules (Capoulade et al., 2001). Notre équipe a ensuite étudié la réactivation de p53 dans les cellules de lymphomes B ayant une p53 sauvage en ciblant le complexe p53/MDM2 à l'aide de la nutline 3, une molécule qui se fixe sur MDM2 au niveau de son site d'interaction avec la p53 et libère ainsi cette dernière. Nos résultats montrent que le traitement des cellules de LB et PTLD par la nutline 3 induit l'activation de p53 dans toutes les lignées testées. Cependant, les cellules EBV- entrent massivement en apoptose, alors que les cellules EBV+ en latence III sont très résistantes (Renouf et al., 2009). La suite de ce travail auquel j'ai participé, a consisté à élucider les mécanismes impliqués dans cette résistance à l'apoptose et à mettre en place des stratégies pour la contourner.

2) Résultats

Sachant qu'EBV peut induire la surexpression de la protéine anti-apoptotique BCL-2 (Henderson et al., 1991), la première hypothèse était la suivante : l'inhibition de BAX par BCL-2 dans les cellules EBV+ en latence III empêche sa relocalisation mitochondriale et par conséquent l'apoptose induite par la nutline 3. Pour tester cette hypothèse, un inhibiteur de BCL-2, ABT-737 a été utilisé et sa capacité à restaurer la sensibilité de ces cellules à la nutline 3 a été analysé.

Dans nos cellules, le pré-traitement avec ABT-737 rompt l'interaction BAX/BCL-2 sans affecter le niveau d'expression de ces deux protéines et augmente la quantité de BAX relocalisée dans la mitochondrie après traitement par la nutline 3. Ceci a pour effet d'augmenter la proportion de BAX activée dans les cellules EBV+ en latence III et de restaurer leur sensibilité au traitement par la nutline 3.

Par ailleurs, les résultats obtenus montrent que le traitement avec ABT-737 seul est capable d'induire fortement l'apoptose dans toutes les lignées de LCL (modèle de PTLD). Ces résultats très intéressants nous ont conduit à poursuivre l'étude de ce composé afin de déterminer son utilité en tant que thérapie alternative dans le traitement des lymphomes B associés à EBV, seul ou en association avec des traitements conventionnels (voir § B).

En parallèle, afin de mieux comprendre les mécanismes mis en jeux : une analyse du transcriptome a été réalisée sur 2 lignées de LB qui ne diffèrent que par leur statut EBV : les BL2, EBV- et BL2 infectées *in vitro* par la souche B95 d'EBV, appelées BL2/B95 qui sont en latence III, traitées ou non pendant différents temps par la nutline 3. Les résultats montrent que les gènes cibles de p53 sont induits après traitement dans les deux lignées, mais que, de manière intéressante, ceux impliqués dans l'autophagie le sont plus fortement dans la lignée EBV+ en latence III. L'autophagie est une voie de dégradation des protéines et organelles qui

maintient l'homéostasie cellulaire dont le rôle physiologique est très discuté puisque ce processus permet la survie cellulaire mais peut également induire la mort.

Nous avons montré que les cellules EBV+ en latence III ont un niveau basal d'autophagie élevé par rapport aux cellules EBV-. De même, des biopsies de patients ayant un lymphome B EBV+ en latence II ou III ont un fort niveau d'autophagie. Cette autophagie constitutive est due notamment à l'activation de NFKB (induite par la protéine virale LMP1) qui provoque une surexpression de l'un des acteurs majeurs de la formation des autophagosomes, la Bécline-1. De plus, le traitement des cellules EBV+ en latence III par la chloroquine, un inhibiteur de l'autophagie, induit l'apoptose des cellules et potentialise l'effet cytotoxique de la nutline, démontrant ainsi que le processus d'autophagie participe à la résistance de ces cellules à l'apoptose.

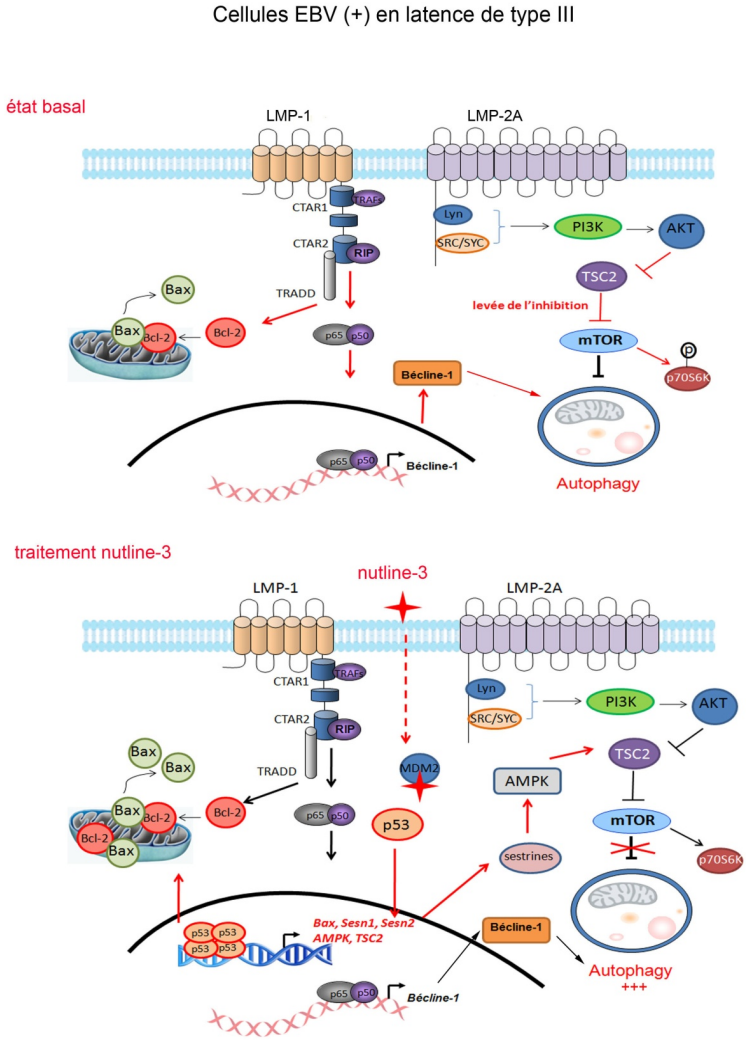

Figure 6 : Schéma illustrant les différents mécanismes impliqués dans la résistance à l'apoptose induite par p53 des cellules EBV+ en latence de type III (D'après la thèse de A. Pujals)

A l'état basal, la LMP-1 induit l'expression de la protéine BCL-2 qui interagit avec BAX. La LMP-1 active également p65 qui se fixe sur le promoteur de bécline-1 et augmente son expression. Ce mécanisme augmente le niveau d'autophagie dans ces cellules. A l'inverse la LMP-2A inhiberait ce processus en favorisant l'activation de mTOR par l'intermédiaire de la voie PIK/AKT qui inhibe TSC2. Le traitement par la nutline-3 induit l'activation de p53 ce qui permet la transcription de ses gènes cibles qui peuvent être impliqués dans l'apoptose et l'autophagie. Dans ces cellules, l'augmentation de l'expression de BAX n'a pas d'effet car la protéine BCL-2 inhibe l'activité pro-apoptotique de cette protéine. L'activation des Sestrines, de l'AMPK et de TSC2 induit une inhibition de mTOR ce qui lève l'inhibition de l'autophagie. Ce mécanisme contribue également à la résistance des cellules à l'apoptose.

Les travaux des doctorantes Anaïs Pujals (2008-2012) et Loëtitia Favre (2012-2016) auxquels j'ai participé montrent donc que la résistance à l'apoptose p53 dépendante induite par EBV repose sur deux mécanismes complémentaires : la surexpression de la protéine anti-apoptotique BCL-2 (Pujals et al., 2011) et une autophagie constitutive (Pujals et al., 2015) (Figure 6).

Publications p.77

Pujals A, Renouf B**, Robert A**, Chelouah S, Hollville E, Wiels J. Treatment with a BH3 mimetic overcomes the resistance of latency III EBV (+) cells to p53-mediated apoptosis. Cell Death Dis. 2011 Jul 28;2:e184. doi: 10.1038/cddis.2011.67.

Pujals A, Fabre L., Durieu C., **Robert A,** Meurice G, Legentil M., Chelouah S, Lecam E., Vassilev L., Lipinski M, Wiels J. Constitutive Autophagy in Epstein-Barr Virus-positive Latency III Cells Protects them from Nutlin-3-induced Apoptosis. Autophagy. 2015

Dans la continuité de ce projet, nous avons accueilli Tiphaine Gaudin pour son stage de M2 de Virologie Moléculaire et Médicale de l'UPMC en janvier 2018 (six mois). Elle a travaillé sur le rôle de la protéine DRAM-1 dans la résistance à l'apoptose des cellules tumorales infectées par le virus d'Epstein-Barr. Parmi les gènes retrouvés lors de l'analyse transcriptomique, DRAM-1 (DNA damage-Regulated Autophagy Modulator 1) est celui qui est le plus fortement exprimé en réponse à la nutline 3 puisque son expression est augmentée de 68 fois dans les cellules EBV+ en latence III et 27 fois dans les cellules EBV-. Pendant son travail de Master 2, l'objectif de Tiphaine a donc été d'approfondir l'étude de la protéine DRAM-1. DRAM-1 a été identifiée en 2006 (Crighton et al., 2006), mais ses différents rôles et mécanismes d'action demeurent méconnus. Il a toutefois été montré que DRAM-1 est une protéine lysosomale, induite par p53, qui régulerait positivement l'autophagie en augmentant l'acidification des lysosomes. Elle induirait aussi l'apoptose par la voie mitochondriale en interagissant avec BAX, une protéine pro-apoptotique (Guan et al., 2015).

Tiphaine a montré que l'EBV augmente le niveau basal de DRAM-1 (en termes d'ARN et de protéine) quel que soit le type de latence II (NPC) ou III (BL). Elle met aussi en évidence une augmentation en ARN et en protéine de DRAM-1 en réponse à l'activation de p53 dans les cellules en latence II, alors que dans les cellules en latence III, cette augmentation de l'ARN n'est pas reflétée par une augmentation de la protéine. Il reste maintenant à comprendre les mécanismes qui induisent une expression basale élevée de DRAM-1 dans les cellules EBV+ et pourquoi celle-ci ne peut être augmentée dans les cellules en latence III après activation de p53. L'inhibition de l'expression de DRAM-1 par CRISPR-Cas9 est l'une des pistes envisagées pour mieux comprendre son rôle à l'état basal et après induction de l'apoptose. J'ai encadré Tiphaine techniquement et scientifiquement, j'ai conçu, avec elle, les expériences qu'elle a réalisées, analysé avec elle ses résultats, corrigé son rapport et je l'ai entrainée pour sa soutenance orale.

B. Stratégies thérapeutiques fondées sur l'utilisation d'inhibiteurs des protéines anti-apoptotiques de la famille de BCL-2 dans le traitement des lymphomes B.

Dans le cadre de ce projet, j'ai encadré Loëtitia Favre (Directrice de thèse : Joëlle Wiels). Elle a réalisé les expérimentations in vitro et participé à celles in vivo sur le projet visant à évaluer le potentiel thérapeutique d'un inhibiteur de BCL-2 dans le traitement des lymphoprolifératons B associées à EBV. Elle a aussi mis au point au laboratoire, le test de BH3 profiling qui permet de tester les membres anti-apoptotique de la famille BCL-2 nécessaires à la survie de nos lignées cellulaires. Notre travail a abouti à une publication et à un article en préparation dont elle est 3ème autrice. Loëtitia a soutenu sa thèse en 2016 et a actuellement un poste d'assistante hospitalo-universitaire à l'hôpital Henri Mondor à Créteil.

En janvier 2016, Crystal Gov a réalisé son stage de 6 mois pour le M2 Biologie Santé spécialité cancérologie sur l'analyse des mécanismes d'apoptose induits par l'action combinée d'inhibiteur de c-myc et de BCL-2 dans les cellules de lymphomes B. Je l'ai aidé à analyser ses résultats et j'ai corrigé une partie de son mémoire. Puis, Crystal est revenue en tant qu'ingénieure d'étude en 2017 pour une durée de cinq mois, je l'ai alors encadré sur un projet étudiant les dérivés de la meiogynine A comme potentiels inhibiteurs des membres de la famille de BCL-2. Mon encadrement a surtout concerné la conception des expériences et leur analyse. Elle signe en 3ème autrice sur l'article paru sur le sujet. Actuellement, Crystal passe des examens pour faire des études de médecine en Italie. En même temps que Crystal, nous avons accueilli sur ce sujet, Ophélie Desachy pour son stage de deux mois de L3 (UPEC), elle poursuit actuellement ses études.

1) Contexte de recherche

Les protéines de la famille de BCL-2 jouent un rôle majeur dans l'homéostasie cellulaire puisqu'elles régulent la mort par apoptose grâce à des interactions dynamiques entre les membres anti- et pro-apoptotiques (Figure 7).

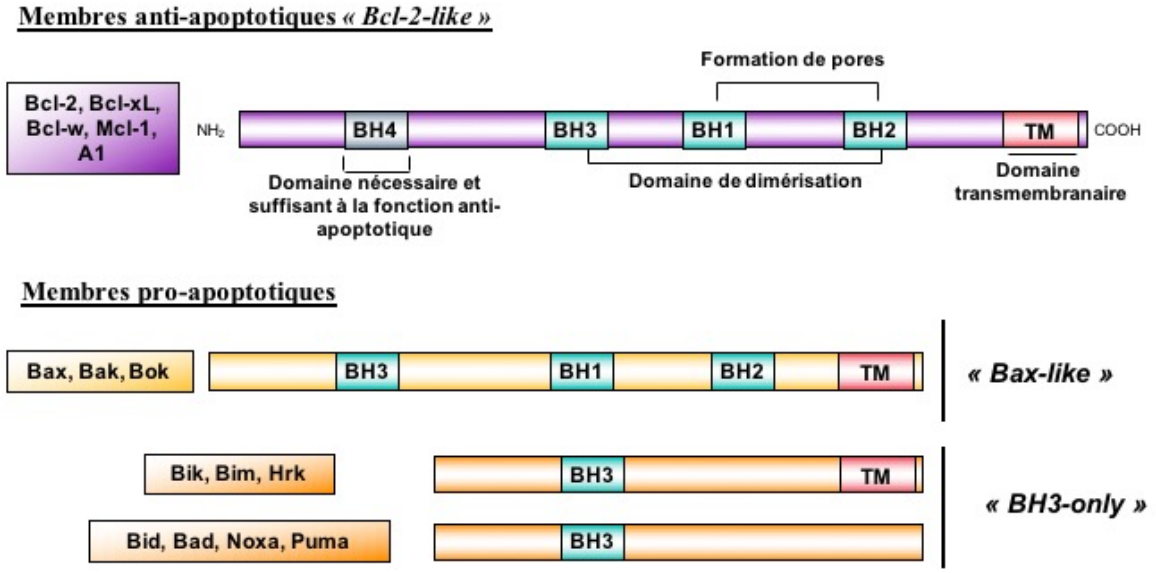

Figure 7 : Les différents membres de la famille BCL-2

Les membres de cette famille peuvent être répartis en trois classes définies selon le nombre de domaines d'homologie à la protéine BCL-2 (BH1, 2, 3 et 4) qu'ils possèdent (Taylor et al., 2008) :

- les anti-apoptotiques ont pour fonction de bloquer l'apoptose. Ces protéines contiennent les 4 domaines BH1, BH2, BH3 et BH4. Ce dernier est spécifique de cette classe. Elles sont principalement localisées à la membrane de la mitochondrie mais aussi retrouvées dans celle de différents organites comme le réticulum endoplasmique (RE) ou le noyau (Korsmeyer et al., 2000). Appartiennent à ce groupe : les protéines BCL-2, BCL-XL, MCL-1, BCL-W, BCL2A1 et BCL-B. Ces protéines sont capables de s'hétérodimériser avec les protéines pro-apoptotiques par l'intermédiaire de leur domaine BH3 et de la poche hydrophobe formée par les domaines BH1, BH2 et BH3 et ainsi d'inhiber spécifiquement l'apoptose. Par exemple : BCL-2 peut inhiber BAX, MCL-1 et BCL-XL peuvent interagir avec BAX et BAK (Willis et al., 2005).

- les pro-apoptotiques « BAX-like » possèdent les trois domaines BH1, BH2 et BH3. Les protéines BAX, BAK et BOK appartiennent à cette classe.

- Les pro-apoptotiques BH3-only possèdent uniquement le domaine BH3. Cette classe regroupe les protéines BIK, HRK, BIM, BAD, BID, PUMA, NOXA et BMF.

Les pro-apoptotiques sont majoritairement localisées dans le cytosol puis après un signal apoptotique, elles changent de conformation pour cibler et intégrer les membranes et particulièrement celle de la mitochondrie (Korsmeyer et al., 2000). Le déclenchement ou non de l'apoptose est donc dépendant du ratio entre les protéines pro et anti-apoptotiques de la famille BCL-2. Un déséquilibre d'expression en faveur des membres anti-apoptotiques participe au développement des tumeurs ainsi qu'à leur résistance aux traitements. De nombreuses études ont montré que BCL-2, BCL-XL ou MCL-1 étaient surexprimées dans la plupart des cancers (Campos et al., 1993; Wuilleme-Toumi et al., 2005). Dans les lymphomes B, la surexpression de la protéine BCL-2 (notamment liée à des anomalies chromosomiques), est corrélée avec une faible réponse à la chimiothérapie (Campos et al., 1993). De même, nous avons montré que la surexpression de BCL-2 engendrée par EBV dans les cellules de lymphome B en latence de type III les rend plus résistantes à l'apoptose que les cellules non infectées (Pujals et al., 2011). Cibler les membres de cette famille constitue donc une alternative thérapeutique prometteuse pour induire l'apoptose ou sensibiliser certaines tumeurs à l'apoptose induite par les chimiothérapies.

Plusieurs laboratoires ont donc développé des molécules de synthèse appelées BH3 mimétiques qui vont se fixer sur le domaine BH3 des protéines anti-apoptotiques afin de les piéger et les inhiber. ABT-737, le premier BH3 mimétique a été mis sur le marché par le laboratoire Abott et cible BCL-2, BCL-XL et BCL-W. Sa version orale, ABT-263, ou Navitoclax est toujours en essais de phase II (NCT02079740) en combinaison avec le Trametinib (inhibiteur de MEK) chez des patients ayant des tumeurs solides avancées ou métastatiques. Cependant, suite aux effets secondaires liés à l'inhibition de BCL-XL (induction de thrombocytopénie chez les patients), les laboratoires ont développé des inhibiteurs plus spécifiques de BCL-2 (Ashkenazi et al., 2017) comme le Venetoclax ou ABT-199 qui est la seule molécule approuvée par la FDA (Food and Drug Administration) pour le moment. Il est utilisé en seconde ligne pour le

traitement des leucémies lymphoïdes chroniques (NDA 208573). En ce qui concerne les inhibiteurs de MCL-1, 4 molécules sont actuellement en tests cliniques : AMG176 (NCT02675452, Amgen,(Caenepeel et al., 2017)), S64315/MIK665 (NCT02979366/ NCT02992483, Servier) et AZD5991 (NCT03218683, Astrazeneca (Hird et al., 2017)).

2) Résultats

Comme nous avions montré précédemment que ABT-737 restaurait en partie la sensibilité des cellules EBV+ en latence III à l'apoptose et que les LCL étaient beaucoup plus sensibles au traitement que les cellules de LB, nous avons ensuite voulu évaluer l'activité anti-tumorale d'ABT-737 (en combinaison ou non avec des drogues conventionnelles) chez des souris xénogreffées avec des cellules de LB ou des LCL (modèle de PTLD). Les cellules ont été injecté en sous cutanée chez des souris NOD/SCID. Quand les tumeurs sont devenues palpables, les souris ont été réparties afin d'obtenir des groupes avec un volume tumoral médian homogène. Les souris ont été traitées quotidiennement en intra péritonéal avec ABT-737 (75 mg/kg) pendant 14 jours seul ou en combinaison avec 50mg/kg de Cyclophosphamide (modèle LB) ou 10 mg/kg de Rituximab (modèle PTLD). Le volume des tumeurs ainsi que le poids des souris ont été contrôlés tous les deux jours. La formulation sanguine a été analysée tous les semaines afin de contrôler la toxicité du composé. Les souris ont été euthanasiées et autopsiées lorsque le volume tumoral atteignait 1500 mm^3.

Nos résultats montrent qu'ABT-737 seul en combinaison avec le rituximab est très efficace dans le modèle PTLD alors qu'il l'est très peu dans le modèle de LB (Figure 8).

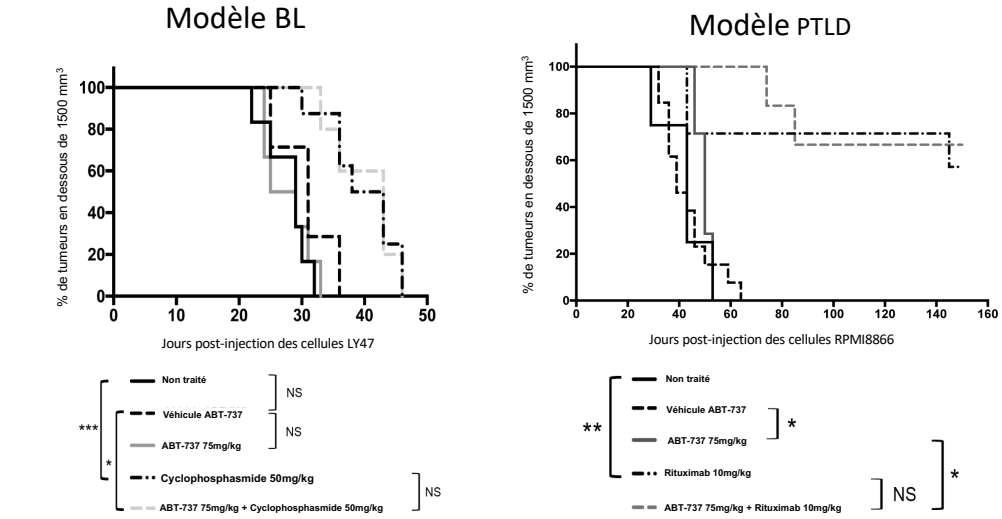

	Médiane de survie
Non traité	29
Véhicule ABT-737	31
ABT-737 75mg/kg	27
ABT-737 75mg/kg + Cyclophosphamide 50mg/kg	40, 5
Cyclophosphamide 50mg/kg	43

	Médiane de survie
Non traité	43
Véhicule ABT-737	39
ABT-737 75mg/kg	50
ABT-737 75mg/kg + Rituximab 10mg/kg	Non défini
Rituximab 10mg/kg	Non défini

Figure 8 : Effet anti tumoral d'ABT-737 in vivo

Courbes de Kaplan Meier pour le modèle du LB à gauche et pour le modèle PTLD à droite. Dans le modèle du LB, AB-737 seul n'a pas d'effet sur la survie des animaux et en combinaison avec le cyclophosphamide, on observe une légère augmentation de la survie. Dans le modèle PTLD, ABT-737 seul augmente la survie des animaux et en combinaison avec le Rituximab, 66% des souris sont en rémission à plus de 160 jours.

De façon plus générale, nous avons montré que des cellules provenant de LB et des LCL exprimant un niveau équivalent de BCL-2 et de BCL-XL ne présentent pas le même niveau de sensibilité aux inhibiteurs de ces protéines. Une piste pour expliquer cette différence est que les lignées de LB surexpriment c-Myc. Des résultats préliminaires obtenus par Loëtitia et de Crystal montrent que l'inhibition de c-myc par 10058-F4 (inhibiteur de l'interaction myc/max) potentialise l'effet d'ABT-737 dans des lignées de LB.

Publication p.83
Pujals A.* **Robert A**.*, Favre L, Desille T., Debernardi J., Joëlle Wiels. The BCL-2 inhibitor, ABT-737 enhances the activity of therapeutic agents against B lymphoproliferations associated with EBV both in vitro and in vivo, en préparation. *Co 1ères autrices

D'autre part, il a été démontré que l'utilisation d'ABT-737 induisait parfois une résistance dans les cellules cancéreuses en raison d'une surexpression des protéines non ciblées notamment MCL-1 (Konopleva et al., 2006). Ceci suggère qu'un traitement efficace peut nécessiter l'inhibition simultanée de multiples protéines anti-apoptotiques.

Notre laboratoire travaille en étroite collaboration avec une équipe de chimiste (ICSN-Gif sur Yvette) qui cherche à développer des inhibiteurs naturels des protéines anti-apoptotiques de la famille de BCL-2 à partir d'extraits de plantes subtropicales.

Depuis les années 40, 75% des 175 molécules utilisées en oncologie sont des molécules naturelles ou en sont dérivées. Les molécules naturelles (ici des métabolites secondaires de plantes) sont, et de loin, la source la plus riche de nouvelles classes de composés. Elles possèdent une vaste et unique diversité chimique. Elles sont souvent très originales, poly-fonctionnalisées et complexes. La complexité des structures des métabolites secondaires résulte d'une optimisation des interactions avec leur cible biologique (en réponse à une agression par exemple) qui a permis la survie des espèces au cours des millénaires. Les produits naturels sont donc en quelque sorte « prévalidés par la Nature » et peuvent être considérés comme des ressources privilégiées pour le developpement de drogues (Lachance et al., 2012). Un crible de 5000 extraits de plantes a permis d'identifier 12 composés capables de déplacer l'interaction BCL-XL/BAK ou MCL-1/BID en polarisation de fluorescence (Fotsop et al., 2010; Litaudon et al., 2009a; Litaudon et al., 2009b). Parmi ces molécules, la Meiogynine A est un antagoniste naturel de l'association BCL-XL/BAK et le Drimane serait un antagoniste de l'association MCL-1/BAK.

Un premier travail sur les dérivés de la Meiogynine A a permis aux chimistes de synthétiser totalement un inhibiteur ciblant à la fois MCL-1 et BCL-XL (Desrat et al., 2014) ainsi qu'un inhibiteur ciblant MCL-1 et BCL-2 (Abou Samra et al., 2018).

Pour ce projet, Loëtitia Favre a mis au point dans le laboratoire une nouvelle approche fonctionnelle, le BH3 profiling qui permet prédire la dépendance des tumeurs à certains membres de la famille de BCL-2 pour survivre. En effet, en théorie, connaître le taux des différentes protéines anti-apoptotiques dans les cellules tumorales devrait permettre de prévoir l'efficacité du traitement mais cela ne semble pas suffisant. Cette technique consiste à

exposer les mitochondries de cellules à des concentrations connues de peptides BH3 et à mesurer la perméabilisation de la membrane mitochondriale qui en résulte. Loëtitia a ainsi déterminé que les BL2 étaient dépendantes de BCL-XL et de MCL-1, et que les Remb1 étaient dépendantes de BCL-XL. Dans la littérature, les H929 et RS4;11 sont réciproquement dépendantes de MCL-1 et BCL-2.

Ainsi, nous avons pu confirmer que parmi les composés synthétisés par les chimistes, l'analogue appelé AAS-312-F1 induisait l'apoptose des BL2, des H929, des RS4;11 et pas des Remb1 (Travail de Crystal Gov). Il était donc spécifique de MCL-1 et de BCL-2 (Figure 9). Ce composé est issu d'une synthèse totale ne permettant malheureusement pas d'avoir assez de produit pour le tester *in vivo*.

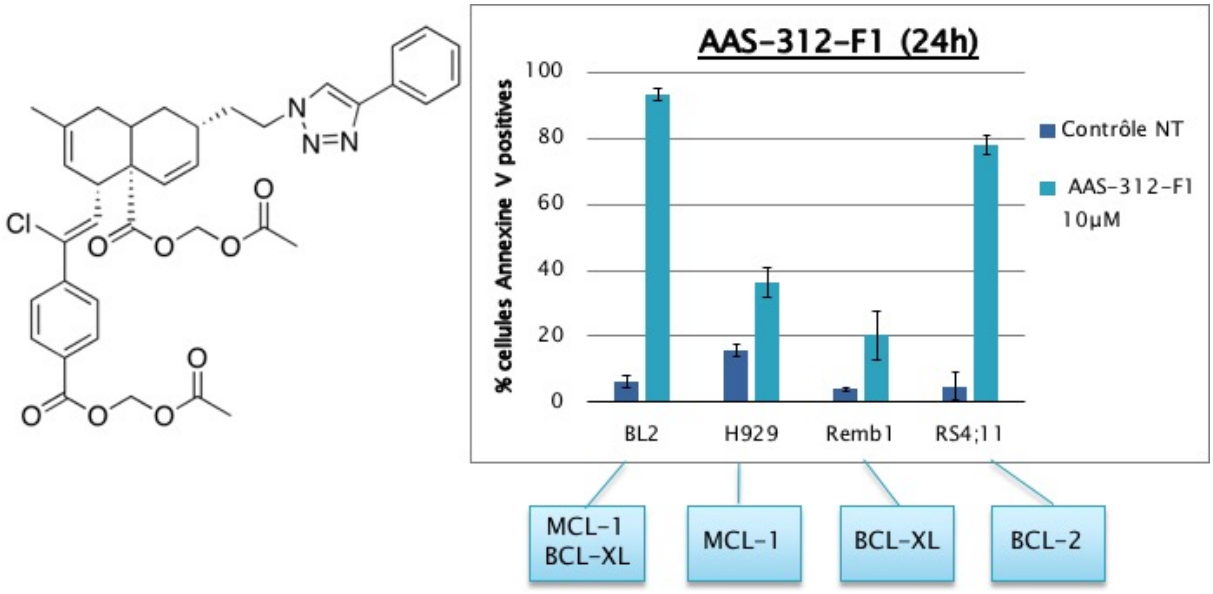

Figure 9 : AAS-312-F1 est un inhibiteur naturel de BCL-2 et de MCL-1

Les différentes lignées cellulaires ont été traitées ou non par 10 µM de AAS-312-F1 pendant 24h puis les cellules sont analysées en cytométrie de flux après marquage à l'iodure de propidium et à l'annexine V afin d'évaluer l'apoptose.

Publication p.79

Abou Samra A., **Robert A.**, Gov C., Favre L., Eloy L., Jacquet E., Bignon J., Wiels J., Desrat,S., Roussi F. Dual Inhibitors of the Pro-Survival Proteins Bcl-2 and Mcl-1 Derived from Natural Compound Meiogynin A, European Journal of Medicinal Chemistry, 2018

C. Apoptose induite par la vérotoxine-1 dans les cellules de lymphome de Burkitt

Dans le cadre de ce projet, nous avons accueilli Delphine Pion pour un stage de deux mois pour son M1 « Biologie Santé » de l'université de Créteil (UPEC) en avril 2010. Delphine a analysé l'implication de la protéine « BH3 only » BIK dans le mécanisme d'activation de BAK et de BAX lors de l'apoptose induite par la VT-1. J'ai défini son projet, je l'ai encadré techniquement, j'ai corrigé son mémoire et préparé avec elle sa soutenance orale. Elle a actuellement un poste d'assistante ingénieure à l'hôpital Necker-Enfants malades.

En janvier 2012, Justine Debernardi a rejoint notre équipe pour son stage de M2 de « toxicologie humaine, évaluation des risques et vigilance » de la faculté de pharmacie de

Chatenay Malabry pour étudier le rôle de la protéine BID. Justine a ensuite obtenu une allocation doctorale de la ligue contre le cancer qui lui a permis de poursuivre en thèse de Sciences à partir de novembre 2012 (co-encadrement avec J. Wiels) et elle a également présenté notre sujet pour l'obtention de sa thèse de Pharmacie (mai 2013). Tout au long de ces 4 années, je l'ai aidé à définir son projet, je l'ai encadré techniquement, j'ai corrigé ses mémoires, ses demandes de financements (allocations 1ères et 4ème année), participé à la préparation de ses différentes soutenances orales. Justine a soutenu sa thèse en 3 ans et signe un article en première autrice que je signe en dernière. Elle a eu aussi une bourse pour présenter ses résultats à la 23ème Euroconférence sur l'apoptose organisée par l'ECDO (European Cell Death Organisation) en 2015 où elle a obtenu le prix Harlan pour son poster. Justine a maintenant un poste de pharmacien de surveillance des produits de santé chez Novonordisk.

1) Contexte de Recherche

La glycosylation est un processus enzymatique complexe. Chez l'humain, plusieurs centaines de glycosyltransferases (qui catalysent l'ajout de monosaccharide) et de glycosidases (qui hydrolysent les liaisons glycosidiques) orchestrent la diversité de structure des glycanes liés aux protéines et aux lipides. Il existe 3 groupes de glycolipides : les glycérolipides, les glycosylphosphatidylinositoles, et les glycosphingolipides (GSLs). Les GSLs présents dans les membranes cellulaires de tous les vertébrés sont le groupe majoritaire. Leur partie lipidique, ancrée dans la membrane plasmique, est un céramide (Cer) formé par l'association d'un acide gras et d'une sphingosine. Leur partie exposée à la surface des cellules est une chaine oligosaccharidique hydrophile plus ou moins longue (de 1 à une dizaine de sucres). L'ajout des sucres se fait séquentiellement par les glycosyltransférases. Le premier sucre ajouté sur le céramide est soit un galactose (Gal) soit un glucose (Glc). Lorsque du GlcCer est formé, il sert de substrat à la lactosylcéramide synthétase qui ajoute un Gal pour former le lactosylcéramide (LacCer). Le LacCer est le précurseur de trois grandes familles de GSLs : la lacto-série, la ganglio-série, et la globo-série. La présence d'un GSL en surface d'une cellule dépend d'un équilibre entre l'activation des enzymes en amont et en aval du GSL, de la disponibilité du GSL en amont et également de sa dégradation. Par exemple, pour faire du Gb3 (premier composé de la globo-série), il faut que la Gb3 synthétase soit active, qu'il y ait du LacCer disponible, que la Gb4 synthétase ne soit pas activée et qu'il y ait peu ou pas de dégradation de Gb3 (Figure 10).

Les GSLs jouent un rôle fondamental pendant le développement et la différenciation cellulaire. Par ailleurs, durant l'oncogenèse, leurs voies de synthèse sont modifiées ce qui entraine des altérations du profil de glycosylation des cellules. Ces altérations peuvent modifier le potentiel invasif des tumeurs et la formation de métastases (revu dans , (Hakomori et al., 1997)) et sont aussi à la base de l'expression spécifique de certains GSLs sur des tumeurs (GD2 sur le neuroblastome par exemple).

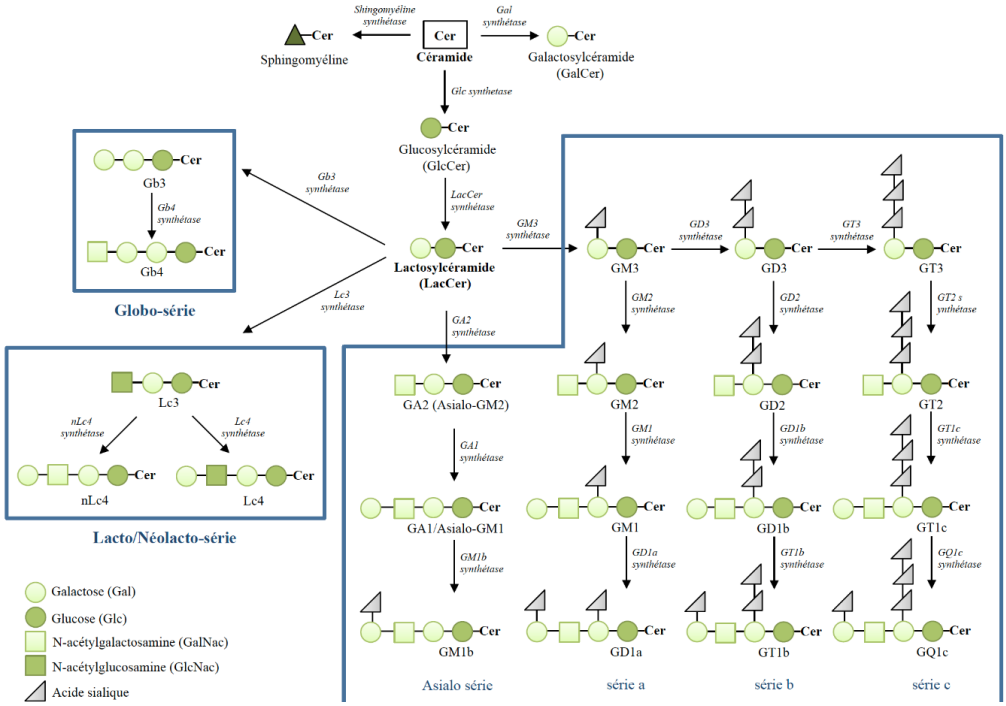

Figure 10 : Schéma général de la synthèse des glycosphingolipides

Lors de travaux précédents, l'équipe a montré qu'un GSL, le globotriaosylceramide (Gb3), est fortement exprimé à la surface des cellules de LB (Nudelman et al., 1983; Wiels et al., 1981). Reconnu aussi comme un Ag de différenciation des lymphocytes B (CD77), sa fonction biologique précise à la surface des cellules B normales du centre germinatif, reste indéterminée (Mangeney et al., 1991). Enfin, Gb3/CD77 est le récepteur de certaines toxines bactériennes de la famille des Shiga toxines (stx) aussi appelées vérotoxines (VT). L'équipe a montré dans un modèle de cellules de LB, que la VT-1 induisait un processus apoptotique classique dépendant des caspases et de la mitochondrie. La fixation de la VT-1 sur le récepteur Gb3/CD77 conduit au clivage de la forme entière de BID (FL-BID, Full-lengh BID) en t-BID (truncated BID) par la caspase 8, à la relocalisation mitochondriale de BAX ainsi qu'à la perméabilisation membranaire de la mitochondrie (Garibal et al., 2010; Mangeney et al., 1993; Tetaud et al., 2003). Cependant, les résultats montraient aussi que le clivage de BID n'était pas impliqué dans l'activation de BAX. **Le but de ce travail était donc de comprendre ce qui permettait l'activation de BAX dans notre modèle.**

2) Résultats

Dans ce travail, nous avons mis en évidence que la forme entière et la forme tronquée de la protéine BH3-only BID agissent toutes deux dans cette voie de signalisation (Figure 11). Nous avons analysé le rôle de ces deux formes par deux approches complémentaires : l'utilisation d'un inhibiteur de la caspase 8 et celle d'un vecteur lentivirus codant pour un shRNA ayant pour cible l'ARN de BID. Nous avons aussi réexprimé dans les cellules où l'expression de BID est inhibée de façon stable, un mutant de cette protéine non clivable par la caspase 8. Si le rôle de t-BID est incontesté dans les voies de signalisations apoptotiques, la participation de FL-BID reste, en revanche, encore largement méconnue. Nous avons montré que ces deux

protéines contrôlent de manière concertée la sortie des facteurs apoptogéniques CYTOCHROME C (CYT C) et Smac/DIABLO de l'espace intermembranaire mitochondrial vers le cytosol. En effet, FL-BID contrôle l'activation des protéines BAK et BAX ainsi que leur homo-oligomérisation ce qui permet la formation de pores dans la membrane de la mitochondrie et la sortie initiale du CYT C et de Smac/DIABLO. En revanche, t-BID est nécessaire à l'hétéro-oligomérisation de BAK et BAX qui permettrait une amplification de ce processus (Debernardi et al., 2018). Selon le modèle de libération biphasique du CYT C proposé par *Scorrano et al.* (Scorrano et al., 2002), notre hypothèse est que la sortie du premier pool de CYT C déjà présent dans l'espace intermembranaire (et par extension de celui de Smac/DIABLO) s'effectuerait par les pores homo-oligomériques BAK/BAK et/ou BAX/BAX alors que les pores hétéro-oligomériques favoriseraient le passage du pool libéré par le remodelage des crêtes mitochondriales.

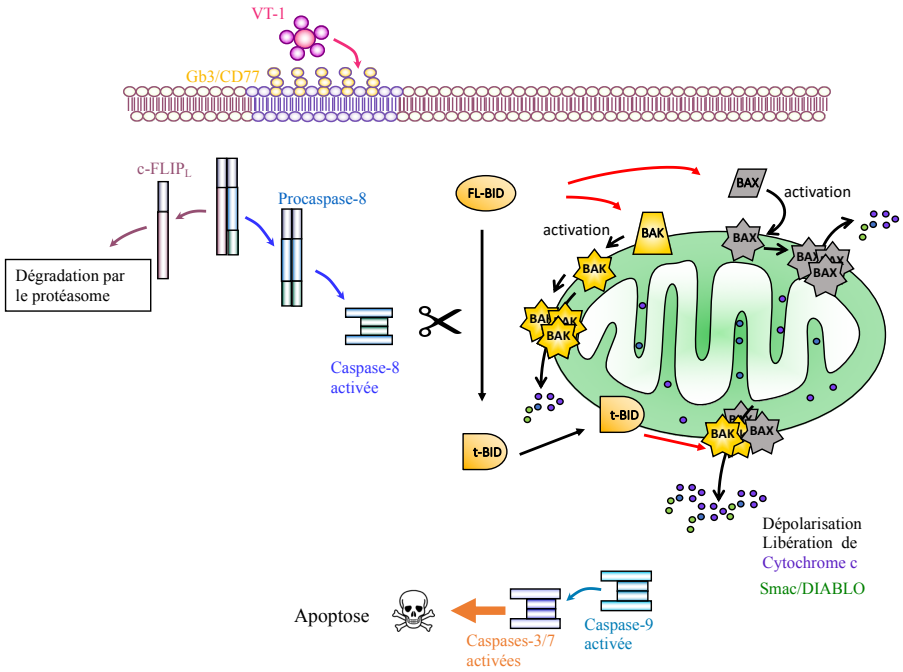

Figure 11 : Apoptose induite par la Vérotoxine-1 dans les cellules de lymphome de Burkitt

Nous avons montré, dans ce modèle, que BID joue un rôle crucial dans l'apoptose induite par la VT-1. T-BID et FL-BID sont impliqués dans la libération des protéines de l'espace intermembranaire de la mitochondrie (CYTOCHROME C et Smac/DIABLO) vers le cytosol. FL-BID contrôle l'homodimérisation de BAX et de BAK ce qui contribuerait à la libération initiale des protéines de l'espace intermembranaire de la mitochondrie alors que t-BID est nécessaire à leur hétérodimérisation et participerait à l'amplification de cette libération. L'ensemble de ces résultats montre une coopération fonctionnelle entre BAX et BAK au cours de l'apoptose induite par la VT-1 et que l'activation de la voie caspase-8/t-BID n'est absolument pas requise pour initier la mort cellulaire.

En conclusion, l'ensemble de nos résultats révèle, donc, l'existence d'une coopération fonctionnelle entre BAX et BAK au cours de l'apoptose induite par la VT-1 et, surtout, que l'activation de la voie caspase-8/t-BID n'est absolument pas nécessaire au déclenchement de la mort cellulaire.

Publication p.81

Debernardi J, Hollville E, Wiels J, **Robert A**. Differential role of FL-BID and t-BID during Verotoxin-1-induced apoptosis in Burkitt's lymphoma cells, oncogene 2018.

Chapitre 2. Projets en cours et futures directions

Mon projet de recherche s'articule autour de deux grands axes qui sont dans la continuité des projets développés précédemment et vise à mettre en place de nouvelles stratégies thérapeutiques pour contourner les résistances à la mort des cellules tumorales. Le premier consiste à explorer le potentiel thérapeutique d'un anticorps dirigé contre l'Ag Gb3/CD77 dans le traitement du LB et de certaines tumeurs chimiorésistantes. Le deuxième vise à développer (comme évoqué précédemment) toujours en collaboration avec le laboratoire de F. Roussi à l'ICSN, des inhibiteurs des membres de la famille de BCL-2 pour contrecarrer les résistances dues à la surexpression des membres anti-apoptotiques de cette famille.

I. Gb3/CD77 comme cible thérapeutique et diagnostique

Ce projet m'a déjà permis d'encadrer Benjamin Morin lors de son stage de M2 de Biologie Moléculaire et Cellulaire de l'université Pierre et Marie Curie (UPMC, janvier-juin 2016) et Sophie Cheverry lors de son stage de quatrième année d'école d'ingénieur (SupBiotech, août-décembre 2016). Je les ai encadrés techniquement et scientifiquement, j'ai conçu les expériences qu'ils ont réalisé, analysé leurs résultats, corrigé leur rapport et je les ai préparés à leur oral. Benjamin a obtenu après son M2, un poste d'ingénieur d'étude en CDD à l'université de Poitiers et Sophie a poursuivi en 5ème année dans son école. Le recrutement d'un·e étudiant·e en M2 pour ce projet est prévu pour janvier 2019.

Pour ce projet, nous avons obtenu un financement de la fondation de France (2012-2014) et un financement dans le cadre d'un appel à projet « innovation et entreprenariat-prématuration » de l'Idex Paris-Saclay (2016-2017). J'ai déposé une demande de financement à laLligue contre le cancer Ile de France en juillet 2018.

A. Contexte

Gb3/CD77 est, comme nous l'avons déjà vu, fortement et spécifiquement exprimé en surface des cellules de LB et de certains lymphomes B (cf § III. C. Apoptose induite par la vérotoxine-1 dans les cellules de lymphome de Burkitt). Plus récemment, sa surexpression dans différents types de tumeurs solides (sein, ovaires) en comparaison avec les tissus normaux respectifs (Arab et al., 1997; Gupta et al., 2012) a été rapportée. De plus, son haut niveau d'expression est notamment associé à certains cancers résistants aux chimiothérapies (carcinomes pulmonaires non à petites cellules et ovariens) que cette résistance soit primaire ou acquise après traitement (Arab et al., 1997; Johansson et al., 2010). Ces données sont des arguments en faveur de l'exploration de Gb3/CD77 comme nouvelle cible thérapeutique.

La principale cause de résistance des cellules tumorales aux agents cytotoxiques, la résistance dite « multidrogues (MDR) », est associée aux membres de la superfamille des transporteurs ABC. La suractivation de ces pompes membranaires d'efflux dépendantes de l'ATP a pour effet un rejet par les cellules de divers types de drogues chimiothérapeutiques empêchant ainsi leurs actions cytotoxiques. Cette suractivation est majoritairement due à

l'augmentation de l'expression du produit d'un gène fortement conservé, le gène *MDR1*, codant pour une protéine appelée glycoprotéine P (P-gp ou MDR1). Récemment, plusieurs études ont suggéré une association entre MDR1 et la glycosylation du céramide qui, comme indiqué précédemment, constitue la base lipidique des GSLs. En effet, de nombreuses cellules cancéreuses surexprimant MDR1 ont des niveaux élevés de GlcCer, et de son enzyme de synthèse, la glucosylcéramide synthétase (GCS) (revu dans (Liu et al., 2013)). De même, la transfection de *MDR1* augmente les niveaux de trois GSLs : GlcCer, LacCer et Gb3/CD77 (De Rosa et al., 2004). Par ailleurs, cette régulation semble se faire dans les deux sens puisque la surexpression de la GCS induit une augmentation du niveau de MDR1 (Liu et al., 2010). Outre ces liens entre la GCS et MDR1, un autre travail a aussi montré que MDR1 aurait une fonction de « flippase » qui permet le transfert du GlcCer de la face cytosolique à la lumière de l'appareil de Golgi, là où se trouve les glycosyltransférases (De Rosa et al., 2004). Au final, et même si les mécanismes restent encore peu clairs, il apparaît qu'il existe une association préférentielle entre l'expression de Gb3/CD77 et celle de MDR1 à la surface de différents types de cellules chimiorésistantes ce qui fait de Gb3/CD77 une cible qui pourrait permettre de contourner cette résistance aux traitements.

Comme dit précédemment, Gb3/CD77 est aussi le récepteur de toxines bactériennes de la famille Shiga, notamment de la VT-1, et différents essais précliniques ont été donc menés avec cette toxine. Des régressions de la masse tumorale ont été observées dans divers modèles de xénogreffes mais il existe un effet cytotoxique de la VT-1 lié à son inhibition très efficace de la synthèse protéique induisant l'apoptose ce qui peut entrainer des effets secondaires importants notamment sur les cellules normales exprimant Gb3/CD77. Ainsi, certaines équipes cherchent à diminuer les doses utilisées et/ou à utiliser des versions modifiées de la toxine (revu dans (Engedal et al., 2011)). Cependant, le problème majeur de son utilisation comme agent thérapeutique reste son immunogénicité résiduelle. En effet, des anticorps anti-VT-1 ont été retrouvés dans des populations en bonne santé, ce qui peut être associé avec une immunité protégeant ces différentes populations (Ludwig et al., 2002). L'ensemble de ces données nous incitent donc à penser que l'utilisation d'un anticorps monoclonal dirigé contre Gb3/CD77 pourrait constituer une nouvelle stratégie thérapeutique.

Les anticorps monoclonaux (AcM), que ce soit en monothérapie ou en association avec une chimiothérapie, ont pris place aujourd'hui dans le traitement standard de nombreuses formes de cancers. Le Rituximab est le premier anticorps autorisé par la FDA en oncologie en 1997. Cet AcM est dirigé contre la molécule CD20 présente à la surface des lymphocytes B du stade pré-B au stade mature. Depuis sa mise sur le marché d'autres anti-CD20 ont été développés et des réponses importantes ont été observées dans différents désordres lymphoprolifératifs (revu dans (Coiffier, 2007)). Les cibles des AcM sont généralement des protéines mais des études récentes ont montré que les GSLs pouvaient aussi constituer de bonnes cibles. Ainsi, un AcM dirigé contre GD2, le dinuximab, a été approuvé par la FDA en 2005, et est utilisé en combinaison avec d'autres drogues, notamment chez les enfants ayant un neuroblastome à hauts risques (Ozkaynak et al., 2018). Nous avons produit au laboratoire un anticorps anti-Gb3/CD77 (clone 38.13) qui est une immunoglobuline de rat de classe M

(IgM). Même si la majorité des anticorps thérapeutiques sont de classe G (IgG), les IgM offrent certains avantages. En effet, ce sont des pentamères qui possèdent 3 sites de fixation du complément ce qui leur confèrent une meilleure efficacité pour activer ce dernier. De plus, les IgM sont des molécules avec une forte avidité pour leur cible et leur haute valence facilite les cross-linkings des récepteurs ce qui conduit à une mort cellulaire plus efficace (Vollmers et al., 2009). Récemment, une équipe de Nantes a démontré qu'un AcM anti-Gb3/CD77 murin de classe M appelé 3E2 avait un effet sur la croissance tumorale dans des modèles où les tumeurs n'expriment pas Gb3/CD77 (neuroblastome) mais où les cellules endothéliales en prolifération environnant la tumeur l'expriment. Cet anti-Gb3/CD77 a un effet anti-tumoral via l'inhibition de l'angiogénèse *in vivo*. De façon intéressante, ces expériences montrent une absence de toxicité de l'anticorps sur les autres cellules normales exprimant Gb3/CD77 ce qui est sans doute lié au fait que le Gb3/CD77 est plus fortement exprimé en surface des cellules endothéliales en prolifération qu'en surface des cellules normales (Desselle et al., 2012). L'ensemble de ces données suggère que des AcM anti-Gb3/CD77 devraient spécifiquement permettre l'élimination des cellules malignes sans toxicité pour les cellules normales. De plus, nous pouvons espérer un effet de ces AcM sur l'angiogenèse de la tumeur. L'utilisation d'un anticorps monoclonal humanisé dirigé contre Gb3/CD77 pourrait donc constituer une nouvelle stratégie thérapeutique.

Les objectifs de ce projet consistent à étudier le potentiel thérapeutique d'un AcM dirigé contre le Gb3/CD77 dans le traitement des tumeurs chimiorésistantes. Il est réalisé selon deux axes. Nous étudions, d'une part, les liens entre la surexpression de Gb3/CD77 et la résistance aux traitements due à la surexpression de MDR1 afin de comprendre les mécanismes moléculaires mis en jeux et évaluons, d'autre part, l'effet de l'anti-Gb3/CD77 *in vivo* dans des modèles de xénogreffes de tumeurs qui expriment Gb3/CD77 corrélativement à leur résistance aux traitements (projet ayant déjà reçu un avis favorable du comité d'éthique, CEEA-26). En parallèle, nous avons débuté une collaboration avec le département de biologie et de pathologie médicales et celui d'hématologie de GR afin d'analyser l'expression de Gb3/CD77 chez des patients atteints de différents types de lymphomes B folliculaires. Cette étude nous permettra de mieux cibler les pathologies susceptibles d'être traitées par les anti-Gb3/CD77 mais aussi éventuellement d'utiliser ces Ac pour le diagnostic de certains lymphomes.

B. Etat des travaux

Dans le modèle du LB, nous avons montré que l'Ag Gb3/CD77 est capable de transmettre un signal d'apoptose. Nous avons, en effet, pu mettre en évidence que la fixation de deux ligands sur ce récepteur (un AcM anti-Gb3/CD77 et la Vérotoxine-1) induisait la mort des cellules de LB par apoptose. Cependant, deux voies de signalisation différentes sont mises en jeux : une cascade apoptotique dépendante des caspases et de la mitochondrie en ce qui concerne la VT-1 (cf. Chapitre 1 III. C) et une voie apoptotique dépendante des ROS pour l'AcM (Debernardi et al., 2018; Garibal et al., 2010; Tetaud et al., 2003).

1) Etude du lien entre la surexpression de Gb3/CD77 et de MDR1 dans certains cancers résistants aux chimiothérapies

Afin de mieux comprendre le lien entre MDR-1 et Gb3/CD77, Benjamin Morin a évalué leur expression dans différentes lignées comme les lignées Ramos et P3HR1 (LB), OV-1 (cancer de l'ovaire), OV-1/VCR, OV-1/DXR et OV-1/CDDP (établies dans le laboratoire par J. Bénard à partir d'un prélèvement de patiente de GR et résistantes respectivement à la vincristine, la doxorubicine et au cisplatine, (Benard et al., 1985)). Dans les cellules de LB, nos tests réalisés par cytométrie en flux montrent que l'expression de Gb3/CD77 n'est pas associée à l'expression de MDR-1 même dans des cellules résistantes à de nombreux traitements comme les P3HR1. Ceci suggère que dans le modèle du LB, l'expression de Gb3/CD77 est seulement due à l'origine des cellules (centre germinatif) sans lien avec MDR-1. En revanche, une corrélation entre l'expression de MDR-1 et celle de Gb3/CD77 a été observée dans les lignées de cancer de l'ovaire : les cellules parentales OV-1 et les cellules OV-1/CDDP n'expriment ni MDR-1 ni Gb3/CD77 alors que les cellules résistantes OV-1/DXR et OV-1/VCR, expriment en parallèle MDR-1 et Gb3/CD77 (Figure 12).En revanche, l'expression de Gb3/CD77 et la résistance aux drogues de ces cellules ne sont pas corrélées avec l'expression de MRP1, un autre membre de la superfamille ABC.

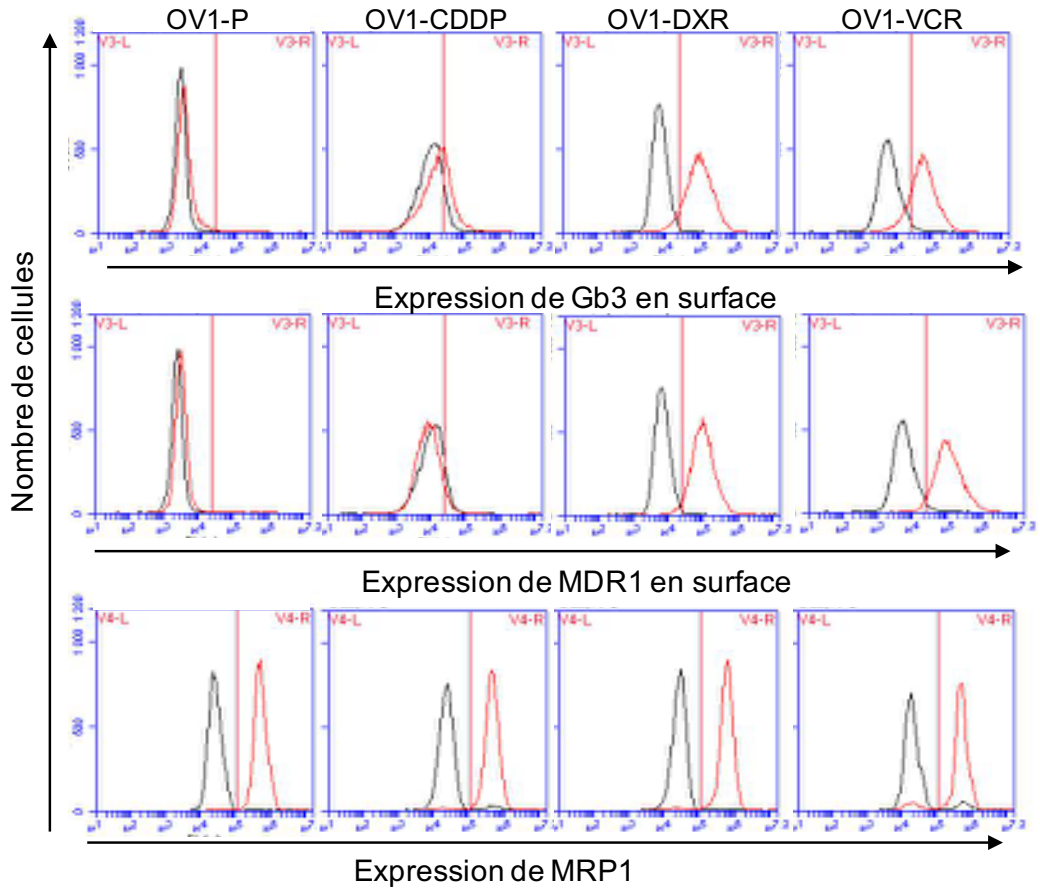

Figure 12 : Expression de Gb3/CD77, MDR-1 et MRP-1 en surface de différents clones de carcinome ovarien.
Analyse par cytométrie de flux. Noir : isotype contrôle, rouge : anticorps couplé

D'autre part, et de manière un peu paradoxale vu les résultats publiés par d'autres groupes, nous avons observé que l'inhibition globale de la synthèse des GSLs par le PPMP (inhibiteur de la GCS) dans les cellules résistantes à la Doxorubicine ou à la Vincristine, entrainait une augmentation de l'expression de MDR1 en surface (Figure 13).

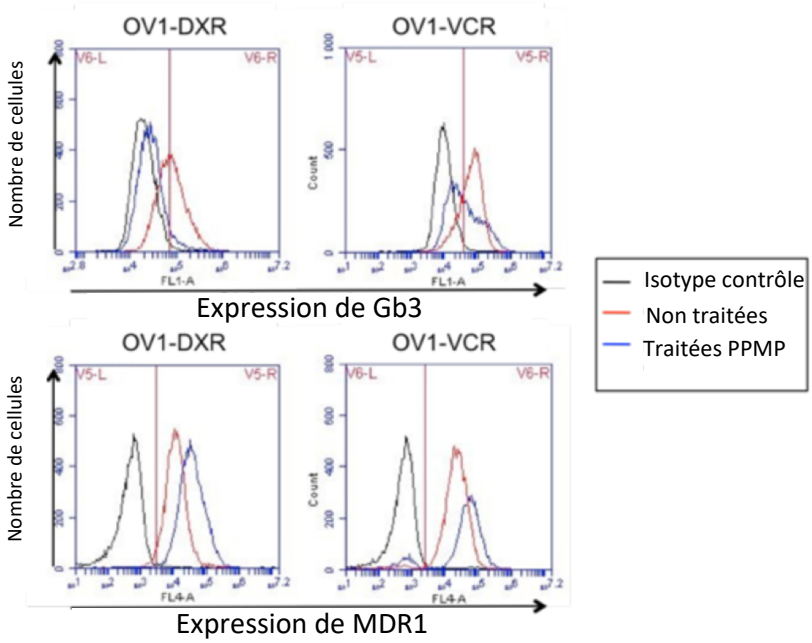

Figure 13 : L'inhibition de la synthèse des glycolipides par le PPMP augmente l'expression en surface des clones de carcinome ovarien résistants à la DXR ou à la VCR.

2) Evaluation thérapeutique d'un AcM anti-Gb3/CD77

L'étape suivante était d'évaluer le potentiel thérapeutique de nos anticorps monoclonaux dirigés contre Gb3/CD77. Nous avons utilisé l'AcM anti 38.13 et un autre AcM anti-Gb3/CD77 (1A4, IgM souris) que nous avions à disposition. Nous avons montré précédemment que ces anticorps utilisés seuls induisent la mort des cellules de LB par apoptose (Tetaud et al., 2003). Il restait donc à évaluer leur capacité à activer l'ADCC (Antibody-dependent cell-mediated cytotoxicity) et/ou la CDC (complement-dependent cytotoxicity). Sophie Cheverry a montré que ces anticorps activent la CDC mais qu'ils ne déclenchent pas l'ADCC en utilisant pour cibles des lignées de BL (Figure 14).

Ensuite, nous avons testé nos anticorps sur deux autres modèles tumoraux. Tout d'abord, notre modèle de carcinome de l'ovaire (OV1) où nous avons montré que les clones résistants à la Doxorubicine ou à la Vincristine (OV-1/DXR et OV-1/VCR) qui expriment le Gb3/CD77 sont efficacement tués par les anti-Gb3/CD77 alors que les cellules parentales OV-1 et les cellules OV-1/CDDP qui n'expriment pas le Gb3/CD77, ne sont pas sensibles à l'AcM (Figure 14A). Le second modèle repose sur une collaboration avec la plateforme de pharmacologie préclinique de GR qui vient d'obtenir des PDX (patient-derived xenografts) à partir d'une biopsie d'un lymphome de Burkitt. Les PDX sont aujourd'hui considérés comme de très bons modèles de la

réalité clinique en oncologie car les cellules tumorales n'ont jamais été cultivées *in vitro* et ont donc des caractéristiques moléculaires et une hétérogénéité tumorale proches de la tumeur d'origine. Nous avons montré que ces cellules expriment le Gb3/CD77 et que nos anti-Gb3/CD77 les tuent efficacement. Nous avons pour la suite des expériences concentré nos effort sur le clone 38.13 pour lequel nous disposons des droits d'exploitation.

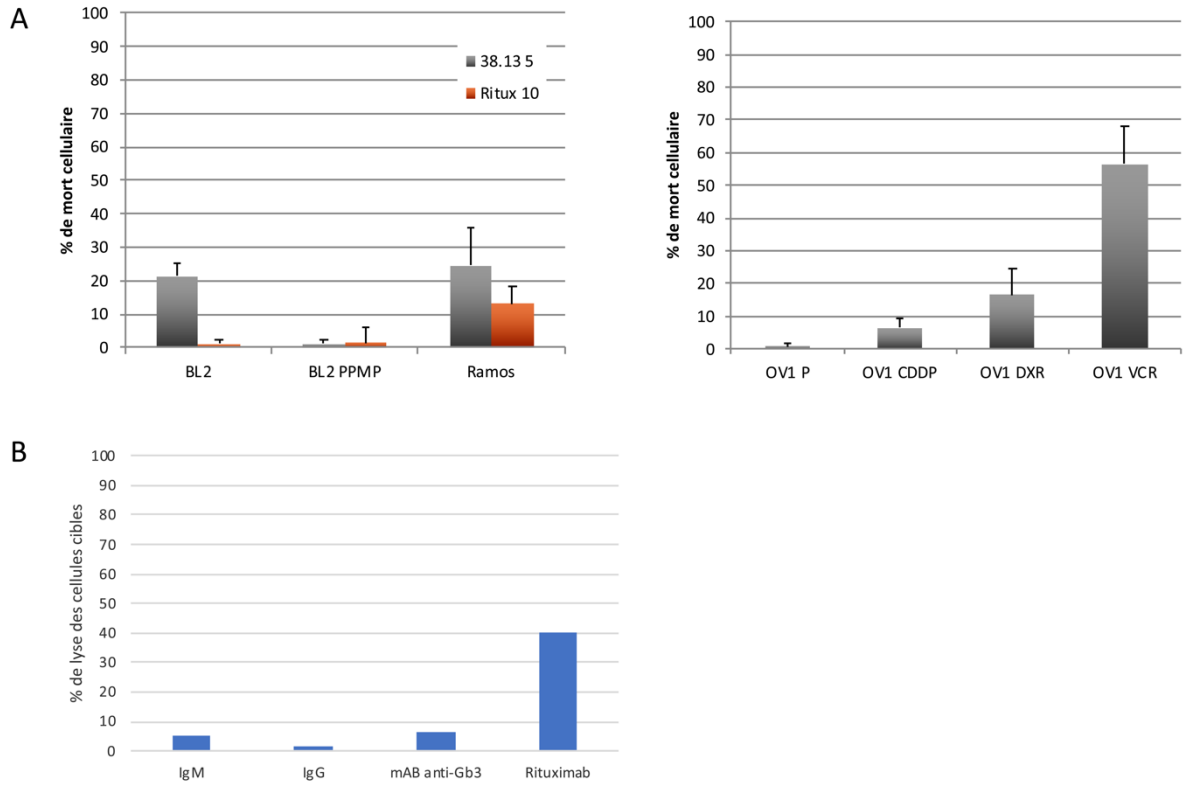

Figure 14 : 38.13 induit la mort des cellules cibles par la cytotoxicité du complément et pas par l'ADCC.

A. Les cellules cibles (les LB à gauche et les différents clones OV-1 à droite) ont été incubées ou non avec différents anticorps (5µ g/mL pour 38.13, 10 µg/mL pour le Rituximab) pendant 2h à 37°C en présence de sérum humain (source de complément). Puis la cytotoxicité est évaluée après marquage à l'Iodure de propidium et analysée en cytométrie de flux.
B. Les cellules cibles (ici, des LB) sont marquées à la Calcéine-AM puis mises en présence d'anticorps (2µg/mL) et de PBMC humain pendant 4h à 37°C. La cytotoxicité est ensuite évaluée par la perte d'intensité de fluorescence.

Afin de pouvoir évaluer la pharmacocinétique et la pharmacodynamique de notre anticorps, nous avons tout d'abord mis au point le dosage de l'anticorps dans le sérum par la méthode immuno-enzymatique Elisa (Travail de Sophie Cheverry). Ensuite une première expérience *in vivo* a été lancée sur des souris nude xénogreffées avec des cellules de LB qui ont été traitées 2 fois par semaine avec deux doses d'AcM anti-Gb3/CD77 (10 et 40 mg/kg) en injections intraveineuses et comparées à un groupe contrôle. Le sang a été prélevé à J0 (avant traitement) puis à J7, J10 et J14. Les résultats du dosage de l'anti-Gb3/CD77 dans le sérum des souris ont montré que la dose 40 mg/kg induit l'atteinte d'un plateau dès 7 jours avec une concentration sérique maximale de 5,3µg/ml. A la dose 10mg/kg, il n'y a pas de plateau atteint même après J14 et la concentration maximale est de 6 µg/ml. Ceci suggère qu'une dose intermédiaire de 20 mg/kg devrait permettre d'augmenter la concentration sérique de l'Ac assez rapidement sans atteindre de plateau. Cette expérience a aussi montré que la prise des

tumeurs est très hétérogène chez la souris nude, et les résultats obtenus, même s'ils étaient encourageants, étaient difficilement interprétables quant à l'effet de l'anti-Gb3/CD77.

C. Axes de recherche et Méthodologie

1) Etude du lien entre la surexpression de Gb3/CD77 et de MDR1 dans certains cancers résistants aux chimiothérapies

Afin de compléter notre étude, nous souhaitons élargir à d'autres types de tumeurs (sein, poumon) notre analyse du lien entre l'expression de Gb3/CD77 et la résistance aux traitements. Sur l'ensemble des lignées sélectionnées, nous mesurerons le niveau d'expression de Gb3/CD77 et l'activité de son enzyme de synthèse, la Gb3 synthétase (méthode établie depuis de longues années au laboratoire (Taga et al., 1995a), ainsi que l'expression de MDR1 (par western blot et cytométrie en flux). Comme l'expression de MDR1 en surface des cellules ne reflète pas forcément son activité, nous mesurerons aussi cette dernière (cytométrie de flux en utilisant la calcéine-AM, ce composé fluorescent entre de façon passive dans la cellule et sa sortie reflète l'activité des pompes). Nous établirons également le contenu global en GSLs de ces différentes lignées par chromatographie sur couche mince de gel de silice.

Nous collaborons avec une équipe Danoise (Henrik Clausen, Copenhaguen Center for Glycomics) qui a récemment mis au point une stratégie permettant l'étude fonctionnelle précise de la glycosylation en supprimant chaque glycosyltransférase individuellement (technique CRISPR-Cas9)(Narimatsu et al., 2018). Les lignées cellulaires isogéniques ainsi obtenues permettent de caractériser le glycoprotéome et le glycolipidome des cellules par spectrométrie de masse nLC-MS/MS. Dans le but de déterminer plus précisément le rôle de Gb3/CD77 dans la résistance aux traitements, nous allons inhiber les glycosyltransférases impliquées dans la série globo (il s'agit de la GCS, la LacCer synthétase et la Gb3 synthétase) dans les clones d'OV-1 résistants à la Doxorubicine (DXR) ou à la Vincristine (VCR). Nous mesurerons ensuite l'expression et l'activité de MDR1 ainsi que la résistance aux drogues de ces cellules mono ou multi-KO. Le glycome des lignées présentant une modulation de la résistance aux drogues sera ensuite analysé. Par ailleurs, afin de contrôler l'effet spécifique de chaque enzyme, nous nous proposons aussi de les ré-exprimer dans ces cellules KO avec un système inductible (doxocycline). En effet, ce système développé également dans l'équipe de Henrik Clausen a l'avantage d'induire une expression de l'enzyme proportionnelle à la dose de doxocycline et donc de contrôler les niveaux d'induction. Une étude récente ayant montré que la surexpression de la GCS pourrait induire une activation de la voie Akt/ERK1/2 entrainant une augmentation de MDR1, nous testerons aussi la phosphorylation de différents molécules cibles de cette voie dans notre modèle (Wegner et al., 2018). Ces travaux devraient nous permettre de mieux appréhender les relations entre Gb3/CD77 et MDR1 et de façon plus globale, le lien entre MDR1 et la synthèse des glycolipides.

En parallèle, nous collecterons différentes tumeurs (cancer du sein, de l'ovaire, du testicule, etc …) provenant du centre de ressource biologique (CRB) de GR et du CHU Henri Mondor (Collaboration Anaïs Pujals) afin d'évaluer l'expression de Gb3/CD77, de la Gb3

synthétase et de MDR-1 *in vivo*. Ce travail sera réalisé par immunohistochimie sur des cryosections et des coupes en paraffine.

2) Evaluation thérapeutique d'un AcM anti-Gb3/CD77

Pour ce qui concerne la partie *in vivo* grâce aux résultats obtenus lors de la première expérience, nous avons réajusté le schéma d'injection pour les souris xénogreffées ainsi que les analyses qui seront faites. En bref, les souris porteuses de tumeurs atteignant 100 mm^3 seront randomisées (6 à 8 animaux par groupe) et traitées 2 fois par semaine avec une dose d'AcM (20 mg/kg) en injections intraveineuses et comparées à un groupe contrôle et ce, pendant au moins 8 semaines. Les souris seront pesées, les tumeurs mesurées et les effets secondaires évalués. Nous avons donc changé de modèle : nous avons utilisé des souris Rag2-/- γc -/- ce qui a permis de nettement améliorer la prise des tumeurs. Cette expérience en cours devrait nous permettre d'analyser la distribution et la persistance de l'anticorps dans les différents tissus ainsi que sa pharmacocinétique et la pharmacodynamique.

En ce qui concerne les tumeurs chimiorésistantes, nous utiliserons tout d'abord, notre modèle de cancer de l'ovaire (5ème cancer féminin, taux de survie de 30% à 5 ans) puis un modèle de NSCLC (85% des cas de cancer du poumon, première cause de mortalité chez l'homme) (Arriagada et al., 2010; Janne, 2003). Ces tumeurs xénogreffées seront traitées selon le schéma établi pour le lymphome de Burkitt. La suite de cette partie du projet consistera à tester l'association de l'anti-Gb3/CD77 avec le traitement de référence des différentes tumeurs à des doses plus faibles que celles qui induisent seules la régression tumorale afin d'obtenir une régression tumorale efficace, tout en limitant les effets secondaires.

3) Gb3/CD77 dans le diagnostic des lymphomes B

En parallèle, nous avons initié une collaboration avec le Département de biologie et de pathologie médicale (Dr. Véronique Vergé) et celui d'hématologie de GR (Dr. Julien Lazarovici) afin d'analyser l'expression de Gb3/CD77 chez des patients atteints de différents types de lymphomes B.

En effet, quand les cellules B deviennent cancéreuses, elles gardent souvent certaines caractéristiques de leur cellule d'origine comme notamment le stade de différenciation. Les études histologiques et immunohistologiques ont été d'une importance capitale pour la classification des tumeurs B. Par exemple, dans le cas du lymphome folliculaire (FL), la tumeur ressemble morphologiquement à des cellules du CG, expriment des marqueurs typiques (comme CD10) et prolifèrent en structures qui ressemblent aux CG. Le lymphome de Burkitt a, quant à lui, une prolifération diffuse, rarement folliculaire, marquée avec de nombreuses cellules en apoptoses et en mitose, un aspect en ciel étoilé fréquent dû à de nombreux macrophages à corps tingibles qui englobent les restes apoptotiques. Cependant, les cellules ressemblent à des centroblastes, elles expriment des marqueurs du centre germinatifs (IgM^+, $CD10^+$, $Bcl6^+$) et ont des mutations somatiques des Ig confirmant leur origine folliculaire. Le développement d'outils permettant l'analyse de l'expression de tous les gènes comme le GEP (gene expression profil) ont permis de classifier un groupe hétérogène comme le DLBCL

démontrant qu'il pouvait être subdivisé en plusieurs groupes. : les GCB-like (germinal center like), les ABC-like (activated B cell like), et les DLBCL de type 3.

Ainsi, la majorité des lymphomes B est dérivée des cellules du CG ou post-CG (Figure 15) ce qui rend leur classification très compliquée. La classification globale des LNH est établie par l'Organisation Mondiale de la Santé (OMS) et est utilisée par les médecins des différentes spécialités, leur permettant d'avoir une même approche du diagnostic et un langage international commun. Elle prend en compte les critères morphologiques, immunologiques, génétiques et cliniques des tumeurs.

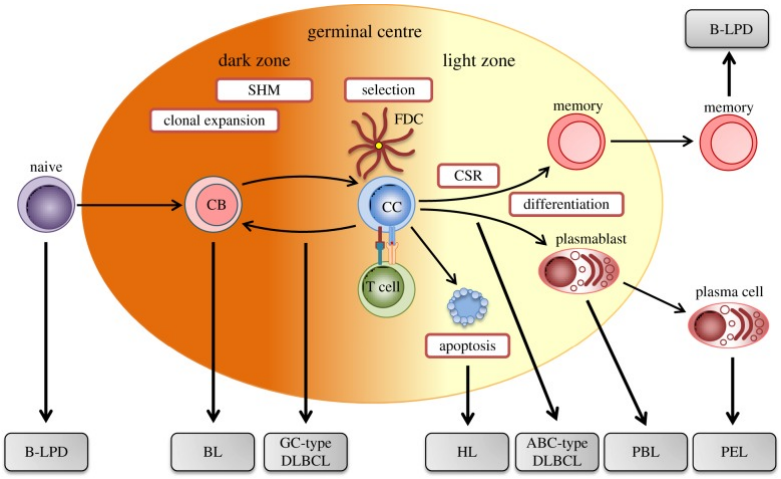

Figure 15 : Origine centro-germinale des différents lymphomes B.
Figurent sur ce schéma, les étapes principales de la différenciation B au niveau du CG. Les centroblastes suivent une expansion clonale massive dans la zone sombre et activent le processus d'hypermutation somatique (SHM, somatic hypermutation). Dans la zone claire, les cellules B centrocytes sont sélectionnées pour les mutations qui augmentent l'affinité. Les cellules sélectionnées positivement vont subir plusieurs tours de prolifération/mutation et sélection avant de se différencier en cellules B mémoires ou plasmocytes et quitter le CG après avoir subi la commutation isotypique ou de classe (CSR, class switch recombination).

Par exemple, pour le DLBCL, plusieurs algorithmes d'immunohistochimie sont utilisés comme celui de Hans (utilisé à GR) qui combine 3 marqueurs en immunohistochimie : CD10, MUM1 et BCL-6 (Figure 16). Cependant, la concordance de la classification des patients par les différents algorithmes est parfois très faible (Coutinho et al., 2013). L'idéal serait de combiner une analyse des profils d'expression génique des tumeurs avec la cytométrie mais cela aurait un coût élevé et nécessiterait beaucoup de temps. En effet, il faudrait avoir un soutien bio statistique et mettre en place des algorithmes standards pour l'analyse des données. De plus, jusqu'à récemment, ce type d'analyse GEP nécessitait des coupes cryoconservées ce qui est beaucoup contraignant que les coupes en paraffine (Ott, 2017). La connaissance de l'origine cellulaire de la tumeur est d'une importance capitale pour prédire la réponse du patient au traitement. En effet, par exemple, les patients souffrant d'un DLBCL-GC ont une survie à 5 ans de 80% contre 45% pour ceux souffrant d'un DLBCL-ABC (Gutierrez-Garcia et al., 2011). **Il semble donc nécessaire d'inclure de nouveaux marqueurs dans ces algorithmes pour améliorer la classification des patients**.

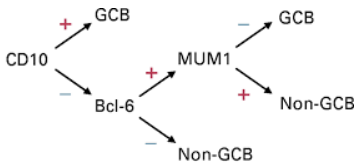

Figure 16 : Algorithme de Hans

Gb3 a été validé comme un marqueur de différenciation B et nommé CD77 (Wiels, 1989). Il est en effet présent à la surface d'un petit contingent de cellules dans les centres germinatifs. Son expression est transitoire : il est absent en surface des lymphocytes pro et pré B et son expression est induite après stimulation du BCR par l'antigène. Seulement 15% des cellules B des amygdales sont $CD77^+$ (Bailey et al., 2005). Il disparaît de la surface des lymphocytes B (L_B) en phase terminale de différenciation (Wiels et al., 1991). Cette expression restreinte du récepteur est corrélée à une activation séquentielle des glycosyltransférases. Une fois les L_B des CG activés par l'Ag, la Gb4 synthétase est exprimée et le Gb3/CD77 est métabolisé en Gb4 (Taga et al., 1995a; Taga et al., 1995b).

Le Gb3/CD77 a longtemps été considéré comme un marqueur discriminant les centroblastes (IgM^+ IgD- $CD38^+$ $CD77^+$) des centrocytes (IgM^+ IgD^- $CD38^+$ $CD77^-$). En effet, par séquençage et cytométrie en flux, les cellules exprimant CD77 ont été caractérisées comme des centroblastes engagés dans des hypermutations somatiques alors que celles ne l'exprimant plus correspondaient aux centrocytes subissant la commutation de classe (Feuillard et al., 1995; Fyfe et al., 1987; Liu et al., 1996). L'analyse histologique des centres germinatifs par un anticorps anti-Gb3/CD77 (38.13) a montré une diminution du marquage Gb3/CD77 de la zone sombre vers la zone claire. Les cellules Gb3/$CD77^+$ sont donc enrichies dans la zone sombre ce qui, là encore, indique une association avec les centroblastes. Cependant, une étude transcriptomique des gènes des populations Gb3/$CD77^-$ et Gb3/$CD77^+$ n'a montré que peu de différences dans leur programme d'expression. En effet, elles présentent un statut de prolifération équivalent et les composés impliqués dans la maintenance et la réparation de l'ADN montrent des niveaux de transcrits similaires (Hogerkorp et al., 2006; Klein et al., 2003; Nakayama et al., 2006).

Un modèle dans lequel la maturation des lymphocytes B suit une voie unidirectionnelle entre la zone sombre et la zone claire a longtemps été retenu pour expliquer l'efficacité de l'affinité de la maturation. Cependant, nous savons maintenant que les cellules B subiraient des cycles itératifs de mutation et de sélection dans les centres germinatifs dans un processus appelé « réentrée cyclique ». Victoria et al. ont observé qu'environ 30% des cellules B des centres germinatifs réintègrent la zone sombre après chaque tour de sélection dans la zone claire (Victora et al., 2010). Même s'il apparaît aujourd'hui que l'expression de Gb3/CD77 ne permet pas de discriminer les centroblastes des centrocytes, il n'en reste pas moins vrai que son expression au cours de la différenciation des cellules B est limité aux centres germinatifs ce qui suggère que ce récepteur pourrait jouer dans la sélection des lymphocytes B lors de leur différenciation dans les centres germinatifs. **Ainsi, Gb3/CD77 pourrait constituer un nouveau marqueur pour le diagnostic des lymphomes B.**

Des résultats préliminaires obtenus sur des lignées de DLBCL et de BL nous ont permis de montrer que les cellules de BL sont CD10$^+$, CD77$^+$ (cytométrie) et BCL6$^+$ (Western blot) ce qui est cohérent avec leur origine GC. Les lignées de DBLCL identifiées comme GC grâce aux diagnostics établis pour les patients dont elles sont issues (Karpas, Val, SU-DHL-4, SU-DHL-6 et RL) sont CD10$^+$, CD77$^+$, ce qui est cohérent avec les résultats obtenus avec l'algorithme de Hans. Les lignées identifiées comme ABC (OCI-LY10 et OCI-LY3) sont CD10$^-$, CD77$^-$ et BCL-6$^-$ ce qui est toujours en accord avec les résultats obtenus par l'algorithme de Hans. Nous disposions de deux autres lignées identifiées simplement en tant que DLBCL : les NU-DHL-1 qui sont CD10$^-$, BCL-6$^+$ et CD77$^-$ et les U2940 qui sont CD10$^-$, CD77$^+$ et BCL-6$^+$. Selon l'algorithme de Hans, il faudrait donc connaître leur statut MUM1 pour conclure. Dans la littérature les U2940 sont MUM1$^-$ (Fridberg et al., 2007) donc GCB selon Hans. Or, elles sont CD77$^+$ ce qui est cohérent. Nous n'avons pas évalué le statut MUM1 des NU-DHL-1 mais nous pensons qu'elles sont MUM1$^+$ vu qu'elles sont CD77$^-$ et que leur profil est de type ABC (figure 17). Ceci reste bien entendu des résultats préliminaires mais nous a permis de poser l'hypothèse suivante : le marquage Gb3/CD77 permet de discriminer les DLBCL GC des DLBCL ABC. J'ai donc mis au point un triple marquage CD19-APC, CD10-PE et Gb3/CD77-FITC afin d'analyser les biopsies de patients provenant de GR selon un protocole standardisé. Les résultats obtenus sont comparés au diagnostic réalisé en cytométrie et en immunohistochimie à l'hôpital.

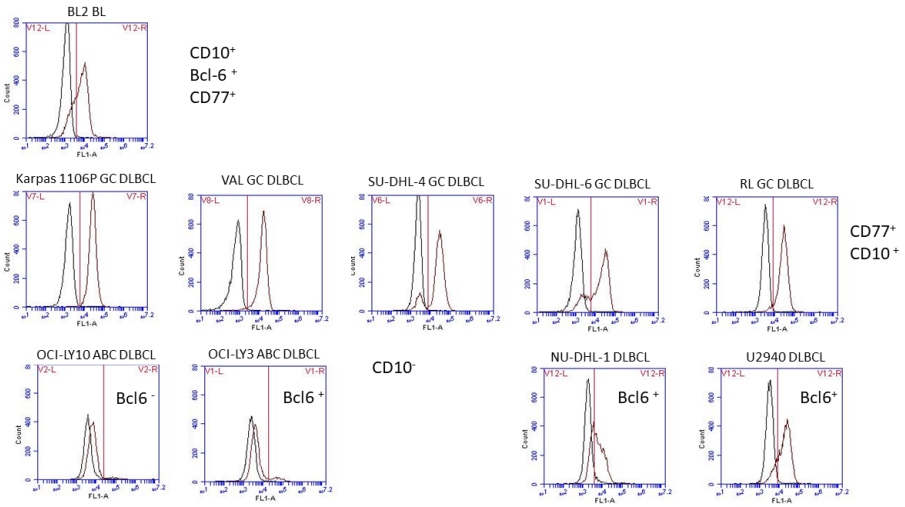

Figure 17 : L'expression de Gb3/CD77 en surface permet de discriminer les DLBCL GC des DLBCL ABC.
Après marquage par l'Ac 38.13, les cellules sont analysées en cytométrie. Noir : Isotype contrôle, Rouge : CD77.

Cette étude toujours en cours nous permettra de mieux cibler les pathologies susceptibles d'être traitées par les anti-Gb3/CD77 mais aussi éventuellement d'utiliser les anti-Gb3/CD77 pour le diagnostic de certains lymphomes comme le FL dont une étude a montré récemment l'hétérogénéité cellulaire par une analyse « single cell » de l'expression génique (Milpied et al., 2018).

En résumé, ce projet devrait nous permettre de comprendre le rôle de Gb3/CD77 dans des voies de signalisation impliquées dans la résistance aux traitements et pourrait mener à plus long terme à la mise en place de stratégies thérapeutiques utilisant un AcM anti-Gb3 qui cible spécifiquement les cellules tumorales, dont les effets toxiques pour les patients

seront limités et qui constituerait une stratégie de contournement des résistances aux traitements conventionnels.

II. Développement d'inhibiteurs spécifiques de MCL-1 : Les drimanes

Pour ce projet, j'ai encadré techniquement et scientifiquement plusieurs étudiantes, j'ai conçu les expériences qu'elles ont réalisées, analysé leurs résultats, corrigé leurs rapports et je les ai préparées à leurs oraux. Laura Bousset est venue de l'université de Clermont Ferrand pour faire son stage de M1 (deux mois) de Génétique et Physiologie en juillet 2015. Elle a travaillé sur les composés dérivés du drimane et a continué les expériences commencées par Loëtitia Favre concernant la caractérisation de leur mode d'action. Laura est maintenant en 3ème année de thèse au laboratoire GreD (Génétique Reproduction et Développement) à Clermont-Ferrand. Puis en 2017, nous avons accueilli Anaïs Marchi pour un stage de M1 (Clermont-Ferrand, deux mois) qui poursuit ses études en biologie. Depuis octobre 2017, je participe à l'encadrement technique et scientifique de Florian Daressy (Directrice J. Wiels) doctorant qui a repris ce projet. Florian bénéficie d'une bourse Initiative Doctorale Interdisciplinaire (IDI 2017) de l'IDEX Paris Saclay. Il a reçu une bourse pour participer et présenter son projet à la conférence de l'ECDO à Saint Pétersbourg en octobre 2018. En janvier 2019, Sophia Lahlil rejoindra notre équipe pour travailler sur ce sujet pour son M2 de de « toxicologie humaine, évaluation des risques et vigilance » à la faculté de pharmacie de Chatenay Malabry.

A. Travaux préliminaires

Après le travail sur la meiogynine A, un second travail a permis à l'équipe de chimiste d'isoler une autre molécule naturelle appelée Drimane qui est plus spécifique de MCL-1 (Ki=61nM±15) que de BCL-XL (Ki>100µM) en polarisation de fluorescence. Les différents analogues de cette molécule, les composés NA1 sont présentées dans le tableau 1.

Tableau 1 Constantes de dissociation du Drimane et de ses analogues, les composés NA-1

Référence	Structure	PF Mcl-1/Bid	PF Bcl-xL/Bak
SE2-190-6 Na1-26-2 **(Drimane)**	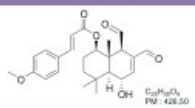	Ki = 61 nM ± 15 IC_{50} = 258 nM ± 45	> 100 µM
NA1-99-5	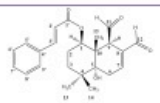	Ki = 1.4 µM ± 0.2 IC_{50} = 4.4 µM ± 0.7	> 100 µM
NA1-115-7	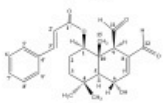	Ki = 97 nM ± 11 IC_{50} = 367 nM ± 32	> 100 µM
NA1-120-1	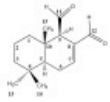	>100 µM	> 100 µM
NA1-122-5	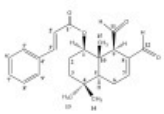	Inactive, à réévaluer	> 100 µM
NA1-119-1	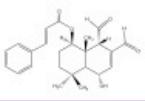	Ki = 4.9 µM ± 0.5 IC_{50} = 15 µM ± 1.4	> 100 µM

Ce tableau résume les résultats des expériences de polarisation de fluorescence (PF) obtenus par les chimistes ainsi que les formules chimiques du Drimane (SE2-190-6/Na1-26-2) et de ses analogues, les composés NA1). La PF permet d'étudier les interactions protéines/peptides selon la dépolarisation ou non de la lumière émise. Les protéines MCL-1 et BCL-XL ont été incubées en présence d'un peptide BH3 couplé à la fluorescéine (peptide BH3 de BID et de BAK, respectivement). Les résultats obtenus permettent de calculer les constantes de dissociation (Ki) et de déterminer les concentrations inhibitrices médianes (IC50), qui sont indiquées ci-dessus.

Comme pour la meiogynine, la cytotoxicité de ces molécules a été mesurée par le test MTT. Les cellules ont été incubées 24h avec 0, 1, 2, 5 et 10 µM de chaque composé et la figure 18 résume les résultats obtenus. Comme observé par les chimistes en polarité de fluorescence (PF), le composé NA1-120-1 n'a aucun effet quelle que soit la lignée. Contrairement aux résultats obtenus en PF, notre test montre que les composés NA1-99-5 et NA1-119-1 sont des inhibiteurs pan-BCL-2 (cf. tableau, Figure 17). Les composés NA1-122-5 et NA1-115-7 sont eux spécifiques de MCL-1. Pour des raisons de disponibilité et de stabilité des produits, nous avons donc continué nos expériences avec les composés NA1-115-7 et NA1-119-1.

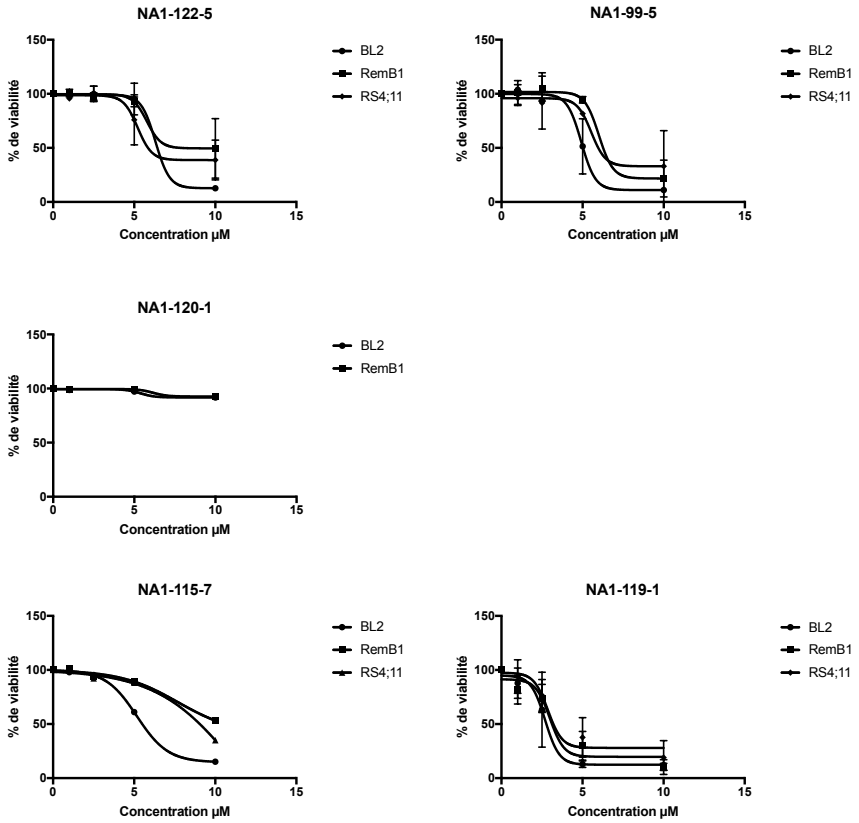

		LC50 µM						
Lignée	Dépendance	ABT-737	ABT-199	NA1-122-5	NA1-99-5	NA1-120-1	NA1-115-7	NA1-119-1
BL2	BCL-XL/ MCL-1	>10	>10	6,35	4	>10	5,2	2,695
Remb1	BCL-XL	1,4	5,5	>10	6	>10	>10	2,985
RS4;11	BCL-2	0,33	0,33	>7,5	5,5	>10	>10	2,872
H929	MCL-1	ND	ND	ND	ND	ND	ND	5,229

Figure 18 : Détermination de la LC50 (concentration léthale 50) des différents composés dérivés du Drimane

Nous avons ensuite testé leur capacité à induire l'apoptose pour cela, les lignées cellulaires ont été traitées par 4 µM de NA1-119-1 ou de NA1-115-7 pendant 24 heures. Les cellules ont été marquées à l'annexine V/PI puis analysées par cytométrie en flux. Les résultats confirment la meilleure spécificité de NA1-115-7 qui tue plus de 50% des cellules décrites comme dépendantes de MCL-1 (BL2 : 80%, H929 : 55%) et moins de 30% des Remb1 et des

RS4;11 (dépendantes de BCL-XL et de BCL-2 respectivement). Le NA1-119-1 est efficace sur les H929, les BL2 et les Remb1 (pourcentage d'apoptose respectivement de 83, 55 et 59%) mais n'a que très peu d'effet sur RS4;11 (pourcentage d'apoptose : 26%, Figure 19).

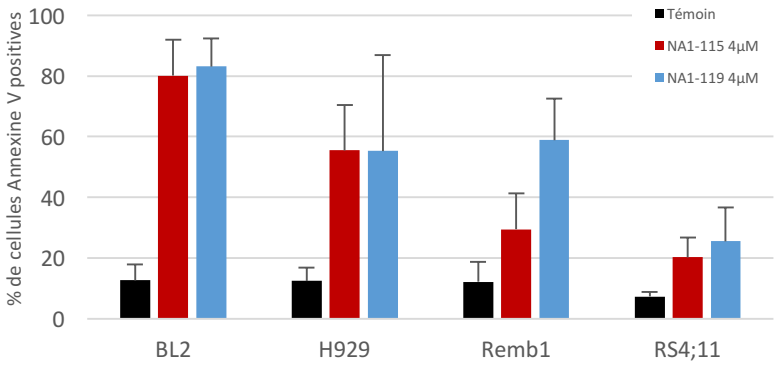

Figure 19 : NA1-115-7 et NA1-119-1 induisent la mort des cellules par apoptose.
Analyse en cytométrie de flux du marquage Annexine V/PI après traitement des différentes lignées pendant 24h à 4 µM

Les dérivés du Drimane testés sont théoriquement capables de déplacer l'interaction entre les membres anti-apoptotiques et pro-apoptotiques et ainsi lever l'inhibition de l'apoptose. Ce mécanisme d'action s'apparente à celui des protéines « BH3-only » et devrait conduire à l'activation des protéines pro-apoptotiques. Afin de voir si les inhibiteurs influent effectivement sur l'activation de protéines pro-apoptotiques, le changement de conformation de BAX et BAK a été étudié par cytométrie en flux grâce à des anticorps conformationnels reconnaissant leur forme active (Figure 20A). L'activation de BAX est aussi caractérisée par sa relocalisation du cytosol (à l'état basal) vers à la mitochondrie ce que nous avons également analysé. Dans les BL2, nos deux inhibiteurs entrainent la relocalisation de BAX à la mitochondrie. Cette activation de BAX et de BAK déclenche la voie mitochondriale de l'apoptose comme en témoignent les sorties de CYT C et de Smac/DIABLO de la mitochondrie vers le cytosol. En revanche, dans les Remb1, NA1-115-7 est moins efficace que NA1-119-1 (Figure 20B).

Les résultats représentés dans la figure 21 montrent qu'après traitement avec NA1-119-1, les caspases 8 et 3 sont clivées et donc activées dans les BL2 et dans Remb1 alors qu'avec NA1-115-7, elles le sont uniquement dans les BL2. Ceci est confirmé par l'observation du clivage de la PARP, substrat des caspases 3 et 7. De façon intéressante, nous observons une diminution de la protéine MCL-1 dans les BL2 avec NA1-119-1 et NA1-115-7. Il semblerait que dans les RemB1, la protéine soit complètement dégradée après traitement par le NA1-119-1.

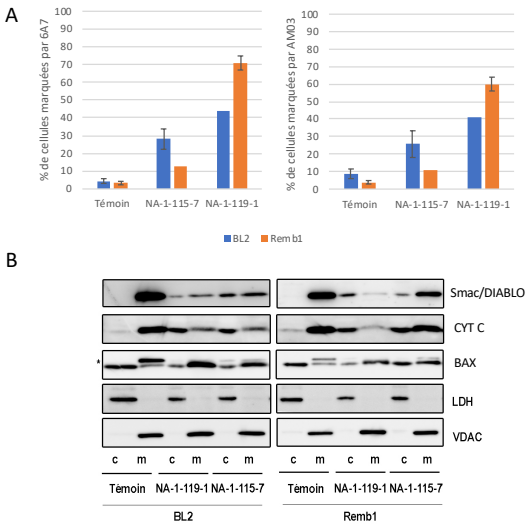

Figure 20 : Le traitement des cellules B par des inhibiteurs de MCL-1 induit l'activation de la mitochondrie

A. Analyse par cytométrie en flux des formes actives des protéines BAX et BAK. Les cellules BL2 et REMB1 ont été traitées ou non par 4 µM de NA1-119-1 ou de NA1-115-7 pendant 4 heures puis marquées par un anticorps conformationnel (6A7) reconnaissant la forme active de BAX ou par un anticorps conformationnel (AM03) reconnaissant la forme active de BAK. B. Analyse par Western Blot des extraits protéiques cytosoliques et mitochondriaux des cellules BL2 et REMB1 traitées ou non par 4 µM de NA-1-119-1 ou de NA-1-115-7 pendant 7 heures. c : fraction cytosolique ; m : fraction mitochondriale. * hybridation résiduelle non spécifique de Smac/DIABLO.

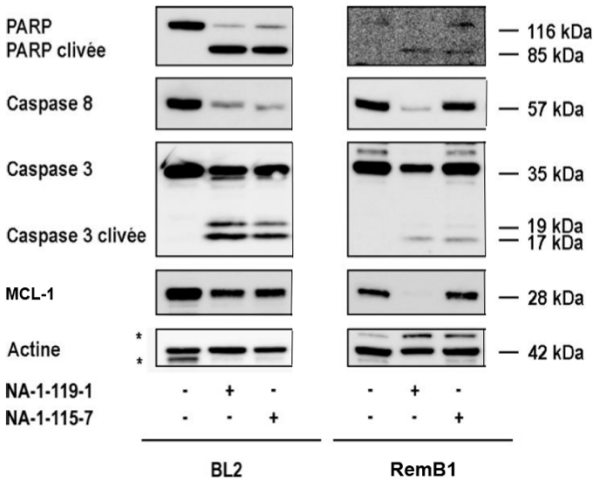

Figure 21 : Les inhibiteurs potentiels de MCL-1 activent les caspases et semblent dégrader MCL-1

Après 7h de traitement avec NA1-115-7 ou avec NA1-119-1 (4 µM)., les cellules ont ensuite été lysées et les extraits protéiques ont été analysés par western blot pour évaluer les clivages de la PARP, des caspases 8 et 3 ainsi que l'expression de MCL-1.

Afin de vérifier une inhibition de l'interaction entre MCL-1 et son/ses partenaire(s) par nos composés, nous avons, dans un premier temps, testé les partenaires pro-apoptotiques connus pour interagir avec MCL-1. Pour cela, nous avons immunoprécipité MCL-1 et testé la co-immunoprécipitation de BAK, NOXA ET BIM ainsi que de BAX et BID (Travail de Loëtitia Favre). Nous avons réussi à montrer que, dans la lignée BL2, MCL-1 interagit bien avec BAK et NOXA mais pas avec BAX et BID (Figure 22A). Quant aux résultats obtenus avec BIM, ils ne nous ont pas permis d'identifier avec certitude la présence ou non d'une interaction. Nous avons ensuite voulu vérifier si le traitement des cellules avec l'inhibiteur potentiel de MCL-1, NA1-

119-1, induisait la dissociation de MCL-1/BAK. Pour cela, nous avons traité les lignées BL2 et Remb1 avec NA1-119-1 pendant 5h, un temps suffisant pour déclencher l'apoptose sans avoir une dégradation trop importante de MCL-1. Les résultats confirment qu'en l'absence de traitement, MCL-1 interagit avec BAK dans les BL2 et Remb1 et qu'un traitement avec l'inhibiteur conduit bien à une diminution de la co-immunoprécipitation de BAK avec MCL-1, diminution plus importante dans la lignée Remb1 que la lignée BL2 (Figure 22B).

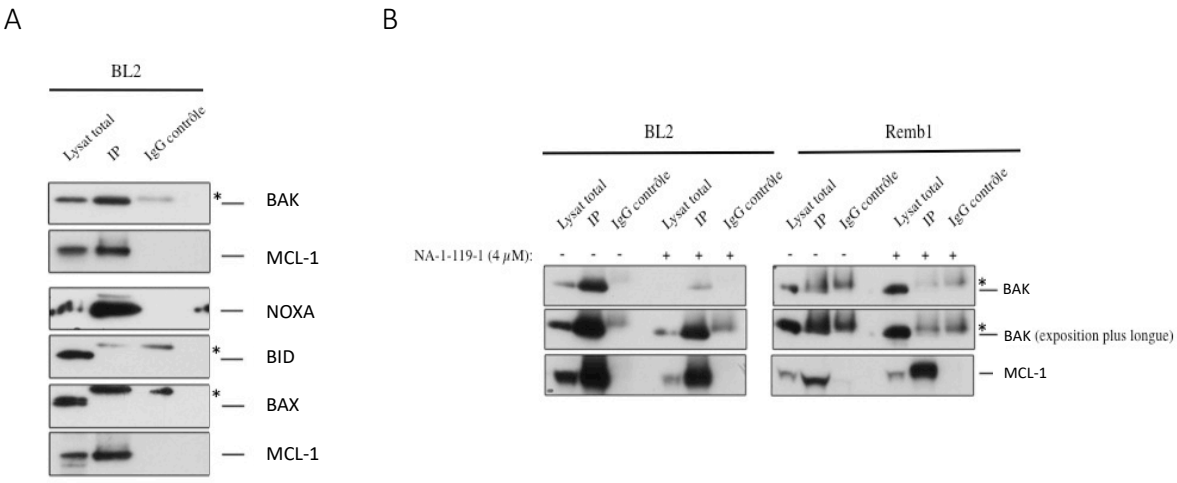

Figure 22: NA1-119-1 induit la rupture d'interaction entre MCL-1 et BAK

A. Des lysats de BL2 ont été incubés en présence de billes de sépharose G couplées avec un anti-MCL-1 (IP) ou des billes de sépharose G couplées avec un IgG contrôle de lapin (contrôle IgG). Les protéines immunoprécipitées ont été analysées par western blot. Afin de contrôler le niveau protéique avant immunoprécipitation, une portion de lysat total (3%) a été inclus dans le western blot. B. Les lignées BL2 et Remb1 ont été traitées ou non avec NA1-119-1 (4 µM) pendant 5h avant d'être lysées pour imunoprécipiter MCL-1. Les lysats ont été incubés et analysés comme en A. * Signal des chaînes légères des Ig.

A ce stade, nos résultats nous amènent à proposer le modèle d'action pour la molécule NA1-119-1 schématisé dans la Figure 23. Dans cette hypothèse, en l'absence de traitement, MCL-1 est localisée à la mitochondrie et interagit avec NOXA, BAK et potentiellement BIM. Lorsque les cellules sont traitées avec NA-1-119-1, MCL-1 n'interagit plus avec ses partenaires (BAK et NOXA) qui sont donc libérés. MCL-1 devient alors la cible d'ubiquitine-ligases entraînant ainsi sa dégradation par le protéasome. L'hétérodimérisation BAX/BAK génère des pores au niveau de la membrane mitochondriale, qui permettent la libération de SMAC et du CYT C. La caspase 8 est clivée et activée et permet le clivage de ses substrats tels que les caspases effectrices 7 et 3 ainsi que la protéine BID. L'activation des caspases effectrices permet de déclencher l'apoptose.

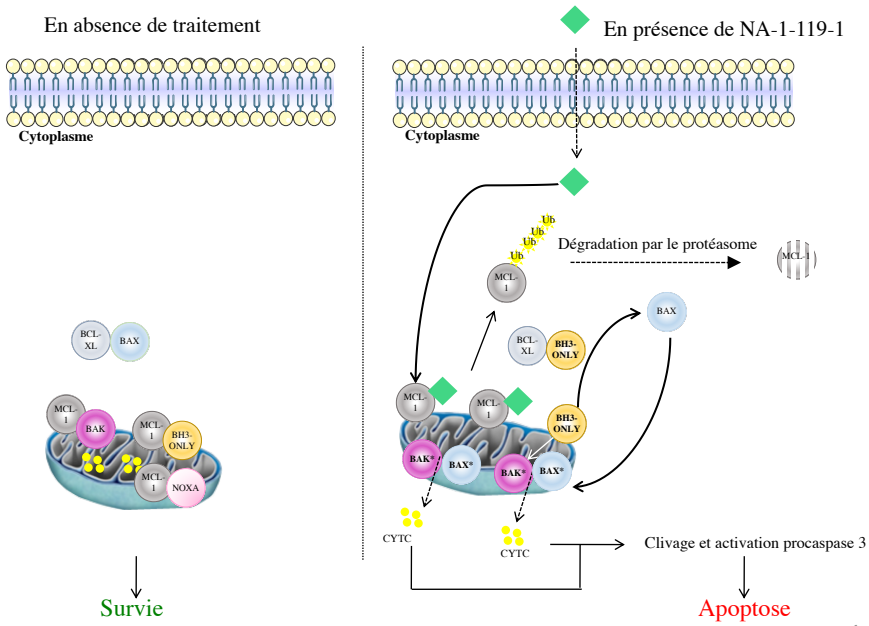

Figure 23: Schéma du mécanisme d'action de NA1-119-1 (D'après la thèse de L. Favre)

En l'absence de traitement, la protéine pro-apoptotique BAX (représentée en bleu ciel) est localisée dans le cytoplasme des cellules. Elle est sous forme inactive et peut interagir avec les membres anti-apoptotiques tels que BCL-2 et/ou BCL-xL (représentés en gris clair). MCL-1 (représentée en gris foncé), fortement exprimée, est localisée au niveau des mitochondries et interagit avec des membres pro-apoptotiques BAK (en rose foncé) et NOXA (en rose clair). Les cellules survivent. Lorsque les cellules sont traitées avec NA1-119-1, cette molécule provoque la dissociation des complexes formés entre MCL-1 et BAK. MCL-1 est dégradée, BAX se relocalise à la mitochondrie (par un mécanisme qui reste à déterminer) ; BAX et BAK s'activent. Les facteurs apoptogènes (CYT C et Smac/DIABLO) initialement séquestrés dans les mitochondries sont alors libérés dans le cytoplasme des cellules traitées induisent le clivage et l'activation des caspases 8 et 3. La caspase 3 clive ses substrats dont la PARP et les cellules entrent en apoptose

B. Perspectives de travail et méthodologie

1) In vitro

Nous avons identifié deux énantiomères NA1-119-1, NA1-115-7 capables de dissocier les interactions MCL-1/membres pro-apoptotiques avec une forte affinité en polarisation de fluorescence et montré qu'ils étaient capables de déclencher l'apoptose des lignées cellulaires par la voie mitochondriale.

Dans la suite du travail, il semble important de définir si ces molécules répondent à la définition d'un BH3 mimétique qui doit :

- Lier la cible avec un haute affinité
- Induire une apoptose dépendante de BAK et de BAX

En ce qui concerne le premier point, dans le cadre d'une collaboration entre l'équipe de F. Roussi et une équipe de RMN de l'ICSN, des études d'interaction entre les molécules élaborées et la protéine MCL-1 seront effectuées afin de déterminer leur site de fixation plus précisément.

De plus, les expériences de co-immunoprécipitation nous ont montré que MCL-1 interagit avec BAK et NOXA dans nos lignées non traitées, ce qui est en accord avec la

littérature. Quant aux résultats obtenus après traitement des cellules avec NA1-119-1, ils semblent indiquer qu'il existe une rupture d'interaction entre MCL-1 et BAK. Toutefois, ces résultats doivent être reproduits pour affirmer que NA1-119-1 entraîne une rupture d'interaction et des expériences similaires avec NA1-115-7 devront être réalisées. Il faudra aussi analyser l'interaction MCL-1/NOXA après traitement. Les expériences de polarisation de fluorescence des chimistes indiquent que les composés de la famille NA1 rompent les interactions MCL-1/protéines pro-apoptotiques avec une plus grande affinité que les liaisons BCL-XL/BAX. Il faudra vérifier si dans les cellules qui meurent après traitement par les composés NA1, BCL-XL interagit avec BAX ou BAK à l'état basal. Si cette interaction est réelle, il faudrait alors vérifier si le traitement induit une rupture d'interaction ou non. Si cette interaction n'est pas rompue, cela constituerait une preuve supplémentaire que les inhibiteurs sont spécifiques de MCL-1 notamment pour le composé NA1-115-7.

Pour confirmer la spécificité d'action de ces composés, nous envisageons aussi de traiter des lignées MEF sauvages, invalidées pour MCL-1 (KO MCL-1), BCL-XL (KO BCL-XL) et d'analyser l'apoptose dans ces cellules après traitement par nos composés.

En ce qui concerne le deuxième point, après traitement, nous observons que BAX se relocalise à la mitochondrie et que BAX et BAK s'activent. Le relargage de la mitochondrie vers le cytoplasme de facteurs apoptogènes (CYT C et Smac/DIABLO) reflète la perméabilisation de la membrane mitochondriale, due aux pores formés par BAX et BAK. L'interaction BAX/BAK, ainsi que les interactions BAX/BAX et BAK/BAK pourront être confirmées par co-immunoprécipitations et par des expériences de pontage au BMH pour valider l'implication de ces protéines dans la formation des pores. De plus, il sera nécessaire de vérifier que nos composés n'induisent pas l'apoptose dans des cellules invalidées pour BAX (KO BAX), BAK (KO BAK) et BAX/BAK (DKO BAX/BAK).

Nous élargirons aussi le nombre de lignées utilisées après les avoir caractérisées par « BH3 profiling ». Nous souhaiterions notamment tester des lignées issues de tumeurs solides.

Enfin, l'entrée des cellules en apoptose est concomitante à la dégradation de MCL-1 ce qui suggère que les inhibiteurs rompent l'interaction MCL-1/ protéine(s) pro-apoptotique(s), libérant MCL-1 et démasquant les sites d'ubiquitination qui seront les cibles d'ubiquitine-ligases, permettant alors sa dégradation par le protéasome. Or, les autres BH3 mimétique ciblant MCL-1 comme S63845 et A1210, stabilisent MCL-1 ce qui est plutôt en accord avec les connaissances sur les mécanismes de dégradation de MCL-1 (Kotschy et al., 2016). En effet, MULE/HUWEI, la principale ubiquitine ligase permettant la dégradation de MCL-1 se fixe sur le site BH3 donc les inhibiteurs devraient l'en empêcher. Au vu de nos résultats, on peut supposer que soit nos inhibiteurs ne lient pas exactement le site BH3, soit l'interaction MULE/MCL-1 peut déplacer les composés, soit cette dégradation est le fait d'une autre ubiquitine ligase comme SCF/FBW7 ou SCF/bTRCP (Figure 24). Il faudra tester cette hypothèse par exemple en utilisant des cellules KO pour MULE et en regardant si nos composés déclenchent toujours l'apoptose et si MCL-1 est toujours dégradé. Les phosphorylations de MCL-1 sont aussi importante pour sa stabilisation, il faudra donc s'y intéresser. Même si cela nous semble peu probable au vu de l'ensemble de nos résultats, Il reste aussi possible que nos inhibiteurs dans

la cellule ne ciblent pas directement les protéines de la famille de BCL-2. Il faudra alors regarder si on a une activation de l'UPR (unfolded protein response) et/ou une induction de NOXA comme c'est le cas pour le gossypol ou l'obatoclax par exemple (Revu dans (Soderquist et al., 2016)).

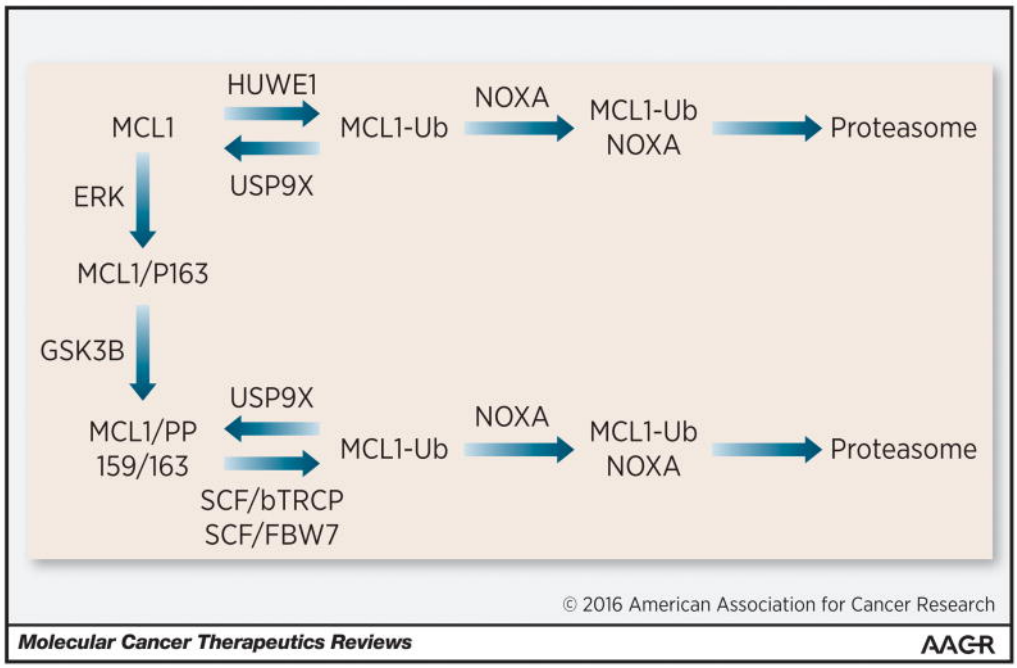

Figure 24 : Régulation du turnover de la protéine MCL-1 (Soderquist and Eastman, 2016)

MCL-1 peut être ubiquitinylée par au moins 3 E3 ligases en fonction de sa phosphorylation. NOXA stabiliserait MCL-1 ubiquitinylée et l'hétérodimère MCL-1/NOXA est ensuite dégradé par le protéasome.

2) In vivo

Par la suite, nous envisageons d'utiliser ces deux inhibiteurs pour des expériences *in vivo* sur des modèles de tumeurs xénogreffées (souris nude) de BL et de DLBCL qui sont déjà en place dans l'équipe. Un système de tumeurs syngéniques établi avec des lignées de lymphomes murins *Eμ-Myc* sera également utilisé afin de valider nos molécules dans un modèle immunocompétent.

Le premier obstacle pour l'évaluation des composés de la famille NA-1 *in vivo* est leur formulation. En effet, de nombreux essais ont été réalisés pour les solubiliser mais sans succès. Grâce à Fanny Roussi, nous avons donc mis en place une collaboration avec des galénistes de l'université de Pharmacie de Caen (équipe d'Aurélie Malzert-Fréon) afin d'encapsuler nos composés dans des nanoémulsions (Groo et al., 2017). Cette équipe a déjà réalisé ce type d'expérience pour une autre molécule inhibant MCL-1 : le pyridoclax (Gloaguen et al., 2015) et a réussi à stabiliser le composé afin de pouvoir l'administrer oralement ou en intraveineuse Cette formulation a même permis d'augmenter son efficacité *in vitro* en augmentant sa biodisponibilité (communication personnelle). Des tests avec différents formulations de nanoémulsions sont en cours pour nos molécules et seront évaluées *in vitro* avant le passage *in vivo*.

Les protocoles d'injection seront définis en collaboration avec la plateforme d'Evaluation et de Pharmacologie Précliniques de GR. Les inhibiteurs seront testés seuls ou en combinaison avec le cyclophosphamide (l'un des composants du traitement chimiothérapeutique des BL et DLBCL) ou en combinaison avec des anti-CD20 (Rituximab).

L'objectif de nos travaux est de produire et d'évaluer par des études précliniques un composé capable d'inhiber spécifiquement et avec une forte affinité la protéine anti-apoptotique MCL-1. Le but recherché, à terme, est la mise en place d'un nouvel outil thérapeutique ciblé qui permettra de contourner des résistances aux outils thérapeutiques conventionnels (chimiothérapie et radiothérapie) ou qui pourra potentialiser l'effet de ces outils. Ces travaux ne sont possibles que grâce à une interaction forte et à des échanges constants entre une équipe de chimistes et une équipe de biologistes qui permettent de tester de nombreux composés et de les optimiser le plus rapidement et efficacement possible.

Bibliographie

-Abou Samra, A., Robert, A., Gov, C., Favre, L., Eloy, L., Jacquet, E., Bignon, J., Wiels, J., Desrat, S., and Roussi, F. (2018). Dual inhibitors of the pro-survival proteins Bcl-2 and Mcl-1 derived from natural compound meiogynin A. Eur J Med Chem 148, 26-38.

-Arab, S., Russel, E., Chapman, W.B., Rosen, B., and Lingwood, C.A. (1997). Expression of the verotoxin receptor glycolipid, globotriaosylceramide, in ovarian hyperplasias. Oncol Res 9, 553-563.

-Arriagada, R., Auperin, A., Burdett, S., Higgins, J.P., Johnson, D.H., Le Chevalier, T., Le Pechoux, C., Parmar, M.K., Pignon, J.P., Souhami, R.L., et al. (2010). Adjuvant chemotherapy, with or without postoperative radiotherapy, in operable non-small-cell lung cancer: two meta-analyses of individual patient data. Lancet 375, 1267-1277.

-Ashkenazi, A., Fairbrother, W.J., Leverson, J.D., and Souers, A.J. (2017). From basic apoptosis discoveries to advanced selective BCL-2 family inhibitors. Nat Rev Drug Discov 16, 273-284.

-Bailey, S., Mardell, C., Wheatland, L., Zola, H., and Macardle, P.J. (2005). A comparison of Verotoxin B-subunit (Stx1B) and CD77 antibody to define germinal centre populations. Cell Immunol 236, 167-170.

-Benard, J., Da Silva, J., De Blois, M.C., Boyer, P., Duvillard, P., Chiric, E., and Riou, G. (1985). Characterization of a human ovarian adenocarcinoma line, IGROV1, in tissue culture and in nude mice. Cancer Res 45, 4970-4979.

-Brodsky, W.Y., and Uryvaeva, I.V. (1977). Cell polyploidy: its relation to tissue growth and function. Int Rev Cytol 50, 275-332.

-Burkitt, D. (1958). A sarcoma involving the jaws in African children. Br J Surg 46, 218-223.

-Caenepeel, S.R., Belmontes, B., Sun, J., Coxon, A., Moody, G., and Hughes, P.E. (2017). Abstract 2027: Preclinical evaluation of AMG 176, a novel, potent and selective Mcl-1 inhibitor with robust anti-tumor activity in Mcl-1 dependent cancer models. Cancer Research 77, 2027-2027.

-Campos, L., Rouault, J.P., Sabido, O., Oriol, P., Roubi, N., Vasselon, C., Archimbaud, E., Magaud, J.P., and Guyotat, D. (1993). High expression of bcl-2 protein in acute myeloid leukemia cells is associated with poor response to chemotherapy. Blood 81, 3091-3096.

-Capoulade, C., Bressac-de Paillerets, B., Lefrere, I., Ronsin, M., Feunteun, J., Tursz, T., and Wiels, J. (1998). Overexpression of MDM2, due to enhanced translation, results in inactivation of wild-type p53 in Burkitt's lymphoma cells. Oncogene 16, 1603-1610.

-Capoulade, C., Mir, L.M., Carlier, K., Lecluse, Y., Tetaud, C., Mishal, Z., and Wiels, J. (2001). Apoptosis of tumoral and nontumoral lymphoid cells is induced by both mdm2 and p53 antisense oligodeoxynucleotides. Blood 97, 1043-1049.

-Chen, C.F., Yeh, S.H., Chen, D.S., Chen, P.J., and Jou, Y.S. (2005). Molecular genetic evidence supporting a novel human hepatocellular carcinoma tumor suppressor locus at 13q12.11. Genes Chromosomes Cancer 44, 320-328.

-Coiffier, B. (2007). Rituximab therapy in malignant lymphoma. Oncogene 26, 3603-3613.

-Coutinho, R., Clear, A.J., Owen, A., Wilson, A., Matthews, J., Lee, A., Alvarez, R., Gomes da Silva, M., Cabecadas, J., Calaminici, M., et al. (2013). Poor concordance among nine

immunohistochemistry classifiers of cell-of-origin for diffuse large B-cell lymphoma: implications for therapeutic strategies. Clin Cancer Res 19, 6686-6695.

-Crighton, D., Wilkinson, S., O'Prey, J., Syed, N., Smith, P., Harrison, P.R., Gasco, M., Garrone, O., Crook, T., and Ryan, K.M. (2006). DRAM, a p53-induced modulator of autophagy, is critical for apoptosis. Cell 126, 121-134.

-Davoli, T., and de Lange, T. (2011). The causes and consequences of polyploidy in normal development and cancer. Annu Rev Cell Dev Biol 27, 585-610.

-De Rosa, M.F., Sillence, D., Ackerley, C., and Lingwood, C. (2004). Role of multiple drug resistance protein 1 in neutral but not acidic glycosphingolipid biosynthesis. J Biol Chem 279, 7867-7876.

-Debernardi, J., Hollville, E., Lipinski, M., Wiels, J., and Robert, A. (2018). Differential role of FL-BID and t-BID during verotoxin-1-induced apoptosis in Burkitt's lymphoma cells. Oncogene 37, 2410-2421.

-Delaval, B., Bright, A., Lawson, N.D., and Doxsey, S. (2011). The cilia protein IFT88 is required for spindle orientation in mitosis. Nat Cell Biol 13, 461-468.

-Desrat, S., Pujals, A., Colas, C., Dardenne, J., Geny, C., Favre, L., Dumontet, V., Iorga, B.I., Litaudon, M., Raphael, M., et al. (2014). Pro-apoptotic meiogynin A derivatives that target Bcl-xL and Mcl-1. Bioorg Med Chem Lett 24, 5086-5088.

-Desselle, A., Chaumette, T., Gaugler, M.H., Cochonneau, D., Fleurence, J., Dubois, N., Hulin, P., Aubry, J., Birkle, S., and Paris, F. (2012). Anti-Gb3 monoclonal antibody inhibits angiogenesis and tumor development. PLoS One 7, e45423.

-Engedal, N., Skotland, T., Torgersen, M.L., and Sandvig, K. (2011). Shiga toxin and its use in targeted cancer therapy and imaging. Microb Biotechnol 4, 32-46.

-Feuillard, J., Taylor, D., Casamayor-Palleja, M., Johnson, G.D., and MacLennan, I.C. (1995). Isolation and characteristics of tonsil centroblasts with reference to Ig class switching. Int Immunol 7, 121-130.

-Fotsop, D.F., Roussi, F., Leverrier, A., Breteche, A., and Gueritte, F. (2010). Biomimetic total synthesis of meiogynin A, an inhibitor of Bcl-xL and Bak interaction. J Org Chem 75, 7412-7415.

-Fridberg, M., Servin, A., Anagnostaki, L., Linderoth, J., Berglund, M., Soderberg, O., Enblad, G., Rosen, A., Mustelin, T., Jerkeman, M., et al. (2007). Protein expression and cellular localization in two prognostic subgroups of diffuse large B-cell lymphoma: higher expression of ZAP70 and PKC-beta II in the non-germinal center group and poor survival in patients deficient in nuclear PTEN. Leuk Lymphoma 48, 2221-2232.

-Fyfe, G., Cebra-Thomas, J.A., Mustain, E., Davie, J.M., Alley, C.D., and Nahm, M.H. (1987). Subpopulations of B lymphocytes in germinal centers. J Immunol 139, 2187-2194.

-Ganem, N.J., Godinho, S.A., and Pellman, D. (2009). A mechanism linking extra centrosomes to chromosomal instability. Nature 460, 278-282.

-Garibal, J., Hollville, E., Renouf, B., Tetaud, C., and Wiels, J. (2010). Caspase-8-mediated cleavage of Bid and protein phosphatase 2A-mediated activation of Bax are necessary for Verotoxin-1-induced apoptosis in Burkitt's lymphoma cells. Cell Signal 22, 467-475.

-Gloaguen, C., Voisin-Chiret, A.S., Sopkova-de Oliveira Santos, J., Fogha, J., Gautier, F., De Giorgi, M., Burzicki, G., Perato, S., Petigny-Lechartier, C., Simonin-Le Jeune, K., et al. (2015). First evidence that oligopyridines, alpha-helix foldamers, inhibit Mcl-1 and sensitize ovarian carcinoma cells to Bcl-xL-targeting strategies. J Med Chem 58, 1644-1668.

-Groo, A.C., De Pascale, M., Voisin-Chiret, A.S., Corvaisier, S., Since, M., and Malzert-Freon, A. (2017). Comparison of 2 strategies to enhance pyridoclax solubility: Nanoemulsion delivery system versus salt synthesis. Eur J Pharm Sci 97, 218-226.

-Guan, J.J., Zhang, X.D., Sun, W., Qi, L., Wu, J.C., and Qin, Z.H. (2015). DRAM1 regulates apoptosis through increasing protein levels and lysosomal localization of BAX. Cell Death Dis 6, e1624.

-Gupta, S. (2000). Hepatic polyploidy and liver growth control. Semin Cancer Biol 10, 161-171.

-Gupta, V., Bhinge, K.N., Hosain, S.B., Xiong, K., Gu, X., Shi, R., Ho, M.Y., Khoo, K.H., Li, S.C., Li, Y.T., et al. (2012). Ceramide glycosylation by glucosylceramide synthase selectively maintains the properties of breast cancer stem cells. J Biol Chem 287, 37195-37205.

-Gutierrez-Garcia, G., Cardesa-Salzmann, T., Climent, F., Gonzalez-Barca, E., Mercadal, S., Mate, J.L., Sancho, J.M., Arenillas, L., Serrano, S., Escoda, L., et al. (2011). Gene-expression profiling and not immunophenotypic algorithms predicts prognosis in patients with diffuse large B-cell lymphoma treated with immunochemotherapy. Blood 117, 4836-4843.

-Hakomori, S., and Zhang, Y. (1997). Glycosphingolipid antigens and cancer therapy. Chem Biol 4, 97-104.

-Haycraft, C.J., Swoboda, P., Taulman, P.D., Thomas, J.H., and Yoder, B.K. (2001). The C. elegans homolog of the murine cystic kidney disease gene Tg737 functions in a ciliogenic pathway and is disrupted in osm-5 mutant worms. Development 128, 1493-1505.

-Henderson, S., Rowe, M., Gregory, C., Croom-Carter, D., Wang, F., Longnecker, R., Kieff, E., and Rickinson, A. (1991). Induction of bcl-2 expression by Epstein-Barr virus latent membrane protein 1 protects infected B cells from programmed cell death. Cell 65, 1107-1115.

-Hird, A.W., Secrist, J.P., Adam, A., Belmonte, M.A., Gangl, E., Gibbons, F., Hargreaves, D., Johannes, J.W., Kazmirski, S.L., Kettle, J.G., et al. (2017). Abstract DDT01-02: AZD5991: A potent and selective macrocyclic inhibitor of Mcl-1 for treatment of hematologic cancers. Cancer Research 77, DDT01-02-DDT01-02.

-Hogerkorp, C.M., and Borrebaeck, C.A. (2006). The human CD77- B cell population represents a heterogeneous subset of cells comprising centroblasts, centrocytes, and plasmablasts, prompting phenotypical revision. J Immunol 177, 4341-4349.

-Isfort, R.J., Cody, D.B., Doersen, C.J., Richards, W.G., Yoder, B.K., Wilkinson, J.E., Kier, L.D., Jirtle, R.L., Isenberg, J.S., Klounig, J.E., et al. (1997). The tetratricopeptide repeat containing Tg737 gene is a liver neoplasia tumor suppressor gene. Oncogene 15, 1797-1803.

-Janke, C., and Kneussel, M. (2010). Tubulin post-translational modifications: encoding functions on the neuronal microtubule cytoskeleton. Trends Neurosci 33, 362-372.

-Janne, P.A. (2003). Chemotherapy for malignant pleural mesothelioma. Clin Lung Cancer 5, 98-106.

-Johansson, D., Andersson, C., Moharer, J., Johansson, A., and Behnam-Motlagh, P. (2010). Cisplatin-induced expression of Gb3 enables verotoxin-1 treatment of cisplatin resistance in malignant pleural mesothelioma cells. Br J Cancer 102, 383-391.

-Klein, U., Tu, Y., Stolovitzky, G.A., Keller, J.L., Haddad, J., Jr., Miljkovic, V., Cattoretti, G., Califano, A., and Dalla-Favera, R. (2003). Transcriptional analysis of the B cell germinal center reaction. Proc Natl Acad Sci U S A 100, 2639-2644.

-Konopleva, M., Contractor, R., Tsao, T., Samudio, I., Ruvolo, P.P., Kitada, S., Deng, X., Zhai, D., Shi, Y.X., Sneed, T., et al. (2006). Mechanisms of apoptosis sensitivity and resistance to the BH3 mimetic ABT-737 in acute myeloid leukemia. Cancer Cell 10, 375-388.

-Korsmeyer, S.J., Wei, M.C., Saito, M., Weiler, S., Oh, K.J., and Schlesinger, P.H. (2000). Pro-apoptotic cascade activates BID, which oligomerizes BAK or BAX into pores that result in the release of cytochrome c. Cell Death Differ 7, 1166-1173.

-Kotschy, A., Szlavik, Z., Murray, J., Davidson, J., Maragno, A.L., Le Toumelin-Braizat, G., Chanrion, M., Kelly, G.L., Gong, J.N., Moujalled, D.M., et al. (2016). The MCL1 inhibitor S63845 is tolerable and effective in diverse cancer models. Nature 538, 477-482.

-Lachance, H., Wetzel, S., Kumar, K., and Waldmann, H. (2012). Charting, navigating, and populating natural product chemical space for drug discovery. J Med Chem 55, 5989-6001.

-Litaudon, M., Bousserouel, H., Awang, K., Nosjean, O., Martin, M.T., Dau, M.E., Hadi, H.A., Boutin, J.A., Sevenet, T., and Gueritte, F. (2009a). A Dimeric sesquiterpenoid from a Malaysian Meiogyne as a new inhibitor of Bcl-xL/BakBH3 domain peptide interaction. J Nat Prod 72, 480-483.

-Litaudon, M., Jolly, C., Le Callonec, C., Cuong, D.D., Retailleau, P., Nosjean, O., Nguyen, V.H., Pfeiffer, B., Boutin, J.A., and Gueritte, F. (2009b). Cytotoxic pentacyclic triterpenoids from Combretum sundaicum and Lantana camara as inhibitors of Bcl-xL/BakBH3 domain peptide interaction. J Nat Prod 72, 1314-1320.

-Liu, Y.J., Arpin, C., de Bouteiller, O., Guret, C., Banchereau, J., Martinez-Valdez, H., and Lebecque, S. (1996). Sequential triggering of apoptosis, somatic mutation and isotype switch during germinal center development. Semin Immunol 8, 169-177.

-Liu, Y.Y., Gupta, V., Patwardhan, G.A., Bhinge, K., Zhao, Y., Bao, J., Mehendale, H., Cabot, M.C., Li, Y.T., and Jazwinski, S.M. (2010). Glucosylceramide synthase upregulates MDR1 expression in the regulation of cancer drug resistance through cSrc and beta-catenin signaling. Mol Cancer 9, 145.

-Liu, Y.Y., Hill, R.A., and Li, Y.T. (2013). Ceramide glycosylation catalyzed by glucosylceramide synthase and cancer drug resistance. Adv Cancer Res 117, 59-89.

-Ludwig, K., Sarkim, V., Bitzan, M., Karmali, M.A., Bobrowski, C., Ruder, H., Laufs, R., Sobottka, I., Petric, M., Karch, H., et al. (2002). Shiga toxin-producing Escherichia coli infection and antibodies against Stx2 and Stx1 in household contacts of children with enteropathic hemolytic-uremic syndrome. J Clin Microbiol 40, 1773-1782.

-Mangeney, M., Lingwood, C.A., Taga, S., Caillou, B., Tursz, T., and Wiels, J. (1993). Apoptosis induced in Burkitt's lymphoma cells via Gb3/CD77, a glycolipid antigen. Cancer Res 53, 5314-5319.

-Mangeney, M., Richard, Y., Coulaud, D., Tursz, T., and Wiels, J. (1991). CD77: an antigen of germinal center B cells entering apoptosis. Eur J Immunol 21, 1131-1140.

-Milpied, P., Cervera-Marzal, I., Mollichella, M.L., Tesson, B., Brisou, G., Traverse-Glehen, A., Salles, G., Spinelli, L., and Nadel, B. (2018). Human germinal center transcriptional programs are de-synchronized in B cell lymphoma. Nat Immunol 19, 1013-1024.

-Moyer, J.H., Lee-Tischler, M.J., Kwon, H.Y., Schrick, J.J., Avner, E.D., Sweeney, W.E., Godfrey, V.L., Cacheiro, N.L., Wilkinson, J.E., and Woychik, R.P. (1994). Candidate gene associated with a mutation causing recessive polycystic kidney disease in mice. Science 264, 1329-1333.

-Murcia, N.S., Richards, W.G., Yoder, B.K., Mucenski, M.L., Dunlap, J.R., and Woychik, R.P. (2000). The Oak Ridge Polycystic Kidney (orpk) disease gene is required for left-right axis determination. Development 127, 2347-2355.

-Nakayama, Y., Stabach, P., Maher, S.E., Mahajan, M.C., Masiar, P., Liao, C., Zhang, X., Ye, Z.J., Tuck, D., Bothwell, A.L., et al. (2006). A limited number of genes are involved in the differentiation of germinal center B cells. J Cell Biochem 99, 1308-1325.

-Narimatsu, Y., Joshi, H.J., Zhang, Y., Gomes, C., Chen, Y.H., Lorenzetti, F., Furukawa, S., Schjoldager, K., Hansen, L., Clausen, H., et al. (2018). A validated gRNA library for CRISPR/Cas9 targeting of the human glycosyltransferase genome. Glycobiology.

-Nigg, E.A., and Holland, A.J. (2018). Once and only once: mechanisms of centriole duplication and their deregulation in disease. Nat Rev Mol Cell Biol 19, 297-312.

-Nourse, J.P., Jones, K., and Gandhi, M.K. (2011). Epstein-Barr Virus-related post-transplant lymphoproliferative disorders: pathogenetic insights for targeted therapy. Am J Transplant 11, 888-895.

-Nudelman, E., Kannagi, R., Hakomori, S., Parsons, M., Lipinski, M., Wiels, J., Fellous, M., and Tursz, T. (1983). A glycolipid antigen associated with Burkitt lymphoma defined by a monoclonal antibody. Science 220, 509-511.

-Ohta, S., Nishio, K., Kubota, N., Ohmori, T., Funayama, Y., Ohira, T., Nakajima, H., Adachi, M., and Saijo, N. (1994). Characterization of a taxol-resistant human small-cell lung cancer cell line. Jpn J Cancer Res 85, 290-297.

-Ott, G. (2017). Aggressive B-cell lymphomas in the update of the 4th edition of the World Health Organization classification of haematopoietic and lymphatic tissues: refinements of the classification, new entities and genetic findings. Br J Haematol 178, 871-887.

-Ozkaynak, M.F., Gilman, A.L., London, W.B., Naranjo, A., Diccianni, M.B., Tenney, S.C., Smith, M., Messer, K.S., Seeger, R., Reynolds, C.P., et al. (2018). A Comprehensive Safety Trial of Chimeric Antibody 14.18 With GM-CSF, IL-2, and Isotretinoin in High-Risk Neuroblastoma Patients Following Myeloablative Therapy: Children's Oncology Group Study ANBL0931. Front Immunol 9, 1355.

-Pazour, G.J., Dickert, B.L., Vucica, Y., Seeley, E.S., Rosenbaum, J.L., Witman, G.B., and Cole, D.G. (2000). Chlamydomonas IFT88 and its mouse homologue, polycystic kidney disease gene tg737, are required for assembly of cilia and flagella. J Cell Biol 151, 709-718.

-Peris, L., Thery, M., Faure, J., Saoudi, Y., Lafanechere, L., Chilton, J.K., Gordon-Weeks, P., Galjart, N., Bornens, M., Wordeman, L., et al. (2006). Tubulin tyrosination is a major factor affecting the recruitment of CAP-Gly proteins at microtubule plus ends. J Cell Biol 174, 839-849.

-Pihan, G.A., Purohit, A., Wallace, J., Knecht, H., Woda, B., Quesenberry, P., and Doxsey, S.J. (1998). Centrosome defects and genetic instability in malignant tumors. Cancer Res 58, 3974-3985.

-Pihan, G.A., Purohit, A., Wallace, J., Malhotra, R., Liotta, L., and Doxsey, S.J. (2001). Centrosome defects can account for cellular and genetic changes that characterize prostate cancer progression. Cancer Res 61, 2212-2219.

-Pujals, A., Favre, L., Pioche-Durieu, C., Robert, A., Meurice, G., Le Gentil, M., Chelouah, S., Martin-Garcia, N., Le Cam, E., Guettier, C., et al. (2015). Constitutive autophagy contributes to resistance to TP53-mediated apoptosis in Epstein-Barr virus-positive latency III B-cell lymphoproliferations. Autophagy, 0.

-Pujals, A., Renouf, B., Robert, A., Chelouah, S., Hollville, E., and Wiels, J. (2011). Treatment with a BH3 mimetic overcomes the resistance of latency III EBV (+) cells to p53-mediated apoptosis. Cell Death Dis 2, e184.

-Renouf, B., Hollville, E., Pujals, A., Tetaud, C., Garibal, J., and Wiels, J. (2009). Activation of p53 by MDM2 antagonists has differential apoptotic effects on Epstein-Barr virus (EBV)-positive and EBV-negative Burkitt's lymphoma cells. Leukemia 23, 1557-1563.

-Ribrag, V., Koscielny, S., Bosq, J., Leguay, T., Casasnovas, O., Fornecker, L.M., Recher, C., Ghesquieres, H., Morschhauser, F., Girault, S., et al. (2016). Rituximab and dose-dense

chemotherapy for adults with Burkitt's lymphoma: a randomised, controlled, open-label, phase 3 trial. Lancet 387, 2402-2411.

-Richards, W.G., Yoder, B.K., Isfort, R.J., Detilleux, P.G., Foster, C., Neilsen, N., Woychik, R.P., and Wilkinson, J.E. (1996). Oval cell proliferation associated with the murine insertional mutation TgN737Rpw. Am J Pathol 149, 1919-1930.

-Richards, W.G., Yoder, B.K., Isfort, R.J., Detilleux, P.G., Foster, C., Neilsen, N., Woychik, R.P., and Wilkinson, J.E. (1997). Isolation and characterization of liver epithelial cell lines from wild-type and mutant TgN737Rpw mice. Am J Pathol 150, 1189-1197.

-Rowe, M., Rowe, D.T., Gregory, C.D., Young, L.S., Farrell, P.J., Rupani, H., and Rickinson, A.B. (1987). Differences in B cell growth phenotype reflect novel patterns of Epstein-Barr virus latent gene expression in Burkitt's lymphoma cells. EMBO J 6, 2743-2751.

-Sangrajrang, S., Denoulet, P., Laing, N.M., Tatoud, R., Millot, G., Calvo, F., Tew, K.D., and Fellous, A. (1998). Association of estramustine resistance in human prostatic carcinoma cells with modified patterns of tubulin expression. Biochem Pharmacol 55, 325-331.

-Scorrano, L., Ashiya, M., Buttle, K., Weiler, S., Oakes, S.A., Mannella, C.A., and Korsmeyer, S.J. (2002). A distinct pathway remodels mitochondrial cristae and mobilizes cytochrome c during apoptosis. Dev Cell 2, 55-67.

-Shannon-Lowe, C., Rickinson, A.B., and Bell, A.I. (2017). Epstein-Barr virus-associated lymphomas. Philos Trans R Soc Lond B Biol Sci 372.

-Si-Tayeb, K., Lemaigre, F.P., and Duncan, S.A. (2010). Organogenesis and development of the liver. Dev Cell 18, 175-189.

-Sigal, S.H., Gupta, S., Gebhard, D.F., Jr., Holst, P., Neufeld, D., and Reid, L.M. (1995). Evidence for a terminal differentiation process in the rat liver. Differentiation 59, 35-42.

-Sigal, S.H., Rajvanshi, P., Gorla, G.R., Sokhi, R.P., Saxena, R., Gebhard, D.R., Jr., Reid, L.M., and Gupta, S. (1999). Partial hepatectomy-induced polyploidy attenuates hepatocyte replication and activates cell aging events. Am J Physiol 276, G1260-1272.

-Soderquist, R., and Eastman, A. (2016). BCL2 Inhibitors as Anticancer Drugs: A Plethora of Misleading BH3 Mimetics. Mol Cancer Ther 15, 2011-2017.

-Soucek, K., Kamaid, A., Phung, A.D., Kubala, L., Bulinski, J.C., Harper, R.W., and Eiserich, J.P. (2006). Normal and prostate cancer cells display distinct molecular profiles of alpha-tubulin posttranslational modifications. Prostate 66, 954-965.

-Storchova, Z., and Pellman, D. (2004). From polyploidy to aneuploidy, genome instability and cancer. Nat Rev Mol Cell Biol 5, 45-54.

-Taga, S., Mangeney, M., Tursz, T., and Wiels, J. (1995a). Differential regulation of glycosphingolipid biosynthesis in phenotypically distinct Burkitt's lymphoma cell lines. Int J Cancer 61, 261-267.

-Taga, S., Tetaud, C., Mangeney, M., Tursz, T., and Wiels, J. (1995b). Sequential changes in glycolipid expression during human B cell differentiation: enzymatic bases. Biochim Biophys Acta 1254, 56-65.

-Taylor, R.C., Cullen, S.P., and Martin, S.J. (2008). Apoptosis: controlled demolition at the cellular level. Nat Rev Mol Cell Biol 9, 231-241.

-Tetaud, C., Falguieres, T., Carlier, K., Lecluse, Y., Garibal, J., Coulaud, D., Busson, P., Steffensen, R., Clausen, H., Johannes, L., et al. (2003). Two distinct Gb3/CD77 signaling pathways leading to apoptosis are triggered by anti-Gb3/CD77 mAb and verotoxin-1. J Biol Chem 278, 45200-45208.

-Thomas, D.A., Faderl, S., O'Brien, S., Bueso-Ramos, C., Cortes, J., Garcia-Manero, G., Giles, F.J., Verstovsek, S., Wierda, W.G., Pierce, S.A., et al. (2006). Chemoimmunotherapy with

hyper-CVAD plus rituximab for the treatment of adult Burkitt and Burkitt-type lymphoma or acute lymphoblastic leukemia. Cancer 106, 1569-1580.

-Thompson, M.P., and Kurzrock, R. (2004). Epstein-Barr virus and cancer. Clin Cancer Res 10, 803-821.

-Vasiliev, J.M., Omelchenko, T., Gelfand, I.M., Feder, H.H., and Bonder, E.M. (2004). Rho overexpression leads to mitosis-associated detachment of cells from epithelial sheets: a link to the mechanism of cancer dissemination. Proc Natl Acad Sci U S A 101, 12526-12530.

-Vegso, G., Hajdu, M., and Sebestyen, A. (2011). Lymphoproliferative disorders after solid organ transplantation-classification, incidence, risk factors, early detection and treatment options. Pathol Oncol Res 17, 443-454.

-Veland, I.R., Awan, A., Pedersen, L.B., Yoder, B.K., and Christensen, S.T. (2009). Primary cilia and signaling pathways in mammalian development, health and disease. Nephron Physiol 111, p39-53.

-Victora, G.D., Schwickert, T.A., Fooksman, D.R., Kamphorst, A.O., Meyer-Hermann, M., Dustin, M.L., and Nussenzweig, M.C. (2010). Germinal center dynamics revealed by multiphoton microscopy with a photoactivatable fluorescent reporter. Cell 143, 592-605.

-Vinogradov, A.E., Anatskaya, O.V., and Kudryavtsev, B.N. (2001). Relationship of hepatocyte ploidy levels with body size and growth rate in mammals. Genome 44, 350-360.

-Vollmers, H.P., and Brandlein, S. (2009). Natural antibodies and cancer. N Biotechnol 25, 294-298.

-Wasylyk, C., Zambrano, A., Zhao, C., Brants, J., Abecassis, J., Schalken, J.A., Rogatsch, H., Schaefer, G., Pycha, A., Klocker, H., et al. (2010). Tubulin tyrosine ligase like 12 links to prostate cancer through tubulin posttranslational modification and chromosome ploidy. Int J Cancer 127, 2542-2553.

-Wegner, M.S., Schomel, N., Gruber, L., Ortel, S.B., Kjellberg, M.A., Mattjus, P., Kurz, J., Trautmann, S., Peng, B., Wegner, M., et al. (2018). UDP-glucose ceramide glucosyltransferase activates AKT, promoted proliferation, and doxorubicin resistance in breast cancer cells. Cell Mol Life Sci.

-Wiels, J., Fellous, M., and Tursz, T. (1981). Monoclonal antibody against a Burkitt lymphoma-associated antigen. Proc Natl Acad Sci U S A 78, 6485-6488.

-Wiels, J., Mangeney, M., Tetaud, C., and Tursz, T. (1991). Sequential shifts in the three major glycosphingolipid series are associated with B cell differentiation. Int Immunol 3, 1289-1300.

-Wiels, J., Tursz T. (1989). Leucocyte Typing IV: White Cell Differentiation: BLA, aglycolipd marker of Burkitt's lymphoma and a subset of germinal-centre B-cells. Paper presented at: International Workshop and Conference on Human Leucocyte Differentiation Antigens (Vienna, Austria: Oxford University Press).

-Willis, S.N., Chen, L., Dewson, G., Wei, A., Naik, E., Fletcher, J.I., Adams, J.M., and Huang, D.C. (2005). Proapoptotic Bak is sequestered by Mcl-1 and Bcl-xL, but not Bcl-2, until displaced by BH3-only proteins. Genes Dev 19, 1294-1305.

-Wuilleme-Toumi, S., Robillard, N., Gomez, P., Moreau, P., Le Gouill, S., Avet-Loiseau, H., Harousseau, J.L., Amiot, M., and Bataille, R. (2005). Mcl-1 is overexpressed in multiple myeloma and associated with relapse and shorter survival. Leukemia 19, 1248-1252.

-Yoder, B.K., and Blumberg, D.D. (1994). The promoter of a gene encoding a novel Dictyostelium spore coat protein. Dev Biol 163, 38-48.

-You, N., Tan, Y., Zhou, L., Huang, X., Wang, W., Wang, L., Wu, K., Mi, N., Li, J., and Zheng, L. (2017). Tg737 acts as a key driver of invasion and migration in liver cancer stem cells and

correlates with poor prognosis in patients with hepatocellular carcinoma. Exp Cell Res 358, 217-226.

-Young, L.S., and Rickinson, A.B. (2004). Epstein-Barr virus: 40 years on. Nat Rev Cancer 4, 757-768.

-Zitouni, S., Nabais, C., Jana, S.C., Guerrero, A., and Bettencourt-Dias, M. (2014). Polo-like kinases: structural variations lead to multiple functions. Nat Rev Mol Cell Biol 15, 433-452.

ANNEXES

CURRICULUM VITAE

ROBERT Aude
27 mars 1979
Ingénieure de Recherche 1ère classe

Coordonnées Professionnelles :

UMR8126, Institut Gustave Roussy
114 rue Edouard Vaillant
94805 Villejuif Cedex
☏ 00 331 42 11 46 41
✉ aude.robert@gustaveroussy.fr
ORCID ID: https://orcid.org/0000-0003-3095-4190
ResearcherID : F-9584-2015

Formations et Diplôme Universitaires

2009 ***Formation spéciale à l'expérimentation animale*** *-Niveau 1-*

2006 **Doctorat spécialité Interfaces de la chimie, de la physique et de l'informatique avec la Biologie**. Mention Très honorable, *Université P. et M. Curie, Paris VI.*

2002 **DEA de Biologie Cellulaire et Moléculaire : approches pluridisciplinaires de la biologie.** Mention bien, *Université P. et M. Curie, Paris VI.*

2001 **Maîtrise de Biologie Cellulaire et Physiologie mention Génétique Moléculaire et Cellulaire.** Mention bien, *Université P. et M. Curie, Paris VI.*

Parcours Scientifique

Depuis décembre 2007,
Ingénieure de Recherche, dans l'équipe du ***Dr Joëlle Wiels****. UMR8126 CNRS/Université Paris Sud 11, Signalisation, noyaux et innovations en oncologie, Institut Gustave Roussy, Villejuif, France.*
Sujet : Oncogenèse et résistance à l'apoptose dans les lymphomes B

2007
Post-Doctorante, sous la direction de ***Pr Jan De Mey,*** *à l'ESBS, Institut Gilbert Laustriat, UMR - 7175 CNRS/Université Louis Pasteur, Illkirch, France.*
Sujet : Caractérisation du rôle de la protéine TTLL12, une nouvelle tubuline tyrosine like, dans le cycle cellulaire.

2006
Post-Doctorante (2 mois), sous la direction du ***Dr Chantal Desdouets****. INSERM U567, laboratoire Régénération, Ploïdisation, et biothérapie du foie, Institut Cochin, Paris, France*
Sujet : Caractérisation de la souris transgénique centrine-1-GFP.

2002-2006
Doctorante, sous la direction du ***Dr Chantal Desdouets.*** *INSERM U567, laboratoire Régénération, Ploïdisation, et biothérapie du foie, Institut Cochin, Paris, France.*
Sujet : Cycle cellulaire et Centrosome : Rôle de la protéine du transport intraflagellaire, Polaris, dans la transition G_1/S et Rôle des centrosomes dans le maintien de la tétraploïdie hépatocytaire.

Activités liées à l'administration et à la recherche

Membre du comité des utilisateurs de l'animalerie
Membre du comité des utilisateurs du laboratoire P3. Formatrice.
Membre du comité de pilotage du logiciel de gestion du centre des Ressources Biologiques de l'Institut Gustave Roussy.
Membre du comité scientifique du « Congrès jeunes chercheurs en Biologie-Prix René Descartes » 2011-2013
Membre du Cervo (Comité Ethique en Recherche clinique et épidémiologique Vétérinaire d'Oniris) depuis 2016

Contrats et Subventions

2012-2015 Allocation doctorale de la ligue contre le cancer de Justine Debernardi. Apoptose induite par la vérotoxine-1 dans les cellules de lymphome de Burkitt : *Analyse des mécanismes et implication du stress du réticulum endoplasmique dans la résistance des cellules EBV+.*

2014-2016 Subvention Fondation de France…Recherche fondamentale et translationnelle sur le cancer (Tumeurs solides et Leucémies) « étude de la résistance aux traitements » 50K€ Porteuse de projet Joëlle Wiels… *Caractérisation et évaluation du potentiel thérapeutique d'un anticorps monoclonal ciblant le glycolipide Gb3/CD77 dans le traitement du lymphome de Burkitt et de certaines tumeurs chimiorésistantes*.

2016-2017 Idex Paris Saclay…68K€ porteuse de projet Joëlle Wiels. *Evaluation du potentiel thérapeutique d'un anti-Gb3/CD77 dans le traitement du lymphome de Burkitt et de tumeurs chimiorésistantes.*

Collaborations internationales

Université de Pennsylvanie
Andrei Thomas-Tikhonenko/ Colleen Harrington

Copenhagen Center for Glycomics, Copenhague
Henri Clausen

Collaborations nationales

ICSN Institut de chimie des substances naturelles, Gif sur Yvette
Fanny Roussi

CERMN Centre d'études et de recherche sur le médicament de Normandie, Caen
Aurélie Malzert-Fréon

PFEP Plateforme d'évaluation Préclinique, Gustave Roussy, Villejuif
Karine Ser-Leroux

Département de cancérologie de l'enfant et de l'adolescent, Gustave Roussy, Villejuif
Birgit GEOERGER

CHU Henri Mondor
Anaïs Pujals

Encadrements

Doctorant·e·s :
Loetitia Favre (2012-2016) 20%
Justine Debernardi (2012 -2015) 50%
Florian Daressy (2017-2020) 30%

Master 2 (6 mois):
Justine Debernardi 50% (2012)
Benjamin Morin 50% (2016)
Crystal Gov 20% (2016)
Tiphaine Gaudin 50% (2018)

Master 1 :
Delphine Pion 50% (2010) 2 mois
Laura Bousset 100% (2015) 2 mois
Anaïs Marchi 100% (2017) 2 mois
Mélanie Levasseur 100% (2003) 2 mois

Autres :
Sophie Cheverry 4ème année école d'ingénieur (SupBiotech) 100% (2016) 5 mois
Ophélie Desachy L3 100% (2017) 2 mois
Florian Sirmain-Bousquet 4ème année école d'ingénieur (ESBS, école supérieure de biotechnologie de Strasbourg) 100% (2007) 2 mois
Pauline Chang Yane L3 (2004) 1 mois

LISTE DES TRAVAUX, PUBLICATIONS

Articles dans des revues internationales avec comité de lecture

- Wu X., Kabalane H., Kahli M, Petryk N, Laperrousaz B., Jaszczyszyn J., Drillon G., Nicolini FE., Perot G., **Robert A.,** Fund C., Chibon F., Xia R., Wiels J., Argoul F., Maguer-Satta V., Arneodo A., Audit B., Hyrien O. *Developmental and cancer-associated plasticity of DNA replication program preferentially targets late-replicating gene deserts, Nucleic Acids Research 2018.*

- Abou Samra A., **Robert A.,** Gov C., Favre L., Eloy,L Jacquet,E Bignon J, Wiels,J, Desrat,S., Roussi F. *Dual Inhibitors of the Pro-Survival Proteins Bcl-2 and Mcl-1 Derived from Natural Compound Meiogynin A, European Journal of Medicinal Chemistry 2018 Feb.*

- Debernardi J, Hollville E, Wiels *J*, **Robert A**. *Differential role of FL-Bid and t-Bid during Verotoxin-1-induced apoptosis in Burkitt's lymphoma cells*, *oncogene 2018*

- Chelouah S, Cochet E, Couve-Privat S, Balkaran S, **Robert A,** May E., Ogryzko V. and Wiels *J. New interactors of the truncated EBNA-LP protein identified by mass spectrometry in P3HR1 Burkitt's lymphoma cells, Cancers 2018 Jan*

- Pujals A, Fabre L., Durieu C., **Robert A,** Meurice G, Legentil M., Chelouah S, Lecam E., Vassilev L., Lipinski M, Wiels J. *Constitutive Autophagy in Epstein-Barr Virus-positive Latency III Cells Protects them from Nutlin-3-induced Apoptosis. Autophagy 2015*

- Brants J., Semenchenko K., Wasylyk C., **Robert A.,** Carles A., Zambrano A., Pradeau-Aubreton K., Birck C., Schalken J., Poch O., de Mey J., and Wasylyk B. *Tubulin Tyrosine Ligase Like 12, a novel TTLL family member with SET- and TTL-like domains and roles in histone and tubulin modifications and mitosis. Plos One décembre 2012*

- Pujals A, Renouf B, **Robert A,** Chelouah S, Hollville E, Wiels J. *Treatment with a BH3 mimetic overcomes the resistance of latency III EBV (+) cells to p53-mediated apoptosis. Cell Death Dis. 2011 Jul*

- **Robert A.,** Margall Ducos G., Guidotti J.E., Bregerie O., Celati C., Brechot C, Desdouets C. *The Intraflagellar component Polaris is a centrosomal protein regulating G_1/S transition in nonciliated cells. J cell science. 2007, Feb 15*

- Guidotti JE, Bregerie O., **Robert A.,** Debey P., Brechot C., Desdouets C. *Liver cell polyploidization : a pivotal role for binuclear hepatocytes. J. Biol. Chem. 2003*

Articles dans des conférences internationales avec comité de lecture

- Margall-Ducos, G., Morizur, S., D, Couton C., **Robert, A.,** & Desdouets, C. (2006, Octobre). *Liver cell binucleation: A physiological process triggered by an unorganized microtubules network. Hepatology Vol. 44, No. 4, pp. 483A-483A.*

Posters, communications orales dans des conférences nat & int.

Posters

- Colloque "Recherche et maladies rares à Paris-Sud", Kremlin-Bicêtre, France, 2018.
The Bcl-2 inhibitor, ABT-737 enhances the activity of therapeutic agents against B lymphoproliferations associated with EBV both in vitro and in vivo. Pujals A.*, **Robert A.***, Favre L, Desille T., Debernardi J., Wiels J.

- *European Cell Death organisation, Saint Pétersbourg, Russia, 2018*
New inhibitors of the BCL-2 family members derived from natural drimane sesquiterpenes Daressy F., Favre L., Bousset L., Litaudon M., Apel C., Bignon J., Pamlard O., Malard F., Roussi F., Wiels J. and **Robert A.**

- *European Cell Death organisation, Genève, Suisse, 2015*
Differential role of FL-Bid and t-Bid during Verotoxin-1-induced apoptosis in Burkitt's lymphoma cells. - Debernardi J, Hollville E, Wiels *J* and **Robert A**. Prix Harlan

- *Congrès Jeunes chercheurs en Biologie-Prix René Descartes, Paris, France, 2013.*
Apoptotic Signaling Induced by Verotoxin-1 via Gb3/CD77 Receptor in Burkitt's Lymphoma Cells. Debernardi, J., **Robert, A.***, Hollville, E., Wiels, J.* *Co 1ères autrices

- *Cell Death in cancer, Amsterdam, Pays Bas, 2012*
Treatment with a BH3 mimetic overcomes the resistance of latency III EBV (+) cells to p53-mediated apoptosis. Pujals A, Renouf B, **Robert A**, Chelouah S, Hollville E, Wiels J.

- *EMBO workshop: Molecular Mechanisms of Cell cycle, Spetses, Grèce, 2007*

Incomplete cytokinesis in the liver: a new developmental program colled by insulin. Celton-Morizur S., Margall-Ducos G., Couton D., Brégerie O., **Robert A.** and Desdouets C.

- *The Cell Cycle-Cold Spring Harbor, New York, Etats-Unis, 2006.*

Physiological incompleted cytokinesis: a lesson from liver. Margall-Ducos, G., Morizur, S., D, Brégerie, O., **Robert, A**., & Desdouets, C

T*he Intraflagellar component Polaris is a centrosomal protein regulating G_1/S transition in nonciliated cells.* **Robert A**., Margall Ducos G., Guidotti J.E., Bregerie O., Desdouets C.

- *ELSO - European Life Scientist Organization, Dresden, Allemagne, 2005.*

Polaris, a new centrosomal protein involved in cell progression control. **Robert A**., Margall Ducos G., Guidotti J.E., Bregerie O., Desdouets C.

- *Congrès annuel de l'ARC pour les jeunes chercheurs, Paris, France, 2005.*
Trafic des Centrosomes : Polaris et ploïdisation hépatocytaire. **Robert A**., Margall Ducos G., Guidotti J.E., Bregerie O., Desdouets C.

- *Congrès Jeunes chercheurs de Paris 5, Paris, France, 2005.*

Polaris, a new centrosomal protein involved in cell progression control. **Robert A**., Margall Ducos G., Guidotti J.E., Bregerie O., Desdouets C.

Communications orales

- *Vth International Meeting "Early events in Human Pathologies"* 2012. Listvyanka, Baikal, Russia. Apoptotic signaling induced by Verotoxin-1 in Burkitt's lymphoma cells.

- *ISREC, Lausanne, Suisse 2006.* The intraflagellar transport component, Polaris is a centrosomal protein regulating G_1/S transition.

- *ETH, institut de Biochimie, Zurich, Suisse 2006. The* intraflagellar transport component, Polaris is a centrosomal protein regulating G_1/S transition.

- *UMR 7098, P. and M. Curie University, Paris VI, France 2005.* Polaris, une nouvelle protéine centrosomienne impliquée dans le contrôle du cycle cellulaire.

Rapports de recherche, papiers soumis etc.

- Pujals A.*, **Robert A.***, Favre L, Desille T., Debernardi J., Wiels J. *The Bcl-2 inhibitor, ABT-737 enhances the activity of therapeutic agents against B lymphoproliferations associated with EBV both in vitro and in vivo, en préparation.* *Co 1ères autrices

ARTICLES

- Guidotti JE, Bregerie O., **Robert A.,** Debey P., Brechot C., Desdouets C. *Liver cell polyploidization : a pivotal role for binuclear hepatocytes. J. Biol. Chem. 2003*

THE JOURNAL OF BIOLOGICAL CHEMISTRY
Vol. 278, No. 21, Issue of May 23, pp. 19095–19101, 2003
Printed in U.S.A.

Liver Cell Polyploidization: A Pivotal Role for Binuclear Hepatocytes*[S]

Received for publication, January 29, 2003, and in revised form, March 6, 2003
Published, JBC Papers in Press, March 7, 2003, DOI 10.1074/jbc.M300982200

Jacques-Emmanuel Guidotti‡§, Olivier Brégerie‡§, Aude Robert‡, Pascale Debey¶, Christian Brechot‡, and Chantal Desdouets‡‖

From ‡INSERM U370, CHU Necker, 156 Rue de Vaugirard, 75015 Paris, France and ¶Unité Mixte de Recherche 8646 CNRS-MNHN, U565 INSERM, Muséum National d'Histoire Naturelle, 53 Rue Buffon, 75005 Paris, France

Polyploidy is a general physiological process indicative of terminal differentiation. During liver growth, this process generates the appearance of tetraploid (4n) and octoploid (8n) hepatocytes with one or two nuclei. The onset of polyploidy in the liver has been recognized for quite some time; however, the cellular mechanisms that govern it remain unknown. In this report, we observed the sequential appearance during liver growth of binuclear diploid (2 × 2n) and mononuclear 4n hepatocytes from a diploid hepatocyte population. To identify the cell cycle modifications involved in hepatocyte polyploidization, mitosis was then monitored in primary cultures of rat hepatocytes. Twenty percent of mononuclear 2n hepatocytes failed to undergo cytokinesis with no observable contractile movement of the ring. This process led to the formation of binuclear 2 × 2n hepatocytes. This tetraploid condition following cleavage failure did not activate the p53-dependent checkpoint in G_1. In fact, binuclear hepatocytes were able to proceed through S phase, and the formation of a bipolar spindle during mitosis constituted the key step leading to the genesis of two mononuclear 4n hepatocytes. Finally, we studied the duplication and clustering of centrosomes in the binuclear hepatocyte. These cells exhibited two centrosomes in G_1 that were duplicated during S phase and then clustered by pairs at opposite poles of the cell during metaphase. This event led only to mononuclear 4n progeny and maintained the tetraploidy status of hepatocytes.

Polyploidy is a general physiological process that prevails in many cellular systems including plants, insects, and mammals (1). The onset of cellular polyploidization is associated with late fetal development and postnatal maturation. Advanced polyploidy in mammalian cells is indicative of terminal differentiation and senescence (2). Hepatocytes come under the former category. During growth, the liver parenchyma undergoes dramatic changes characterized by gradual polyploidization during which hepatocytes of several ploidy classes emerge as a result of modified cell division cycles. This process generates the successive appearance of tetraploid and octoploid cell classes with one or two nuclei. Thus, in the liver of a newborn rat, hepatocytes are exclusively diploid (2n),[1] and polyploidization starts after weaning. In adult rats, about 10% of hepatocytes are diploid, 70% are tetraploid, and 20% octoploid. If we consider the polyploid fraction, 20–30% of hepatocytes are binuclear (either 2 × 2n or 2 × 4n) (3, 4). The degree of polyploidization varies among mammals (5) and particularly in humans, where the number of polyploid cells averages 20–30% in the adult liver (6, 7). Interestingly, in different liver pathologies, hepatocarcinoma for example, hepatocellular growth shifts to a nonpolyploidizing growth pattern, and expansion of the diploid hepatocyte population has been found to take place (4, 7).

Polyploidization is a general strategy of cell growth that enables an increase in metabolic output, cell mass, and cell size, and may constitute an alternative to cell division (1). In addition, the status of ploidy is likely to affect the expression profile of specific genes, as has been described in a yeast system (8). The biological significance of hepatic polyploidy remains unclear. It has been suggested that the polyploid genome may provide protection against the dominant expression of mutated oncogenes, a safety measure that might be helpful for an organ heavily engaged in drug detoxification (9).

The onset of polyploidy in the liver has been recognized for quite some time. However, the cellular mechanisms that govern the passage from mononuclear 2n to binuclear 2 × 2n and/or mononuclear 4n hepatocytes remain unknown. One possible explanation is that binuclear 2 × 2n hepatocytes may play a pivotal role in the genesis of mononuclear 4n hepatocytes. Hepatocyte binucleation results from either a defect in the cytokinesis of mononuclear 2n cells (3, 7) or the fusion of two mononuclear 2n cells (10). Thereafter, binuclear 2 × 2n hepatocytes may divide, leading to the genesis of two daughter mononuclear 4n hepatocytes. A mononuclear 4n hepatocyte then embarks upon a new round of binucleation/polyploidization with the formation of 2 × 4n and 8n cells. An alternative explanation for liver polyploidization is that a mononuclear 2n hepatocyte gives rise directly to mononuclear 4n cells through endoreplication. This process has already been described in plants, *Drosophila*, and mammals, notably in megakaryocyte and trophoblast cells, and results from uncoupling of the normal link between S phase and mitosis (1). In murine models exhibiting an absence or deregulated expression of genes such as *p21*, S-phase kinase associated protein 2 (*Skp2*), and excision repair cross-complementing protein 1 (*ERCC1*), endoreplication induces premature liver polyploidization. In these mice, the liver has been characterized by an increase in the number of mononuclear polyploid fractions (11–13).

The aim of this work was to define the cellular mechanisms

* This study was supported by grants from INSERM and the Ligue Nationale Contre le Cancer. The costs of publication of this article were defrayed in part by the payment of page charges. This article must therefore be hereby marked "*advertisement*" in accordance with 18 U.S.C. Section 1734 solely to indicate this fact.

[S] The on-line version of this article (available at http://www.jbc.org) contains three videos depicting cell mitosis (Videos 1–3).

§ These authors contributed equally to this work.
‖ To whom correspondence should be addressed. Tel.: 33-1-40615545; Fax: 33-1-40-615581; E-mail: desdouet@necker.fr.

[1] The abbreviations used are: 2n, diploid; 4n, tetraploid; 8n, octaploid; 2 × 2n (or 2 × 4n), binuclear; BrdUrd, 5-bromo-2′-deoxyuridine.

involved in liver polyploidization by studying the hepatocyte cell cycle. We demonstrated that the binuclear hepatocyte is central to the polyploidization process. Having characterized the *in vivo* kinetic of liver polyploidization, we showed that the abortion of cytokinesis induced the formation of binuclear hepatocytes. This tetraploid condition following cleavage failure did not activate the p53-dependent checkpoint in G_1; binuclear cells could divide and generate two mononuclear 4n daughter cells. This event was driven by the clustering of two centrosomes at each pole of the cell, leading to the formation of a bipolar spindle.

EXPERIMENTAL PROCEDURES

Animals—Male Wistar rats (Iffacredo, Lyon, France) were treated in accordance with European Union regulations on animal care. The rats were housed under standard light/dark conditions and received pelleted food and water *ad libitum*. All rats were weaned 17 days after birth (weaning and the commencement of feeding influence hepatic polyploidy) (5).

In Situ Detection of Ploidy—Liver tissues were fixed in 10% phosphate-buffered formalin and then embedded in paraffin. Three-micrometer-thick tissue sections were deparaffinized in xylene and, after rehydration, boiled for 3× 5 min in 10 mmol/liter citrate buffer, pH 6.2, in a microwave oven. Immunohistochemistry was performed as described below. Plasma membranes were labeled with anti-β-catenin antibody (diluted 1:50, BD Transduction Laboratories). Hoechst 33342 (0.2 μg/ml) was used to stain and quantify DNA in each nucleus. Tissue sections were analyzed under a Zeiss (Axiovert 35) (Carl Zeiss, Gottingen, Germany) inverted microscope equipped for epi-illumination. Zeiss Plan Neofluar 40× objectives (numerical aperture, 0.75) were chosen that enabled the collection of light from the entire thickness of the nucleus, these conditions being essential for adequate DNA content determinations. Images were captured using a cooled CCD camera (Photometrics, Tucson, Arizona; KAF 1400-G2, class 2) on 4056 gray levels. Automatic quantitative image analysis was performed in 12 bits using IPLab Spectrum software. Nuclei were assigned as mono or binucleated hepatocytes by comparing fluorescent and membrane-labeling images. Other liver cell types (defined by their morphological characteristics), overlapping nuclei, or debris were eliminated interactively. Parameters such as integrated fluorescence intensity (IntF) were stored in computer files for analysis using the KaleidaGraph and Imastat software (Imastat as developed by P. Debey) (14). A minimum of 300 hepatocytes were studied and observed on eight to twelve separate fields; these observations concerned specimens from four animals for each point analyzed. This number of hepatocytes was within the range covered by other imaging-based studies.

Live Cell Videomicroscopy and Immunofluorescence Microscopy on Primary Rat Hepatocytes—Primary rat hepatocytes were isolated by liver perfusion with a collagenase blend (Liberase, Roche Applied Science). After isolation, cells were collected in William's medium E enriched with 1 mg/ml bovine serum albumin and left to sediment for 20 min. After three centrifugations (65 × *g* for 1 min), hepatocytes were seeded at 5×10^5 cells/cm^2 on plastic dishes in William's medium E, supplemented with 10% fetal bovine serum, 1 mg/ml bovine serum albumin, and 5 μg/ml bovine insulin in a 37 °C incubator with 5% CO_2 atmosphere. All culture medium used contained penicillin (100 units/ml), streptomycin (100 μg/ml), and fungizone (250 ng/ml). Hepatocyte viability was assessed to be >90% using trypan blue dye exclusion. After cell attachment (4 h later), the medium was removed and replaced by fresh serum-free William's medium E containing 0.5 mg/ml bovine serum albumin, 5 μg/ml bovine insulin, and $7\ 10^{-7}$ M hydrocortisone hemisuccinate. The medium was changed every day thereafter. Twenty-four h after plating, the cells were placed in the mitogenic stimulation medium, *i.e.* the same medium describe above supplemented with epidermal growth factor (EGF) at 50 ng/ml and pyruvate at 20 mM (mitogenic stimulation medium). This medium was used throughout the culture time. Under these conditions, maximal DNA synthesis occurs from 48–60 h, depending on the cell culture (15).

For live cell microscopy, hepatocytes were grown on 35 × 10-mm tissue culture plates and mounted on the microscope after 48 h of culture. During imaging, hepatocytes were maintained in William's medium E on a stage heated at 37 °C under a 5% CO_2 atmosphere. Cells were imaged at 3 min intervals for 24 h with a Leica DMIRBE using a 63× lens (numerical aperture, 0.7), a condenser (working distance, 23 mm; numerical aperture, 0.53), and a Pentamax cooled CCD camera (Popper Scientific) coupled to an electronic shutter. Metamorph 4.6 was used for computer-based image acquisition and analysis of live cell data. The single images shown were prepared using Adobe Photoshop® 5.5.

For immunofluorescence microscopy, hepatocytes were grown on chambered coverslips and fixed with methanol at −20 °C for 10 min. The coverslips were then washed and blocked with the Biotin blocking system (Dako). Incubations with primary mouse antibodies (anti-γ−tubulin (1:200, GTU88, Sigma), anti-β-tubulin (1:200, TUB2.1, Sigma), and anti-p53 (1:100, FL-393, Santa Cruz Biotechnology)) were carried out for 1 h at room temperature. For the detection of primary antibodies, biotinylated swine anti-mouse or anti-rabbit immunoglobulin solutions were used (1:200, Dako) followed by FITC-conjugated streptavidin (1:200, DAKO). Hoechst 33342 (0.2 μg/ml) was included in the final incubation to stain DNA.

Western Blot Analyzes—Hepatocyte protein extracts were prepared in lysis buffer containing 50 mM Tris, pH 7.5, 250 mM NaCl, 2 mM EDTA, 0.5% Nonidet P-40, 50 mM NaF, 0.1 mM Na3VO4, 1 mM dithiothreitol, 1 mM phenylmethylsulfonyl fluoride, and 2 μg/ml leupeptin, pepstatin, and aprotinin. Protein concentration was determined by the Bradford method (Bio-Rad); 30 μg of protein were fractionated on SDS-PAGE and then transferred to Hybond C membrane (Amersham Biosciences). p53, cyclin E, and β-tubulin proteins were detected using specific antisera (FL-393 against p53 and M20 against cyclin E with incubation overnight at 4 °C; both antisera were from Santa Cruz Biotechnology). Horseradish peroxidase-conjugated antibody (Amersham Biosciences) was used as second antibody (dilution 1:2000, incubation for 1 h at room temperature). Immunoreactive bands were visualized with enhanced chemiluminescence (ECL, Amersham Biosciences) according to the manufacturer's instructions.

5-Bromo-2′-deoxyuridine (BRD) Labeling—The percentage of cells undergoing DNA synthesis was estimated by counting the number of BrdUrd-labeled cells using the BrdUrd detection kit II (Roche Applied Science). Cells were incubated with BrdUrd labeling medium for 12 h. The medium was then removed and the cells were fixed in ethanol/acetic acid (70:30) and stained according to manufacturer's instructions. Ten separate fields were counted per plate, and averages were representative of three independent experiments.

RESULTS

Kinetics of Polyploidization during Liver Growth—Although several studies have described changes in ploidy at various stages of liver development, none has established the *in vivo* emergence of tetraploid hepatocytes (binuclear 2 × 2n or mononuclear 4n cells). For this purpose, we used an approach based on quantitative fluorescence imaging (14). The simultaneous nuclear and plasma membrane labeling of liver tissue sections made it possible to determine the number of nuclei per cell (Fig. 1*A*) and thus calculate the binuclear hepatocyte fraction (Fig. 1*C*). The use of a stoichiometric DNA labeling agent, Hoechst 33342, enabled determination of the DNA content in all cells by measuring the integrated fluorescence emitted by each nucleus. A typical histogram of integrated fluorescence values for mononuclear cells is shown in Fig. 1*B*. Because of the clear bimodal distribution around two main values separated by a factor of 2, the distribution of 2n and 4n mononuclear hepatocytes was assessed with accuracy even in a small number of nuclei. Using this technique, we examined the hepatic ploidy status of 12–39-day-old rats. The relative proportions of different hepatocyte ploidy classes during liver development are shown in Fig. 1*C*. We found that hepatocytes were mostly diploid in the livers of young rats (99% at day 12). From day 22 the proportion of diploid cells started to fall significantly, with the successive appearance of binuclear 2 × 2n and mononuclear 4n hepatocytes. Binuclear 2 × 2n cells were first detected at day 22 (4.6% of hepatocytes), and then their proportion rose rapidly between days 25 and 30 to reach 27.5% of the total hepatocyte population (Fig. 1*C*). The relative proportion of the binuclear population decreased gradually and comprised only 2 × 2n DNA content until at least day 39 (data not shown). The mononuclear 4n hepatocyte population was only present at significant levels 25 days after birth and represented 5.2% of the total hepatocyte population. Up to day 25, the fraction of

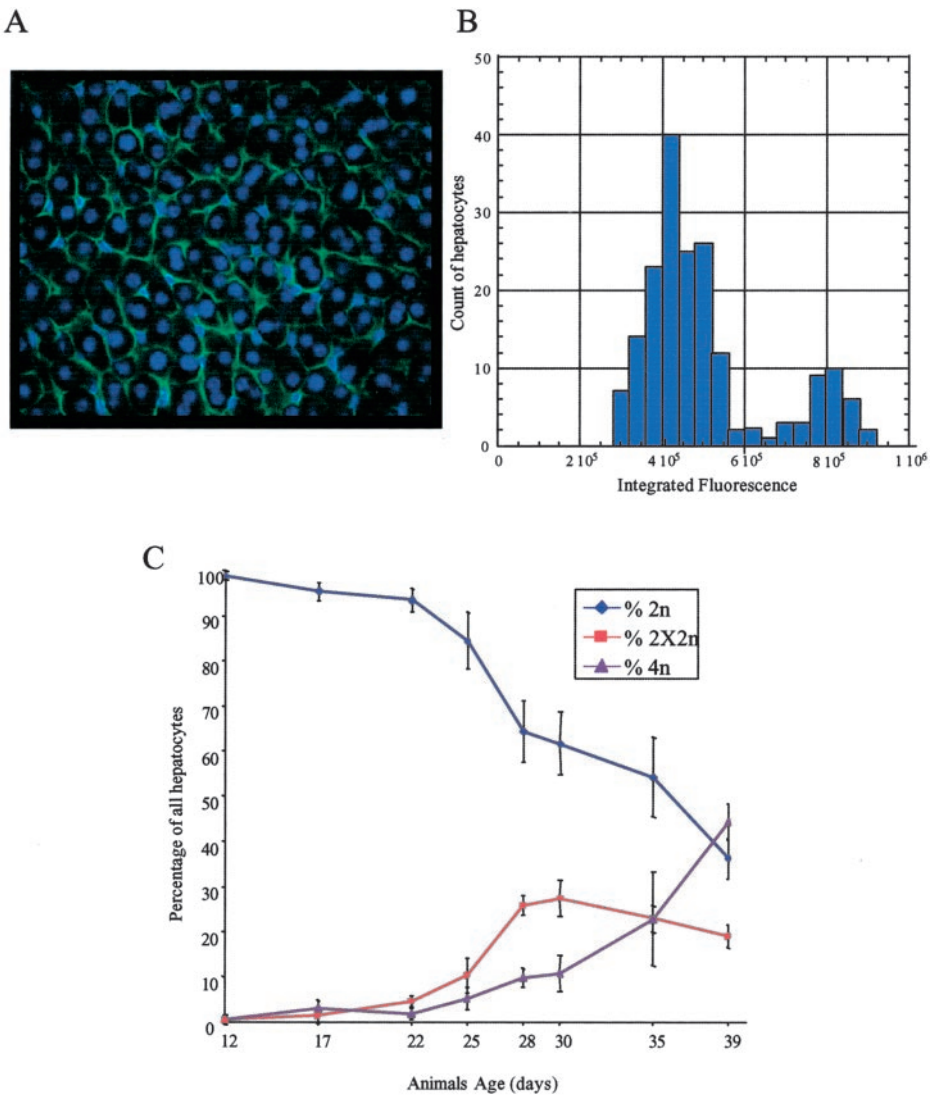

FIG. 1. ***In situ* analysis of hepatocyte polyploidy during liver growth.** *A*, imaging of a liver section after double staining with Hoechst (nuclear labeling, *blue*) and β-catenin (plasma membrane labeling, *green*) enabled a distinction between mononuclear and binuclear hepatocytes. *B*, representative histogram of the DNA content distribution of mononuclear hepatocytes from a 35-day-old rat. DNA content was evaluated by recording the Hoechst-integrated fluorescence in each nucleus. Integrated fluorescence is expressed in arbitrary units. The first peak is representative of hepatocytes with 2n DNA content. The second peak is positioned at twice the value of the first peak and is representative of hepatocytes with 4n DNA content. *C*, polyploidization during liver growth. At each point, four rats were independently analyzed. Percentages of mononuclear 2n (♦), binuclear 2 × 2n (■), and mononuclear 4n (▲) cells were calculated as described under "Experimental Procedures." The average percentage of each population is shown on the curve. S. E. values were in all cases below 10%.

nuclei with a 4n DNA content represented only cycling mononuclear 2n cells in G_2, as determined by the percentage of replicating nuclei in control rats injected with BrdUrd (data not shown and Ref. 16). These cells were not present at significant levels after 25 days. At day 30, a sharp increase was observed in the number of mononuclear 4n hepatocytes (10.9% of the total population), and this hepatocyte population was in the majority at day 39, reaching 44.4% of the total population (Fig. 1*C*). These results clearly demonstrated *in vivo* that binuclear 2 × 2n and mononuclear 4n hepatocytes appear successively during liver growth.

Genesis of Binuclear Hepatocytes and Abortion of Cytokinesis—To define the genesis of binuclear hepatocytes, we monitored the division of hepatocytes isolated from 24-day-old rats corresponding to the moment of appearance of these cells *in vivo*. After 48 h of culture, mononuclear 2n hepatocytes were observed for 24 h to visualize their passage through mitosis; during this period, 60% of mononuclear 2n hepatocytes were in S phase or had already proceeded through this phase (BrdUrd labeling, data not shown). At least 50 mononuclear 2n hepatocytes were inspected during four independent experiments, and no morphological evidence of cell apoptosis was observed at any time during the study. In 80% of the mononuclear 2n hepatocytes analyzed division was normal (example on Fig. 2*A* and on Video 1), the cell initiated prophase, and the chromosome then lined up along the metaphase plate (Fig. 2*A*, *panel 2*). Cells then pinched off in the middle during telophase/cytokinesis (Fig. 2*A*, *panel 3*). Once mitosis was complete, the resulting two daughter mononuclear 2n hepatocytes became individualized (Fig. 2*A*, *panel 4*). In contrast, 20% of the mononuclear 2n cells observed exited from mitosis inappropriately (example on Fig. 2*B* and on Video 2). The initial steps (prophase, metaphase, and anaphase) took place as expected, but during telophase, cytokinesis aborted. The cells established an acto-myosin ring-like structure (Fig. 2*B*, *panel 3*) but no contractile movement could be seen. Ultimately, disappearance of the ring led to the formation of a binuclear hepatocyte (Fig. 2*B*, *panel 4*). The average length of mitosis was similar during the two types of division (61 ± 5 min; from three independent experiments). In particular, the duration of telophase was not reduced by the abortion of cytokinesis. We conclude, therefore, that acytokinesis is the basis of hepatocyte binucleation.

Binuclear Hepatocyte Is a Pivotal Cell for the Genesis of Tetraploid Hepatocytes—We then determined whether binuclear hepatocytes could proceed through a complete subsequent cell cycle. In fact, under certain experimental conditions recent results have demonstrated the existence of a p53-dependent checkpoint control acting in G_1 to recognize tetraploid cells and induce their arrest (17–19). For this purpose, we first analyzed whether binuclear hepatocytes were able to progress through S phase. We performed BrdUrd labeling on hepatocytes isolated from 28 days-old male rats (the maximum level of binuclear

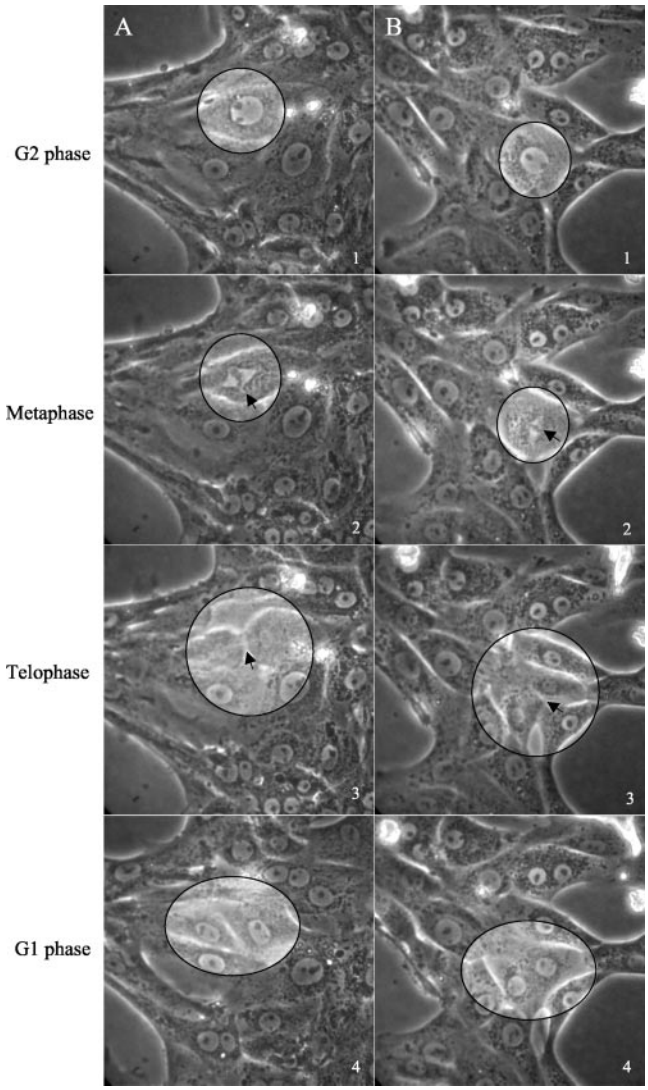

FIG. 2. **Genesis of binuclear 2 × 2n hepatocytes because of the failure of cytokinesis.** Hepatocytes were isolated from 24 day-old male rats and cultured in serum-free medium with epidermal growth factor (5 nM), insulin (100 nM), and dexamethasone (25 nM). Epidermal growth factor was added 24 h after plating. Hepatocytes were mounted on time-lapse videomicroscopy 48 h after plating. The mitosis of mononuclear 2n cells was monitored for 24 h. Images are shown at selected time points. *A*, division of a mononuclear 2n hepatocyte leads to two mononuclear daughter 2n cells (80% of cases). *Arrows* indicate the metaphase plate on *panel 2* and the contractile ring on *panel 3*. *B*, division of a mononuclear 2n hepatocyte leads to a binuclear 2 × 2n cell (20% of cases). *Arrows* indicate the metaphase plate on *panel 2* and the deficient contractile ring on *panel 3*. Complete movies (Video 1 and 2) are available as supplementary information.

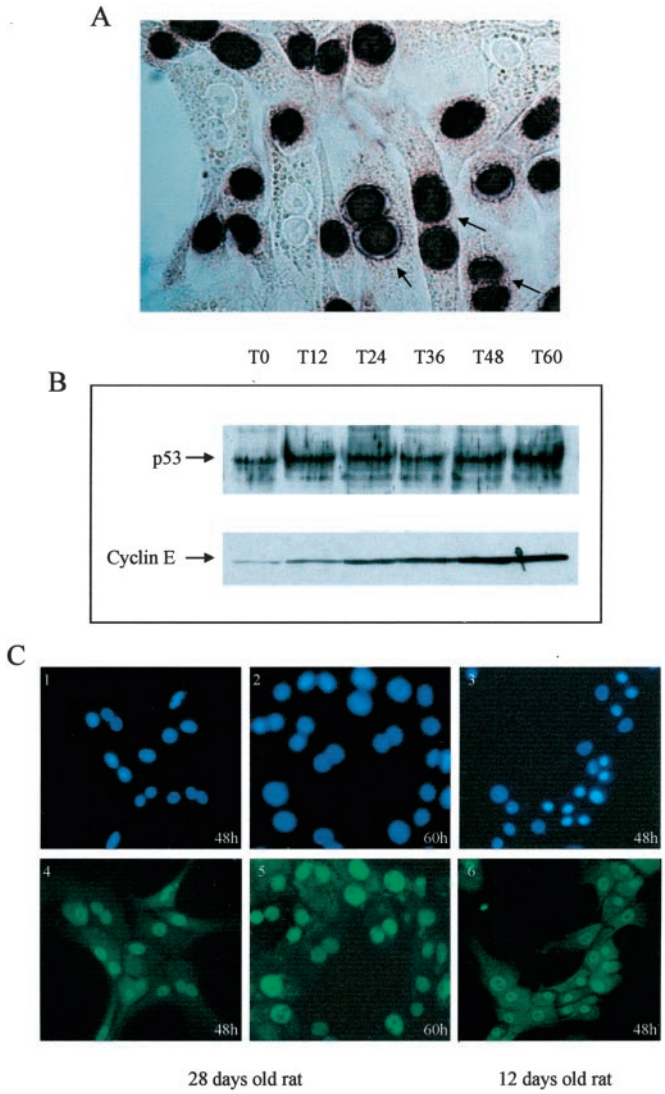

FIG. 3. **Binuclear hepatocytes progress through S phase.** *A*, hepatocytes were isolated from 28-day-old male rats. The cell cycle progression was evaluated by determining BrdUrd incorporation. Hepatocytes were incubated with BrdUrd for 12 h and subsequently fixed and labeled. In this experiment, BrdUrd was incorporated between 48 and 60 h of culture (maximal DNA synthesis). *B*, cell lysates were prepared at different times during a primary culture of hepatocytes isolated from the same rat. The expression of p53 and cyclin E was analyzed by immunoblotting as described under "Experimental Procedures." *C*, p53 protein was detected by immunofluorescence in hepatocytes isolated either from 28-day-old male rats (48 and 60 h of culture; *panels 1*, *2*, *4*, and *5*) or from 12-day-old male rats (48 h of culture; *panels 3* and *6*). Visualization of DNA by Hoechst staining (*panels 1–3*) and p53 staining with the antibody FL393 (*panels 4–6*) is shown. The same expression pattern was observed at different time points during the culture.

cells is found in the liver at this age). Analysis of BrdUrd incorporation revealed that DNA replication occurred in binuclear as well as mononuclear hepatocytes (Fig. 3*A*); maximum labeling (35%) was observed between 48 and 60 h of culture, which corresponds to the peak of S phase for the mononuclear 2n fraction. We next determined whether the absence of the p53-dependent checkpoint could explain the cell cycle progression of binuclear cells. We monitored the level of p53 by Western blot and immunofluorescence on primary hepatocyte cultures (28 day-old male rats) (Fig. 3, *B* and *C*). We did not observe any significant changes to the expression of p53 at different times during culture compared with the increasing expression of cyclin E (Fig. 3*B*). Moreover, p53 was expressed in both mononuclear 2n and binuclear 2 × 2n hepatocytes with a predominant nuclear localization. (Fig. 3*C*, 48 and 60 h of culture, *panels 1*, *2*, *4*, and *5*). Furthermore, we observed the same p53 pattern in hepatocytes isolated from 12 day-old male rats (Fig. 3*C*, 48 h of culture, *panels 3* and *6*). Taken together, these results indicate that p53 was expressed in hepatocytes of different ploidy classes; moreover, its expression did not prevent the cell cycle progression of binuclear hepatocytes.

Thereafter, we monitored the mitosis of binuclear cells using time-lapse videomicroscopy. After 48 h of culture in four different experiments, 20 binuclear cells were analyzed for up to 24 h. We observed that all of the binuclear cells monitored proceeded identically through mitosis. An example is shown in Fig. 4 and on Video 3. We observed that both nuclei of the binuclear hepatocyte entered mitosis simultaneously. The key step occurred during

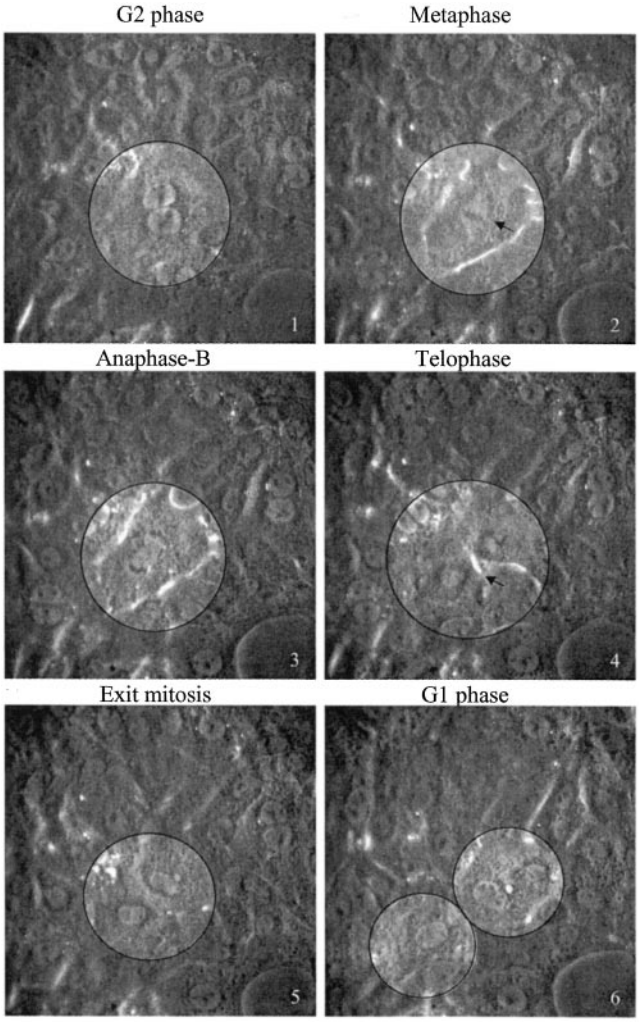

FIG. 4. **Outcome of binuclear 2 × 2n cells.** Primary hepatocytes from 28 day-old rats were mounted under time-lapse videomicroscopy 48 h after plating. The mitosis of binuclear 2 × 2n cells was monitored over a 24-h period. Images are shown at selected time points. The division of a binuclear 2n hepatocyte generated two mononuclear 4n cells. *Arrows* indicate the two-pole spindle and metaphase plate (*panel 2*) and the contractile ring (*panel 3*). The complete movie (Video 3) is available as supplementary information.

metaphase; a bipolar spindle was formed, leading to the alignment of all chromosomes along the same plate (Fig. 4, *panel 2*). Thereafter, during anaphase sister chromatids separated and migrated toward the two opposing poles as expected (Fig. 4, *panel 3*). Cytokinesis occurred correctly at the end of telophase (Fig. 4, *panel 4*). Ultimately, this gave rise to two mononuclear 4n daughter hepatocytes (Fig. 4, *panels 5* and *6*). Taken together, these experiments show that binuclear hepatocyte is the pivotal cell giving rise to mononuclear 4n progeny.

Centrosome Traffic during the Division of Binuclear Hepatocytes—To explain the formation of a unique bipolar spindle during the division of binuclear hepatocytes, we studied centrosome duplication and separation in these cells. During the G_1 phase, in a diploid mammalian cell the centrosome comprises a pair of centrioles connected via a proteinaceous linkage (20). The centrosome is duplicated during S phase when a procentriole buds from each parental centriole. During prophase, the centriolar linkage is disrupted, and the two centrosomes separate and migrate apart to form the bipolar spindle. During our study, we scored the number of centrosomes at different stages of the cell cycle to characterize bipolar spindle formation in binuclear hepatocytes. Using immunofluorescence analysis on primary cell cultures, we showed that a binuclear hepatocyte displayed two centrosomes during G_1 phase (2n DNA content per nucleus) and four centrosomes during G_2 phase (4n DNA content per nucleus) (Fig. 5*A*). Thus a binuclear hepatocyte inherited two parental centrosomes from mononuclear 2n cells, which duplicated. We then studied their movement during mitosis. The nuclei entered prophase simultaneously (Fig. 5*B*). At this point, the four centrosomes moved apart and, at metaphase, clustered in pairs at opposite poles of the cell (Fig. 5*B*). During telophase, centrosome clustering was maintained (Fig. 5*B*). Finally, leaving mitosis, the two daughter mononuclear 4n cells will inherit two centrosomes from the binuclear 2 × 2n hepatocyte. This phenomenon was always observed. At last, we determined whether each centrosome was capable of nucleating microtubules. During prophase, the four centrosomes of binuclear hepatocytes nucleated microtubule asters like the two centrosomes of a mononuclear cell (Fig. 5*C*) and therefore participated in the formation of the bipolar spindle. We were therefore able to demonstrate that, in the binuclear hepatocyte, centrosome clustering appeared to constitute a key event during formation of the bipolar spindle, giving rise solely to mononuclear 4n progeny.

DISCUSSION

In this report, we demonstrate that liver cell polyploidization is an original physiological process passing through a binucleation step. A proportion of mononucleated 2n hepatocytes aborted cytokinesis and thus generated a binuclear hepatocyte 2 × 2n. This binuclear cell was able to pass through a new cell cycle and subsequently divide into two mononuclear 4n cells. Moreover, we showed that the clustering of centrosomes during mitosis was a key step in the genesis of mononuclear 4n hepatocytes.

First of all, we were interested in characterizing changes to hepatocyte polyploidization during liver growth *in vivo*. In fact, only *ex vivo* studies utilizing methods such as karyometry (3), cytophotometry (21), flow cytometry (22), and fluorescence microscopy (23) have so far described this phenomenon after cell isolation and purification. In this study, we developed a method that accurately distinguished mononuclear and binuclear cells and measured the DNA content of each nucleus in tissue sections. Our methodology provides the first direct assessment of hepatocyte ploidy status during liver growth and, interestingly, the results of previous *ex vivo* studies were in line with ours. We demonstrated *in vivo* during post-natal development that the liver is almost solely made up of diploid hepatocytes for the first 22 days; thereafter, between the ages of 22 and 28 days the decline of this population is strictly correlated with the appearance of the binuclear population. These results strongly suggest that the mononuclear 2n hepatocyte is the precursor of the binuclear hepatocyte. Moreover, we observed that the mononuclear 4n population appeared 30 days after birth, by which stage the binuclear population was slowly declining. These observations suggest that a binuclear status may constitute an intermediate step prior to the generation of mononuclear 4n hepatocytes.

To analyze more precisely the cellular mechanisms involved in hepatocyte polyploidization, we followed the division of cells during primary culture. We directly demonstrated that mononuclear 2n hepatocytes were the precursors of binuclear 2 × 2n cells using time-lapse videomicroscopy. We showed that 20% of mononuclear 2n hepatocytes abort cytokinesis; no movement of the contractile ring was observed, and its disappearance led to the genesis of a binuclear cell. This report therefore provides the first direct evidence that acytokinesis forms the basis for hepatocyte binucleation. Previous studies (based on other cell types) had described the binucleation processes as a result of

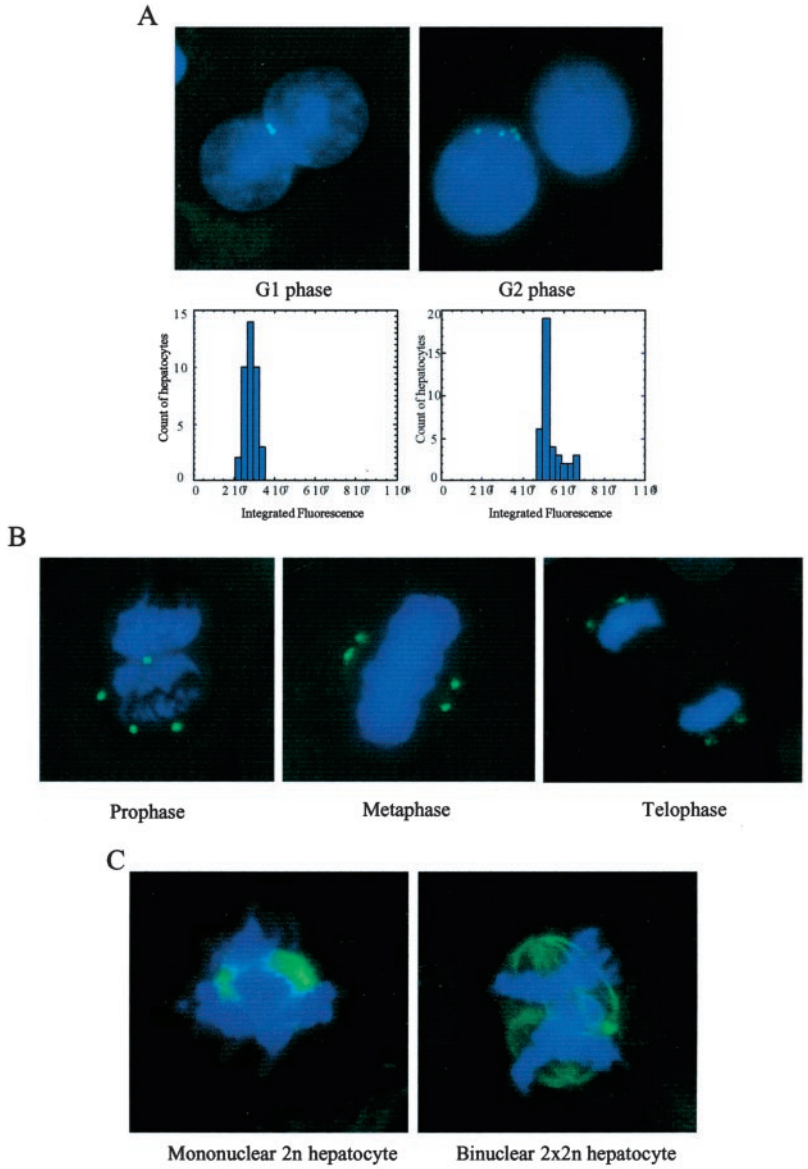

FIG. 5. **Centrosomes of binuclear hepatocytes duplicated during S phase and by their specific migration induced the formation of a bipolar spindle.** *A*, hepatocytes were cultured for 24 h (G_1 phase) or 52 h (G_2 phase) and then fixed for immunofluorescence microscopy. Double staining was performed using specific antibody against γ-tubulin (*green*) to reveal centrosomes, followed by counterstaining with Hoechst coloration (*blue*) for DNA. DNA content was evaluated by recording Hoechst fluorescence in the nuclei of binuclear cells. The peak DNA content of cells with four centrosomes ($2 \times 4n$) was positioned at twice the value of one of the cells with two centrosomes ($2 \times 2n$). *B* and *C*, hepatocytes were cultured for 60 h. At this stage of the culture, the higher mitotic index was detected (data not shown). Cells were permeabilized and fixed in order to observe the localization of centrosomes and the mitotic spindle. *B*, anti-γ-tubulin antibody was used to visualize the centrosome (*green*) and, Hoechst was used to visualize DNA (*blue*). *C*, anti-β-tubulin was used to visualize microtubule asters (*green*), and Hoechst was used to visualize DNA (*blue*).

exit from mitosis because of either the absence or abortion of cytokinesis (18, 24–33). However, this process has been observed following antibody suppression or overexpression or the mutagenesis of several proteins involved in cell cleavage. These proteins include passenger proteins such as INCENP (24) and survivin (25); protein kinases such as polo-like kinase and aurora A and B (18, 26, 27); small G-proteins and their regulators such as citron kinase, MgcRacGap, and Vav3 (28–30); and microtubule motor proteins such as CENP-E (31), MKLP1 (32), and PRC1 (33). Our study offers an experimental model to investigate whether one or several of these proteins are also involved in the physiological hepatocyte binucleation process. In this context, it is interesting to note that a recent study suggested that citron kinase is not implicated in the binucleation process during post-natal liver development (34).

Furthermore, we have shown that binuclear hepatocytes divide into two mononuclear 4n hepatocytes. Binuclear hepatocytes were able to progress through S phase in primary culture, and this observation was not due to the culture conditions, since binuclear hepatocytes were also BrdUrd-labeled *in vivo* during liver growth (data not shown). Intriguingly, recent studies in other cell types (for example HeLa cells and embryo fibroblasts) have shown that tetraploidy, induced by an inappropriate exit of cells from mitosis following the failure of spindle assembly, chromosome segregation, or cytokinesis, causes all cells to arrest in G_1 (17, 18). In that model, the function of the p53 protein was required to impose G_1 arrest in response to tetraploidization. Its inactivation caused a failure to arrest at this G_1 checkpoint, and tetraploid cells then rapidly progressed to aneuploidy. In these cells, amplified numbers of centrosomes and their abnormal clustering led to the formation of multipolar mitotic spindles (19). Contrastingly, in our experimental system p53 was expressed in all binuclear and mononuclear hepatocytes. Thus, our observations demonstrate that G_1 checkpoint control by p53 is not activated by physiological acytokinesis in hepatocytes. Three studies in p53-deficient mice have addressed the implication of p53 in hepatocyte ploidization (13, 21, 35). Although discrepant results were obtained in one of these studies, the other two showed that the p53 genotype (p53+/+, p53±, p53−/−) did not influence hepatocyte polyploidization (13, 35). Our study therefore provides direct support for this hypothesis. It will be interesting in the future to search for other potential checkpoints, including (in particular) the retinoblastoma (Rb) pocket protein family (19).

Following the mitosis of binuclear hepatocytes, we established that 100% of these cells formed a bipolar spindle, leading

to the alignment of all chromosomes on one metaphase plate, a prerequisite for correct chromosome segregation, thus ensuring the tetraploidy status of progeny cells. Interestingly, we found that the two centrosomes of a G_1 binuclear hepatocyte duplicated during S phase and then associated in pairs at metaphase at the two opposite poles of the cell. Formation of the bipolar spindle with two active centrosomes at each pole may be necessary to ensure spindle stability and correct segregation of the 8n DNA content. How the centrosomes migrate in pairs to the two opposite poles of the cell is still to be determined. In diploid cells, at G_2/M transition the dynamic structure linking parental centrioles is disrupted, and the two centrosomes then move apart to form the mitotic spindle (36). In binuclear hepatocytes, the lack of disruption to this structure may prevent separation of the pair of centrosomes and lead to their specific positioning at the two poles of the cell in metaphase.

In conclusion, the hepatocyte constitutes a particularly interesting model of a ploidy process leading first to binuclear cells, which then evolve into mononuclear tetraploid cells. Further work will make it possible to decode the molecular mechanisms controlling hepatocyte tetraploidization and the prevention of aneuploidy.

Acknowledgments—We thank F. Demaugre, D. Kremsdorf, and N. Ferry for helpful discussions and D. Euphrasie and G. Pivert for technical assistance. We also thank the imaging facility at the Jacques Monod Institute (Paris, France) for live cell videomicroscopy analysis.

REFERENCES

1. Ravid, K., Lu, J., Zimmet, J. M., and Jones, M. R. (2002) *J. Cell. Physiol.* **190,** 7–20
2. Sigal, S. H., Rajvanshi, P., Gorla, G. R., Sokhi, R. P., Saxena, R., Gebhard, D. R., Jr., Reid, L. M., and Gupta, S. (1999) *Am. J. Physiol.* **276,** G1260–G1272
3. Nadal, C., and Zajdela, F. (1967) *Exp. Cell Res.* **48,** 518–528
4. Saeter, G., Schwarze, P. E., Nesland, J. M., Juul, N., Pettersen, E. O., and Seglen, P. O. (1988) *Carcinogenesis* **9,** 939–945
5. Wheatley, D. N. (1972) *Exp. Cell Res.* **74,** 455–465
6. Kudryavtsev, B. N., Kudryavtseva, M. V., Sakuta, G. A., and Stein, G. I. (1993) *Virchows Arch. B Cell Pathol.* **64,** 387–393
7. Seglen, P. O. (1997) *Cell Biol. Toxicol.* **13,** 301–315
8. Galitski, T., Saldanha, A. J., Styles, C. A., Lander, E. S., and Fink, G. R. (1999) *Science* **285,** 251–254
9. Schwarze, P. E., Pettersen, E. O., Shoaib, M. C., and Seglen, P. O. (1984) *Carcinogenesis* **5,** 1267–1275
10. Gomez-Lechon, M. J., Barbera, E., Gil, R., and Baguena, J. (1981) *Cell. Mol. Biol.* **27,** 695–701
11. Wu, H., Wade, M., Krall, L., Grisham, J., Xiong, J., and Van Dyke, T. (1996) *Genes Dev.* **10,** 245–260
12. Minamishima, Y. A., and Nakayama, K. (2002) *Cancer Res.* **62,** 995–999
13. Nunez, F., Chipchase, M. D., Clarke, A. R., and Melton, D. W. (2000) *FASEB J.* **14,** 1073–1082
14. Chassoux, D., Franchi, J., Cao, T. T., and Debey, P. (1999) *Anal. Quant. Cytol. Histol.* **21,** 489–497
15. McIntyre, M., Desdouets, C., Senamaud-Beaufort, C., Laurent-Winter, C., Lamas, E., and Brechot, C. (1999) *Oncogene* **18,** 4577–4585
16. Sigal, S. H., Gupta, S., Gebhard, D. F., Jr., Holst, P., Neufeld, D., and Reid, L. M. (1995) *Differentiation* **59,** 35–42
17. Andreassen, P. R., Lohez, O. D., Lacroix, F. B., and Margolis, R. L. (2001) *Mol. Biol. Cell* **12,** 1315–1328
18. Meraldi, P., Honda, R., and Nigg, E. A. (2002) *EMBO J.* **21,** 483–492
19. Borel, F., Lohez, O. D., Lacroix, F. B., and Margolis, R. L. (2002) *Proc. Natl. Acad. Sci. U. S. A.* **99,** 9819–9824
20. Lange, B. M. (2002) *Curr. Opin. Cell Biol.* **14,** 35–43
21. Yin, L., Ghebranious, N., Chakraborty, S., Sheehan, C. E., Ilic, Z., and Sell, S. (1998) *Hepatology* **27,** 73–80
22. Mossin, L., Blankson, H., Huitfeldt, H., and Seglen, P. O. (1994) *Exp. Cell Res.* **214,** 551–560
23. Martin, N. C., McCullough, C. T., Bush, P. G., Sharp, L., Hall, A. C., and Harrison, D. J. (2002) *J. Cell. Physiol.* **191,** 138–144
24. Mackay, A. M., Ainsztein, A. M., Eckley, D. M., and Earnshaw, W. C. (1998) *J. Cell Biol.* **140,** 991–1002
25. Skoufias, D. A., Mollinari, C., Lacroix, F. B., and Margolis, R. L. (2000) *J. Cell Biol.* **151,** 1575–1582
26. Lee, K. S., Yuan, Y. L., Kuriyama, R., and Erikson, R. L. (1995) *Mol. Cell. Biol.* **15,** 7143–7151
27. Terada, Y., Tatsuka, M., Susuki, F., Yasuda, Y., Fujita, S., and Otsu, M. (1998) *EMBO* **3,** 667–676
28. Madaule, P., Eda, M., Watanabe, N., Fujisawa, K., Matsuoka, T., Bito, H., Ishizaki, T., and Narumiya, S. (1998) *Nature* **394,** 491–494
29. Hirose, K., Kawashima, T., Iwamoto, I., Nosaka, T., and Kitamura, T. (2001) *J. Biol. Chem.* **276,** 5821–5828
30. Fujikawa, K., Inoue, Y., Sakai, M., Koyama, Y., Nishi, S., Funada, R., Alt, F. W., and Swat, W. (2002) *Proc. Natl. Acad. Sci. U. S. A.* **99,** 4313–4318
31. Martineau-Thuillier, S., Andreassen, P. R., and Margolis, R. L. (1998) *Chromosoma* **107,** 461–470
32. Nislow, C., Lombillo, V. A., Kuriyama, R., and McIntosh, J. R. (1992) *Nature* **359,** 543–547
33. Mollinari, C., Kleman, J. P., Jiang, W., Schoehn, G., Hunter, T., and Margolis, R. L. (2002) *J. Cell Biol.* **157,** 1175–1186
34. Liu, H., Di Cunto, F., Imarisio, S., and Reid, L. M. (2003) *J. Biol. Chem.* **278,** 2541–2548
35. Bellamy, C. O., Clarke, A. R., Wyllie, A. H., and Harrison, D. J. (1997) *FASEB J.* **11,** 591–599
36. Mayor, T., Stierhof, Y. D., Tanaka, K., Fry, A. M., and Nigg, E. A. (2000) *J. Cell Biol.* **151,** 837–846

- Robert A., Margall Ducos G., Guidotti J.E., Bregerie O., Celati C., Brechot C, Desdouets C. *The Intraflagellar component Polaris is a centrosomal protein regulating G1/S transition in nonciliated cells. J cell science. 2007, Feb 15*

The intraflagellar transport component IFT88/polaris is a centrosomal protein regulating G1-S transition in non-ciliated cells

Aude Robert[1,2,3,4], Germain Margall-Ducos[1,2,3,4], Jacques-Emmanuel Guidotti[1,2,3,4], Olivier Brégerie[5], Claude Celati[6], Christian Bréchot[5] and Chantal Desdouets[1,2,3,4,*]

[1]Institut Cochin, Département Génétique et Développement, [2]INSERM, U567, [3]CNRS, UMR8104 and [4]Université Paris 5, Faculté de médecine R. Descartes, UM 3, Paris, F-75014 France
[5]INSERM U785. Université Paris XI, CHB Paul Brousse, Villejuif Cedex, F-94804 France
[6]Laboratoire de Biologie du Cycle Cellulaire et de la Motilité, UMR144 Institut Curie/CNRS, 12 rue Lhomond, Paris cedex 05, F-75248 France
*Author for correspondence (e-mail: desdouets@cochin.inserm.fr)

Accepted 1 December 2006
Journal of Cell Science 120, 628-637 Published by The Company of Biologists 2007
doi:10.1242/jcs.03366

Summary

Loss of normal primary cilia function in mammals is linked to proliferative diseases, such as polycystic kidney disease, suggesting a regulatory relationship between cilia and cell cycle. The primary cilium expressed by most mammalian cells is nucleated from the elder centriole of the centrosome. The relationship between centrosome and cilia suggests that these structures share functions and components. We now show that IFT88/polaris, a component of the intraflagellar transport, remains associated to the centrosome in a proliferative state. IFT88/polaris is tightly associated with the centrosome throughout the cell cycle in a microtubule- and dynein-independent manner. IFT88/polaris tetratricopeptide repeat motifs are essential for this localization. Overexpression of IFT88/polaris prevents G1-S transition and induces apoptotic cell death. By contrast, IFT88/polaris depletion induced by RNA interference promotes cell-cycle progression to S, G2, and M phases. Finally, we demonstrate that IFT88/polaris interacts with Che-1, an Rb-binding protein that inhibits the Rb growth suppressing function. We propose that IFT88/polaris, a protein essential for ciliogenesis, is also crucial for G1-S transition in non-ciliated cells.

Key words: Polaris, Centrosome, Cilium, Intraflagellar transport, G1-S transition

Introduction

The centrosome functions as an organizing center for cytoskeletal components, especially microtubules (Doxsey, 2001; Nigg, 2002; Salisbury et al., 1999). A vertebrate centrosome comprises two barrel-shaped centrioles which are embedded within a protein-dense matrix known as the pericentriolar matrix (PCM). By nucleating and anchoring microtubules, centrosome influences most microtubule-dependent processes, including cell shape, polarity, adhesion and motility, as well as intracellular transport and positioning of organelles (Bornens, 2002; Fukasawa, 2002; Rieder et al., 2001). The centrosome also has a crucial role in cell division, mediating assembly and organization of the mitotic spindle that is required for correct chromosome segregation, and the positioning of the cleavage plane during cytokinesis (Doxsey, 2001; Piel et al., 2001). Consistent with this role, centriole duplication is coordinated with the cell cycle (Hinchcliffe and Sluder, 2001). Centrosomes are also the precursors of primary cilia, nonmotile sensory organelles found on most vertebrate cells (Badano et al., 2005; Quarmby and Parker, 2005). Typically, a single cilium projects from each cell, emerging from the elder centriole of the centrosome that has become a basal body (Sorokin, 1962). The presence of a cilium is associated with the establishment of polarity and differentiation of the cell (Wheatley et al., 1996). Thus, cilia are most abundant on non-proliferating G0 cells and entry into the cell cycle is preceded by ciliary resorption, whereas exit from mitosis is accompanied by ciliary assembly, a relationship that may reflect the use of the basal bodies and/or centrioles as mitotic spindle poles (Rieder et al., 1979).

Primary cilia assembly occurs by a process called intraflagellar transport (IFT) that was first described in *Chlamydomonas* (Kozminski et al., 1993; Rosenbaum and Witman, 2002). This process has recently become the focus of intense research interest owing to its association with human disease and developmental abnormalities, including polycystic kidney disease (PKD), hepatic and pancreatic defects, blindness and obesity, as well as skeletal patterning abnormalities and randomization of the left-right body axis (Hildebrandt and Otto, 2005). The first evidence that defective cilia are the proximal cause for PKD originated with the discovery that the gene mutated in the Oak Ridge polycystic kidney (*Tg737*^{orpk}) mouse (Moyer et al., 1994) is homologous to a gene essential for ciliary assembly in *Chlamydomonas*, *ift88* (Pazour et al., 2000) and in *C. elegans, osm-5* (Haycraft et al., 2001; Qin et al., 2001). Whereas *Tg737*^{orpk} mutants are viable, complete knockout of the mouse *Tg737* gene (*Tg737*$^{\Delta 2\text{-}3\beta\text{-}gal}$) is embryonic lethal (Murcia et al., 2000). Homozygous *Tg737*$^{\Delta 2\text{-}3\beta\text{-}gal}$ mutants die in early to mid-gestation and exhibit neural tube defects, random left-right

body axis specification and a pronounced expansion of the anterior-posterior (AP) limb bud axis. In *Tg737*^{orpk} and *Tg737*$^{\Delta 2\text{-}3\beta\text{-}gal}$ mutant mice, cilia are severely malformed or absent (Murcia et al., 2000; Pazour et al., 2000; Yoder et al., 2002a). In fact, in mammals, IFT88/polaris, the protein encoded by *Tg737*, is a core component of the intraflagellar transport machinery and is required for the formation of all cilia (Murcia et al., 2000; Pazour et al., 2000).

Growing evidence suggest a link between cilia, centrosome and proliferating disorders. Here, we show that the IFT protein IFT88/polaris, essential for cilia function, is also crucial for cell cycle progression. We demonstrated by immunofluorescence and biochemical analysis in proliferating cells, either ciliated or not, that IFT88/polaris is tightly associated with the centrosome throughout the cell cycle. Expression of a series of deletion constructs revealed the presence of two independent centrosome-targeting domains. Moreover, we tested whether IFT88/polaris participates in the regulation of cell cycle progression. Our results show that altered levels of IFT88/polaris concentration influence the G1-S cell cycle progression.

Results

Subcellular localization of IFT88/polaris in proliferating ciliated or non-ciliated cells

IFT88/polaris is known as an IFT protein localized to basal body and axoneme of cilia from *Chlamydomonas* to mammals (Cole et al., 1998; Pazour et al., 2000; Qin et al., 2001). To provide insight into its cellular distribution in proliferating ciliated cells (resorpted cilia) or in non ciliated cells, we generated polyclonal antiserum against the C-terminal region of the protein. As expected, in quiescent ciliated cells IFT88/polaris was localized to the basal body and along the axoneme (Fig. 1A). We investigated IFT88/polaris localization in proliferating cells either ciliated or not (ciliated cells, RPE-1 and CHO; non-ciliated cells, HeLa, 2A1.6) (shown for RPE-1 cells, Fig. 1B). Endogenous IFT88/polaris was found at one or two perinuclear focal points that colocalized with γ-tubulin in cells in G1 or G2 phase (Fig. 1B). This localization was confirmed biochemically (Fig. 1C). Low-speed Triton-X-100-soluble and -insoluble fractions of unsynchronized 2A1.6 cell lysates were prepared as described previously (Moudjou and Bornens, 1994) and submitted to western blot analysis together with centrosome sucrose-gradient preparations. IFT88/polaris was detected both in the Triton-insoluble fraction and, to a lesser extent, in the Triton-soluble fraction (Fig. 1C, left panel). Clearly, IFT88/polaris was as enriched in the centrosomal fraction as γ-tubulin (Fig. 1C, left panel). Exposure of the centrosomal fraction to various solubilizing treatments, including detergents and chaotropic agents, was done to assess the strength of this association. We found that IFT88/polaris, as well as γ-tubulin, can partly be solubilized in 2D buffer and about half of the protein can be solubilized in 8M urea (Fig. 1C, right panel). These results demonstrated a tight association

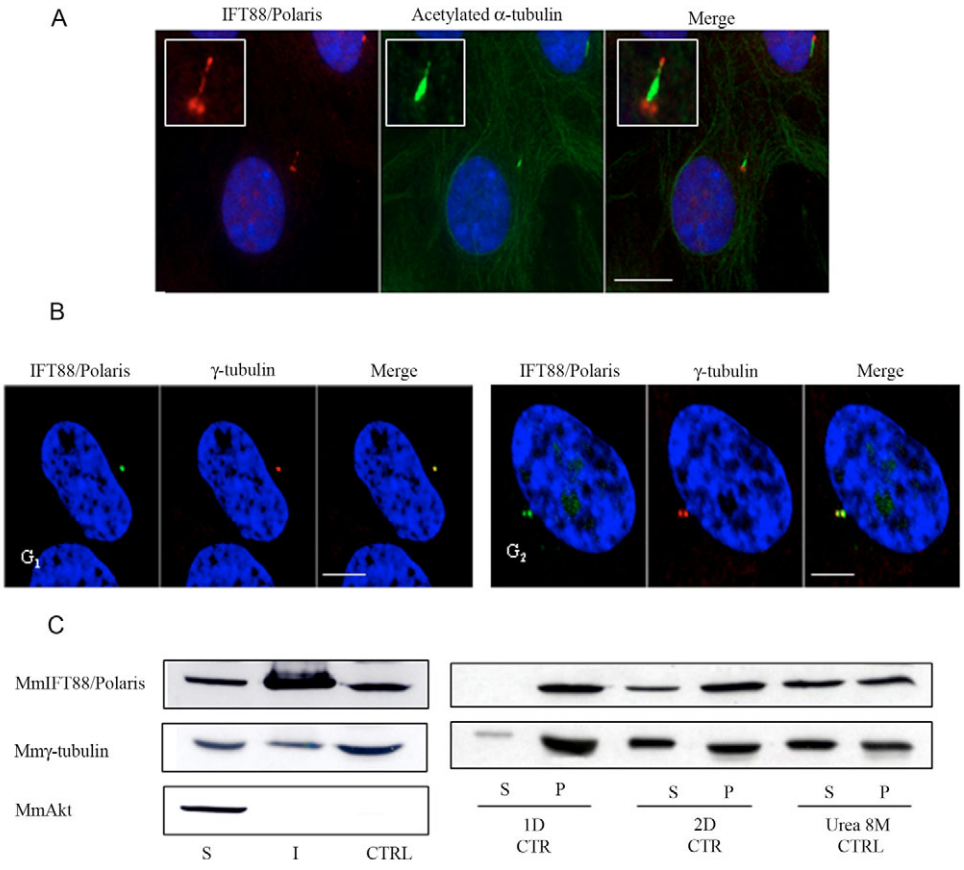

Fig. 1. IFT88/polaris localizes to basal bodies and axonemes in quiescent ciliated cells and to centrosomes in proliferating cells. (A) RPE-1 cell immunostained with an antibody against acetylated-tubulin (6-11B-1, green) to label the axoneme of the cilium, and with anti-IFT88/polaris (740, red) to stain IFT88/polaris which was localized to the axoneme and the basal body. Insets, higher magnifications of cilium. Ciliary assembly was induced by culturing RPE-1 cells in medium supplemented with 0.25% serum for 48 hours. Bar, 10 μm. (B) Confocal immunofluorescence microscopy analysis, using anti-IFT88/polaris 740 (green) and anti-γ-tubulin (GTU88, red), were performed on exponentially growing RPE-1 cells. Bars, 5 μm. Nuclei in A and B are stained with Hoechst 33342 dye. (C) Left panel, western blot analysis of Triton-X-100-soluble (S) and -insoluble (I) protein fractions from 2A1.6 cells, and of a highly enriched centrosomal fraction (CTR). Right panel, biochemical extraction of centrosome-associated IFT88/polaris. Supernatant (S) and pellet (P) of centrosomal fractions obtained under different extraction conditions (see Materials and Methods) were immunoblotted with anti-IFT88/polaris (02078), anti-γ-tubulin (GTU88) and anti-Akt antibodies. Detection of Akt, a well-characterized cytoplasmic protein, was used as a negative control to verify the purity of the centrosomal fraction.

of IFT88/polaris with the centrosome, which can only be disrupted in denaturing conditions.

IFT88/polaris localizes to the centrosome throughout the cell cycle, independently of the microtubules network and the dynein motor

We next examined whether IFT88/polaris has a cell-cycle-dependent behaviour. For that, we used HeLa HC1 cells that constitutively expressed the centriole protein centrin1 fused to GFP (Piel et al., 2000). During G1, IFT88/polaris was present at the proximal ends of maternal centrioles (Fig. 2). In early S phase, centrioles begin to duplicate, and by G2/M, duplication is usually completed. At G2-M transition process, IFT88/polaris was still localized at the proximal ends of the mother and the daughter centrioles (Fig. 2; G2, prophase cells). By metaphase, when centrosomes become mature, IFT88/polaris staining was brighter at centrosomes than at any other cell cycle stage; by telophase IFT88/polaris staining reached its lowest levels (Fig. 2). We next asked how IFT88/polaris assembles at centrosomes, which serve as nucleation and organizing sites for cytoplasmic microtubules. In nocodazole-treated cells, IFT88/polaris remained centrosomal, as did the core centrosomal protein γ-tubulin (Fig. 3). We also investigated whether centrosomal assembly of IFT88/polaris depends on dynein-dynactin molecular motor by overexpressing a mutant of $p150^{glued}$ that antagonizes the function of the motor in vivo. We confirmed that overexpression of Dsred-$p150^{217\text{-}548}$ in HeLa cells causes PCM1 mislocalization (Fig. 3). By contrast, as found for γ-tubulin, the centrosomal localization of IFT88/polaris was not affected in cells overexpressing Dsred-$p150^{217\text{-}548}$ (Fig. 3). These data demonstrate that IFT88/polaris is assembled at the centrosome throughout the cell cycle in a microtubule- and dynein-independent manner.

IFT88/polaris TPR domains are essential for centrosome targeting

Polaris is known to have an evolutionary conserved role in ciliogenesis (Han et al., 2003; Haycraft et al., 2001; Murcia et al., 2000; Pazour et al., 2000; Qin et al., 2001; Yoder et al., 2002b). To circumvent any phenotypes due to defects of cilia, all the following experiments have been performed in non-ciliated cells. To define sub-regions of IFT88/polaris involved in centrosomal targeting, we generated deletion mutant constructs fused to GFP either at the N-terminus or the C-terminus (mutants Δ1 to Δ7, see Materials and Methods for details) and expressed these truncated polypeptides into transiently transfected HeLa cells. As shown in Fig. 4A, the full-length sequence of IFT88/polaris contains ten copies of a tetratricopeptide repeat (TPR), with three copies located towards the N-terminus and seven repeats located closer to the C-terminus. Sequence analysis indicated also the presence of two putative coiled-coil domains. At low expression levels, exogenous full-length IFT88/polaris localized almost exclusively to the centrosome (Fig. 4B, left panel). At higher expression levels, multiple dots of various sizes were detected in cells (Fig. 4B, right panel) as previously described for the overexpression of other centrosomal proteins (Kim et al., 2004; Mayor et al., 2002); nevertheless, of several dots present, only one stained positive for γ-tubulin (Fig. 4B, right panel, Arrow). By analyzing the localization of truncated mutants, we demonstrated that mutants Δ2, Δ3, Δ6 and Δ7 were successfully recruited to the centrosome (Fig. 4C, example for Δ6). Like the full-length protein, these fusion proteins were

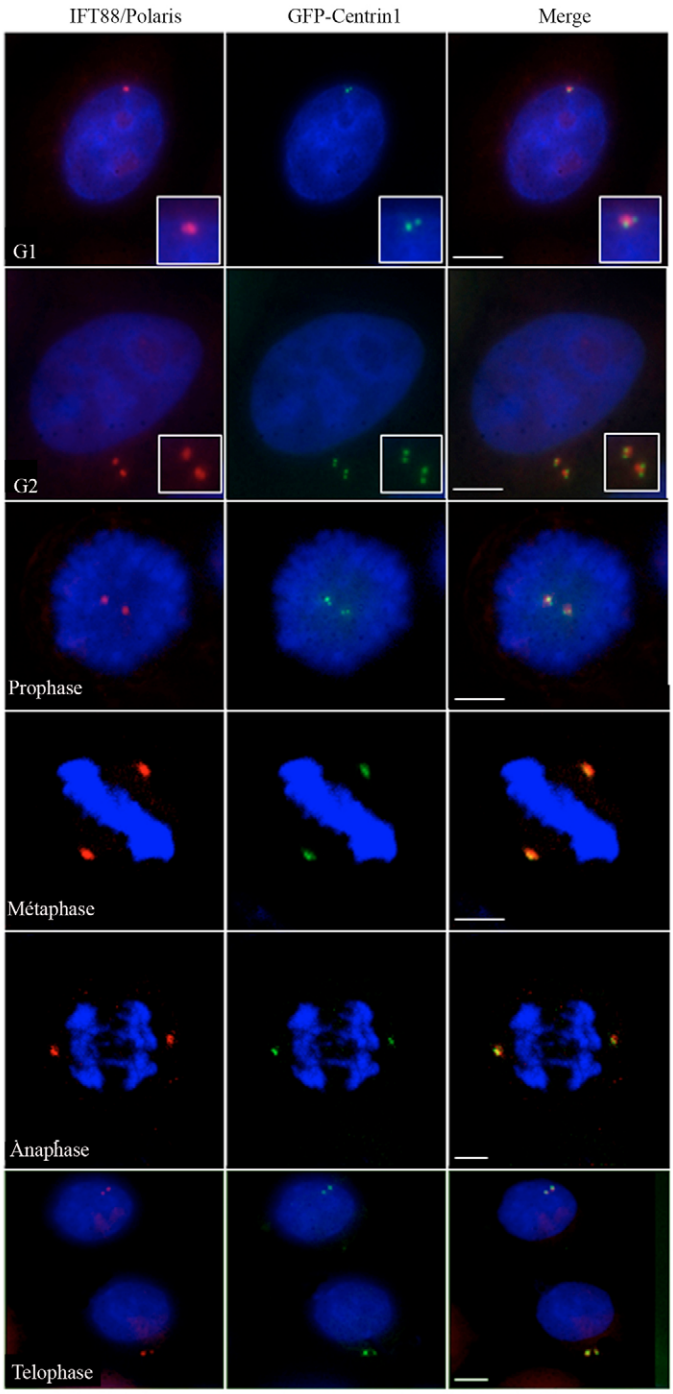

Fig. 2. IFT88/polaris is localized to the centrosome throughout the cell cycle. Immunofluorescence images of endogenous IFT88/polaris in HeLa cells at different stages of cell cycle that stably express GFP-centrin1. Right panel, merged images of IFT88/polaris (red), centrin1 (green), and nuclei (blue) from cells in G1, G2, prophase, metaphase, anaphase and telophase. Insets, higher magnifications of centrioles stained for GFP-centrin1 (left) and IFT88/polaris (anti-IFT88/polaris 740, middle) in cells at G1 and G2. Bars, 5 μm.

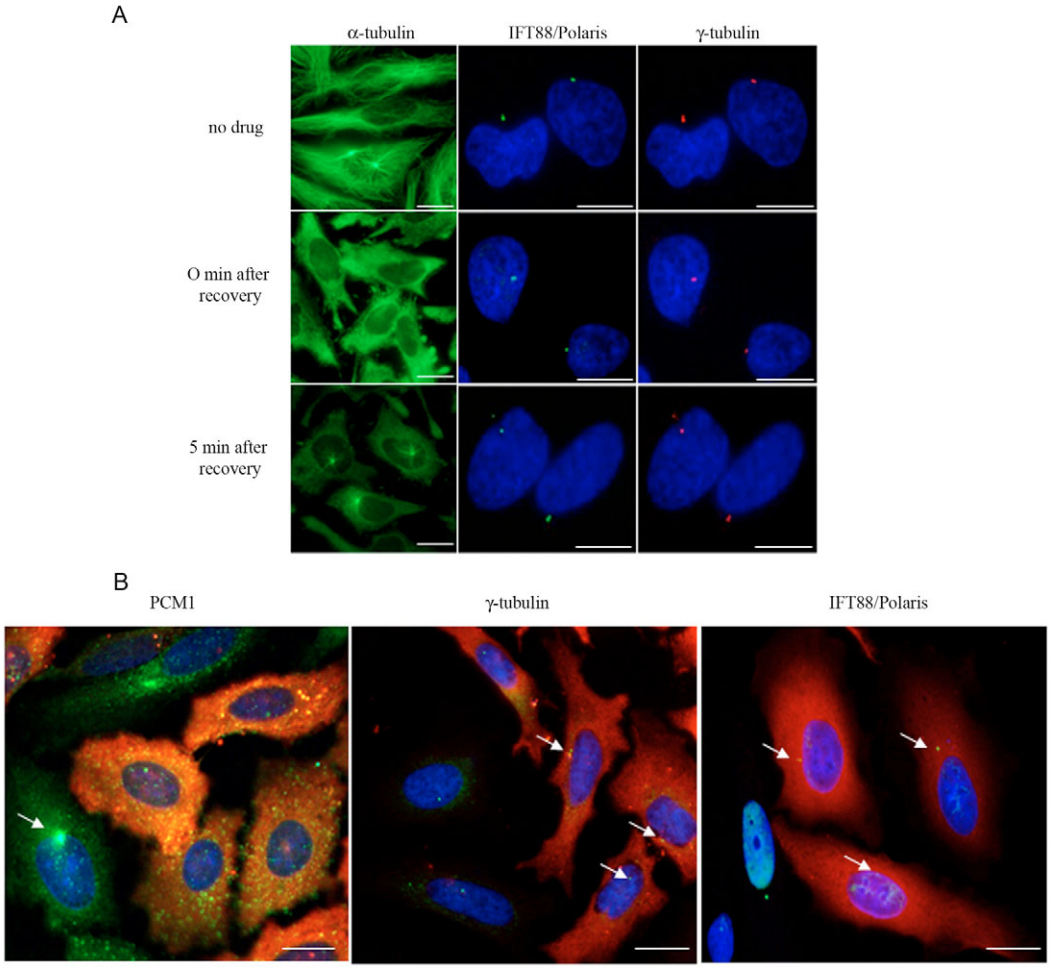

Fig. 3. Centrosomal assembly of IFT88/polaris is not dependent on polymerized microtubules or the dynein-dynactin molecular motor. (A) Hela cells were either mock-treated (no drug) or treated with nocodazole for 1 hour and allowed to recover for 0 or 5 minutes. Cells were stained with α-tubulin antibody (methanol fixation, Tub2.1, green) to follow depolymerization (0 minutes) or polymerization (5 minutes after recovery) of microtubules, or co-stained with anti-IFT88/polaris 740 (PFA 4% fixation, green) and anti-γ-tubulin (PFA 4% fixation, red) antibodies. IFT88/polaris and γ-tubulin localizations were analyzed on cells treated or not with the nocodazole (n=200). Bars, 10 μm. (B) HeLa cells were transiently transfected with DsRed-p150$^{217\text{-}548}$, which inhibits dynein-dynactin motor function, and co-stained with antibodies against PCM1, γ–tubulin or IFT88/polaris (green). The left panel shows untransfected cells with expected PCM1 localisation (greens staining, arrow) and transfected DsRed-p150$^{217\text{-}548}$ cells with PCM1 mislocalization (scattered staining). Middle and right panels show that, after expression of plasmid DsRedp150$^{217\text{-}548}$, centrosomal localization in transfected cells is unchanged for γ-tubulin and IFT88/polaris (arrows). Bars, 10 μm.

identified as multiple dots with one that colocalized with γ-tubulin (Fig. 4C, example for Δ6) when expressed at high levels. By contrast, mutants Δ1 and Δ5 were distributed diffusely in the cytoplasm, like the GFP control protein, and colocalization with γ-tubulin was not observed (Fig. 4C, example for Δ5). Finally, distribution of mutant Δ4 was visible in the cytoplasm as multiple dots, but more irregular in shape and did not colocalize with γ-tubulin (Fig. 4C). From these experiments, we concluded that the two TPR domains were independently essential to target IFT88/polaris to the centrosome.

Overexpression of IFT88/polaris prevents entry into S phase and induces apoptotic cell death

Since no late stages of mitosis were observed in transfected cells overexpressing IFT88/polaris, we sought to determine whether its ectopic expression caused changes in cell cycle progression. C-Nap1, a protein involved in centrosome cohesion, was used as control. Expression of GFP–C-Nap1 resulted in the formation of multiple dots without altering mitosis progression (Mayor et al., 2002). Nocodazole treated cells expressing only GFP or GFP–C-Nap1, showed a prominent accumulation of phases G2 and M (without treatment 16% of cells, with nocodazole 40%) (Fig. 5A). By contrast, the proportion of cells at G2/M was not significantly changed in cells expressing GFP-IFT88/polaris treated or not with nocodazole (19% or 21%, respectively, Fig. 5A). Thereafter, we determined whether its ectopic expression changed the progression into S phase. IFT88/polaris overexpression dramatically decreased the fraction of BrdU-positive cells at 36 hours post transfection (Fig. 5B, 4% compare with 25% and 32% for GFP and GFP–C-Nap1, respectively). The impairment of G1-S transition was confirmed by thymidine block experiments (Fig. 5C). In a final

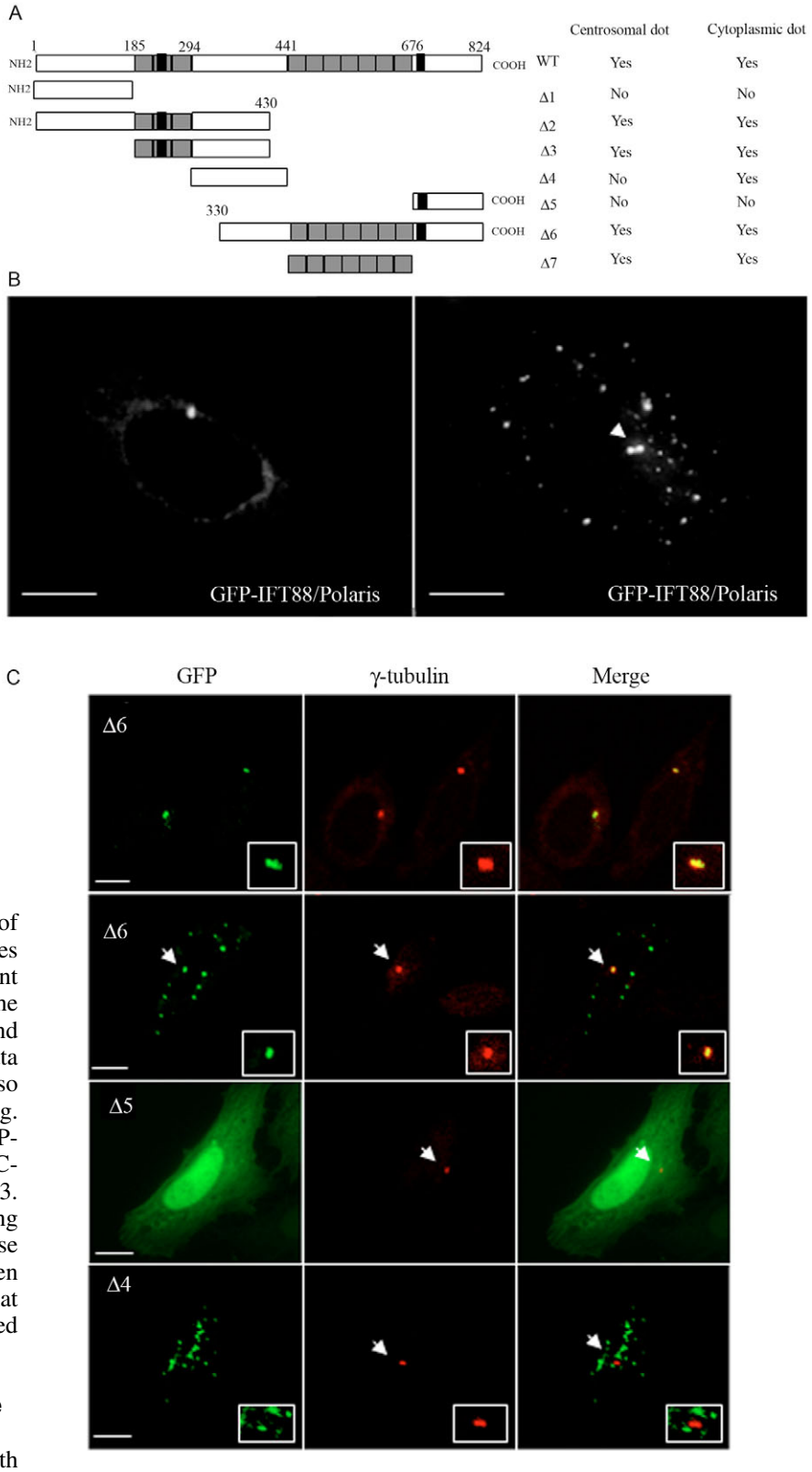

Fig. 4. IFT88/polaris is targeted to the centrosome by its TRP domains. (A) Deletion constructs. Numbers indicate the positions of amino acids, black boxes designate the predicted coiled-coil domain of IFT88/polaris, grey boxes designate the tetratricopeptide repeat domains (TPR). Results of the immunolocalization of GFP-tagged polypeptides are summarized on the right. (B) HeLa cells were transiently transfected with GFP-IFT88/polaris full-length and, 24 hours later, processed for immunofluorescence microscopy (GFP staining). Depending on the expression level, ectopic IFT88/polaris expression resulted in the formation of a single dot (left panel) or multiple dots (right panel). The arrowhead points to the dot containing the centrosome (γ-tubulin labeling, data not shown). Bars, 10 μm. (C) Phenotypes observed after ectopic expression of GFP-tagged truncated IFT88/polaris polypeptides (green). Transfected cells were stained with γ-tubulin (red) 24 hours post transfection. Although polypeptides Δ1, Δ4 and Δ5 produced proteins that were not found at the centrosome (see Δ4 and Δ5), other polypeptides containing TRP domains (Δ2, Δ3, Δ6 and Δ7) produced proteins that were recruited to the centrosome (see Δ6). Depending on expression levels, ectopic expression of mutants Δ2, Δ3, Δ6 and Δ7 resulted in the formation of a single dot (Δ6 first panel) or of multiple dots (Δ6, second panel). Bars, 10 μm.

set of experiments, we studied the outcome of these cells. Morphological evaluation of cultures using Hoechst 33342 staining and fluorescent microscopy revealed a marked increase in the number of cells with nuclear condensation and fragmentation 48 hours after transfection (data not shown). Caspase 3 activity was also examined on transfected cells. As shown on Fig. 5D, only 4% of cells transfected with the GFP-control vector and 6% transfected with GFP–C-Nap1, expressed the activated form of caspase 3. By contrast, 40% of cells overexpressing IFT88/polaris were positive for cleaved caspase 3 at 48 hours post transfection (Fig. 5D). Taken together, the above results demonstrated that cells overexpressing IFT88/polaris arrested before S phase and then died by apoptosis.

IFT88/polaris silencing promotes cell cycle progression to S, G2 and M phases

These results prompted us to analyze the growth characteristics of cells depleted from IFT88/polaris. Two non-overlapping IFT88/polaris small interference RNAs (siRNAs) (siPol1 and siPol2) were tested and produced similar results. Cells transfected with siPol1or siPol2 showed a specific reduction of about 60% of IFT88/polaris expression compared with control (scramble) transfected cells (Fig. 6A, left panel). We also confirmed by immunofluorescence staining that IFT88/polaris was greatly reduced at the centrosome in most cells (Fig. 6A, right panel). In contrast to cells overexpressing IFT88/polaris, reduction of the endogenous protein activated entry into S phase as

demonstrated by BrdU labeling (from 21.1%±0.4 in control cells to 45.6%±2.3 in siPol1 cells at 48 hours, Fig. 6B). In fact, cells expressing reduced levels of IFT88/polaris protein exhibited an increased rate of proliferation (Fig. 6C). Furthermore, flow cytometric analysis for DNA content showed that inhibition of IFT88/polaris resulted in a significant reduction in cells in G1 (70.8%±2 with scramble siRNA, 50.3%±2.7 with siPol1) and a significant increase in cells in S phase (18.1%±3.6 with scramble siRNA, 31.1%±3.4 with siPol1) and in G2 and M phases (11.1%±1.9 with scramble siRNA, 18.6%±1 with siPol1) (Fig. 6D). In conclusion, IFT88/polaris silencing promoted cell-cycle progression to S and G2/M phases.

Identification of IFT88/polaris downstream signaling partners involved in cell cycle regulation

To identify IFT88/polaris targets in cell-cycle regulation, we performed a yeast two-hybrid screening. The mouse full-length IFT88/polaris protein was used to screen a human fetal liver cDNA library. From the 3×10^6 yeast transformants obtained, we selected six clones that fulfilled our selection criteria. One of these clones contained the cDNA encoding amino acids 392 to 558 of Che-1 protein. Che-1 is known to interact with Rb protein and this binding affects the growth-suppressing function of Rb by relieving its inhibition of E2F1 transcriptional activity essential for G1-S transition (Bruno et al., 2002; Fanciulli et al., 2000). To test the specificity of this interaction in mammalian cells, we immunoprecipitated extracts from HEK293T cells that had been transfected with Myc-tagged full-length IFT88/polaris plasmid, with anti-Myc or anti-Che-1 antibodies. We demonstrated that Myc-tagged full-length IFT88/polaris could be coimmunoprecipitated by endogenous Che-1 (Fig. 7A, upper panel) and conversely, endogenous Che-1 could be coimmunoprecipitated with full-length IFT88/polaris (Fig. 7A, lower panel). More importantly, we observed interaction between endogenous IFT88/polaris and Che-1 (Fig. 7B). In order to understand the mechanism of action of IFT88/polaris at the G1-S transition, we analyzed whether the interaction between Che-1 and Rb is affected by IFT88/polaris overexpression. As shown in Fig. 7C, a reduced amount of Rb was immunoprecipitated by Che-1 in the cells overexpressing IFT88/polaris. Taken together, these results demonstrated that IFT88/polaris interacted with Che-1 and, thus, modulated its binding to Rb protein.

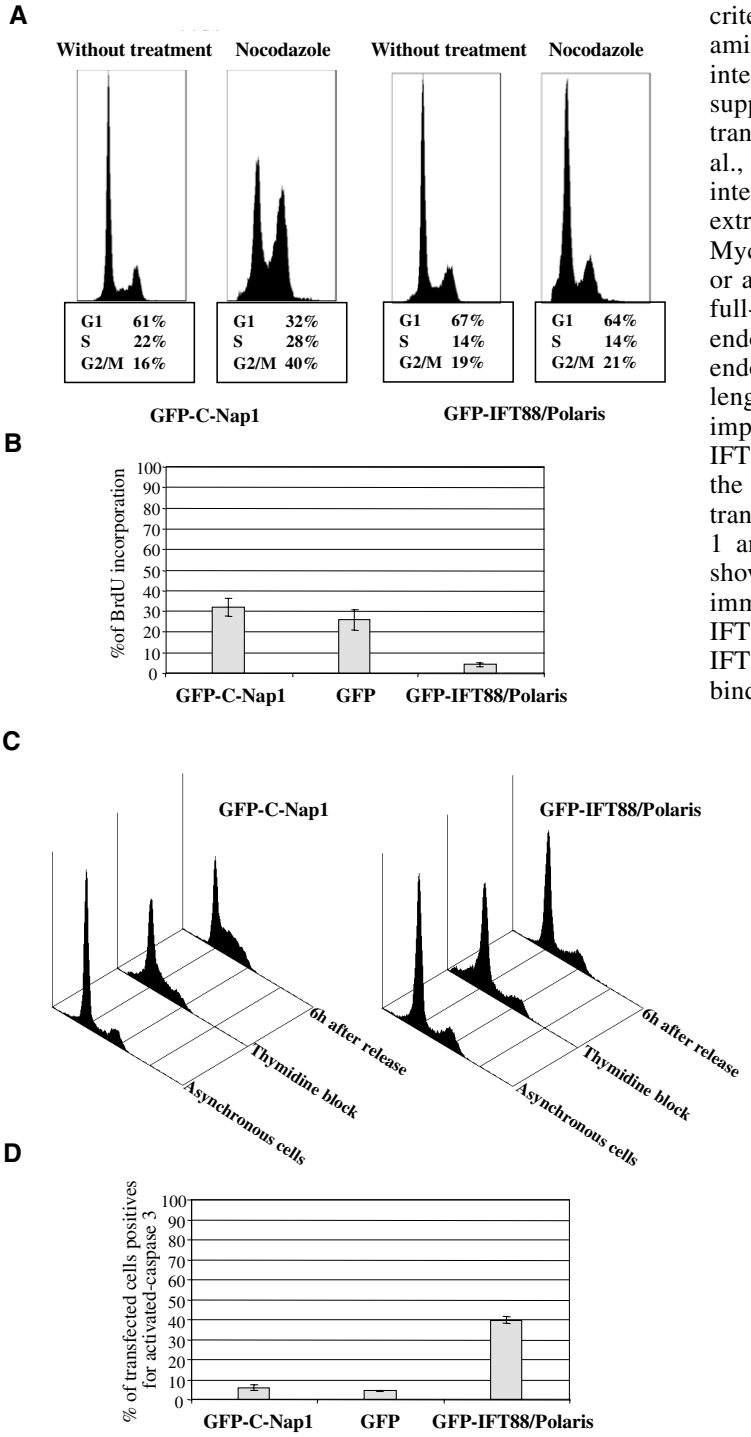

Fig. 5. Overexpression of IFT88/polaris induces an arrest in the cell cycle before S phase and an apoptotic death. (A) HeLa cells were transfected for 36 hours to express either GFP-IFT88/polaris or GFP–C-Nap1 and these cells were treated or not with nocodazole for 12 hours. Cell-cycle-phase distribution of GFP-positive cells was assessed using propidium iodide. Proportions were estimated by triplicate measurements using FACS analysis and the software Wincycle™. (B) HeLa cells were transfected for 36 hours to express GFP-IFT88/polaris, GFP–C-Nap1 or GFP. BrdU staining was analyzed on GFP-positive cells after labeling with anti-BrdU monoclonal antibody (n=150). (C) HeLa cells were transfected for 36 hours to express GFP-IFT88/polaris, GFP–C-Nap1. These cells were synchronized by thymidine block for 12 hours and released for 6 hours. Cell-cycle-phase distribution of GFP-positive cells was assessed using iodide propidium and FACS analysis. (D) Caspase-3-like activity was measured 48 hours after transfection in GFP-positive cells (n=150). Data are from three independent experiments and presented as the mean ± s.d.

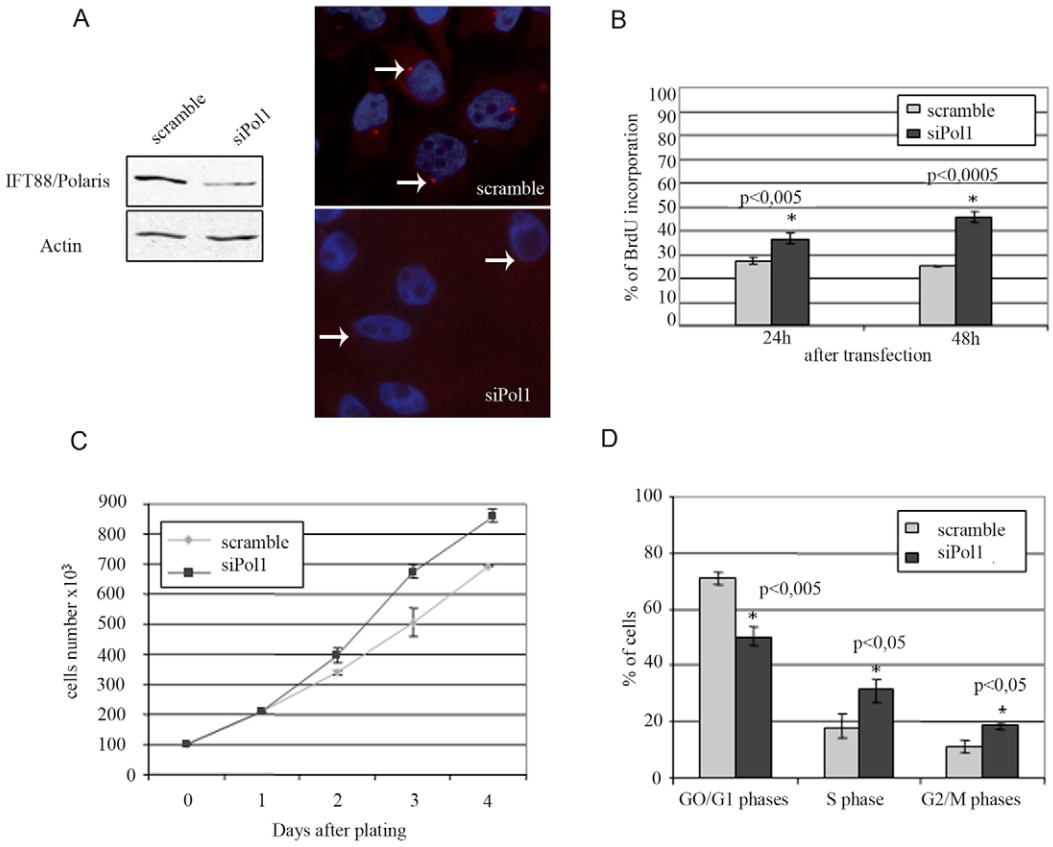

Fig. 6. IFT88/polaris downregulation causes cells proliferation. (A) Two non-overlapping IFT88/polaris siRNAs (siPol1 and siPol2) were tested and were found to produce similar results. Data obtained with siPol1 are illustrated in this figure. HeLa cells were transfected with scramble or IFT88/polaris siRNA (siPol1). Cell lysates (48 hours post transfection) were subject to western blot (left panel) using either the anti-IFT88/polaris antibody 740 (top) or an anti-actin antibody (I-19, bottom). HeLa cells transfected with scramble or IFT88/polaris siRNA (siPol1) were also immunostained (right panel) with anti-IFT88/polaris antibody 740. (B) HeLa cells were transfected with scramble or siPol1, treated with BrdU during 4 hours before the indicated time and BrdU-positive cells were analyzed (n=300). (C) Growth curves of cells transiently transfected with scramble or siPol1. (D) FACS analysis, 48 hours post tranfection. The histogram indicates the percentage of cells at a given cell cycle phase. Data are from three independent experiments and presented as the mean ± s.d.

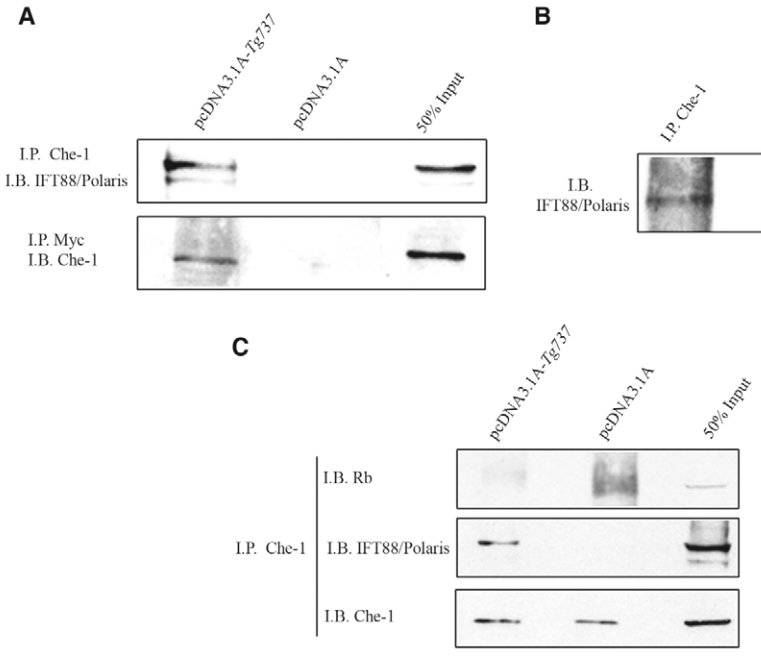

Fig. 7. IFT88/polaris interacts with Che-1 and inhibits its interaction with Rb protein. (A) HEK293T cells were transfected with control plasmid (pcDNA3.1A) or Myc-tagged full-length IFT88/polaris (pcDNA3.1A-*Tg737*). Lysates (500 μg) from transfected cells were immunoprecipitated with anti-Myc antibody or anti-Che-1 antibody and analyzed by western blot using specific anti-IFT88/polaris (740) or Che-1 antibodies. (B) Lysates (1 mg) from non transfected HEK293T cells were immunoprecipitated with anti-Che-1 antibody and analyzed by western blot using a specific anti-IFT88/polaris (740) antibody. (C) HEK293T cells were transfected with control plasmid or Myc-tagged full-length IFT88/polaris. Lysates (500 μg) from transfected cells were immunoprecipitated with anti-Che-1 antibody and analyzed by western blot using specific anti-Rb, anti-IFT88/polaris (740) or Che-1 antibodies. I.P., immunoprecipitation; I.B, immunoblot.

Discussion

We have demonstrated with this study that IFT88/polaris localizes in proliferating mammalian cells at the centrosome and participates to cell cycle progression by controlling G1-S transition. In differentiated ciliated cells, IFT88/polaris is known to have an essential and evolutionarily conserved role for the formation of all cilia (Rosenbaum and Witman, 2002). Here, we show that IFT88/polaris is tightly associated at the proximal end of centrioles throughout the cell cycle. This association is dependent on IFT88/polaris TPR domains and independent of the microtubule network and the dynein-dynactin motors. IFT88/polaris centrosomal localization is conserved in non-ciliated cells, suggesting an additional role beyond the classic IFT system.

A recent convergence of data has indicated an intimate regulatory relationship between ciliogenesis and cell cycle progression. Thus, members of protein families known for their mitotic functions play roles in ciliary assembly. For instance, a distant paralog of aurora kinase is essential for flagellar disassembly in *Chlamydomonas* (Pan et al., 2004). The centrosomal protein pericentrin, essential for correct spindle organization (Zimmerman et al., 2004), forms a complex with IFT proteins and is required for assembly of primary cilia (Jurczyk et al., 2004). However, proteins that are essential for cilia function appear to be indispensable for cell cycle progression. The FA2p protein, discovered in a genetic screen for *Chlamydomonas* mutants defective in deflagellation (Finst et al., 1998), is essential for G2-M transition (Mahjoub et al., 2002). Rootletin, a major structural component of the ciliary rootlet (Yang et al., 2002), regulates centrosome cohesion and separation during the cell cycle (Bahe et al., 2005; Yang et al., 2006). Indeed, the association between cilia and proliferative diseases has already raised the idea that cystoproteins provide a functional signal relay between the cilium, the centrosome and the cell cycle. Inversin, a protein of the axoneme, basal body and centrosome, binds to the anaphase-promoting-complex protein Apc2 (Morgan et al., 2002). Moreover, the Bardet-Bield syndrome protein BBS4, a protein of the basal body and the centrosome, has been shown to target pericentriolar material 1 (PCM1) to the pericentriolar region and, therefore, to control cell division (Kim et al., 2004). Here, we show for the first time that an IFT protein controls also cell cycle progression. Recently, another IFT component, IFT20 has also been shown to localize to the centrosome; nevertheless, its knockdown has no effect on cell cycle progression (Follit et al., 2006). In our case, alteration of the levels of IFT88/polaris in non-ciliated cells induces the following cell cycle defects: (1) overexpression of IFT88/polaris interferes with the G1-S cell cycle transition leading to a higher incidence of apoptotic cell death; (2) by contrast, inhibition of IFT88/polaris expression leads to cell-cycle progression to S and G2/M phases. Previous studies report in *Tg737*^{orpk} mouse model that the pathology is associated with epithelial cell hyperproliferation (Richards et al., 1996; Zhang et al., 2005). On the basis of our findings, we propose that IFT88/polaris controls proliferation by regulating G1-S transition. Consistent with this idea, we demonstrate that IFT88/polaris interacts with Che-1, a key regulator for S phase entry. The role of Che-1 in cell proliferation is clearly linked to the growth-suppressing function of Rb (Bruno et al., 2002). Furthermore, we show that IFT88/polaris modulates Che-1 binding to Rb. Thus, we hypothesize that the overexpression of IFT88/polaris interferes with the G1-S cell cycle transition by titrating out Che-1, which is normally required at this crucial stage. It is tempting to speculate that, during cell cycle progression, IFT88/polaris, by interacting with Che-1, regulates its localization and/or its activity. It will be of interest to test this possibility and to identify other partners in order to better understand the molecular mechanisms by which IFT88/polaris controls G1-S transition.

The challenge is now to determine how dysfunction of primary cilia impacts upon processes such as cell cycle regulation. In vertebrates, primary cilia function as environmental sensors to transfer information from the extracellular space into the cell body (Davenport and Yoder, 2005). The ciliary membrane and cytoplasm are relatively isolated from cell body which offers the advantage of compartmentalization (Anderson, 1972), whereas IFT proteins allow for rapid transport of proteins between cilium and cell body (Kozminski et al., 1993). Cilia may provide information that help cells to remain in a differentiated state. Because cystoproteins change their subcellular localization according to the cell-cycle stage (Mollet et al., 2005; Morgan et al., 2002; Nurnberger et al., 2004; Sayer et al., 2006), cilia resorption may permit the redistribution of IFT proteins and/or ciliary proteins in the rest of the cell and, thus, promote cell-cycle progression. This model is fully compatible with our results on IFT88/polaris and suggests the existence of a mechanism that regulates proteins by shuttling them to the nucleus, the centrosome or to cilia.

Finally, we report a new cellular function for a component of the mammalian IFT by demonstrating that IFT88/polaris has a direct role in cell cycle progression. *C. elegans*, *Trypasoma brucei* and *Chlamydomonas* mutants for IFT88/polaris have not been shown to have defects in cell proliferation (Haycraft et al., 2001; Kohl et al., 2003; Pazour et al., 2000). This suggests that IFT88/polaris has others functions in higher eukaryotic organisms. In agreement with this idea, recent studies have demonstrated that IFT88/polaris is implicated in the regulation of the Sonic hedgehog signaling in mice (Liu et al., 2005); however, IFT mutations in *Drosophila* do not disrupt this pathway (Han et al., 2003). We can assume that polaris and, more generally, IFT proteins play roles in signaling pathways in vertebrates.

We are convinced that certain ciliary proteins are components of the cell cycle. Defining their role in this process will lead to a better understanding of the molecular mechanism involved in proliferative diseases such as PKD. Our findings may facilitate the understanding of the link between ciliary function and cellular response, and provide an entry point to define the dysfunctions associated with abnormal cilia formation.

Materials and Methods

Cell lines

HEK293T cells and HeLa cells that express or not centrin1-GFP were grown in Dulbecco's modified Eagle's medium (DMEM) (Gibco, BRL) with 10% foetal bovine serum (FBS), and penicillin and streptomycin (100 international unit (IU)/ml and 100 μg/ml, respectively). Human RPE1 cells were grown in DMEM–F-12 medium supplemented as above. Mouse lymphocytes (2A1.6) were grown in RPMI medium with 10% FBS, 1% β-mercaptoethanol, 5 mM sodium pyruvate, and penicillin and streptomycin (100 IU/ml and 100 μg/ml, respectively). All the cell lines were incubated at 37°C with 5% CO_2 atmosphere.

Construction of expression vectors

Constructs encoding the different domains of IFT88/polaris were engineered by PCR using the IFT88/polaris encoding cDNA as a template (*Tg737* cDNA 5.5). PCR fragments were then subcloned into the multicloning site of eukaryotic expression vectors: (1) pEGFP-N2 (Clontech), in fusion with GFP in C-terminal, (2) pGFP-C2, in fusion with GFP in N-terminal and (3) pcDNA3.1A (Invitrogen). All constructs were sequenced to verify intact reading frames. The series of deletion constructs used in this study is listed in Fig. 4A and were cloned in pEGFP-N2 (Clontech): Δ1 (amino acids 1-185), Δ2 (amino acids 1-430), Δ3 (amino acids 185-430), Δ4 (amino acids 294-441), Δ5 (amino acids 676-824), Δ6 (amino acids 330-824), Δ7 (amino acids 441-676).

Antibodies

Two antibodies against IFT88/polaris were generated according to the protocol of Agro-Bio (La Ferté St Aubin, France). The first antibody, IFT88/polaris-02078, was generated in rabbits by using a 21-residue-long peptide (NVHLAPETDEDDLYSGFNDYN) starting at position 3 of the mouse protein. For the anti-IFT88/polaris-740, a 1050-bp *Eco*RI digestion fragment of mouse IFT88/polaris (corresponding to amino acids 474-824) was cloned into the *Eco*RI site of the glutathione-S-transferase (GST) expression vector pGEX 4T1 (Pharmacia). Large-scale protein inductions were carried out, and the GST-IFT88/polaris fusion proteins were injected into rabbits for the production of polyclonal antibody. Commercial antibodies against γ-tubulin (GTU88, Sigma), α-tubulin (B-5-1-2, Sigma), acetylated tubulin (6-11B-1, Sigma), actin (I-19, Santa Cruz), Myc (9E10, Santa Cruz), Rb (sc-50, Santa Cruz), Akt (Cell Signaling) and cleaved caspase 3 (Asp175, Cell Signaling) were also used according to the manufacturer's instructions. Secondary antibodies against rabbit and mouse IgG conjugated to Alexa Fluor-488 (Molecular Probes) or Texas Red (Jackson) were used as well.

Centrosome subfractionation

Soluble, insoluble and centrosome fractions were isolated from 2A1.6 lymphocytes as described previously (Moudjou and Bornens, 1994). Pelleted centrosomes were incubated for 1 hour at 4°C with extraction buffer (20 mM Tris-HCl pH 7.4, 2 mM EDTA) alone, with 1D buffer (extraction buffer containing 0.5% NP-40 and 0.5% deoxycholate), with 2D buffer (extraction buffer containing 0.5% NP-40, 0.5% deoxycholate and 0.1% SDS) or with 8 M urea. Proteins were then fractionated into pellet (P) and supernatant (S) by centrifugation at 10,000 ***g*** for 15 minutes. Proteins were detected by various antibodies and visualized by enhanced chemiluminescence (ECL, Amersham Biosciences).

Transfections, drug treatments, and FACS analysis

For transient transfection, HeLa cells were seeded onto glass coverslips (22×22 mm; 3×10^5 cells) and transfected with 1 μg of plasmid DNA using transfecting reagent exgen500 (Euromedex). At the indicated time point post transfection, cells were washed with PBS and fixed either with 4% paraformaldehyde (PFA) (15 minutes at 4°C) or methanol (6 minutes at –20°C). For synchronization experiments, cells were treated with either thymidine (2.5 mM, for 16 hours) or with nocodazole (165 nM, for 12 hours). For microtubule depolymerization and regrowth, HeLa cells were incubated in 25 μM nocodazole at 37°C for 1 hour. Following drug removal, cells were incubated for the indicated times to allow microtubule regrowth, and fixed and processed for immunofluorescence as described above. For FACS analysis, cells were collected by trypsinization and fixed in 70% ethanol-PBS overnight at 4°C. Cells were then incubated with RNAse (100 μg/ml) for 30 minutes at room temperature, stained with 15 μg/ml propidium iodide and analyzed on a Beckman Coulter flow cytometer using a gate on GFP-positive cells. The percentages of cells in G1 and S phases and at G2-M transition were determined using the software Wincycle™.

Immunofluorescence

Cells grown on glass coverslips were fixed either in 4% PFA for 15 minutes at 4°C and permeabilized for 2 minutes with ice cold methanol or fixed and permeabilized directly for 6 minutes with ice cold methanol. After blocking with 10% goat serum in PBS (30 minutes), cells were incubated for 1 hour with primary antibodies, washed in PBS containing 0.1% Tween 20 and incubated in secondary antibodies for 30 minutes, all at room temperature. Hoechst 33342 (0.2 μg/ml, Sigma) was included in the final wash to counterstain nuclei. Samples were mounted on slides in fluorescent mounting medium (DakoCytomation). The percentage of cells undergoing DNA synthesis was estimated by counting the number of BrdU-labeled cells using the BrdU Detection Kit II (Roche). Images were usually taken using a Nikon Statif Eclipse E600 microscope with 63× magnification, 1.4-0.7 NA PL-APO objectives, a DXM1200 cooled CCD camera (Nikon) and ACT-1 (Universal Imaging). For studies of colocalizations with centriolar markers, *z*-axis stacks were collected using a piezoelectric device mounted at the base of a 63× magnification, 1.4 NA PL-APO objective on a Leica DMRA2 microscope, a Coolsnap HQ camera controlled by Metamorph software (Universal Imaging) was used. The *z*-axis stacks were compiled as single 2D projections using ImageJ software. All images were imported into Adobe Photoshop v5.0 for contrast adjustment and figure assembly.

Knockdown of IFT88/polaris expression using siRNA

We synthesized 21-mer nucleotide siRNA duplexes (designed by oligoengine), comprised of a 19 nucleotide duplex corresponding to IFT88/polaris in HeLa cells (siPol1, position 667 from start codon: CCGAAGCACUUAACACUUA; siPol2, position 1650 from start codon: CUGAAACUUCACGCAAUCC) and dTdT overhangs at each 3′-end (Sigma-Proligo). A non-silencing siRNA-scramble was also used as control. For transfection, each duplex was mixed with oligofectamine (Invitrogen) according to the manufacturer's protocol and introduced (24 hours after plating) into cells cultured in 6-well plates. Analyses were performed 24 and 48 hours post transfection.

Yeast two hybrid screen

The entire coding sequence of mouse IFT88/polaris was subcloned into the bait plasmid pBTM116 to create pBTM116-Tg737. The *Saccharomyces cerevisiae* strain Y190, carrying *Gal4-LacZ* and *Gal4*-histidine fusion genes, was transformed with the bait construct and a human liver cDNA library (clontech) in the prey plasmid, pACT2. Transformants were first selected for histidine prototrophy and then assayed for induction of β-galactosidase activity. Plasmids from positive clones were rescued into *Escherichia coli* and re-transformed into L40 containing either pBTM116-Tg737 or pBTM116. The sequences were compared with the database using the blast program.

Immunoprecipitation

For immunoprecipitation experiments cells were lysed at 4°C for 30 minutes in lysis buffer (50 mM Tris-HCl pH 8, 150 mM NaCl, 10% glycerol, 1% Nonidet P-40, 0.5 mM EDTA, and 0.5 mM EGTA, protease inhibitor cocktail (Roche). After high-speed centrifugation, the lysates were immunoprecipitated by standard procedures using mouse anti-Myc monoclonal antibody clone 9E10 (Santa Cruz) or as described previously with Che-1 antibody (Bruno et al., 2002).

Data analysis and statistic

All values for statistical significance represent the mean ± standard deviation (s.d.). Mean values were compared using the Student's *t*-test. All comparisons of statistical significance have *P* values of $P<0.05$.

The authors thank M. Bornens and P. Bastin for their critical evaluation of this manuscript and all members of the lab for fruitful discussion. A.R. was supported by a doctoral fellowship from the Research Minister and from the Association pour la Recherche sur le Cancer (ARC). This study was supported by grants from Institut National de la Santé et de la Recherche Médicale (INSERM) and by ARC3259. We thank E. Nigg for GFP–C-Nap1 plasmid, M. Fanciulli for the anti-Che-1 antibody and the Myc-Che-1 plasmid, T. Schoer for the Dsred-p150$^{217\text{-}548}$ plasmid and B. Yoder for *Tg737* cDNA 5.5.

References

Anderson, R. G. (1972). The three-dimensional structure of the basal body from the rhesus monkey oviduct. *J. Cell Biol.* **54**, 246-265.

Badano, J. L., Teslovich, T. M. and Katsanis, N. (2005). The centrosome in human genetic disease. *Nat. Rev. Genet.* **6**, 194-205.

Bahe, S., Stierhof, Y. D., Wilkinson, C. J., Leiss, F. and Nigg, E. A. (2005). Rootletin forms centriole-associated filaments and functions in centrosome cohesion. *J. Cell Biol.* **171**, 27-33.

Bornens, M. (2002). Centrosome composition and microtubule anchoring mechanisms. *Curr. Opin. Cell Biol.* **14**, 25-34.

Bruno, T., De Angelis, R., De Nicola, F., Barbato, C., Di Padova, M., Corbi, N., Libri, V., Benassi, B., Mattei, E., Chersi, A. et al. (2002). Che-1 affects cell growth by interfering with the recruitment of HDAC1 by Rb. *Cancer Cell* **2**, 387-399.

Cole, D. G., Diener, D. R., Himelblau, A. L., Beech, P. L., Fuster, J. C. and Rosenbaum, J. L. (1998). *Chlamydomonas* kinesin-II-dependent intraflagellar transport (IFT): IFT particles contain proteins required for ciliary assembly in Caenorhabditis elegans sensory neurons. *J. Cell Biol.* **141**, 993-1008.

Davenport, J. R. and Yoder, B. K. (2005). An incredible decade for the primary cilium: a look at a once-forgotten organelle. *Am. J. Physiol. Renal Physiol.* **289**, F1159-F1169.

Doxsey, S. (2001). Re-evaluating centrosome function. *Nat. Rev. Mol. Cell Biol.* **2**, 688-698.

Fanciulli, M., Bruno, T., Di Padova, M., De Angelis, R., Iezzi, S., Iacobini, C., Floridi, A. and Passananti, C. (2000). Identification of a novel partner of RNA polymerase II subunit **11**, Che-1, which interacts with and affects the growth suppression function of Rb. *FASEB J.* **14**, 904-912.

Finst, R. J., Kim, P. J. and Quarmby, L. M. (1998). Genetics of the deflagellation pathway in *Chlamydomonas*. *Genetics* **149**, 927-936.

Follit, J. A., Tuft, R. A., Fogarty, K. E. and Pazour, G. J. (2006). The intraflagellar transport protein IFT20 is associated with the golgi complex and is required for cilia assembly. *Mol Biol. Cell* **17**, 3781-3792.

Fukasawa, K. (2002). Introduction. Centrosome. *Oncogene* **21**, 6140-6145.

Han, Y. G., Kwok, B. H. and Kernan, M. J. (2003). Intraflagellar transport is required in Drosophila to differentiate sensory cilia but not sperm. *Curr. Biol.* **13**, 1679-1686.

Haycraft, C. J., Swoboda, P., Taulman, P. D., Thomas, J. H. and Yoder, B. K. (2001). The C. elegans homolog of the murine cystic kidney disease gene Tg737 functions in a ciliogenic pathway and is disrupted in osm-5 mutant worms. *Development* **128**, 1493-1505.

Hildebrandt, F. and Otto, E. (2005). Cilia and centrosomes: a unifying pathogenic concept for cystic kidney disease? *Nat. Rev. Genet.* **6**, 928-940.

Hinchcliffe, E. H. and Sluder, G. (2001). "It takes two to tango": understanding how centrosome duplication is regulated throughout the cell cycle. *Genes Dev.* **15**, 1167-1181.

Jurczyk, A., Gromley, A., Redick, S., San Agustin, J., Witman, G., Pazour, G. J., Peters, D. J. and Doxsey, S. (2004). Pericentrin forms a complex with intraflagellar transport proteins and polycystin-2 and is required for primary cilia assembly. *J. Cell Biol.* **166**, 637-643.

Kim, J. C., Badano, J. L., Sibold, S., Esmail, M. A., Hill, J., Hoskins, B. E., Leitch, C. C., Venner, K., Ansley, S. J., Ross, A. J. et al. (2004). The Bardet-Biedl protein BBS4 targets cargo to the pericentriolar region and is required for microtubule anchoring and cell cycle progression. *Nat. Genet.* **36**, 462-470.

Kohl, L., Robinson, D. and Bastin, P. (2003). Novel roles for the flagellum in cell morphogenesis and cytokinesis of trypanosomes. *EMBO J.* **22**, 5336-5346.

Kozminski, K. G., Johnson, K. A., Forscher, P. and Rosenbaum, J. L. (1993). A motility in the eukaryotic flagellum unrelated to flagellar beating. *Proc. Natl. Acad. Sci. USA* **90**, 5519-5523.

Liu, A., Wang, B. and Niswander, L. A. (2005). Mouse intraflagellar transport proteins regulate both the activator and repressor functions of Gli transcription factors. *Development* **132**, 3103-3111.

Mahjoub, M. R., Montpetit, B., Zhao, L., Finst, R. J., Goh, B., Kim, A. C. and Quarmby, L. M. (2002). The FA2 gene of *Chlamydomonas* encodes a NIMA family kinase with roles in cell cycle progression and microtubule severing during deflagellation. *J. Cell Sci.* **115**, 1759-1768.

Mayor, T., Hacker, U., Stierhof, Y. D. and Nigg, E. A. (2002). The mechanism regulating the dissociation of the centrosomal protein C-Nap1 from mitotic spindle poles. *J. Cell Sci.* **115**, 3275-3284.

Mollet, G., Silbermann, F., Delous, M., Salomon, R., Antignac, C. and Saunier, S. (2005). Characterization of the nephrocystin/nephrocystin-4 complex and subcellular localization of nephrocystin-4 to primary cilia and centrosomes. *Hum. Mol. Genet.* **14**, 645-656.

Morgan, D., Eley, L., Sayer, J., Strachan, T., Yates, L. M., Craighead, A. S. and Goodship, J. A. (2002). Expression analyses and interaction with the anaphase promoting complex protein Apc2 suggest a role for inversin in primary cilia and involvement in the cell cycle. *Hum. Mol. Genet.* **11**, 3345-3350.

Moudjou, M. and Bornens, M. (1994). *Cell Biology: A Laboratory Handbook*. New York: Academic Press.

Moyer, J. H., Lee-Tischler, M. J., Kwon, H. Y., Schrick, J. J., Avner, E. D., Sweeney, W. E., Godfrey, V. L., Cacheiro, N. L., Wilkinson, J. E. and Woychik, R. P. (1994). Candidate gene associated with a mutation causing recessive polycystic kidney disease in mice. *Science* **264**, 1329-1333.

Murcia, N. S., Richards, W. G., Yoder, B. K., Mucenski, M. L., Dunlap, J. R. and Woychik, R. P. (2000). The Oak Ridge Polycystic Kidney (orpk) disease gene is required for left-right axis determination. *Development* **127**, 2347-2355.

Nigg, E. A. (2002). Centrosome aberrations: cause or consequence of cancer progression? *Nat. Rev. Cancer* **2**, 815-825.

Nurnberger, J., Kribben, A., Opazo Saez, A., Heusch, G., Philipp, T. and Phillips, C. L. (2004). The Invs gene encodes a microtubule-associated protein. *J. Am. Soc. Nephrol.* **15**, 1700-1710.

Pan, J., Wang, Q. and Snell, W. J. (2004). An aurora kinase is essential for flagellar disassembly in *Chlamydomonas*. *Dev. Cell* **6**, 445-451.

Pazour, G. J., Dickert, B. L., Vucica, Y., Seeley, E. S., Rosenbaum, J. L., Witman, G. B. and Cole, D. G. (2000). *Chlamydomonas* IFT88 and its mouse homologue, polycystic kidney disease gene tg737, are required for assembly of cilia and flagella. *J. Cell Biol.* **151**, 709-718.

Piel, M., Meyer, P., Khodjakov, A., Rieder, C. L. and Bornens, M. (2000). The respective contributions of the mother and daughter centrioles to centrosome activity and behavior in vertebrate cells. *J. Cell Biol.* **149**, 317-330.

Piel, M., Nordberg, J., Euteneuer, U. and Bornens, M. (2001). Centrosome-dependent exit of cytokinesis in animal cells. *Science* **291**, 1550-1553.

Qin, H., Rosenbaum, J. L. and Barr, M. M. (2001). An autosomal recessive polycystic kidney disease gene homolog is involved in intraflagellar transport in C. elegans ciliated sensory neurons. *Curr. Biol.* **11**, 457-461.

Quarmby, L. M. and Parker, J. D. (2005). Cilia and the cell cycle? *J. Cell Biol.* **169**, 707-710.

Richards, W. G., Yoder, B. K., Isfort, R. J., Detilleux, P. G., Foster, C., Neilsen, N., Woychik, R. P. and Wilkinson, J. E. (1996). Oval cell proliferation associated with the murine insertional mutation TgN737Rpw. *Am. J. Pathol.* **149**, 1919-1930.

Rieder, C. L., Jensen, C. G. and Jensen, L. C. (1979). The resorption of primary cilia during mitosis in a vertebrate (PtK1) cell line. *J. Ultrastruct. Res.* **68**, 173-185.

Rieder, C. L., Faruki, S. and Khodjakov, A. (2001). The centrosome in vertebrates: more than a microtubule-organizing center. *Trends Cell Biol.* **11**, 413-419.

Rosenbaum, J. L. and Witman, G. B. (2002). Intraflagellar transport. *Nat. Rev. Mol. Cell Biol.* **3**, 813-825.

Salisbury, J. L., Whitehead, C. M., Lingle, W. L. and Barrett, S. L. (1999). Centrosomes and cancer. *Biol. Cell* **91**, 451-460.

Sayer, J. A., Otto, E. A., O'Toole, J. F., Nurnberg, G., Kennedy, M. A., Becker, C., Hennies, H. C., Helou, J., Attanasio, M., Fausett, B. V. et al. (2006). The centrosomal protein nephrocystin-6 is mutated in Joubert syndrome and activates transcription factor ATF4. *Nat. Genet.* **38**, 674-681.

Sorokin, S. (1962). Centrioles and the formation of rudimentary cilia by fibroblasts and smooth muscle cells. *J. Cell Biol.* **15**, 363-377.

Wheatley, D. N., Wang, A. M. and Strugnell, G. E. (1996). Expression of primary cilia in mammalian cells. *Cell Biol. Int.* **20**, 73-81.

Yang, J., Liu, X., Yue, G., Adamian, M., Bulgakov, O. and Li, T. (2002). Rootletin, a novel coiled-coil protein, is a structural component of the ciliary rootlet. *J. Cell Biol.* **159**, 431-440.

Yang, J., Adamian, M. and Li, T. (2006). Rootletin interacts with C-Nap1 and may function as a physical linker between the pair of centrioles/basal bodies in cells. *Mol. Biol. Cell* **17**, 1033-1040.

Yoder, B. K., Hou, X. and Guay-Woodford, L. M. (2002a). The polycystic kidney disease proteins, polycystin-1, polycystin-2, polaris, and cystin, are co-localized in renal cilia. *J. Am. Soc. Nephrol.* **13**, 2508-2516.

Yoder, B. K., Tousson, A., Millican, L., Wu, J. H., Bugg, C. E., Jr, Schafer, J. A. and Balkovetz, D. F. (2002b). Polaris, a protein disrupted in orpk mutant mice, is required for assembly of renal cilium. *Am. J. Physiol. Renal Physiol.* **282**, F541-F552.

Zhang, Q., Davenport, J. R., Croyle, M. J., Haycraft, C. J. and Yoder, B. K. (2005). Disruption of IFT results in both exocrine and endocrine abnormalities in the pancreas of Tg737(orpk) mutant mice. *Lab. Invest.* **85**, 45-64.

Zimmerman, W. C., Sillibourne, J., Rosa, J. and Doxsey, S. J. (2004). Mitosis-specific anchoring of gamma tubulin complexes by pericentrin controls spindle organization and mitotic entry. *Mol. Biol. Cell* **15**, 3642-3657.

Journal of Cell Science

- Brants J., Semenchenko K., Wasylyk C., Robert A., Carles A., Zambrano A., Pradeau-Aubreton K., Birck C., Schalken J., Poch O., de Mey J., and Wasylyk B. *Tubulin Tyrosine Ligase Like 12, a novel TTLL family member with SET- and TTL-like domains and roles in histone and tubulin modifications and mitosis. Plos One décembre 2012*

OPEN ACCESS Freely available online

PLOS ONE

Tubulin Tyrosine Ligase Like 12, a TTLL Family Member with SET- and TTL-Like Domains and Roles in Histone and Tubulin Modifications and Mitosis

Jan Brants[1], Kostyantyn Semenchenko[1], Christine Wasylyk[1], Aude Robert[2], Annaick Carles[1], Alberto Zambrano[1], Karine Pradeau-Aubreton[1], Catherine Birck[1], Jack A. Schalken[3], Olivier Poch[1], Jan de Mey[2], Bohdan Wasylyk[1]*

1 Institut de Génétique et de Biologie Moléculaire et Cellulaire, UMR 7104 CNRS UDS - U 964 INSERM , Illkirch, France, **2** Université de Strasbourg, Ecole Supérieure de Biotechnologie de Strasbourg C.N.R.S. - U.M.R.7100, Equipe ''Microtubules et Morphogenèse'', Parc d'Innovation, Illkirch, France, **3** Department of Urology, Radboud University Nijmegen Medical Centre, Nijmegen, The Netherlands

Abstract

hTTLL12 is a member of the tubulin tyrosine ligase (TTL) family that is highly conserved in phylogeny. It has both SET-like and TTL-like domains, suggesting that it could have histone methylation and tubulin tyrosine ligase activities. Altered expression of hTTLL12 in human cells leads to specific changes in H4K20 trimethylation, and tubulin detyrosination, hTTLL12 does not catalyse histone methylation or tubulin tyrosination in vitro, as might be expected from the lack of critical amino acids in its SET-like and TTLL-like domains. hTTLL12 misexpression increases mitotic duration and chromosome numbers. These results suggest that hTTLL12 has non-catalytic functions related to tubulin and histone modification, which could be linked to its effects on mitosis and chromosome number stability.

Citation: Brants J, Semenchenko K, Wasylyk C, Robert A, Carles A, et al. (2012) Tubulin Tyrosine Ligase Like 12, a TTLL Family Member with SET- and TTL-Like Domains and Roles in Histone and Tubulin Modifications and Mitosis. PLoS ONE 7(12): e51258. doi:10.1371/journal.pone.0051258

Editor: Axel Imhof, Ludwig-Maximilians-Universität München, Germany

Received September 13, 2012; **Accepted** October 30, 2012; **Published** December 12, 2012

Funding: The authors are thankful for the financial support from the European Union (FP5 Procure project QLK6-2000-00159 and FP6 Prima project #504587), the Ligue Nationale Française contre le Cancer, the Ligues Départementales de Lutte contre le Cancer (Haut- and Bas-Rhin), the Association pour la Recherche sur le Cancer, the Centre National de la Recherche Scientifique, and the Institut National de la Santé et de la Recherche Médicale, the Cancéropôle Grand-Est (Axe IV and DKFZ-CGE projects) and INCa (PL099). The funders had no role in study design, data collection and analysis, decision to publish, or preparation of the manuscript.

Competing Interests: The authors have declared that no competing interests exist.

* E-mail: boh@igbmc.fr

Introduction

The human genome codes for may proteins that have not been assigned a validated function. In our screens of RNAs that are differentially expressed in tumours, we identified a number of encoded proteins with unknown functions that could potentially be targeted for therapeutic intervention [1]. We selected hTTLL12 for further study, since it has enzymic features. We showed that hTTLL12 is expressed in the proliferating layer of benign human prostate, and expression increases during cancer progression to metastasis. Overexpression alters chromosomal ploidy. These results raise the possibility that hTTLL12 could contribute to tumorigenesis through effects on chromosome number stability [2]. In order to study whether hTTLL12 may have enzymatic activity, we used sequence homology searches to reveal the presence of SET-like and TTL-like domains in the N- and C-terminal parts of the molecule, respectively.

SET domains are approximately 130 amino acids long and have been found in all eukaryotic organisms studied so far. Their principle function is to transfer a methyl group from S-adenosyl-L-methionine (SAM) to the ε-amino group of lysine residues on histones or other proteins. Various histone lysine residues are methylated, and the combination of these methylations and other covalent modifications constitutes ''the histone code'' that has epigenetic functions and regulates various cellular processes, such as transcription and the organization of chromatin. Chromatin condensation and compaction are essential for rapid chromosome congression and accurate chromosome segregation during cell division [reviews: [3,4,5,6,7]].

TTL domains are approximately 350 amino acid modules that catalyze ligation of amino acids to tubulins or other substrates. The TTL domain contains ATP-grasp-like motifs that correspond to the ATP/Mg^{2+} binding site typical of enzymes with ATP-dependent carboxylate-amine/thiol ligase activity [8]. This domain is present in a family of proteins that has 14 members in mouse. They have been shown to ligate tyrosine (TTL), glutamate (TTLL1, 4, 5, 6, 7, 9, 11 and 13) or glycine (TTLL3, 8 and 10) to the C-terminal tails of α/β tubulin. TTL re-adds tyrosine to α-tubulin that has been terminally detyrosinated, in a process called the TTL cycle. TTLL1, 4, 5 and 7 ligate an initial glutamate to a glutamic acid side chain through iso-peptide bonds, whereas TTLL 6, 7, 9, 11 and 13 elongate polyglutamate chains through peptide bonds. In related reactions, TTLL3 and 8 ligate glycine to a glutamic acid side chain, whereas TTLL3 and 10 elongate polyglycine chains. Tubulin C-terminal tails are hotspots for complex patterns of modifications, with important roles in cellular processes that include subcellular organization, intracellular transport, cell movement and mitosis [reviews: [9,10,11,12,13]]. The complexity and importance of tubulin

modifications has led to the analogy being made between the "tubulin code" and the better established "histone code" [14,15].

hTTLL12 is the least characterized and most unusual member of the TTL family. We report its effects on histone and tubulin modifications, mitotic duration and chromosome numbers. hTTLL12 does not appear to have detectable in-vitro enzymatic activity related to the changes observed in cells. We raise the possibility that hTTLL12 is an inactive pseudo-enzyme that has important regulatory roles, similar to pseudo-enzymes in other protein families.

Materials and Methods

Materials

Details for vector constructs, siRNAs, antibody generation, commercial antibodies and their dilutions used for western blotting (WB) and immunocytochemistry, are described in Supporting Information.

Databases searches

The initial step was an iterated PSI-BLAST search with the full-length human hTTLL12 CDS against the nr database of NCBI until convergence occurred. Similar PSI-BLAST searches were performed using the C-terminal TTL-like domain and the N-terminal unknown region [16].

Multiple sequence alignments and phylogenetic trees

For each domain or region, the detected homologs were included in a clustered multiple alignment of complete sequences (MACS) constructed using the PipeAlign program suite [17] and subsequently manually adjusted. For the MACS of the N-terminal of hTTLL12, SET domain containing proteins were retrieved from PFAM (PF00856). Human SET domain proteins were retained and aligned with the hTTLL12 sequence through ClustalX and manually adjusted. The MACS of the TTL domain was made using representative sequences for each human TTL-like and TTL protein. All MACSs and details about the proteins included are available in data. The PhyloWin program [18] was used to generate the phylogenetic tree based on 212 positions of the TTL domain MACS and using the neighbour-joining reconstruction algorithm with pair-wise gap removal option and 1000 bootstrap replicates. The trees were edited and displayed with TreeView [19].

Cell culture, transfection and generation of stable clones

HEp-2 cells (ATCC CCL-23) were grown in modified Eagle's medium (MEM), 10% foetal calf serum, 0.1 mM nonessential amino acids, 1 mM Na-pyruvate, 40 μg/ml gentamicin at 37°C in a humidified 5% CO_2 atmosphere. siRNA transfections were performed using Lipofectamine (Invitrogen) according to the manufacturer's protocol. In brief, 100,000 cells per well were seeded in a 12 well plate, grown for 18 hours followed by 3 hours OPTIMEM incubation and transfection during 6 hours. After transfection, medium was changed to normal growth medium and incubated as indicated until cell lysis. To obtain stable clones, HEp-2 cells were transfected with the Flag-*hTTLL12* expression plasmid, the empty pSG5-puro-Flag plasmid [20] or the as*hTTLL12* expression plasmid using the BBS calcium phosphate method [21]. 48 hours post-transfection, cells were passaged into selection medium containing 3 μg/ml puromycin, renewed every three days. 10–14 days post-transfection, we characterized five positive clones per stable transfection by immunofluorescence and WB giving rise to hTTLL12 clones A-E and Control clones A–E. Since we did not observe significant difference between as*hTTLL12* clones and empty vector clones by various criteria we considered the ashTTLL12 clones as additional negative controls (Control clones F–G).

SDS-PAGE and WB

Standard procedures were used (see Supporting Experimental Procedures S1 for details).

Co-immunoprecipitation

Nuclear extracts from hTTLL12_A, _B and _C clones were prepared using the Nuclear Complex Co-IP Kit (Active Motif) according to the manufacturer's instructions. For tubulin co-immunoprecipitation, 75% confluent hTTLL12 or control clones were washed thrice with cold 1× PBS, lysed in RIPA buffer (30 minutes, ice), scraped and cleared (12,000 g, 2 minutes). After protein quantification of the supernatants (Bradford assay, BioRad), 1 mg of proteins was pre-cleared with 100 μl of protein A-Sepharose (Sigma-Aldrich, 30 minutes, 4°C). After centrifugation, supernatants were mixed to 100 μl of M2-sepharose (Sigma-Aldrich) and incubated for 90 minutes at 4°C. Beads were washed thrice, bound proteins were eluted by boiling in 100 μl 2× SDS sample buffer (10 minutes) and centrifuged (10,000 g, 30 seconds). The resulting supernatants were fractionated on a 8.5% SDS-PAGE gel and WB was performed as described above.

Immunocytochemistry and Confocal Microscopy

Standard procedures were used (see Supporting Experimental Procedures S1 for details).

Cell cycle synchronisation by double thymidine block

Cells were plated on 10 cm dishes in an amount (≈750,000) that would give 80% confluence in 4–5 days. After about 24 h after plating, medium with 0.2 μM thymidine was applied for 23 h, then changed for fresh medium for 9 h, and again with thymidine for 23 h. Cells were collected at 2 h time intervals for 18–24 h for FACS analysis for DNA content. Time points in which cells were predominantly in the S1, G2/M and G1 phase were selected for WBs.

Time-lapse microscopy

Control clones, hTTLL12 clones or parental HEp-2 cells were seeded at a density of 200,000 cells/2 ml in six well cell culture plates. siRNA transfection of parental HEp-2 cells was performed as described above. 48 hours after seeding of the stable clones, or 72 hours after siRNA transfection [3 non-targeting control siRNAs (siScramble, siLuciferase and siCtrl), or one of 6 hTTLL12-sepecific siRNAs (sihTTLL12_1-6)], cell cultures were stained with vital Hoechst (3.3 μg/ml, Hoechst 33258, Molecular Probes) during 30 minutes at 37°C and grown on a video microscopy platform in a humidified 5% CO_2 atmosphere. Images were acquired in phase contrast and UV at 1 minute intervals during 4 hours (Control and hTTLL12 clones) or 3 minutes intervals during 10 hours (siRNA transfected cells) using a CCD camera with a 40×//0.55 N-Plan objective in an inverted motorized microscope (DMIRE2, Leica). Analyses were performed using ImageJ software (http://rsb.info.nih.gov/ij/). Mitotic duration was scored from cells that had one, normal-sized, nucleus. The following numbers of cells were used to analyse: (a) mitotic duration, 205 (HEp-2), 263 (Control clones), 372 (hTTLL12 clones), 591 (siControl transfected Hep-2), and 899 (sihTTLL12 transfected Hep-2); (b) spindle positioning, 262 (HEp-2), 420 (Control clones), 380 (hTTLL12 clones), 502 (siControl transfected Hep-2), and 973 (sihTTLL12 transfected Hep-2); (c)

congression delay, 420 (Control clones), 491 (hTTLL12 clones), 502 (siControl transfected Hep-2), and 852 (sihTTLL12 transfected Hep-2).

Cell growth

3,000 cells of hTTLL12 and Control clones (hTTLL12_A-E and Control_A-E) were seeded per well of a 96 well plate. Cell proliferation was assayed using the MTT-based colorimetric assay (Chemicon Int.) following the manufacturer's instructions.

Cell cycle analysis

Unsynchronized exponentially growing cells were fixed in 70% ethanol (−20°C), washed and stained with propidium iodide. Detached cell populations were collected and combined with adherent cells for all experiments. FACScalibur cytometer (Becton Dickinson) and Cellquest software were used for acquisition, and Modifit software (Verity) for cell cycle analysis.

In-vitro assays for histone methyl transferase and tubulin tyrosine ligase and purification of proteins

Standard procedures were used as detailed in the Experimental Procedures.

Statistics

Statistical analyses were carried out by Student's *t*-test.

Results

Domain structure and phylogenetic distribution of hTTLL12

We initially characterised human hTTLL12 using bioinformatics. There are thirteen human proteins with homology to the hTTLL12 C-terminal TTL domain (Figure 1A, Alignment S1) [22,23]. The phylogenetic tree, based on the sequences of the TTL domains (Figure 1B), has a relatively long branch for hTTLL12 compared to the other hTTL-like proteins, indicating that it is one of the most divergent. The core TTL domain (416–642) of hTTLL12 has a N-terminal extension (353–415) with weak homology to the extended domains of the other hTTL family members (Alignment S1 and data not shown). Despite the overall similarity, the TTL domain of hTTLL12 has distinct features. It lacks 2 of the six sequences predicted to bind ATP and Mg^{2+} in the other TTL domains (Figure 1A, grey lines). It also lacks three of the seven conserved motifs found in the other TTL family members (Table S1). In addition, it contains specific residues that are conserved in TTLL12s from other species (Table S1). Interestingly, TTLL12 is widely conserved; it is found in simple eukaryotes (Entamoeba, Trypanosomes, Paramecium, Tetrahymena, Hydra), plants [monocots (*Oryza sativa*, Indian rice), eudicots (*Arabidopsis thaliana*)], nematodes (*Caenorhabditis elegans*, etc.), flies (*Drosophila melanogaster*, etc.) and higher eukaryotes (data not shown). The conserved sequences include the N-terminal region, which has a SET-like domain according to PSI-BLAST [16] (amino acids 91 to 249 of hTTLL12; Figure 1A). This sequence aligns with human SET domain proteins from PFAM (Alignment S2), and is most related to the SET domains of SETD3, SETD4 and SETD6 (Figure 1C). Some of its sequences are highly conserved in other human SET domains (see Table S2; letters colours indicate degrees of conservation; red: absolutely conserved; blue: very highly conserved; black: highly conserved). The highly conserved sequences correspond to SET domain structural elements, including β-strands, an α-helix and a linker region [6]. The hTTLL12 SET-like domain appears to contain an insert, as found in iSET domains [24]. This insert lies between amino acids 158–188 (Alignment S2). Several plant and protozoan orthologues have an additional sequence inserted in a position equivalent to 160 of hTTLL12, indicating that these orthologues have an iSET domain with a large insert. In summary, hTTLL12 appears to be an atypical member of the TTL protein family, from the presence of a SET-like domain, the loss of conserved residues found in other TTL family proteins, and the conservation of hTTLL12-specific features throughout many species.

hTTLL12 selectively affects trimethylation of histone H4K20 in cells

Since SET domain proteins methylate histone lysines [reviewed in [25]], we studied whether hTTLL12 affects methylation of histones H3 and H4. We generated stable clones of HEp-2 that overexpress Flag-hTTLL12 (hTTLL12_A-E), and control clones with the corresponding empty Flag-expression vector (Control_A-E). Western blots (WBs) of total cell extracts were probed with antibodies against hTTLL12, specific methylated forms of H4K20, H3K9, H3K4 and H3K27, and a loading control (TBP); suitably exposed films were quantitated (Figure 2A, see lanes 1–6 for representative blots and the histogram for quantification). hTTLL12 overexpression increased the levels of H4K20 trimethylation ($p = 0.005$), without affecting total H4 protein levels (data not shown), or any of the other modifications investigated. We then studied knockdown of hTTLL12 with siRNAs. Decreasing hTTLL12 levels decreased H4K20me3 levels ($p = 0.029$; Figure 2B; a representative WB is shown; the histogram combines the results from four sihTTLL12 and four control siRNAs in replicated experiments), whereas H3K9me3 levels were not changed. These results show that up and down regulation of hTTLL12 have opposing effects on H4K20 trimethylation. In order to investigate whether there is a direct connection between hTTLL12 and chromatin, we tested whether hTTLL12 interacts with histones and chromatin components such as HP1 isoforms [26,27]. We found that immunoprecipitates of Flag-hTTLL12 from nuclear extracts of hTTLL12 overexpressing clones contained HP1γ the nucleosomal component histone H3 and H4K20me3 (Figure 2C). These proteins were not detected in the controls, in which Flag-hTTLL12 pull down was inhibited with the Flag peptide, indicating that the interactions were specific. These results show that hTTLL12 interacts with chromatin components.

hTTLL12 affects the levels of detyrosinated tubulin

hTTLL12 has a TTL-like domain, suggesting that it might affect tubulin tyrosination. We measured the effects of increasing and decreasing hTTLL12 levels in HEp-2 on detyrosinated tubulin levels by WB with a specific antibody. hTTLL12 overexpression in the stable clones resulted in a significant nearly two-fold increase in detyrosinated tubulin levels, compared to the control clones ($p = 0.003$; Figure 3A, see the representative WB and the combined data from 4 overexpression and 5 control clones). Knockdown of endogenous hTTLL12 in HEp-2 cells also resulted in a significant increase in detyrosinated tubulin levels ($p = 8.8\ 10^{-5}$; Figure 3B; a representative WB is shown; the histogram combines the results from six sihTTLL12 and four control siRNAs in replicated experiments). As expected, TTL knockdown also increased detyrosinated tubulin levels, but to a greater extent than knockdown of hTTLL12, even though the extents of knockdown were similar (80% or more, 2 siTTLs and 6 sihTTLL12s; data not shown). We were not able to detect corresponding changes in tyrosinated tubulin, most likely due to the technical limitations of WB and dot-blots. These techniques

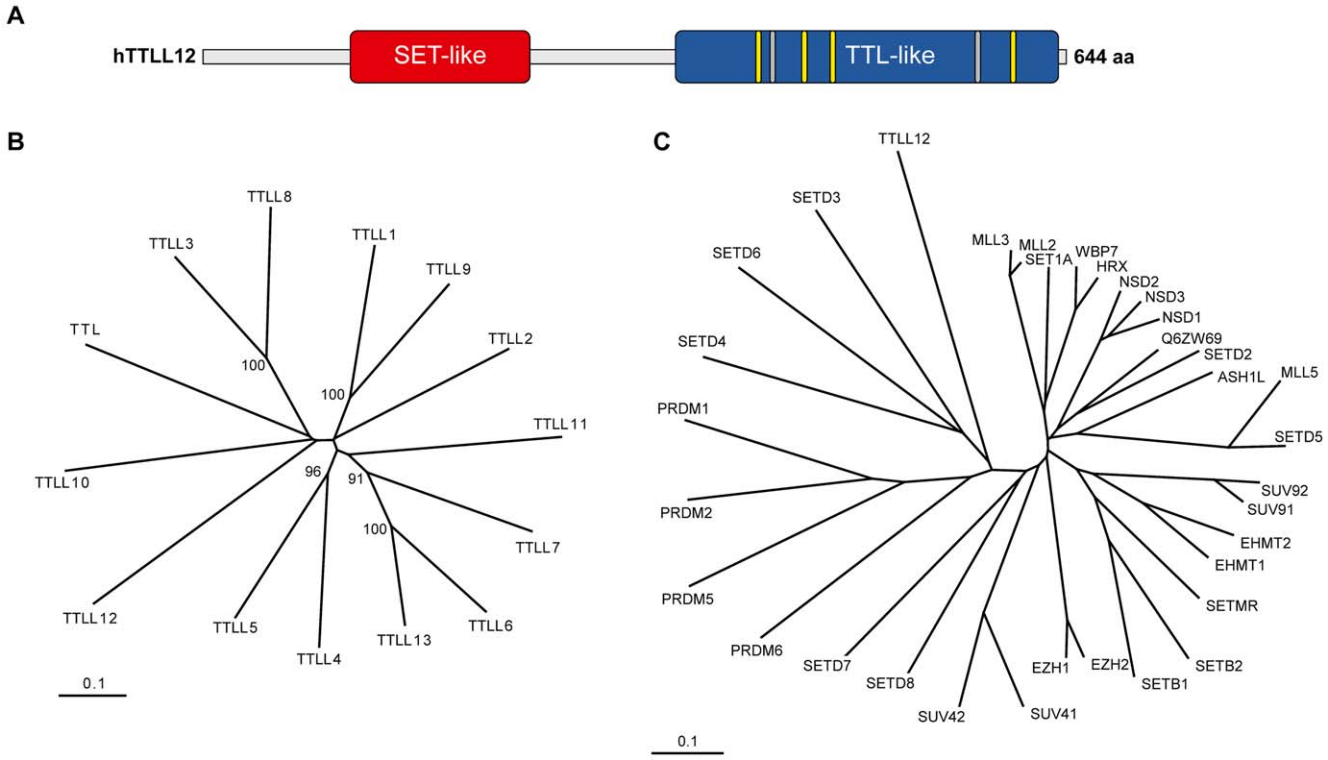

Figure 1. hTTLL12, domain organisation and similarity with other proteins. *A.* Schematic representation. Red indicates the SET-like domain (amino acids 91–249), blue the TTL-like domain (amino acids 353–642), yellow or grey the predicted ATP and Mg^{2+} binding amino acid motifs that are respectively conserved (WICK$^{416–419}$, SKYI$^{450–453}$, DIRY$^{470–473}$, EVN$^{605–607}$), or non-conserved (SLDT$^{426–429}$ and RAMYAVD$^{578–584}$) in hTTLL12. *B, C.* Phylogenetic trees of the TTL domains of the human TTL family based on Alignment S1 *(B)* and the SET-like domain of hTTLL12 and human SET domains based on Alignment S2 *(C)*. Bootstrap values are provided for significant nodes when they are >80%. Multiple sequence alignments are available as data.
doi:10.1371/journal.pone.0051258.g001

did not accurately detect the small proportional changes that we would expect to find (about 10%). Hep-2 express a high proportion of tyrosinated tubulin relatively to detyrosinated tubulin (data not shown), which reduces the proportional change of tyrosinated tubulin that would result from conversion to detyrosinated tubulin. Nevertheless, we did find that changes in hTTLL12 levels increase tubulin detyrosination.

The effects of hTTLL12 on tubulin modification may result from interactions with α-tubulin and tubulin-associated structures in the cell. To detect interacting proteins, we immuno-purified Flag-hTTLL12 from overexpressing clones with anti-Flag affinity columns. Proteins that co-purified with Flag-hTTLL12 from overexpressing clones were dissociated by boiling in loading buffer and analysed by WB. α-tubulin was detected in extracts prepared from the Flag-hTTLL12 overexpressing clones (Figure 3C, lane 3, and data not shown), but not from cells that overexpress Flag-NudCD2 (a different protein, lane 2) or from parental cells (lane 1). We also analysed proteins eluted with the FLAG peptide by SDS-PAGE electrophoresis, silver staining and mass spectrometry. One of the bands, that migrated around 50 kDa (the size of α-tubulin) and that was not present in the sample purified from a control clone, was shown to be α-tubulin by mass spectrometry (Figure S1 and Table S3). These results suggest that hTTLL12 interacts specifically with α-tubulin.

We have previously reported that hTTLL12 co-localises with the mitotic spindle during mitosis [2]. We verified that hTTLL12 has a similar location in HEp-2 cells. Cells were fixed, permeabilised and stained with antibodies against hTTLL12 and fluorescently labelled secondary antibodies, and observed by confocal microscopy. The staining was specific, since knockdown with different sihTTLL12s strongly decreased staining intensity (data not shown). hTTLL12 (red; Figure S2) localised to dots on mitotic spindle MTs that co-stained with α-tubulin antibodies (green, Figure S2A). hTTLL12 also appeared to localize to centrosomes, which were co-stained with beta/gamma-tubulin (green; Figure S2B & C). These results indicate that hTTLL12 localises to the tubulin-rich mitotic spindle, which is consistent with its ability to affect tubulin C-terminal modification.

H4K20me3 and tubulin detyrosination levels are altered by TTLL2 expression at defined stages of the cell cycle

H4K20 methylation and tubulin tyrosination levels change during the cell cycle [28,29]. hTTLL12 can affect cell cycle distribution in some cell lines [2], suggesting that hTTLL12's effects on histone and tubulin modifications in HEp-2 could be an indirect consequence of changes in cell cycle distribution. We checked whether hTTLL12 expression affects cell cycle progression of HEp-2 cells. Using the MTT assay, we found that hTTLL12 clones grew significantly more slowly from day 6 onwards (Figure S3A). Using WBs of cell extracts, we found that the hTTLL12 clones expressed increased levels of Rb ($p = 0.1\ 10^{-3}$) and decreased levels of HP1α ($p = 0.4\ 10^{-4}$), without changes in HP1β and HP1γ (Figure S3B), as expected for inhibition of cell cycle progression by hTTLL12 [30,31]. FACS analysis showed that hTTLL12 clones also had a larger proportion of cells in G2/M with tetraploid chromosome content (4c; Figure

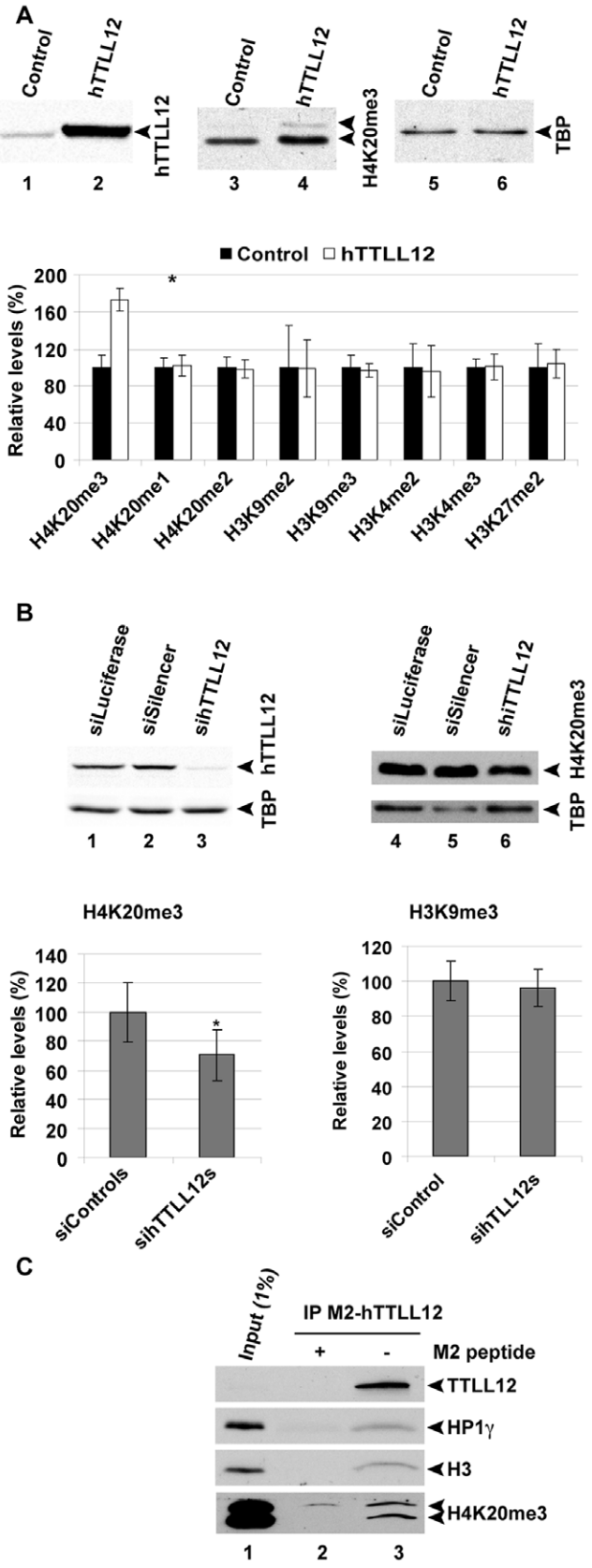

Figure 2. hTTLL12 changes H4K20me3 levels and co-immunoprecipitates with HP1γ, H3 and H4K20me3. *A.* hTTLL12 (hTTLL12_A-E) or Control (Control_A, _B, _D, _E) clones were harvested in Laemmli buffer and subjected to SDS-PAGE and WB. Representative WBs (upper part; hTTLL12_A and Control_E) are shown for hTTLL12 (30 μg protein/lane) or H4K20me3 and TBP (20 μg protein/lane). Similar WBs were probed with different antibodies, quantified by densitometry and normalized to TBP levels (lower part), to determine methylated H4K20me3, H4K20me1, H4K20me2, H3K9me2, H3K9me3, H3K4me2, H3K4me3 and H3K27me2 levels. Data represent average protein levels ± SEM in hTTLL12 lysates relative to average levels in Control lysates (n = 2 except for H4K20me3 (n = 5) and H3K9me3 (n = 3)). *B.* HEp-2 cells were transfected with 10 nM control siRNAs (siLuciferase, siCtrl, siGFP or siSilencer) or 10 nM hTTLL12-specific siRNA (sihTTLL12_2-5). 72 hours after transfection, cells were lysed in Laemmli buffer and analysed by SDS-PAGE and WB. Chemiluminescent signals were detected using a Versadoc image station (hTTLL12) or film (H4K20me3). Representative WBs (upper part) for hTTLL12 (40 μg of total protein/lane), H4K20me3 (5 μg total protein/lane) and respective TBP signals in siLuciferase, siSilencer and sihTTLL12_2 lysates. H4K20me3 levels were quantified using Quantity One software and normalized to TBP (lower left part). Data represent average H4K20me3 levels ± SEM in sihTTLL12 lysates relative to average levels in control siRNA lysates (siControl; n = 3). * Statistically significant difference to the levels in siControl ($P<0.05$, Student's *t*-test). To evaluate H3K9me3 levels (lower right part), HEp-2 cells were transfected with non-targeting control siRNA (siGFP or siCtrl) or hTTLL12-specific siRNA (20 nM sihTTLL12_3 or 10 nM sihTTLL12_4). 48 hours after transfection, cells were harvested in Laemmli buffer and subjected to SDS-PAGE and WB. H3K9me3 levels were quantified by densitometry and normalized to TBP. Data represent average protein levels ± SEM in sihTTLL12 lysates relative to average levels in non-targeting siRNA lysates (siControl; n = 2). *C.* WB showing co-immunoprecipitation of HP1γ, Histone H3 and H4K20me3 with M2-Flagged hTTLL12 from nuclear extract of stable clone hTTLL12_A. Similar results were obtained with two other clones (hTTLL12_B and hTTLL12_C, data not shown). Lane 1: 1% of the input; lane 2: IP of M2-Flagged hTTLL12 in the presence of 500 μg M2-peptide, lane 3: IP M2-Flagged hTTLL12 in the absence of M2-peptide. * Statistically significant ($P<0.05$, Student's *t*-test) difference to the levels in Control or siControl.
doi:10.1371/journal.pone.0051258.g002

S3C). As observed previously [2], there were also cells with a greater DNA content (8c), as expected from increased chromosome numbers. To measure this increase, we counted chromosomes in metaphase spreads of HEp-2, and hTTLL12 and Control clones (Figure S3C; hTTLL12 red; Control green). The modal chromosome number for HEp-2 (data not shown) and Control clone cells was 74. hTTLL12 overexpressing cells had significantly more cells with greater modal chromosome numbers ($p = 4.84\ 10^{-12}$). This shows that hTTLL12 overexpression increases the number of chromosomes per cell in HEp-2, similar to HCT-116 cells [2].

Since the difference in H4K20me3 and detyrosinated tubulin levels could have been a consequence of differences in cell cycle distribution of the cell populations that were compared, we studied whether there were differences when cells were at the same stage of the cell cycle. Cells were synchronised by double thymidine block, released, collected every 2 hours for 24 hours, analysed by FACS for DNA content, and time points were selected at which the cells were predominantly in the S, G2/M and G1 phases (Figure 4A). Western blot analysis showed that there were differences in modifications in the selected populations (Figure 4B), suggesting that the differences are not due to differences in cell cycle distributions of the hTTLL12 overexpressing and control clones. Interestingly, we observed that the time to transit G2 and M and then enter into G1 was delayed in the hTTLL12 overexpressing cells (Figure 4C), suggesting that hTTLL12 could have an effect on the length of the G2 or M phases of the cell cycle.

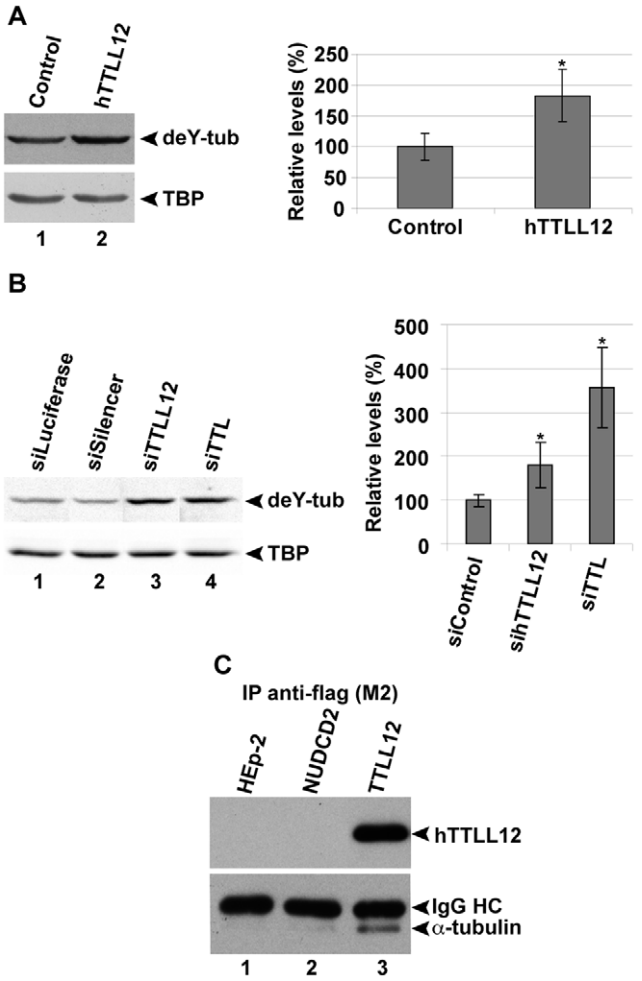

Figure 3. hTTLL12 alters detyrosinated tubulin levels and co-immunoprecipitates with α-tubulin. *A.* hTTLL12 (hTTLL12_A-E) or Control (Control_A, _B, _D, _E) clones were harvested in Laemmli buffer and analysed by SDS-PAGE and WB. Representative WBs (left part) for detyrosinated tubulin (deY-tub) and TBP (40 μg total protein/lane; Control_D and hTTLL12_B shown). deY-tub levels from similar WBs were quantified by densitometry and normalised to TBP (right part). Data represent average detyrosinated tubulin levels ± SEM in hTTLL12 lysates relative to average levels in control lysates (n = 2). * Statistically significant difference to the controls ($P<0.05$, Student's *t*-test). *B.* HEp-2 cells were transfected with 10 nM control siRNAs (siLuciferase, siCtrl, siGFP or siSilencer), 10 nM hTTLL12-specific siRNA (sihTTLL12_1-6), or 10 nM positive control siRNA (siTTL_1-2). 72 hours after transfection, cells were lysed in Laemmli buffer and analysed by SDS-PAGE and WB. Chemiluminescent signals were detected using a Versadoc image station. Representative WBs (left part) for detyrosinated tubulin (40 μg of total protein/lane) and TBP signals (note that lanes 1–3 of the TBP blot are identical to the ones shown in the upper left part of Figure 2B) in siLuciferase, siSilencer, sihTTLL12_2 and siTTL_2 lysates. Detyrosinated tubulin levels were quantified using Quantity One software and normalized to TBP (right part). Data represent average detyrosinated tubulin levels ± SEM in sihTTLL12 and siTTL lysates relative to average levels in control siRNA lysates (siControl; n = 5). * Statistically significant difference to the levels in siControl ($P<0.05$, Student's *t*-test). *C.* Representative WB showing the co-immunoprecipitation of α-tubulin with Flag-hTTLL12 immunoprecipitated from the stable clone hTTLL12_A (lane 3). Similar results were obtained with 4 other clones (hTTLL12_B-E, data not shown). Parental HEp-2 cells (lane1) and a stable HEp2-clone overexpressing Flag-NudCD2 (lane 2) were used as negative controls. IgG HC: IgG heavy chain.
doi:10.1371/journal.pone.0051258.g003

Mitotic phenotypes induced by hTTLL12 up and down regulation

Microscopy of individual living cells was used to study the effects of altering hTTLL12 levels on the duration of different phases of the cell cycle. Chromosomes were detected by fluorescent labelling with Hoechst vital stain and cells by phase contrast (Figure 5A). Ten clones (5 hTTLL12, 5 Control) and HEp-2 were plated and after 48h the unsynchronized cultures were observed every minute for 4 hours. hTTLL12 overexpressing cells had a longer mitotic duration than Control clones and HEp-2 [61±9 versus 40±4 and 37±1 minutes; Figure 5A, Figure 5B and Figure S5A]. The increased duration of mitosis resulted from increases in both prometaphase and metaphase [hTTLL12 versus Control clones: prometaphase 34±6 versus 25±2 min ($p = 0.016$), metaphase 27±3 min versus 16±2 min ($p = 1.3\ 10^{-4}$)]. There were no significant overall differences in other parameters (data not shown), including: (1) chromosome "delay" and "lag" [the presence of chromosomes that did not congress immediately to the metaphase plate (Figure S4A), or that remained stranded at the spindle equator after anaphase, respectively]; (2) chromatin fragmentation and membrane blebbing (markers of cell death), (3) variations in sharpness and centring, and reorientation of the metaphase plate (markers for spindle positioning defects), (4) multipolar spindles (a marker for centrosome duplication and spindle assembly defects); and (5) ingression of the furrow during cytokinesis (a marker for cytokinesis defects). This indicated that the predominant effect of hTTLL12 overexpression is prolongation of prometaphase and metaphase that cumulate to increase mitotic duration.

In parallel, hTTLL12 was depleted from HEp-2 cells with siRNAs (6 sihTTLL12 and 3 controls, used individually; hTTLL12 was decreased by more than 70% 72–80 hours post-transfection). The unsynchronized cultures were observed every 3 minutes for 10 hours. hTTLL12 down regulation increased mitotic duration to 63±15 minutes, compared to 38±2 minutes for the controls (Figure 5C & Figure S4A). About 17% of the hTTLL12 down regulated cells displayed very long mitotic durations, of more than 90 minutes, compared to about 4% of the control cells (Figure S4C). hTTLL12 down regulation did not grossly alter chromosome segregation and cytokinesis compared to the controls. These results show that down regulation as well as up regulation of hTTLL12 had similar effects on mitotic duration. Up and down regulation also had similar effects on the levels of detyrosinated tubulin (see above), suggesting that cells are exquisitely sensitive to hTTLL12 levels.

To facilitate identification of mitotic defects, we focussed on cells with a mitotic duration longer than 50 minutes. Within the hTTLL12 overexpressing cell population, these cells were significantly delayed in chromosome congression to the metaphase plate (Figure S5). They also had differences in spindle positioning prior to anaphase (Figure S6). Control cells displayed a sharp chromosome plate at the equator of the cell very soon after NEB, even before completion of chromosomes congression, indicating that they achieved spindle alignment parallel to the substrate during prometaphase. Modifications of hTTLL12 expression affected spindle positioning, as shown by displacement of the chromosome plate from the cell centre, rotational reorientation of the plate within the cell, and oscillations between a sharp and a fuzzy plate (Figure S6B & C). These are typical characteristics of spindles that are not stably maintained in the cell centre and that change the spatial orientation of their axis. We deduce that hTTLL12 has effects on the spindle that affect congression and positioning, which could affect mitotic timing.

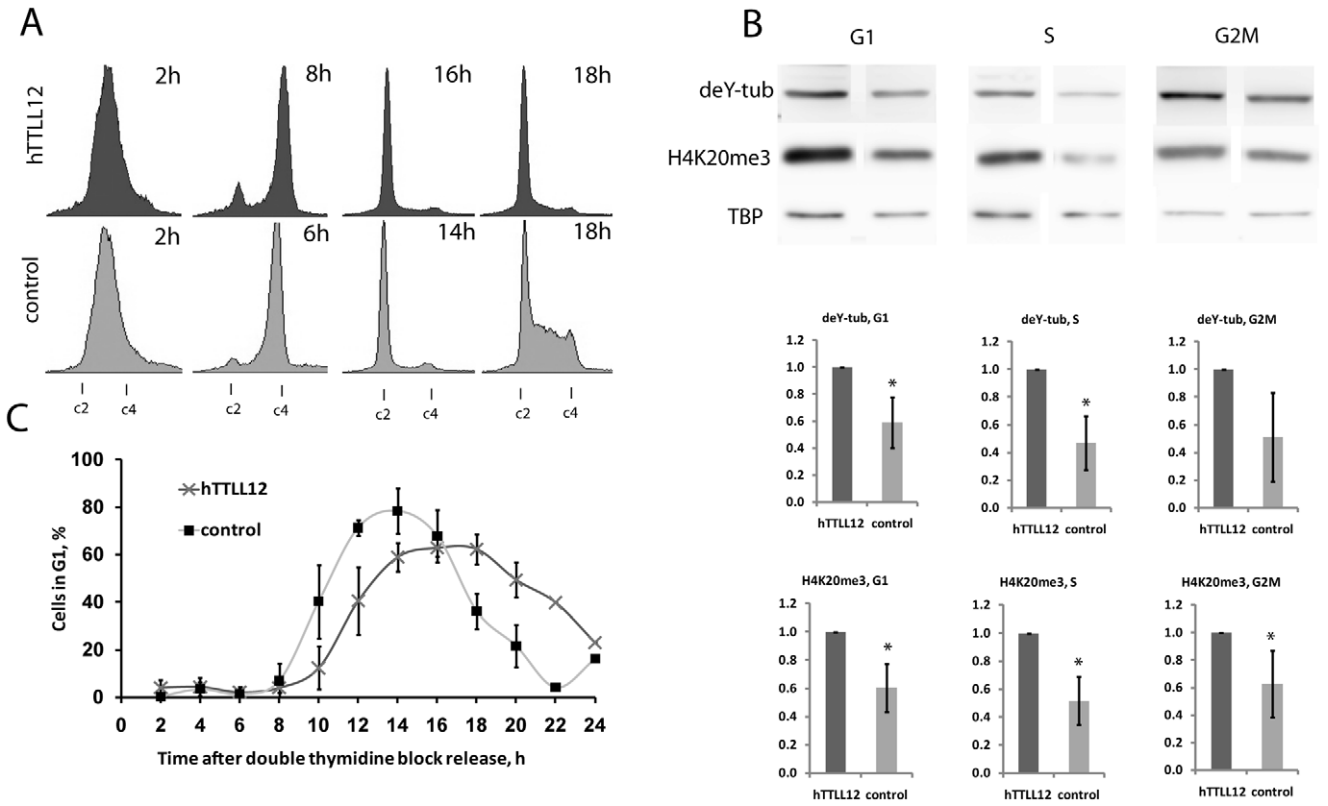

Figure 4. Cell cycle phase dependence of the levels of detyrosinated tubulin (deY-tub) and H4K20me3 in clones overexpressing hTTLL12 compared to control clones. *A.* FACS scans of cells released from a double thymidine block at the indicated times. The times shown are those at which the cells were predominantly in S, G2/M and G1, except for the 18 hour time point. One representative synchronisation is shown. *B.* WBs, from one experiment, of whole cell lysates from cells synchronised in the G1, S and G2/M phases, respectively. The graphs are the averages from 3 independent experiments. * $p<0.05$. *C.* Proportion of cells in G1 at different times after release from double thymidine block. The average from 3 different experiments (up to 18 h) is shown. c2, c4 = DNA complements as measured by propidium iodide.
doi:10.1371/journal.pone.0051258.g004

hTTLL12 lacks HMTase activity in vitro

The presence of a SET-like domain and the effects of hTTLL12 on the levels of H4K20me3 raised the possibility that hTTLL12 could have HMTase activity. In order to investigate this possibility, we used in vitro HMT assays in which the transfer of radiolabelled methyl groups from SAM to purified histones is followed by fluorography. The positive control was NSD1, which has HMTase activity towards both H4K20 and H3K36 [32]. We expressed hTTLL12 in bacteria using the Glutathione S-transferase (GST) Gene Fusion system and in mammalian BHK21 cells using Vaccinia virus Ankara strain (MVA) vectors [33] or establishing stable clones of HEp-2 cells that express Flag-tagged hTTLL12. Tagged proteins were purified by affinity chromatography. The bacterial proteins were essentially pure, whereas the mammalian proteins contained substantial levels of EEF1A1. EEF1A1 was identified by mass spectrometry and WB in both mammalian expression systems, and was shown to co-immunoprecipitate with hTTLL12 (see Figure S1). As expected, we found that a fragment of NSD1 that contains the SET domain [GST-NSD1 (1700–1987)] catalyses the methylation of core histones [Figure 6A; compare lanes 2 & 3 containing different amounts of GST-NSD1 (1700–1987) with lane 1 lacking histones]. In comparison, GST-hTTLL12 (50–250), which contains the SET domain of hTTLL12 and which was purified in parallel with GST-NSD1 (1700–1987), did not have detectable HMTase activity (Figure 6A, lanes 4–6). The same results were obtained in several independent experiments in which the NSD1 and hTTLL12 recombinants were purified in parallel. Similar lack of activity was observed with full length hTTLL12 purified from vaccinia virus infected cells, whether or not the hTTLL12 fraction contained EEF1A1 (Figure 6A, lanes 7–10 and 12). TTL, expressed and purified using the same system, also lacked HMTase activity, as expected from the lack of a SET domain (lane 11). However, this protein was enzymatically active in tubulin tyrosine ligase assays [[33] and see below]. This suggests that the experimental procedure used is compatible with the isolation of enzymatically active proteins. We also purified hTTLL12 from the clones in which endogenous H4K20me3 levels were altered due to hTTLL12 overexpression. Flag-tagged hTTLL12 was purified from fractionated cell extracts from two overexpressing clones (hTTLL12_C & hTTLL12_D). Control clones (Control_C, Control_D) were processed in parallel to give control extracts. We used fractionated cells since hTTLL12 is located in the cytoplasm and the nucleus of cells, in different proportions depending on the cell type [2]. Three fractions were prepared, the cytoplasmic fraction, a nuclear 0.4 M NaCl wash, and a subsequent 1 M salt wash. The relative levels of hTTLL12 in the three fractions were approximately 100:2:0.4 in HEp-2. Purified hTTLL12 did not have any additional HMTase activity compared to the control extracts [Figure 6B, lower panel; compare lanes 4, 5 with 3, lanes 8, 9 with 7, and see the lack of detectable incorporation in lane 11; see also the signal for the positive control GST-NSD1 (1700–1987)]. There was background incorporation of radioactivity that was histone dependent (compare lanes 2 and

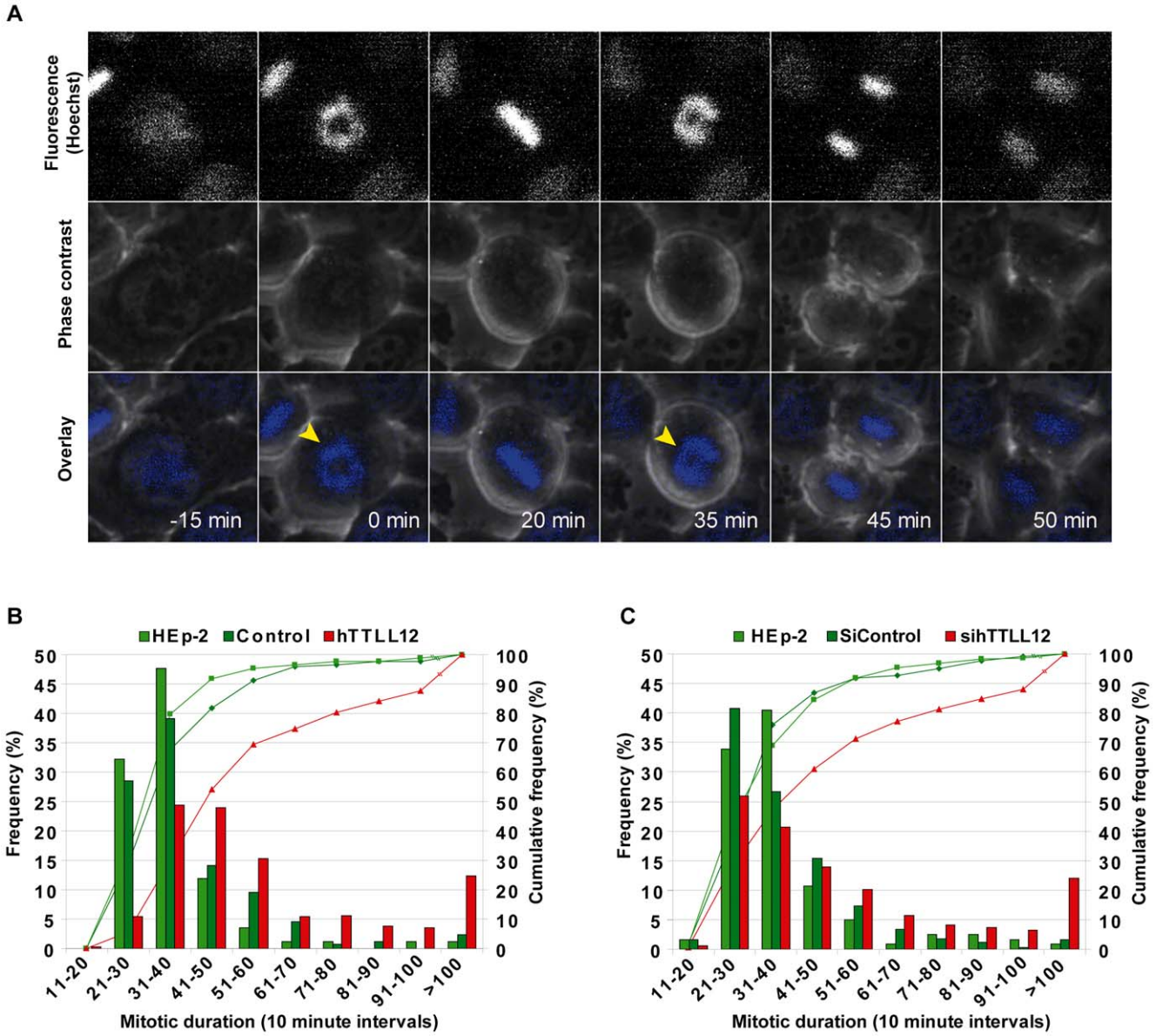

Figure 5. hTTLL12 up and down regulation prolong mitotic duration of HEp-2 cells. *A.* Example frames from live cell movies of a HEp-2 cell stained with vital Hoechst. The time between nuclear envelope breakdown (NEB, first arrowhead, 0 min) and anaphase onset (second arrowhead) are indicated. Upper panel: fluorescent images (Hoechst), middle panel: phase contrast images, lower panel: overlay. *B–C.* Cumulative frequency (plot, right axis) and frequency distribution (histogram, left axis) of mitotic duration for hTTLL12 clones *(B)* and siRNA transfected HEp-2 *(C)*. *B.* hTTLL12 (hTTLL12_A-E) or Control (Control_A-E) clones were seeded in 6-well plates. 48 hours post seeding, cells were treated with vital Hoechst and analysed (Experimental Procedures). Parental HEp-2 cells (light green), and the averages of the hTTLL12 (red) and Control (dark green) clones are plotted. *C.* HEp-2 cells were transfected separately with 12.5 nM sihTTLL12_1-6 or controls (siLuciferase, siCtrl, siScramble). 72 hours post transfection, cells were stained with vital Hoechst and analysed. HEp-2 cells; light green; averages of sihTTLL12s; red; averages of siControls; dark green. More detailed information and statistical analysis can be found in Figure S1.
doi:10.1371/journal.pone.0051258.g005

3, 4 and 5, and 9 and 10). In some cases the background activity appeared to be lower in the hTTLL12 containing extracts, suggesting that the hTTLL12 extracts could contain inhibitors. However, adding hTTLL12 extracts to either GST-NSD1 (1700–1987)] or control extracts did not significantly decrease their activities (data not shown). The results were reproducible, using independent protein preparations (data not shown). Taken together, our results suggest that hTTLL12 does not have HMTase activity.

hTTLL12 lacks TTL activity in vitro

Since hTTLL12 has a TTL-like domain, we studied whether it has TTL activity. We used in vitro assays with [^{14}C] labelled tyrosine, purified tubulin, and either extracts from transiently transfected cells or proteins purified from mammalian cells infected with appropriate viral expression vectors. Extracts from cells transfected with the TTL expression vector exhibited increased TTL activity compared to mock-transfected cell extracts (Figure 7A, lanes 9 and 4, respectively). The reactions were specific, as shown by dependence on cell extract (1), ATP (lane 2),

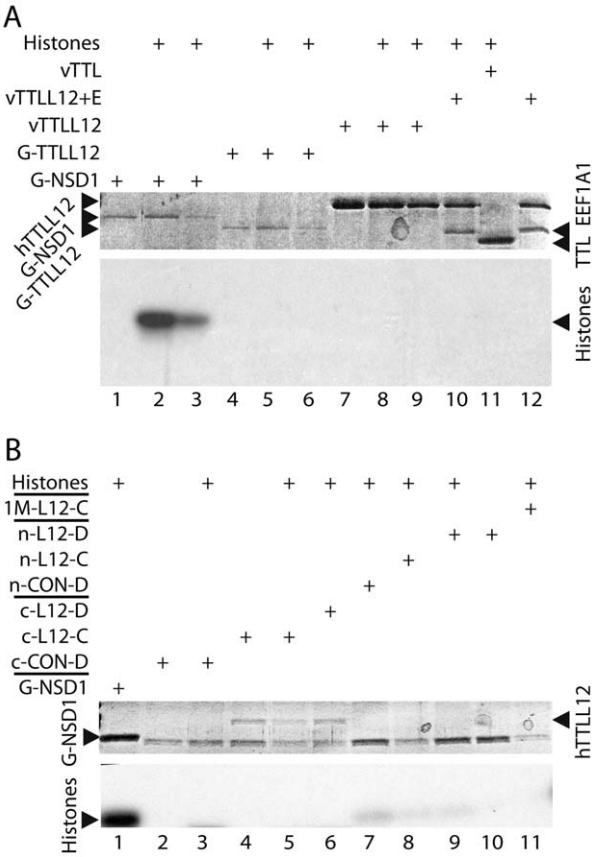

Figure 6. hTTLL12 lacks HMTase activity. The assays included histones purified from calf thymus (*A*, lanes 2, 3,5, 6, 8–11; *B* lanes 1, 3, 5–9, 11) as substrate and proteins to be tested for HMT activity that were purified from bacterial, viral and mammalian cell expression systems. The upper panels in each part (*A* & *B*) are Coomassie Blue stained SDS-polyacrylamide gels of the expressed proteins and the lower panels are the corresponding fluorograms centred on the core histones (Histones). The proteins tested for HMTase activity were expressed and purified from appropriate pGEX vector transformed E. coli [GST-NSD1 (1700–1987) (G-NSD1), GST-TTLL12 (50–250) (G-TTLL12)], recombinant vaccinia virus Ankara strain (MVA) infected mammalian cells [vTTLL12, vTTLL12 and vTTLL12 + E (a fraction that contains EEF1A1)] and HEp-2 cell clones transformed with pSG5-puro-Flag (CON-D) or pSG5-puro-Flag TTLL12 (L12-C & L-12-D). The HEp-2 proteins were purified from cytoplasmic (c-CON-D, c-L12-c, c-L12-D), nuclear (n-CON-D, n-L12-C, n-L12-D) and 1M KCl (1M-L12-C) fractions. 10 μl reactions were loaded on 15% SDS-PAGE gels. In *A*, the approximate amounts of protein used per reaction were: GST-NSD1 (1700–1987) (1 μg, lanes 1, 2; 0.5 μg, lane 3), GST-TTLL12 (50–250) (0.5 μg, lanes 4, 5; 0.25 μg, lane 6), TTLL12 (3 μg, lanes 7, 8; 1.5 μg lane 9), TTLL12 + EEF1A1 (2 μg, lanes 10, 12) and TTL (4 μg, lane 11). In *B*, they were GST-NSD1 (1700–1987) (2 μg, lanes 1, 12), TTLL12 (0.25 μg, lanes 4–6; 0.005 μg lanes 8–10, 0.001 μg lane 11). TTLL12 was not detected in the equivalent fractions purified from the control HEp-2 clone (CON-D). In *B*, lanes 2–11, the band migrating slightly faster than GST-NSD1 (1700–1987)) is IgH from the affinity column that is eluted under the harsh denaturing conditions used for sample preparation for SDS-PAGE.
doi:10.1371/journal.pone.0051258.g006

tubulin (lane 3) and the use of an expression vector with the appropriate orientation (lane 8). Extracts from cells transfected with expression vectors for hTTLL12 (6) and Flag-hTTLL12 (7) did not increase endogenous TTL activity. As might be expected, transfection of the hTTLL12 anti-sense construct did not affect TTL activity. hTTLL12 and TTL were efficiently expressed in these experiments (Figure 7B), showing that lack of activity was not due to absence of expression. We also tested the activity of TTL and hTTLL12 purified from mammalian BHK21 cells infected with appropriate Vaccinia virus Ankara strain (MVA) vectors [33]. As expected, TTL catalysed ligation of labelled tyrosine to tubulin in a dose dependent manner (Figure 7C). In contrast, equivalent amounts of hTTLL12 or hTTLL12 complexed to EF1A1 did not exhibit any activity relative to control reactions lacking purified proteins (the first bar). Adding hTTLL12 or hTTLL12 +EEF1A1 to TTL did not affect its activity, showing that these preparations did not contain contaminants that may have inhibited the reactions. Overall, these results suggest that hTTLL12 is devoid of TTL activity.

Discussion

hTTLL12 is the most divergent member of the 14-gene TTL family in humans. It has a phylogenetically conserved association of two domains (SET- and TTL- like) that predict that it could be involved in histone and tubulin modification. We found that changes in hTTLL12 expression affect histone and tubulin modifications in cells. They also affect mitotic duration, which could be linked to both types of modification. However hTTLL12 appears to lack these histone and tubulin modification activities in vitro. These results suggest that hTTLL12 is an inactive enzyme homologue that may have a regulatory function.

TTLL12 is an unusual member of the TTL family, according to bioinformatics analysis. TTLL12 has a unique phylogenic distribution and it has features that distinguish it from the other family members in humans. For example, it is the only member of the TTLL family to be identified in plant genomes, such as Arapidopsis thaliana [34]. The TTL domain of hTTLL12 lacks three of the seven motifs that are conserved in the other family members. Furthermore, it has several residues that are specific to hTTLL12 and conserved orthologues in different species. The N-terminal region of hTTLL12 has homology to SET domains in a number of human proteins. The overall sequence similarity is low, which is a general characteristic of SET domains [for reviews see [5,6,7,24]]. The TTLL12 SET domain has also been detected by Aravind et al [3], who studied the natural history of the eukaryotic chromatin protein modification system. They propose that the TTLL12 clade is one of at least 5 types of SET domains that were present in the LECA (last eukaryotic common ancestor). TTLL12 is one of the major lineages of SET domains that might have played the initial role in the establishment of multiple distinct heterochromatic and euchromatic states that are likely to have been present throughout much of eukaryotic evolution.

The presence of a SET-like domain in hTTLL12 prompted us to investigate its role in histone lysine methylation. We found that hTTLL12 is functionally linked to at least one histone methylation. Altering hTTLL12 levels affects H4K20me3 levels, without influencing other methylation states of H4K20 (me2 and me1) and methylation of H3K4 and H3K9. However, we did not detect histone methyl transferase activity in vitro with hTTLL12 proteins purified from various sources. hTTLL12 interacts with EEF1A1, raising the possibility that hTTLL12 may methylate this protein. EEF1A1 has been shown to be methylated and two histone methyltranferases that mediate this modification have been identified in Saccharomyces cerevisiae [35]. However, we did not detect methylation of EEF1A1 by hTTLL12 in our in-vitro methylation experiments. We propose that hTTLL12 affects H4K20 trimethylation in cells by an indirect mechanism, perhaps by altering the expression and/or interactions with factors implicated in this modification. hTTLL12's SET-like domain appears to lack a critical asparagine residue that is important for

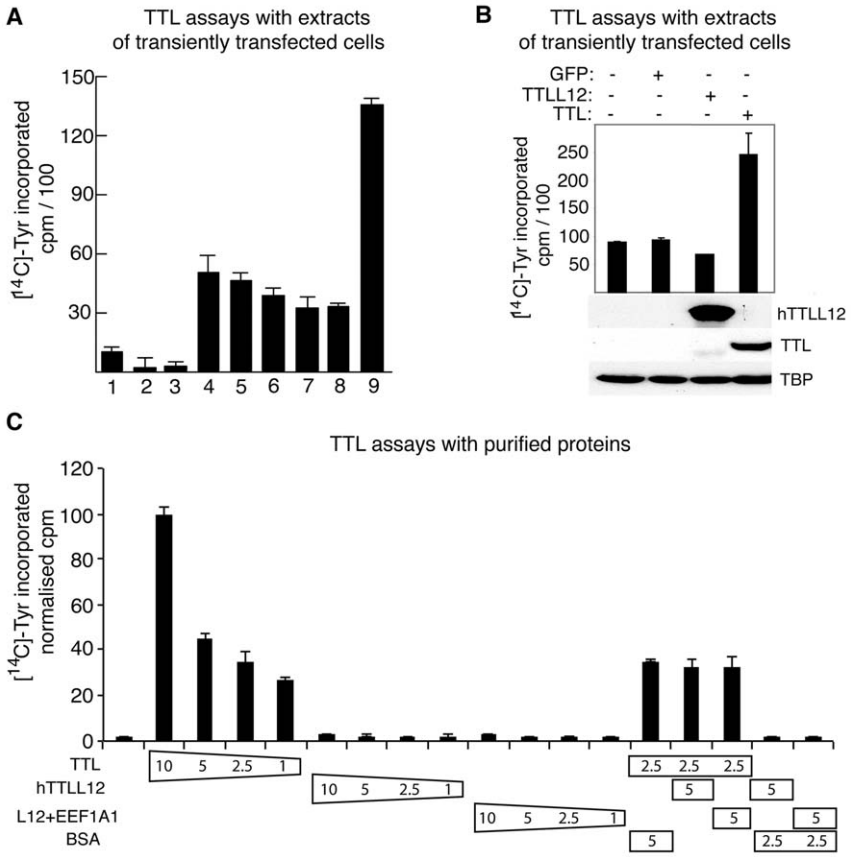

Figure 7. hTTLL12 lacks tubulin tyrosine ligase activity, as shown with tubulin tyrosine ligase (TTL) assays using cell extracts (*A, B*) or purified proteins (*C*). (A) TTL assays on extracts of transfected HEp-2 cells. Control reactions lacked cell extract (1), ATP (2) or purified tubulin (3). Test reactions contained extracts from cells transfected with: no DNA (4, mock), pc-AS 153 (5, antisense hTTLL12), pcDNA3-hTTLL12 (6), pSG5-puro-hFlag TTLL12 (7, Flag-hTTLL12), pc-AS TTL (8, antisense hTTL), and pcDNA3-TTL (9). (B) Expression of TTLL12 and TTL in transfected cell extracts. WBs were used to detect hTTLL12, TTL and TBP (loading control) in the extracts used for the activity tests. (C). TTL activity of purified proteins. The in-vitro reactions contained the indicated quantities (µg) of TTL, hTTLL12 and hTTLL12 complexed to EEF1A1 that had been purified from mammalian cells infected with corresponding recombinant Ankara strain (MVA) vaccinia viruses. The counts were normalised to 100 for 10 µg TTL. Error bars indicate standard deviations.

doi:10.1371/journal.pone.0051258.g007

methyltransferase activity. A single asparagine to glutamine mutation in the SET domain of *Neurospora* DIM-5 strongly reduces the enzyme activity and binding to the cofactor SAM [S-Adenosyl-L-methionine, N241Q, [36]]. The predicted corresponding position in hTTLL12 (position 458; Alignment S2) is in fact a glutamine residue. hTTLL12 alters the expression levels of proteins that have indirect effects on trimethylation of H4K20 [Rb, HP1α; [26,27,37]]. TTLL12 has been shown to interact with SAP25 [38] and Arid1A [39], which are involved in nucleosome remodelling. It remains to be seen whether these interactions account for its effects on histone modification.

hTTLL12 is also functionally linked to tubulin tyrosination [this report and [2]]. This effect appears to be indirect, for a number of reasons. Increasing and decreasing hTTLL12 levels increase the levels of detyrosinated tubulin, which would be difficult to explain by a direct effect. In our experiments, hTTLL12 purified from a number of sources does not have tubulin tyrosine ligase activity. In other studies it was shown to lack polyglutamylation [23] and polyglycylation [40] activities. Lack of activity is also suggested by its sequence. In the alignment of TTL domains (Alignment S1) hTTLL12 seems to lack residues that are important for ATP/Mg^{2+} binding [GXGI→SLDT$^{426–429}$ and FEψψGFD→RA-MYAVD$^{578–584}$[41,42,43]]. The GXGI ATP/Mg^{2+} binding motif in hTTL is important for TTL activity, since this activity is abolished by mutation of the corresponding ^{157}GEGI^{160} in the human TTL protein to ^{157}GAAA^{160} (our unpublished data). Overall, our results suggest that hTTLL12 has indirect and perhaps regulatory roles in histone modification and tubulin detyrosination, rather than direct enzymatic activity.

Altered tubulin tyrosination and H4K20 methylation is compatible with the phenotypic effects of hTTLL12. hTTLL12 up- and down-regulation prolong mitotic duration. There are also more subtle defects in chromosome congression and positioning, in cells with the longest mitotic durations. Detyrosinated tubulin is enriched in the mitotic spindle, but less so in astral microtubules of the spindle [44]. Detyrosination could be an essential regulator of chromosome segregation, since the tyrosination state of α-tubulin regulates the activity of the depolymerizing kinesin MCAK [45], which is essential for proper chromosome segregation in anaphase [46]. H4K20 mono-methylation has been implicated in mitosis, but the link with tri-methylation is weaker [reviews: [47,48,49,50]]. There are high levels of H4K20me3 in centromeric heterochromatin, which is required for the proper segregation of chromosomes during mitosis [51,52]. hTTLL12 affects HP1α levels. HP1 proteins are required for correct chromosome segregation in Drosophila embryos [53], and during

metaphase only HP1α, and not HP1β and HP1γ, co-localises with centromeric heterochromatin [54].

A role for hTTLL12 in mitosis is also supported by the MitoCheck consortium [55,56]. They systematically analyzed genes and proteins that are required for chromosome segregation and cell division in human cells. 22,000 human genes were inactivated individually by RNA interference (RNAi) in cultured human cells. Cellular phenotypes were recorded by high-throughput live cell imaging. Automated analyses of images and movies revealed that about 600 out of the 22,000 genes play a role in mitosis. One of these genes is hTTLL12. The phenotypes observed were dynamic changes, segregation problems, strange nuclear shapes, nuclei that stay together and apoptosis. Different aspects of this phenotype were observed with 2 out of 4 dsRNAs used to down regulate hTTLL12 (http://www.mitocheck.org/cgi-bin/mtc?query = ttll12&query_type = genes). These phenotypes are compatible with our observations. Significantly, these phenotypes were not observed with any of the other members of the TTL family. hTTL and hTTLL1 were found to have effects on secretion, and hTTLL4 on apoptosis.

We found that hTTLL12 induces changes in DNA content and chromosome numbers by FACS and karyotype analysis, respectively. The changes in chromosome number are observed in some cells in each clone, which are composed of a mixed population of cells with different chromosome numbers. This suggests that hTTLL12 overexpression favours relatively rare events that are not completely eliminated by cell death. A strong effect on chromosome number would be expected to be lethal to the cell. hTTLL12 appears to predispose cells to low frequency events that may accumulate with time, and perhaps help cells adapt during tumour progression. hTTLL12 has been linked to altered chromosome numbers by others. In a study of amniotic fluid from fetuses with the two most common human autosomal aneuploidies, trisomies 21 and 18, in which RNA expression was compared to euploid fetuses matched for sex and gestational age, one of the four RNAs that was upregulated in both comparisons was hTTLL12. hTTLL12 does not map to the chromosomes with altered copy number, suggesting that copy number did not account for the differences [57,58]. It remains to be seen whether there is any connection between these studies and our observations.

Our working hypothesis is that hTTLL12 could be a pseudo-enzyme that regulates histone and tubulin modifications and thereby microtubule dynamics, mitosis and chromosome number instability. hTTLL12 may exploit its ability to bind the same substrates and cofactors as other TTLs and SET domain factors. Consequently, hTTLL12 would be well placed to directly or indirectly regulate the biological processes in which its cognate enzymes act. Such enzymes could include the many tubulin-modifying and -demodifying enzymes that have been recently characterised and shown to regulate microtubule functions through different modifications. Combinatorial use of tubulin modifications could generate a dynamic microtubule code [10,12]. hTTLL12 would thus resemble the numerous other inactive enzyme homologues that contain conserved substitutions in their catalytic sites and have regulatory roles [59]. Most enzyme families have inactive homologues (pseudo-enzymes) that are well conserved. They appear to have sufficient functional importance to resist selective pressure during evolution. hTTLL12 may be another example of a dead enzyme with an important physiological role. It is possible that the study of hTTLL12 could offer novel insights into biochemical pathways controlled by its active counterparts.

Supporting Information

Supporting Experimental Procedures S1.
(PDF)

Figure S1 KIAA0153 might be part of a complex containing EF1A1, α- and β-tubulin. *A* Purification of flag-hTTLL12 by affinity and further Coomassie staining revealed an extra band identified as EF1A1 by Mass Spectrometry. 1: total cell extract, 2: column flow through, 3: column wash, 4: proteins eluted by peptide competition. *B* Silver stained gels and bands identified by Mass Spectrometry. 1: marker, 2 and 3: proteins eluted from columns loaded with cell extract from vector stable transfectant (2), and sense stable transfectant. Major proteins identified are indicated. The other bands correspond to heat shock proteins and degradation products from either hTTLL12 or EF1A1 (not indicated). 75, 50, 37 correspond to molecular weight markers ($\times 10^{-3}$ kD).
(PDF)

Figure S2 hTTLL12 localises to mitotic spindle microtubules and centrosomes. HEp-2 cells were fixed and co-stained with hTTLL12 (2065, red) and β-tubulin (green) (panel A), hTTLL12 (2089, red) and β-tubulin (green) (panel B) or hTTLL12 (2089, red) and γ-tubulin (green) (panel C) specific antibodies. Images were taken by confocal microscopy.
(PDF)

Figure S3 hTTLL12 expression deregulation in HEp-2 cells alters growth and DNA-profiles. *A.* Growth of Control (Control_A-E) and hTTLL12 (hTTLL12_A-E) clones was measured by MTT in quadruplicate during ten days. Data represent average values ± average deviation of Control (black) and hTTLL12 (white) clones. * Statistically significant difference to Control cells ($P<0.05$, Student's *t*-test). *B.* hTTLL12 (hTTLL12_A-E) or Control (Control_A, _B, _D, _E) clones were seeded, harvested in Laemmli buffer and subjected to SDS-PAGE and WB (20 μg protein/lane). Histone H4 (H4), Rb, HP1α, HP1β and HP1gamma levels were quantified by densitometry and normalized to TBP. Data represent average protein levels ± SEM in hTTLL12 lysates relative to average levels in Control lysates (n = 3 for Rb, HP1β, HP1gamma, n = 4 for H4, HP1α). *C.* The DNA profile of controls (HEp-2, Control_A, _B, _F, and _G; purple bars) and hTTLL12 clones (hTTLL12_A-E; red bars) was analyzed by FACs after propidium iodide staining. 2c, 4c and 8c: diploid, tetraploid and octaploid DNA contents. D. Chromosome numbers per cell. For each clone (Control_A-E: "triangle" A, "dot" B, "cross" C, "square" D, "diamond" E, green; hTTLL12_A-E: "dot" A, "cross" B, "square" C, "diamond" D, "triangle" E, red), sixty-five metaphase spreads (1–65, y axis) were stained with Giemsa and the number of chromosomes per mitosis was counted (X-axis). The modal chromosome number of HEp-2 cells is 74. * Statistically significant difference between the average chromosome numbers in hTTLL12 and Control clones ($P<0.05$, Student's *t*-test).
(PDF)

Figure S4 Altering hTTLL12 expression prolongs mitotic duration (see Fig. 5). Mitotic duration was scored from time-lapse movies (Experimental Procedures). The total numbers of clone or transfected cells analysed were: 205 HEp-2, 263 Control_A-E, 372 hTTLL12_A-E, 591 control siRNAs (siCtrl, siLuciferase, siScramble, used separately and combined), and 899 sihTTLL12_1-6, used separately). *A.* Data represent average mitotic duration ± STDEV (standard deviation) for HEp-2, hTTLL12 and Control clones, and control siRNAs (siControl) and sihTTLL12 transfected cells. * Statistically significant difference

between hTTLL12 clones and Control clones or Hep-2, as well as between sihTTLL12 and siControl or HEp-2 ($P<0.05$, Student's *t*-test). *B.* Average percentages for each clone type (HEp-2, Control_A-E and hTTLL12_A-E) ± STDEV divided into time intervals. * Statistically significant difference between hTTLL12 clones and Control clones or HEp-2 ($P<0.05$, Student's *t*-test). *C.* Average percentages for each siRNA type (non-transfected (HEp-2), siControl (siCtrl, siLuciferase, siScramble) and siTTLL12 (sihTTLL12_1-6)) ± STDEV divided into time intervals. * Statistically significant difference between sihTTLL12 transfected cells and siControl or HEp-2 ($P<0.05$, Student's *t*-test).
(PDF)

Figure S5 hTTLL12 overexpression leads to chromosome congression delay in HEp-2 cells. The total numbers of cells analysed by time lapse movies (Experimental Procedures) were 420 for Control_A-E and 491 for hTTLL12_A, _B, _D, and _E. *A.* Representative fluorescent (Hoechst) images of metaphases of a HEp-2 cell (Control), and a hTTLL12 overexpressing cell showing congression delay. Red arrows mark chromosomes that are delayed. 0 min is the time of NEB. *B.* Average percentages for each clone type ± STDEV having congression delay divided in time intervals (mitotic duration ≤50 min or >50 min) scored from time lapse movies of hTTLL12 and Control clones. * Statistically significant difference between Control and hTTLL12 clones ($P<0.05$, Student's *t*-test).
(PDF)

Figure S6 hTTLL12 up and down regulation leads to a spindle positioning phenotype in HEp-2 cells. The orientation and placement of mitotic spindles was scored from time-lapse movies (Experimental Procedures). The numbers of cells analysed were: 262 HEp-2, 420 Control_A-E, 380 hTTLL12_A, _B, _D clones, 502 control siRNAs (siCtrl, siLuciferase, siScramble, used separately and combined), and 973 sihTTLL12 (sihTTLL12_1-6, used separately). *A.* Phase contrast and fluorescent (Hoechst) image overlays of metaphases from representative cells: a HEp-2 (Control, upper panel), a hTTLL12 clone (hTTLL12, middle panel) and a sihTTLL12 transfected cell (sihTTLL12, lower panel). Red lines and grey circles highlight metaphase plate position with respect to the circumference of the cell. 0 min is the time of anaphase onset. *B.* Average percentages for each cell type ± STDEV with the spindle positioning phenotype divided into time intervals (mitotic duration ≤50 min or >50 min) for HEp-2 cells, hTTLL12 and Control clones. * Statistically significant ($P<0.05$, Student's *t*-test) difference between hTTLL12 clones and Control clones or HEp-2 cells. *C.* Average percentage for each clone or cell type ± STDEV with the spindle positioning phenotype divided into time intervals (mitotic duration ≤50 min or >50 min) scored from time lapse movies with HEp-2 or cell transfected with control siRNAs or sihTTLL12s. * Statistically significant difference between sihTTLL12 and control siRNA transfected cells or HEp-2 ($P<0.05$, Student's *t*-test).
(PDF)

Table S1 Amino acid conservation in the TTL core domain of TTL family members. The consensus sequence for the human family and the corresponding sequence in hTTLL12 are from Alignment S1. The alignment for different species is not shown.
(PDF)

Table S2 The sequences and their positions in hTTLL12 that are highly conserved in other human SET domains (see Alignment S2) are listed. Letters are coloured according to Fig. 1 in Qian et al. (38): red: absolutely conserved; blue: very highly conserved; black: highly conserved). The corresponding conserved structural elements are indicated (38). Amino acids 158–188 are the approximate limit of a predicted insert in the SET domain that is deduced from Alignment S2. Sequence alignments of hTTLL12 with several plant and unicellular ciliate protozoan orthologues (e.g. NP_177879.3, *Arabidopsis thaliana*; XP_002326123 *Populus trichocarpa*; ABF94289, *Oryza sativa*; XP_001020206, *Tetrahymena thermophila* SB210; XP_001454840, *Paramecium tetraurelia* strain d4-2; XP_001580810, *Trichomonas vaginalis* G3) indicate that these orthologues have an insert that has an additional sequence inserted in this position (data not shown).
(PDF)

Table S3 The 55 kDa co-immunoprecipitated protein band (Fig. 3C) corresponds to α-tubulin. The table summarizes tryptic peptide sequences, their relative positions on the α-tubulin primary protein sequence, their measured masses and computed masses. * oxidized methionine.
(PDF)

Alignment S1 Multiple sequence alignment of the TTL domains of the human TTL protein family members.
(PDF)

Alignment S2 Multiple sequence alignment of the hTTLL12 SET-like domain and the SET domains of human proteins.
(PDF)

Acknowledgments

We thank: Vivek Tripathi and Jérome L. Lemoine for their inputs for the manuscript; all the members of Procure (FP5), Prima (FP6), Dr A McEwen, Dr JP Samama, Dr JM Zahm, and the Wasylyk laboratory for useful discussions, support and encouragement; Dr M Argentini for invaluable help with the mass spectrometry; A Mertz for assisting in karyotype analyses; the IGBMC mass spectrometry platform and core facilities; and A Lux for perfect technical assistance.

Author Contributions

Conceived and designed the experiments: JB KS CW AR AZ CB JAS OP JdM BW. Performed the experiments: JB KS CW AR AC AZ KP-A CB. Analyzed the data: JB KS CW AR AC AZ JAS OP JdM BW. Wrote the paper: JB BW.

References

1. Carles A, Millon R, Cromer A, Ganguli G, Lemaire F, et al. (2006) Head and neck squamous cell carcinoma transcriptome analysis by comprehensive validated differential display. Oncogene 25: 1821–1831.
2. Wasylyk C, Zambrano A, Zhao C, Brants J, Abecassis J, et al. (2010) Tubulin tyrosine ligase like 12 links to prostate cancer through tubulin posttranslational modification and chromosome ploidy. Int J Cancer 127: 2542–2553.
3. Aravind L, Abhiman S, Iyer LM (2011) Natural history of the eukaryotic chromatin protein methylation system. Prog Mol Biol Transl Sci 101: 105–176.
4. Xu D, Bai J, Duan Q, Costa M, Dai W (2009) Covalent modifications of histones during mitosis and meiosis. Cell Cycle 8: 3688–3694.
5. Cheng X, Zhang X (2007) Structural dynamics of protein lysine methylation and demethylation. Mutat Res 618: 102–115.
6. Qian C, Zhou MM (2006) SET domain protein lysine methyltransferases: Structure, specificity and catalysis. Cell Mol Life Sci 63: 2755–2763.
7. Dillon SC, Zhang X, Trievel RC, Cheng X (2005) The SET-domain protein superfamily: protein lysine methyltransferases. Genome Biol 6: 227.
8. Szyk A, Deaconescu AM, Piszczek G, Roll-Mecak A (2011) Tubulin tyrosine ligase structure reveals adaptation of an ancient fold to bind and modify tubulin. Nat Struct Mol Biol 18: 1250–1258.

9. Garnham CP, Roll-Mecak A (2012) The chemical complexity of cellular microtubules: Tubulin post-translational modification enzymes and their roles in tuning microtubule functions. Cytoskeleton (Hoboken) 69: 442–463.
10. Janke C, Bulinski JC (2011) Post-translational regulation of the microtubule cytoskeleton: mechanisms and functions. Nat Rev Mol Cell Biol 12: 773–786.
11. Ikegami K, Setou M (2010) Unique post-translational modifications in specialized microtubule architecture. Cell Struct Funct 35: 15–22.
12. Wloga D, Gaertig J (2010) Post-translational modifications of microtubules. J Cell Sci 123: 3447–3455.
13. Etienne-Manneville S (2010) From signaling pathways to microtubule dynamics: the key players. Curr Opin Cell Biol 22: 104–111.
14. Jenuwein T, Allis CD (2001) Translating the histone code. Science 293: 1074–1080.
15. Verhey KJ, Gaertig J (2007) The tubulin code. Cell Cycle 6: 2152–2160.
16. Altschul SF, Madden TL, Schaffer AA, Zhang J, Zhang Z, et al. (1997) Gapped BLAST and PSI-BLAST: a new generation of protein database search programs. Nucleic Acids Res 25: 3389–3402.
17. Plewniak F, Bianchetti L, Brelivet Y, Carles A, Chalmel F, et al. (2003) PipeAlign: A new toolkit for protein family analysis. Nucleic Acids Res 31: 3829–3832.
18. Galtier N, Gouy M, Gautier C (1996) SEAVIEW and PHYLO_WIN: two graphic tools for sequence alignment and molecular phylogeny. Comput Appl Biosci 12: 543–548.
19. Page RD (1996) TreeView: an application to display phylogenetic trees on personal computers. Comput Appl Biosci 12: 357–358.
20. Nielsen AL, Oulad-Abdelghani M, Ortiz JA, Remboutsika E, Chambon P, et al. (2001) Heterochromatin formation in mammalian cells: interaction between histones and HP1 proteins. Mol Cell 7: 729–739.
21. Chen C, Okayama H (1987) High-efficiency transformation of mammalian cells by plasmid DNA. Mol Cell Biol 7: 2745–2752.
22. Ikegami K, Mukai M, Tsuchida J, Heier RL, Macgregor GR, et al. (2006) TTLL7 is a mammalian beta-tubulin polyglutamylase required for growth of MAP2-positive neurites. J Biol Chem 281: 30707–30716.
23. van Dijk J, Rogowski K, Miro J, Lacroix B, Edde B, et al. (2007) A targeted multienzyme mechanism for selective microtubule polyglutamylation. Mol Cell 26: 437–448.
24. Couture JF, Trievel RC (2006) Histone-modifying enzymes: encrypting an enigmatic epigenetic code. Curr Opin Struct Biol 16: 753–760.
25. Morgunkova A, Barlev NA (2006) Lysine methylation goes global. Cell Cycle 5: 1308–1312.
26. Schotta G, Lachner M, Sarma K, Ebert A, Sengupta R, et al. (2004) A silencing pathway to induce H3-K9 and H4-K20 trimethylation at constitutive heterochromatin. Genes Dev 18: 1251–1262.
27. Gonzalo S, Garcia-Cao M, Fraga MF, Schotta G, Peters AH, et al. (2005) Role of the RB1 family in stabilizing histone methylation at constitutive heterochromatin. Nat Cell Biol 7: 420–428.
28. Pesavento JJ, Yang H, Kelleher NL, Mizzen CA (2008) Certain and progressive methylation of histone H4 at lysine 20 during the cell cycle. Mol Cell Biol 28: 468–486.
29. Forrest GL, Klevecz RR (1978) Tyrosyltubulin ligase and colchicine binding activity in synchronized Chinese hamster cells. J Cell Biol 78: 441–450.
30. De Koning L, Savignoni A, Boumendil C, Rehman H, Asselain B, et al. (2009) Heterochromatin protein 1alpha: a hallmark of cell proliferation relevant to clinical oncology. EMBO Mol Med 1: 178–191.
31. Manning AL, Dyson NJ (2012) RB: mitotic implications of a tumour suppressor. Nat Rev Cancer 12: 220–226.
32. Rayasam GV, Wendling O, Angrand PO, Mark M, Niederreither K, et al. (2003) NSD1 is essential for early post-implantation development and has a catalytically active SET domain. Embo J 22: 3153–3163.
33. Hebben M, Brants J, Birck C, Samama JP, Wasylyk B, et al. (2007) High level protein expression in mammalian cells using a safe viral vector: modified vaccinia virus Ankara. Protein Expr Purif 56: 269–278.
34. Gardiner J, Marc J (2011) Arabidopsis thaliana, a plant model organism for the neuronal microtubule cytoskeleton? J Exp Bot 62: 89–97.
35. Lipson RS, Webb KJ, Clarke SG (2010) Two novel methyltransferases acting upon eukaryotic elongation factor 1A in Saccharomyces cerevisiae. Arch Biochem Biophys 500: 137–143.
36. Zhang X, Tamaru H, Khan SI, Horton JR, Keefe LJ, et al. (2002) Structure of the Neurospora SET domain protein DIM-5, a histone H3 lysine methyltransferase. Cell 111: 117–127.
37. Yang H, Pesavento JJ, Starnes TW, Cryderman DE, Wallrath LL, et al. (2008) Preferential dimethylation of histone H4 lysine 20 by Suv4-20. J Biol Chem 283: 12085–12092.
38. Shiio Y, Rose DW, Aur R, Donohoe S, Aebersold R, et al. (2006) Identification and characterization of SAP25, a novel component of the mSin3 corepressor complex. Mol Cell Biol 26: 1386–1397.
39. Hastie AR, Pruitt SC (2007) Yeast two-hybrid interaction partner screening through in vivo Cre-mediated Binary Interaction Tag generation. Nucleic Acids Res 35: e141.
40. Rogowski K, Juge F, van Dijk J, Wloga D, Strub JM, et al. (2009) Evolutionary divergence of enzymatic mechanisms for posttranslational polyglycylation. Cell 137: 1076–1087.
41. Artymiuk PJ, Poirrette AR, Rice DW, Willett P (1996) Biotin carboxylase comes into the fold. Nat Struct Biol 3: 128–132.
42. Dideberg O, Bertrand J (1998) Tubulin tyrosine ligase: a shared fold with the glutathione synthetase ADP-forming family. Trends Biochem Sci 23: 57–58.
43. Galperin MY, Koonin EV (1997) A diverse superfamily of enzymes with ATP-dependent carboxylate-amine/thiol ligase activity. Protein Sci 6: 2639–2643.
44. Gundersen GG, Bulinski JC (1986) Distribution of tyrosinated and nontyrosinated alpha-tubulin during mitosis. J Cell Biol 102: 1118–1126.
45. Peris L, Wagenbach M, Lafanechere L, Brocard J, Moore AT, et al. (2009) Motor-dependent microtubule disassembly driven by tubulin tyrosination. J Cell Biol 185: 1159–1166.
46. Maney T, Hunter AW, Wagenbach M, Wordeman L (1998) Mitotic centromere-associated kinesin is important for anaphase chromosome segregation. J Cell Biol 142: 787–801.
47. Yang H, Mizzen CA (2009) The multiple facets of histone H4-lysine 20 methylation. Biochem Cell Biol 87: 151–161.
48. Wu S, Rice JC (2011) A new regulator of the cell cycle: the PR-Set7 histone methyltransferase. Cell Cycle 10: 68–72.
49. Brustel J, Tardat M, Kirsh O, Grimaud C, Julien E (2011) Coupling mitosis to DNA replication: the emerging role of the histone H4-lysine 20 methyltransferase PR-Set7. Trends Cell Biol 21: 452–460.
50. Beck DB, Oda H, Shen SS, Reinberg D (2012) PR-Set7 and H4K20me1: at the crossroads of genome integrity, cell cycle, chromosome condensation, and transcription. Genes Dev 26: 325–337.
51. Pidoux AL, Allshire RC (2005) The role of heterochromatin in centromere function. Philos Trans R Soc Lond B Biol Sci 360: 569–579.
52. Kourmouli N, Jeppesen P, Mahadevhaiah S, Burgoyne P, Wu R, et al. (2004) Heterochromatin and tri-methylated lysine 20 of histone H4 in animals. J Cell Sci 117: 2491–2501.
53. Kellum R, Alberts BM (1995) Heterochromatin protein 1 is required for correct chromosome segregation in Drosophila embryos. J Cell Sci 108 (Pt 4): 1419–1431.
54. Hayakawa T, Haraguchi T, Masumoto H, Hiraoka Y (2003) Cell cycle behavior of human HP1 subtypes: distinct molecular domains of HP1 are required for their centromeric localization during interphase and metaphase. J Cell Sci 116: 3327–3338.
55. Hutchins JR, Toyoda Y, Hegemann B, Poser I, Heriche JK, et al. (2010) Systematic analysis of human protein complexes identifies chromosome segregation proteins. Science 328: 593–599.
56. Neumann B, Walter T, Heriche JK, Bulkescher J, Erfle H, et al. (2010) Phenotypic profiling of the human genome by time-lapse microscopy reveals cell division genes. Nature 464: 721–727.
57. Bianchi DW, Maron JL, Johnson KL (2010) Insights into fetal and neonatal development through analysis of cell-free RNA in body fluids. Early Hum Dev 86: 747–752.
58. Koide K, Slonim DK, Johnson KL, Tantravahi U, Cowan JM, et al. (2011) Transcriptomic analysis of cell-free fetal RNA suggests a specific molecular phenotype in trisomy 18. Hum Genet 129: 295–305.
59. Adrain C, Freeman M (2012) New lives for old: evolution of pseudoenzyme function illustrated by iRhoms. Nat Rev Mol Cell Biol 13: 489–498.

- Pujals A, Renouf B, **Robert A,** Chelouah S, Hollville E, Wiels J. *Treatment with a BH3 mimetic overcomes the resistance of latency III EBV (+) cells to p53-mediated apoptosis. Cell Death Dis. 2011 Jul*

- Pujals A, Fabre L., Durieu C., **Robert A,** Meurice G, Legentil M., Chelouah S, Lecam E., Vassilev L., Lipinski M, Wiels J. *Constitutive Autophagy in Epstein-Barr Virus-positive Latency III Cells Protects them from Nutlin-3-induced Apoptosis. Autophagy 2015*

Citation: Cell Death and Disease (2011) 2, e184; doi:10.1038/cddis.2011.67

www.nature.com/cddis

Treatment with a BH3 mimetic overcomes the resistance of latency III EBV (+) cells to p53-mediated apoptosis

A Pujals[1,2], B Renouf[1,2,3], A Robert[1], S Chelouah[1], É Hollville[1,4] and J Wiels*[,1]

P53 inactivation is often observed in Burkitt's lymphoma (BL) cells due to mutations in the p53 gene or overexpression of its negative regulator, murine double minute-2 (MDM2). This event is now considered an essential part of the oncogenic process. Epstein–Barr virus (EBV) is strongly associated with BL and is a cofactor in its development. We previously showed that nutlin-3, an antagonist of MDM2, activates the p53 pathway in BL cell lines harboring wild-type p53. However, nutlin-3 strongly induced apoptosis in EBV (−) or latency I EBV (+) cells, whereas latency III EBV (+) cells were much more resistant. We show here that this resistance to apoptosis is also observed in latency III EBV (+) lymphoblastoid cell lines. We also show that, in latency III EBV (+) cells, B-cell lymphona 2 (Bcl-2) is selectively overproduced and interacts with Bcl-2-associated X protein (Bax), preventing its activation. The treatment of these cells with the Bcl-2-homology domain 3 mimetic ABT-737 disrupts Bax/Bcl-2 interaction and allows Bax activation by nutlin-3. Furthermore, treatment with these two compounds strongly induces apoptosis. Thus, a combination of Mdm2 and Bcl-2 inhibitors might be a useful anti-cancer strategy for diseases linked to EBV infection.
Cell Death and Disease (2011) **2,** e184; doi:10.1038/cddis.2011.67; published online 28 July 2011
Subject Category: Cancer

The p53 tumor suppressor is a transcription factor that is activated in response to DNA or cell damage, such as oncogene activation, radiation, mitotic stress, ribosomal stress or chemical challenge.[1] When activated, p53 has a key role in protecting against tumor development, by inducing cell cycle arrest or apoptosis.[2] This physiological function of p53 is frequently altered in malignant cells, through mutation, cytoplasmic sequestration, interaction with viral oncoproteins or an increase in interactions with its main cellular regulator murine double minute-2 (MDM2).[3] MDM2 is an E3 ubiquitin ligase that binds p53 and induces its ubiquitin-dependent degradation.[4] MDM2 also inhibits the transcriptional activity of p53 through direct protein–protein interactions.[5] MDM2 overproduction, leading to p53 inactivation, has been observed in various types of cancer.[6,7] Given the key role of p53 in determining cell fate, several strategies for disrupting the p53–MDM2 interaction have been explored.[8,9] Potent, stable and selective small-molecule antagonists of MDM2 have recently been synthesized. These molecules include nutlins, *cis*-imidazoline compounds that act by binding to the p53 pocket of MDM2, thereby overcoming the inhibitory effects of this molecule and inducing the release and activation of p53.[10] Nutlin treatment has been shown to enhance apoptosis in various tumor cells *in vitro*,[11,12] to inhibit tumor growth *in vivo*[10,13] and to act in synergy with genotoxic drugs or irradiation in cancer therapy (reviewed in Vassilev[14]).

The anti-cancer activity of p53 results principally from the ability of this molecule to induce apoptosis through the intrinsic mitochondrial pathway.[15] The crucial event in the initiation of this pathway is mitochondrial outer membrane permeabilization (MOMP), leading to the release of signaling molecules from the intermembrane space into the cytosol.[16] This process is controlled by members of the B-cell lymphoma 2 (Bcl-2) protein family.[17] This family has pro-apoptotic members, classified into 'effectors' (Bcl-2-associated X protein (Bax) and Bak), which participate directly in membrane permeabilization, and 'Bcl-2-homology domain 3 (BH3)-only members' (Puma, Noxa, Bad, Bim and Bid), which act as 'direct activators' or 'sensitizers' of the apoptotic pathway.[18] However, this family also has anti-apoptotic members, such as Bcl-2, B-cell lymphoma-extra large (Bcl-xL) and myeloid cell factor-1 (Mcl-1), which antagonize MOMP. The levels of the pro-apoptotic Bcl-2 family proteins Bax, Noxa, Bid and Puma are directly regulated by p53.[19]

The p53 pathway is frequently disrupted in Burkitt's lymphoma (BL) cells, and this disruption is now considered

[1]UMR 8126 CNRS, Univ Paris-Sud, Institut Gustave Roussy, Villejuif, France
*Corresponding author: J Wiels, UMR 8126 CNRS, Univ Paris-Sud, Institut Gustave Roussy, 114 rue Edouard Vaillant, Villejuif, Cedex 94805, France. Tel: +33 1 4211 4740; Fax: +33 1 4211 5494; E-mail: wiels@igr.fr
[2]These authors contributed equally to this work.
[3]Current address: INSERM U682, Hôpital de Hautepierre, Strasbourg, France
[4]Current address: Molecular Cell Biology Laboratory, Department of Genetics, The Smurfit Institute, Trinity College, Dublin, Ireland
Keywords: p53; Bax; Bcl-2; EBV; apoptosis; Burkitt's lymphoma
Abbreviations: Bax, Bcl-2-associated X protein; Bcl-xL, B-cell lymphoma-extra large; Bcl-2, B-cell lymphoma 2; BH3, Bcl-2-homology domain 3; caspase, cysteinyl aspartate-specific protease; $DiOC_6(3)$, 3′-dihexyloxacarbocyanine iodide; BL, Burkitt's lymphoma; EBV, Epstein–Barr virus; PI, propidium iodide; LCL, lymphoblastoid cell lines; LMP, latent membrane protein; Mcl-1, myeloid cell factor-1; MDM2, murine double minute-2; MFI, mean fluorescence intensity; MOMP, mitochondrial outer membrane permeabilization; NFκB, nuclear factor-κ B; PARP, poly (ADP-ribose) polymerase
Received 26.1.11; revised 15.6.11; accepted 16.6.11; Edited by A Stephanou

as an essential part of the tumorigenic process.[20] In a previous study, we therefore investigated the consequences of activating wt p53 and determined whether Epstein–Barr virus (EBV) infection of the cells had an effect on these consequences.[21] The EBV genome is present in the vast majority of BL cases. The virus remains latent in infected tumor cells, producing only a very small number of viral proteins.[22] Most EBV-infected BL cells harbor the latency I phenotype (Epstein–Barr nuclear antigen 1 (EBNA1) is the only viral protein produced). However, cases with the latency III profile (all latent EBV proteins are produced: EBNA1, 2, 3a, 3b, 3c, EBNA leader protein, latent membrane protein 1 (LMP1) and 2 (LMP2)) have also been identified.[23] Latent EBV does not specifically target p53, but it nonetheless interferes with cell cycle checkpoints regulated by p53 in the G1/S and G2/M phases[24] and modulates p53-induced apoptosis.[25] We have shown that, regardless of EBV status, the treatment of BL cells with nutlin-3 induces p53 activation, as shown by the induction of $p21^{WAF1}$ MDM2 and Bax. However, although nutlin-3-treated EBV (−) BL cells display massive apoptosis, latency III EBV (+) cells are much more resistant.[21]

In this study, we investigated the mechanism responsible for the resistance to p53-mediated apoptosis induced by EBV in lymphoid cells. We analyzed two types of EBV (+) latency III cells: BL cells and lymphoblastoid cell lines (LCLs), a recognized model for the study of post-transplantation lymphoproliferative disorders. Both types of cell were found to be more resistant to treatment with nutlin-3 than EBV (−) cells. In EBV (−) cells, Bax was activated by nutlin-3 treatment, promoting apoptosis. By contrast, in EBV (+) latency III cells, Bax accumulated in mitochondria but was poorly activated by nutlin-3. Our findings indicate that Bcl-2 is selectively overproduced in these cells and forms stable complexes with Bax. Treatment with nutlin-3 has no significant impact on these complexes. Finally, we also demonstrated that ABT-737, a potent and selective small molecule that binds and antagonizes Bcl-xl, Bcl-2 and Bcl-w, sensitizes EBV (+) latency III cells to nutlin-3 treatment.

Results

Latency III EBV (+) cells are more resistant than EBV (−) cells to p53-dependent apoptosis. We have previously shown that, in BL cell lines, the induction of apoptosis by nutlin-3 depends on the EBV status of the cells: EBV (−) and EBV (+) latency I cells are highly sensitive to this antagonist of MDM2, whereas EBV (+) latency III cells are much more resistant.[21] We investigated whether other EBV (+) latency III cells were also resistant to p53-dependent apoptosis by evaluating the response to nutlin-3 treatment in LCLs. All cell lines were treated with 10 μM nutlin-3 for 24 h and apoptosis was assessed by flow cytometry after labeling the cells with annexin-V-FITC and propidium iodide (PI). Nutlin-3 induced slightly higher levels of apoptosis in LCL (52 ± 10%, 49 ± 4%, 48 ± 7% apoptotic cells for RPMI8866, Priess and Remb1 cells, respectively) than in latency III BL cell lines (40 ± 4%, 18 ± 5%, 36 ± 2%, for BL2/B95, Seraphina and LY47 cells, respectively) but these levels of apoptosis remained lower than those in EBV (−) BL cell lines (76 ± 4%, 95 ± 4% for BL2 and BL28 cells, respectively; Figure 1a).

We characterized the apoptotic cell death induced by nutlin-3 in more detail by measuring the loss of mitochondrial membrane potential ($\Delta_{\Psi m}$) by flow cytometry with the carbocyanine dye 3′-dihexyloxacarbocyanine iodide ($DiOC_6(3)$). Loss of $\Delta_{\Psi m}$ occurs early in apoptosis and was therefore measured after 16 h of treatment with nutlin-3. In EBV (−) BL cells treated with nutlin-3, mitochondrial depolarization was observed in 53 ± 6 % of BL2 cells and 89 ± 5% of BL28 cells (Figure 1b). By contrast, in EBV (+) latency III cells (BL and LCL), the loss of $\Delta_{\Psi m}$ was much milder, with 25 ± 2%, 9 ± 3%, 5 ± 4%, 19 ± 4%, 22 ± 1%, 23 ± 2 % mitochondrial depolarization in BL2/B95, Seraphina, LY47, RPMI8866, Priess and Remb1 cells, respectively.

We then carried out western blotting to assess the cleavage of poly (ADP-ribose) polymerase (PARP), a DNA repair enzyme directly targeted by caspase-3 (cysteinyl aspartate-specific protease-3). After 7 h of treatment with nutlin-3, the 85 kDa PARP cleavage product was observed in EBV (−) BL2 and BL28 cell extracts, whereas no cleavage was observed in EBV (+) BL and LCL extracts, except for Remb1 cells, in which low levels of cleavage were detected (Figure 1c). After 24 h of treatment, PARP was almost totally (BL2) or totally (BL28) cleaved in EBV (−) cells. By contrast, in EBV (+) cells, PARP cleavage occurred either at very low rates (BL2/B95, RPMI8866, Priess and Remb1 cells) or not at all (Seraphina and LY47 cells). Thus, both BL and LCL latency III EBV (+) cells are more resistant than EBV (−) cells to p53-mediated apoptosis.

The activation of p53 increases Bax levels similarly in EBV (−) and EBV (+) cell lines. In susceptible EBV (−) BL cells, nutlin-3-induced apoptosis involves permeabilization of the mitochondrial outer membrane. This mechanism is generally controlled and mediated by Bcl-2 family proteins. The pro-apoptotic protein Bax, encoded by a p53 target gene, is one member of this family. We showed in a previous study that nutlin-3 activated the p53 pathway similarly in all BL cell lines.[21] In this study, we measured the accumulation of Bax in both EBV (−) BL cell lines and EBV (+) latency III BL and LCL treated with nutlin-3 for various periods of time (3, 7 or 24 h). Western blot analysis was carried out to determine the levels of p53 (as a control of its activation) and of Bax. Bax-specific bands were quantified by densitometry and normalized with respect to β-actin levels. In all cell lines, treatment with nutlin-3 induced a gradual increase in Bax levels until 24 h of treatment (Figure 2). These results are consistent with our previous findings and confirm that the accumulation of Bax in response to p53 activation is not correlated with the EBV status of the cells and that the resistance of EBV (+) cells to apoptosis does not result from a defect in Bax accumulation.

Following p53 activation, Bax accumulates in the mitochondria of latency III EBV (+) cells but is not activated. For Bax to be active, it must be translocated from the cytosol (where it is found in healthy cells) to the outer mitochondrial membrane. The redistribution of Bax was assessed by western blot analysis of the mitochondrial and

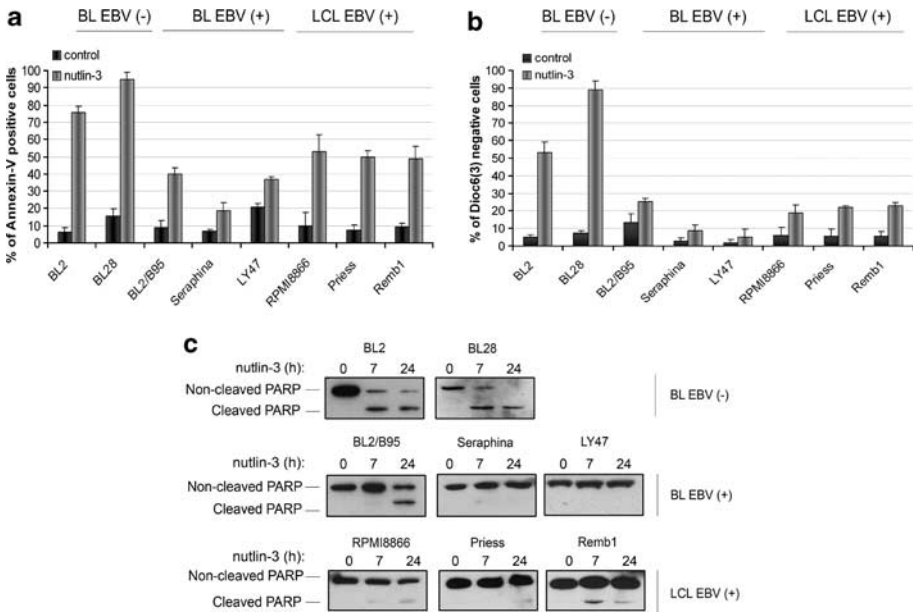

Figure 1 Effect of nutlin-3 treatment on the induction of apoptosis in Epstein–Barr virus (EBV) (−), EBV (+) Burkitt's lymphoma (BL) and lymphoblastoid cell lines (LCLs). (**a**) Cells were treated with 10 μM nutlin-3 or with the solvent dimethyl sulfoxide for 24 h. The cells were labeled with annexin V-FITC and PI and analyzed with a FACSCalibur flow cytometer to determine the percentage of cells that were apoptotic. The values presented (means ± s.d.) are from three independent experiments. (**b**) Cells were treated with 10 μM nutlin-3 or the solvent dimethyl sulfoxide for 16 h. The cells were stained with $DIOC_6(3)$ and analyzed on a FACSCalibur flow cytometer. $DiOC_6(3)$ stains mitochondria in a potential-dependent fashion. Cells with a low $\Delta\Psi_m$ are therefore only weakly fluorescent, and are described as '$DiOC_6(3)$ negative'. The values presented (means ± s.d.) are from three independent experiments. (**c**) Cells were treated with 10 μM nutlin-3 for the indicated periods of time. Apoptosis levels were determined by assessing polyadenosine diphosphate-ribose polymerase (PARP) cleavage on western blots. Results are representative of at least three independent experiments

cytosolic fractions of untreated cells and of cells treated with nutlin-3 for 24 h (Figure 3a). Fractionation quality was checked by probing blots with antibodies recognizing proteins known to be localized to mitochondria (Bcl-2) or the cytosol (vinculin). Bax-specific bands were then quantified by densitometry and the results were normalized with respect to Bcl-2 or vinculin levels. In EBV (−) BL cells, nutlin-3 treatment either strongly decreased the amount of Bax in the cytosolic fractions (BL2) or resulted in this protein being undetectable (BL28) in these fractions, whereas Bax levels in the mitochondrial fractions clearly increased. By contrast, in EBV (+) cell lines (BL and LCL), Bax accumulated in both the cytosolic and mitochondrial fractions after treatment with nutlin-3.

We investigated whether the Bax accumulating in the mitochondria was in the activated form by labeling cells with the 6A7 conformation-specific Bax mAb (Figure 3b). This antibody recognizes an N-terminal epitope of Bax that is occluded in the inactive form of the protein but exposed after the activation and insertion of the protein into membranes.[26] After treatment with nutlin-3, 52% of EBV (−) BL2 cells were positive for 6A7 labeling (mean fluorescence intensity (MFI): 105 *versus* 48 for control), whereas latency III EBV (+) cells were only weakly stained (2% (MFI: 38 *versus* 36), 25% (MFI: 66 *versus* 39) and 32% (MFI: 68 *versus* 28) for LY47, BL2/B95 and Remb1 cells, respectively).

To confirm that the activation of Bax is involved in nutlin-3-mediated apoptosis of BL2 cells, we next inhibited the production of this protein with a specific small-interfering RNA, treated the cells with nutlin-3 and then measured apoptosis levels by assessing PARP cleavage on western blots. In BL2 cells with low levels of Bax, lower levels of PARP cleavage were observed than in controls cells (Supplementary Figure 1). These data show that, in EBV (−) cells treated with nutlin-3, Bax accumulates in mitochondria in its activated form and takes part in the apoptotic process. By contrast, in EBV (+) latency III cells, most of the Bax accumulating in the mitochondria is not in the active conformation.

Bcl-2 is overproduced in latency III EBV (+) cells. At least three EBV-encoded proteins (LMP1, LMP2A and EBNA2) have been shown to induce the upregulation of various anti-apoptotic Bcl-2 family members able to sequester Bax.[27–29] We therefore carried out western blotting to evaluate the endogenous levels of these anti-apoptotic proteins (Bcl-2, Bcl-xL and Mcl-1) in our cell lines (Figure 4). There was no direct correlation between the EBV status of the various cell lines and basal levels of Bcl-xL or Mcl-1. By contrast, a strong correlation was observed between basal levels of Bcl-2 and EBV status: all latency III EBV (+) cells contained high levels of Bcl-2, whereas EBV (−) cells had low levels of this protein. To confirm that high levels of Bcl-2 were correlated with LMP1 expression,[28] we also assessed the level of this viral protein. Large amounts of LMP1 were observed in all EBV (+) cell lines except BL2/B95, which had only low levels of this protein. As LMP1 has also been shown to induce the downregulation of Bax,[30] we determined endogenous Bax levels in our various cell lines. No correlation was observed between the EBV status and Bax levels.

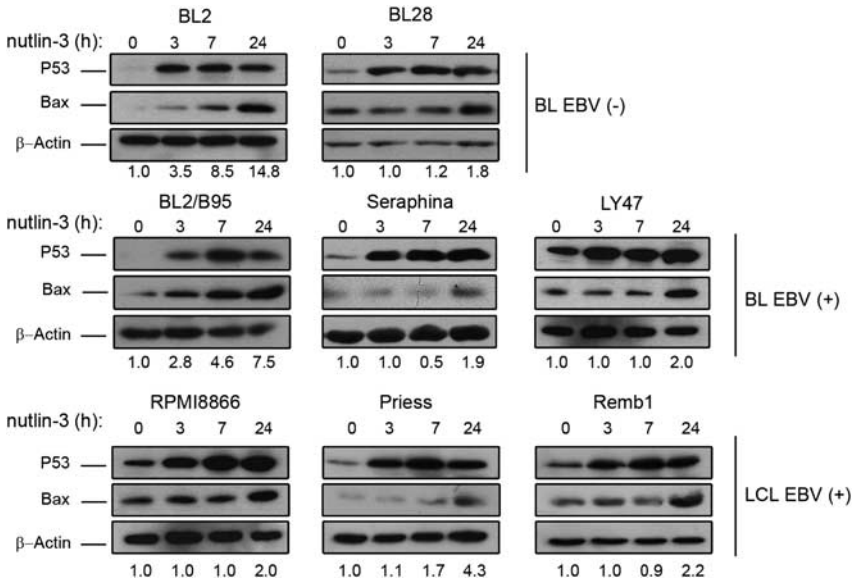

Figure 2 Effect of nutlin-3 treatment on p53 and Bax levels in Burkitt's lymphoma (BL) and lymphoblastoid cell lines (LCLs). Cells were treated with 10 μM nutlin-3 for the indicated periods of time. The levels of p53 and Bax protein were assessed by western blot analysis. Fold-change values for Bax *versus* the untreated control (0 h), normalized with respect to β-actin levels are shown under the blots

Bcl-2 interacts with Bax in latency III EBV (+) cells, but not in EBV (−) cells. We investigated the role of Bcl-2 in the resistance to apoptosis observed in latency III EBV (+) cells by studying the interactions between Bax and Bcl-2. BL2 EBV (−) cells and BL2/B95 EBV (+) cells (which differ only in terms of their EBV status) were left untreated or treated with nutlin-3 for 7 h. Proteins were then extracted and immunoprecipitation was carried out with an anti-Bax pAb. The immunoprecipitates were then probed for Bax and Bcl-2 (Figure 5). These western blots showed that treatment with nutlin-3 induced a stronger accumulation of Bax in BL2 than in BL2/B95 cells, but that Bcl-2 was coprecipitated with Bax only in BL2/B95 cells, with nutlin-3 treatment having no significant impact on this co-immunoprecipitation. Thus, in EBV (+) latency III cells, Bax and Bcl-2 form stable complexes that may be at least partly responsible for the resistance to apoptosis.

An inhibitor of Bcl-2 disrupts the interactions between Bax and Bcl-2 and allows Bax activation in BL2/B95 EBV (+) cells treated with nutlin-3. We investigated the involvement of interactions between Bax and Bcl-2 in resistance to nutlin-3-induced apoptosis using ABT-737, a BH3 mimetic that antagonizes pro-survival members of the Bcl-2 family, promoting the release of Bax.[31] We first investigated the effect of this Bcl-2 inhibitor on Bax/Bcl-2 interaction. BL2/B95 EBV (+) cells were treated for 1 h with ABT-737 (10 μM), incubated with nutlin-3 for 7 h and protein extracts were prepared. We then assessed Bax and Bcl-2 levels by western blotting and interaction between these two molecules by co-immunoprecipitation. Treatment with ABT-737 had no effect on Bcl-2 or Bax levels (Figure 6a), but abolished the co-immunoprecipitation of Bax with Bcl-2, in both untreated cells and cells treated with nutlin-3 (Figure 6b).

We also evaluated the effect of treatment with ABT-737 on the distribution of Bax in untreated cells and cells treated with nutlin-3. ABT-737 decreased the accumulation of Bax in the cytosol induced by nutlin-3 alone and concomitantly increased the level of Bax in the mitochondria (Figure 6c). We investigated whether the Bax accumulating in the mitochondria was in the activated form by labeling the cells with the 6A7 conformation-specific Bax mAb (Figure 6d). After treatment with ABT-737 alone or nutlin-3 alone, 10% (MFI: 39 *versus* 31) and 23% (MFI: 62) of BL2/B95 cells, respectively, were weakly positive for 6A7 labeling, whereas when the two compounds were used in combination, 41% (MFI: 74) of the cells were strongly labeled with the 6A7 mAb. Thus, a combined treatment with ABT-737 and nutlin-3 induces the release of Bax from the Bax/Bcl-2 complexes and its activation in mitochondria.

An inhibitor of Bcl-2 restores the susceptibility of latency III EBV (+) cells to p53-dependent apoptosis. We then used flow cytometry to determine whether treatment with ABT-737 sensitized the EBV (+) latency III BL and LCL cells to nutlin-3-induced apoptosis (Figure 7a). Consistent with our previous observations, treatment with nutlin-3 for 24 h induced $<50\%$ apoptosis in these cells. Treatment with ABT-737 (10 μM) alone had no cytotoxic effect on BL2/B95 and Seraphina cells but induced $42 \pm 7\%$ apoptosis in LY47 cells. An even stronger effect was observed in LCL cells, in which treatment with 10 μM ABT-737 for 24 h induced $>70\%$ apoptosis (data not shown). In these cell lines, we therefore decreased the concentration of ABT-737 used to reduce its cytotoxic effect. Treatment with 0.25 μM ABT-737 induced $32 \pm 8\%$, $47 \pm 3\%$ and $39 \pm 2\%$ apoptosis in RPMI8866, Priess and Remb1 cells, respectively. When the two drugs were used in combination, a synergic effect on the induction of apoptosis was observed in BL2/B95 and Seraphina cells ($78 \pm 5\%$ and $81 \pm 3\%$ apoptotic cells, respectively). In the other cell lines, no synergy between ABT-737 and nutlin-3 was observed, these

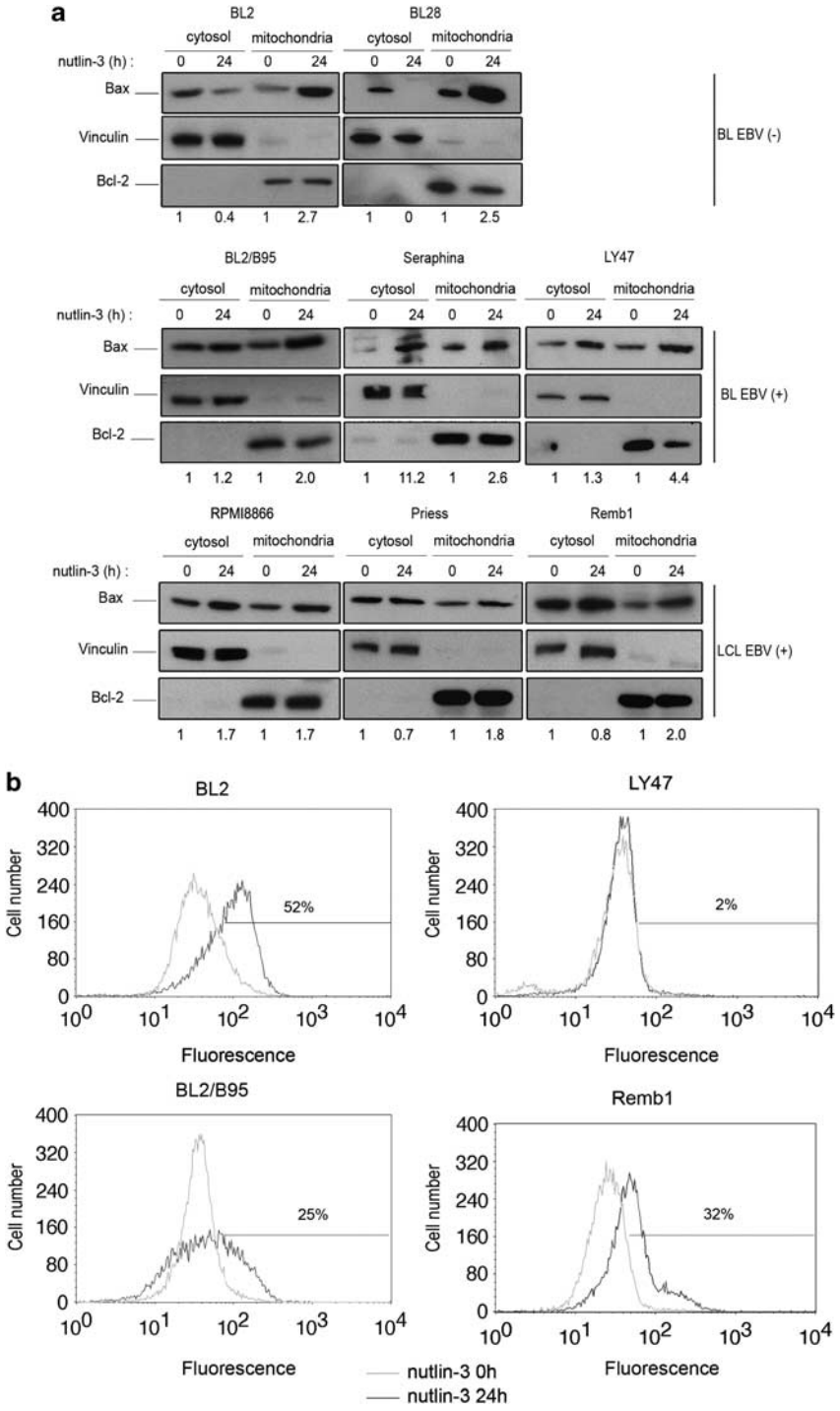

Figure 3 Effect of nutlin-3 treatment on Bax relocalization and activation in EBV (−) and EBV (+) cells. (**a**) Cells were treated with 10 μM nutlin-3 or the solvent dimethyl sulfoxide for 24 h. Cytosolic and mitochondrial fractions were analyzed by western blotting with an anti-Bax pAb. Vinculin and Bcl-2 were used as cytosolic and mitochondrial markers, respectively. Fold-change values *versus* the untreated control (0 h), after normalization with respect to vinculin or Bcl-2 protein levels, are shown under the blots. Results are representative of three independent experiments. (**b**) BL2 EBV (−) cells and BL2/B95, LY47 and Remb1 EBV (+) cells were treated with 10 μM nutlin-3 or the solvent dimethyl sulfoxide for 24 h. Cells were fixed in 0.25% paraformaldehyde and labeled with a conformation-specific 6A7 Bax antibody, which recognizes only the active conformation of the protein and Alexa 488-conjugated goat anti-mouse IgG. Cells were then analyzed with a FACSCalibur flow cytometer

compounds instead having an additive effect (65 ± 1%, 71 ± 8%, 73 ± 7% and 81 ± 5% apoptosis in LY47, RPMI8866, Priess and Remb1 cells, respectively). We also evaluated the effect of nutlin-3 and ABT-737 on three cell lines originating from the same individual: BL40, BL40/B95 and IARC 211. BL2 and BL2/B95 were used as controls. Apoptosis was determined by assessing PARP cleavage on western blots (Figure 7b). No cleavage of PARP was

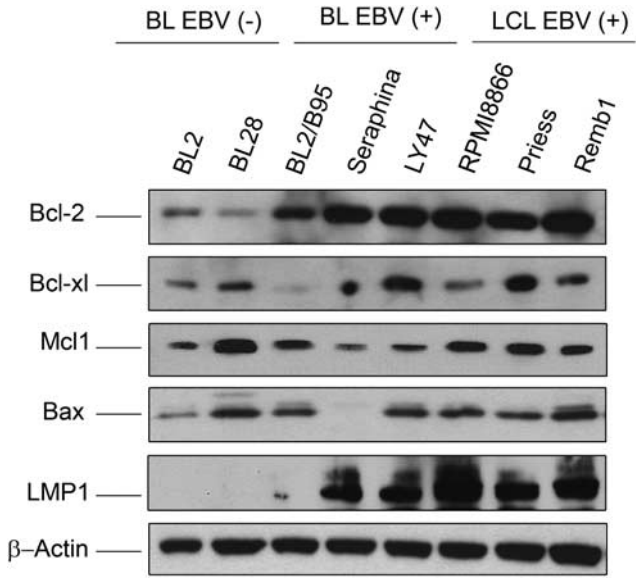

Figure 4 Levels of Bcl-2 family members in EBV (−) and EBV (+) lymphoid cell lines. Levels of the Bax, Bcl-2, Bcl-xl and Mcl-1 proteins as well as these of the viral LMP1 protein were assessed by western blot analysis

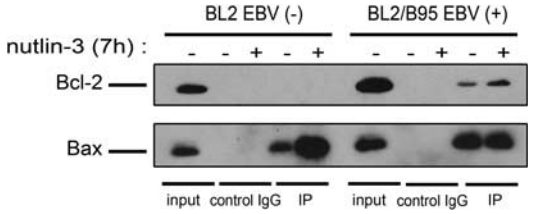

Figure 5 Interaction of Bax with Bcl-2 in BL2 EBV (−) and BL2/B95 EBV (+) cells untreated or treated with nutlin-3. Cells were treated with 10 μM nutlin-3 or the solvent dimethyl sulfoxide for 7 h. Lysates were subjected to immunoprecipitation with agarose-conjugated anti-Bax pAb (IP) or agarose-conjugated control rabbit IgG (IgG control) and then subjected to western blotting with an anti-Bcl-2 mAb or an anti-Bax pAb. As a control for protein levels before IP, a portion of cell lysate (input) corresponding to 15% of the input for IP was also included in the western blot. All results are representative of three independent experiments

observed after treatment with ABT-737 alone in BL2 and BL2/B95 cells, whereas a strong or partial cleavage was observed in BL40, BL40/B95 and IARC 211 cells. Treatment with nutlin-3 alone induced strong (BL2) or complete (BL40) cleavage of PARP in EBV (−) cell lines, moderate cleavage in BL2/B95 cells and almost no cleavage in BL40/B95 and IARC 211 cells. As expected, treatment with both compounds had an additive effect on cell viability and PARP was totally cleaved in all cell lines.

Finally, as EBV reactivation might also reduce cell viability, we tested the effects of nutlin-3 and ABT-737 on production of the viral BZLF1 protein, a transcriptional activator that mediates the transition between the latent and lytic cycles of EBV. Except in LY47 cells, in which nutlin-3 slightly increased the very low basal levels of BZLF1 protein, nutlin-3, ABT-737 and the combination of these two molecules were unable to induce the production of this protein in any of the EBV (+) cell lines tested, (Supplementary Figure 2). Thus, a combined treatment with ABT-737 and nutlin-3 efficiently induces the apoptosis of latency III EBV (+) cells producing large amounts of Bcl-2 protein, without affecting the latent stage of the virus.

Discussion

The activation of wt p53, or even the reactivation of mutant p53, alone or in combination with cytotoxic agents (chemotherapy drugs or radiation) is now considered a promising new approach for cancer treatment.[15,32] Various elements must be considered during the development of such new therapies, including the cellular context, which may greatly modulate the consequences of p53 activation. In this study, we showed that the type III latent EBV infection of lymphoid cells does not prevent the p53 activation induced by an inhibitor of Mdm2, but strongly decreases p53-induced apoptosis. We also found that the activation of p53 induced Bax accumulation similarly in all cell lines and that this pro-apoptotic member of the Bcl-2 family was involved in the apoptotic pathway in EBV (−) cell lines. Bax is primarily a cytosolic protein in healthy living cells. Following the induction of apoptosis, it undergoes a conformational change and is translocated to the mitochondria.[33] After nutlin-3 treatment, Bax underwent conformational changes and relocalization in EBV (−) cells, whereas in EBV (+) cells, it accumulated in both the cytosol and the mitochondria but underwent no conformational changes. Thus, the accumulation of Bax in the mitochondria of EBV (+) cells is not sufficient to induce apoptosis.

Several studies have shown that latent infection with EBV protects cells from apoptosis. For example, the viral proteins LMP1 and LMP2A have been shown to upregulate various anti-apoptotic members of the Bcl-2 family by activating the nuclear factor-κ B (NFκB) pathway,[28] or to inhibit the transcription of the pro-apoptotic Bax protein.[30] We determined the endogenous levels of Bax, Bcl-2, Bcl-xl and Mcl-1 in our cell lines. Consistent with the results of Rowe *et al.*,[28] we observed a strong correlation between basal Bcl-2 level and EBV status: all latency III EBV (+) cells had high levels of Bcl-2, whereas EBV (−) cells had low levels of this protein. By contrast, Bax levels, similar to those of Bcl-xl and Mcl-1, were variable in all cell lines, regardless of EBV status. It has been reported that Bcl-2 inhibits both changes in the conformation of the N-terminus of Bax and the translocation of Bax from the cytosol to the mitochondria.[34,35] Our results are consistent with these observations, as we observed no specific translocation of Bax to the mitochondria after the treatment with nutlin-3 of cells overproducing Bcl-2. We also showed that Bcl-2 interacted with Bax in EBV (+) cells, but not in EBV (−) cells. This sequestration of Bax may account, at least in part, for the resistance to nutlin-3 observed in EBV (+) latency III cells. Our results are also consistent with those of Forte and Luftig,[36] who previously showed that, in LCL, nutlin-3 induced p53 activation and a moderate level of apoptosis (around 40% of annexin-V (+) cells after 48 h of treatment), which was enhanced by previous treatment of the cells with an inhibitor of NFκB activity. They showed that NFκB activity controlled steady-state levels of MDM2 protein and concluded that the NFκB inhibitor sensitized cells to nutlin-3 by decreasing MDM2 levels. However, as the upregulation of

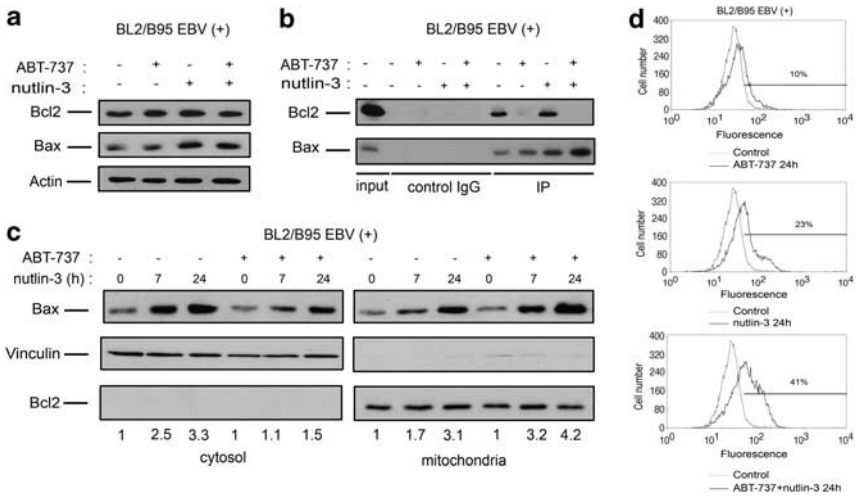

Figure 6 Effect of a combination of nutlin-3 and ABT-737 in the EBV (+) cell lines. BL2B95 EBV (+) cells were or were not subjected to prior treatment with 10 μM ABT-737 for 1 h, and were then treated with nutlin-3 for 7 h. (**a**) The levels of Bcl-2 and Bax proteins were assessed by western blot analysis. (**b**) Lysates were subjected to immunoprecipitation with agarose-conjugated anti-Bax pAb (IP) or agarose-conjugated control rabbit IgG (IgG control) and then subjected to western blotting with an anti-Bcl-2 mAb or an anti-Bax pAb. As a control for protein levels before IP, a portion of cell lysate (Input) corresponding to 15% of the input for IP was also included in the western blot. All results are representative of three independent experiments. (**c**) BL2/B95 EBV (+) cells were or were not subjected to prior treatment with 10 μM ABT-737 for 1 h and were then treated with nutlin-3 for the indicated periods of time. Cytosolic and mitochondrial fractions were analyzed by western blotting with an anti-Bax pAb. Vinculin and Bcl-2 were used as cytosolic and mitochondrial markers, respectively. Fold-change values *versus* the untreated control (0 h), after normalization with respect to the levels of vinculin or Bcl-2 protein, are shown under the blots. The results shown are representative of three independent experiments. (**d**) BL2/B95 cells were or were not subjected to prior treatment with ABT-737 for 1 h and were then left untreated or treated with nutlin-3 for 24 h. Cells were fixed in 0.25% paraformaldehyde and labeled with a conformation-specific 6A7 Bax antibody, which recognizes only the active conformation of the protein and Alexa 488-conjugated goat anti-mouse IgG. Cells were then analyzed with a FACSCalibur flow cytometer

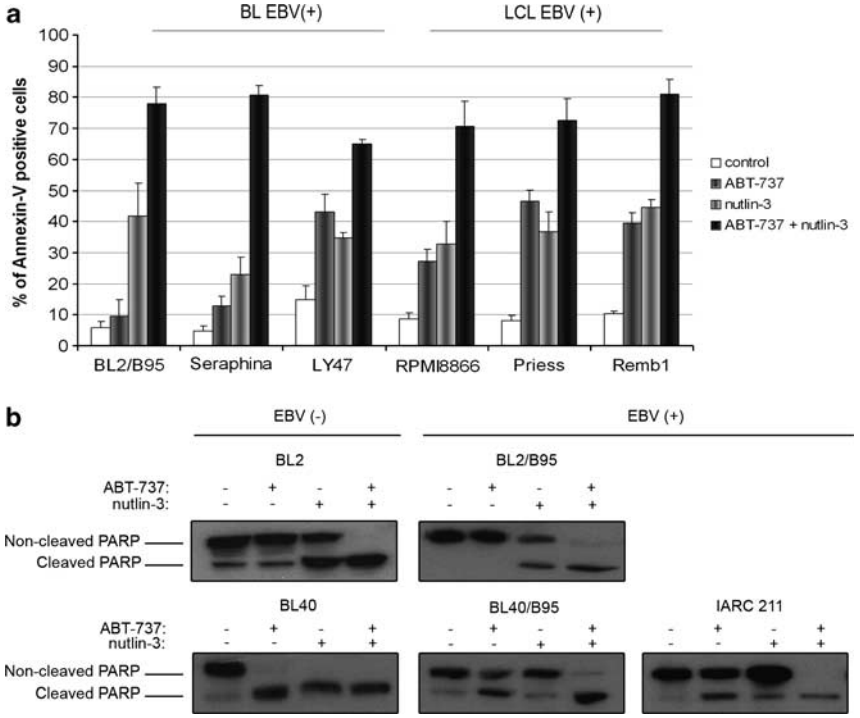

Figure 7 Effect of a combination of nutlin-3 and ABT-737 on the induction of apoptosis in EBV (+) Burkitt's lymphoma (BL) and lymphoblastoid cell lines (LCL). (**a**) EBV (+) cell lines were or were not subjected to prior treatment with ABT-737 (BL2/B95, Seraphina, LY47: 10 μM; 8866, Priess, Remb1: 0.25 μM) for 1 h and were then left untreated or treated with nutlin-3 for 24 h. The cells were labeled with annexin V-FITC and PI and analyzed with a FACSCalibur flow cytometer, to determine the percentage of cells that were apoptotic. The values presented (means ± s.d.) are from three independent experiments. (**b**) Cell lines were treated as in (**a**) and apoptosis levels were determined by assessing polyadenosine diphosphate-ribose polymerase (PARP) cleavage on western blots. Results are representative of at least three independent experiments

Bcl-2 in B cells containing LMP1 is due to NFκB activation,[28,37] it could also be deduced from their data that the NFκB inhibitor sensitizes cells by decreasing Bcl-2 levels.

ABT-737 is a BH3 mimetic that efficiently antagonizes various pro-survival members of Bcl-2 family and promotes the release of Bax and Bak.[31] In latency III EBV (+) cells, the disruption of Bax/Bcl-2 interaction by treatment with ABT-737 before nutlin-3 treatment promoted the relocalization of Bax to the mitochondria and its activation. Treatment with these two compounds also strongly induced the apoptosis of these cells. The combined inhibition of the MDM2 and Bcl-2 proteins has been reported to strongly induce apoptosis in acute myelogenous leukemia cells overproducing Bcl-2[38] and in tumors (including BL) in which Hdmx limits the p53 activation induced by nutlin-3.[39] Combined treatment with nutlin-3 and an inhibitor of the anti-apoptotic members of the Bcl-2 family, such as ABT-737, may therefore constitute an attractive new treatment strategy for tumors harboring wild-type p53 but with defects in the p53-induced apoptotic pathway. *In vivo* studies in murine models are now required to evaluate the effects of this combined treatment in terms of side effects and tumor regression and to compare these effects with those of conventional chemotherapy.

Concerning latency III EBV (+) cells, it will also be interesting to use *in vivo* models to assess the efficiency of ABT-737 alone, as we found that, even at very low doses, this compound promoted apoptosis in LCL cells. This treatment may be particularly beneficial in patients with EBV (+) post-transplant lymphoproliferative disorder or nasopharyngeal carcinoma, because both these types of tumor overproduce Bcl-2 or Bcl-xL.[40]

Materials and Methods

Cell lines. All BL cell lines were originally established from endemic or sporadic cases of BL. BL2, BL28, BL40, BL2/B95, BL40/B95 and LY47 were kindly provided by the International Agency for Research on Cancer (IARC, Lyon); Seraphina cells were provided by Professor G Klein (Stockholm); BL2/B95 and BL40/B95 cells were generated by stable infection of the original EBV (−) BL2 and BL40 cells with the B95-8 EBV strain. LCLs were obtained by the *in vitro* immortalization of normal B lymphocytes. IARC 211 cells were established from the normal B lymphocytes of patient BL40 and were obtained from IARC. Priess and Remb1 cells were kindly provided by Dr JG Bodmer (London). These cell lines were cultured in RPMI 1640 medium (PAA) containing 2 mM L-glutamine, 1 mM sodium pyruvate, 20 mM glucose, 100 U/ml penicillin and 100 μg/ml streptomycin and supplemented with 10% heat-inactivated fetal calf serum.

Antibodies and reagents. Nutlin-3 was obtained from Cayman Chemical (SPI-Bio, Montigny-le-Bretonneux, France); ABT-737 was kindly provided by Abbott Laboratories (Chicago, IL, USA).

PARP mAb (Ab-2, clone c-2-10) and anti-p53 mAb (Ab-6, OP43) were purchased from Calbiochem (Meudon, France). Anti-Bax pAb (N-20), anti-Bcl-2 mAb (clone 100), anti-Mcl-1 mAb (clone 22), anti-Bcl-xl mAb (7B2.5) and anti-BZLF1 mAb (BZ1) were purchased from Santa Cruz Biotechnology Inc. (Heidelberg, Germany). Anti-vinculin (clone VIN-11-5) and anti-β actin (clone AC-74) mAbs were obtained from Sigma-Aldrich (Saint-Quentin Fallavier, France). Anti-LMP1 mAb (CS1-4) was obtained from Dako France SAS (Trappes, France). Horseradish peroxidase (HRP)-conjugated rabbit anti-mouse IgG and HRP-conjugated donkey anti-rabbit IgG for western blotting were purchased from GE Healthcare (Velizy, France) and Jackson ImmunoResearch Laboratories (Newmarket, UK), respectively.

Induction and quantification of apoptosis. We treated 0.5×10^6 cells for various periods of time, at 37 °C, with nutlin-3 (10 μM), ABT-737 (10 μM) or both these compounds. Cells were washed in PBS, resuspended in annexin buffer (10 mM HEPES/NaOH (pH 7.4), 150 mM NaCl, 5 mM KCl, 1 mM $MgCl_2$, 1.8 mM $CaCl_2$) supplemented with 2.5 μg/ml FITC-labeled annexin-V (Roche Applied Science, Meylan, France) and incubated at room temperature for 10 min. Cells were then washed, resuspended in annexin buffer supplemented with PI (10 μg/ml) and analyzed by flow cytometry ($n = 10\,000$; FACSCalibur, Becton-Dickinson, Pont-de-Claix, France). Annexin-V-positive cells (PI negative or PI positive) were considered to be apoptotic.

Determination of mitochondrial membrane potential. After treatment with nutlin-3, ABT-737 or both these compounds, for various periods of time, $DIOC_6(3)$ was added (40 nm) and cells were incubated for an additional 30 min at 37 °C. Cells were washed, resuspended in PBS supplemented with PI and analyzed by flow cytometry ($n = 10\,000$; FACSCalibur, Becton-Dickinson).

Intracellular labeling. Cells (2×10^6), either untreated or treated with nutlin-3 (10 μM), were fixed by incubation in 0.25% paraformaldehyde for 20 min at room temperature. They were then washed twice and stained with primary antibody (monoclonal anti-Bax antibody, clone 6A7, Sigma-Aldrich) in digitonin (200 μg/ml) for 30 min at room temperature. The cells were then washed again with PBS and incubated for 30 min with goat anti-mouse IgG conjugated to Alexa 488 (GAM-Alexa-488, Molecular Probes, Leiden, The Netherlands). Samples were than analyzed on a FACSCalibur flow cytometer. Cells labeled with GAM-Alexa-488 only were used as a control.

Preparation of mitochondrial and cytosolic fractions. We resuspended 2×10^6 cells in 100 μl of ice-cold cell lysis and mitochondria intact buffer (250 mM sucrose, 70 mM KCl, 200 μg/ml digitonin) and incubated the suspension at 4 °C for 5 min. The samples were then centrifuged at $1000 \times g$ for 5 min at 4 °C. The supernatants (cytosolic fractions) were recovered and stored at −80 °C. The pellets were resuspended in 50 μl of IP buffer (30 mM Tris HCl (pH 7.4), 150 mM NaCl, 2 mM EDTA, 2 mM EGTA, 0.2% Triton × 100, 0.3% NP40, complete protease inhibitor cocktail) and incubated for 10 min at 4 °C. The suspension was then centrifuged at $10\,000 \times g$ for 10 min at 4 °C and the supernatants (mitochondrial fractions) were stored at −80 °C until use.

Immunoprecipitation. We subjected 5×10^6 cells to disruption by sonication (10 s on ice) in 1 ml of CHAPS buffer (1% CHAPS, 1 M Hepes, 5 M NaCl, complete protease inhibitor cocktail). We mixed the resulting lysates with 2 μg of agarose-conjugated rabbit anti-Bax pAb (clone N-20) or agarose-conjugated control rabbit IgG pAb (Santa Cruz Biotechnology Inc.) and incubated the mixture overnight at 4 °C, with end-over-end rotation. Immune complexes were washed twice with ice-cold CHAPS buffer, twice with PBS and resuspended in loading buffer. The samples were boiled for 5 min and the proteins were separated by electrophoresis in 4–12% Bis-Tris precast gels (Invitrogen, Cergy Pontoise, France) and analyzed by western blotting.

Western-blot analysis. A pellet containing 1×10^6 cells was solubilized by incubation in ice-cold lysis buffer (150 mM NaCl, 50 mM Tris (pH 7.4), 5 mM EDTA, 0.1% NP40, 0.5% sodium deoxycholate, 0.1% SDS, complete protease inhibitor cocktail) for 10 min. Sample loading buffer was added and the mixture was boiled for 5 min. Proteins were separated by electrophoresis in 12% polyacrylamide gels or 4–12% Bis-Tris precast gels (Invitrogen) and transferred to PVDF membranes (Millipore, Molsheim, France). Blots were blocked by incubation overnight at 4 °C in 3% non-fat milk powder, 2% glycine in PBS and incubated for 1 h at room temperature with primary antibodies. The blots were then washed and incubated with HRP-conjugated RAM-IgG or HRP-conjugated DAR-IgG. Antibody complexes were detected by enhanced chemiluminescence (Millipore).

Conflict of Interest

The authors declare no conflict of interest.

Acknowledgements. This work was supported by grants from the Fondation de France 00012093 (JW), the Cancéropole and Région Ile-de-France (ERABL, IF09-2092/R), the Association pour la recherche sur le Cancer 3454 (JW and EH) and the Université Paris-Sud 11 (BQR 2009). We thank Yann Lécluse for expert technical assistance in performing flow cytometry analysis.

1. Lane DP. Cancer. p53, guardian of the genome. *Nature* 1992; **358**: 15–16.
2. Levine AJ. p53, the cellular gatekeeper for growth and division. *Cell* 1997; **88**: 323–331.
3. Vousden KH, Lu X. Live or let die: the cell's response to p53. *Nat Rev Cancer* 2002; **2**: 594–604.
4. Honda R, Tanaka H, Yasuda H. Oncoprotein MDM2 is a ubiquitin ligase E3 for tumor suppressor p53. *FEBS Lett* 1997; **420**: 25–27.
5. Momand J, Zambetti GP, Olson DC, George D, Levine AJ. The mdm-2 oncogene product forms a complex with the p53 protein and inhibits p53-mediated transactivation. *Cell* 1992; **69**: 1237–1245.
6. Capoulade C, Bressac-de Paillerets B, Lefrere I, Ronsin M, Feunteun J, Tursz T *et al.* Overexpression of MDM2, due to enhanced translation, results in inactivation of wild-type p53 in Burkitt's lymphoma cells. *Oncogene* 1998; **16**: 1603–1610.
7. Oliner JD, Kinzler KW, Meltzer PS, George DL, Vogelstein B. Amplification of a gene encoding a p53-associated protein in human sarcomas. *Nature* 1992; **358**: 80–83.
8. Dickens MP, Fitzgerald R, Fischer PM. Small-molecule inhibitors of MDM2 as new anticancer therapeutics. *Semin Cancer Biol* 2010; **20**: 10–18.
9. Yang Y, Ludwig RL, Jensen JP, Pierre SA, Medaglia MV, Davydov IV *et al.* Small molecule inhibitors of HDM2 ubiquitin ligase activity stabilize and activate p53 in cells. *Cancer Cell* 2005; **7**: 547–559.
10. Vassilev LT, Vu BT, Graves B, Carvajal D, Podlaski F, Filipovic Z *et al. In vivo* activation of the p53 pathway by small-molecule antagonists of MDM2. *Science* 2004; **303**: 844–848.
11. Stuhmer T, Chatterjee M, Hildebrandt M, Herrmann P, Gollasch H, Gerecke C *et al.* Nongenotoxic activation of the p53 pathway as a therapeutic strategy for multiple myeloma. *Blood* 2005; **106**: 3609–3617.
12. Sarek G, Kurki S, Enback J, Iotzova G, Haas J, Laakkonen P *et al.* Reactivation of the p53 pathway as a treatment modality for KSHV-induced lymphomas. *J Clin Invest* 2007; **117**: 1019–1028.
13. Van Maerken T, Ferdinande L, Taildeman J, Lambertz I, Yigit N, Vercruysse L *et al.* Antitumor activity of the selective MDM2 antagonist nutlin-3 against chemoresistant neuroblastoma with wild-type p53. *J Natl Cancer Inst* 2009; **101**: 1562–1574.
14. Vassilev LT. MDM2 inhibitors for cancer therapy. *Trends Mol Med* 2007; **13**: 23–31.
15. Vazquez A, Bond EE, Levine AJ, Bond GL. The genetics of the p53 pathway, apoptosis and cancer therapy. *Nat Rev Drug Discov* 2008; **7**: 979–987.
16. Spierings D, McStay G, Saleh M, Bender C, Chipuk J, Maurer U *et al.* Connected to death: the (unexpurgated) mitochondrial pathway of apoptosis. *Science* 2005; **310**: 66–67.
17. Youle RJ, Strasser A. The BCL-2 protein family: opposing activities that mediate cell death. *Nat Rev Mol Cell Biol* 2008; **9**: 47–59.
18. Chipuk JE, Green DR. How do BCL-2 proteins induce mitochondrial outer membrane permeabilization? *Trends Cell Biol* 2008; **18**: 157–164.
19. Schuler M, Green DR. Transcription, apoptosis and p53: catch-22. *Trends Genet* 2005; **21**: 182–187.
20. Lindstrom MS, Wiman KG. Role of genetic and epigenetic changes in Burkitt lymphoma. *Semin Cancer Biol* 2002; **12**: 381–387.
21. Renouf B, Hollville E, Pujals A, Tetaud C, Garibal J, Wiels J. Activation of p53 by MDM2 antagonists has differential apoptotic effects on Epstein-Barr virus (EBV)-positive and EBV-negative Burkitt's lymphoma cells. *Leukemia* 2009; **23**: 1557–1563.
22. Thompson MP, Kurzrock R. Epstein-Barr virus and cancer. *Clin Cancer Res* 2004; **10**: 803–821.
23. Rowe M, Rowe DT, Gregory CD, Young LS, Farrell PJ, Rupani H *et al.* Differences in B-cell growth phenotype reflect novel patterns of Epstein-Barr virus latent gene expression in Burkitt's lymphoma cells. *EMBO J* 1987; **6**: 2743–2751.
24. O'Nions J, Allday MJ. Epstein-Barr virus can inhibit genotoxin-induced G1 arrest downstream of p53 by preventing the inactivation of CDK2. *Oncogene* 2003; **22**: 7181–7191.
25. Okan I, Wang Y, Chen F, Hu LF, Imreh S, Klein G *et al.* The EBV-encoded LMP1 protein inhibits p53-triggered apoptosis but not growth arrest. *Oncogene* 1995; **11**: 1027–1031.
26. Hsu YT, Youle RJ. Bax in murine thymus is a soluble monomeric protein that displays differential detergent-induced conformations. *J Biol Chem* 1998; **273**: 10777–10783.
27. Portis T, Longnecker R. Epstein-Barr virus (EBV) LMP2A mediates B-lymphocyte survival through constitutive activation of the Ras/PI3K/Akt pathway. *Oncogene* 2004; **23**: 8619–8628.
28. Rowe M, Peng-Pilon M, Huen DS, Hardy R, Croom-Carter D, Lundgren E *et al.* Upregulation of *bcl-2* by the Epstein-Barr virus latent membrane protein LMP1: a B-cell-specific response that is delayed relative to NF-kappa B activation and to induction of cell surface markers. *J Virol* 1994; **68**: 5602–5612.
29. Wang S, Rowe M, Lundgren E. Expression of the Epstein Barr virus transforming protein LMP1 causes a rapid and transient stimulation of the Bcl-2 homologue Mcl-1 levels in B-cell lines. *Cancer Res* 1996; **56**: 4610–4613.
30. Grimm T, Schneider S, Naschberger E, Huber J, Guenzi E, Kieser A *et al.* EBV latent membrane protein-1 protects B cells from apoptosis by inhibition of BAX. *Blood* 2005; **105**: 3263–3269.
31. Oltersdorf T, Elmore SW, Shoemaker AR, Armstrong RC, Augeri DJ, Belli BA *et al.* An inhibitor of Bcl-2 family proteins induces regression of solid tumours. *Nature* 2005; **435**: 677–681.
32. Farnebo M, Bykov VJ, Wiman KG. The p53 tumor suppressor: a master regulator of diverse cellular processes and therapeutic target in cancer. *Biochem Biophys Res Commun* 2010; **396**: 85–89.
33. Nechushtan A, Smith CL, Hsu YT, Youle RJ. Conformation of the Bax C-terminus regulates subcellular location and cell death. *EMBO J* 1999; **18**: 2330–2341.
34. Murphy KM, Ranganathan V, Farnsworth ML, Kavallaris M, Lock RB. Bcl-2 inhibits Bax translocation from cytosol to mitochondria during drug-induced apoptosis of human tumor cells. *Cell Death Differ* 2000; **7**: 102–111.
35. Murphy KM, Streips UN, Lock RB. Bcl-2 inhibits a Fas-induced conformational change in the Bax N terminus and Bax mitochondrial translocation. *J Biol Chem* 2000; **275**: 17225–17228.
36. Forte E, Luftig MA. MDM2-dependent inhibition of p53 is required for Epstein-Barr virus B-cell growth transformation and infected-cell survival. *J Virol* 2009; **83**: 2491–2499.
37. Feuillard J, Schuhmacher M, Kohanna S, Asso-Bonnet M, Ledeur F, Joubert-Caron R *et al.* Inducible loss of NF-kappaB activity is associated with apoptosis and Bcl-2 down-regulation in Epstein-Barr virus-transformed B lymphocytes. *Blood* 2000; **95**: 2068–2075.
38. Kojima K, Konopleva M, Samudio IJ, Schober WD, Bornmann WG, Andreeff M. Concomitant inhibition of MDM2 and Bcl-2 protein function synergistically induce mitochondrial apoptosis in AML. *Cell Cycle* 2006; **5**: 2778–2786.
39. Wade M, Rodewald LW, Espinosa JM, Wahl GM. BH3 activation blocks Hdmx suppression of apoptosis and cooperates with Nutlin to induce cell death. *Cell Cycle* 2008; **7**: 1973–1982.
40. Murray PG, Swinnen LJ, Constandinou CM, Pyle JM, Carr TJ, Hardwick JM *et al.* BCL-2 but not its Epstein-Barr virus-encoded homologue, BHRF1, is commonly expressed in posttransplantation lymphoproliferative disorders. *Blood* 1996; **87**: 706–711.

Supplementary Information accompanies the paper on Cell Death and Disease website (http://www.nature.com/cddis)

BASIC RESEARCH PAPER

Autophagy 11:12, 2275–2287; December 2015; © 2015 Taylor & Francis Group, LLC

Constitutive autophagy contributes to resistance to TP53-mediated apoptosis in Epstein-Barr virus-positive latency III B-cell lymphoproliferations

Anaïs Pujals,[1,‡,†] Loëtitia Favre,[1,‡] Catherine Pioche-Durieu,[1] Aude Robert,[1] Guillaume Meurice,[2] Marion Le Gentil,[2] Sonia Chelouah,[1] Nadine Martin-Garcia,[3] Eric Le Cam,[1] Catherine Guettier,[4] Martine Raphaël,[1] Lyubomir T Vassilev,[5] Philippe Gaulard,[3] Patrice Codogno,[6] Marc Lipinski,[1] and Joëlle Wiels[1,*]

[1]UMR 8126 CNRS; Univ Paris-Sud; Institut Gustave Roussy; Villejuif, France; [2]Functional Genomic Platform; Institut Gustave Roussy; Villejuif, France; [3]CHU Henri Mondor; Assistance Publique-Hôpitaux de Paris; Département de Pathologie; Inserm U955; Université Paris-Est Créteil; Créteil, France; [4]Service d'Anatomie Pathologique; Hôpital Bicêtre; Le Kremlin-Bicêtre; Le Kremlin-Bicêtre, France ; [5]Roche Research Center; Hoffmann-La Roche Inc.; Nutley, NJ USA; [6]INSERM U845; Necker Growth and Signaling Research Center; University Paris Descartes; Paris, France

[†]Current affiliation: CHU Henri Mondor; Assistance Publique-Hôpitaux de Paris; Département de Pathologie; Inserm U955; Université Paris-Est Créteil; Créteil, France

[‡]These authors contributed equally to this work.

Keywords: autophagy, BECN1, Burkitt lymphoma, EBV, nulin-3, TP53

Abbreviations: ACTB, actin beta; AMPK, AMP-activated protein kinase; BAF, bafilomycin A_1; BAX, BCL2–associated X protein; BCL2, B-cell CLL/lymphoma 2; BECN1, Beclin 1 autophagy related; BL, Burkitt lymphoma; DLBCL, diffuse large B cell lymphoma; EBNA, Epstein-Barr nuclear antigen; EBV, Epstein-Barr virus; HRP, horseradish peroxidase; LCL, lymphoblastoid cell lines; LMP, latent membrane protein; mAb, monoclonal antibody; MAP1LC3/LC3, microtubule-associated protein 1 light chain 3; MDC, monodansylcadaverine; MDM2, MDM2 proto-oncogene; E3, ubiquitin protein ligase; MFI, mean fluorescence intensity; MTOR, mechanistic target of rapamycin (serine/threonine kinase); NFKB, nuclear factor of kappa light polypeptide gene enhancer in B-cells; pAb, polyclonal antibody; PI, propidium iodide; PTLD, post-transplant lymphoproliferative disorder; RELA/p65, v-rel avian reticuloendotheliosis viral oncogene homolog A; RPS6KB/p70S6K, ribosomal protein S6 kinase 70kDa; SESN1, sestrin 1; ShRNA, short hairpin RNA; TP53, tumor protein p53

The Epstein-Barr virus (EBV) is associated with various lymphoproliferative disorders and lymphomas. We have previously demonstrated that treating wild-type TP53-expressing B cell lines with the TP53 pathway activator nutlin-3 induced apoptosis in EBV-negative and EBV-positive latency I cells whereas EBV-positive latency III cells remained much more apoptosis-resistant. Here, we report a constitutively high level of autophagy in these resistant cells which express high levels of the proautophagic protein BECN1/Beclin 1 based, at least in part, on the activation of the NFKB signaling pathway by the viral protein LMP1. Following treatment with nutlin-3, several autophagy-stimulating genes were upregulated both in EBV-negative and EBV-positive latency III cells. However the process of autophagy was only triggered in the latter and was associated with an upregulation of SESN1/sestrin 1 and inhibition of MTOR more rapid than in EBV-negative cells. A treatment with chloroquine, an inhibitor of autophagy, potentiated the apoptotic effect of nutlin-3, particularly in those EBV-positive cells which were resistant to apoptosis induced by nutlin-3 alone, thereby showing that autophagy participates in this resistant phenotype. Finally, using immunohistochemical staining, clinical samples from various B cell lymphoproliferations with the EBV-positive latency II or III phenotype were found to harbor a constitutively active autophagy.

Introduction

The Epstein-Barr virus (EBV), a γ-Herpes virus, is associated with various B cell malignancies including Burkitt lymphoma (BL) and post-transplant lymphoproliferative disorders (PTLD). Its ability to efficiently immortalize B lymphocytes thus generating lymphoblastoid cell lines (LCL) underlies its oncogenic role. In EBV-infected tumor cells, the virus remains latent, with only a small subset of viral proteins being expressed. These include 6 nuclear antigens (EBNA) and 3 membrane proteins (LMP), which are differentially expressed between the various EBV-associated tumors. For instance, virtually all EBV-positive

*Correspondence to: Joëlle Wiels; Email: wiels@igr.fr
Submitted: 12/13/2013; Revised: 10/17/2015; Accepted: 10/29/2015
http://dx.doi.org/10.1080/15548627.2015.1115939

BL cells only express EBNA1 (latency I phenotype) while most of PTLD cases express the full spectrum of latent proteins (latency III phenotype). However, rare cases of BL with a latency III phenotype have been reported as well as some cases of PTLD with a latency II phenotype (expression of EBNA1, LMP1 and LMP2). Among the viral products, it is mostly the membrane protein LMP1, which has been implicated in tumor formation. This versatile protein initiates the activation of the mitogen-activated protein kinases MAPK8/JNK1 and MAPK14/p38, the Janus kinase-signal transducers and activators of transcription (JAK-STAT) and the NFKB (nuclear factor of kappa light polypeptide gene enhancer in B-cells) signaling cascades, with an overall effect on cell survival.

TP53 (tumor protein p53) is a stress-activated transcription factor which plays a key role in protecting cells against tumor development, either promoting the inhibition of cell proliferation or inducing cell apoptosis.[1] Mutation in its coding sequence, sequestration in the cytoplasm or increased interactions with its main cellular regulator MDM2 are but a few of the possible ways whereby the physiological functions of the TP53 protein can be disrupted in tumor cells.[2] As recently demonstrated, TP53 is also involved in the regulation of autophagy, a lysosomal degradation pathway that contributes to cell homeostasis. The autophagy process starts with the formation of large double-membrane vesicles called autophagosomes. These in turn fuse with lysosomes to form autolysosomes whose internal content is then degraded by hydrolases, thus clearing the cell from damaged organelles and protein aggregates.[3] Numerous proteins have been reported to regulate autophagy. On the negative side, MTOR (mechanistic target of rapamycin [serine/threonine kinase]) is a key factor. On the positive side, BECN1, a critical component in the class III phosphatidylinositol 3-kinase (PtdIns3K) complexes regulates autophagy by inducing the formation of autophagosomes.[4] Other positive regulators of autophagy include various transcriptional targets of TP53 such as sestrins whose effects result in MTOR inhibition,[5] and DRAM1 (DNA-damage regulated autophagy modulator 1), a lysosomal membrane protein whose mechanism of action remains uncharacterized.[6] In contrast, cytoplasmic TP53 inhibits autophagy, thus implying that it plays a dual role in the modulation of this catabolic pathway.[7] Given its key function in determining cell fate, several strategies have been developed to restore TP53 activity in tumor cells. Several low molecular mass compounds can disrupt its interaction with MDM2 (MDM2 proto-oncogene, E3 ubiquitin protein ligase) (for a review see refs.8, 9). For example, nutlin-3, a *cis*-imidazoline, binds the TP53 pocket of MDM2 thereby inducing both the release and the activation of TP53.[10] In vitro, nutlin-3 has been found to enhance apoptosis in various experimental systems.[11-13] In preclinical studies, a treatment with this drug inhibited tumor growth and exerted a synergistic effect with genotoxic drugs or irradiation. This opened the way to phase I clinical trials (with the second generation nutlin, RG7112) which are currently carried out for various tumor types (reviewed in refs. 14, 15).

In previous studies, we have shown that wild-type (WT) TP53-containing EBV-negative and -positive cells treated with nutlin-3 exhibit TP53 activation as assessed by the induction of CDKN1A/p21 (cyclin-dependent kinase inhibitor 1A [p21, Cip1]), MDM2 and BAX (BCL2–associated X protein). However, whereas nutlin-3-treated EBV-negative BL cells die massively through an apoptotic process involving BAX, EBV-positive latency III BL and LCL cells prove much more resistant,[16] in relation with their strong level of expression of BCL2 (BCL2, B-cell CLL/lymphoma 2).[17] We also observed that treating latency III cells with an inhibitor of BCL2 only partially restored their sensitivity to nutlin-3, which prompted us to study these cells further. Here, autophagy was found to be constitutively activated in EBV-positive latency III cells and to participate in their mechanisms of resistance to nutlin-3-induced apoptosis. A treatment with chloroquine, an inhibitor of autophagy, provided an apoptosis-inducing effect complementary to the action of nutlin-3. Autophagy was also constitutively activated in EBV-positive latency II and latency III primary B cell lymphoproliferations (diffuse large B cell lymphoma [DLBCL] and PTLD) but neither in EBV-negative nor in EBV-positive latency I BL.

Results

Constitutive levels of autophagy differ between EBV-negative and EBV-positive latency III cells

The MAP1LC3/LC3 (microtubule-associated protein 1 light chain 3) protein exists under 2 forms. The cytosolic LC3-I moiety can be converted by lipidation into LC3-II, which can then be recruited into the membrane of phagophores, the precursors to autophagosomes. A western blot analysis revealing the relative importance of these 2 forms in cell populations provides a convenient way to assess their level of basal autophagy. Since EBV is a known activator of the autophagic machinery,[18] we tested the presence of the 2 LC3 forms in a panel of EBV-negative BL cell lines (BL2, BL28 and BL40), in their in vitro EBV-infected counterparts (BL2/B95, BL28/B95 and BL40/B95), in LY47, an EBV-positive latency III BL cell line, and in 2 LCL (IARC211, derived from the same patient as BL40, and RPMI8866). As shown in **Figure 1A**, LC3-II was detected in the EBV-positive cells only, whereas the presence of LC3-I appeared independent of the EBV status of the cell lines. We also used staining of the cells with monodansylcadaverine (MDC) for monitoring autophagy in our cell lines. This autofluorescent compound associates with acidic and lipid-rich compartments and thus gives an indication of the presence of late autophagic vacuoles in the cells.[19] As shown in **Figure 1B**, higher levels of punctate MDC staining were observed in BL2/B95 (23± 10%) and RPMI8866 (46±5%), 2 EBV-positive latency III cell lines, than in EBV-negative BL2 cells (11±2%). Together, these data suggest that the level of basal autophagy is higher in EBV-positive latency III cells than in EBV-negative cells.

BECN1 and autophagy are upregulated in EBV-positive latency III cells through NFKB activation

The viral LMP1 protein is a known inducer of the NFKB signaling cascade [20,21] which, under certain circumstances, positively modulates canonical autophagy.[22,23] We thus reasoned that the NFKB complex could play a part in the activation of autophagy in these cells. As expected, its RELA/p65 (v-rel avian

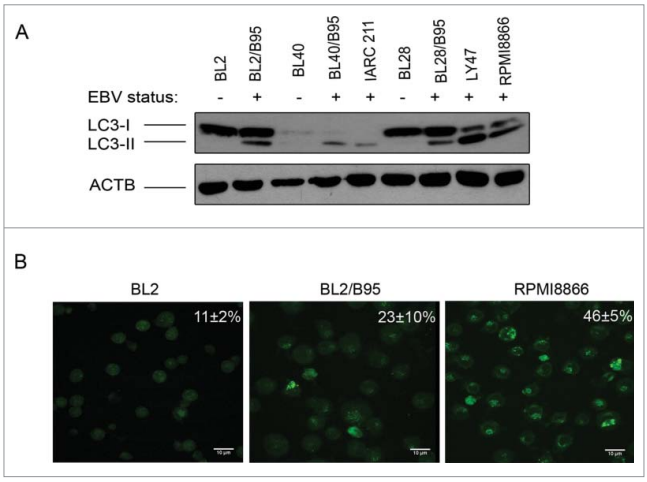

Figure 1. Analysis of constitutive autophagy in EBV-negative and EBV-positive latency III lymphoid cell lines. (**A**) Whole cell lysates from the indicated cell lines were submitted to western blot analysis for detection of LC3-I, LC3-II and ACTB. (**B**) Cells stained with MDC were examined by confocal fluorescence microscopy. Mean percentages of MDC-stained cells indicative of autophagy were calculated from 3 independent experiments.

reticuloendotheliosis viral oncogene homolog A) subunit was found to be more abundant in the EBV-positive latency III than in the EBV-negative cell lines (**Fig. 2A**). As RELA/p65 binds to and activates the *BECN1* gene promoter,[24] we then tested the same cell lines for expression of the BECN1 protein which was found to follow that of RELA (**Fig. 2A** and **Fig. S1**). To examine RELA expression levels more precisely, cytosolic and nuclear extracts were prepared from both EBV-positive latency III and EBV-negative cell lines. Levels of RELA were found to be higher in the nuclear fraction of EBV-positive cell lines than in their EBV-negative counterparts, contrasting with the cytosolic fractions where no such relation was observed (**Fig. S2**). This is consistent with RELA playing a role in the process leading to BECN1 expression based on its transcriptional regulatory function. To confirm that LMP1 regulates BECN1 expression through the NFKB pathway we used stable transfectants of DG75 cells, which express LMP1 only in the absence of tetracycline. In these conditions of LMP1 expression, levels of both RELA and BECN1 increased as compared to control cells cultivated in the presence of tetracycline (**Fig. 2B**). We also used an shRNA approach to test for a direct correlation between the status of the NFKB-BECN1 pathway and the level of autophagy in EBV-positive latency III cells. To this end, RPMI8866 cells were transduced with an shRNA directed against *RELA* and the levels of expression of RELA, BECN1, LC3-I and LC3-II were tested. As seen in **Figure 2C**, levels of BECN1 and LC3-II were found strongly decreased in transduced cells where RELA expression was virtually abolished as compared to control cells transduced with an shRNA that does not target any known human gene. LC3-I expression was not affected by inhibition of RELA. Altogether, these data indicate that an LMP1-dependent activation of the NFKB signaling pathway upregulates the expression of BECN1 and the level of autophagy in EBV-positive latency III cells.

Treatment with nutlin-3 induces the expression of a subset of genes involved in autophagy in EBV-negative and EBV-positive latency III cells

We have previously shown that nutlin-3 similarly induced TP53 activation in EBV-negative and EBV-positive B cells whereas the induction of apoptosis by this compound depended upon their EBV status: EBV-negative and -positive latency I cells are highly sensitive to this antagonist of MDM2 whereas EBV-positive latency III cells are much more resistant.[16] Having detected higher levels of basal autophagy in the latter, we decided to examine the transcriptional effect of nutlin-3 treatment on EBV-negative BL2 and EBV-positive latency III BL2/B95 cells. A genome-wide transcriptome analysis was performed at various times of incubation in the presence of 10 μM of nutlin-3. Over time, an increasing number of genes were found to be upregulated in both cell lines (**Fig. S3**). As expected, these genes encode proteins involved in cellular functions that are regulated by TP53. Among them, 5 genes have been previously implicated in the autophagy process. They are reported in **Figure 3A** where it can be seen that their mRNA expression levels increased during treatment in both cell types with an apparently more powerful induction in the EBV-converted BL2/B95 cell line than in its EBV-negative parent. These changes in the mRNA expression levels induced by 16 h of treatment with nutlin-3 were then quantified as compared to untreated cells (**Fig. 3B**). *DRAM1*, the TP53 target gene most strongly induced in both BL2 and BL2/B95 (fold change 26.8 and 66.8, respectively), encodes a lysosomal protein that induces macroautophagy.[25] Treatment of BL2 and BL2/B95 with nutlin-3 also induced higher transcription levels of *SESN1* (fold change 6.9 and 13.3), *SESN2* (Sestrin 2) (fold change 5.2 and 9.2), *PRKAB1*, the β-1 regulatory subunit of AMPK (AMP-activated protein kinase) (fold change 2.7 and 3) and *TSC2* (tuberous sclerosis 2) (fold change 2, only in BL2/B95). The proteins encoded by these genes are involved in a cascade of events: AMPK is activated by direct interactions with SESN1 and SESN2 and phosphorylates TSC2 which, in turn, inhibits MTOR thus leading to autophagy activation.[5] Treatment of BL2 and BL2/B95 with nutlin-3 did not modify the mRNA level of *BECN1* (data not shown).

Treatment with nutlin-3 promotes autophagy in EBV-positive latency III cells but not in EBV-negative cells

Since nutlin-3 treatment increases the level of expression of several genes involved in autophagy, we decided to assess if this compound is able to increase the autophagic flux in EBV-negative and -positive cell lines. To this end, BL2, BL2/B95 and RPMI8866 cells were treated with nutlin-3 for 3, 5, 7 or 24 h followed by assessment of autophagy measured by western blot analysis of LC3-I and LC3-II levels. Since LC3-II accumulation may result from either increased autophagosome formation or impaired autophagosome-lysosome fusion, cells were treated either with or without bafilomycin A_1 (BAF) which inhibits intralysosomal acidification thereby blocking the degradation of

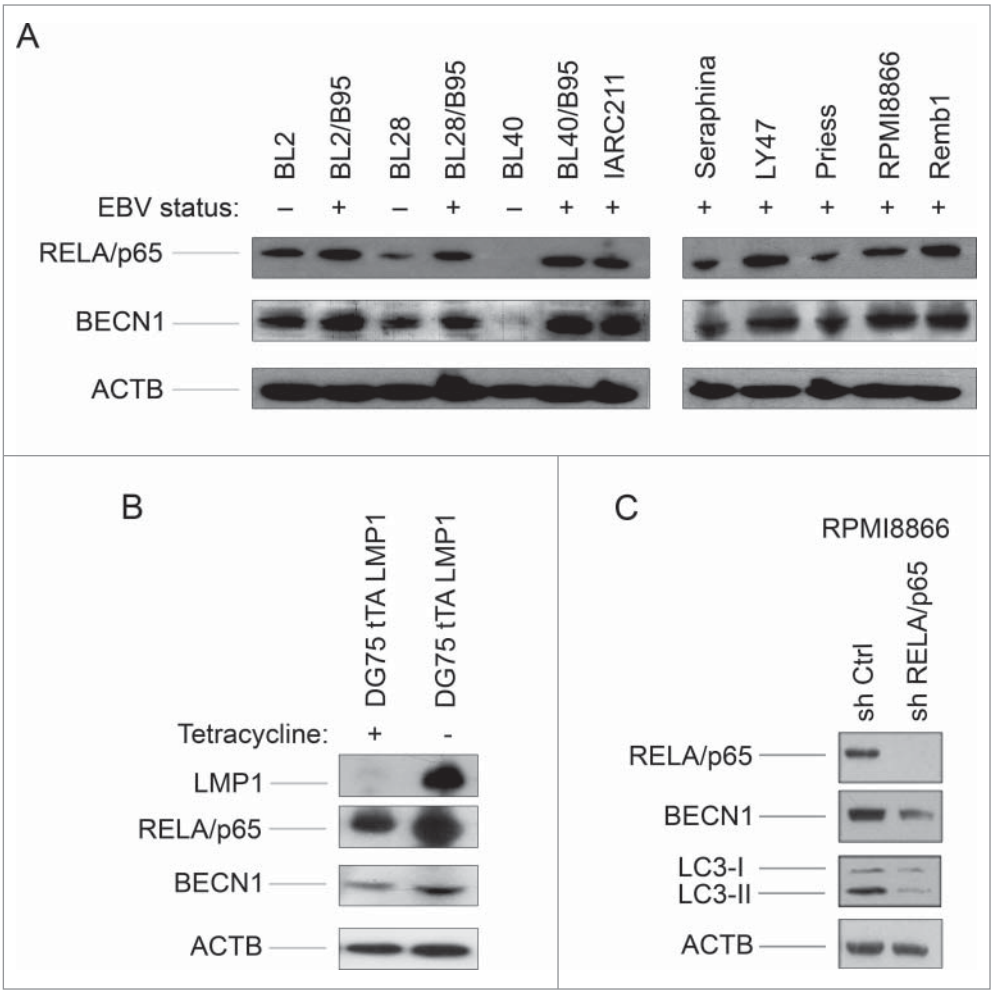

Figure 2. RELA activation and BECN1 expression in EBV-negative and EBV-positive latency III lymphoid cell lines. (**A**) Whole cell lysates were analyzed by western blotting for RELA and BECN1 expression. (**B**) Whole cell lysates prepared from DG75 cells, expressing LMP1 in a tetracycline-regulated system, were tested for expression of LMP1, RELA and BECN1. (**C**) Whole cell lysates prepared from RPMI8866 stably transduced with a *RELA*-specific shRNA or a control shRNA were submitted to western blot analysis for detection of RELA and BECN1 expression. The western blots shown are representative of 3 independent experiments.

LC3-II.[26] It can be seen in **Figure 4A** that in the absence of BAF, the levels of the autophagosome-specific LC3-II form detected after nutlin-3 treatment differed between cell lines: in BL2 cells, LC3-II remained hardly detectable; in BL2/B95 cells, the amount of LC3-II increased as early as 3 h after treatment and became the major form of LC3 at 24 h; in RPMI 8866 cells, the level of LC3-II, already high in untreated cells, remained stable until 7 h and slightly increased at 24 h. In the latter, the level of the cytosolic LC3-I form decreased progressively all along the 24 h nutlin-3 treatment. When these cell lines were pretreated with BAF (100 nM), the increase of LC3-II levels observed after 3, 5 and 7 h of nutlin-3 treatment was further enhanced particularly in BL2/B95 and RPMI8866 cells (**Fig. 4A** and **Fig. S4**). Altogether, these results indicate that in EBV-positive cells, the LC3-II increase induced by nutlin-3 is due to an increase in autophagic activity and not to an impaired autophagosome turnover.

To further explore this matter, EBV-negative and -positive latency III cells treated with nutlin-3 for 16 h were stained with MDC and observed by fluorescence confocal microscopy (**Fig. 4B**). From a comparison with results shown in **Figure 1B**, it can be concluded that the percentage of MDC-stained vacuoles increased after treatment with nutlin-3, and that this increase was much more pronounced in EBV-positive latency III cells (41 ± 2% *vs* 23 ±10 % and 65 ± 11% vs 46 ± 5% cells stained in BL2/B95 and RPMI8866, respectively) than in EBV-negative BL2 cells (16 ± 7% cells stained vs 11 ± 2%). MDC staining was also measured by flow cytometry after 16 and 24 h of treatment with nutlin-3. Results shown in **Figure 4C** confirmed that nutlin-3 had a greater effect in EBV-positive than in EBV-negative cells. In addition, induction of autophagy by nutlin-3 treatment was assessed with a new dye (cyto-ID) that makes it possible to selectively stain autophagic compartments. Flow cytometry analysis of cells (**Fig. 4D**) indicated that treating cells with nutlin-3 for 16 h did not result in increased autophagy in BL2 (mean fluorescence intensity [MFI]: 4549 vs 4682 for untreated cells) whereas such a treatment substantially increased autophagy in BL2/B95 (MFI: 7690 vs 4770) and RPMI8866 (MFI: 17322 vs 13287).

Finally, the EBV-positive BL2/B95 and RPMI8866 cells were submitted to electron microscopy observation. Typical autophagosomes were detected between 7 and 10 h of nutlin-3 treatment (**Fig. 5**). In contrast, at these time points, such autophagosomes were not detectable in BL2 cells (data not shown). Altogether, these results are thus consistent with a differential effect of nutlin-3 treatment on the level of autophagy in EBV-negative and EBV-positive latency III cells.

Treatment with nutlin-3 inhibits MTOR activity more rapidly in EBV-positive latency III cells than in EBV-negative cells

We next decided to test whether the induction of an autophagic flux after nutlin-3 treatment correlated with MTOR

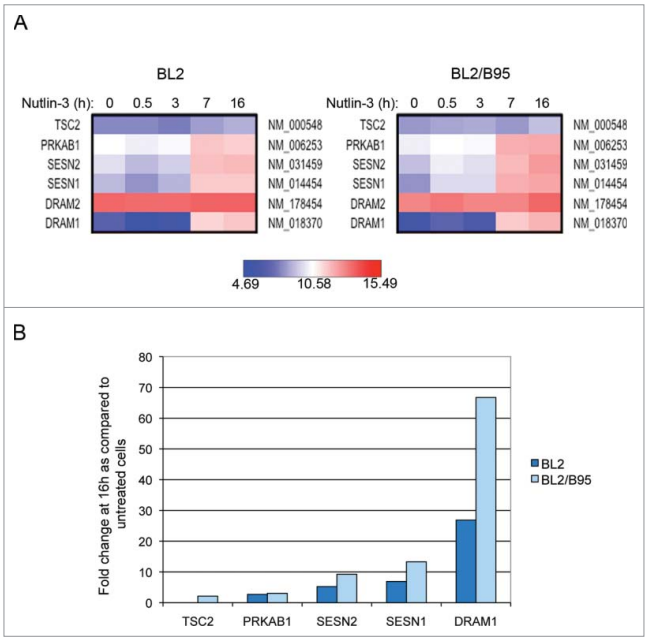

Figure 3. Changes in global gene expression analysis of EBV-negative BL2 and EBV-positive latency III BL2/B95 cells according to nutlin-3 treatments. (**A**) Probes corresponding to genes relative to autophagy are represented using heatmaps. (**B**) Fold change in mRNA levels for autophagy-related genes in both cell lines treated for 16 h as compared to untreated cells.

inhibition, which could potentially be induced by activation of the SESN-AMPK-TSC pathway suggested by the transcriptomic analysis. First, BL2 and BL2/B95 as well as LY47 and RPMI8866 cells were treated with 10 μM nutlin-3 and tested at various time points for expression of SESN1 (**Fig. 6A**). SESN1-specific bands observed on western blots were quantified by densitometry and normalized to ACTB/β-actin levels. In the EBV-positive cells, increased amounts of SESN1 were readily detectable after 1 h (for LY47) or 3 h (for BL2/B95 and RPMI8866) of treatment with nutlin-3. In the EBV-negative BL2 cell line, the accumulation of SESN1 was only detected after 5 h of treatment. To determine whether the induction of SESN1 expression correlated with an inhibition of MTOR kinase activity, we then analyzed the phosphorylation status of its target protein RPS6KB (ribosomal protein S6 kinase, 70kDa)[27] using an antibody specific for RPS6KB phosphorylated at Thr389 (the main target of MTOR). In EBV-positive BL2/B95 cells, treatment with nutlin-3 induced a strong inhibition of RPS6KB phosphorylation with kinetics similar to that of SESN1 induction. In contrast, there was virtually no effect in EBV-negative BL2 cells (**Fig. 6B**). Reblotting with an anti-RPS6KB verified that the treatment with nutlin-3 had not resulted in a decrease in the levels of the protein (**Fig. 6B**). Since the effects of nutlin-3 appeared to be delayed in EBV-negative as compared to EBV-positive cells, we then tested the expression of phospho-RPS6KB in BL2, BL2/B95, LY47 and RPMI8866 cells after 7 and 24 h of treatment. At these later time points, phospho-RPS6KB was decreased in all 4 cell lines regardless of their EBV status (**Fig. 6C**). Reblotting with an anti-RPS6KB again verified that the treatment had virtually no effect on the endogenous form of the protein (except for its virtually complete disappearance in BL2 cells treated for 24 h which might be due to the high level of apoptosis observed at that time in these cells). Together, these results are consistent with the interpretation that treatment with nutlin-3 inhibits MTOR activity in both EBV-negative and EBV-positive latency III cells but with more rapid kinetics in the latter.

An inhibitor of autophagy induces apoptosis in EBV-positive latency III cells and enhances the effect of nutlin-3

Having observed that nutlin-3 induced higher levels of autophagy in EBV-positive latency III cells than in EBV-negative cells and since the former are much more resistant to nutlin-3-induced apoptosis than the latter, we wished to test the hypothesis that a high level of autophagy had a causative effect on the resistance to apoptosis induction. To this end, we used chloroquine to inhibit autophagy in EBV-positive latency III BL and LCL cells which were then submitted to nutlin-3 treatment for 24 h. Chloroquine is a lysosomotropic agent that raises intralysosomal pH and impairs autophagic protein degradation, resulting in the accumulation of ineffective autophagosomes and blockade of autophagosomes-lysosomes fusion, with ensuing death in cells relying on autophagy for survival.[28] In these experiments the level of apoptosis was assessed by flow cytometry analysis (**Fig. 7** and **Figure S5** for representative flow cytometry plots). Treatment with chloroquine alone (100 μM) had a variable effect on the 4 cell lines tested. Apoptosis was induced to a very limited extent in BL2 and BL2/B95 cells (20 ± 5% and 27 ± 5%, respectively), RPMI8866 cells were moderately sensitive (38 ± 7%) and LY47 cells proved much more prone to apoptosis (58 ± 5%). Consistent with our previous report,[17] a 24-h treatment with nutlin-3 (10 μM) alone also had a variable effect on the various cell lines, with the EBV-negative BL2 cells being very sensitive (64 ± 5% of apoptotic cells) and the EBV-positive latency III cells being more resistant (37 ±4 %, 34 ± 7% and 34 ± 6% in BL2/B95, LY47 and RPMI8866, respectively). When the 2 drugs were used in combination, an additive effect on the induction of apoptosis was observed in all 4 cell lines. Treatment of cells performed with chloroquine alone or nutlin-3 alone were compared to a combination thereof using the Mann-Whitney test and the Bonferroni correction to account for multiple testing. The differences observed between treatments were found statistically significant in all cell lines ($P < 0.005$ for BL2 and BL2/B95 and $P < 0.0005$ for LY47 and RPMI8866).

Additional experiments were performed with BAF used in place of chloroquine to inhibit autophagy. BL2, BL2/B95, LY47 and RPMI8866 were incubated with or without BAF (100 nM; 2 h) and then in the absence or presence of nutlin-3 (10 μM). The level of apoptosis was assessed 24 h later by flow cytometry (**Fig. S6**). Unexpectedly, treatment with BAF alone induced a very high level of apoptosis in the EBV-negative cell line BL2 (53 ±11 %), an effect which was more moderate in the 3 EBV-positive cell lines (36 ± 10%, 31 ± 3% and 21 ± 1% for BL2/B95, LY47 and RPMI8866 respectively). A treatment with both drugs induced either no increase of apoptosis (BL2/B95) or a moderate

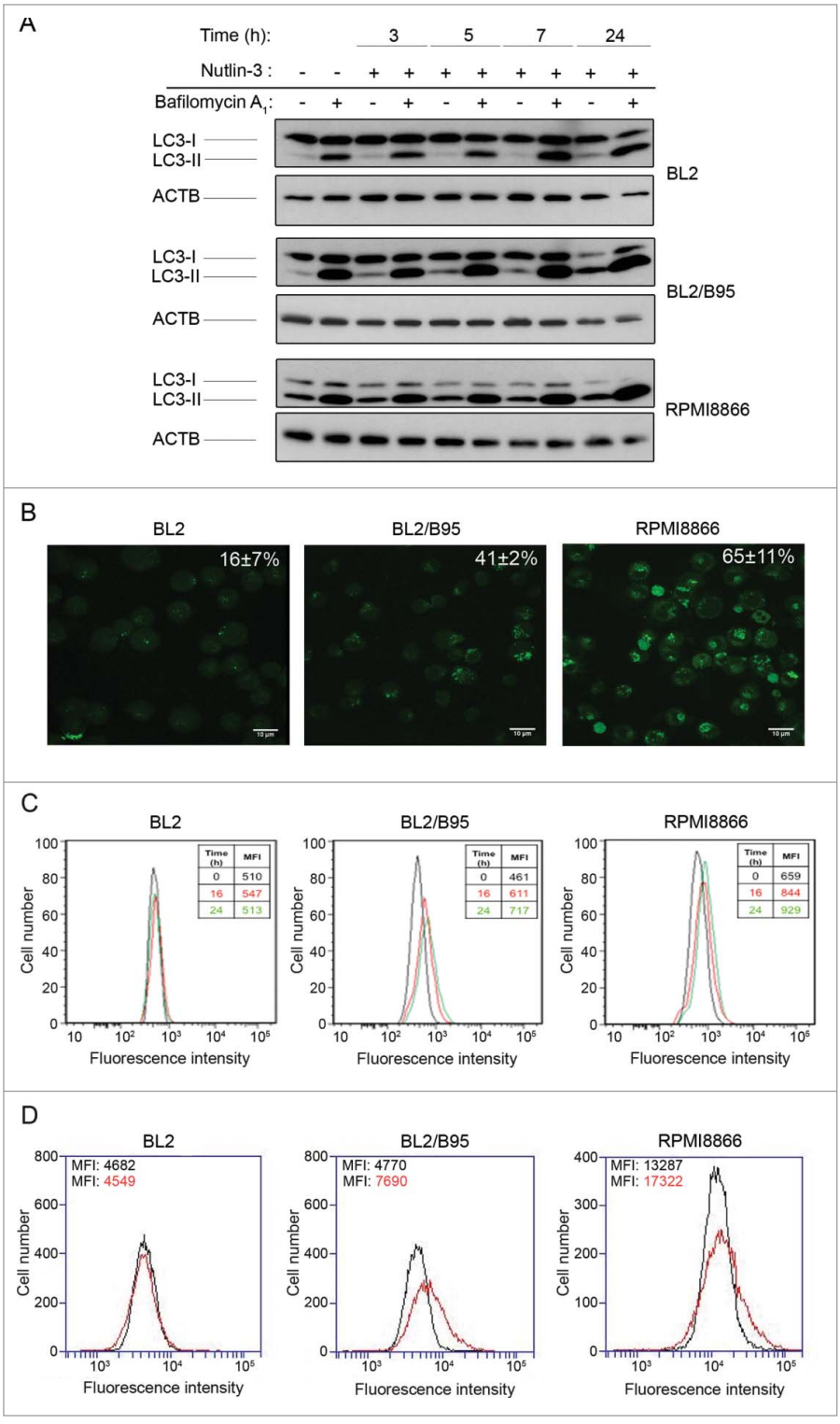

Figure 4. Effect of nutlin-3 treatment on autophagy induction in EBV-negative and EBV-positive latency III lymphoid cell lines. (**A**) Cells preincubated (30 min) with or without BAF (100 nM) were treated with nutlin-3 for various times. Expression of LC3-I and LC3-II was tested by western blotting of whole cell lysates. (**B** and **C**) Cells treated with nutlin-3 for 16 h were stained with MDC. The percentages of cells (means from 3 independent experiments) with MDC stained dots were assessed by fluorescence microscopy (**B**). The MFI of MDC stained dots was assessed by flow cytometry (**C**). (**D**) Cells incubated with or without nutlin-3 for 16 h were stained with the Cyto-ID Autophagy detection kit. The MFI of cyto-ID staining was assessed by flow cytometry.

one (BL2, LY47 and RPMI8866) as compared to treatments with either drug alone.

Dose-response curves of the cytotoxic effect of nutlin-3 (5, 10, 20 and 30 μM) and chloroquine (50, 100, 150, and 200 μM) were also measured by MTT (3-(4,5-dimethylthiazol-2-yl)-2,5-diphenyltetrazolium) assays and the IC_{50} of each compound were determined (**Table S1**). The results confirmed that LY47 cells were more sensitive to chloroquine treatment than the other cell lines (IC_{50}: 108 μM for LY47 as compared to 154, 200 and 174 μM for BL2, BL2/B95 and RPMI8866 respectively). They also showed that a lower dose of nutlin-3 was needed to kill the EBV-negative cells than the EBV-positive latency III cells (IC_{50}: 5 μM for BL2 as compared to 14, 26 and 25 μM for BL2/B95 LY47 and RPMI8866, respectively). Cells were then treated with a sublethal dose of choloroquine (50 μM) in combination with the same concentrations of nutlin-3 to determine if chloroquine can sensitize the cells to nutlin-3. Results in **Table S1** showed that chloroquine efficiently lowered the IC_{50} of nutlin-3 for LY47 (from 26 μM to 5 μM) and for RPMI8866 (from 25 μM to 18 μM). Altogether, these results show that in EBV-positive latency III cells which have a constitutive activation of autophagy and are poorly sensitive to nutlin-3 alone, treatment with the autophagy inhibitor chloroquine and nutlin-3 offers an efficient way to trigger cell death. Surprisingly, this additive effect was much less pronounced or even absent with BAF, another inhibitor of autophagy.

EBV-positive latency II and III B cell lymphoproliferations exhibit a constitutively active autophagy

It has been shown by immunohistochemical (IHC) staining of tissue sections that LC3-I displays a diffuse cytoplasmic staining whereas LC3-II appears as distinct puncta.[29] To compare the constitutive level of autophagy between EBV-negative or EBV-positive latency I and EBV-positive latency II or III lymphoproliferations, we used IHC to evaluate the expression pattern of LC3 in 3 cases of BL (EBV-negative or EBV-positive latency I), 2 of DLBCL (EBV-positive latency II), 5 of PTLD (EBV-positive latency II or III) and

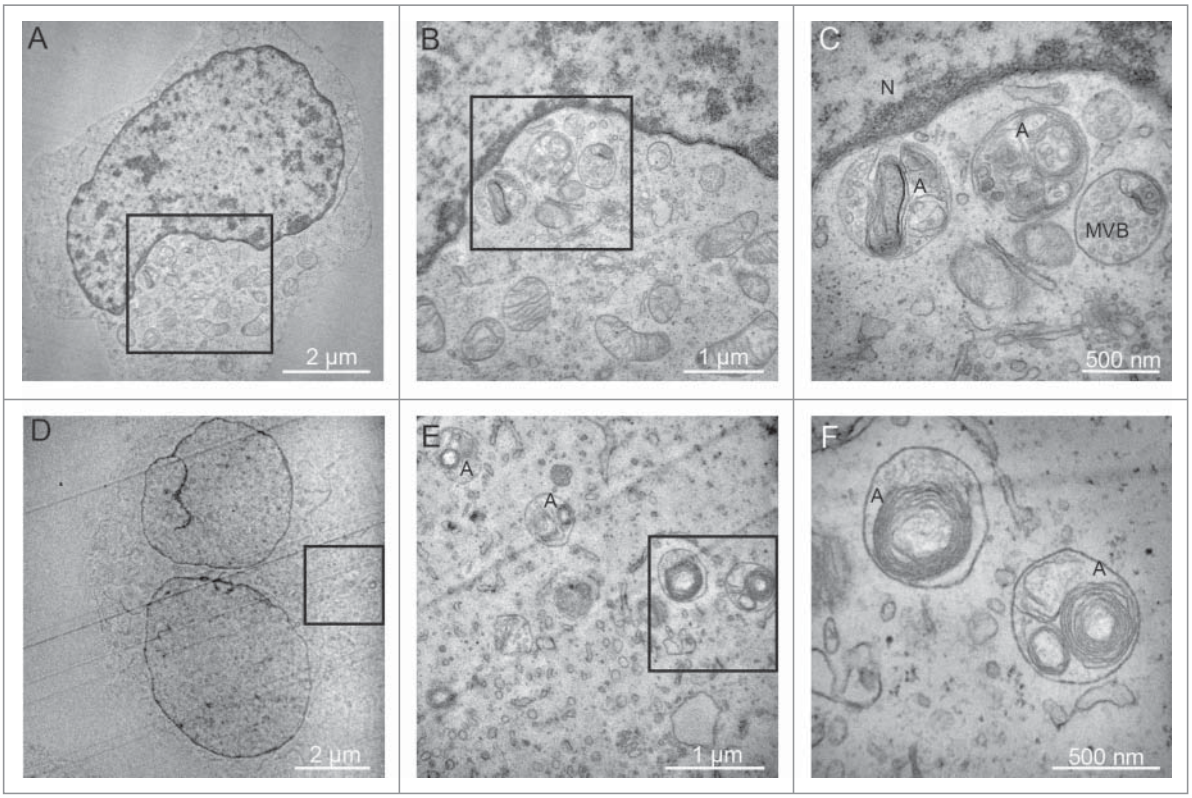

Figure 5. Effect of nutlin-3 treatment on autophagy induction observed by electron microscopy. (**A, B** and **C**) BL2/B95 cells, (**D, E** and **F**) RPMI8866 cells. **B** and **C**, and **E** and **F**, are successive magnifications of **A** and **D**, respectively. Nucleus (N), multivesicular body (MVB) and autophagosomes (A) as indicated.

one case of infectious mononucleosis (EBV-positive latency III). All EBV-positive DLBCL and PTLD cases as well as the one infectious mononucleosis case (all LMP1-positive) exhibited low (+) or moderate (++) levels of LC3-positive puncta, indicative of the presence of autophagosomes in these samples. This contrasted with the absence of any puncta in the 3 BL cases which displayed an homogeneous LC3 staining, reflecting its diffuse distribution in the cytoplasm (**Table 1** and **Fig. S7**). A representative staining of EBNA2, LMP1 and LC3 puncta is shown in **Figure 8**. These in vivo results suggest that LMP1 expression is associated with constitutive autophagy in a subset of EBV-positive latency II and III lymphoproliferations.

Discussion

In this study, we have further analyzed molecular mechanisms involved in the resistance to nutlin-3-induced apoptosis in EBV-positive latency III lymphoblastoid cells. We have shown that these cells possess a high level of constitutive autophagy which was further enhanced by nutlin-3 treatment and that autophagy contributes to their resistance to apoptosis. Two distinct pathways are involved in this process. Constitutive autophagy correlates with an increased expression of BECN1 (as compared to EBV-negative cells), which is due, at least partially, to an LMP1-induced activation of NFKB. On the other hand, nutlin-3 treatment, which, as previously shown, induces activation of TP53 in these cells,[16] results in: a) an accumulation of SESN1, a protein that can modulate the AMPK-MTOR pathway; b) the inhibition of MTOR kinase activity; c) the delivery of an additional autophagic stimulation. Finally, we have also shown that LMP1-positive B cell lymphoproliferations (latency II or III types) have a high autophagy level, as assessed by the expression of LC3-II in tissue sections.

Lee and Sugden have previously reported that LMP1 enhanced autophagy of EBV-infected cells in a process that regulated its own level of expression.[30] Contrasting with our own observations, this upregulation of autophagy by LMP1 was not NFKB-dependent. Indeed, these authors showed that only the transmembrane domains 3 to 6 of the LMP1 protein, which are not involved in the activation of the NFKB signaling pathway, were required for induction of autophagy. This difference between our 2 reports may be due to the distinct cell systems we have been using. In our study, the latency III EBV-positive cell lines which have been used contained the whole EBV genome; in Lee and Sugden's experiments, the effects of the different domains of LMP1 on autophagy are analyzed in cell lines expressing either a mutant or a wild-type version of the LMP1 protein. Furthermore, it is also conceivable that both the C-terminal and the transmembrane domains of LMP1 be involved in the induction of autophagy in EBV-positive cells, the former through activation of NFKB, the latter via an unknown

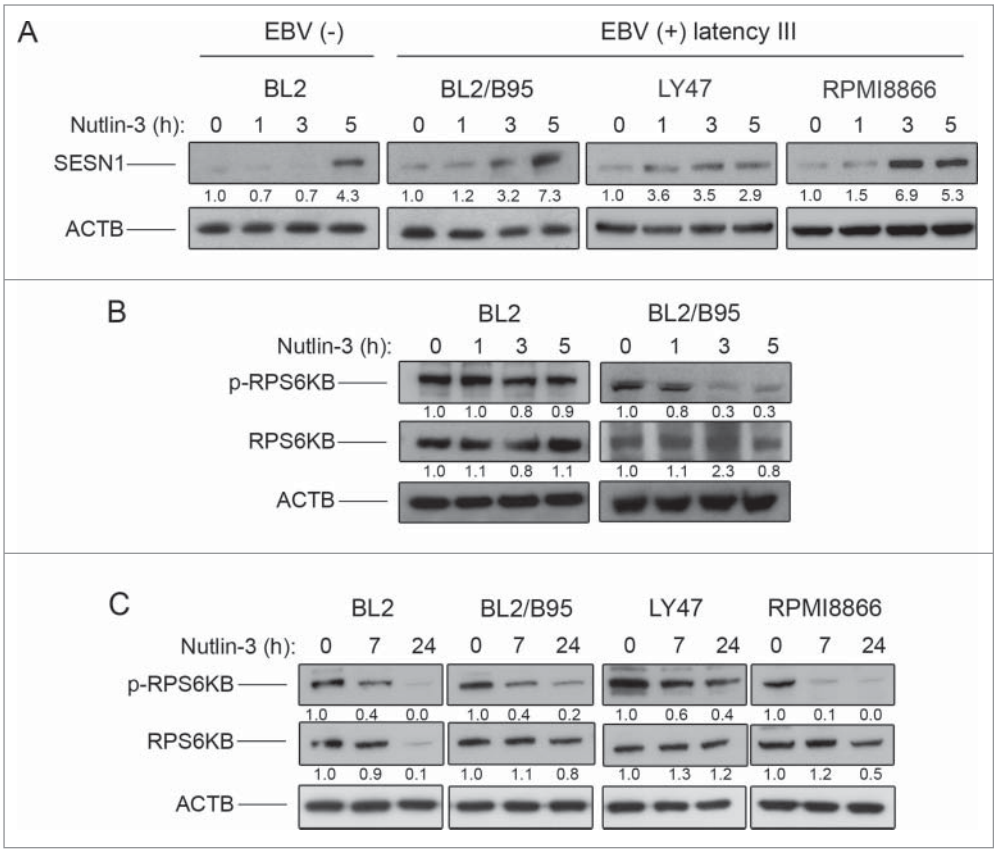

Figure 6. Effect of nutlin-3 treatment on SESN1 expression and MTOR kinase activity in EBV-negative and EBV-positive latency III lymphoid cell lines. SESN1 (**A**), p70S6K and phospho-P70S6K (**B** and **C**) expression was tested by western blot analysis of whole cell lysates at indicated times of treatment. Fold-change values reported under each blot were calculated in reference to untreated (0 h) controls and normalized to ACTB levels. The blots shown are representative of 3 independent experiments.

mechanism. Recent data from the Sugden's group have further emphasized the complexity of the signals activated by LMP1.[31] Thus, the 6 transmembrane domains of LMP1 were shown to trigger autophagy eventually leading to apoptosis in a process that was blocked by the signaling activated by its C-terminal domain. The study of Sommermann et al., also underlines the importance of the role of LMP1-induced NFKB activation for the fate of the EBV-positive latency III B cells. Indeed in such cells, LMP1 expression increases glucose uptake through NFKB signaling whereas inhibition of NFKB decreased glucose import and induced autophagy. These authors also reported that a treatment of these autophagic cells with chloroquine resulted in cell death thereby suggesting that autophagy is a protective mechanism set up by the cells when NFKB is turned off.[32]

Other recent studies have examined the role of autophagy during viral infections. For instance, autophagy protects infected cells by degrading intracellular viruses through xenophagy, a form of autophagy whereby foreign molecules are degraded in autophagosomes, or by contributing to both the innate and adaptative immune responses (reviewed in ref. 33). With regard to EBV, it has been shown that autophagy contributes to MHC class II presentation of the viral EBNA1 antigen[34] but it remains debated whether CD4-positive T cell clones specific for EBNA1 epitopes efficiently recognize LCL cells or not.[35] On the other hand, some viruses utilize mechanisms that counteract autophagy to escape these antiviral processes or may even be able to use autophagy to promote their own replication (reviewed in refs.18, 36). In the present study, we have shown that B cells infected by EBV in vitro have a high constitutive level of autophagy in contrast to EBV-negative cells and, most importantly, we have extended these data on primary EBV-positive and -negative lymphoproliferations. We have also found that treating EBV-positive latency III cell lines with chloroquine, an autophagy inhibitor, induced apoptosis thereby suggesting that autophagy corresponds to a strategy developed by the virus to promote survival of its host cell. This process comes in addition to various other ways EBV utilizes to subvert the cellular machinery and induce transformation in B cells.[37]

Surprisingly, treatment with another inhibitor of autophagy, BAF, induced only a moderate level of apoptosis in EBV-positive latency III cells but had a strong effect in EBV-negative cells. Moreover, BAF treatment hardly sensitized both types of cells to nutlin-3-induced apoptosis. Since we have shown by various methods that EBV-negative BL2 cells have a much lower level of basal autophagy than EBV-positive latency III cells, this would suggest that the cytotoxicity induced by BAF in our B cell lines is not related to its ability to inhibit autophagy. Further studies are certainly needed to better understand the discrepancies observed between chloroquine and BAF treatments in EBV-positive latency III cells but also to address why inhibition of vacuolar ATP-ases but not deacidification of vacuoles by a weak base induces apoptosis in EBV-negative cells.

We have previously reported that in EBV-positive latency III cells, BCL2 forms complexes with the proapoptotic BAX protein, inhibits its activation and thereby participates in the resistance of these cells to apoptosis.[17] Since BCL2 also negatively regulates autophagy by interacting with BECN1, the intriguing question remains: how is a high level of expression of BCL2 in these cells compatible with a high constitutive level of autophagy? The interactions of BCL2 with BAX and BECN1 are both regulated by multisite phosphorylation of BCL2 but it has been proposed

by Wei et al. that a low level of BCL2 phosphorylation is sufficient to disrupt BCL2-BECN1 complexes whereas higher levels of phosphorylation are required to disrupt BCL2-BAX complexes.[38] Our preliminary results (data not shown) indicate that BCL2 is phosphorylated in EBV-positive latency III cells suggesting that this occurs at a level sufficiently low to preclude interaction with BECN1 but not with BAX.

In a previous study, Chaumorcel et al. have reported that a high level of BCL2 induced by virus infection does not necessarily lead to inhibition of autophagy. In this study, it was shown that human cytomegalovirus (HCMV) infection induced a robust increase of BCL2 protein levels but that this upregulation of BCL2 was not involved in the HCMV-induced inhibition of autophagy. Indeed, in infected cells, BCL2 was phosphorylated by the JUN kinase and thereby unable to associate with BECN1.[39] Further experiments including coimmunoprecipitations of BCL2 and BECN1 are clearly needed to determine if the situation is similar in our model. On the other hand, since phosphorylation of BECN1 also regulates its interaction with BCL2,[4] it will be necessary to check its level of phosphorylation. Finally, Pattingre et al. have shown that only those BCL2/BECN1 complexes, which are localized to the endoplasmic reticulum effectively inhibit autophagy, suggesting that it would be worth investigating the subcellular localization of BCL2 in EBV-positive latency III cells.[40]

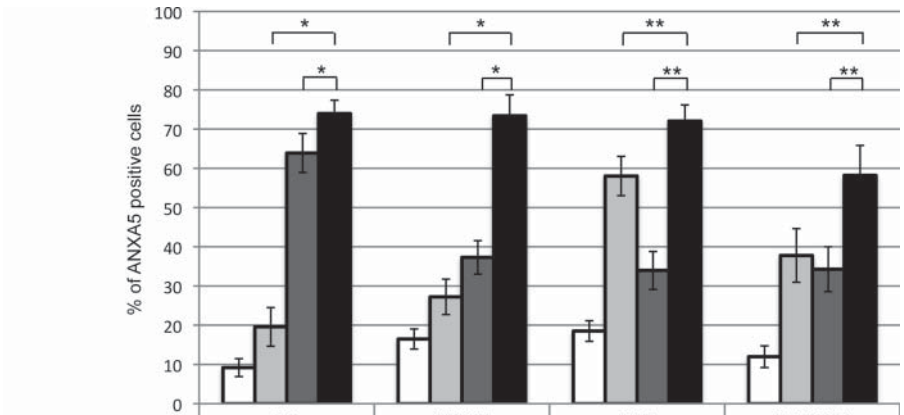

	BL2	BL2B95	LY47	RPMI8866
Untreated	9 ±2	16 ±3	19 ±3	12 ±3
Chloroquine	20 ±5	27 ±5	58 ±5	38 ±7
Nutlin-3	64 ±5	37 ±4	34 ±5	34 ±6
Chloroquine + Nutlin-3	74 ±3	73 ±5	72 ±4	58 ±8

Figure 7. Combined effect of nutlin-3 and chloroquine treatments on apoptosis in EBV-negative and -positive latency III lymphoid cell lines. Cells were incubated with or without chloroquine (100 μM) for 2 h, followed by an incubation in the absence or presence of nutlin-3 for 24 h. Apoptosis was then measured by flow cytometry detection of ANXA5-FITC-positive cells (whether PI-positive or not). Values are means from at least 5 independent experiments, error bars represent standard deviation (SD). Statistical analyses were performed using the nonparametric Mann-Whitney test with Bonferroni correction to compare results obtained after treatment with chloroquine and nutlin-3 to those obtained after treatment with only one of these compounds. Statistical significance is as follows: *, $P < 0.005$; **$P < 0.0005$.

We have also reported here that nutlin-3 treatment enhanced expression of several genes involved in autophagy in both EBV-negative and -positive latency III cells. However, the nutlin-3 treatment resulted in the induction of very moderate levels of autophagy, if at all, in EBV-negative cells whereas in EBV-positive latency III cells, nutlin-3 strongly enhanced the basal level of autophagy. Part of this differential induction of autophagy could be related to the different kinetics of SESN1 upregulation and MTOR inhibition that we observed between EBV-negative and -positive cells. Recent studies have highlighted the dual role played by TP53 with regard to autophagy: when nuclear, TP53 transactivates target genes thus stimulating autophagy;[25,41] when cytoplasmic, TP53 negatively regulates autophagy by interacting with RB1CC1 (RB1-inducible coiled-coil 1), the human ortholog of yeast Atg17 which is involved in autophagosome formation.[42] In EBV-negative cells where autophagy is hardly induced, it would be interesting to test the level of RB1CC1 and of cytoplasmic TP53 after nutlin-3 treatment to determine whether their interaction could regulate this catabolic process. Similarly, it would be worth determining the role of DRAM1, the gene most strongly induced by nutlin-3 in both EBV-negative and -positive cells, since this protein is an inducer of autophagy but also contributes to apoptosis.[25]

The role of autophagy in cancer is complex and controversial. Autophagy can result in tumor suppression through various mechanisms but it can also be involved in tumor survival and in resistance to cancer treatment (reviewed in refs.43, 44). In this study, we have found that using chloroquine, an inhibitor of lysosome and autophagosome fusion, was sufficient to promote apoptosis in EBV-positive latency III cells. Also, pretreating with chloroquine sensitized these cells to nutlin-3-induced apoptosis.

In vitro experiments and preclinical studies in various mouse xenograft tumor models have demonstrated that chloroquine potentiates antitumoral treatments through its capacity to inhibit autophagy.[45-47] So far, chloroquine (and its derivative hydroxychloroquine) is the only autophagy inhibitor under clinical testing—in combination with conventional drugs or targeted tools—for the treatment of refractory tumors. Although its mechanisms of action in vivo remain unclear, the first results are encouraging with tumor growth stabilized or median survival times increased observed in patients treated with chloroquine.[48]

Finally, it is worth noting that in the work reported by Amaravadi et al., the induction of TP53 in mice carrying a *Myc*-induced lymphoma promotes tumor cell apoptosis but with surviving tumor cells which display a high level of autophagy. In this murine model, inhibiting autophagy using chloroquine or

Table 1. Pattern of expression of LC3 by immunohistochemistry in B cell lymphoproliferations.

Patient	Diagnosis	EBV latency type	EBER expression	EBNA2 expression	LMP1 expression	LC3 puncta
1	BL	Not EBV infected	–	–	–	–
2	BL	I	+	–	–	–
3	BL	I	+	–	–	–
4	EBV+ DLBCL of the elderly	II	+	–	+	+
5	EBV+ DLBCL of the elderly	II	+	–	+	+
6	Polymorphic PTLD	II	+	–	+	++
7	Polymorphic PTLD	III	+	+	+	+
8	Monomorphic PTLD	III	+	+	+	++
9	PTLD, early lesion: infectious mononucleosis-like	II`I	+	+	+	+
10	Infectious mononucleosis	III	+	+	+	+

ATG5 shRNA enhances apoptosis and stimulates tumor regression.[49] Our in vitro results, fully consistent with those obtained in vivo, confirm that the autophagy induced by TP53 activation can result in tumor cell survival and resistance to treatment. Since EBV-positive latency III cells have a high level of expression of BCL2, our results are also in accordance with those of MacLean et al. showing that chloroquine-induced cell death of *Tp53*$^{+/+}$ *Eμ-Myc* murine B cells is not impaired by overexpression of the antiapoptotic protein BCL2.[50] Using chloroquine thus appears interesting to prevent induction of autophagy and enhance cytotoxic efficacy of TP53 activation in cells treated with nutlin-3 or other drugs, which induce a TP53-dependent apoptosis. However, since such an induction of autophagy by TP53 occurs only in cells with a high level of basal autophagy associated with a high expression of BECN1, it could be of interest to test for BECN1 levels prior to any chloroquine treatment.

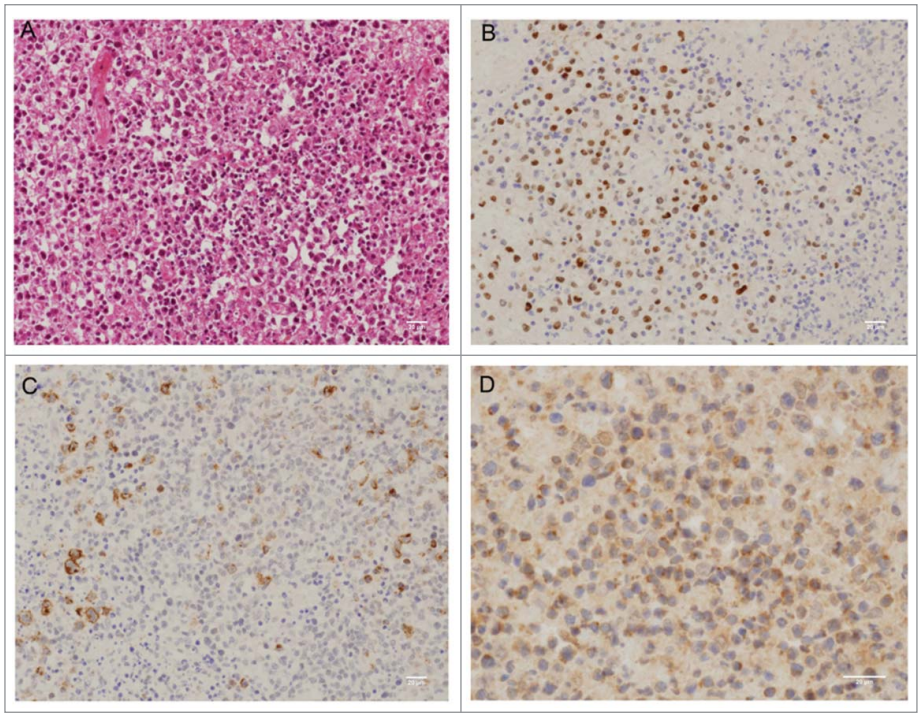

Figure 8. Pattern of expression of EBNA2, LMP1 and LC3 in a case of EBV-positive latency III lymphoproliferation. Immunohistochemical staining obtained from tonsil biopsy. Panels are representative of images taken at 25x (**A, B** and **C**) or 40x magnification (**D**). (**A**) hematoxylineosin-Safran staining. (**B**) EBNA2 nuclear staining. (**C**) LMP1 cell membrane staining. (**D**) cytosolic LC3 staining with visible puncta.

Materials and Methods

Cell lines

All BL cell lines were originally established from endemic or sporadic cases of BL. BL2, BL28, BL40, BL2/B95, BL28/B95, BL40/B95, and LY47 were kindly provided by the International Agency for Research on Cancer (IARC, Lyon, France); Seraphina was provided by Prof. G. Klein (Stockholm, Sweden); BL2/B95, BL28/B95 and BL40/B95 were generated by stable infection of the original EBV-negative BL2, BL28 and BL40 cells with the B95–8 EBV strain. LCLs were obtained by the in vitro immortalization of normal B lymphocytes. IARC 211 cells were established from the normal B lymphocytes of patient BL40. Priess and Remb1 cells were kindly provided by Dr J.G. Bodmer (London, UK) and RMPI8866 by Dr J. Banchereau (Dardilly, France). DG75 tTA LMP1, a stable transfectant of the DG75 cell line with a tetracycline-regulated LMP1 expression,[51] was kindly provided by Dr O. Dellis (Orsay, France). All cell lines, except DG75, express wt TP53. They were cultured in complete RPMI 1640 medium (containing 2 mM L-glutamine, 1 mM sodium pyruvate, 20 mM glucose, 100 U/ml penicillin and 100 μg/ml streptomycin and supplemented with 10% heat-inactivated fetal calf serum). Tetracycline hydrochloride (1 μg/ml; MP Biochemicals, 02194542) was used to silence tetracycline-regulated LMP1 expression in the DG75 tTA LMP1 cell line.

Antibodies and reagents

Nutlin-3 was kindly provided by Roche Laboratories. Chloroquine (C6628) and bafilomycin A_1 (B1793) were obtained from Sigma-Aldrich. Anti-RELA/p65 monoclonal antibody (mAb) was purchased from Santa Cruz Biotechnology (sc-8008). Anti-ACTB/β-actin (A5316) mAb was obtained from Sigma-Aldrich. Anti-SESN1 polyclonal antibody (pAb; ab67156) was obtained from Abcam. Anti-BECN1 pAb (3738), anti-RPS6KB/p70S6K pAb (9202), anti-phospho-RPS6KB/p70S6K mAb (Thr389, 9206) and anti-LC3B pAb (2775) were purchased from Cell Signaling technology. Anti-LMP1 mAb (M 0897) was obtained from Dako France SAS. Anti-LC3B mAb (0231–100/LC3–5F10) used for immunohistochemistry was obtained from Nanotools and anti-EBNA2 (NVL-EBV-PE2) from Novocastra. Horseradish peroxidase (HRP)-conjugated rabbit anti-mouse IgG (NA 931) and HRP-conjugated donkey anti-rabbit IgG (NA 934) were purchased from GE Healthcare.

Western blot analysis

A pellet containing 1×10^6 cells was solubilized by incubation in ice-cold lysis buffer (150 mM NaCl, 50 mM Tris. pH 7.4, 5 mM EDTA, 0.1% NP40 (IGEPAL-CA630, Sigma Aldrich, I3021), 0.5% sodium deoxycholate (Sigma Aldrich, D6750), 0.1% SDS (Fluka, 05030), complete protease inhibitor cocktail (Roche, 11 873 580 001) for 15 min or directly in loading buffer (60 mM Tris, pH 6.8, 2% SDS, 10% glycerol, 1% β-mercaptoethanol) for further detection of phosphoproteins. Sample loading buffer was added and the mixture was boiled for 5 min. Proteins were separated by electrophoresis and western blotting was realized as previously described.[17]

Lentivirus and stable transduction of shRNAs

RPMI8866 cells were cultured in a 96-well plate with lentiviral particules containing a control shRNA (MISSION TRC2 pLKO.5-puro Control Transduction Particle, SHC202V, Sigma Aldrich) or a shRNA targetting *RELA*/*p65* (MISSION Lentiviral Transduction Particles, SHCLNV-NM_021975, clone ID: TRCN0000014686, Sigma Aldrich) at a multiplicity of infection of 5 in complete RPMI medium supplemented with hexadimethrine bromide (4 μg/ml; Sigma Aldrich, D6750). After 24 h, 100 μl of complete RPMI medium was added. After 48 h, transduced cells were washed with phosphate-buffered saline (Life technologies, 18912–014) and then cultured in complete RPMI medium containing puromycin (0.6 μg/ml). Stable transduced cells were obtained after 3 to 4 wk of puromycin selection.

Gene expression analysis

Cells were treated with 10 μM nutlin-3 for various periods of time. Three replicates per condition were done. RNA extracted from each replicate (RNeasy Micro kit, Qiagen, 74004) was used for gene expression with Agilent® 4×44 Human Gene Expression arrays (Agilent Technologies). After single color hybridization and array scanning, performed as recommended by the manufacturer, data were carefully checked using several quality control. Raw data were extracted from image with Feature Extraction (10.5.1.1, Agilent). These data were log2-transformed and then normalized using the quantile method. An unsupervised cluster was computed using Euclidian distance and Ward method for clusterisation, and validated by bootstrapping. PCA analysis was also performed to analyze sources of variance between samples. Supervised analysis of genes differentially expressed between groups of interest was performed using the moderated *t* test from the LIMMA package. The expression profile of the set of significant differentially expressed genes was used to compute a supervised cluster using the same parameters as for unsupervised cluster.

Detection of autophagy by immunofluorescence staining

EBV-positive latency III and EBV-negative cells were incubated with or without nutlin-3 (10 μM) for 16 h at 37°C. Cells were stained with MDC (100 μM; Sigma-Aldrich, 30432) for 10 min at 37°C. After 2 washes in phosphate-buffered saline, cells were plated on glass slides pretreated with poly-D-lysine. Cells were then fixed in 3% paraformaldehyde for 20 min, washed and examined by fluorescence microscopy (Leica confocal microscope SPE, Leica Microsystèmes SA, Nanterre, France). For each condition, the percentage of cells with characteristic MDC staining dots indicative of autophagy was assessed. MDC staining was also assessed by flow cytometry using an LSR II Becton Dickinson flow cytometer equipped with a 355 nm UV laser (BD Biosciences, Le Pont de Claix, France). Data were analyzed, and MFI values calculated, using the BD FACSDiva software (BD Biosciences). Graphs were done with the FlowJo software (Flow Jo, Tree Star Inc.).

Autophagic vesicles were detected using the CYTO-ID autophagy detection kit according to the manufacturer's instructions (Enzo Life Science, ENZ-51031). The cationic amphilic tracer dye used in this assay selectively labels pre-autophagosomes, autophagosomes and autolysosomes but not lysosomes. Cells incubated with or without nutlin-3 were washed, resuspended in 0.5 ml of freshly diluted Cyto-ID Green stain reagent and incubated at 37°C for 30 min in the dark. Cells were then washed and analyzed by flow cytometry using an Accuri C6 Flow cytometer (BD Biosciences, Le Pont de Claix, France).

Electron microscopy

Cells were incubated with or without 10 μM nutline-3 for 7 h. For Epon embedding, cell pellet fractions were fixed for 1 h at room temperature in 2% glutaraldehyde in 0.1 M cacodylate buffer, pH 7.4. Cells pellets were postfixed for 1 h with 1% osmium tetroxide in 0.1M cacodylate buffer and 1.5% potassium ferrocyanide. Cells were dehydrated in increasing concentrations of ethanol and embedded in Epon812 (EMS, 14120). Polymerization was carried out for 72 h at 56°C. Ultrathin sections (70 nm) were collected on collodion-carbon-coated copper grids (EMS, G200-Cu). Sections were contrasted by uranyl acetate and lead citrate. Cells were observed with a Zeiss 902 electron microscope (Carl Zeiss microscopy GmbH, Jena, Germany) in filtered zero-loss mode using a CCD Megaview III camera and a

SIS system (Olympus Soft Imaging Solutions GmbH, Münster, Germany).

Induction and quantification of apoptosis

5×10^5 cells were treated for 24 h, at 37°C, with nutlin-3 (10 μM), chloroquine (100 μM) or both of these compounds. Cells were stained with FITC-labeled ANXA5/annexin-V (Roche Applied Science, 11–828–681–001) and propidium iodide (PI) and analyzed by flow cytometry as previously described.[17] Apoptosis is assessed by the number of ANXA5-positive cells whether PI-positive or not.

Statistical analysis

Data are expressed as mean ± standard deviation (SD). Statistical differences between each treatment alone (chloroquine or nutlin-3) and the combination of these drugs were analyzed by the nonparametric Mann-Whitney 2-tailed test. A Bonferroni correction was applied to account for multiple testing (8 pairwise comparisons performed) and tests with a P value < 0.006 were considered statistically different ($\alpha = 0.05/8$).

Patients

Lymphoma cases were retrieved from the pathology departments in 2 French university hospitals (Créteil and Kremlin-Bicêtre). All cases were independently reviewed by at least 2 pathologists specialized in hematology and were classified as EBV (+) DLBCL of the elderly (n = 2), BL (n = 3), infectious mononucleosis (n = 1) or PTLD (n = 4). In accordance to French laws, all patients have given informed consent.

Immunohistochemistry

Staining was performed as described in ref.29 Briefly, paraffin-embedded tissue sections were deparaffinized with xylene, dehydrated through graded alcohols and subjected to antigen retrieval using 10 mM Tris-EDTA buffer (Diapath, T0013) for 25 min at 98°C. After cooling, sections were incubated in BLOXALL blocking solution (Vector Laboratories, SP6000) for 5 min to block for endogenous peroxidase. Sections were then washed with TBS and incubated with primary antibodies (anti-LC3, anti-EBNA2, anti-LMP1 mAbs) for 45 min at room temperature. After 2 washes in TBS-Tween for 5 min, sections were incubated with secondary anti-mouse antibody (Dako EnVision + System-HRP labeled polymer, K4000) for 30 min at room temperature. After washing, sections were incubated with DAB (3,3′-diaminobenzidine, Vector Laboratories, SK-4100) for 10 min at room temperature and then washed in TBS. Sections were then counter-stained with Mayer hematoxylin, mounted (Shandon, Immu-Mount, 9990402) and observed under a microscope Axioskop 2 (Zeiss, Marly le Roi, France).

Disclosure of Potential Conflict of interest

The authors declare no conflict of interest.

Acknowledgments

We thank Sophie Salome-Desnoulez and Yann Lécluse (Imaging and Cytometry Platform, Institut Gustave Roussy) for expert technical assistance in performing confocal microscopy and flow cytometry analyses. We are very grateful to Agnès Laplanche (Department of Biostatistics and Epidemiology, Institut Gustave-Roussy) for her great help in statistical analyses and to Evelyne May (UMR 8126 CNRS) for helpful discussions and suggestions.

Funding

This work was supported by grants from the Fondation de France 00012093 (JW), the Cancéropole and Région Ile-de-France (ERABL, IF09–2092/R), the Fondation pour la Recherche Médicale (doctoral fellowship to AP) and the Université Paris-Sud (BQR 2009).

Supplemental material

Supplemental data for this article can be accessed on the publisher's website.

References

1. Levine AJ. p53, the cellular gatekeeper for growth and division. Cell 1997; 88:323-31; PMID:9039259; http://dx.doi.org/10.1016/S0092-8674(00)81871-1
2. Vousden KH, Lu X. Live or let die: the cell's response to p53. Nat Rev Cancer 2002; 2:594-604; PMID:12154352; http://dx.doi.org/10.1038/nrc864
3. Mizushima N. Autophagy: process and function. Genes Dev 2007; 21:2861-73; PMID:18006683; http://dx.doi.org/10.1101/gad.1599207
4. Kang R, Zeh HJ, Lotze MT, Tang D. The Beclin 1 network regulates autophagy and apoptosis. Cell Death Differ 2011; 18:571-80; PMID:21311563; http://dx.doi.org/10.1038/cdd.2010.191
5. Budanov AV, Karin M. p53 target genes sestrin1 and sestrin2 connect genotoxic stress and mTOR signaling. Cell 2008; 134:451-60; PMID:18692468; http://dx.doi.org/10.1016/j.cell.2008.06.028
6. Liu EY, Ryan KM. Autophagy and cancer–issues we need to digest. J Cell Sci 2012; 125:2349-58; PMID:22641689; http://dx.doi.org/10.1242/jcs.093708
7. Tasdemir E, Chiara Maiuri M, Morselli E, Criollo A, D'Amelio M, Djavaheri-Mergny M, Cecconi F, Tavernarakis N, Kroemer G. A dual role of p53 in the control of autophagy. Autophagy 2008; 4:810-4; PMID:18604159; http://dx.doi.org/10.4161/auto.6486
8. Dickens MP, Fitzgerald R, Fischer PM. Small-molecule inhibitors of MDM2 as new anticancer therapeutics. Semin Cancer Biol 2010; 20:10-8; PMID:19897042; http://dx.doi.org/10.1016/j.semcancer.2009.10.003
9. Vu BT, Vassilev L. Small-molecule inhibitors of the p53-MDM2 interaction. Curr Top Microbiol Immunol 2011; 348:151-72; PMID:21046355
10. Vassilev LT, Vu BT,Graves B, Carvajal D, Podlaski F, Filipovic Z, Kong N,Kammlott U, Lukacs C,Klein C, et al. In vivo activation of the p53 pathway by small-molecule antagonists of MDM2. Science 2004; 303:844-8; PMID:14704432; http://dx.doi.org/10.1126/science.1092472
11. Stuhmer T, Chatterjee M, Hildebrandt M, Herrmann P, Gollasch H, Gerecke C, Theurich S, Cigliano L, Manz RA, Daniel PT, et al. Nongenotoxic activation of the p53 pathway as a therapeutic strategy for multiple myeloma. Blood 2005; 106:3609-17; PMID:16081689; http://dx.doi.org/10.1182/blood-2005-04-1489
12. Sarek G, Kurki S, Enback J, Iotzova G, Haas J, Laakkonen P, Laiho M, Ojala PM. Reactivation of the p53 pathway as a treatment modality for KSHV-induced lymphomas. J Clin Invest 2007; 117:1019-28; PMID:17364023; http://dx.doi.org/10.1172/JCI30945
13. Secchiero P, Barbarotto E, Tiribelli M, Zerbinati C, di Iasio MG, Gonelli A, Cavazzini F, Campioni D, Fanin R, Cuneo A, et al. Functional integrity of the p53-mediated apoptotic pathway induced by the nongenotoxic agent nutlin-3 in B-cell chronic lymphocytic leukemia (B-CLL). Blood 2006; 107:4122-9; PMID:16439677; http://dx.doi.org/10.1182/blood-2005-11-4465

14. Vassilev LT. MDM2 inhibitors for cancer therapy. Trends Mol Med 2007; 13:23-31; PMID:17126603; http://dx.doi.org/10.1016/j.molmed.2006.11.002
15. Khoo KH, Verma CS, Lane DP. Drugging the p53 pathway: understanding the route to clinical efficacy. Nat Rev Drug Discov 2014; 13:217-36; PMID:24577402; http://dx.doi.org/10.1038/nrd4288
16. Renouf B, Hollville E, Pujals A, Tetaud C, Garibal J, Wiels J. Activation of p53 by MDM2 antagonists has differential apoptotic effects on Epstein-Barr virus (EBV)-positive and EBV-negative Burkitt's lymphoma cells. Leukemia 2009; 23:1557-63; PMID:19421231; http://dx.doi.org/10.1038/leu.2009.92
17. Pujals A, Renouf B, Robert A, Chelouah S, Hollville E, Wiels J. Treatment with a BH3 mimetic overcomes the resistance of latency III EBV (+) cells to p53-mediated apoptosis. Cell Death Dis 2011; 2:e184; PMID:21796156; http://dx.doi.org/10.1038/cddis.2011.67
18. Cavignac Y, Esclatine A. Herpesviruses and autophagy: catch me if you can! Viruses 2010; 2:314-33; PMID:21994613; http://dx.doi.org/10.3390/v2010314
19. Klionsky DJ, Abdalla FC, Abeliovich H, Abraham RT, Acevedo-Arozena A, Adeli K, Agholme L, Agnello M, Agostinis P, Aguirre-Ghiso JA, et al. Guidelines for the use and interpretation of assays for monitoring autophagy. Autophagy 2012; 8:445-544; PMID:22966490; http://dx.doi.org/10.4161/auto.19496
20. Huen DS, Henderson SA, Croom-Carter D, Rowe M. The Epstein-Barr virus latent membrane protein-1 (LMP1) mediates activation of NF-kappa B and cell surface phenotype via two effector regions in its carboxy-terminal cytoplasmic domain. Oncogene 1995; 10:549-60; PMID:7845680
21. Laherty CD, Hu HM, Opipari AW, Wang F, Dixit VM. The Epstein-Barr virus LMP1 gene product induces A20 zinc finger protein expression by activating nuclear factor kappa B. J Biol Chem 1992; 267:24157-60; PMID:1332946
22. Nivon M, Richet E, Codogno P, Arrigo AP, Kretz-Remy C. Autophagy activation by NFkappaB is essential for cell survival after heat shock. Autophagy 2009; 5:766-83; PMID:19502777; http://dx.doi.org/10.4161/auto.8788
23. Ryu HJ, Kim JE, Yeo SI, Kang TC. p65/RelA-Ser529 NF-kappaB subunit phosphorylation induces autophagic astroglial death (Clasmatodendrosis) following status epilepticus. Cell Mol Neurobiol 2011; 31:1071-8; PMID:21598036; http://dx.doi.org/10.1007/s10571-011-9706-1
24. Copetti T, Demarchi F, Schneider C. p65/RelA binds and activates the beclin 1 promoter. Autophagy 2009; 5:858-9; PMID:19458474; http://dx.doi.org/10.4161/auto.8822
25. Crighton D, Wilkinson S, O'Prey J, Syed N, Smith P, Harrison PR, Gasco M, Garrone O, Crook T, Ryan KM. DRAM, a p53-induced modulator of autophagy, is critical for apoptosis. Cell 2006; 126:121-34; PMID:16839881; http://dx.doi.org/10.1016/j.cell.2006.05.034
26. Mizushima N, Yoshimori T, Levine B. Methods in mammalian autophagy research. Cell 2010; 140:313-26; PMID:20144757; http://dx.doi.org/10.1016/j.cell.2010.01.028
27. Isotani S, Hara K, Tokunaga C, Inoue H, Avruch J, Yonezawa K. Immunopurified mammalian target of rapamycin phosphorylates and activates p70 S6 kinase alpha in vitro. J Biol Chem 1999; 274:34493-8; PMID:10567431; http://dx.doi.org/10.1074/jbc.274.48.34493
28. Glaumann H, Ahlberg J. Comparison of different autophagic vacuoles with regard to ultrastructure, enzymatic composition, and degradation capacity–formation of crinosomes. Exp Mol Pathol 1987; 47:346-62; PMID:3678466; http://dx.doi.org/10.1016/0014-4800(87)90018-9
29. Rosenfeldt MT, Nixon C, Liu E, Mah LY, Ryan KM. Analysis of macroautophagy by immunohistochemistry. Autophagy 2012; 8:963-9; PMID:22562096; http://dx.doi.org/10.4161/auto.20186
30. Lee DY, Sugden B. The latent membrane protein 1 oncogene modifies B-cell physiology by regulating autophagy. Oncogene 2008; 27:2833-42; PMID:18037963; http://dx.doi.org/10.1038/sj.onc.1210946
31. Pratt ZL, Zhang J, Sugden B. The latent membrane protein 1 (LMP1) oncogene of Epstein-Barr virus can simultaneously induce and inhibit apoptosis in B-cells. J Virol 2012; 86:4380-93; PMID:22318153
32. Sommermann TG, O'Neill K, Plas DR, Cahir-McFarland E. IKKbeta and NF-kappaB transcription govern lymphoma cell survival through AKT-induced plasma membrane trafficking of GLUT1. Cancer Res 2011; 71:7291-300; PMID:21987722; http://dx.doi.org/10.1158/0008-5472.CAN-11-1715
33. Jackson WT. Viruses and the autophagy pathway. Virology 2015; 479-480:450-6; PMID:25858140; http://dx.doi.org/10.1016/j.virol.2015.03.042
34. Paludan C, Schmid D, Landthaler M, Vockerodt M, Kube D, Tuschl T, Munz C. Endogenous MHC class II processing of a viral nuclear antigen after autophagy. Science 2005; 307:593-6; PMID:15591165; http://dx.doi.org/10.1126/science.1104904
35. Leung CS, Haigh TA, Mackay LK, Rickinson AB, Taylor GS. Nuclear location of an endogenously expressed antigen, EBNA1, restricts access to macroautophagy and the range of CD4 epitope display. Proc Natl Acad Sci U S A 2010; 107:2165-70; PMID:20133861; http://dx.doi.org/10.1073/pnas.0909448107
36. Kirkegaard K. Subversion of the cellular autophagy pathway by viruses. Curr Top Microbiol Immunol 2009; 335:323-33; PMID:19802573
37. Klein G, Klein E, Kashuba E. Interaction of Epstein-Barr virus (EBV) with human B-lymphocytes. Biochem Biophys Res Commun 2010; 396:67-73; PMID:20494113; http://dx.doi.org/10.1016/j.bbrc.2010.02.146
38. Wei Y, Sinha S, Levine B. Dual role of JNK1-mediated phosphorylation of Bcl-2 in autophagy and apoptosis regulation. Autophagy 2008; 4:949-51; PMID:18769111; http://dx.doi.org/10.4161/auto.6788
39. Chaumorcel M, Lussignol M, Mouna L, Cavignac Y, Fahie K, Cotte-Laffitte J, Geballe A, Brune W, Beau I, Codogno P, et al. The human cytomegalovirus protein TRS1 inhibits autophagy via its interaction with Beclin 1. J Virol 2012; 86:2571-84; PMID:22205736; http://dx.doi.org/10.1128/JVI.05746-11
40. Pattingre S, Tassa A, Qu X, Garuti R, Liang XH, Mizushima N, Packer M, Schneider MD, Levine B. Bcl-2 antiapoptotic proteins inhibit Beclin 1-dependent autophagy. Cell 2005; 122:927-39; PMID:16179260; http://dx.doi.org/10.1016/j.cell.2005.07.002
41. Feng Z, Zhang H, Levine AJ, Jin S. The coordinate regulation of the p53 and mTOR pathways in cells. Proc Natl Acad Sci U S A 2005; 102:8204-9; PMID:15928081; http://dx.doi.org/10.1073/pnas.0502857102
42. Morselli E, Shen S, Ruckenstuhl C, Bauer MA, Marino G, Galluzzi L, Criollo A, Michaud M, Maiuri MC, Chano T, et al. p53 inhibits autophagy by interacting with the human ortholog of yeast Atg17, RB1CC1/FIP200. Cell Cycle 2011; 10:2763-9; PMID:21775823; http://dx.doi.org/10.4161/cc.10.16.16868
43. Eskelinen EL. The dual role of autophagy in cancer. Curr Opin Pharmacol 2011; 11:294-300; PMID:21498118; http://dx.doi.org/10.1016/j.coph.2011.03.009
44. Rosenfeldt MT, Ryan KM. The multiple roles of autophagy in cancer. Carcinogenesis 2011; 32:955-63; PMID:21317301; http://dx.doi.org/10.1093/carcin/bgr031
45. Guo XL, Li D, Hu F, Song JR, Zhang SS, Deng WJ, Sun K, Zhao QD, Xie XQ, Song YJ, et al. Targeting autophagy potentiates chemotherapy-induced apoptosis and proliferation inhibition in hepatocarcinoma cells. Cancer Lett 2012; 320:171-9.
46. Sasaki K, Tsuno NH, Sunami E, Tsurita G, Kawai K, Okaji Y, Nishikawa T, Shuno Y, Hongo K, Hiyoshi M, et al. Chloroquine potentiates the anti-cancer effect of 5-fluorouracil on colon cancer cells. BMC Cancer 2010; 10:370; PMID:20630104; http://dx.doi.org/10.1186/1471-2407-10-370
47. Yang ZJ, Chee CE, Huang S, Sinicrope FA. The role of autophagy in cancer: therapeutic implications. Mol Cancer Ther 2011; 10:1533-41; PMID:21878654; http://dx.doi.org/10.1158/1535-7163.MCT-11-0047
48. Maes H, Rubio N, Garg AD, Agostinis P. Autophagy: shaping the tumor microenvironment and therapeutic response. Trends Mol Med 2013; 19:428-46; PMID:23714574; http://dx.doi.org/10.1016/j.molmed.2013.04.005
49. Amaravadi RK, Yu D, Lum JJ, Bui T, Christophorou MA, Evan GI, Thomas-Tikhonenko A, Thompson CB. Autophagy inhibition enhances therapy-induced apoptosis in a Myc-induced model of lymphoma. J Clin Invest 2007; 117:326-36; PMID:17235397; http://dx.doi.org/10.1172/JCI28833
50. Maclean KH, Dorsey FC, Cleveland JL, Kastan MB. Targeting lysosomal degradation induces p53-dependent cell death and prevents cancer in mouse models of lymphomagenesis. J Clin Invest 2008; 118:79-88; PMID:18097482; http://dx.doi.org/10.1172/JCI33700
51. Floettmann JE, Ward K, Rickinson AB, Rowe M. Cytostatic effect of Epstein-Barr virus latent membrane protein-1 analyzed using tetracycline-regulated expression in B cell lines. Virology 1996; 223:29-40; PMID:8806537; http://dx.doi.org/10.1006/viro.1996.0452

- Abou Samra A., **Robert A.,** Gov C., Favre L., Eloy,L Jacquet,E Bignon J, Wiels,J, Desrat,S., Roussi F. *Dual Inhibitors of the Pro-Survival Proteins Bcl-2 and Mcl-1 Derived from Natural Compound Meiogynin A, European Journal of Medicinal Chemistry 2018 Feb.*

European Journal of Medicinal Chemistry 148 (2018) 26–38

Contents lists available at ScienceDirect

European Journal of Medicinal Chemistry

journal homepage: http://www.elsevier.com/locate/ejmech

Research paper

Dual inhibitors of the pro-survival proteins Bcl-2 and Mcl-1 derived from natural compound meiogynin A

Alma Abou Samra [a], Aude Robert [b], Crystal Gov [b], Loëtitia Favre [b], Laure Eloy [a], Eric Jacquet [a], Jérôme Bignon [a], Joëlle Wiels [b], Sandy Desrat [a, *], Fanny Roussi [a, **]

[a] Institut de Chimie des Substances Naturelles, CNRS, ICSN UPR2301, Université Paris-Saclay, 91198, Gif-sur-Yvette, France
[b] UMR CNRS 8126, Univ. Paris Sud, Université Paris-Saclay, Institut Gustave Roussy, 114 rue Edouard-Vaillant, 94805, Villejuif Cedex, France

ARTICLE INFO

Article history:
Received 22 November 2017
Received in revised form
29 January 2018
Accepted 31 January 2018
Available online 5 February 2018

Keywords:
Natural compound
Apoptosis
Bcl-2 proteins
Protein-protein interactions
Cancer

ABSTRACT

Thirty analogues of natural meiogynin A, a pan-Bcl-2 inhibitor, were prepared in order to elaborate cytotoxic compounds on specific cancer cells overexpressing one or more proteins of the Bcl-2 family. The interaction of all the new analogues with Bcl-xL, Mcl-1 and Bcl-2 proteins was first evaluated by fluorescence polarization assay (FPA) and showed that modulation of the lateral chain has a dramatic impact as subtle changes significantly modify the activity on the target proteins. The acetoxymethyl prodrugs of the two most active compounds were then elaborated to determine their cytotoxicity on B cell lines. A strong cytotoxic effect on BL2, RS4;11 and H929 cells was observed with a triazole prodrug that induces apoptosis.

1. Introduction

Apoptosis is a physiological form of programmed cell death that is essential for tissue homeostasis through the elimination of useless or potentially harmful cells [1]. Evasion of apoptosis is a hallmark of cancer. It is often correlated with the deregulation of the Bcl-2 family of proteins that control the intrinsic pathway of apoptosis [2]. All the proteins of this family share one or more of the four Bcl-2 homology (BH) domains, namely BH1, BH2, BH3 and BH4. This complex family comprises multi-domain-anti-apoptotic members such as Bcl-2, Bcl-xL or Mcl-1 and pro-apoptotic ones which are either multi-domain effector proteins (Bax and Bak) or BH3-only proteins such as Bim, Bid, Bad, and Noxa. The intrinsic pathway of apoptosis is initiated by cellular stress signals such as DNA damage that lead to the transcriptional upregulation and/or activation of pro-apoptotic BH3-only proteins. These proteins are able to bind to anti-apoptotic members of the family and inhibit their activity. In addition, direct activator BH3-only proteins (e.g., BID and BIM) also bind to and activate the multi-domain proteins BAK and BAX. Once activated, BAK and BAX oligomerize and form pores in the outer mitochondrial membrane, inducing its permeabilization (MOMP) and the release of two apoptogenic factors (CYT C and SMAC/DIABLO) which triggers caspase activation leading *in fine* to cell death [3].

Despite tremendous progress, many important questions concerning the mechanism of action of the Bcl-2 family proteins remain unanswered. Nevertheless, numerous studies have shown that anti-apoptotic Bcl-2, Bcl-xL or Mcl-1 proteins are overexpressed in many types of cancers [4,5]. Alongside being part of the oncogenesis process, their overexpression confers resistance to apoptosis that is induced by standard anticancer therapies. The anti-apoptotic proteins sequester and neutralize the BH3 death domain of the pro-apoptotic proteins within a binding groove formed by their BH1, BH2 and BH3 regions through protein-protein interactions, thus preventing cell death. Consequently, anti-apoptotic members of the Bcl-2 family represent highly interesting targets for cancer treatment. Over the years, the development of small synthetic BH3 mimetics that are able to bind to the anti-apoptotic Bcl-2 family members in order to release Bax and Bak and to restore apoptosis, proved highly successful [6–8]. Schematically, anti-apoptotic protein inhibitors can be classified in three distinct groups:

* Corresponding author.
** Corresponding author.
E-mail addresses: sandy.desrat@cnrs.fr (S. Desrat), fanny.roussi@cnrs.fr (F. Roussi).

https://doi.org/10.1016/j.ejmech.2018.01.100
0223-5234/

- Pan-Bcl-2 inhibitors that target several proteins of this family, at least Bcl-xL, Bcl-2 and Mcl-1. This is the case for natural gossypol and its derivatives *R*-(−)-gossypol (AT-101) [9], TW-37 that has reached phase I/II clinical trials [10,11], apogossypolone [12] and (−)-BI-97D6 [13]. This is the case as well for obatoclax that is active on a low micromolar range and operates through a combination of on- and off-target effects [14].
- Dual inhibitors either of Bcl-xL and Bcl-2 like ABT-737 and ABT 263 [15] or BM-957 and BM-1197 [16], or of Bcl-xL/Mcl-1 [17].
- Selective inhibitors of a protein, targeting either Bcl-xL like WEHI-539 [18], or Bcl-2 like ABT-199 that was recently approved by the FDA for the treatment of CLL [19] or Mcl-1 like S63845 [20]. All these compounds are highly active with a *Ki* at a nano- or even a sub-nanomolar level. Nevertheless, the use of these specific inhibitors was shown to induce resistance in cancer cells because of an overexpression of the non-targeted proteins (Mcl-1 or Bcl-xL) [21]. This suggests that efficient treatment may require simultaneous inhibition of multiple anti-apoptotic Bcl-2 proteins.

During the past years, our team has been involved in the isolation and synthesis of natural compounds that target the anti-apoptotic proteins of the Bcl-2 family [22–24]. Particularly, we have performed a bio-inspired synthesis of meiogynin A **1** [25], a sesquiterpene dimer that was isolated from a Malaysian Annonaceae [26] and elaborated further analogues like **2** and **3** [27–29] (Fig. 1). It should be pointed out that, contrarily to the replacement of the cyclohexane core by a phenyl, introduction of aromatics on the lateral chain had a tremendous impact, and induced significant improvements of the activity on Bcl-xl and Mcl-1 [30]. Recently, the activity of compounds **1**–**3** on Bcl-2 has also been evaluated: depending on the nature of the lateral chain, they are either pan-Bcl-2 inhibitors (compounds **1** and **2**) or dual Mcl-1/Bcl-2 inhibitors (compound **3**).

Nevertheless, albeit very potent on proteins of the Bcl-2 family, meiogynin A **1** [28] and analogues **2** and **3** are devoid of cytotoxic activity on cancer cells that overexpress these proteins. This is probably due to the presence of the carboxylic acid functions, which are important for the interactions with the proteins *via* hydrogen bonding with two arginine residues [29] but make cells penetration difficult. In addition, compounds **2** and **3** possess an ester linkage on the lateral chain that are readily hydrolyzed by cellular esterases leading to an inactive alcohol **4**.

In this publication, we report our attempts to elaborate cytotoxic derivatives of meiogynin A **1** by replacement of the ester linkage and protection of the two acid functions. At least one acid function seems important for a good activity on the proteins. Transient protections of these functions that are able to release the acids in cells were envisaged.

2. Results & discussion

Among the chemical functions that could be used to install the aromatic lateral chain on the meiogynin A core, we first investigated the carbamate. This function has a double advantage: it can be formed directly on the alcohol **4** without any protecting group on the diacid by addition of commercially-available isocyanates. Moreover, it should give a better stability to these analogues in physiologic medium. The precursor **7** was prepared in nine steps with 44% overall yield [30] based on a key bio-inspired Diels Alder cycloaddition (Scheme 1) between triene **5** and chiral dienophile **6** (*e.r.* > 94:6). This decalin **7** was isolated as a single diastereoisomer thanks to an excellent stereoselectivity in favor of the *endo* product in the cycloaddition reaction (>95%). The benzoate group was saponified in presence of lithium hydroxide to give the alcohol intermediate **4** in quantitative yield. Then, addition of aromatic isocyanates led, in 79–92% yield, to a series of carbamate analogues **8a-f** carrying different aromatic rings: chloro- and bromo-benzyl derivatives, 4-acetophenone and 3-pyridine compounds.

Synthesis of amide analogues from intermediate **4** required beforehand the protection of the acid functions. Installing transient methyl ester was chosen first. Carboxylic acid **10** was obtained by treatment of **4** with trimethylsilyldiazomethane to give the dimethyl ester **9** followed by TEMPO-mediated oxidation in presence of sodium chlorite (Scheme 2). Then, classical peptide coupling conditions using HATU led to various aromatic amides **11a-g** in moderate to quantitative yields. Although complete conversions were observed, the lowest isolated yields could be explained by the difficulties encountered during the purification process at this scale (20–30 mg). Halogenated phenyl or pyridine amide derivative have been prepared as these types of modifications on meiogynin analogues gave the best results in terms of Bcl-xL and Mcl-1 interaction [30]. To restore the carboxylic acid functions, different conditions have been tested. However, neither led to the desired compounds, even the harsher of conditions. Only the methyl benzoate function could be saponified using lithium hydroxide. When heating the reaction mixture to hydrolyze the remaining ester, degradation was observed. This explains why some of the compounds could not be isolated. Indeed, only 4-chlorobenzyl **12a**, 4-chlorophenyl **12c**, 4-morpholino-phenyl **12g** amide derivatives could be isolated as mono-carboxylic acid. The methyl ester on the ring junction of the decalin seems to be hindered and stable under basic conditions. Subsequently, in order to obtain diacid amide derivatives, another protecting group had to be selected.

As the carbonyl of the decalin **4** seems to be too hindered for hydroxide nucleophilic addition, acycloxymethyl groups were installed as protecting groups assuming that the resulting terminal ester would be more accessible. This ester group, which is cleaved in cell medium by non-specific esterases, is generally employed to increase lipophilicity of polar drugs, thus enabling cell penetration [31–34]. Very few publications deal with its stability towards organic reagents, as it is usually added at the last step of the synthesis. Anyhow, if stable enough, it could have a twofold utility in this specific case: be a protecting group for the acids and a cell penetrating facilitator. Thus, an acetoxymethyl prodrug **15** of the 4-chlorobenzylamide analogue **16** was prepared. The acycloxymethyl group was introduced in the first step on the diacid **4** in quantitative yield (Scheme 3). The diacetoxymethyl alcohol **13** obtained was then oxidized into the corresponding carboxylic acid **14**, in the same conditions previously used. Finally, a peptide coupling with 4-chlorobenzylamine led to the amide analogue **15** in 50% yield. The cleavage of the protecting group was then evaluated under different conditions. Both carboxylic acid functions were restored in few hours at rt using either lithium hydroxide in THF/water or potassium carbonate in MeOH, leading to compound **16** in 99% yield.

The last class of meiogynin analogues that has been developed was the triazole derivatives, obtained by Huisgens 1,3-dipolar cycloaddition. The click chemistry reaction was performed between an azide **17** and commercially available alkynes. Azide **17** was obtained in one step from the alcohol **13** (Scheme 4), already in hands. Then click chemistry reaction with phenyl, benzyl, and 3-pyridyl acetylene led to the desired triazole derivatives **18a-c** in moderate yields (30–50%). Acetoxymethyl protecting group removal in presence of potassium carbonate in methanol finally gave the dicarboxytriazole compounds **19a-c** in quantitative yields.

The interactions of all the new analogues **8a**-**19** with Bcl-xL, Mcl-1 and Bcl-2 proteins have been evaluated (Table 1). The modulation of the lateral chain has a dramatic impact, as subtle changes

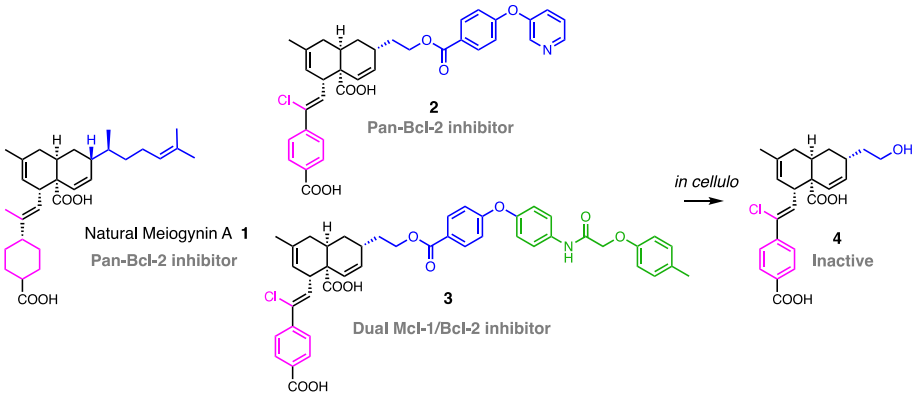

Compd.	Bcl-xL/Bak binding affinity[a] K_i[b] (μM)	Mcl-1/Bid binding affinity[a] K_i[b] (μM)	Bcl-2/Bim binding affinity[a] K_i[b] (μM)
1	8.30 ±1.20	5.20 ± 1.20	1.46 ± 0.12
2	0.15 ± 0.005	0.11 ± 0.01	1.80 ± 0.15
3	> 23	0.46 ± 0.06	0.09 ± 0.01

[a] Binding affinities were measured by fluorescence polarization after competition between the ligand and a fluorescein-labeled peptide. [b] K_i is the concentration of the ligand corresponding to 50% of the binding of the labelled reference compound, corrected for experimental conditions

Fig. 1. Meiogynin A **1**, two unnatural analogues **2**–**3** and their assumed inactive metabolite **4**.

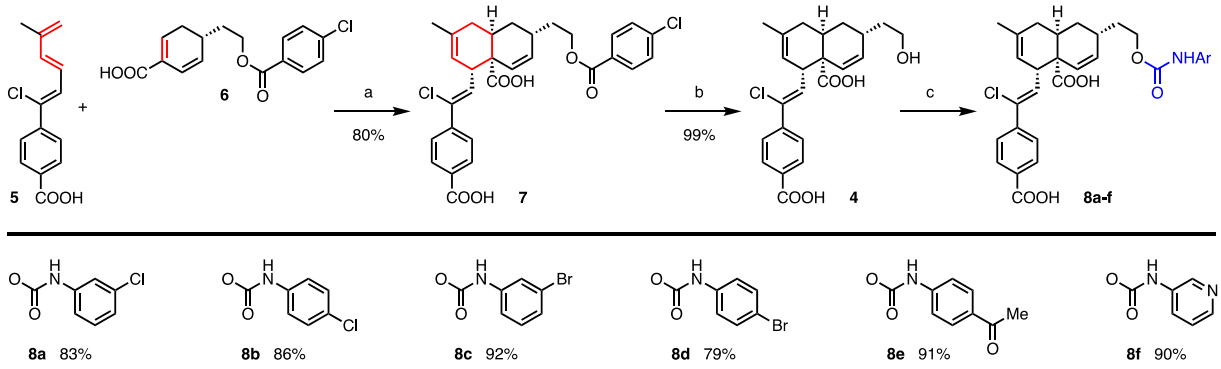

Scheme 1. Synthesis of meiogynin carbamate analogues: (a) 2-Bromophenylboronic acid (20 mol%), DCE, 80 °C, 18 h; (b) LiOH·H_2O (5 eq), MeOH/THF/H_2O 1:1:1, rt, 6 h; (c) ArNCO (1.2 eq), NEt_3 (3 eq), DCM, 0 °C to rt, 18 h.

on the linker (from an ester to a carbamate, an amide or a triazole) can significantly modify the activity on the proteins. The most potent derivatives are the carbamates, mainly **8c** and **8d** that are pan-Bcl-2 inhibitors. It is worth mentioning that both carry meta- or para-bromo-phenyl substituent. Their chloro-equivalents (**8a-b**) are about three times less potent.

Compound **8c** has similar activity to that of compound **7** (*i.e.* on a sub-micromolar range), the latter representing the common intermediate of compounds **2** and **3**. As expected, diester amides **11** and **15** are globally inactive except compound **11c**, which is an Mcl-1-selective inhibitor (*K*i= 738 nM). This represents the only compound that is active on a sub-micromolar range and for which the acids are protected. Saponification of one ester to give compounds **12a**, **12c** and **12g** restores the activity on the three proteins. Moreover, compounds **12a** and **12c** are remarkably potent on Bcl-2. Surprisingly, the diacid amide **16**, corresponding to the formerly saponified mono-ester **12a**, is practically inactive. This may indicate that compounds **11c**, **12a** and **12c** have a different binding mode compared to that of compounds **2** and **3**. In addition, shifting the carbonyl of the lateral chain *one notch* compared to the ester series is detrimental for the activity. Finally, among compounds of the triazole series, **19a** is the most interesting with dual activity on Mcl-1 and Bcl-2.

Based on their activity on Bcl-2 family proteins, the most potent compound in each series (**8c**, **11e**, **19a**) was evaluated for its cytotoxic activity on cancer cells. In addition, in order to determine the impact of the acid functions on cell penetration, acetoxymethyl-protected triazole **18a** (the putative precursor of **19a** in cells) and carbamate **20** (elaborated in one step from **8c** as shown in Scheme 5) were also tested.

As proteins of the Bcl-2 family play a central role in lymphocytes cell death and are very often deregulated in haematological malignancies [37–39], compounds **8c**, **11e**, **18a**, **19a** and **20** have been tested on four human B cell lines that overexpress one or more proteins of the Bcl-2 family, and whose profile of dependence on pro-survival family members has been determined [20]: BL2, a Burkitt lymphoma cell line is dependent on Bcl-xL and Mcl-1 for their survival; Remb1, a lymphoblastoid cell line (EBV-transformed normal B lymphocytes) is dependent on Bcl-xL; RS4;11, an acute lymphoblastic leukemia (ALL) cell line is dependent on Bcl-2 and H929, a multiple myeloma cell line is dependent on Mcl-1. Cells were treated (or not) with 10 μM of each compound for 24 h and apoptosis was measured by flow cytometry after labelling the cells with Annexin V-FITC and PI. Compounds **8c**, **11e**, **19a** and **20** – and

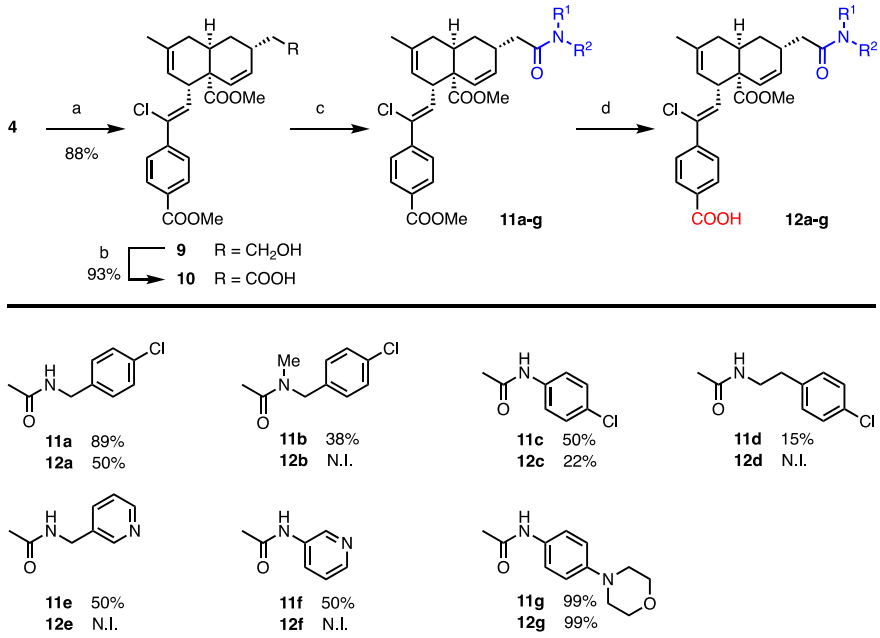

Scheme 2. Synthesis of meiogynin amide analogues: (a) $TMSCHN_2$ (2.2 eq), MeOH/Tol. 1:1, 0 °C, 6 h; (b) TEMPO (0.07 eq), $NaClO_2$ (4 eq), MeCN, 35 °C, 24 h; (c) Amine (1.6 eq), DIPEA (3 eq), HATU (1.6 eq), DMF, rt, 24 h; (d) $LiOH{\cdot}H_2O$ (5 eq), THF/H_2O 2:1, rt, 6 h.

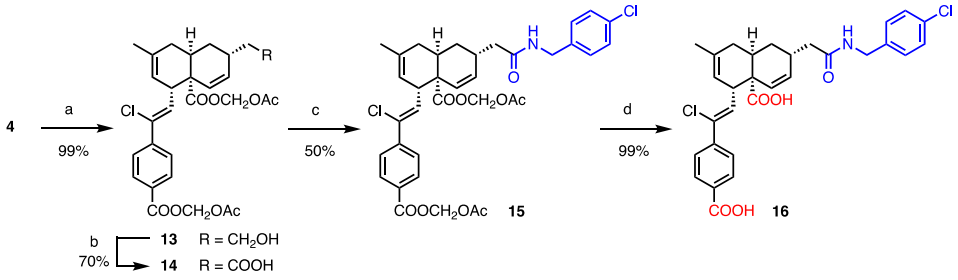

Scheme 3. Use of acycloxymethyl as protecting group to prepare dicarboxyamide analogues: (a) Bromomethyl acetate (2 eq), K_2CO_3 (3 eq), DMF, rt, 18 h; (b) TEMPO (0.07 eq), $NaClO_2$ (4 eq), MeCN, 35 °C, 24 h; (c) 4-chlorobenzylamine (1.6 eq), DIPEA (3 eq), HATU (1.6 eq), DMF, rt, 24 h; (d) K_2CO_3 (3 eq), MeOH, rt, 6 h.

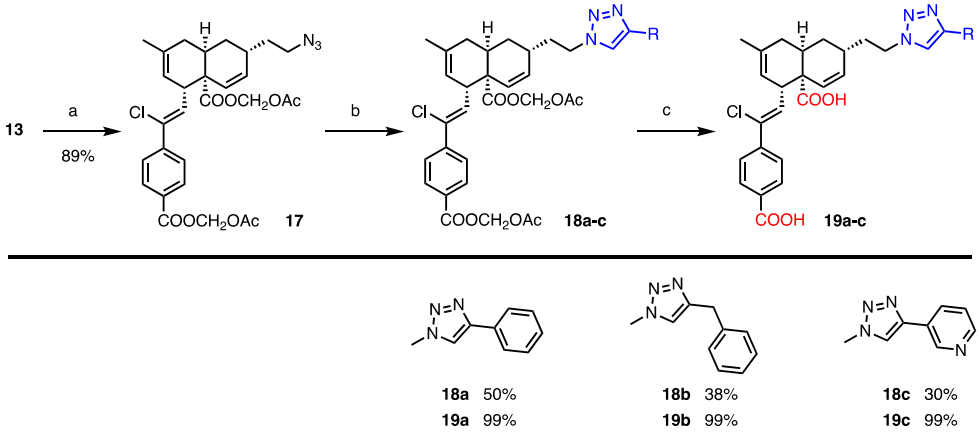

Scheme 4. Synthesis of triazole analogues: (a) PPh_3 (2 eq), DIAD (2 eq), DPPA (2 eq), THF, rt, 48 h; (b) Alkyne (4.5 eq), $CuSO_4{\cdot}5H_2O$ (0.01 eq), PhCOOH (0.05 eq), *t*-BuOH/H_2O (2:1), 60 °C, 24 h; (c) K_2CO_3 (3 eq), MeOH, rt, 4 h.

despite their strong binding affinity to Bcl-2 or Bcl-xL or Mcl-1 as shown by fluorescence polarization assay (FPA) in Table 1 – did not induce apoptosis of any cell lines (Fig. 2). By contrast, the protected triazole **18a** which is inactive by FPA, induced apoptosis in 93 ± 1% of BL2, 75.5 ± 7% of RS4;11, 37.5 ± 6% of H929 and 20.5 ± 5% of Remb1 cells. These results indicate that, as expected, compound **18a** undergoes hydrolysis *in cellulo* by unspecific esterases to afford the diacid analogue **19a**. Moreover, these findings are in accordance

Table 1
Biological evaluation of the ligands **1**–**19** on Bcl-xL/Bak, Mcl-1/Bid and Bcl-2/Bim displacement assays.

Compd.	Bcl-xL/Bak binding **affinity**[a] ***Ki***[b] (μM)	Mcl-1/Bid binding **affinity**[a] ***Ki***[b] (μM)	Bcl-2/Bim binding **affinity**[a] ***Ki***[b] (μM)
1	8.30 ± 1.20	5.2 ± 1.20	1.46 ± 0.12
2	0.15 ± 0.005	0.11 ± 0.01	1.8 ± 0.15
3	>23	0.46 ± 0.06	0.09 ± 0.001
7	0.51 ± 0.08	0.49 ± 0.06	0.45 ± 0.04
8a	3.92 ± 0.14	1.08 ± 0.04	1.08 ± 0.11
8b	4.40 ± 0.16	1.38 ± 0.10	1.42 ± 0.24
8c	0.840 ± 0.02	0.34 ± 0.02	0.37 ± 0.13
8d	2.19 ± 0.09	0.46 ± 0.03	0.83 ± 0.16
8e	1.91 ± 0.03	1.52 ± 0.21	2.92 ± 0.40
8f	8.48 ± 0.40	5.92 ± 0.47	>23
9	>23	>23	>23
10	>23	>23	>23
11a	>23	>23	>23
11b	>23	17.54 ± 1.52	>23
11c	>23	>23	>23
11d	>23	8.38 ± 0.45	>23
11e	>23	0.74 ± 0.06	>23
11f	>23	>23	>23
11g	>23	>23	>23
12a	2.73 ± 0.39	4.46 ± 1.42	0.62 ± 0.02
12c	2.74 ± 0.17	1.00 ± 0.17	0.70 ± 0.03
12g	9.91 ± 0.96	6.80 ± 1.35	>23
13	>23	4.74 ± 0.48	>23
14	15.63 ± 1.72	3.55 ± 0.39	1.82 ± 0.92
15	20.73 ± 0.51	6.83 ± 0.40	>23
16	14.08 ± 0.40	3.60 ± 1.09	>23
17	5.31 ± 0.07	2.25 ± 1.42	1.45 ± 0.26
18a	16.47 ± 1.92	13.68 ± 5.01	2.58 ± 0.21
18b	>23	>23	>23
18c	>23	>23	>23
19a	2.44 ± 0.02	0.56 ± 0.04	1.54 ± 0.44
19b	>23	2.07 ± 0.32	2.22 ± 1.12
19c	>23	>23	>23

[a] Binding affinities were measured by fluorescence polarization [35] after competition between the ligand and a fluorescein-labelled peptide.
[b] *Ki* is the concentration of the ligand corresponding to 50% of the binding of the labelled reference compound, corrected for experimental conditions [36].

with the FPA results showing that this compound mainly inhibited Bcl-2 and Mcl-1.

However, as compound **18a** weakly induced apoptosis of the Bcl-xL-dependent Remb1 cells, we decided to test the cytotoxicity of this compound by another technique (MTT assay) that measures the cellular enzymatic activity and hence estimates the number of active living cells. Based on MTT assay results, IC_{50} of compound **18a** were determined on these cell lines (Table 2). These results confirmed that the prodrug **18a** had a strong cytotoxic effect on BL2, RS4;11 and H929 cells and a much weaker effect on Remb1. Considering the low or sub-micromolar affinity of its active form **19a** towards the anti-apoptotic proteins Bcl-2 and Mcl-1, we can conclude that this triazole targets both anti-apoptotic proteins Mcl-1 and Bcl-2. In conclusion, compound **18a** is a dual inhibitor of Mcl-1 and Bcl-2 able to induce apoptosis of B cell lymphomas which are Bcl-2- and/or Mcl-1- dependent.

3. Conclusions

Inspired by the structure of meiogynin A **1**, pharmacomodulations were previously initiated and led to new pan-Bcl-2 inhibitors up to fifty times more active than the natural product on Bcl-xL, Mcl-1 and Bcl-2; but devoid of cytotoxicity on various cell lines. In this work, 30 analogues were prepared by replacing the ester linkage on the lateral chain by carbamate, amide and triazole functions. According to FPA, whereas the carbamate **8c** acts as pan-Bcl-2 inhibitor, the amide **11e** and the triazole **19a** are dual Mcl-1/Bcl-2 inhibitors. As no cytotoxicity on B cell lines was observed for these compounds, the acetoxymethyl prodrugs of **8c** and **19a** were elaborated and their cytotoxicity evaluated on the same cell lines. While the prodrug **20** exhibits no cytotoxic effect, the acetoxymethyl triazole prodrug **18a** induces apoptosis and had a strong cytotoxic effect on BL2, RS4;11 and H929 cells. In addition to being used as drug protecting group to facilitate cell penetration, the acetoxymethyl has proved to be an excellent protecting group in organic synthesis that could be easily removed under mild conditions.

4. Experimental section

4.1. General experimental details

All reagents and solvents were used as purchased from commercial suppliers or were purified/dried according to Armarego and Chai [40]. Purifications by column chromatography on silica gel were performed using Merck Silica Gel 60 (70–230 mesh). ^1H and ^{13}C NMR spectra were recorded on Bruker ARX300 and ARX500 instruments using $CDCl_3$, acetone-d_6 or methanol-d_4 as internal references. Chemical shifts (δ values) are given in parts per million (ppm), and multiplicity of signals are reported as follows: s, singlet; bs, broad singlet; d, doublet; t, triplet; q, quartet; dd, doublet of doublets; m, multiplet. HRMS analyses were performed using a Waters LCT Premier instrument by ElectroSpray Ionization (ESI). IR spectra were recorded on a PerkinElmer Spectrum BX-FTIR spectrometer.

4.2. Synthetic procedures and description of compounds 4-16

4.2.1. Cycloadduct 7

A solution of triene **5** (460 mg, 1.84 mmol, 1 eq), dienophile **6** (624 mg, 2.03 mmol, 1.1 eq) and 2-bromophenylboronic acid (74 mg, 0.37 mmol, 0.2 eq) in 1,2-dichloroethane (15 mL) was heated at reflux overnight. The reaction mixture was then concentrated under reduced pressure and purified by column chromatography on silica gel using CH_2Cl_2/AcOH 99:1 to obtain the cycloadduct **7** as a white solid (818 mg, 1.47 mmol, 80%). $R_f = 0.15$

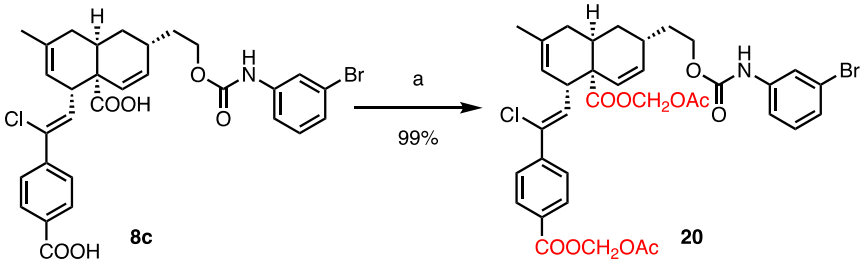

Scheme 5. Protection of the acid functions of carbamate **8c** as acycloxymethyl esters: (a) Bromomethyl acetate (2 eq), K_2CO_3 (3 eq), DMF, rt, 18 h.

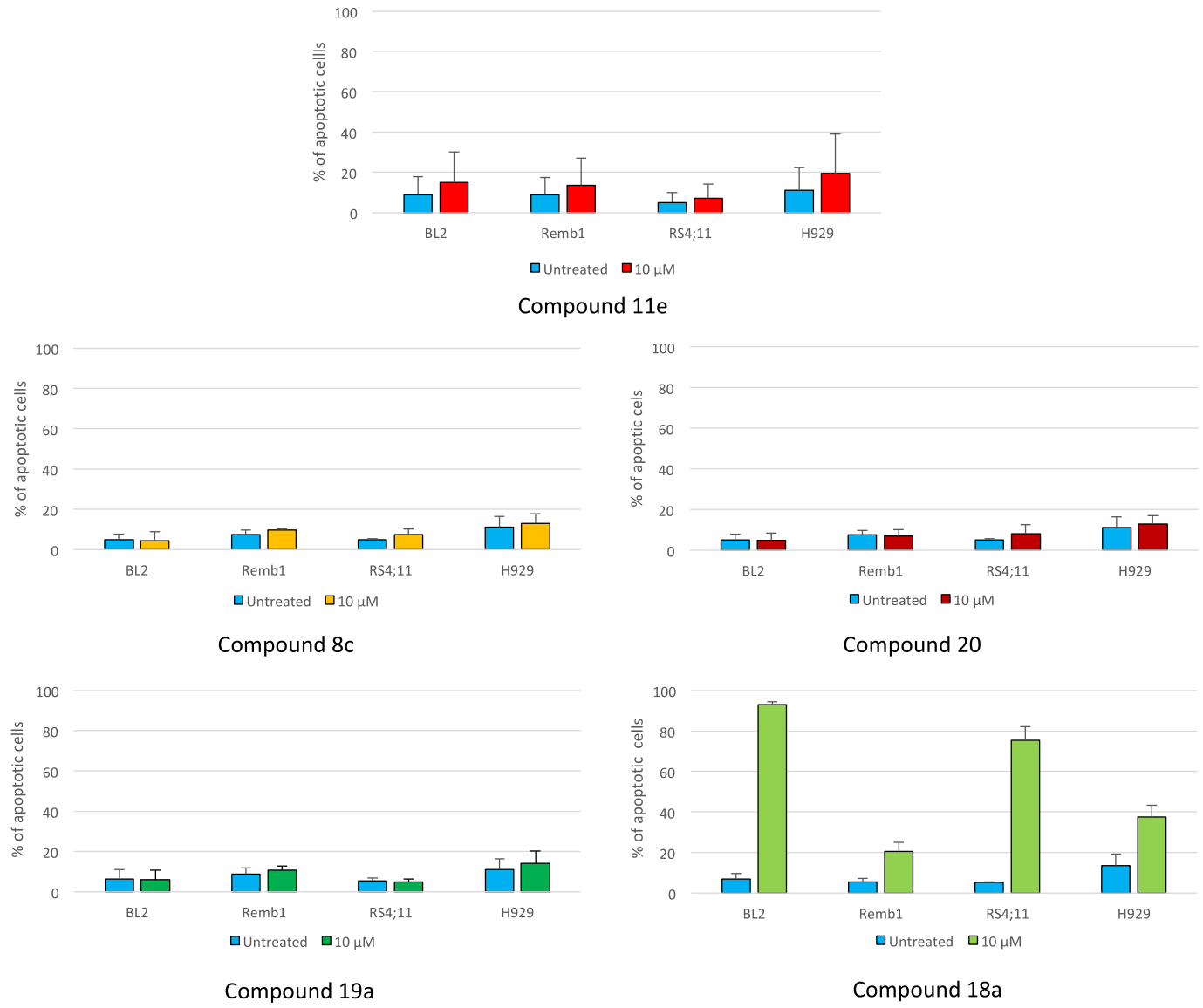

Fig. 2. Effects of compounds **8c**, **11e**, **18a, 19a** and **20** treatments on the induction of apoptosis in B cell lines. Cells were treated (or not) with 10 µM of each compound for 24 h and the proportion of cells in apoptosis was determined by flow cytometry after labelling with annexin V-FITC and PI. The values presented (mean ± S.D.) are from three independent experiments.

Table 2
IC_{50} of compounds **18a**, **ABT-737** and **ABT-199** on various B cell lines.

Cell lines	Dependency	**IC_{50} (µM)**[a]		
		ABT-737	ABT-199	18a
BL2	Mcl-1/Bcl-xL	>10	>10	9.4
Remb1	Bcl-xL	1.4	5.5	>20
RS4;11	Bcl-2	0.33	0.33	9.6
H929	Mcl-1	ND	ND	9.6

[a] IC_{50} measures the drug concentrations required for 50% cell death.

(CH_2Cl_2/AcOH 99:1); $[\alpha]_D^{20}$ -239.0° (*c* 0.5, MeOH); IR: *ν* 3197 (OH), 2925 (C=C), 1713 (C=O), 1606 (C=O), 1399 (C=C) cm^{-1}; ^1H NMR (500 MHz, acetone-d_6): *δ* 13.00–9.00 (brs, 2H), 8.03 (d, *J* = 8.2 Hz, 4H), 7.69 (d, *J* = 8.2 Hz, 2H), 7.55 (d, *J* = 8.2 Hz, 2H), 6.33 (d, *J* = 9.8 Hz, 1H), 5.77 (dd, *J* = 9.9, 2.7 Hz, 1H), 5.70 (d, *J* = 9.9 Hz, 1H), 5.31–5.26 (m, 1 H), 4.46–4.36 (m, 2H), 3.78–3.69 (m, 1H), 2.77–2.69 (m, 1H), 2.64–2.55 (m, 1H), 2.10 (dd, *J* = 18.1, 7.2 Hz, 1H), 1.99–1.83 (m, 4H), 1.78–1.70 (m, 1H), 1.65 (s, 3H) ppm; ^{13}C NMR (125 MHz, acetone-d_6): *δ* 175.6, 167.1, 165.9, 143.0, 139.6, 136.5, 133.1, 132.0 (2C), 131.6, 131.4, 131.1, 130.7, 130.6 (2C), 130.2, 129.7 (2C), 127.3 (2C), 117.9, 63.8, 48.6, 35.7, 32.5, 31.6, 30.4, 30.2, 29.7, 23.5 ppm; HRMS (ESI): *m/z* calcd. for $C_{30}H_{27}Cl_2O_6^-$ $[M\text{-}H]^-$ 553.1190; found 553.1199.

4.2.2. Alcohol **4**

To a solution of cycloadduct **7** (730 mg, 1.28 mmol, 1 eq) in MeOH/THF/H_2O 1:1:1 (12 mL) was added $LiOH{\cdot}H_2O$ (270 mg, 6.41 mmol, 5 eq). The mixture was stirred for 6 h at rt and water was added. The aqueous phase was acidified with a 2 M solution of HCl. The product was then extracted with MTBE (3 times) and the combined organic phases dried over $MgSO_4$ and concentrated under reduced pressure. The crude product was purified on silica gel using CH_2Cl_2:MeOH:AcOH (94:5:1) to obtain a light yellow solid (532 mg, 1.19 mmol, 99%). R_f = 0.2 (heptane/EtOAc/AcOH 50:49:1); $[\alpha]_D^{20}$ -25.1° (*c* 1, MeOH); IR: *ν* 3358 (OH), 2876 (C=C), 1689 (C=O)

cm^{-1}; ^{1}H NMR (500 MHz, methanol-d_4): δ 7.99 (d, J = 8.2 Hz, 2H), 7.64 (d, J = 8.2 Hz, 2H), 6.19 (d, J = 9.7 Hz, 1H), 5.69 (dd, J = 10.1, 2.7 Hz, 1H), 5.61 (d, J = 10.1, 1H), 5.27–5.24 (m, 1H), 3.70–3.65 (m, 1H), 3.65–3.58 (m, 2H), 2.67–2.60 (m, 1H), 2.52–2.44 (m, 1H), 2.08 (dd, J = 18.3, 7.3 Hz, 1H), 1.94 (dd, J = 18.3, 7.3 Hz, 1H), 1.87–1.81 (m, 1H), 1.75–1.69 (m, 1H), 1.67 (s, 3H), 1.64–1.58 (m, 1H), 1.51–1.42 (m, 1H) ppm; ^{13}C NMR (125 MHz, methanol-d_4): δ 178.1, 169.2, 143.8, 136.8, 133.9, 132.3, 131.8, 130.9, 130.8, 130.8 (2C), 127.5 (2C), 118.3, 60.5, 48.6, 46.3, 40.0, 32.9, 32.2, 30.1, 29.8, 23.6 ppm; HRMS (ESI): *m/z* calcd. for $C_{23}H_{24}ClO_5^-$ [M-H]$^-$ 415.1318; found 415.1313.

*4.2.3. General procedure for carbamates **8a-f** synthesis*

To a solution of alcohol **4** (1 eq) in anhydrous dichloromethane (0.2 M) at 0 °C was added NEt_3 (3 eq) followed by isocyanate ArNCO (1.2 eq). The mixture was stirred for 18 h at rt water was added. The compound was then extracted with MTBE (3 times) and the combined organic phases were dried over $MgSO_4$, filtered and concentrated under reduced pressure. The crude residue was purified by flash chromatography on silica gel using heptane/EtOAc mixture as eluent.

*4.2.4. Carbamate **8a***

The compound was isolated as a white solid (113 mg, 0,20 mmol, 83%). R_f = 0.3 (CH_2Cl_2/MeOH/AcOH 97:2:1); $[\alpha]_D^{20}$ -203.6° (*c* 0.5, acetone); IR: ν 3306 (OH), 2926 (C=C), 1694, (C=O), 1599 (C=C), 1405 (C=C) cm^{-1}; ^{1}H NMR (500 MHz, acetone-d_6): δ 8.80–8.72 (brs, 1H), 8.03 (d, J = 8.6 Hz, 2H), 7.69 (d, J = 8.6 Hz, 2H), 7.58 (d, J = 9.0 Hz, 2H), 7.31 (d, J = 9.0 Hz, 2H), 6.32 (d, J = 9.7 Hz, 1H), 5.74 (dd, J = 10.0, 2,5 Hz, 1H), 5.68 (d, J = 10.0 Hz, 1H), 5.31–5.26 (m, 1H), 4.29–4.16 (m, 2H), 3.75–3.67 (m, 1H), 2.75–2.68 (m, 1H), 2.55–2.46 (m, 1H), 2.13–2.03 (m, 1H), 1.97–1.88 (m, 2H), 1.87–1.80 (m, 2H), 1.78–1.71 (m, 1H), 1.65 (s, 3H), 1.64–1.57 (m, 1H) ppm; ^{13}C NMR (125 MHz, acetone-d_6): δ 175.7, 167.1, 154.4, 142.9, 139.2, 136.4, 133.1, 131.6, 131.3, 131.1, 130.9, 130.6, 130.5 (2C), 129.5 (2C), 127.3 (2C), 120.6 (2C), 117.9, 63.5, 48.6, 45.8, 36.0, 32.4, 31.6, 29.8, 29.5, 23.5 ppm; HRMS (ESI): *m/z* calcd. for $C_{30}H_{30}Cl_2NO_6^+$ [M+H]$^+$ 570.1445; found 570.1450.

*4.2.5. Carbamate **8b***

The compound was isolated as a white solid (118 mg, 0.21 mmol, 86%). R_f = 0.3 (CH_2Cl_2/MeOH/AcOH 97:2:1); $[\alpha]_D^{20}$ -217.8° (*c* 0.5, acetone); IR: ν 3299 (OH), 2926 (C=C), 1692 (C=O), 1599 (C=C), 1529 (C=C), 1404 (C=C) cm^{-1}; ^{1}H NMR (500 MHz, acetone-d_6): δ 8.80–8.72 (brs, 1H), 8.03 (d, J = 8.6 Hz, 2H), 7.69 (d, J = 8.6 Hz, 2H), 7.58 (d, J = 9.0 Hz, 2H), 7.31 (d, J = 9.0 Hz, 2H), 6.32 (d, J = 9.7 Hz, 1H), 5.74 (dd, J = 10.0, 2,5 Hz, 1H), 5.68 (d, J = 10.0 Hz, 1H), 5.31–5.26 (m, 1H), 4.29–4.16 (m, 2H), 3.75–3.67 (m, 1H), 2.75–2.68 (m, 1H), 2.55–2.46 (m, 1H), 2.13–2.03 (m, 1H), 1.97–1.88 (m, 2H), 1.87–1.80 (m, 2H), 1.78–1.71 (m, 1H), 1.65 (s, 3H), 1.64–1.57 (m, 1H) ppm; ^{13}C NMR (125 MHz, acetone-d_6): δ 175.7, 167.1, 154.4, 142.9, 139.2, 136.4, 133.1, 131.6, 131.3, 131.1, 130.9, 130.6, 130.5 (2C), 129.5 (2C), 127.3 (2C), 120.6 (2C), 117.9, 63.5, 48.6, 45.8, 36.0, 32.4, 31.6, 29.8, 29.5, 23.5 ppm; HRMS (ESI): *m/z* calcd. for $C_{30}H_{30}Cl_2NO_6^+$ [M+H]$^+$ 570.1445; found 570.1450.

*4.2.6. Carbamate **8c***

The compound was isolated as a white solid (68 mg, 0.11 mmol, 92%). R_f = 0.25 (CH_2Cl_2/MeOH/AcOH 97:2:1); $[\alpha]_D^{20}$ -108.8° (*c* 0.5, acetone); IR: ν 3177 (OH), 2928 (C=C), 1742 (C=O), 1712 (C=O), 1521 (C=C) cm^{-1}; ^{1}H NMR (500 MHz, acetone-d_6): δ 8.84–8.76 (brs, 1H), 8.03 (d, J = 8.4 Hz, 2H), 7.90 (s, 1H), 7.69 (d, J = 8.4 Hz, 2H), 7.49 (d, J = 8.1 Hz, 1H), 7.24 (t, J = 8.1 Hz, 1H), 7.18 (d, J = 8.1 Hz, 1H), 6.32 (d, J = 9.7 Hz, 1H), 5.74 (dd, J = 10.0, 2,5 Hz, 1H), 5.68 (d, J = 10.0 Hz, 1H), 5.32–5.25 (m, 1H), 4.29–4.16 (m, 2H), 3.79–3.66 (m, 1H), 2.75–2.68 (m, 1H), 2.55–2.46 (m, 1H), 2.13–2.06 (m, 1H), 1.97–1.88 (m, 1H), 1.89–1.81 (m, 2H), 1.80–1.71 (m, 1H), 1.65 (s, 3H), 1.64–1.57 (m, 1H) ppm; ^{13}C NMR (125 MHz, acetone-d_6): δ 175.7, 167.1, 154.3, 142.9, 142.0, 136.4, 133.1, 131.6, 131.4, 131.3, 131.0, 130.7, 130.5 (2C), 127.3 (2C), 126.1, 122.9, 121.7, 117.9, 117.8, 63.6, 48.6, 45.8, 35.9, 32.4, 31.6, 29.8, 29.5, 23.5 ppm; HRMS (ESI): *m/z* calcd. for $C_{30}H_{30}ClBrNO_6^+$ [M+H]$^+$ 614.0940; found 614.0936.

*4.2.7. Carbamate **8d***

The compound was isolated as a white solid (58 mg, 0,09 mmol, 79%). R_f = 0.25 (CH_2Cl_2/MeOH/AcOH 97:2:1); $[\alpha]_D^{20}$ -71.1° (*c* 0.5, acetone); IR: ν 3163 (OH), 2924 (C=C), 1701 (C=O), 1667 (C=O), 1520 (C=C), 1399 (C=C) cm^{-1}; ^{1}H NMR (500 MHz, acetone-d_6): δ 8.79–8.73 (brs, 1H), 8.03 (d, J = 8.6 Hz, 2H), 7.69 (d, J = 8.6 Hz, 2H), 7.54 (d, J = 8.4 Hz, 2H), 7.45 (d, J = 8.4 Hz, 2H), 6.32 (d, J = 9.7 Hz, 1H), 5.73 (dd, J = 10.0, 2,5 Hz, 1H), 5.68 (d, J = 10.0 Hz, 1H), 5.31–5.26 (m, 1H), 4.29–4.15 (m, 2H), 3.77–3.71 (m, 1H), 2.75–2.67 (m, 1H), 2.55–2.46 (m, 1H), 2.13–2.07 (m, 1H), 1.97–1.89 (m, 1H), 1.88–1.80 (m, 2H), 1.78–1.71 (m, 1H), 1.65 (s, 3H), 1.63–1.57 (m, 1H) ppm; ^{13}C NMR (125 MHz, acetone-d_6): δ 175.6, 167.1, 154.4, 143.0, 139.7, 136.4, 133.1, 132.5 (2C), 131.6, 131.4, 131.0, 130.6, 130.5 (2C), 127.3 (2C), 120.9 (2C), 117.9, 115.2, 63.5, 48.6, 45.8, 36.0, 32.4, 31.6, 29.8, 29.5, 23.5 ppm; HRMS (ESI): *m/z* calcd. for $C_{30}H_{30}ClBrNO_6^+$ [M+H]$^+$ 614.0940; found 614.0938.

*4.2.8. Carbamate **8e***

The compound was isolated as a white solid (63 mg, 0,11 mmol, 91%). R_f = 0.1 (CH_2Cl_2/MeOH/AcOH 97:2:1); $[\alpha]_D^{20}$ -154.0° (*c* 0.5, acetone); IR: ν 3307 (OH), 2922 (C=C), 1710 (C=O), 1599 (C=C), 1531 (C=C), 1407 (C=C) cm^{-1}; ^{1}H NMR (500 MHz, acetone-d_6): δ 9.05–8.98 (brs, 1H), 8.05 (d, J = 8.6 Hz, 2H), 7.96 (d, J = 8.6 Hz, 2H), 7.74–7.69 (m, 4H), 6.34 (d, J = 9.7 Hz, 1H), 5.76 (dd, J = 10.0, 2,5 Hz, 1H), 5.70 (d, J = 10.0 Hz, 1H), 5.33–5.28 (m, 1H), 4.33–4.21 (m, 2H), 3.78–3.71 (m, 1H), 2.77–2.70 (m, 1H), 2.55 (s, 3H), 2.54–2.46 (m, 1H), 2.16–2.08 (m, 1H), 1.98–1.91 (m, 1H), 1.90–1.82 (m, 2H), 1.81–1.77 (m, 1H), 1.67 (s, 3H), 1.66–1.61 (m, 1H) ppm; ^{13}C NMR (125 MHz, acetone-d_6): δ 196.5, 175.6, 167.1, 154.3, 144.6, 142.9, 136.4, 133.1, 132.6, 131.6, 131.1, 130.7, 130.6 (2C), 130.4 (2C), 127.3 (2C), 118.5, 118.3 (2C), 117.9, 63.7, 48.6, 45.8, 35.9, 32.5, 31.7, 29.8, 29.5, 26.4, 23.5 ppm; HRMS (ESI): *m/z* calcd. for $C_{32}H_{32}ClNO_7^+$ [M+H]$^+$ 578.1940; found 578.1946.

*4.2.9. Carbamate **8f***

The compound was isolated as a white solid (58 mg, 0.11 mmol, 90%). R_f = 0.25 (CH_2Cl_2/MeOH/AcOH 97:2:1); $[\alpha]_D^{20}$ -172.7° (*c* 0.5, methanol); IR: ν 3256 (OH), 2922 (C=C), 1697 (C=O), 1606 (C=C), 1543 (C=C) cm^{-1}; ^{1}H NMR (500 MHz, methanol-d_6): δ 8.64–8.58 (brs, 1H), 8.18 (d, J = 4.5 Hz, 1H), 8.02–7.96 (m, 3H), 7.63 (d, J = 8.4 Hz, 2H), 7.36 (dd, J = 9.1, 4.5 Hz, 1H), 6.19 (d, J = 9.6 Hz, 1H), 5.72 (dd, J = 10.1, 2,5 Hz, 1H), 5.66 (d, J = 10.1 Hz, 1H), 5.29–5.23 (m, 1H), 4.31–4.17 (m, 2H), 3.74–3.65 (m, 1H), 2.71–2.62 (m, 1H), 2.57–2.44 (m, 1H), 2.09 (dd, J = 17.9, 8.9 Hz, 1H), 1.98–1.85 (m, 2H), 1.83–1.74 (m, 2H), 1.66 (s, 3H), 1.65–1.59 (m, 1H) ppm; ^{13}C NMR (125 MHz, methanol-d_6): δ 178.1, 169.4, 155.7, 143.9, 143.6, 140.6, 138.0, 136.7, 133.2, 132.4, 132.1, 131.5, 130.8 (2C), 130.7, 127.6, 127.5 (2C), 125.3, 118.3, 64.3, 46.3, 36.2, 32.8, 32.0, 30.3, 30.1, 27.2, 23.5 ppm; HRMS (ESI): *m/z* calcd. for $C_{29}H_{30}ClN_2O_6^+$ [M+H]$^+$ 537.1787; found 537.1794.

*4.2.10. Diester **9***

To a solution of alcohol **4** (300 mg, 0.72 mmol, 1 eq) in a 1:1 mixture of methanol/toluene (6 mL) at 0 °C was added a 2 M solution of trimethylsilyldiazomethane in Et_2O (1.16 mL, 2.32 mmol, 3.2 eq). The reaction was allowed to warm to rt and stirred for 6 h. The reaction mixture was concentrated under reduced pressure. The crude product was then purified by flash chromatography on

silica gel using heptane/EtOAc from 10:0 to 5:5 to obtain a yellow oil (316 mg, 0.71 mmol, 99%). $R_f = 0.45$ (heptane/EtOAc 50:50); $[\alpha]_D^{20}$ -172.0° (*c* 0.05, MeOH); IR: *ν* 3480 (OH), 2924 (C=C), 1721 (C=O), 1606 (C=C), 1434 (C=C) cm^{-1}; ^1H NMR (500 MHz, methanol-d_4): *δ* 8.00 (d, *J* = 8.1 Hz, 2H), 7.64 (d, *J* = 8.1 Hz, 2H), 6.10 (d, *J* = 9.8 Hz, 1H), 5.70 (dd, *J* = 9.8, 2.9 Hz, 1H), 5.58 (d, *J* = 10.0 Hz, 1H), 5.25–5.20 (m, 1H), 3.90 (s, 3H), 3.68–3.65 (m, 1H), 3.63–3.57 (m, 2H), 3.56 (s, 3H), 2.70–2.63 (m, 1H), 2.51–2.45 (m, 1H), 2.06 (dd, *J* = 18.2, 7.0 Hz, 1H), 1.95 (dd, *J* = 18.2, 7.0 Hz, 1H), 1.86–1.81 (m, 1H), 1.84–1.76 (m, 1H), 1.67 (s, 3H), 1.63–1.57 (m, 1H), 1.45–1.39 (m, 1H) ppm; ^{13}C NMR (125 MHz, methanol-d_4): *δ* 176.6, 167.9, 143.8, 137.1, 134.4, 132.3, 131.3, 130.9, 130.7 (2C), 130.2, 127.6 (2C), 118.1, 60.4, 52.7, 52.2, 49.8, 46.6, 39.9, 32.7, 32.1, 30.1, 29.7, 23.5 ppm; HRMS (ESI): *m/z* calcd. for $C_{25}H_{30}ClO_5^+$ $[M+H]^+$ 445.1782; found 445.1792.

4.2.11. Carboxylic acid **10**

A fresh solution of sodium phosphate buffer (40 mL, pH ~ 6.5) consisting of a 1:1 solution of NaH_2PO_4 (20 mL, 0.67 M, 1.608 g) and Na_2HPO_4 (20 mL, 0.67 M, 1.902 g) was prepared. A mixture of the alcohol **9** (200 mg, 0.45 mmol, 1 eq), TEMPO (5 mg, 0.03 mmol, 0.07 eq), and sodium phosphate buffer (1.68 mL, 0.67 M, 2.5 eq) in MeCN (1.6 mL) was heated to 35 °C. Solutions of $NaClO_2$ (162.8 mg, 1.8 mmol, 4 eq) in water (0.26 mL) and bleach (0.6 mL, 2.6% wt) were added simultaneously. The reaction was monitored by TLC. Upon completion, the reaction mixture was quenched by the slow addition of solution of sodium sulphite (285 mg, 2.25 mmol, 5 eq) in H_2O (5 mL) at 0 °C. After addition of HCl 1 M, the product was extracted with MTBE (3 times). The organic phases were combined, washed with H_2O (1 mL), brine (1 mL), dried ($MgSO_4$), and concentrated under reduced pressure to provide the product. The product was then purified by flash chromatography on silica gel using heptane/EtOAc from 8:2 to 5:5 to afford the carboxylic acid **10** as a white solid (191 mg, 0.42 mmol, 93%). $R_f = 0.5$ (heptane/EtOAc 5:5); $[\alpha]_D^{20}$ -27.0° (*c* 0.2, MeOH); IR: *ν* 3202 (OH), 2943 (C=C), 1720 (C=O), 1698 (C=O), 1607 (C=C), 1432 (C=C) cm^{-1}; ^1H NMR (500 MHz, methanol-d_4): *δ* 13.00–9.00 (brs, 1H), 8.00 (d, *J* = 8.7 Hz, 2H), 7.64 (d, *J* = 8.7 Hz, 2H), 6.10 (d, *J* = 10.1 Hz, 1H), 5.69 (dd, *J* = 10.1, 2.8 Hz, 1H), 5.63 (d, *J* = 10.0 Hz, 1H), 5.23 (d, *J* = 4.6 Hz, 1H), 3.91 (s, 3H), 3.71–3.66 (m, 1H), 3.58 (s, 3H), 2.80–2.72 (m, 1H), 2.71–2.64 (m, 1H), 2.27 (dd, *J* = 15.2, 6.9 Hz, 1H), 2.18 (dd, *J* = 15.8, 7.6 Hz, 1H), 2.10 (dd, *J* = 18.8, 6.7 Hz, 1H), 2.00–1.93 (m, 1H), 1.93–1.87 (m, 1H), 1.74–1.70 (m, 1H), 1.67 (s, 3H) ppm; ^{13}C NMR (125 MHz, methanol-d_4): *δ* 176.3, 174.7, 166.1, 143.8, 137.2, 133.2, 132.5, 131.4, 131.3, 130.9, 130.7 (2C), 127.7 (2C), 118.2, 52.8, 52.4, 49.8, 46.6, 41.4, 32.6, 31.9, 30.5, 30.1, 23.5 ppm; HRMS (ESI): *m/z* calcd. for $C_{25}H_{28}ClO_6^+$ $[M+H]^+$ 459.1574; found 459.1558.

4.2.12. General procedure for amides **11a-g** synthesis

To a solution of carboxylic acid **10** (1 eq), amine (1.6 eq) and HATU (1.6 eq) in dry DMF (0.1 M) was added *N*,*N*,diispropylethylamine (3 eq). The reaction mixture was stirred for 24 h at rt, and then washed with a saturated solution of HCl 1 N. The amide was then extracted by MTBE (3 times), dried over $MgSO_4$, and concentrated under reduced pressure. The crude product was purified by flash chromatography on silica gel using heptane/EtOAc from 8:2 to 5:5 to obtain the desired amide **11**.

4.2.13. Amide **11a**

The compound was isolated as a yellow solid (44 mg, 0.08 mmol, 89%). $R_f = 0.32$ (heptane/EtOAc 5:5); $[\alpha]_D^{20}$ -114.6° (*c* 1, MeOH); IR: *ν* 3298 (NH), 2918 (C=C), 1722 (C=O), 1646 (C=O), 1536 (C=C), 1434 (C=C) cm^{-1}; ^1H NMR (500 MHz, methanol-d_4): *δ* 8.00 (d, *J* = 8.3 Hz, 2H), 7.63 (d, *J* = 8.3 Hz, 2H), 7.33 (d, *J* = 8.3 Hz, 2H), 7.27 (d, *J* = 8.3 Hz, 2H), 6.10 (d, *J* = 9.3 Hz, 1H), 5.66 (dd, *J* = 9.6, 1.9 Hz, 1H), 5.63 (dd, *J* = 9.6, 1.9 Hz, 1H), 5.24–5.21 (m, 1H), 4.34 (d, *J* = 3.9 Hz, 2H), 3.91 (s, 3H), 3.69–3.66 (m, 1H), 3.55 (s, 3H), 2.84–2.77 (m, 1H), 2.70–2.65 (m, 1H), 2.23 (dd, *J* = 14.6, 6.7 Hz, 1H), 2.12 (dd, *J* = 14.6, 6.7 Hz, 1H), 2.08 (dd, *J* = 18.8, 9.0 Hz, 1H), 1.94 (dd, *J* = 18.8, 9.0 Hz, 1H), 1.84–1.79 (m, 1H), 1.72–1.69 (m, 1H), 1.67 (s, 3H) ppm; ^{13}C NMR (125 MHz, methanol-d_4): *δ* 176.5, 174.4, 168.0, 143.8, 139.1, 137.2, 135.3, 133.4, 132.5, 131.4, 131.3, 130.9, 130.8 (2C), 130.4 (2C), 129.7 (2C), 127.7 (2C), 118.3, 52.8, 52.4, 49.9, 46.6, 43.5, 43.3, 32.6, 31.8, 31.1, 30.1, 23.6 ppm; HRMS (ESI): *m/z* calcd. for $C_{32}H_{34}Cl_2NO_5^+$ $[M+H]^+$ 582.1814; found 582.1808.

4.2.14. Amide **11b**

The compound was isolated as a white solid (16 mg, 0.03 mmol, 38%). $R_f = 0.7$ (heptane/EtOAc 5:5); $[\alpha]_D^{20}$ -63.0° (*c* 0.2, MeOH); IR: *ν* 3321 (NH), 2923 (C=C), 1721 (C=O), 1614 (C=C), 1436 (C=C) cm^{-1}; ^1H NMR (500 MHz, methanol-d_4): *δ* 8.00 (d, *J* = 8.6 Hz, 2H), 7.64 (d, *J* = 8.6 Hz, 2H), 7.31 (d, *J* = 8.4 Hz, 2H), 7.26 (d, *J* = 8.3 Hz, 2H), 6.11 (d, *J* = 10.0 Hz, 1H), 5.70 (dd, *J* = 10.0, 2.8 Hz, 1H), 5.63 (d, *J* = 9.7 Hz, 1H), 5.24–5.22 (m, 1H), 4.24 (s, 2H), 3.91 (s, 3H), 3.70–3.66 (m, 1H), 3.57 (s, 3H), 3.04 (s, 3H), 2.84–2.77 (m, 1H), 2.70–2.63 (m, 1H), 2.33 (dd, *J* = 13.9, 7.0 Hz, 1H), 2.25 (dd, *J* = 13.9, 7.0 Hz, 1H), 2.11 (dd, *J* = 19.2, 7.7 Hz, 1H), 1.97 (dd, *J* = 19.2, 7.7 Hz, 1H), 1.92–1.87 (m, 1H), 1.72–1.68 (m, 1H), 1.67 (s, 3H) ppm; ^{13}C NMR (125 MHz, methanol-d_4): *δ* 176.5, 174.1, 168.0, 143.9, 140.4, 137.2, 134.1, 133.7, 132.5, 131.5, 131.1, 130.9, 130.8 (2C), 129.9 (2C), 129.6 (2C), 127.8 (2C), 118.3, 52.8, 52.4, 46.6, 44.2, 40.1, 38.1, 35.9, 32.7, 32.2, 30.6, 30.2, 23.6 ppm; HRMS (ESI): *m/z* calcd. for hydrodechlorination product $C_{33}H_{38}ClNO_5^+$ $[M+H]^+$ 564.2517; found 564.2511.

4.2.15. Amide **11c**

The compound was isolated as a white solid (12 mg, 0.02 mmol, 50%). $R_f = 0.7$ (heptane/EtOAc 5:5); $[\alpha]_D^{20}$ -45.5° (*c* 0.02, MeOH); IR: *ν* 3283 (NH), 2921 (C=C), 1724 (C=O), 1642 (C=O), 1537 (C=C), 1436 (C=C) cm^{-1}; ^1H NMR (500 MHz, methanol-d_4): *δ* 8.00 (d, *J* = 8.6 Hz, 2H), 7.64 (d, *J* = 8.6 Hz, 2H), 7.56 (d, *J* = 8.8 Hz, 2H), 7.30 (d, *J* = 8.3 Hz, 2H), 6.10 (d, *J* = 10.0 Hz, 1H), 5.72 (dd, *J* = 9.9, 2.3 Hz, 1H), 5.66 (d, *J* = 10.0 Hz, 1H), 5.25–5.22 (m, 1H), 4.57 (s, 1H), 3.91 (s, 3H), 3.71–3.67 (m, 1H), 3.55 (s, 3H), 2.90–2.87 (m, 1H), 2.71–2.68 (m, 1H), 2.36 (dd, *J* = 13.8, 6.7 Hz, 1H), 2.27 (dd, *J* = 13.8, 6.7 Hz, 1H), 2.10 (dd, *J* = 17.6, 7.1 Hz, 1H), 1.97 (dd, *J* = 17.6, 7.1 Hz, 1H), 1.91–1.86 (m, 1H), 1.80–1.75 (m, 1H), 1.67 (s, 3H) ppm; ^{13}C NMR (125 MHz, methanol-d_4): *δ* 176.5, 174.5, 169.1, 143.8, 137.2, 135.6, 133.2, 132.5, 131.4, 130.8, 130.7 (2C), 129.8 (2C), 127.7 (2C), 127.5, 125.1, 122.7 (2C), 118.2, 52.8, 52.4, 49.9, 46.6, 44.1, 32.6, 31.8, 31.1, 30.1, 23.5 ppm; HRMS (ESI): *m/z* calcd. for $C_{31}H_{32}Cl_2NO_5^+$ $[M+H]^+$ 568.1689; found 568.1699.

4.2.16. Amide **11d**

The compound was isolated as a white solid (3 mg, 0.01 mmol, 15%). $R_f = 0.3$ (heptane/EtOAc 5:5); $[\alpha]_D^{20}$ -39.0° (*c* 0.1, MeOH); IR: *ν* 3307 (NH), 2919 (C=C), 1723 (C=O), 1644 (C=O), 1492 (C=C), 1435 (C=C) cm^{-1}; ^1H NMR (500 MHz, methanol-d_4): *δ* 8.00 (d, *J* = 8.6 Hz, 2H), 7.64 (d, *J* = 8.6 Hz, 2H), 7.29 (d, *J* = 8.4 Hz, 2H), 7.22 (d, *J* = 8.4 Hz, 2H), 6.09 (d, *J* = 10.1 Hz, 1H), 5.60 (d, *J* = 10.1 Hz, 1H), 5.55 (dd, *J* = 10.1, 2.7 Hz, 1H), 5.24–5.21 (m, 1H), 3.90 (s, 3H), 3.69–3.64 (m, 1H), 3.55 (s, 3H), 3.48–3.37 (m, 2H), 2.79 (t, *J* = 7.9 Hz, 2H), 2.73–2.67 (m, 1H), 2.66–2.62 (m, 1H), 2.12 (dd, *J* = 14.3, 6.9 Hz, 1H), 2.06 (dd, *J* = 18.3, 6.9 Hz, 1H), 1.99 (dd, *J* = 14.3, 6.9 Hz, 1H), 1.89 (dd, *J* = 18.3, 6.9 Hz, 1H), 1.67 (s, 3H), 1.60 (dd, *J* = 9.9, 3.5 Hz, 1H), 1.57 (dd, *J* = 9.9, 3.5 Hz, 1H) ppm; ^{13}C NMR (125 MHz, methanol-d_4): *δ* 176.5, 174.5, 168.1, 143.8, 139.4, 137.2, 134.1, 133.3, 132.5, 131.6 (2C), 131.5, 131.2, 130.9, 130.8 (2C), 129.7 (2C), 127.8 (2C), 118.2, 52.8, 52.4, 49.9, 46.5, 43.4, 41.5, 35.9, 32.6, 31.8, 31.1, 30.1, 23.6 ppm; HRMS (ESI): *m/z* calcd. for $C_{33}H_{36}Cl_2NO_5^+$ $[M+H]^+$ 596.1971; found 596.1982.

*4.2.17. Amide **11e***

The compound was isolated as a yellow oil (12 mg, 0.02 mmol, 50%). $R_f = 0.5$ (heptane/EtOAc 5:5); $[\alpha]_D^{20}$ -114.0° (*c* 0.2, MeOH); IR: *ν* 3312 (NH), 2929 (C=C), 1722 (C=O), 1672 (C=O), 1432 (C=C), 1406 (C=C) cm^{-1}; ^1H NMR (500 MHz, methanol-d_4): *δ* 8.50 (s, 1H), 8.44 (d, *J* = 4.0 Hz, 1H), 8.00 (d, *J* = 8.3 Hz, 2H), 7.79 (d, *J* = 8.3 Hz, 1H), 7.63 (d, *J* = 8.3 Hz, 2H), 7.42 (q, 1H), 6.10 (d, *J* = 8.1 Hz, 1H), 5.70 (dd, *J* = 10.0, 3.1 Hz, 1H), 5.64 (s, 1H), 5.63 (d, *J* = 8.1 Hz, 1H), 5.26–5.21 (m, 1H), 4.41 (d, *J* = 4.2 Hz, 2H), 3.90 (s, 3H), 3.70–3.65 (m, 1H), 3.55 (s, 3H), 2.85–2.77 (m, 1H), 2.71–2.64 (m, 1H), 2.24 (dd, *J* = 14.5, 7.1 Hz, 1H), 2.12 (dd, *J* = 14.5, 7.1 Hz, 1H), 2.08 (dd, *J* = 18.5, 8.8 Hz, 1H), 1.93 (dd, *J* = 18.5, 8.8 Hz, 1H), 1.85–1.78 (m, 1H), 1.74–1.69 (m, 1H), 1.67 (s, 3H) ppm; ^{13}C NMR (125 MHz, methanol-d_4): *δ* 176.4, 174.6), 168.0, 149.6, 148.9, 143.8, 137.8, 137.1, 136.9, 133.4, 133.2, 132.5, 131.3, 131.1, 130.7 (2C), 127,7 (2C), 125.4, 118.2, 52.8, 52.4, 49.9, 46.5, 43.2, 41.7, 32.6, 31.9, 31.1, 30.1, 23.5 ppm; HRMS (ESI): *m/z* calcd. for $C_{31}H_{34}ClN_2O_5^+$ $[M+H]^+$ 549.2156; found 549.2161.

*4.2.18. Amide **11f***

The compound was isolated as a yellow oil (23 mg, 0.04 mmol, 99%). $R_f = 0.5$ (heptane/EtOAc 5:5); $[\alpha]_D^{20}$ -94.0° (*c* 0.1, MeOH); IR: *ν* 3319 (NH), 2973 (C=C), 1704 (C=O), 1454 (C=C), 1379 (C=C) cm^{-1}; ^1H NMR (500 MHz, methanol-d_4): *δ* 8.73 (d, *J* = 2.73 Hz, 1H), 8.25 (d, *J* = 4.5 Hz, 1H), 8.11 (d, *J* = 8.3 Hz, 1H), 8.00 (d, *J* = 8.6 Hz, 2H), 7.39 (dd, *J* = 8.3, 4.5 Hz, 2H), 6.10 (d, *J* = 10.1 Hz, 1H), 5.73 (dd, *J* = 10.1, 2.5 Hz, 1H), 5.67 (d, *J* = 10.2 Hz, 1H), 5.26–5.20 (m, 1H), 3.90 (s, 3H), 3.70–3.65 (m, 1H), 3.55 (s, 3H), 2.94–2.88 (s, 1H), 2.74–2.68 (m, 1H), 2.41 (dd, *J* = 14.2, 7.9 Hz, 1H), 2.32 (dd, *J* = 14.2, 7.9 Hz, 1H), 2.11 (dd, *J* = 18.3, 7.4 Hz, 1H), 1.98 (dd, *J* = 18.3, 7.4 Hz, 1H), 1.93–1.88 (m, 1H), 1.83–1.77 (m, 1H), 1.67 (s, 3H) ppm; ^{13}C NMR (125 MHz, methanol-d_4): *δ* 176.5, 173.4, 168.0, 145.3, 143.8, 142.6, 142.0, 137.5, 137.2, 133.2), 132.5, 131.5, 130.8, 130.7 (2C), 129.1, 127,7 (2C), 125.4, 118.2, 52.8, 52.4, 49.9, 46.6, 43.9, 32.6, 31.8, 31.1, 30.1, 23.5 ppm; HRMS (ESI): *m/z* calcd. for $C_{30}H_{32}ClN_2O_5^+$ $[M+H]^+$ 535.2000; found 535.2015.

*4.2.19. Amide **11g***

The compound was isolated as a colorless oil (11 mg, 0.02 mmol, 99%). $R_f = 0.6$ (heptane/EtOAc 5:5); $[\alpha]_D^{20}$ -95.4° (*c* 0.5, MeOH); IR: *ν* 3372 (NH), 2919 (C=C), 1709 (C=O), 1678 (C=O), 1596 (C=C), 1515 (C=C), 1437 (C=C) cm^{-1}; ^1H NMR (500 MHz, methanol-d_4): *δ* 8.00 (d, *J* = 8.3 Hz, 2H), 7.64 (d, *J* = 8.3 Hz, 2H), 7.43 (d, *J* = 8.8 Hz, 2H), 6.93 (d, *J* = 8.8 Hz, 2H), 6.10 (d, *J* = 9.8 Hz, 1H), 5.72 (dd, *J* = 10.1, 2.5 Hz, 1H), 5.66 (d, *J* = 10.4 Hz, 1H), 5.25–5.22 (m, 1H), 3.90 (s, 3H), 3.82 (t, *J* = 4.8 Hz, 4H), 3.72–3.66 (m, 1H), 3.55 (s, 3H), 3.10 (t, *J* = 4.8 Hz, 4H), 2.92–2.83 (m, 1H), 2.74–2.67 (m, 1H), 2.33 (dd, *J* = 13.7, 7.2 Hz, 1H), 2.24 (dd, *J* = 13.7, 7.2 Hz, 1H), 2.11 (dd, *J* = 18.5, 7.2 Hz, 1H), 1.98 (dd, *J* = 18.5, 7.2 Hz, 1H), 1.92–1.86 (m, 1H), 1.81–1.75 (m, 1H), 1.67 (s, 3H) ppm; ^{13}C NMR (125 MHz, methanol-d_4): *δ* 176.5, 172.7, 168.0, 149.9, 143.9, 137.3, 133.4, 132.7, 132.5, 131.5, 131.4, 130.9, 130.8 (2C), 127.8 (2C), 122.8 (2C), 118.2, 117.5 (2C), 68.1 (2C), 52.8, 52.4, 51.2 (2C), 49.9, 46.6, 44.1, 32.6, 31.8, 31.3, 30.1, 23.6 ppm; HRMS (ESI): *m/z* calcd. for $C_{35}H_{40}ClN_2O_6^+$ $[M+H]^+$ 619.2575; found 619.2592.

*4.2.20. General procedure for monoacid **12a, 12c** and **12g** synthesis*

To a solution of the amide **11a-g** (1 eq) in MeOH/THF/water 1:1:1 (0.1 M) was added $LiOH \cdot H_2O$ (10 eq). The mixture was stirred 6 h at rt and water was added. The aqueous phase was acidified with a 2 M solution of HCl. The product was then extracted with MTBE (3 times) and the combined organic phases dried over $MgSO_4$ and concentrated under reduced pressure. The product was then purified by flash chromatography on silica gel using heptane/EtOAc/AcOH from 99:0:1 to 50:49:1.

*4.2.21. Monoacid **12a***

The compound was isolated as a colorless oil (5 mg, 0.01 mmol, 50%). $R_f = 0.5$ (heptane/EtOAc/AcOH 80:19:1); $[\alpha]_D^{20}$ -14.0° (*c* 0.1, MeOH); IR: *ν* 3372 (OH), 2917 (C=C), 1716 (C=O), 1648 (C=O), 1434 (C=C) cm^{-1}; ^1H NMR (500 MHz, methanol-d_4): *δ* 8.49 (t, *J* = 6.2 Hz, 1H), 8.00 (d, *J* = 8.5 Hz, 2H), 7.62 (d, *J* = 8.5 Hz, 2H), 7.33 (d, *J* = 8.3 Hz, 2H), 7.28 (d, *J* = 8.5 Hz, 2H), 6.09 (d, *J* = 10.2 Hz, 1H), 5.66 (dd, *J* = 9.6, 1.9 Hz, 1H), 5.63 (dd, *J* = 9.6, 1.9 Hz, 1H), 5.24–5.21 (m, 1H), 4.34 (t, 2H), 3.71–3.65 (m, 1H), 3.55 (s, 3H), 2.88–2.78 (m, 1H), 2.72–2.65 (m, 1H), 2.30–2.20 (m, 1H), 2.15–2.10 (m, 1H), 2.10–2.04 (m, 1H), 1.99–1.90 (m, 1H), 1.86–1.79 (m, 1H), 1.74–1.69 (m, 1H), 1.67 (s, 3H) ppm; ^{13}C NMR (125 MHz, methanol-d_4): *δ* 176.5, 174.5, 169.4, 143.6, 139.1, 137.2, 134.1, 133.3, 132.7, 132.3, 131.4, 131.0 (2C), 130.6, 130.4 (2C), 129.7 (2C), 127.7 (2C), 118.3, 52.4, 49.9, 46.6, 43.5, 43.3, 32.7, 31.9, 31.2, 30.1, 23.6 ppm; HRMS (ESI): *m/z* calcd. for $C_{31}H_{32}Cl_2NO_5^+$ $[M+H]^+$ 568.1658; found 568.1667.

*4.2.22. Monoacid **12c***

The compound was isolated as a colorless oil (2 mg, 0.002 mmol, 22%). $R_f = 0.5$ (heptane/EtOAc/AcOH 50:49:1); $[\alpha]_D^{20}$ -74.0° (*c* 0.1, MeOH); IR: *ν* 3401 (OH), 2922 (C=C), 1723 C=O), 1679 (C=O), 1606 (C=C), 1539 (C=C), 1403 (C=C) cm^{-1}; ^1H NMR (500 MHz, methanol-d_4): *δ* 7.94 (d, *J* = 8.5 Hz, 2H), 7.56 (d, *J* = 8.0 Hz, 2H), 7.54 (d, *J* = 9 Hz, 2H), 7.30 (d, *J* = 8.8 Hz, 2H), 6.03 (d, *J* = 10.0 Hz, 1H), 5.72 (dd, *J* = 10.0, 2.7 Hz, 1H), 5.67 (d, *J* = 10.3 Hz, 1H), 5.25–5.22 (m, 1H), 3.70–3.66 (m, 1H), 3.55 (s, 3H), 2.92–2.85 (m, 1H), 2.72–2.68 (m, 1H), 2.36 (dd, *J* = 13.8, 6.6 Hz, 1H), 2.27 (dd, *J* = 13.8, 6.6 Hz, 1H), 2.36 (dd, *J* = 16.6, 7.2 Hz, 1H), 2.11 (dd, *J* = 16.6, 7.2 Hz, 1H), 1.91–1.86 (m, 1H), 1.80–1.75 (m, 1H), 1.67 (s, 3H) ppm; ^{13}C NMR (125 MHz, methanol-d_4): *δ* 176.5, 173.0, 171.3, 143.0, 136.9, 136.0, 134.3, 133.2, 132.7, 131.6, 130.6 (2C), 130.1, 129.9 (2C), 129.6, 127.3 (2C), 122.7 (2C), 118.5, 52.4, 49.6, 46.6, 44.2, 32.6, 31.9, 31.2, 30.1, 23.6 ppm; HRMS (ESI): *m/z* calcd. for $C_{30}H_{30}Cl_2NO_5^+$ $[M+H]^+$ 554.1501; found 554.1514.

*4.2.23. Monoacid **12g***

The compound was isolated as a colorless oil (5 mg, 0.01 mmol, 99%). $R_f = 0.3$ (heptane/EtOAc/AcOH 50:49:1); $[\alpha]_D^{20}$ -100.0° (*c* 0.01, MeOH); IR: *ν* 3358 (OH), 2977 (C=C), 1652 (C=O), 1406 (C=C), 1384 (C=C) cm^{-1}; ^1H NMR (500 MHz, methanol-d_4): *δ* 7.99 (d, *J* = 8.5 Hz, 2H), 7.61 (d, *J* = 8.5 Hz, 2H), 7.43 (d, *J* = 9.0 Hz, 2H), 6.93 (d, *J* = 9.0 Hz, 2H), 6.08 (d, *J* = 10.1 Hz, 1H), 5.73 (dd, *J* = 10.1, 2.6 Hz, 1H), 5.67 (d, *J* = 10.4 Hz, 1H), 5.26–5.22 (m, 1H), 3.82 (t, *J* = 4.8 Hz, 4H), 3.72–3.66 (m, 1H), 3.55 (s, 3H), 3.10 (t, *J* = 4.8 Hz, 4H), 2.92–2.83 (m, 1H), 2.74–2.67 (m, 1H), 2.33 (dd, *J* = 13.7, 7.2 Hz, 1H), 2.26 (dd, *J* = 13.7, 7.2 Hz, 1H), 2.11 (dd, *J* = 18.5, 7.2 Hz, 1H), 1.98 (dd, *J* = 18.5, 7.2 Hz, 1H), 1.92–1.86 (m, 1H), 1.81–1.75 (m, 1H), 1.67 (s, 3H) ppm; ^{13}C NMR (125 MHz, methanol-d_4): *δ* 176.5, 173.0, 169.2, 148.6, 143.7, 137.2, 133.3, 132.7, 132.2, 131.5, 131.4, 131.0 (2C), 130.7, 127.7 (2C), 122.6 (2C), 120.5, 118.3 (2C), 66.8 (2C), 54.2 (2C), 52.4, 49.9, 46.6, 44.1, 32.6, 31.8, 31.2, 30.1, 23.6 ppm; HRMS (ESI): *m/z* calcd. for $C_{34}H_{38}ClN_2O_6^+$ $[M+H]^+$ 605.2413; found 605.2407.

*4.2.24. Diester **13***

To a solution of the diacid **4** (80 mg, 0.19 mmol, 1 eq) in DMF was added potassium carbonate (53 mg, 0.38 mmol, 2 eq). The suspension was stirred during 2 min after which bromomethyl acetate (37 μL, 0.38 mmol, 2 eq) was added. After 18 h at rt, dichloromethane was added to the mixture and the resulting organic phase was successively washed with water (3 times) and brine (3 times). The organic phase was concentrated under reduced pressure and the residue was submitted to flash chromatography using heptane/EtOAc from 10:0 to 5:5 to yield the corresponding diester **13** as a yellow oil (89 mg, 0.19 mmol, **99%**). $R_f = 0.3$ (heptane/EtOAc 4:6); $[\alpha]_D^{20}$ -117.5° (*c* 1, MeOH); IR: *ν* 3348 (OH), 2973 (C=C), 2926 (C=C),

1742 (C=O), 1605 (C=C), 1408 (C=C), 1372 (C=C) cm^{-1}; ^1H NMR (500 MHz, methanol-d_4): δ 8.03 (d, $J = 8.5$ Hz, 2H), 7.69 (d, $J = 8.5$ Hz, 2H), 6.18 (d, $J = 9.8$ Hz, 1H), 5.97 (s, 2H), 5.74 (dd, $J = 9.9$, 3.1 Hz, 1H), 5.65 (ABq, $J = 5.8$ Hz, $\Delta\delta = 19.0$ Hz, 2H), 5.57 (d, $J = 10.2$ Hz, 1H), 5.25–5.22 (m, 1H), 3.70–3.65 (m, 1H), 3.63–3.58 (m, 2H), 2.72–2.66 (m, 1H), 2.53–2.46 (m, 1H), 2.11 (s, 3H), 2.08 (dd, $J = 17.9$, 6.6 Hz, 1H), 1.95 (dd, $J = 17.9$, 6.6 Hz, 1H), 1.88–1.83 (m, 1H), 1.80 (s, 3H), 1.74–1.69 (m, 1H), 1.67 (s, 3H), 1.63–1.58 (m, 1H), 1.53–1.47 (m, 1H) ppm; ^{13}C NMR (125 MHz, methanol-d_4): δ 174.7, 171.3, 171.0, 165.9, 144.3, 137.5, 135.2, 132.6, 131.1 (2C), 130.7, 130.5, 129.6, 127.9 (2C), 117.8, 81.1, 80.3, 60.5, 49.8, 46.2, 39.9, 32.7, 31.9, 30.1, 29.8, 29.2, 23.5, 20.6 ppm; HRMS (ESI): *m/z* calcd. for $C_{29}H_{33}ClNaO_9^+$ $[M+Na]^+$ 583.1711; found 583.1736.

4.2.25. Carboxylic acid **14**

The compound was isolated as a colorless oil (41 mg, 0.07 mmol, 70%) using the procedure described for compound **10**. $R_f = 0.5$ (heptane/EtOAc/AcOH 40:59:1); $[\alpha]_D^{20}$ -91.6° (*c* 1, MeOH); IR: ν 3307 (OH), 2919 (C=C), 1735 (C=O), 1606 (C=C), 1408 (C=C), 1369 (C=C) cm^{-1}; ^1H NMR (500 MHz, methanol-d_4): δ 8.02 (d, $J = 8.7$ Hz, 2H), 7.68 (d, $J = 8.7$ Hz, 2H), 6.18 (d, $J = 9.7$ Hz, 1H), 5.97 (s, 2H), 5.73 (dd, $J = 10.1$, 2.8 Hz, 1H), 5.67 (ABq, $J = 5.8$ Hz, $\Delta\delta = 19.0$ Hz, 2H), 5.62 (d, $J = 10.3$ Hz, 1H), 5.25–5.22 (m, 1H), 3.70–3.65 (m, 1H), 2.80–2.74 (m, 1H), 2.73–2.64 (m, 1H), 2.29 (dd, $J = 16.2$, 6.9 Hz, 1H), 2.20 (dd, $J = 16.2$, 6.9 Hz, 1H), 2.11 (s, 3H), 2.10–2.07 (m, 1H), 1.98–1.94 (m, 1H), 1.92–1.88 (m, 1H), 1.80 (s, 3H), 1.77–1.70 (m, 1H), 1.67 (s, 3H) ppm; ^{13}C NMR (125 MHz, methanol-d_4): δ 176.6, 174.5, 171.3, 171.0, 165.9, 144.2, 137.2, 134.0, 132.7, 131.2 (2C), 130.6, 130.5, 130.4, 127.9 (2C), 117.9, 81.1, 80.4, 49.4, 46.1, 41.5, 32.6, 31.7, 30.9, 30.5, 30.5, 23.6, 20.7 ppm; HRMS (ESI): *m/z* calcd. for $C_{29}H_{31}ClNaO_9^+$ $[M+Na]^+$ 597.1503; found 597.1512.

4.2.26. Amide **15**

Following the procedure described for compounds **11a-g**, the amide **15** was isolated as a colorless oil (7 mg, 0.01 mmol, 50%). $R_f = 0.4$ (heptane/EtOAc 4:6); $[\alpha]_D^{20}$ -102.3° (*c* 0.4, MeOH); IR: ν 3293 (NH), 2925 (C=C), 1738 (C=O), 1646 (C=O), 1606 (C=C), 1534 (C=C), 1408 (C=C) cm^{-1}; ^1H NMR (500 MHz, methanol-d_4): δ 8.04 (d, $J = 8.6$ Hz, 2H), 7.70 (d, $J = 8.6$ Hz, 2H), 7.34 (d, $J = 8.6$ Hz, 2H), 7.28 (d, $J = 8.6$ Hz, 2H), 6.19 (d, $J = 9.5$ Hz, 1H), 5.97 (s, 2H), 5.72–5,67 (m, 2H), 5.64–5.62 (m, 1H), 5.61 (d, $J = 8.2$ Hz, 1H), 5.26–5.23 (m, 1H), 4.35 (ABq, $J = 15.1$ Hz, $\Delta\delta = 19.0$ Hz, 2H), 3.72–3.67 (m, 1H), 2.86–2.79 (m, 1H), 2.73–2.68 (m, 1H), 2.29–2.23 (m, 1H), 2.16–2.11 (m, 1H), 2.10–2.07 (m, 1H), 2.11 (s, 3H), 1.96–1.93 (m, 1H), 1.87–1.82 (m, 1H), 1.78 (s, 3H), 1.75–1.70 (m, 1H), 1.67 (s, 3H) ppm; ^{13}C NMR (125 MHz, methanol-d_4): δ 174.5, 174.4, 171.3, 169.8, 167.3, 144.3, 139.1, 137.2, 134.0, 132.7, 131.2 (2C), 130.6, 130.5, 130.4 (2C), 129.7 (2C), 128.1, 127.9 (2C), 127.8, 117.8, 81.1, 80.4, 49.9, 46.1, 43.6, 43.2, 32.7, 31.6, 31.2, 30.0, 23.7, 23.6, 20.7 ppm; HRMS (ESI): *m/z* calcd. for $C_{36}H_{38}Cl_2NO_9^+$ $[M+H]^+$ 698.1924; found 698.1944.

4.2.27. Diacid **16**

To a solution of amide **15** (50 mg, 0.09 mmol, 1 eq) in MeOH was added K_2CO_3 (36 mg, 0.26 mmol, 3 eq) was added. After 6 h at rt, HCl 1 N was added and the product was extracted by MTBE (3 times), dried over $MgSO_4$ and concentrated under reduced pressure to afford a white solid (47 mg, 0.09 mmol, **99%**). $R_f = 0.4$ (heptane/EtOAc/AcOH 30:69:1); $[\alpha]_D^{20}$ -80.8° (*c* 0.5, MeOH); IR: ν 3287 (OH), 2922 (C=C), 1694 (C=O), 1607 (C=C), 1539 (C=C), 1408 (C=C) cm^{-1}; ^1H NMR (500 MHz, methanol-d_4): δ 7.99 (d, $J = 8.5$ Hz, 2H), 7.64 (d, $J = 8.5$ Hz, 2H), 7.33 (d, $J = 8.4$ Hz, 2H), 7.28 (d, $J = 8.5$ Hz, 2H), 6.20 (d, $J = 9.7$ Hz, 1H), 5.69–5,61 (m, 2H), 5.27–5.23 (m, 1H), 4.35 (ABq, $J = 15.9$ Hz, $\Delta\delta = 20.3$ Hz, 2H), 3.72–3.65 (m, 1H), 2.86–2.77 (m, 1H), 2.68–2.61 (m, 1H), 2.30–2.22 (m, 1H), 2.18–2.12 (m, 1H), 2.13–2.06 (m, 1H), 1.96–1.88 (m, 1H), 1.86–1.79 (m, 1H), 1.76–1.70 (m, 1H), 1.67 (s, 3H) ppm; ^{13}C NMR (125 MHz, methanol-d_4): δ 178.1, 174.6, 169.7, 143.6, 139.0, 136.7, 134.0, 132.7, 132.5, 132.1, 130.9 (2C), 130.8, 130.6, 130.4 (2C), 129.7 (2C), 127.6 (2C), 118.4, 49.9, 46.4, 43.5, 43.4, 32.9, 32.0, 31.3, 30.1, 23.6 ppm; HRMS (ESI): *m/z* calcd. for $C_{30}H_{28}Cl_2NO_5^-$ $[M-H]^-$ 552.1345; found 552.1366.

4.2.28. Azide **17**

A solution of the alcohol **13** (20 mg, 0.036 mmol, 1 eq), triphenylphosphine (19 mg, 0.072 mmol, 2 eq), diisopropylazidocarboxylate (14 μL, 0.072 mmol, 2 eq), and diphenylphosphoryl azide (DPPA) (16 μL, 0.072 mmol, 2 eq) in THF was stirred at rt for 48 h. The solvent was removed under reduced pressure and the residue was purified by flash chromatography on silica gel using heptane/EtOAc from 10:0 to 4:6 to afford the corresponding azide **17** as a transparent oil (17 mg, 0.032 mmol, 89%). $R_f = 0.3$ (heptane/EtOAc 6:4); $[\alpha]_D^{20}$ -93.5° (*c* 0.2, MeOH); IR: ν 3335 (OH), 2973 (C=C), 2099 (N_3), 1744 (C=O), 1454 (C=C) cm^{-1}; ^1H NMR (500 MHz, methanol-d_4): δ 8.03 (d, $J = 8.6$ Hz, 2H), 7.68 (d, $J = 8.6$ Hz, 2H), 6.17 (d, $J = 9.7$ Hz, 1H), 5.97 (s, 2H), 5.72 (dd, $J = 9.9$, 2.9 Hz, 1H), 5.65 (ABq, $J = 5.7$ Hz, $\Delta\delta = 8.5$ Hz, 2H), 5.61 (d, $J = 10.1$ Hz, 1H), 5.27–5.23 (m, 1H), 3.71–3.63 (m, 1H), 3.37–3.32 (m, 2H), 2.74–2.63 (m, 1H), 2.51–2.43 (m, 1H), 2.11 (s, 3H), 2.08 (dd, $J = 17.9$, 6.6 Hz, 1H), 1.95 (dd, $J = 17.9$, 6.6 Hz, 1H), 1.88–1.83 (m, 1H), 1.80 (s, 3H), 1.74–1.69 (m, 1H), 1.67 (s, 3H), 1.66–1.61 (m, 1H), 1.55–1.48 (m, 1H) ppm; ^{13}C NMR (500 MHz, methanol-d_4): δ 174.6, 171.3, 171.0, 165.9, 144.3, 137.3, 134.4, 132.7, 131.2 (2C), 130.6, 130.5, 130.3, 127.9 (2C), 117.8, 81.1, 80.4, 70.8, 50.0, 46.2, 35.9, 32.7, 31.5, 30.7, 30.1, 23.6, 22.1, 20.6 ppm; HRMS (ESI): *m/z* calcd. for $C_{29}H_{32}ClNaN_3O_8^+$ $[M+Na]^+$ 608.1776; found 608.1793.

4.2.29. General procedure for triazoles **18a-c** synthesis

Copper(II) sulfate (0.01 eq) was added to a solution of the azide **17** (1 eq), and the alkyne (4.5 eq) in a mixture of *t*-butanol/water 2:1 (0.1 M), and a fivefold excess of benzoic acid (0.05 eq). The reaction mixture was stirred at 60 °C for 24 h. Water was then added to the mixture and the compound was extracted with MTBE (3 times), dried over MgSO4 and concentrated under reduced pressure. The desired triazole **18** was isolated after purification by flash chromatography on silica gel heptane/EtOAc from 10:0 to 6:4.

4.2.30. Triazole **18a**

The compound was isolated as a colorless oil (7 mg, 0.01 mmol, 50%). $R_f = 0.4$ (heptane/EtOAc 6:4); $[\alpha]_D^{20}$ -40.0° (*c* 0.1, MeOH); IR: ν 2923 (C=C), 1737 (C=O), 1606 (C=C), 1368 (C=C) cm^{-1}; ^1H NMR (500 MHz, methanol-d_4): δ 8.35 (s, 1H), 8.04 (d, $J = 8.4$ Hz, 2H), 7.82 (d, $J = 7.2$ Hz, 2H), 7.69 (d, $J = 7.2$ Hz, 2H), 7.44 (t, $J = 7.4$ Hz, 2H), 7.35 (t, $J = 7.5$ Hz, 1H), 6.19 (d, $J = 10.1$ Hz, 1H), 5.97 (s, 2H), 5.77 (dd, $J = 10.1$, 3.0 Hz, 1H), 5.68 (s, 2H), 5.65 (d, $J = 9.9$ Hz, 1H), 5.27–5.23 (m, 1H), 4.50 (t, $J = 7.3$ Hz, 2H), 3.73–3.67 (m, 1H), 2.77–2.70 (m, 1H), 2.44–2.37 (m, 1H), 2.11 (s, 3H), 2.08–2.06 (m, 1H), 2.05–2.02 (m, 1H), 1.97–1.94 (m, 1H), 1.93–1.92 (m, 1H), 1.91–1.88 (m, 1H), 1.85–1.81 (m, 1H), 1.79 (s, 3H), 1.65 (s, 3H) ppm; ^{13}C NMR (125 MHz, methanol-d_4): δ 174.5, 171.3, 171.0, 165.9, 149.1, 144.2, 137.3, 133.9, 132.7, 131.8, 131.1 (2C), 130.8, 130.5, 130.1 (2C), 129.5), 127.9 (2C), 127.2, 126.8 (2C), 122.3, 117.8, 82.7, 81.1, 80.5, 49.2, 46.2, 37.5, 32.7, 31.4, 30.1, 29.3, 29.2, 23.9, 20.6 ppm; HRMS (ESI): *m/z* calcd. for $C_{37}H_{39}ClN_3O_8^+$ $[M+H]^+$ 688.2354; found 688.2375.

4.2.31. Triazole **18b**

The compound was isolated as a light yellow oil (5 mg, 0.01 mmol, 38%). $R_f = 0.5$ (heptane/EtOAc 5:5); $[\alpha]_D^{20}$ -38.9° (*c* 0.8, MeOH); IR: ν 2924 (C=C), 1736 (C=O), 1454 (C=C), 1380 (C=C) cm^{-1}; ^1H NMR (500 MHz, methanol-d_4): δ 8.67 (s, 1H), 8.24 (d, $J = 8.4$ Hz, 2H), 8.04 (d, $J = 8.4$ Hz, 2H), 7.69 (d, $J = 8.4$ Hz, 2H), 7.67 (t, $J = 3.9$ Hz, 1H), 7.56 (t, $J = 4.2$ Hz, 2H), 6.19 (d, $J = 9.7$ Hz, 1H), 5.97

(s, 2H), 5.75 (dd, $J = 9.8$, 3.0 Hz, 1H), 5.68 (s, 2H), 5.65 (d, $J = 10.5$ Hz, 1H), 5.27–5.23 (m, 1H), 4.56 (t, $J = 7.3$ Hz, 2H), 3.73–3.67 (m, 1H), 3.30 (s, 2H), 2.77–2.70 (m, 1H), 2.47–2.38 (m, 1H), 2.11 (s, 3H), 2.08–2.06 (m, 1H), 2.05–2.02 (m, 1H), 1.97–1.94 (m, 1H), 1.93–1.92 (m, 1H), 1.91–1.88 (m, 1H), 1.85–1.81 (m, 1H), 1.79 (s, 3H), 1.65 (s, 3H) ppm; ^{13}C NMR (125 MHz, methanol-d_4): δ 174.5, 171.3, 171.1, 165.9, 148.3, 144.3, 138.4, 137.3, 134.6, 133.8, 132.8, 131.4 (2C), 130.8, 130.5, 131.2 (2C), 130.6, 130.3, 129.7 (2C), 127.9 (2C), 117.8, 81.1, 80.5, 71.3, 66.6, 49.2, 46.2, 37.3, 32.6, 31.3, 30.9, 30.7, 30.1, 23.6, 20.6 ppm; HRMS (ESI): *m/z* calcd. for benzylic oxidation product $C_{38}H_{39}ClN_3O_9^+$ $[M+H]^+$ 716.2369; found 716.2358.

4.2.32. Triazole ***18c***

The compound was isolated as a light yellow oil (4 mg, 0.01 mmol, 30%). $R_f = 0.5$ (heptane/EtOAc/Et_3N 20:79:1); $[\alpha]_D^{20}$ -181.7° (*c* 0.3, MeOH); IR: ν 2931 (C=C), 1729 (C=O), 1606 (C=C), 1455 (C=C) cm^{-1}; ^{1}H NMR (500 MHz, methanol-d_4): δ 8.58 (s, 1H), 8.46 (s, 1H), 8.08 (d, $J = 7.9$ Hz, 1H), 8.04 (d, $J = 8.4$ Hz, 2H), 7.92 (t, $J = 8.0$ Hz, 1H), 7.69 (d, $J = 8.4$ Hz, 2H), 7.38 (t, $J = 6.6$ Hz, 1H), 6.19 (d, $J = 9.7$ Hz, 1H), 5.97 (s, 2H), 5.76 (dd, $J = 10.1$, 2.8 Hz, 1H), 5.68 (s, 2H), 5.65 (d, $J = 10.6$ Hz, 1H), 5.27–5.23 (m, 1H), 4.54 (t, $J = 7.4$ Hz, 2H), 3.73–3.67 (m, 1H), 2.77–2.70 (m, 1H), 2.44–2.37 (m, 1H), 2.11 (s, 3H), 2.08–2.06 (m, 1H), 2.05–2.02 (m, 1H), 1.97–1.94 (m, 1H), 1.93–1.92 (m, 1H), 1.91–1.88 (m, 1H), 1.85–1.81 (m, 1H), 1.79 (s, 3H), 1.65 (s, 3H) ppm; ^{13}C NMR (125 MHz, methanol-d_4): δ 174.5, 171.1, 169.7, 165.9, 151.2, 150.6, 148.9, 144.2, 139.1, 137.3, 133.9, 132.7, 131.2 (2C), 130.8, 130.5, 127.9 (2C), 127.4, 124.7, 124.3, 121.7, 117.8, 81.1, 80.5, 71.7, 49.2, 46.2, 37.5, 32.7, 31.4, 30.9, 30.7, 30.1, 23.5, 20.6 ppm; HRMS (ESI): *m/z* calcd. for $C_{36}H_{38}ClN_4O_8^+$ $[M+H]^+$ 689.2378; found 689.2396.

4.2.33. Triazole ***19a***

Following the procedure described for compound **16**, the triazole **19a** was isolated as a white solid (2 mg, 0.003 mmol, 99%). $R_f = 0.3$ (heptane/EtOAc/AcOH 40:59:1); $[\alpha]_D^{20}$ -77.3° (*c* 0.3, MeOH); IR: ν 3365 (OH), 2926 (C=C), 1704 (C=O), 1612 (C=C), 1407 (C=C) cm^{-1}; ^{1}H NMR (500 MHz, methanol-d_4): δ 8.36 (s, 1H), 7.99 (d, $J = 8.4$ Hz, 2H), 7.82 (d, $J = 7.3$ Hz, 2H), 7.65 (d, $J = 8.4$ Hz, 2H), 7.44 (t, $J = 7.4$ Hz, 2H), 7.35 (t, $J = 7.5$ Hz, 1H), 6.20 (d, $J = 9.8$ Hz, 1H), 5.71 (dd, $J = 18.4$, 8.7 Hz, 2H), 5.28–5.22 (m, 1H), 4.52 (t, $J = 7.3$ Hz, 2H), 3.73–3.67 (m, 1H), 2.72–2.63 (m, 1H), 2.43–2.36 (m, 1H), 2.08–2.06 (m, 1H), 2.05–2.02 (m, 1H), 1.97–1.94 (m, 1H), 1.93–1.92 (m, 1H), 1.91–1.88 (m, 1H), 1.85–1.81 (m, 1H), 1.65 (s, 3H) ppm; ^{13}C NMR (125 MHz, methanol-d_4): δ 177.4, 169.3, 148.4, 144.2, 137.5, 134.2, 132.4, 131.8, 131.1 (2C), 130.8, 130.5, 130.1 (2C), 129.5, 127.9 (2C), 127.5, 126.8 (2C), 122.3, 118.5, 82.9, 49.2, 46.5, 37.7, 32.8, 30.9, 30.4, 29.5, 23.6 ppm; HRMS (ESI): *m/z* calcd. for $C_{31}H_{29}ClN_3O_4^-$ $[M-H]^-$ 542.1847; found 542.1831.

4.2.34. Triazole ***19b***

Following the procedure described for compound **16**, the triazole **19b** was isolated as a white solid (2 mg, 0.003 mmol, 99%). $R_f = 0.5$ (heptane/EtOAc/AcOH 30:69:1); $[\alpha]_D^{20}$ -12.7° (*c* 0.6, MeOH); IR: ν 3355 (OH), 2924 (C=C), 1694 (C=O), 1606 (C=C), 1447 (C=C) cm^{-1}; ^{1}H NMR (500 MHz, methanol-d_4): δ 8.67 (s, 1H), 8.24 (d, $J = 8.4$ Hz, 2H), 8.04 (d, $J = 8.4$ Hz, 2H), 7.99 (d, $J = 8.6$ Hz, 2H), 7.67 (t, $J = 5.5$ Hz, 1H), 7.64 (d, $J = 8.6$ Hz, 2H), 6.20 (d, $J = 10.0$ Hz, 1H), 5.71 (dd, $J = 16.0$, 10.2 Hz, 2H), 5.28–5.22 (m, 1H), 4.52 (t, $J = 7.3$ Hz, 2H), 3.73–3.67 (m, 1H), 3.21 (s, 2H), 2.71–2.65 (m, 1H), 2.43–2.36 (m, 1H), 2.08–2.06 (m, 1H), 2.05–2.02 (m, 1H), 1.95–1.93 (m, 1H), 1.93–1.90 (m, 1H), 1.89–1.85 (m, 1H), 1.86–1.80 (m, 1H), 1.66 (s, 3H) ppm; ^{13}C NMR (125 MHz, methanol-d_4): δ 178.0, 169.3, 148.3, 143.9, 138.4, 137.0, 134.5, 132.6, 132.3, 132.0, 131.3 (2C), 130.9 (2C), 130.8, 130.6, 130.1, 129.7 (2C), 127.7 (2C), 118.4, 54.3, 52.8, 49.2, 46.4, 37.6, 32.9, 31.7, 30.9, 30.2, 23.6 ppm; HRMS (ESI): *m/z* calcd. for benzylic oxidation product $C_{32}H_{29}ClN_3O_5^-$ $[M-H]^-$ 570.1801; found 570.1823.

4.2.35. Triazole ***19c***

Following the procedure described for compound **16**, the triazole **19c** was isolated as a white solid (2 mg, 0.003 mmol, 99%). $R_f = 0.5$ (EtOAc/AcOH 99:1); $[\alpha]_D^{20}$ -50.0° (*c* 0.3, MeOH); IR: ν 3326 (OH), 2936 (C=C), 1689 (C=O), 1614 (C=C), 1407 (C=C) cm^{-1}; ^{1}H NMR (500 MHz, methanol-d_4): δ 8.97 (s, 1H), 8.80 (d, $J = 6.5$ Hz, 1H), 8.67 (t, $J = 7.9$ Hz, 1H), 8.46 (d, $J = 7.2$ Hz, 1H), 8.02 (d, $J = 8.5$ Hz, 2H), 7.99 (d, $J = 7.2$ Hz, 1H), 7.67 (d, $J = 8.4$ Hz, 2H), 6.22 (d, $J = 9.9$ Hz, 1H), 5.71 (dd, $J = 14.2$, 11.2 Hz, 2H), 5.28–5.22 (m, 1H), 4.66 (t, $J = 6.9$ Hz, 2H), 3.75–3.70 (m, 1H), 2.74–2.68 (m, 1H), 2.47–2.41 (m, 1H), 2.15–2.12 (m, 1H), 2.11–2.09 (m, 1H), 1.99–1.96 (m, 1H), 1.95–1.93 (m, 1H), 1.91–1.88 (m, 1H), 1.87–1.84 (m, 1H), 1.68 (s, 3H) ppm; ^{13}C NMR (125 MHz, methanol-d_4): δ 177.3, 169.3, 151.2, 149.2, 146.2, 144.2, 139.1, 136.9, 134.0, 132.4, 130.9 (2C), 130.8, 130.4, 127.7 (2C), 127.1, 124.9, 124.1, 121.7, 118.4, 68.3, 49.7, 46.4, 37.5, 32.9, 31.8, 30.9, 30.2, 23.6 ppm; HRMS (ESI): *m/z* calcd. for $C_{30}H_{30}ClN_4O_4^+$ $[M+H]^+$ 545.1956; found 545.1945.

4.2.36. Carbamate ***20***

Following the procedure described for compound **13**, the protected carbamate **20** was isolated as a colorless oil (5 mg, 0.008 mmol, 99%). $R_f = 0.7$ (heptane/EtOAc 5:5); $[\alpha]_D^{20}$ -11.9° (*c* 0.3, MeOH); IR: ν 3344 (OH), 2974 (C=C), 1736 (C=O), 1646 (C=O), 1593 (C=C), 1422 (C=C) cm^{-1}; ^{1}H NMR (500 MHz, acetone-d_6): δ 8.91–8.82 (brs, 1H), 8.04 (d, $J = 8.5$ Hz, 2H), 7.91 (s, 1H), 7.75 (d, $J = 8.5$ Hz, 2H), 7.49 (d, $J = 8.3$ Hz, 1H), 7.25 (t, $J = 7.9$ Hz, 1H), 7.19 (d, $J = 8.3$ Hz, 1H), 6.29 (d, $J = 9.6$ Hz, 1H), 5.98 (s, 2H), 5.77 (dd, $J = 10.0$, 3.0 Hz, 1H), 5.68 (ABq, $J = 5.7$ Hz, $\Delta\delta = 20.1$ Hz, 2H), 5.62 (dt, $J = 10.3$, 1.8 Hz, 1H), 5.28–5.25 (m, 1H), 4.25–4.15 (m, 2H), 3.71–3.67 (m, 1H), 2.78–2.71 (m, 1H), 2.56–2.48 (m, 1H), 2.10 (s, 3H), 1.97–1.92 (m, 1H), 1.92–1.83 (m, 2H), 1.82 (s, 3H), 1.79–1.72 (m, 2H), 1.65 (s, 3H), 1.62–1.53 (m, 1H) ppm; ^{13}C NMR (125 MHz, methanol-d_4): δ 174.7, 171.1, 166.5, 165.9, 162.3, 144.3, 142.1, 137.3, 134.6132.7, 131.5, 131.2 (2C), 130.6, 130.5, 130.2, 127.9 (2C), 126.8, 123.6, 122.5, 118.3, 117.8, 81.1, 80.4, 64.0, 49.8, 46.2, 36.2, 32.7, 31.7, 30.4, 30.1, 23.6, 23.1, 20.7 ppm; HRMS (ESI): *m/z* calcd. for $C_{36}H_{37}ClO_{10}NNaBr$ $[M+Na]^+$ 780.1187; found 780.1263.

4.3. Bcl-xl, Mcl-1 and Bcl-2 binding affinity assays

The binding affinities of compounds for Bcl-2, Bcl-xL and Mcl-1 were evaluated by competition against fluorescently labelled reference compounds, Bim, Bak and Bid, respectively, as described by Qian et al. [35] Human isoform Bcl-2 (isoform 2), human 45–84/C37 Bcl-xL and mouse DN150/DC25 Mcl-1 proteins were recombinantly produced at ICSN. Bim, FITC-Ahx-Bim-OH, Bak, FITC-Ahx-Bak-OH, Bid and FITC-Ahx-Bid-OH peptides were synthetized by GenePep Laboratories (Montpellier, France). Labelled and unlabelled peptides were diluted in assay buffer, which contained 20 mM Na_2HPO_4 (pH 7.4), 50 mM NaCl, 2 μM EDTA, 0.05% Pluronic F-68 (without pluronic acid for storage at −20 °C). Labelled BH3 peptide (15 nM of Bak and Bid, 3 nM of Bim), 100 nM protein, and 100 μM of unlabelled BH3 peptide or compound (first diluted in 10 mM DMSO and then buffer for final concentration from 10^{-9} to 10^{-4} M) into a final volume of 20 μL were distributed in a 384-well black flat-bottomed microplate (PS, Hibase, Small Volume, Med. Binding, VWR Garnier Bio-One 784076). The microplate was then incubated at room temperature for 2 h and shaken before fluorescent polarization was measured. Fluorescence polarization in millipolarization units was measured with a Beckman Coulter Paradigm® using FP cartridge (λ_{ex} 485 nm, λ_{em} 535 nm). The exposure time was 300 ms per channel. All experimental data were collected using the Biomek Software® (Beckman Coulter, Inc, Brea,

CA, USA) and analyzed using Microsoft Excel 2010 (Microsoft, Redmond, WA, USA). Results are expressed as binding activity, *i.e.* percentage of inhibition of the binding of labelled reference compound, converted into K_i, the concentration corresponding to 50% of such inhibition, and corrected for experimental conditions according to Kenakin rearranged equation [41], which is adapted from Cheng and Prusoff equation [35]. Unlabelled peptides Bim, Bak and Bid were used as positive controls. The performance of the assays was monitored by use of Z′ factors as described by Zhang et al. [42]. The Z′ factors for these assays were 0.8 (Bcl-2/Bim and Bcl-xL/Bak) and 0.7 (Mcl-1/Bid) respectively indicating the robustness of such assays.

4.4. Cell lines

BL2 and Remb1 cell lines were kindly provided by the International Agency for Research on Cancer (IARC, Lyon). NCI-H929 and RS4;11 cells were purchased from DSMZ (Braunschweig, Germany). All cell lines were cultured in RPMI 1640 medium (Invitrogen) containing 2 mM L-glutamine, 1 mM sodium pyruvate, 20 mM glucose, 100 U/mL penicillin and 100 μg/mL streptomycin and supplemented with 7% heat-inactivated fetal calf serum (complete RPMI medium). 2-β-mercapto-ethanol (0.05 mM) was also added to the complete medium for H929.

4.5. MTT assays

Cell viability was measured by the MTT (3-(4, 5-dimethylthiazolyl-2)-2, 5-diphenyltetrazolium bromide) assay. 6.10^4 cells (in duplicate) were incubated for 24 h at 37 °C with 2.5, 5, 10 or 20 μM of each compound in 100 μL of complete RPMI medium. Then, 10 μL of MTT reagent (final concentration 0.5 mg/mL) was added and plates were incubated 2 extra hours. Finally, 100 μL of lysis buffer (20% SDS, 45% Dimethylformadide, pH = 4.7) was added and absorbance was recorded at 570 nm after 2 h of incubation. The IC_{50} values were calculated after plotting the dose-response curves using the GraphPad Prism software.

4.6. Quantification of apoptosis

Apoptosis was assessed by labelling cells with annexin-V-FITC and propidium iodide (PI). 1×10^6 cells were incubated for 24 h at 37 °C with 10 μM of each compound in 1 mL of complete RPMI medium. Cells were then washed in PBS, resuspended in annexin buffer (10 mM HEPES/NaOH, pH = 7.4, 150 mM NaCl, 5 mM KCl, 1 mM MgCl2, 1.8 mM CaCl2) containing 2.5 μg/mL annexin V-FITC (eBioscience) and incubated for 5–10 min. After washing, cells were resuspended in annexin buffer supplemented with PI (10 μg/mL; Sigma-Aldrich) and analyzed (n = 10 000) by flow cytometry (Accuri C6 cytometer, Becton-Dickinson). Annexin V-positive cells (PI negative and positive) were considered as apoptotic cells.

Acknowledgments

We gratefully acknowledge “Fondation ARC pour la Recherche sur le Cancer” and Société Française d'Hématologie for the fellowships of A.A.S. and L.F. respectively. We also thankInternational French-Malaysian Natural Product Laboratory (NatProLab) between CNRS-ICSN and University of Malaya and Investissement d'Avenir grant of the Agence Nationale de la Recherche (CEBA: ANR-10-LABX-25-01) for their financial support.

Appendix A. Supplementary data

Supplementary data related to this article can be found at https://doi.org/10.1016/j.ejmech.2018.01.100.

References

[1] A. Strasser, S. Cory, J.M. Adams, EMBO J. 30 (2011) 3667–3683, https://doi.org/10.1038/emboj.2011.307.
[2] P.E. Czabotar, G. Lessene, A. Strasser, J.M. Adams, Nat. Rev. Mol. Cell Biol. 15 (2014) 49–63, https://doi.org/10.1038/nrm3722.
[3] R. Elkholi, K.V. Floros, J.E. Chipuk, Genes & Cancer 2 (2011) 523–537, https://doi.org/10.1177/1947601911417177.
[4] M.R. Warr, J.C. Shore, Curr. Mol. Med. 8 (2008) 138–147, https://doi.org/10.2174/156652408783769580.
[5] J.C. Reed, Blood 111 (2008) 3322–3330, https://doi.org/10.1182/blood-2007-09-078162.
[6] J.L. Yap, L. Chen, M.E. Lanning, S. Fletcher, J. Med. Chem. 60 (2017) 821–838, https://doi.org/10.1021/acs.jmedchem.5b01888.
[7] A.M. Beekman, L.A. Howell, ChemMedChem 11 (2016) 802–813, https://doi.org/10.1002/cmdc.201500497.
[8] L. Vela, I. Marzo, Curr. Opin. Pharmacol. 23 (2015) 74–81, https://doi.org/10.1016/j.coph.2015.05.014.
[9] S. Kitada, M. Leone, S. Sareth, D. Zhai, J.C. Reed, M. Pellecchia, J. Med. Chem. 46 (2003), https://doi.org/10.1021/jm030190z, 4259–4254.
[10] G. Wang, Z. Nikolovska-Coleska, C.-Y. Yang, R. Wang, G. Tang, J. Guo, S. Shangary, S. Qiu, W. Gao, D. Yang, J. Meagher, J. Stuckey, K. Krajewski, S. Jiang, P.P. Roller, H.O. Abaan, Y. Tomita, S. Wang, J. Med. Chem. 49 (2006) 6139–6142, https://doi.org/10.1021/jm060460o.
[11] R.M. Mohammad, A.S. Goustin, A. Aboukameel, B. Chen, S. Banerjee, G. Wang, Z. Nikolovska-Coleska, S. Wang, A. Al-Katib, Clin. Canc. Res. 13 (2007) 2226–2235, https://doi.org/10.1158/1078-0432.
[12] Y. Sun, J. Wu, A. Aboukameel, S. Banerjee, A.A. Arnold, J. Chen, Z. Nikolovska-Coleska, Y. Lin, X. Ling, D. Yang, S. Wang, A. Al-Katib, R.M. Mohammad, Canc. Biol. Ther. 7 (2008) 1418–1426.
[13] J. Wei, J.L. Stebbins, S. Kitada, R. Dash, D. Zhai, W.J. Placzek, B. Wu, M.F. Rega, Z. Zhang, E. Barile, L. Yang, R. Dahl, P.B. Fisher, J.C. Reed, M. Pellecchia, Front. Oncol. 1 (2011) 28, https://doi.org/10.3389/fonc.2011.00028.
[14] C.A. Goard, A.D. Shimmer, Core Evid. 8 (2013) 15–26, https://doi.org/10.2147/CE.S42568.
[15] L. Gandhi, D. Ross Camidge, M. Ribeiro de Oliveira, P. Bonomi, D. Gandara, D. Khaira, C.L. Hann, E.M. McKeegan, E. Litvinovich, P.M. Hemken, C. Dive, S.H. Enschede, C. Nolan, Y.-L. Chiu, T. Busman, H. Xiong, A.P. Krivoshik, R. Humerickhouse, G.I. Shapiro, C.M. Rudin, J. Clin. Oncol. 29 (2011) 909–916, https://doi.org/10.1200/JCO.2010.31.6208.
[16] J. Chen, H. Zhou, A. Aguilar, L. Liu, L. Bai, D. McEachern, C.-Y. Yang, J.L. Meagher, J.A. Stuckey, S. Wang, J. Med. Chem. 55 (2012) 8502–8514, https://doi.org/10.1021/jm3010306.
[17] Y. Tanaka, K. Aikawa, G. Nishida, M. Homma, S. Sogabe, S. Igaki, Y. Hayano, T. Sameshima, I. Miyahisa, T. Kawamoto, M. Tawada, Y. Imai, M. Inazuka, N. Cho, Y. Imaeda, T. Ishikawa, J. Med. Chem. 56 (2013) 9635–9645, https://doi.org/10.1021/jm401170c.
[18] G. Lessene, P.E. Czabotar, B.E. Sleebs, K. Zobel, K.N. Lowes, J.M. Adams, J.B. Baell, P.M. Colman, K. Deshayes, W.J. Fairbrother, J.A. Flygare, P. Gibbons, W.J.A. Kersten, S. Kulasegaram, R.M. Moss, J.P. Parisot, B.J. Smith, I.P. Street, H. Yang, D.S.C. Huang, K.G. Watson, Nat. Chem. Biol. 9 (2013) 390–397, https://doi.org/10.1038/nchembio.1246.
[19] A.J. Souers, J.D. Leverson, E.R. Boghaert, S.L. Ackler, N.D. Catron, J. Chen, B.D. Dayton, H. Ding, S.H. Enschede, W.J. Fairbrother, D.S.C. Huang, S.G. Hymowitz, S. Jin, S.L. Khaw, P.J. Kovar, L.T. Lam, J. Lee, H.L. Maecker, K.C. Marsh, K.D. Mason, M.J. Mitten, P.M. Nimmer, A. Oleksijew, C.H. Park, C.-M. Park, et al., Nat. Med. 19 (2013) 202–208, https://doi.org/10.1038/nm.3048.
[20] A. Kotschy, Z. Szlavik, J. Murray, J. Davidson, A.L. Maragno, G. Le Toumelin-Braizat, M. Chanrion, G.L. Kelly, J.-N. Gong, D.M. Moujalled, A. Bruno, M. Csekei, A. Paczal, Z.B. Szabo, S. Sipos, G. Radics, A. Proszenyak, B. Balint, L. Ondi, G. Blasko, A. Robertson, A. Surgenor, P. Dokurno, I. Chen, N. Matassova, J. Smith, C. Pedder, C. Graham, A. Studeny, G. Lysiak-Auvity, A.-M. Girard, F. Gravé, D. Segal, C.D. Riffkin, G. Pomilio, L.C.A. Galbraith, B.J. Aubrey, M.S. Brennan, M.J. Herold, C. Chang, G. Guasconi, N. Cauquil, F. Melchiore, N. Guigal-Stephan, B. Lockhart, F. Colland, J.A. Hickman, A.W. Roberts, D.C.S. Huang, A.H. Wei, A. Strasser, G. Lessene, O. Geneste, Nature 538 (2016) 477–482, https://doi.org/10.1038/nature19830.
[21] P.S. Jeng, E.H. Cheng, Nat. Chem. Biol. 9 (2013) 351–352, https://doi.org/10.1038/nchembio.1256.
[22] C. Apel, C. Geny, V. Dumontet, N. Birlirakis, F. Roussi, V.C. Pham, D.T.M. Huong, V.H. Nguyen, V.M. Chau, M. Litaudon, J. Nat. Prod. 77 (2014) 1430–1437, https://doi.org/10.1021/np500170v.
[23] M.N. Azmi, T. Péresse, C. Remeur, G. Chan, F. Roussi, M. Litaudon, K. Awang, Fitoterapia 109 (2016) 190–195, https://doi.org/10.1016/j.fitote.2016.01.004.
[24] C. Gény, G. Rivière, J. Bignon, N. Birlirakis, E. Guittet, K. Awang, M. Litaudon, F. Roussi, V. Dumontet, J. Nat. Prod. 79 (2016) 838–844, https://doi.org/10.1021/acs.jnatprod.5b00915.
[25] D. Fomekong Fotsop, F. Roussi, A. Leverrier, A. Bretéché, F. Guéritte, J. Org. Chem. 75 (2010) 7412–7415, https://doi.org/10.1021/jo101088h.
[26] M. Litaudon, H. Bousserouel, K. Awang, O. Nosjean, M.-T. Martin, M.E. Tran Huu Dau, H.A. Hadi, J.A. Boutin, T. Sévenet, F. Guéritte, J. Nat. Prod. 72 (2009)

480–483, https://doi.org/10.1021/np8006292.
[27] J. Dardenne, S. Desrat, F. Guéritte, F. Roussi, Eur. J. Org Chem. (2013) 2116–2122, https://doi.org/10.1002/ejoc.201201628.
[28] S. Desrat, A. Pujals, C. Colas, J. Dardenne, C. Geny, L. Favre, V. Dumontet, B. Iorga, M. Litaudon, M. Raphaël, J. Wiels, F. Roussi, Bioorg. Med. Chem. Lett 24 (2014) 5086–5088, https://doi.org/10.1016/j.bmcl.2014.09.004.
[29] S. Desrat, C. Remeur, F. Roussi, Org. Biomol. Chem. 13 (2015) 5520–5531, https://doi.org/10.1039/C5OB00354G.
[30] S. Desrat, C. Remeur, C. Geny, G. Rivière, C. Colas, V. Dumontet, N. Birlirakis, B. Iorga, F. Roussi, Chem. Commun. 50 (2014) 8593–8596, https://doi.org/10.1039/C4CC01830C.
[31] W.V. Daehne, E. Frederiksen, E. Gundersen, F. Lund, P. Morch, H.J. Petersen, K. Roholt, L. Tybring, W.O. Godtfredsen, J. Med. Chem. 13 (1970) 607–612, https://doi.org/10.1021/jm00298a005.
[32] H. Bundgaard, N. Mørk, A. Hoelgaard, Int. J. Pharm. 55 (1989) 91–97, https://doi.org/10.1016/0378-5173(89)90028-8.
[33] M.E. Lanning, W. Yu, J.L. Yap, J. Chauhan, L. Chen, E. Whiting, L.S. Pidigu, T. Atkinson, H. Bailey, W. Li, B.M. Roth, L. Hynicka, K. Chesko, E.A. Toth, P. Shapiro, A.D. MacKerell Jr., P.T. Wilder, S. Fletcher, Eur. J. Med. Chem. 113 (2016) 273–292, https://doi.org/10.1016/j.ejmech.2016.02.006.
[34] M. Urban, J. Sarek, I. Tislerova, P. Dzubak, M. Hajduch, Biorg. Med. Chem. 13 (2005) 5527–5535.
[35] J. Qian, M.J. Voorbach, J.R. Huth, M.L. Coen, H. Zhang, S.-C. Ng, K.M. Comess, A.M. Petros, S.H. Rosenberg, U. Warrior, D.J. Burns, Anal. Biochem. 328 (2004) 131–138, https://doi.org/10.1016/j.ab.2003.12.034.
[36] Y. Cheng, W.H. Prusoff, Biochem. Pharmacol. 22 (1973) 3099–3108, https://doi.org/10.1016/0006-2952(73)90196-2.
[37] L. Campos, J.-P. Rouault, O. Sabido, P. Oriol, N. Roubi, C. Vasselon, E. Archimbaud, J.-P. Magaud, D. Guyotat, Blood 81 (1993) 3091–3096.
[38] S. Wuillème-Toumi, N. Robillard, P. Gomez, P. Moreau, S. Le Gouill, H. Avet-Loiseau, J.-L. Harousseau, M. Amiot, R. Bataille, Leukemia 19 (2005) 1248–1252, https://doi.org/10.1038/sj.leu.2403784.
[39] G.L. Kelly, S. Grabow, S.P. Glaser, L. Fitzsimmons, B.J. Aubrey, T. Okamoto, L.J. Valente, M. Robati, L. Tai, W.D. Fairlie, E.F. Lee, M.S. Lindstrom, K.G. Wiman, D.C. Huang, P. Bouillet, M. Rowe, A.B. Rickinson, M.J. Herold, A. Strasser, Genes Dev. 28 (2014) 58–70, https://doi.org/10.1101/gad.232009.113.
[40] W.L.F. Armarego, C.L.L. Chai, Purification of Laboratory Chemicals, seventh ed., Butterworth-Heinemann, Elsevier, Oxford, 2013.
[41] Z.W. Nikolovska-Coleska, R. Wang, X. Fang, H. Pan, Y. Tomita, P. Li, P.P. Roller, K. Krajewski, N.G. Saito, J.A. Stuckey, S. Wang, Anal. Biochem. 332 (2004) 261–273, https://doi.org/10.1016/j.ab.2004.05.055.
[42] J.H. Zhang, T.D.Y. Chung, K.R. Oldenburg, J. Biomol. Screen 4 (1999) 67–73, https://doi.org/10.1177/108705719900400206.

- Debernardi J, Hollville E, Wiels *J*, Robert A. *Differential role of FL-Bid and t-Bid during Verotoxin-1-induced apoptosis in Burkitt's lymphoma cells*, *oncogene 2018*

Oncogene
https://doi.org/10.1038/s41388-018-0123-5

ARTICLE

Differential role of FL-BID and t-BID during verotoxin-1-induced apoptosis in Burkitt's lymphoma cells

Justine Debernardi[1] · Emilie Hollville[1] · Marc Lipinski[1] · Joëlle Wiels[1] · Aude Robert[1]

Received: 15 April 2017 / Revised: 8 December 2017 / Accepted: 17 December 2017

Abstract

The globotriaosylceramide Gb3 is a glycosphingolipid expressed on a subpopulation of germinal center B lymphocytes which has been recognized as the B cell differentiation antigen CD77. Among tumoral cell types, Gb3/CD77 is strongly expressed in Burkitt's lymphoma (BL) cells as well as other solid tumors including breast, testicular and ovarian carcinomas. One known ligand of Gb3/CD77 is Verotoxin-1 (VT-1), a Shiga toxin produced in specific *E. coli* strains. Previously, we have reported that in BL cells, VT-1 induces apoptosis via a caspase-dependent and mitochondria-dependent pathway. Yet, the respective roles of various apoptogenic factors remained to be deciphered. Here, this apoptotic pathway was found to require cleavage of the BID protein by caspase-8 as well as activation of two other apoptogenic proteins, BAK and BAX. Surprisingly however, t-BID, the truncated form of BID resulting from caspase-8 cleavage, played no role in the conformational changes of BAK and BAX. Rather, their activation occurred under the control of full length BID (FL-BID). Indeed, introducing a non-cleavable form of BID (BID-D59A) into BID-deficient BL cells restored BAK and BAX activation following VT-1 treatment. Still, t-BID was involved along with FL-BID in the BAK-dependent and BAX-dependent cytosolic release of CYT C and SMAC/DIABLO from the mitochondrial intermembrane space: FL-BID was found to control the homo-oligomerization of both BAK and BAX, likely contributing to the initial release of CYT C and SMAC/DIABLO, while t-BID was needed for their hetero-oligomerization and ensuing release amplification. Together, our results reveal a functional cooperation between BAK and BAX during VT-1-induced apoptosis and, unexpectedly, that activation of caspase-8 and production of t-BID were not mandatory for initiation of the cell death process.

Introduction

The neutral glycosphingolipid globotriaosylceramide (Gb3) is strongly expressed in Burkitt's lymphoma (BL) cells [1] and various solid tumors including breast, testicular and ovarian carcinomas [2–4]. Gb3 is also found expressed in a subpopulation of germinal center B lymphocytes where it defines the CD77 differentiation antigen [5] and in intestine, kidney and brain endothelial cells. In the latter, Gb3 functions as a receptor for Shiga toxins (Stx) which are produced by the bacterial pathogens *Shigella dysenteriae* type 1 and by Stx-producing *Escherichia coli* (STEC), the main causative agent for food-poisoning worldwide [6]. Stxs produced by STECs are sometimes called Verotoxins (VTs), having been first described as lethal to Vero cells. All forms of Stxs consist of a single 32 kDa. A subunit linked non-covalently to a pentamer of B subunits (7.7 kDa each) which is responsible for Gb3/CD77 binding. Once internalized in the cytosol, the A subunit uses its enzymatic activity to remove an adenine residue from the 28S ribosomal RNA, resulting in protein synthesis inhibition (reviewed in [7, 8]).

Treating cells with Stxs/VTs in vitro induces apoptosis in a variety of tumor models. With a few exceptions such as HeLa cells where it is mitochondria-independent [9], the apoptotic process usually depends on both caspases and molecules stored in mitochondria [10–12]. In some cell types, the endoplasmic reticulum (ER) stress response induced by Stxs/VTs contributes to caspase 8 activation and thus also takes part in the apoptotic pathway [13].

Electronic supplementary material The online version of this article (https://doi.org/10.1038/s41388-018-0123-5) contains supplementary material, which is available to authorized users.

✉ Joëlle Wiels
joelle.wiels@gustaveroussy.fr

[1] UMR 8126, CNRS, Univ Paris Sud, Université Paris-Saclay, Institut Gustave Roussy, Villejuif 94805, France

Published online: 14 February 2018

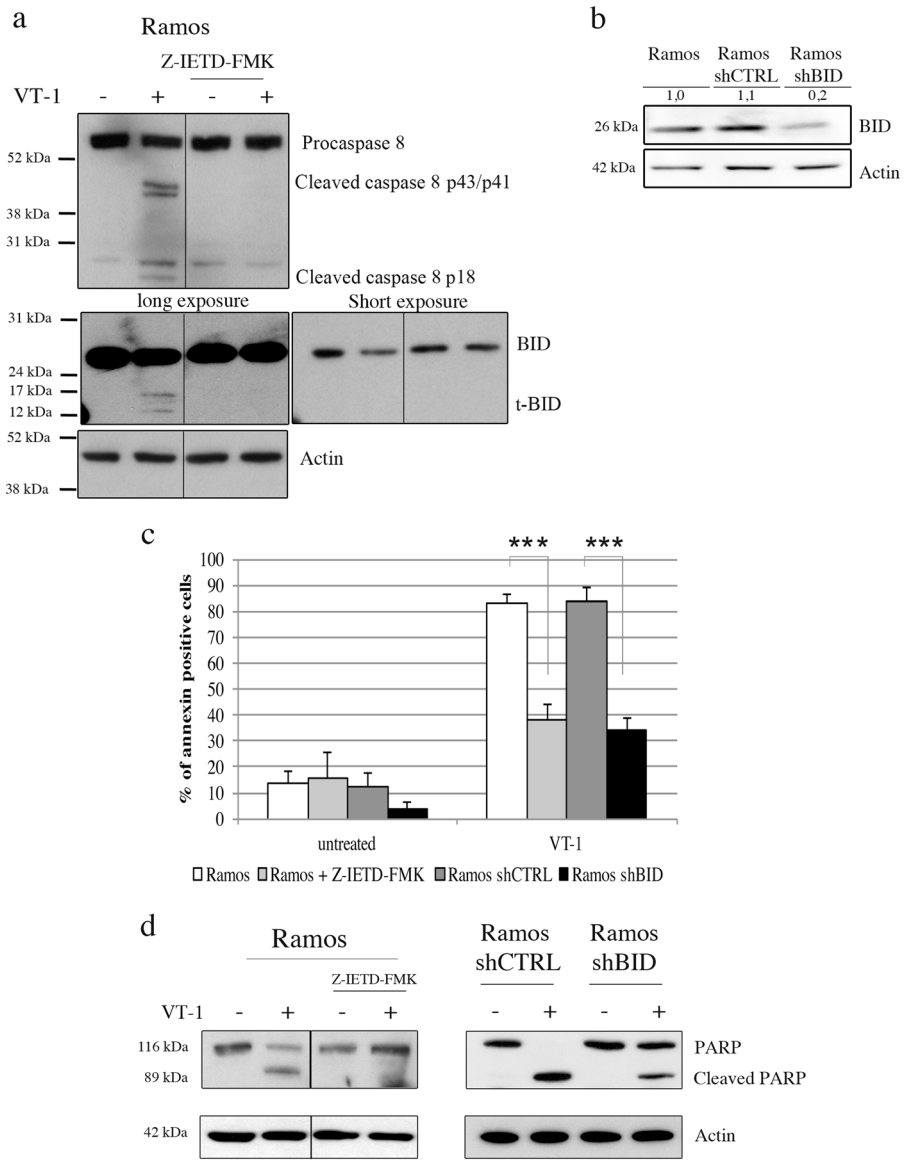

Fig. 1 BID and the caspase-8 pathway are essential for VT-1-induced apoptosis. **a** Ramos cells preincubated (1 h) with or without the caspase-8 inhibitor Z-IETD-FMK were treated or not with VT-1 for 6 h. Whole cell lysates were submitted to western blot analysis for detection of BID, caspase-8 and actin. **b** Whole cell lysates from Ramos cells stably transduced with a control shRNA vector (Ramos shCTRL) or with one directed against BID (Ramos shBID) were submitted to western blot analysis for detection of BID and actin. Fold change values as compared with the non-transduced cells and normalized to β-actin levels are shown above the BID blot. **c** Cells were incubated or not with VT-1 for 6 h and the proportion of apoptotic cells quantified by FACS analysis after labeling with annexin V-FITC and PI. Values (means ± sd) are from five independent experiments. Statistical significance is as follows: $***p < 0.01$. **d** Cells were treated as in (**c**) and whole cell extracts submitted to western blot analysis for detection of PARP cleavage as a marker of apoptosis. Results shown are representative of at least three independent experiments. In **a**, **d** black lines indicate that lanes were not contiguous in the gels

It thus appears that Stxs/VTs can trigger different apoptotic pathways in different cell types and that a number of steps involved in these signaling cascades remain unknown.

Cytochrome C (CYT C) and second mitochondria-derived activator of caspase/direct IAP binding protein with low PI (SMAC/DIABLO) are two apoptogenic factors present in the intermembrane space (IMS) of mitochondria. When liberated into the cytosol following mitochondrial outer membrane permeabilization (MOMP), CYT C and SMAC/DIABLO trigger caspases activation and the downstream cell death machinery. The release of CYT C and SMAC/DIABLO is controlled by a combination of anti-apoptotic and pro-apoptotic members in the B-cell CLL/lymphoma 2 (BCL-2) family which all contain BCL-2 homology (BH) domains referred to as BH1 to BH4. The pro-apoptotic group comprises effectors (mainly the BCL-2-antagonist/killer (BAK) and BCL-2–associated X protein (BAX) proteins) and another subgroup of proteins called "BH3-only" whose role is to regulate the effectors and the anti-apoptotic proteins. How they function precisely, however, remains controversial [14, 15]. There is no doubt that BAK and BAX are key players in MOMP as the two proteins form the pores through which the apoptogenic factors are released from the IMS. To do so, these two proteins must be activated by conformational modifications which result in the formation of oligomers and functional pores in the outer mitochondrial membrane but the precise mechanism thereof is intensely discussed [16, 17]. BID (BH3-interacting domain death agonist) is one of the BH3-only proteins which control BAK and BAX. It is the only one that behaves as a substrate for caspase-8 and other proteases including granzyme B, lysosomal cathepsins and

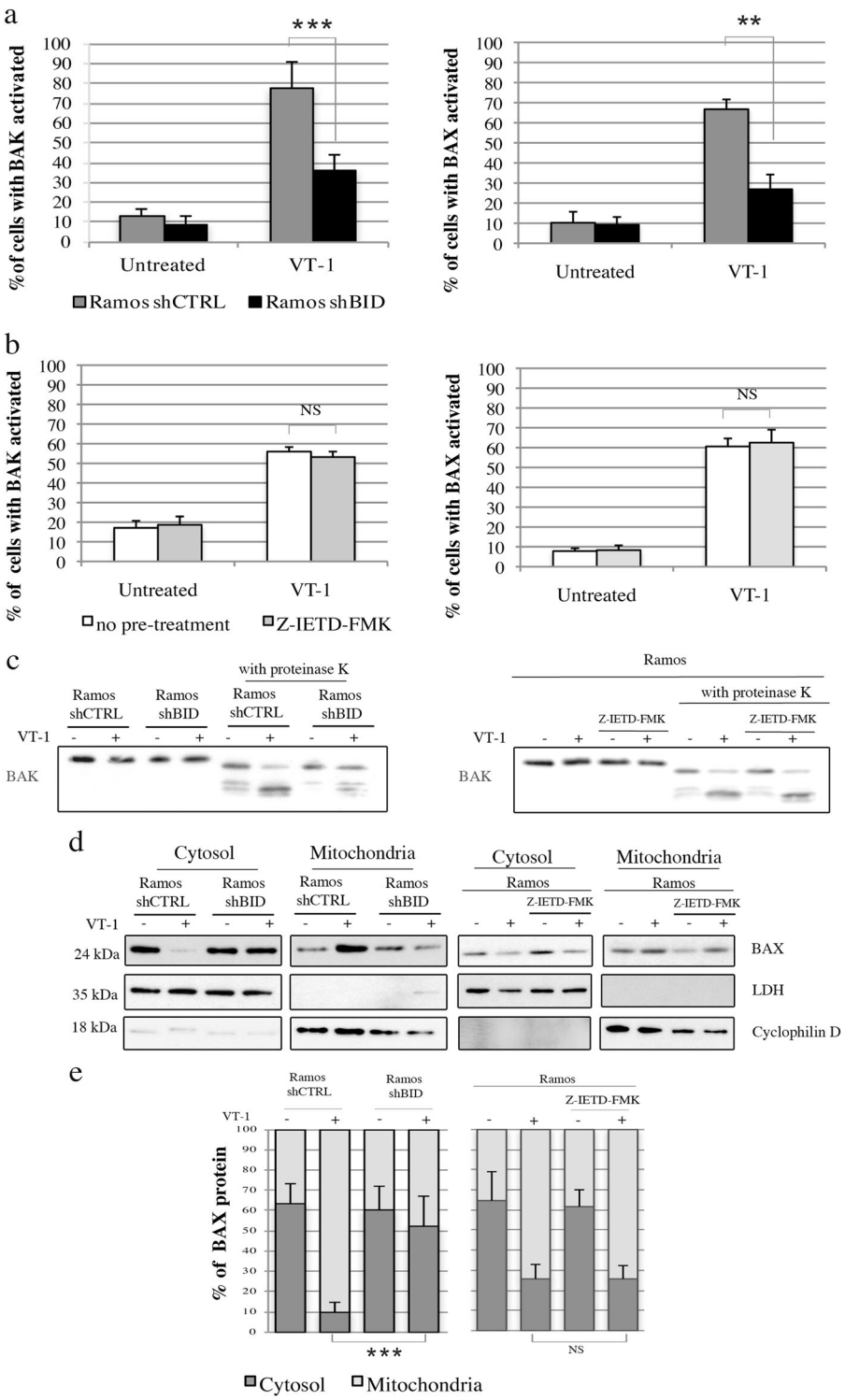

Fig. 2 FL-BID controls BAK and BAX activation during VT-1-induced apoptosis. **a** Ramos shCTRL and Ramos shBID cells were treated or not with VT-1 for 6 h and analyzed by flow cytometry after labeling with anti-BAK (left) or anti-BAX (right) conformational antibodies. Statistical significance is as follows: $**p < 0.025$, $n = 7$; $***p < 0.01$, $n = 4$. **b** Ramos cells preincubated (1 h) with or without the caspase-8 inhibitor Z-IETD-FMK were treated or not with VT-1 for 6 h and analyzed by flow cytometry after labeling with anti-BAK (left) or anti-BAX (right) conformational antibodies. NS non significant, $n = 3$. **c** Membrane fractions were obtained from Ramos shCTRL and Ramos shBID cells (left) or from Ramos cells preincubated (1 h) with or without the caspase-8 inhibitor Z-IETD-FMK (right), all treated or not with VT-1 for 6 h. Extracts were then incubated with proteinase K and analyzed by western blot for detection of BAK. **d** Cytosolic and mitochondrial extracts were obtained from cells treated as in (**c**) and were submitted to western blot analysis for detection of BAX, LDH, and cyclophilin D (used as cytosolic and mitochondrial markers, respectively). Results shown are representative of at least three independent experiments. **e** BAX-specific bands in cytosolic and mitochondrial fractions were quantified by densitometry, normalized to LDH or cyclophilin D levels and reported to the total amount of BAX (cytosolic + mitochondrial). Values (means ± sd) are from four (left) and three (right) independent experiments. Statistical significance is as follows: *** $p < 0.01$; NS non significant

calpains [18–20]. The role of t-BID, the resulting truncation product of BID, is recognized as critical in the apoptotic signaling pathway but how the full-length protein, FL-BID, also participates in the process is still a matter of debate [21, 22].

Previously, we have reported that the apoptosis induced by VT-1 in Gb3/CD77-expressing BL cell lines occurs via caspase-8 activation, a decrease in mitochondrial membrane potential and a cytosolic release of CYT C. BID, which was cleaved by caspase-8, and BAX were both involved in

mitochondrial activation, but the accumulation of the latter at the mitochondrial membrane did not rely on t-BID [10, 23]. Here, this VT-1-induced apoptotic pathway has been further analyzed, revealing a requirement for FL-BID alone for BAK and BAX activation while t-BID and FL-BID were both needed for optimal BAK- and BAX-dependent cytosolic release of CYT C and SMAC/DIABLO. BAK and BAX each formed homo-oligomers under the specific influence of FL-BID but t-BID was additionally needed to trigger BAK-BAX hetero-oligomerization and probably for amplification of the cytosolic release of the apoptogenic factors.

Results

BID and the caspase-8 pathway are essential for VT-1 induced apoptosis

Previously, we demonstrated that the mitochondrial events induced by VT-1 in BL cells involved the cleavage of BID by caspase-8 [23]. To further investigate the role of BID (both full length and cleaved forms) in the apoptotic events induced by VT-1, we used two complementary approaches. First, we pretreated Ramos BL cells with the caspase-8 inhibitor Z-IETD-FMK to prevent cleavage and activation of caspase-8 (Fig. 1a). As expected, this also inhibited the truncation of BID into t-BID (Fig. 1a; long exposure shows that treatment with Z-IETD inhibited the appearance of t-BID and short exposure that this treatment inhibited the decrease of FL-BID). Once treated with Z-IETD-FMK, Ramos cells became resistant to VT-1-induced apoptosis as measured by flow cytometry analysis of annexin-V-positive cells (38 ± 6 vs. $82 \pm 4\%$ in VT-1-treated control cells, $p < 0.01$, Fig. 1c). To directly analyze the role of BID, we then used a lentiviral vector-based shRNA system to stably repress its expression. The shBID reduced BID expression approximately 80% as compared to controls (Ramos shCTRL, Fig. 1b) without affecting the expression of the Gb3/CD77 VT-1 receptor at the cell membrane (Supplemental Fig. 1). These BID-repressed Ramos cells (Ramos shBID) proved much more resistant to VT-1-induced apoptosis than controls transduced with an empty vector (34 ± 4 vs. $83 \pm 6\%$ annexin-V-positive cells, respectively, $p < 0.01$, Fig. 1c). Consequently, and as anticipated, the cleavage of PARP strongly diminished in cells incubated in the presence of VT-1 whether they had been pretreated with Z-IETD-FMK (Fig. 1d, left panel) or if stably expressing shBID (Fig. 1d, right panel). Together, these observations confirmed that in these cells, both BID and the activity of caspase-8 are key elements in VT-1-induced apoptosis.

The activation of BAK and BAX is controlled by FL-BID, not by the caspase-8/t-BID pathway

From our previous studies, the VT-1-induced apoptosis in Ramos cells involves the mitochondrial relocalization of the pro-apoptotic BAX protein followed by MOMP and CYT C release [23]. BAX, and also BAK, get activated following a conformational change which, among other consequences, results in previously inaccessible N-terminal epitopes becoming accessible to conformation-dependent staining antibodies. Flow cytometry analysis with such antibodies showed that both BAK and BAX were activated in Ramos shCTRL cells incubated in the presence of VT-1 (78 ± 12 and $67 \pm 5\%$ of the cells respectively, Fig. 2a), stainings which were significantly inhibited in Ramos shBID cells (36 ± 7 and $27 \pm 7\%$ of the cells, $p < 0.01$ and $p < 0.025$, respectively, Fig. 2a and supplemental Fig. 2a for representative flow cytometry histograms). From these results, it was expected that BID-expressing Ramos cells treated with the caspase-8 inhibitor Z-IETD-FMK would behave similarly to shBID-expressing cells. Surprisingly, however, following VT-1 treatment, both BAK and BAX remained activated in cells pretreated with Z-IETD-FMK (Fig. 2b and supplemental Fig. 2b) suggesting that t-BID played little role if any in BAK and BAX activation.

These results were then confirmed by two other methods, limited proteolysis for BAK and mitochondrial localization for BAX. Indeed, following an apoptotic trigger, the exposure of its N-terminus renders BAK protein sensitive to proteinase K. Western blot analysis with an anti-BAK BH3 domain (Fig. 2c) shows that after treatment with VT-1, BAK became sensitive to proteinase K in Ramos cells, whether or not they had been pre-treated with Z-IETD-FMK. By contrast, after treatment with VT-1, BAK was much more resistant to proteinase K in Ramos shBID than in Ramos shCTRL cells. In healthy cells, BAX shuttles dynamically between cytosol and mitochondria but once activated, its shuttling towards the cytosol is inhibited and it accumulates in mitochondria [24]. Western blot analysis of cytosolic vs. mitochondrial extracts revealed that in Ramos and Ramos shCTRL cells treated with VT-1, BAX indeed accumulated in mitochondria. After VT-1 treatment, such an accumulation was not seen in Ramos shBID cells but was clearly observed in Ramos cells pretreated with Z-IETD-FMK (Fig. 2d and quantification of at least three experiments in Fig. 2e). From all these data, we conclude that it is the expression of full length BID rather than the caspase-8-dependent production of t-BID, which determines the stabilization of BAX and the mitochondrial activation of both BAK and BAX during VT-1-induced apoptosis.

To further substantiate these observations, we performed rescue experiments in Ramos-shBID cells whose

transduction allowed for expression of histidine-tagged murine BID (mBID) proteins, one wild type (BID-WT), the other mutated (BID-D59A) to preclude cleavage of the encoded protein by caspase-8. It can be seen in Supplemental Fig. 3a that after 48 h, transduced shBID Ramos cells expressed large amounts of the murine version of BID with no difference between BID-WT and BID-D59A. As expected, the amount of BID-WT strongly decreased after VT-1 treatment whereas BID-D59A did not (supplemental Fig. 3b). Expression of the murine proteins significantly reconstituted the sensitivity of the Ramos shBID cells to VT-1 as assessed by an MTT cytotoxicity assay (Supplemental Fig. 3c), by annexinV/PI labeling of the cells (supplemental Fig. 3d) or by PARP cleavage (Supplemental Fig. 3e). This effect was observed with both the wild type and the non-cleavable version of mBID. The VT-1-induced activation of BAK and BAX was also measured by flow cytometry in cells expressing murine BID-WT or BID-D59A. Following VT-1 treatment, both BAK and BAX were activated in Ramos shCTRL (71 ± 15 and 74 ± 13% of the cells, respectively, Fig. 3a, b) but not in Ramos shBID cells (29 ± 7 and 30 ± 5% of the cells, respectively, Fig. 3a, b). Transducing the latter with BID-WT or BID-D59A significantly reconstituted the conformational changes of both BAK (in 62 ± 13 and 58 ± 9% of the cells, respectively, Fig. 3a and supplemental Fig. 4a for representative flow cytometry histograms) and BAX (in 52 ± 12 and 47 ± 5% of the cells, respectively, Fig. 3b and supplemental Fig. 4b). Similarly, the stabilization of BAX in mitochondria was significantly reconstituted in cells transduced either with BID WT or with BID-D59A (supplemental Fig. 5a and b). Together, these results further confirmed the implication of the full length BID protein in the activation of both BAK and BAX.

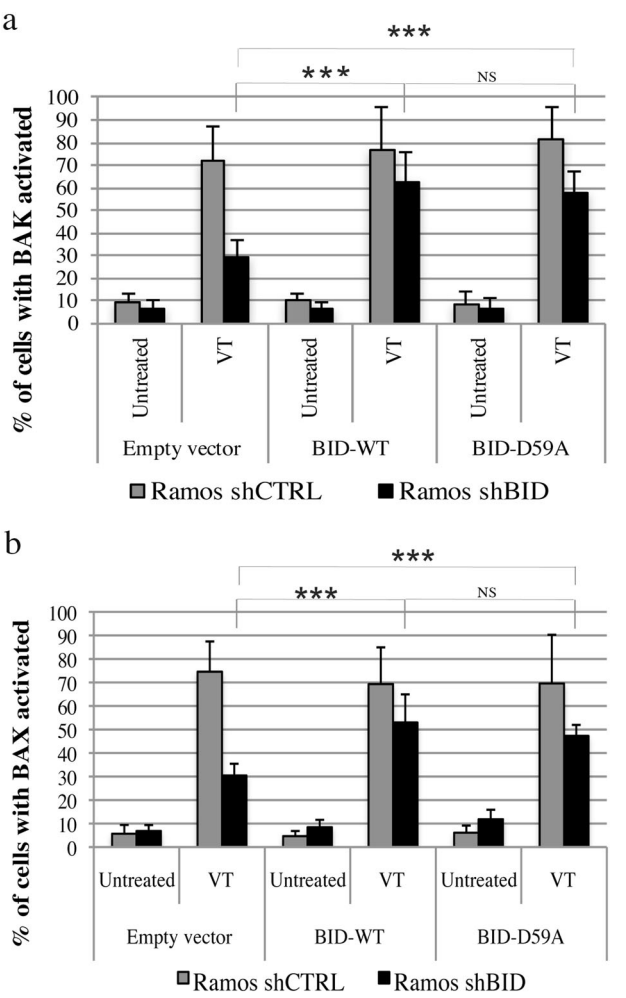

Fig. 3 Expression of FL-BID restores BAK and BAX activation during VT-1-induced apoptosis of Ramos shBID cells. **a** Ramos shCTRL and Ramos shBID cells were transduced with lentiviral vectors encoding either a mutated form of the murine BID protein (BID-D59A) which is not cleavable by caspase-8, a wild type version of murine BID (BID-WT) or a control empty vector. Forty hours after transduction, cells were incubated or not with VT-1 for 6 h and analyzed by flow cytometry after labeling with anti-BAK conformational antibodies. Values (means ± sd) are from seven independent experiments. **b** Cells transduced and treated as in (**a**) were labeled with anti-BAX conformational antibodies. Statistical significance is as follows: ***$p < 0.01$; NS non significant. Values (means ± sd) are from six independent experiments

Both FL-BID and caspase-8 activation are involved in CYT C and SMAC/DIABLO release from mitochondria

Having demonstrated that inhibiting caspase-8 with Z-IETD-FMK changed neither BAK and BAX activation nor BAX mitochondrial stabilization in response to VT-1 treatment, we then wished to explore what the effect would be on the release of apoptogenic IMS proteins from mitochondria to the cytosol. Mitochondrial and cytosolic fractions were prepared from Ramos cells preincubated with Z-IETD-FMK or not, as well as from shBID and shCTRL Ramos cells, all treated or not with VT-1. Western blots shown in Fig. 4a and quantifications of at least three experiments reported in Fig. 4b demonstrate that in VT-1-treated Ramos cells both CYT C and SMAC/DIABLO were released from mitochondria (70 ± 6 and 43 ± 4%, respectively) whereas the release of CYT C was reduced to 34 ± 6% (Fig. 4b upper panel, $p < 0.025$) and that of SMAC/DIABLO to 14 ± 5% (Fig. 4b lower panels, $p < 0.05$) in cells incubated in the presence of Z-IETD-FMK. This indicates that the activity of caspase-8 played a role in the release of these IMS proteins. We assume that this is through the truncation of BID into t-BID but we cannot rule out the possibility that another caspase-8 target may also play a role in conjunction with t-BID.

In Ramos shBID cells, the release of both CYT C and SMAC/DIABLO also decreased as compared to Ramos shCTRL cells (from 67 ± 4 to 24 ± 7%, and from 56 ± 7 to 30 ± 7%, respectively $p < 0.025$ in both cases, Fig. 4b). We

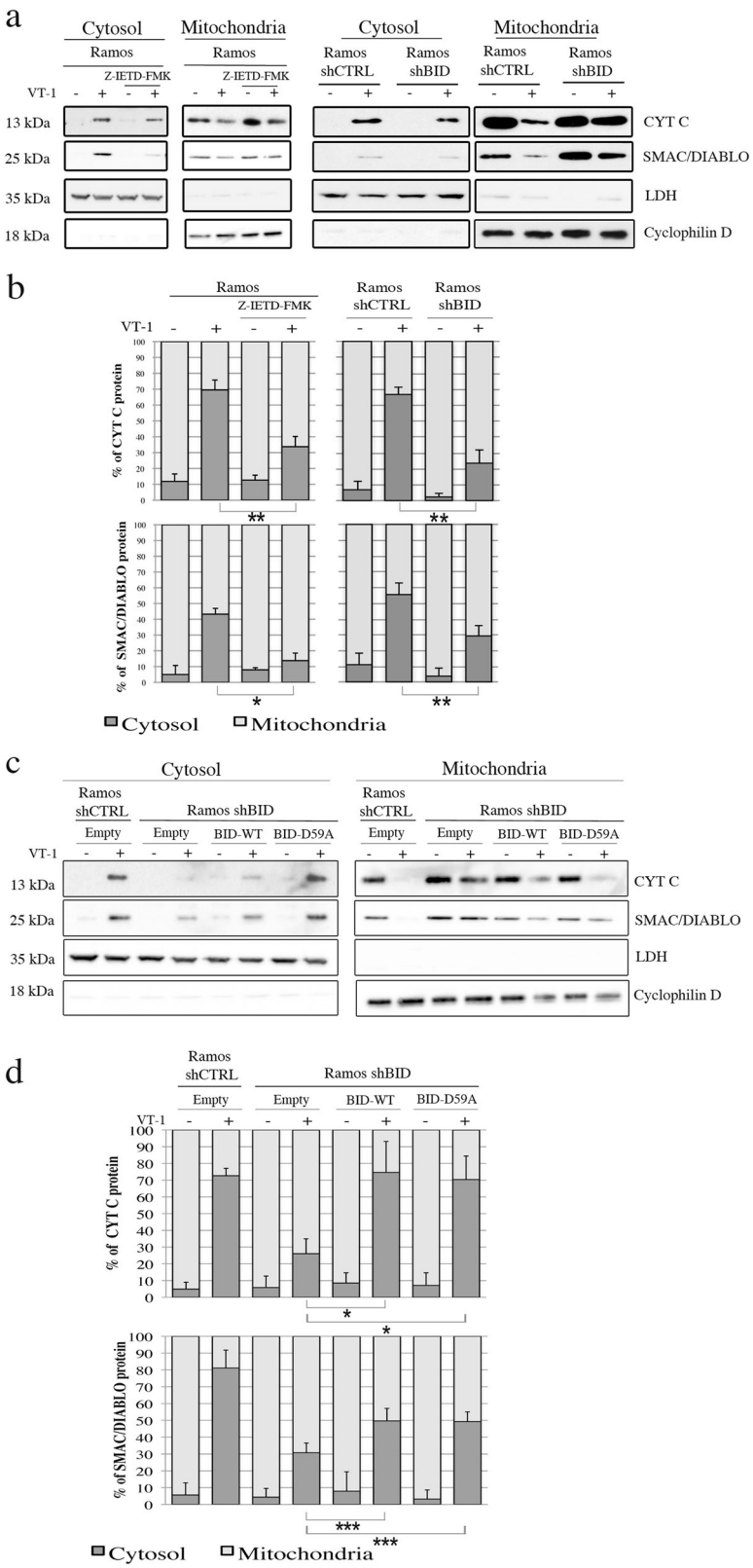

Fig. 4 Both FL-BID and caspase-8 activation are involved in CYT C and SMAC/DIABLO release from mitochondria during VT-1-induced apoptosis. **a** Cytosolic and mitochondrial extracts from Ramos cells preincubated (1 h) with or without the caspase-8 inhibitor Z-IETD-FMK (left) or from Ramos shCTRL and Ramos shBID cells (right), all treated or not with VT-1 for 6 h, were submitted to western blot analysis for detection of CYT C, SMAC/DIABLO, LDH and cyclophilin D (used as cytosolic and mitochondrial markers, respectively). Results shown are representative of at least three independent experiments. **b** CYT C (upper graphics) and SMAC/DIABLO (lower graphics) specific bands in cytosolic and mitochondrial fractions were quantified by densitometry, normalized to LDH or cyclophilin D levels and reported to the total amount (cytosolic + mitochondrial) of CYT C and SMAC/DIABLO. Values (means ± sd) are from four independent experiments. Statistical significance is as follows: $^{**}p < 0.025$; $^{*}p < 0.05$. **c** Ramos shCTRL and Ramos shBID cells were transduced with lentiviral vectors encoding either a mutated form of the murine BID protein (BID-D59A) which is not cleavable by caspase-8, a wild type version (BID-WT) or a control empty vector. Forty hours after transduction, cells were treated or not with VT-1 for 6 h. Cytosolic and mitochondrial extracts were prepared and submitted to western blot analysis for detection of CYT C, SMAC/DIABLO, LDH and cyclophilin D (used as cytosolic and mitochondrial markers, respectively). **d** CYT C (upper graphics) and SMAC/DIABLO (lower graphics) specific bands in cytosolic and mitochondrial fractions were quantified by densitometry, normalized to LDH or cyclophilin D levels and reported to the total amount (cytosolic + mitochondrial) of CYT C and SMAC/DIABLO. Values (means ± sd) are from four independent experiments. Statistical significance is as follows: $^{***}p < 0.01$; $^{*}p < 0.05$

then transduced Ramos shBID cells for expression of murine BID either WT or D59A. As seen in Fig. 4c, d, this resulted in a large increase of both CYT C and SMAC/DIABLO release from mitochondria which did not depend on whether BID could be cleaved into t-BID (BID-WT, 75 ± 19% of CYT C and 50 ± 7% of SMAC/DIABLO release) or not (BID-D59A, 70 ± 14% of CYT C and 49 ± 6% of SMAC/DIABLO release) as compared to Ramos shBID cells transduced with an empty vector (26 ± 9 and 31 ± 6%, respectively). From these data, we conclude that during VT-1-induced apoptosis, FL-BID on one hand and the caspase-8/t-BID pathway on the other hand are both involved in the release of the apoptogenic factors through BAK- and BAX-controlled MOMP.

The caspase-8/t-BID pathway is not involved in BAK and BAX homo-oligomerisation but controls BAK/BAX interaction

Since t-BID was not involved in the activation of BAK or BAX during the VT-1-induced apoptotic process, we wished to further analyze the respective effects of FL-BID and t-BID on the oligomerization of activated BAK and BAX proteins in mitochondria. To this aim, mitochondria were purified from Ramos cells treated with VT-1 or not, followed or not by protein cross-linking using bismaleimidohexane (BMH). Two blots were prepared in parallel with the same samples and blotted with either anti-BAK or anti-BAX antibodies. The BAK protein (apparent MW, 30 kDa) was readily detectable before VT-1 treatment (Fig. 5a, left panel, lanes 1 and 4) but treating the cells with VT-1 induced the formation of oligomers (mostly dimers and trimers) as seen in the crosslinked samples run in lanes 5 and 6 (Fig. 5a, left panel). Staining the second twin blot with anti-BAX antibodies confirmed that the 22 kDa monomeric BAX protein was detectable in these mitochondrial preparations more readily following than prior to VT-1 treatment (Fig. 5a, right panel, compare lanes 1 and 2), confirming the accumulation effect reported above. Here, oligomers and among them, dimers mainly, were the predominant forms observed after VT-1 treatment (Fig. 5a, right panel lane 5 and 6). For both BAK and BAX, the oligomers did not differ when production of t-BID was prevented with Z-IETD-FMK cell treatment (compare lanes 5 and 6 in both left and right panels). Also worth noting, the mobility of the BAK and BAX oligomers clearly differed, thus excluding the existence of hetero-oligomers.

To further investigate whether BAK and BAX directly interacted during the VT-1-induced apoptotic process, we then submitted total Ramos cell extracts to either BAK or BAX immunoprecipitation and then looked for co-immunoprecipitation of the other protein. As seen in Fig. 5b, precipitating BAX coimmunoprecipitated BAK only after VT-1 treatment (compare lanes 2 and 5 in upper panels). Reciprocally, precipitating BAK after VT-1 treatment coimmunoprecipitated BAX, although with less efficiency (compare lanes 2 and 5 in lower panels). These results which contrast with those obtained after protein cross-linking, suggested the existence of direct interactions between BAK and BAX. Two different reasons might explain this apparent contradiction. The failure to cross-link BAK and BAX using BMH might be due to steric factors related to the nature of the cross-linker and/or to the conformation of the proteins. Alternatively, not detecting the hetero-oligomers on gels could reflect their low abundance as compared to the homo-oligomers. When Ramos cells were pre-incubated with Z-IETD-FMK, the co-immunoprecipitation of BAK and BAX was inhibited almost to background levels (compare lanes 5 and 8 in upper and lower panels), indicating that the interaction between these two proteins requires the cleavage of BID by caspase-8.

To further explore the relationship between the caspase-8/t-BID pathway and the interaction between BAX and BAK, we finally submitted Ramos shCTRL and shBID cells to the same coimmunoprecipitation experiments. As can be seen in Fig. 5c, the VT-1 treatment led to BAK/BAX being co-immunoprecipitated in the former (lane 4) but much less in the latter (lane 9). Transducing Ramos shBID cells with the BID-WT expression vector restored the BAK/BAX interaction as detected by co-immunoprecipitation of one protein with antibodies to the other (Fig. 5c, lane 14). This contrasted with Ramos shBID cells transduced with the expression vector for the D59A non-cleavable mutant form of BID in which the BAK/BAX co-immunoprecipitation remained minimal as in Ramos shBID parental cells (Fig. 5c, lane 19). From these results, we conclude that although BAK and BAX can each oligomerize independently of t-BID in VT-1-treated cells, hetero-oligomers form only if the truncated form of BID is produced.

Discussion

Different signaling pathways triggered by Stxs/VTs have been described in various cell types but many steps in these pathways remain to be deciphered [25]. Here, we detail the sequence of events in the VT-1-induced apoptotic pathway and for the first time we demonstrate a cooperative activity between FL-BID and t-BID for a strong and complete apoptosis. In our previous studies, we had shown that the VT-1-induced apoptosis required degradation of the caspase-8 inhibitory molecule c-FLIP$_L$ through the ubiquitin–proteasome pathway and that BAX relocalization

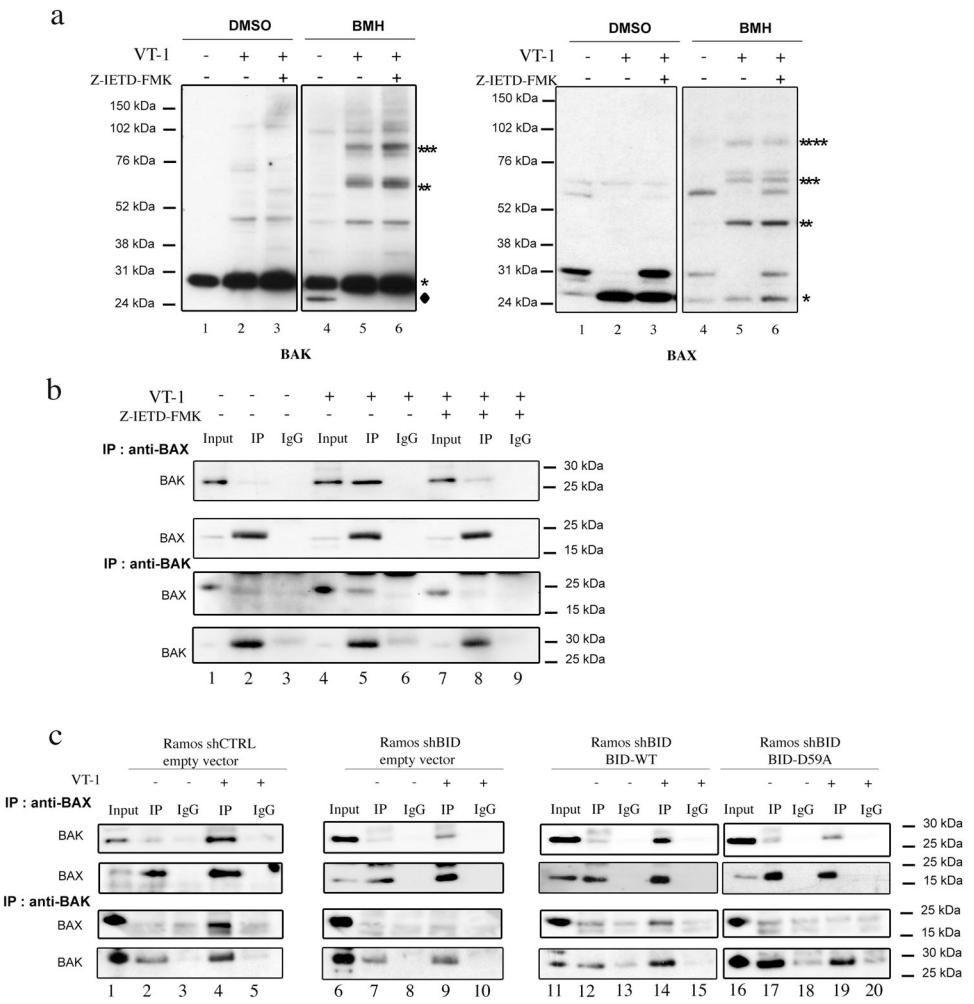

Fig. 5 The Caspase-8/t-BID pathway is not involved in BAK and BAX homo-oligomerisation but controls BAK/BAX interaction. **a** Ramos cells preincubated (1 h) with or without the caspase-8 inhibitor Z-IETD-FMK, were treated or not with VT-1 for 6 h. Enriched mitochondrial fractions were prepared and treated with 0.5 mM bis-maleimidohexane (BMH) crosslinker or DMSO (vehicle control) for 30 min. Protein extracts were analyzed by western blot for detection of BAK (left panel) and BAX (right panel). (*), (**), (***), (****) refer to protein monomers, dimers, trimers and quadrimers, respectively. (♦), intrachain cross-link conformer of inactive BAK. **b** Whole cell lysates from Ramos cells preincubated (1 h) with or without the caspase-8 inhibitor Z-IETD-FMK and treated or not with VT-1 for 6 h were subjected to immunoprecipitation (IP) using a rabbit anti-BAX pAb or control rabbit IgG (upper panel) or using a goat anti-BAK pAb or control goat IgG (lower panel). The immunoprecipitated proteins were submitted to western blot analysis for detection of BAK or BAX. (Input), 15% of the input for IP were included in the blot as a control for pre-IP protein levels. **c** Ramos shCTRL and Ramos shBID cells were transduced with lentiviral vectors encoding either a mutated form of the murine BID protein (BID-D59A) which is not cleavable by caspase-8, a wild type version of murine BID (BID-WT) or an empty control vector. Forty hours after transduction, cells were incubated or not with VT-1 for 6 h and submitted to immunoprecipitations followed by western blots performed as in (**b**)

to mitochondrial membranes participated in the MOMP which leads to CYT C release [10, 23]. In this paper, we have now demonstrated that BAK also is involved in MOMP and that SMAC/DIABLO as well as CYT C are released from the mitochondria during VT-1-induced apoptosis. Most importantly, our results show that the production of t-BID by caspase-8 is involved neither in BAX relocalization and activation nor in BAK activation; rather, both events are controlled by FL-BID. Finally, we have also shown that the caspase-8/t-BID pathway is not involved in the VT-1-induced homo-oligomerization of BAK and BAX but is needed for the BAK/BAX hetero-oligomerization and that both FL-BID and the caspase-8/t-BID pathway are involved in the MOMP-dependent release of CYT C and SMAC/DIABLO. Together, our data strongly suggest that under the control of FL-BID and t-BID, the homo-oli and hetero-oligomers of BAK and BAX act in coordination to insure a maximal release of the apoptogenic proteins and thereby an efficient apoptosis in cells treated with VT-1.

Other groups have reported that endogenous FL-BID functions as an apoptotic regulator for intrinsic cell death

pathways. Studying the role of BID during TNF-α-induced apoptosis, Pei et al. reported that FL-BID directly interacted with BAX in the cytosol after TNF-α treatment and that this interaction induced BAX relocalization to the mitochondria. They also showed that BID cleavage is a relatively late event in the apoptotic process [22]. Sarig et al., who produced the BID-D59A mutated form of BID, showed that expression of this non-cleavable form of BID efficiently induced apoptosis in primary MEFs. They also demonstrated that the apoptosis induced by BID-D59A did not involve its translocation to the mitochondria nor massive CYT C release, but still depended upon BAX and BAK activation [26], On the other hand, Valentijn and Gilmore have reported that FL-BID translocates to the mitochondria during anoikis, a form of apoptosis which occurs upon detachment of epithelial cells from the extracellular matrix, and that its translocation is independent of interactions with BAX [27]. Thus, it will be of interest to determine if during VT-1-induced apoptosis BAX activation requires interaction with FL-BID in the cytosol and whether or not FL-BID translocates to the mitochondria.

It is currently held that the N-terminal protein processing of BID by proteases exposes its BH3 domain and results in the translocation of t-BID to mitochondria where it activates its targets [15]. In contrast, the mechanism of action of FL-BID during apoptosis and its relocalization to the mitochondria is still very poorly understood. Interestingly, it has been shown that FL-BID but not t-BID is able to insert specific lysolipids into the mitochondrial membrane and that these specific changes probably prime mitochondria outer membranes to the actions of BAK and BAX which then induce the release of apoptogenic proteins [28]. Recently, the role of mitochondrial membrane lipids, and most notably of cardiolipin, in the t-BID-promoted activation of BAK and BAX has been confirmed [17]. However, it has also been reported that cardiolipin and the MTCH2 (mitochondrial carrier homolog 2) protein have redundant functions as t-BID receptors in the mitochondrial membrane [29]. Thus, determining the lipid and lysolipid composition of membrane mitochondria before and after treatment with VT-1 will certainly improve our understanding of how FL-BID and t-BID act during this process.

Also importantly, we have shown here that homo-oligomers and hetero-oligomers of BAK and BAX play complementary roles during VT-1-induced apoptosis. The release of IMS proteins from mitochondria is a crucial step in apoptotic signaling [30]. Several studies have pointed towards a major role for BAX in CYT C release based on its ability to form channels in artificial lipid membranes [31, 32] and large oligomeric complexes in the mitochondrial outer membrane [33, 34]. Recently, thanks to super-resolution microscopy approaches, two groups have also reported the presence of large ring-like structures in mitochondria of apoptotic cells [35, 36]. Although the formation of these transmembrane channels by BAX oligomers is a likely explanation, the question of how BAX triggers CYT C release after its translocation to mitochondria continues to be debated. We have now demonstrated that treating cells with VT-1 induced relocalization and formation of BAX oligomers in the mitochondrial outer membrane but also a reorganization of BAK monomers into oligomers. Analyzing the molecular sizes of cross-linked BAX and BAK complexes indicated that both BAX and BAK essentially form homo-oligomers. However, our results also showed that BAK and BAX co-immunoprecipitated, thereby revealing an interaction which occurred after BAX had undergone conformational changes to oligomerize. Although it has been shown that either BAK or BAX can be sufficient to elicit apoptosis, it is generally admitted that the apoptotic process is more complete and efficient when both BAX and BAK are present. Based on the data reported here, it is tempting to speculate that the interactions between these two proteins insure the most efficient MOMP. Inside mitochondria, CYT C and most certainly SMAC/DIABLO are present in different locations: a minor pool is free in the IMS, a major pool enclosed in cristae [37]. Hence, IMS proteins are likely released in two successive steps after MOMP: first, their soluble pool then the pool present in cristae. Interestingly, it has been shown that the oligomerization of a dynamin-related protein of the mitochondrial inner membrane, OPA-1, controls the morphology of cristae and CYT C redistribution during apoptosis. t-BID is involved in this mitochondrial cristae reorganization both by disrupting OPA-1 oligomers [38] and interacting with cardiolipin at mitochondrial contact sites [39]. From these various data and ours, we propose that the soluble pools of the IMS apoptogenic factors are released through BAK and BAX homo-oligomers and only require the action of FL-BID. In contrast, the pools present in cristae would be released only when t-BID is present and involves the formation of BAK/BAX hetero-oligomers. We also assume that BAK and BAX homo-oligomerization triggers the initial release of IMS proteins and that the caspase-8/t-BID pathway activates an amplification loop by inducing BAK/BAX interactions. For such a mechanism, it is likely that the majority of oligomers should be homo-structures, which would explain why we did not detect hetero-oligomers on gels after BMH cross-linking. Interestingly, this scheme is in line with the recent reports of Grosse et al. and Salvador-Gallego et al. who, among homogeneously labeled BAX rings, also noticed the presence of some heterogeneously-labeled structures which they assumed corresponded to assemblies of BAX with other proteins [35, 36].

Materials and methods

Cell lines

Culture conditions of Ramos cell line (ATCC CRL-1596) were previously described in Garibal et al. [23]. Stable BID-repressed Ramos cells (Ramos shBID) were established after transduction of a shRNA targeting BID (Mission® shRNA lentiviral transduction particles SHCLNV-NM 001196, Sigma Aldrich) and control Ramos cells (Ramos shCTRL) after transduction of a control shRNA (Mission® non-target shRNA lentiviral transduction particles, SHC002V). Cells were transduced according to the manufacturer's protocol and then selected by adding puromycin (0.6 mg/ml) to the culture medium.

Vectors and lentiviral transduction

pLVX-IRES-ZS-Green *Bid-wt, Bid-D59A* and empty lentiviral vectors, derived from vectors produced in A. Gross laboratory [26], were a gift from Susin [40]. Viruses were produced into 293T cells by Jetprime (Polyplus) transient transfection of lentiviral constructs and the packaging plasmids pDM2G (gift from Didier Trono, Addgene plasmid # 12259) and pCMVdelta R8.2 (gift from Didier Trono, Addgene plasmid # 12263). Two days after transfection, lentiviral supernatants were harvested, clarified by filtration and concentrated by ultracentrifugation. BL cells (2×10^6) were transduced with lentiviral particles (at a MOI of 15) in 2 ml of fresh medium in six-well plates and incubated 24 h at 37 °C. The medium containing lentiviral particles was then removed and fresh medium was added. The cells were harvested 24 or 48 h after transduction and used for further experiments.

Reagents and antibodies

Purified recombinant verotoxin-1 (VT-1) was purchased from List Biological Laboratories, Inc. Caspase-8 inhibitor (Z-IETD-FMK) was obtained from Calbiochem. Primary antibodies: Mouse anti-caspase-8 mAb (Ab-3, clone 1-3, Calbiochem), mouse anti-poly(ADP-Ribose) polymerase (PARP) mAb (Ab-2, clone c-2-10, Calbiochem), mouse anti-BAK conformational mAb (ab-1, Calbiochem), rabbit anti-BAK pAb (Becton-Dickinson), rabbit anti-BID pAb (FL195, Santa Cruz Biotechnology Inc), rabbit anti-BAX pAb (N-20, Santa Cruz Biotechnology Inc), mouse anti-BAX conformational mAb (6A7, Sigma-Aldrich), mouse anti-CYT C mAb (7H8.2C12, Becton-Dickinson), rabbit anti-SMAC/DIABLO pAb (Imgenex), mouse anti-histidine mAb (His-1, Sigma-Aldrich), mouse anti-β actin mAb (AC-74, Sigma-Aldrich), mouse anti-lactate dehydrogenase (LDH) mAb (H-10, Santa Cruz Biotechnology Inc.) and anti-cyclophilin mAb (E11AE12BD4, Mitosciences). Mouse anti-Gb3/CD77 mAb (1A4) was a gift from Dr. S. Hakomori and rat anti-BAK (4B5) mAb, which recognize the BAK BH3 domain, from Dr. R Kluck [41]. Secondary antibodies: horseradish peroxidase (HRP)-conjugated donkey anti-rabbit IgG and HRP-conjugated goat anti-mouse IgG (GE Healthcare), HRP-conjugated donkey anti-goat IgG (Santa Cruz Biotechnology Inc), Alexa 488-conjugated goat anti-mouse (Life technologies).

Apoptosis measurement

Apoptosis was assessed by labeling cells with annexin-V-FITC and propidium iodide (PI) as previously described [23]. Cells were then analyzed ($n = 10{,}000$) by flow cytometry (Accuri C6 cytometer, Becton-Dickinson). Annexin V-positive cells (PI negative and positive) were counted as apoptotic.

Intracellular immunofluorescence

BAK and BAX conformational changes were tested by flow cytometry using conformational antibodies. Cells, treated or not with VT-1 for 6 h, were harvested, fixed in paraformaldehyde (0.25%, 5 min) and washed three times in PBS before being incubated for 30 min with antibodies diluted (1:100 for anti-BAK (Ab-1), 1:200 for anti-BAX (6A7)) in PBS containing digitonin (500 µg/ml). After three washes in PBS, cells were incubated with Alexa-488-labeled anti-mouse antibodies for 30 min, washed twice, and analyzed by flow cytometry (Accuri C6 cytometer, Becton-Dickinson).

Preparation of whole cell extract

Aliquots of 1×10^6 cells were pelleted, solubilized in ice-cold RIPA buffer (150 mM NaCl, 50 mM Tris, pH 7.5, 5 mM EDTA, 0.5% NP40, 0.5% NaDOC, 0.1% SDS, complete protease inhibitor) and sonicated. Total protein concentration was measured by Bradford assay (Biorad).

Preparation of mitochondrial and cytosolic fractions

Cell fractionation using ice-cold cell lysis and mitochondria intact (CLAMI) buffer was performed as previously described [10].

Isolation of mitochondria and cross-linking

Pellets obtained from 24×10^6 cells were resuspended in sucrose buffer (25 mM sucrose, 5 mM HEPES, 2 mM EDTA, complete protease inhibitor) and incubated 30 min on ice. Sucrose buffer was supplemented with sucrose 1 M

to reach 250 mM concentration and cells were broken by using a dounce. The suspension was centrifuged at 600×*g* for 10 min to remove nucleus and cell debris. The supernatant was then centrifuged at 15,000×*g* at 4 °C for 15 min and the mitochondrial pellet was resuspended in 250 mM sucrose buffer, pH 7. Bis(maleimido)hexane (BMH) crosslinker or DMSO (vehicle control) was added to the mitochondria at 0.5 mM final concentration and the reaction mixture was incubated for 30 min at room temperature. The reaction was then stopped by quenching with DTT (final concentration 50 mM) for 15 min.

Limited proteolysis assay

BAK sensitivity to proteinase K was used to evaluate its conformational change. Membrane extracts enriched for mitochondria were incubated with proteinase K (30 µg/ml) as previously described by Iyer et al. [42]. Samples were then immunoblotted with the 4B5 anti-BAK mAb.

Immunoprecipitation

BAK and BAX immunoprecipitations were performed as previously described [23] using agarose-conjugated rabbit anti-BAX pAb (N-20) or goat anti-BAK pAb (G-23) or agarose-conjugated control rabbit IgG or agarose-conjugated control goat IgG (all from Santa Cruz Biotechnology Inc.)

Western blot analysis

Immunoblotting of protein extracts was carried out as previously described [23]. The blots were imaged with the ImageQuant LAS4000 imager (GE healthcare) and then on film (Amersham). Densitometry analysis of the blots was carried out using Quantity One software, version 4.6 (Bio-Rad).

Data analysis and statistic

All values for statistical significance represent the mean ± standard deviation (sd). Statistical analyses were performed using a non-parametric two-tailed test ($n < 30$): Mann and Whitney for side-by-side comparison and Holm correction was applied for multiple comparisons.

Acknowledgements We thank Yann Lécluse (Imaging and Cytometry Platform, Institut Gustave Roussy) for expert technical assistance in performing flow cytometry analyses. We are very grateful to Hana Raslova and Julie Rivière (INSERM UMR 1170, Institut Gustave-Roussy) for their help in producing lentivirus and to Evelyne May and Martine Raphaël (UMR 8126 CNRS) for helpful discussions and suggestions. This work was supported by grants from the Fondation de France 2014 00047509 (JW), the Ligue National Contre le Cancer (doctoral fellowship to JD) and the Fondation ARC (doctoral fellowship to EH).

Compliance with ethical standards

Conflict of interest The authors declare that they have no competing interests.

References

1. Nudelman E, Kannagi R, Hakomori S, Parsons M, Lipinski M, Wiels J, et al. A glycolipid antigen associated with Burkitt lymphoma defined by a monoclonal antibody. Science. 1983;220:509–11.
2. Arab S, Russel E, Chapman WB, Rosen B, Lingwood CA. Expression of the verotoxin receptor glycolipid, globotriaosylceramide, in ovarian hyperplasias. Oncol Res. 1997;9:553–63.
3. Gupta V, Bhinge KN, Hosain SB, Xiong K, Gu X, Shi R, et al. Ceramide glycosylation by glucosylceramide synthase selectively maintains the properties of breast cancer stem cells. J Biol Chem. 2012;287:37195–205.
4. Ohyama C, Fukushi Y, Satoh M, Saitoh S, Orikasa S, Nudelman E, et al. Changes in glycolipid expression in human testicular tumor. Int J Cancer. 1990;45:1040–4.
5. Mangeney M, Richard Y, Coulaud D, Tursz T, Wiels J. CD77: an antigen of germinal center B cells entering apoptosis. Eur J Immunol. 1991;21:1131–40.
6. Jacewicz M, Clausen H, Nudelman E, Donohue-Rolfe A, Keusch GT. Pathogenesis of shigella diarrhea. XI. Isolation of a shigella toxin-binding glycolipid from rabbit jejunum and HeLa cells and its identification as globotriaosylceramide. J Exp Med. 1986;163:1391–404.
7. Bergan J, Dyve Lingelem AB, Simm R, Skotland T, Sandvig K. Shiga toxins. Toxicon. 2012;60:085–107. 1
8. Johannes L, Romer W. Shiga toxins--from cell biology to biomedical applications. Nat Rev Microbiol. 2010;8:105–16.
9. Fujii J, Matsui T, Heatherly DP, Schlegel KH, Lobo PI, Yutsudo T, et al. Rapid apoptosis induced by Shiga toxin in HeLa cells. Infect Immun. 2003;71:2724–35.
10. Tetaud C, Falguieres T, Carlier K, Lecluse Y, Garibal J, Coulaud D, et al. Two distinct Gb3/CD77 signaling pathways leading to apoptosis are triggered by anti-Gb3/CD77 mAb and verotoxin-1. J Biol Chem. 2003;278:45200–8.
11. Lee SY, Cherla RP, Caliskan I, Tesh VL. Shiga toxin 1 induces apoptosis in the human myelogenous leukemia cell line THP-1 by a caspase-8-dependent, tumor necrosis factor receptor-independent mechanism. Infect Immun. 2005;73:5115–26.

12. Ching JC, Jones NL, Ceponis PJ, Karmali MA, Sherman PM. Escherichia coli shiga-like toxins induce apoptosis and cleavage of poly(ADP-ribose) polymerase via in vitro activation of caspases. Infect Immun. 2002;70:4669–77.
13. Tesh VL. Activation of cell stress response pathways by Shiga toxins. Cell Microbiol. 2012;14:1–9.
14. Tait SW, Green DR. Mitochondrial regulation of cell death. Cold Spring Harbor Perspect Biol. 2013;5:pii:a008706. https://doi.org/10.1101/cshperspect.a008706
15. Zheng JH, Viacava Follis A, Kriwacki RW, Moldoveanu T. Discoveries and controversies in BCL-2 protein-mediated apoptosis. FEBS J. 2016;283:2690–2700.
16. Li MX, Dewson G. Mitochondria and apoptosis: emerging concepts. F1000 prime Rep. 2015;7:42.
17. Renault TT, Chipuk JE. Death upon a kiss: mitochondrial outer membrane composition and organelle communication govern sensitivity to BAK/BAX-dependent apoptosis. Chem Biol. 2014;21:114–23.
18. Chen M, He H, Zhan S, Krajewski S, Reed JC, Gottlieb RA. Bid is cleaved by calpain to an active fragment in vitro and during myocardial ischemia/reperfusion. J Biol Chem. 2001;276:30724–8.
19. Cullen SP, Adrain C, Luthi AU, Duriez PJ, Martin SJ. Human and murine granzyme B exhibit divergent substrate preferences. J Cell Biol. 2007;176:435–44.
20. Li H, Zhu H, Xu CJ, Yuan J. Cleavage of BID by caspase 8 mediates the mitochondrial damage in the Fas pathway of apoptosis. Cell. 1998;94:491–501.
21. Konig HG, Rehm M, Gudorf D, Krajewski S, Gross A, Ward MW, et al. Full length Bid is sufficient to induce apoptosis of cultured rat hippocampal neurons. BMC Cell Biol. 2007;8:7.
22. Pei Y, Xing D, Gao X, Liu L, Chen T. Real-time monitoring full length bid interacting with Bax during TNF-alpha-induced apoptosis. Apoptosis. 2007;12:1681–90.
23. Garibal J, Hollville E, Renouf B, Tetaud C, Wiels J. Caspase-8-mediated cleavage of Bid and protein phosphatase 2A-mediated activation of Bax are necessary for Verotoxin-1-induced apoptosis in Burkitt's lymphoma cells. Cell Signal. 2010;22:467–75.
24. Todt F, Cakir Z, Reichenbach F, Emschermann F, Lauterwasser J, Kaiser A, et al. Differential retrotranslocation of mitochondrial Bax and Bak. EMBO J. 2015;34:67–80.
25. Tesh VL. Induction of apoptosis by Shiga toxins. Future Microbiol. 2010;5:431–53.
26. Sarig R, Zaltsman Y, Marcellus RC, Flavell R, Mak TW, Gross A. BID-D59A is a potent inducer of apoptosis in primary embryonic fibroblasts. J Biol Chem. 2003;278:10707–15.
27. Valentijn AJ, Gilmore AP. Translocation of full-length Bid to mitochondria during anoikis. J Biol Chem. 2004;279:32848–57.
28. Goonesinghe A, Mundy ES, Smith M, Khosravi-Far R, Martinou JC, Esposti MD. Pro-apoptotic Bid induces membrane perturbation by inserting selected lysolipids into the bilayer. Biochem J. 2005;387(Pt 1):109–18.
29. Raemy E, Montessuit S, Pierredon S, van Kampen AH, Vaz FM, Martinou JC. Cardiolipin or MTCH2 can serve as tBID receptors during apoptosis. Cell Death Differ. 2016;23:1165–74.
30. Ghiotto F, Fais F, Bruno S. BH3-only proteins: the death-puppeteer's wires. Cytom A. 2010;77:11–21.
31. Antonsson B, Conti F, Ciavatta A, Montessuit S, Lewis S, Martinou I, et al. Inhibition of Bax channel-forming activity by Bcl-2. Science. 1997;277:370–2.
32. Saito M, Korsmeyer SJ, Schlesinger PH. BAX-dependent transport of cytochrome c reconstituted in pure liposomes. Nat Cell Biol. 2000;2:553–5.
33. Kuwana T, Mackey MR, Perkins G, Ellisman MH, Latterich M, Schneiter R, et al. Bid, Bax, and lipids cooperate to form supramolecular openings in the outer mitochondrial membrane. Cell. 2002;111:331–42.
34. Karch J, Kwong JQ, Burr AR, Sargent MA, Elrod JW, Peixoto PM. et al. Bax and Bak function as the outer membrane component of the mitochondrial permeability pore in regulating necrotic cell death in mice. Elife. 2013;2:e00772
35. Grosse L, Wurm CA, Bruser C, Neumann D, Jans DC, Jakobs S. Bax assembles into large ring-like structures remodeling the mitochondrial outer membrane in apoptosis. EMBO J. 2016;35:402–13.
36. Salvador-Gallego R, Mund M, Cosentino K, Schneider J, Unsay J, Schraermeyer U, et al. Bax assembly into rings and arcs in apoptotic mitochondria is linked to membrane pores. EMBO J. 2016;35:389–401.
37. Scorrano L, Ashiya M, Buttle K, Weiler S, Oakes SA, Mannella CA, et al. A distinct pathway remodels mitochondrial cristae and mobilizes cytochrome c during apoptosis. Dev Cell. 2002;2:55–67.
38. Frezza C, Cipolat S, Martins de Brito O, Micaroni M, Beznoussenko GV, Rudka T, et al. OPA1 controls apoptotic cristae remodeling independently from mitochondrial fusion. Cell. 2006;126:177–89.
39. Kim TH, Zhao Y, Ding WX, Shin JN, He X, Seo YW, et al. Bid-cardiolipin interaction at mitochondrial contact site contributes to mitochondrial cristae reorganization and cytochrome C release. Mol Biol Cell. 2004;15:3061–72.
40. Cabon L, Galan-Malo P, Bouharrour A, Delavallee L, Brunelle-Navas MN, Lorenzo HK, et al. BID regulates AIF-mediated caspase-independent necroptosis by promoting BAX activation. Cell Death Differ. 2012;19:245–56.
41. Dewson G, Kratina T, Sim HW, Puthalakath H, Adams JM, Colman PM, et al. To trigger apoptosis, Bak exposes its BH3 domain and homodimerizes via BH3:groove interactions. Mol Cell. 2008;30:369–80.
42. Iyer S, Anwari K, Alsop AE, Yuen WS, Huang DC, Carroll J, et al. Identification of an activation site in Bak and mitochondrial Bax triggered by antibodies. Nat Commun. 2016;7:11734.

- Pujals A.*, **Robert A.***, Favre L, Desille T., Debernardi J., Joëlle Wiels. *The Bcl-2 inhibitor, ABT-737 enhances the activity of therapeutic agents against B lymphoproliferations associated with EBV both in vitro and in vivo, en préparation.* *Co 1ères autrices

Title: The BCL-2 inhibitor, ABT-737 enhances the activity of therapeutic agents against B lymphoproliferations associated with EBV both *in vitro* and *in vivo*

Anaïs Pujals [1,2]*, Aude Robert[2]*, Loetitia Favre[1,2], Thomas Desille[2], Justine Debernardi[2], Joëlle Wiels[2]

Affiliation
1- Curent affiliation : CHU Henri Mondor; Assistance Publique-Hôpitaux de Paris; Département de Pathologie; Inserm U955; Université Paris-Est Créteil; Créteil, France
2- UMR 8126 CNRS, Université Paris-Sud, Université Paris-Saclay, Institut Gustave Roussy, 94805 Villejuif, France
* These authors contributed equally to this work.

Correspondence to : **Aude ROBERT,** UMR 8126 CNRS, Gustave Roussy, 114 rue Edouard Vaillant, 94805 Villejuif cedex, France. Phone: 33 1 42 11 46 41, Fax: 33 1 42 11 54 94. Email: aude.robert@gustaveroussy.fr.

Keyword: EBV, BCL-2 inhibitor, drug-induced cell death, B lymphoproliferation,

Abstract:
Post-transplant lymphoproliferative disorders (PTLD) and Burkitt lymphoma (BL) are B-cell malignancies strongly associated with EBV infection. In these lymphoproliferations, EBV infection induce an increase of expression of the anti-apoptotic protein BCL-2. Given its chemoprotective effect, BCL-2 constitutes an attractive target for new therapeutic strategies for EBV-positive B-cell malignancies. In this study, we showed that ABT-737, a small molecule inhibitor of BCL-2, BCL-X(L), and BCL-w, strongly induced apoptosis *in vitro* in EBV-positive lymphoblastoid cell lines (LCLs) whereas BL were less sensitive. We assessed the efficiency of this compound *in vivo* on xenograft mouse models in monotherapy or associated with conventional treatments. Results obtained show that as single agent, ABT-737 reduced tumor growth and increased the overall survival of mice xenografted with LCL but had no effect on mice xenografted with BL cell line. Furthermore, the combination ABT-737/Cyclophosphamide reduced tumor growth during treatment but fail to improve the overall survival of mice xenografted with BL cell line whereas the combination ABT-737/Rituximab was very efficient and induced 70% of remission in mice xenografted with LCL. These results suggest that the use of agent targeting BCL-2, either alone or in combination with other conventional drugs, represents a novel promising approach for EBV-positive B lymphoproliferations.

Introduction (913) :

Epstein-Barr virus (EBV), a ubiquitous B-lymphotropic herpes virus, was the first virus directly linked to cancer in human. Since its discovery, EBV has been associated with a heterogenous group of epithelial tumors and various B cell malignancies including Burkitt's lymphoma (BL) and post-transplant lymphoproliferative disorders (PTLD). In infected tumor cells, EBV remains latent in an episomal form, with only a small subset of viral proteins expressed including six nuclear antigens (EBNA) and three latent membrane proteins (LMP). A differential expression of these latent proteins is observed in EBV-associated malignancies, which defines three distinct latency profiles. Most EBV-infected BL cells harbor the latency I phenotype (Epstein-Barr nuclear antigen 1 (EBNA1) is the only viral protein produced). Type II latency (expression of EBNA-1, LMP1 and LMP2) is associated with Hodgkin's lymphoma and nasopharyngeal carcinoma. In type III latency, typically found in PTLD and in some cases of BL, all the latent proteins of the virus are expressed (Reviewed in [1]). The ability of EBV to transform resting B cells to immortalized lymphoblastoïd (LCL) cells underlies its central role in the pathogenesis of these malignancies.

BL is a rare but highly aggressive non-Hodgkin B cell lymphoma that can be classified into three types based on clinical features and disease epidemiology. Endemic BL primarily affects children ages 4 to 7 in equatorial Africa and Papua New Guinea, where it accounts for around 50% of all pediatric cancers. Tumor are EBV-positive in almost every case. By contrast, sporadic BL occurs worldwide. Globally, it accounts for 1% to 2% of adult lymphoma cases. In the U.S. and Western Europe, it accounts for up to 40% of pediatric lymphoma cases. A third type termed "Immunodeficiency-associated" is most common in people with HIV. It accounts for 30% of non-Hodgkin lymphoma in HIV patients. It also can occur in people with congenital conditions that cause immune deficiency and in organ transplant patients who take immunosuppressive drugs. Compared to the endemic type, the incidence of EBV infection is considerably lower in the other two types of Burkitt lymphoma. In the sporadic disease, EBV occurs in about 30% of the patients. With the immunodeficiency-associated type, it occurs in about 25% to 40% of patients.

Post-transplant lymphoproliferative disorder (PTLD) are proliferations that develop as a consequence of immunosuppression in 1%–2% of people who receive a solid organ transplant or a stem cell allograft. It is a heterogeneous clinical and pathologic group of lymphoid

disorders ranging from EBV-driven proliferations to EBV-positive or EBV-negative proliferations indistinguishable from B-cell or less often T-cell lymphomas that occur in immunocompetent individuals. The majority of PTLD are associated with EBV infection, and are monoclonal or, less often, polyclonal B-cell proliferation [2]. Two studies found that gene expression patterns of PTLD tumors were similar to gene expression patterns of EBV-infected LCL, indicating that LCL represent a good in vitro model to examine the effects of the virus on cell function [3, 4]

Significant progress has been made in the treatment of EBV-associated malignancies but multiple challenges remain. At present, the standard treatment of EBV-associated lymphomas is usually identical to that of their EBV-negative counterparts and consist of a few months intensive chemotherapy regimen (CHOP: cyclosphamide, hydroxyadriamycin, vincristin and prednisone) for BL. For PTLD, the usual treatment includes the reduction or withdrawal of immunosuppression, which in some patients leads to regression of PTLD without further intervention. Anti-viral treatment alone with acyclovir/ganciclovir has doubtful efficacy [5] but successful therapy with Rituximab—a chimeric mouse/human anti-CD20 monoclonal antibody—alone or combined to a short low dosis chemotherapy program have been reported [6].

New therapies should focus on exploiting the pathobiology of EBV. Among viral proteins, it is mostly the membrane protein LMP1 that has been implicated in the transforming properties of EBV. LMP1 aggregates at the plasma membrane and enhances the activation of several signaling pathways involved in oncogenesis, such as NF-kappa B, the mitogen-activated protein kinases and the JAK/STAT cascade [7]. The oncogenic functions of LMP1 can be attributed, at least in part, to its ability to inhibit apoptosis through the up-regulation of anti-apoptotic proteins, such as BCL-2, A20 and MCL-1 [8-10]. Moreover, overexpression of BCL-2 was found *in vitro* in LCL and type III BL cell lines [11] and was also described in EBV-positive lymphoproliferations harboring type III latency including PTLD [12, 13]. Given the anti-apoptotic effect of BCL-2, it represents a logical target for new therapeutic strategies in EBV-positive lymphoproliferations. Chemical mimetics of BH3-only proteins represent an exciting new class of cancer therapeutic. ABT-737 is certainly one of the most studied. It efficiently antagonizes various pro-survival members of BCL-2 family (BCL-2, BCL-x(L), BCL-w but not MCL-1 or A1) and increases apoptosis susceptibility in different tumors cells (reviewed in [14]). Here, we reported the efficiency of ABT-737 *in vitro* on EBV-positive

LCL and BL cell lines and *in vivo* on xenograft mouse models. We showed that ABT-737 strongly induced apoptosis *in vitro* in LCL whereas BL were less sensitive. Results obtained *in vivo* show that as monotherapy, ABT-737 reduced tumor growth and increased the overall survival of mice xenografted with LCL but had no effect on BL tumors. Furthermore, the combination ABT-737/Cyclophosphamide reduced tumor growth during treatment but the overall survival of mice xenografted with BL cell line is not improved. In contrast, the combination ABT-737/Rituximab was very efficient and induced around 70% of remission in mice xenografted with LCL. Our results suggest that the use of agent targeting BCL-2, either alone or in combination with other conventional drugs, represents a novel promising approach for EBV-positive B lymphoproliferations.

Results (1179)

Evaluation of ABT-737 efficacy in vitro

We first tested the *in vitro* effect of ABT-737 on a large panel of EBV(+) cell lines including BL cell lines and lymphoblastoid cell lines (LCL), used as a model of PTLD (Figure 1). ABT-737 strongly induced apoptosis in LCL (Figure 1 a, more than 50% of cell death in all cell lines at 10 µM), BL cell lines were relatively resistant to proapoptotic effects of ABT-737 (Figure 1a, less than 50% of cell death in every cell lines at 10µM). In LCL cell lines, a reduced dose to 10 % of the starting dose (0,25µM) was still able to induce apoptosis (figure 1b). Many studies have shown that BCL-2 inhibitors are able to potentiate the effect of conventional treatment in malignant human cells [14, 15]. Cyclophosphamide is a nitrogen mustard alkylating agent central for the treatment of patients with BL. This compound needs to be activated by cytochrome P450 in the body to be efficient. So, for *in vitro* studies, we used Melphalan, another nitrogen mustard alkylating agent that doesn't need to be metabolized. To determine whether ABT-737 augments the antitumor effect of Melphalan *in vitro*, we performed MTT cytotoxique assays on LY47 BL EBV (+) cell line treated with ABT-737 (2,5µM), Mephalan (up to 5µM) and ABT-737 in combination with Melphalan (Supplemental figure 1). At 2,5 µM, ABT-737 had minimal cytotoxic effects compared to mock treated cells (decrease of 14% in cell viability). At 2,5 and 5µM of Melphalan with 2,5 µM of ABT-737, Combination Index (CI) indicated a greater effect than the expected additive effect (CI=0,21) suggesting that ABT-737 can be used to reduce doses of Mephalan used. We thus decided to evaluate the efficacy of

ABT-737 in combination with cyclophosphamide in our *in vivo* models of mice xenografted with BL.

Combination therapy with cyclophosphamide and ABT-737 in mice xenografted with LY47

To confirm the effects of ABT-737 on tumor cell proliferation observed *in vitro*, we tested the combination of ABT-737 and cyclophosphamide, in mice xenografted with LY47 cells. Forty NOD/SCID mice were injected subcutaneously with LY47 cells. Eight days following tumor inoculation, ABT-737 or its vehicle solution were administered every day intraperitoneally at 75 mg/kg for 14 days. A single low dose of cyclophosphamide was administered to mice on day 12 (50 mg/kg, equivalent to 150 mg/m^{2,}[16]). Mice were sacrificed when tumor mass was superior to 1500 mm^3. As shown in Figure 2a, the combination of ABT-737 and cyclophosphamide strongly inhibited the growth of the tumor (grey dashed line, %TGI(D22)=90%), more efficiently than cyclophosphamide alone (black dash-dotted line, %TGI(D22)=82%) whereas ABT-737 alone had no significant antitumor activity (grey solid line, TGI(D22)=4%). However, shortly after stopping treatment with ABT-737 (D22), tumor volume of mice treated with the combination of ABT-737 and cyclophosphamide started to increase. Controls receiving saline (untreated, solid black line), or vehicle (dashed black line) and mice treated with ABT-737 alone (solid grey line) reached end point within 32, 36 and 33 days respectively (Figure 2b). In contrast, mice treated with cyclophosphamide (black dash-dotted line) or with the combination (grey dashed line) reached end point within 46 days. Treatment with ABT-737 and cyclophosphamide did not significantly increase survival over cyclophosphamide alone even if we observed an increase in life span between cyclophosphamide alone and the combination (%ILS=30,6% versus 38,7%) and in the median survival (40,5 days versus 43 days).

Combination therapy with Rituximab and ABT-737 in mice xenografted with RPMI8866

A second study was performed to evaluate the *in vivo* effect of ABT-737 used alone or in combination with the chimeric monoclonal anti-CD20 antibody Rituximab in mice xenografted with LCL (used as a model for PTLD). Fifty nude mice were injected subcutaneously with RPMI8866 cells. Twelve days following tumor inoculation, ABT-737 or its vehicle solution were administered intraperitoneally at 75 mg/kg for 14 consecutive days. Rituximab was administered intraperitoneally once a week (D15; D22; D29; D36) for four weeks at 10 mg/kg.

Results are shown in figure 3 and clearly demonstrated that combination of Rituximab and ABT-737 (grey dashed, TGI(D26)=87%) reduced tumor growth more efficiently than ABT-737 (grey solid line, TG(D26)=68%) and Rituximab alone (black dash-dotted line, TGI(D26)=78%) (Figure 3a). ABT-737 alone can slow tumor growth since at the end of the study, median of survival was increased in the group of mice treated with ABT-737 as compare to the control groups ABT-737 vehicle and untreated (50, 39 and 43 days respectively, %ILS=28%). But shortly after stopping ABT-737 treatment as previously described above, tumor volume of mice treated with ABT-737 alone strongly increased and all tumors reached our experimental end point at D53 (Figure 3b) fared no better than untreated group (D53) and vehicle group (D64). In the Rituximab group, tumors growth was completely suppressed in three mice over seven (43%) and delayed in one mouse (14%). The remaining animals seemed to be refractory since their tumors reached end point volume at D43 (figure 3b, 3 mice/7, 43%). When ABT-737 and Rituximab were used in combination, the anti-tumoral effect was better since tumors growth was delayed in 2 mice/6 (33,3%) or completely suppressed (4 mice/6, 66.7%). The remaining four animals were free of disease at the time of sacrifice (D135).

To evaluate more specifically the effect of the combined treatment of ABT-737 and Rituximab on overall survival of mice, we used the human/SCID chimeric model of PTLD. Indeed, it was previously shown that intraperitoneal injection of LCLs results in the reproducible development of fatal lymphoproliferative disease involving the abdominal cavity and viscera 30–50 days post-inoculation [17, 18]. These tumors share remarkable similarities with EBV (+) PTLD in that they are diffuse large cell lymphomas of human B-cell origin. In these tumors, EBV is uniformly present with a broad pattern of viral gene expression, and BCL-2 is abundantly expressed [17, 19]. Fifty SCID mice were injected intraperitoneally with RPMI8866 cells. The schedule of treatment for ABT-737 and Rituximab was similar to the one described above. Mice were monitored weekly by ultrasound and sacrificed when they developed clinical signs of disease. All animals were subjected to necropsy to determine the growth pattern of tumor development. When abnormal swelling of the abdomen, spiked hair, paralysis or cardiac rhythm acceleration were observed, mice were sacrificed. Otherwise, the end point for the therapeutic trial was death. Survival results obtained for each group are illustrated using a Kaplan-Meier plot (figure 4). Results obtained show that treatment with Rituximab (Black dash-dotted line) or ABT-737 alone (grey solid line) significantly prolonged survival, but all animals (8/8) died with tumors before day 48 (survival median= 39 days and

42 respectively, as compared to 31 and 28 days for untreated and treated with vehicle mice respectively). In contrast, when ABT-737 was combined with Rituximab (dashed grey line), 6 of 9 animals remained tumor free at the time of sacrifice at 130 days (66%). From these experiments, we concluded that in the PTLD model, ABT-737 treatment in combination with Rituximab can induces complete remission. In addition, the combination of ABT-737 and rituximab was well tolerated during the treatment period (no body weight loss, moderate thrombocytopenia, data not shown).

Discussion: 727

High-doses combinations of cytotoxic drugs can be highly effective in treating BL but novel strategies may help to tackle the problem of side effects and relapse. For most patients with aggressive B cell lymphomas, intensive combination chemotherapy is curative. However, in patients who relapse, subsequent intensive salvage chemotherapy rarely results in durable survival and new therapeutic approaches are required. Defect in the apoptotic cascade are a hallmark of cancer and are often associated with chemoresistance. So, agents that restore the ability of cancer cells to undergo apoptosis may enhance the activity of chemotherapy when used in combination. In this context, our preclinical studies on xenografted LY47 mice aimed at determining the potential therapeutic of ABT-737 alone or as an enhancer of chemotherapy in BL EBV (+) treatment. Our results showed that as a single agent, ABT-737 has no effect on overall survival of mice. When combined with low dose cyclophosphamide, ABT-737 delays the tumor growth. However, overall survival of mice was not increased as compared to mice treated with cyclophosphamide alone. Others have shown synergy between ABT-737 and low dose cyclophosphamide, achieving many complete remissions for mice transplanted with Eμmyc/EμBCL-2 lymphomas [20]. This difference in outcome most likely reflects the relative tumor burden at the beginning of treatment (D4 following injection, non-palpable tumors versus animals with established disease D8). Moreover, the Eμmyc/EμBCL-2 mouse develop Burkitt like lymphoma with a high BCL-2 expression that have not the same characteristics such as EBV positive BL cells. The cyclophosphamide administration schedule was also different: two injections were done in their study whereas only one was done in our case. Since in our BL model, treatment with ABT-737 combined with one injection of cyclophosphamide delays tumor growth but has no effect on mice survival, we can hypothesize that repeated (2 or 3) injections of cyclophosphamide combined to ABT-737

would help to maintain a low tumor burden. We can even think that this administration schedule could induce complete remission since standard protocols already included multiple cycles of treatment.

Our data also support the concept that ABT-737 in combination with Rituximab may represent an effective new treatment option for EBV+ BCL-2 expressing lymphoproliferative diseases such as PTLD. EBV-associated lymphomas remain a significant cause of morbidity and mortality in immunosuppressed allograft recipient. Although numerous treatment options have been used (chemotherapy, rituximab, radiation), the overall mortality of the EBV+ lymphoproliferative diseases remains in excess of 50%. Immunosuppressed and non-responder patients complicate therapeutic support, less toxic treatments are needed. Approximately half of treated patients with rituximab are either non-responder or relapse after an initial complete or partial response [21]. We have shown that ABT-737 can slow tumor growth and increase survival of mice xenogafted with LCL. This approach seems to be really promising for treatment of patient with PTLD since ABT-737 is as efficient as rituximab. Moreover, ABT-737 combined with Rituximab increase the number of remission.

Because continuous administration of a parental agent in the clinical setting is problematic, Abbott laboratories have developed an orally available analogue of ABT-737: ABT-263, also known as Navitoclax. Navitoclax has been tested as single agent and in combination with different compounds in B cell malignant xenograft models. Associated with Rituximab, Navitoclax leads to complete remission in 70% of DLBCL xenograft mice [22]. ABT-263 binds with high affinity to BCL-2 but also to BCL-xL which inhibition caused the thrombocytopenia we observed in mice. This side effect was also observed on patient during clinical trial, limiting its development in clinical practice. In our previous study, we have shown that the EBV(+) lymphoid tumoral cells specifically overexpress BCL-2 [11]. ABT-737 binds with high affinity to BCL-2 but also to BCL-xL which inhibition caused the thrombocytopenia we observed in mice. As a result, the use of a more specific compound of BCL-2 such as ABT-199, which is the first FDA-approved treatment that targets BCL-2, should be investigated. So, we think that it would be interesting to test the effect of such a compound alone or in combination in our mice models.

So, our data and results from other suggested that ABT-737 can be an efficient alternative to treat different pathologies associated with EBV and notably for tumors expressing LMP-1. So, this therapeutic strategy could also be evaluated in other EBV

associated malignancies such as NPC (Nasopharyngeal Carcinoma) and NK/T lymphoma. Numerous studies showed that LMP-1 expression is usually found in these tumors [23, 24].

Materials and Methods: 681

Cell lines and reagents

LY47 BL cell line was originally established from an endemic case of BL and kindly provided by the International Agency for Research on Cancer (IARC, Lyon). Seraphina cells were provided by Professor G Klein (Stockholm). BL2/B95 were generated by stable infection of the original EBV (-) BL2 (sporadic case of BL) with B95.8 EBV train. LCLs were obtained by the *in vitro* immortalization of normal B lymphocytes. RPMI 8866 cell line was established from the normal B lymphocytes of a 51-year-old American woman with chronic myelogenous leukaemia (IARC, Lyon). Priess and Remb1 cells were kindly provided by Dr JG Bodmer (London). These cell lines were cultured in RPMI 1640 medium (PAA) containing 2 mM L-glutamine, 1 mM sodium pyruvate, 20 mM glucose, 100 U/ml penicillin and 100 µg/ml streptomycin and supplemented with 10% heat-inactivated fetal calf serum.

ABT-737 was kindly provided by Abbott Laboratories (Chicago, IL, USA). Cyclophosphamide (Sigma-Aldrich), Melphalan (Sigma-Aldrich) and Rituximab (Roche) were reconstituted according to the manufacturer's protocol.

Cell death measurement

Apoptosis was assessed using annexin/ propidium iodide (PI) assay. We treated 0.5×10^6 cells for 24h, at 37°C, with different concentrations of ABT-737. Cells were washed in PBS, resuspended in annexin buffer (10mM HEPES/NaOH (pH 7.4), 150mM NaCl, 5mM KCl, 1mM $MgCl_2$, 1.8mM $CaCl_2$) supplemented with 2.5μg/ml FITC-labeled annexin-V (Roche Applied Science, Meylan, France) and incubated at room temperature for 10 minutes. Cells were then washed, resuspended in annexin buffer supplemented with PI (10μg/ml) and analyzed by flow cytometry (*n*=10000; FACSCalibur, Becton-Dickinson, Pont-de-Claix, France). Annexin-V-positive cells (PI negative or PI positive) were considered to be apoptotic.

Cellular proliferation assay

Cell viability was assessed using MTT assay. Cells (2×10^5) were seeded in 200 µl of RPMI-1640 medium into 96-well plates and treated with ABT-737 or melphalan or both (triplicate). After 24h of incubation, 25 µl of MTT (Sigma-aldrich, 5mg/ml) was added to each well followed by 2 h incubation. Then, 150 µl of lysis buffer (SDS 20%, Dimethylformamide 45%, pH 4,7) was added into each well, and incubated overnight. Optical Density (OD) at 550 nm was measured. Cell viability index was calculated according to the formula: (experimental OD value/control OD value) × 100%. Combination Index (CI) which defines Synergism (CI < 1), Additive Effect (CI = 1) and Antagonism (CI > 1) was calculated using CompuSyn software.

Ethics Statement

Investigation has been conducted in accordance with the ethical standards and according to the Declaration of Helsinki and according to national and international guidelines and has been approved by the authors' institutional review board (Gustave Roussy Animal Care and Use Committee). Mice were sacrificed under general anesthesia by cervical dislocation when deemed unwell (body weight loss superior to 20% from the base-line, tumor mass superior to 1500 mm^3, tumor ulceration, dehydration, paralysis or poor general condition). Necropsy was performed and tumors were resected when it was possible

Subcutaneous xenograft model

For ectopic xenograft, LY47 cells ($1,5 \times 10^6$) or RPMI8866 cells (2×10^6) were suspended in a 1:1 ratio of medium and matrigel (BD Biosciences). Cell suspensions were injected subcutaneously on left hind flanks of female NOD/SCID (LY47) or NUDE (RPMI8866) 6-8 weeks old mice (SCEA, IGR). Mice were randomized according to tumor burden. Drug treatments began between 8-12 days following tumor inoculation. Mice were treated daily with 75 mg/kg ABT-737 or vehicle solution for 14 days. A single low dose of cyclophosphamide was administered intraperitoneally on day 12 (50 mg/kg, equivalent to 150 mg/m2) or Rituximab was administered intraperitoneally once a week (D15; D22; D29; D36) for four weeks at 10 mg/kg. Tumors were measured with a manual calliper every 2-3 days and volumes were calculated using the formula: tumor weight (mg)= [length (mm) x width² (mm^2)]/2. Effects on tumor growth were assessed by determining percent increase in life span (%ILS) as measured by the time for tumors to reach end point: %ILS=[(median time for tumors in treated group to reach

end point / median time for tumors in control group to reach end point)*100]-100 and by dertemining percent of tumor growth inhibition: %TGI=(1-(mean time for tumors in treated group to reach size x / mean time for tumors in control group to reach size x)*100

Disseminated xenograft model

For the human/SCID chimeric model of PTLD (orthotopic xenograft), suspension of RPMI8866 cells ($10x10^6$) was injected intraperitoneally in SCID 6-8 weeks old mice (Charles Rivers). The schedule of treatment for ABT-737 and Rituximab was similar to the one described above.

Statistical analysis

All numeric data are expressed as means. Data plotted on graphs are means and standard deviation (s.d.) or standard error of mean (s.e.m). Statistical analysis were performed using two non-parametric tests: Mann and Whitney for side-by-side comparison and Kruskal and Wallis for multiple comparisons (n>3). All comparisons of statistical significance have P values of $P<0.05$. For survival analysis, Log-rank (Mantel-Cox) test were done using Graphpad Prism.

Abbreviations
PTLD
BL
EBV
BCL-2
BCL-XL
BCL-W
LCL
EBNA
LMP
MCL-1
OD
SCID
ILS
PI

Authors contributions
Acknowledgments
Animalerie
Conflict of interest
The authors declare no conflict of interest.

Funding

This work was supported by grants from the Fondation de France 00012093 (JW), the Canceropole and Region Ile-de-France (ERABL, IF09–2092/R), the Fondation pour la Recherche Medicale (doctoral fellowship to AP) and the Universite Paris-Sud (BQR 2009).

References

1. Neparidze N, Lacy J. Malignancies associated with epstein-barr virus: pathobiology, clinical features, and evolving treatments. Clin Adv Hematol Oncol. 2014; 12: 358-71. doi:
2. Ott G. Aggressive B-cell lymphomas in the update of the 4th edition of the World Health Organization classification of haematopoietic and lymphatic tissues: refinements of the classification, new entities and genetic findings. Br J Haematol. 2017; 178: 871-87. doi: 10.1111/bjh.14744.
3. Craig FE, Johnson LR, Harvey SA, Nalesnik MA, Luo JH, Bhattacharya SD, Swerdlow SH. Gene expression profiling of Epstein-Barr virus-positive and -negative monomorphic B-cell posttransplant lymphoproliferative disorders. Diagn Mol Pathol. 2007; 16: 158-68. doi: 10.1097/PDM.0b013e31804f54a9.
4. Vakiani E, Basso K, Klein U, Mansukhani MM, Narayan G, Smith PM, Murty VV, Dalla-Favera R, Pasqualucci L, Bhagat G. Genetic and phenotypic analysis of B-cell post-transplant lymphoproliferative disorders provides insights into disease biology. Hematol Oncol. 2008; 26: 199-211. doi: 10.1002/hon.859.
5. Pirsch JD, Stratta RJ, Sollinger HW, Hafez GR, D'Alessandro AM, Kalayoglu M, Belzer FO. Treatment of severe Epstein-Barr virus-induced lymphoproliferative syndrome with ganciclovir: two cases after solid organ transplantation. Am J Med. 1989; 86: 241-4. doi:
6. Ganne V, Siddiqi N, Kamaplath B, Chang CC, Cohen EP, Bresnahan BA, Hariharan S. Humanized anti-CD20 monoclonal antibody (Rituximab) treatment for post-transplant lymphoproliferative disorder. Clin Transplant. 2003; 17: 417-22. doi:
7. Eliopoulos AG, Young LS. LMP1 structure and signal transduction. Semin Cancer Biol. 2001; 11: 435-44. doi: 10.1006/scbi.2001.0410
S1044-579X(01)90410-9 [pii].
8. Wang S, Rowe M, Lundgren E. Expression of the Epstein Barr virus transforming protein LMP1 causes a rapid and transient stimulation of the Bcl-2 homologue Mcl-1 levels in B-cell lines. Cancer Res. 1996; 56: 4610-3. doi:
9. Laherty CD, Hu HM, Opipari AW, Wang F, Dixit VM. The Epstein-Barr virus LMP1 gene product induces A20 zinc finger protein expression by activating nuclear factor kappa B. J Biol Chem. 1992; 267: 24157-60. doi:
10. Henderson S, Rowe M, Gregory C, Croom-Carter D, Wang F, Longnecker R, Kieff E, Rickinson A. Induction of bcl-2 expression by Epstein-Barr virus latent membrane protein 1 protects infected B cells from programmed cell death. Cell. 1991; 65: 1107-15. doi:
11. Pujals A, Renouf B, Robert A, Chelouah S, Hollville E, Wiels J. Treatment with a BH3 mimetic overcomes the resistance of latency III EBV (+) cells to p53-mediated apoptosis. Cell Death Dis. 2011; 2: e184. doi: cddis201167 [pii]
10.1038/cddis.2011.67.
12. Chetty R, Biddolph S, Kaklamanis L, Cary N, Stewart S, Giatromanolaki A, Gatter K. bcl-2 protein is strongly expressed in post-transplant lymphoproliferative disorders. J Pathol. 1996; 180: 254-8. doi: 10.1002/(SICI)1096-9896(199611)180:3<254::AID-PATH671>3.0.CO;2-D [pii]
10.1002/(SICI)1096-9896(199611)180:3<254::AID-PATH671>3.0.CO;2-D.
13. Ghigna MR, Reineke T, Rince P, Schuffler P, El Mchichi B, Fabre M, Jacquemin E, Durrbach A, Samuel D, Joab I, Guettier C, Lucioni M, Paulli M, et al. Epstein-Barr virus infection and

altered control of apoptotic pathways in posttransplant lymphoproliferative disorders. Pathobiology. 2013; 80: 53-9. doi: 000339722 [pii] 10.1159/000339722.
14. Labi V, Grespi F, Baumgartner F, Villunger A. Targeting the Bcl-2-regulated apoptosis pathway by BH3 mimetics: a breakthrough in anticancer therapy? Cell Death Differ. 2008; 15: 977-87. doi: cdd200837 [pii] 10.1038/cdd.2008.37.
15. Chen J, Jin S, Abraham V, Huang X, Liu B, Mitten MJ, Nimmer P, Lin X, Smith M, Shen Y, Shoemaker AR, Tahir SK, Zhang H, et al. The Bcl-2/Bcl-X(L)/Bcl-w inhibitor, navitoclax, enhances the activity of chemotherapeutic agents in vitro and in vivo. Mol Cancer Ther. 2011; 10: 2340-9. doi: 10.1158/1535-7163.MCT-11-0415.
16. Nair AB, Jacob S. A simple practice guide for dose conversion between animals and human. J Basic Clin Pharm. 2016; 7: 27-31. doi: 10.4103/0976-0105.177703.
17. Rowe M, Young LS, Crocker J, Stokes H, Henderson S, Rickinson AB. Epstein-Barr virus (EBV)-associated lymphoproliferative disease in the SCID mouse model: implications for the pathogenesis of EBV-positive lymphomas in man. J Exp Med. 1991; 173: 147-58. doi:
18. Cannon MJ, Pisa P, Fox RI, Cooper NR. Epstein-Barr virus induces aggressive lymphoproliferative disorders of human B cell origin in SCID/hu chimeric mice. J Clin Invest. 1990; 85: 1333-7. doi: 10.1172/JCI114573.
19. Guinness ME, Kenney JL, Reiss M, Lacy J. Bcl-2 antisense oligodeoxynucleotide therapy of Epstein-Barr virus-associated lymphoproliferative disease in severe combined immunodeficient mice. Cancer Res. 2000; 60: 5354-8. doi:
20. Mason KD, Vandenberg CJ, Scott CL, Wei AH, Cory S, Huang DC, Roberts AW. In vivo efficacy of the Bcl-2 antagonist ABT-737 against aggressive Myc-driven lymphomas. Proc Natl Acad Sci U S A. 2008; 105: 17961-6. doi: 0809957105 [pii]
10.1073/pnas.0809957105.
21. Milpied N, Vasseur B, Parquet N, Garnier JL, Antoine C, Quartier P, Carret AS, Bouscary D, Faye A, Bourbigot B, Reguerre Y, Stoppa AM, Bourquard P, et al. Humanized anti-CD20 monoclonal antibody (Rituximab) in post transplant B-lymphoproliferative disorder: a retrospective analysis on 32 patients. Ann Oncol. 2000; 11 Suppl 1: 113-6. doi:
22. Tse C, Shoemaker AR, Adickes J, Anderson MG, Chen J, Jin S, Johnson EF, Marsh KC, Mitten MJ, Nimmer P, Roberts L, Tahir SK, Xiao Y, et al. ABT-263: a potent and orally bioavailable Bcl-2 family inhibitor. Cancer Res. 2008; 68: 3421-8. doi: 68/9/3421 [pii]
10.1158/0008-5472.CAN-07-5836.
23. Hila L, Farah F, Ayari H, Ferjaoui M, Dehria W, Ben Jilani S. Epidemiological study, immunohistochemistry and in situ hybridization studies of nasopharyngeal carcinomas: a Tunisian report. Pathol Biol (Paris). 2009; 57: 427-9. doi: S0369-8114(08)00210-1 [pii]
10.1016/j.patbio.2008.07.029.
24. Huang YH, Wu QL, Zong YS, Feng YF, Hou JH. Nasopharyngeal extranodal NK/T-cell lymphoma, nasal type: retrospective study of 18 consecutive cases in Guangzhou, China. Int J Surg Pathol. 2011; 19: 51-61. doi: 1066896910388806 [pii]
10.1177/1066896910388806.

Figure Legend (402)

Figure 1: Effect of ABT-737 on the induction of apoptosis in EBV (+) B malignancies cell lines. The cells were labeled with annexin V-FITC and PI and analyzed with a FACSCalibur flow cytometer, to determine the percentage of cells that were apoptotic. The values presented

(means±s.d.) are from three independent experiments. (a) EBV (+) BL and LCL cell lines were treated with ABT-737 10 µM for 24h. Statistical analysis: Mann and Whitney. (*) means $p<0.05$. (b) EBV (+) lymphoblastoïd cell lines (LCL) were treated with different concentration of ABT-737 for 24h. Statistical analysis: Kruskal and Wallis. (*) means $p<0.05$.

Figure 2: *In vivo* antitumor effect of ABT-737 in combination with cyclophosphamide in LY47 xenograft mice. Mean tumor volume (a) and Kaplan-Meier plot (b) of groups of mice transplanted with 1,5 $x10^6$ LY47 cells treated or not (black solid line, n=6) with ABT-737 (75 mg/kg/d for 14 days; grey solid line, n=6) or vehicle (black dashed line, n=7), or with ABT-737 plus low-dose cyclophosphamide (50 mg/kg, day 12; grey dashed line, n=5), or with low-dose cyclophosphamide alone (Black dash-dotted line, n=8). Statistical analysis: (a) Kruskal-Wallis, (b) Log-rank (Mantel-Cox). (*) means $p<0.05$; (**) means $p<0.005$; (***) means $p<0.0005$; NS: non-significant.

Figure 3: Effect of combination therapy with Rituximab and ABT-737 in mice xenografted with RPMI8866. Mean tumor volume (a) and Kaplan-Meier plot (b) of groups of mice transplanted with 2 $x10^6$ RPMI8866 cells treated or not (black solid line, n=4) with ABT-737 (75 mg/kg/d for 14 days; grey solid line, n=7) or vehicle (black dashed line, n=13), or with ABT-737 plus Rituximab (10 mg/kg; grey dashed line, n=7), or with low-dose of Rituximab alone (black dash-dotted line, n=6). Statistical analysis: (a) Kruskal-Wallis, only the combination was significantly different compared to control group: $p<0,005$ at D18, 22, 25, 29, 32 and 36 and $p<0,05$ at D12, (b) Log-rank (Mantel-Cox). (*) means $p<0.05$; (**) means $p<0.005$; NS: non-significant.

Figure 4: Combination therapy with Rituximab and ABT-737 in mice injected intraperitoneally with RPMI8866. Kaplan–Meier curves of mice ip injected with 10 $x10^6$ RPMI8866 cells treated or not (black solid line) with ABT-737 (75 mg/kg/d for 14 days; grey solid line) or vehicle (black dashed line), or with ABT-737 plus Rituximab (10 mg/kg; grey dashed line), or with low-dose of Rituximab alone (black dash-dotted line) (n = 9 per arm). Statistical significance was determined by log-rank (Mantel-cox) test. NS: non-significant; **: $p<0,005$; ***: $p<0,0005$; ****: $p<0,00005$.

Supplemental figure 1: Effect of combination of Mephalan and ABT-737 on cell proliferation in EBV (+) Burkitt lymphoma (BL) cells. LY47 cells were or were not subjected to prior treatment with ABT-737 (2,5 µM) for 1h and were then left untreated or treated with different doses of Mephalan for 24h. Cell viability was determined using MTT assay. The values presented (means±s.d.) are from four independent experiments.

Figure 1

a

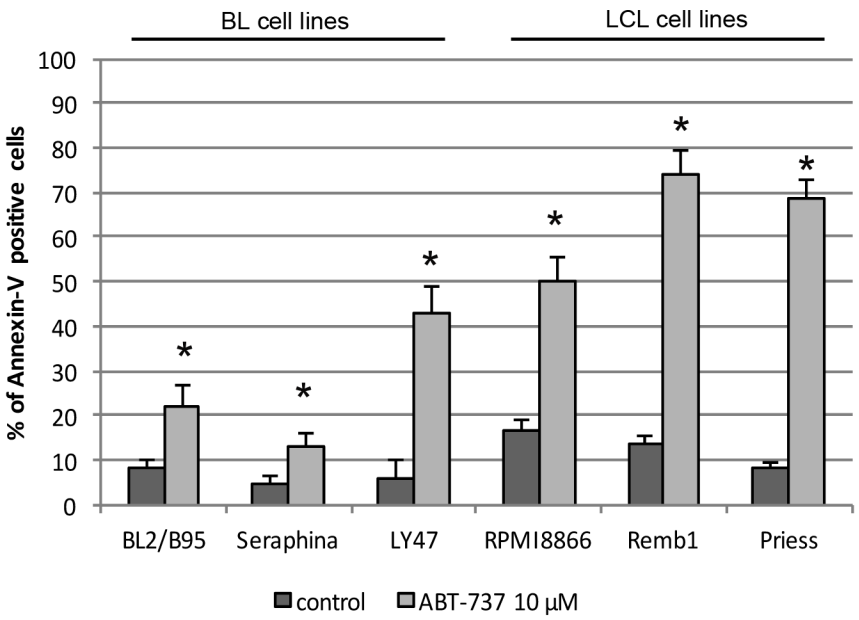
BL cell lines
LCL cell lines
% of Annexin-V positive cells
100
90
80
70
60
50
40
30
20
10
0
BL2/B95
Seraphina
LY47
RPMI8866
Remb1
Priess
control
ABT-737 10 µM

b

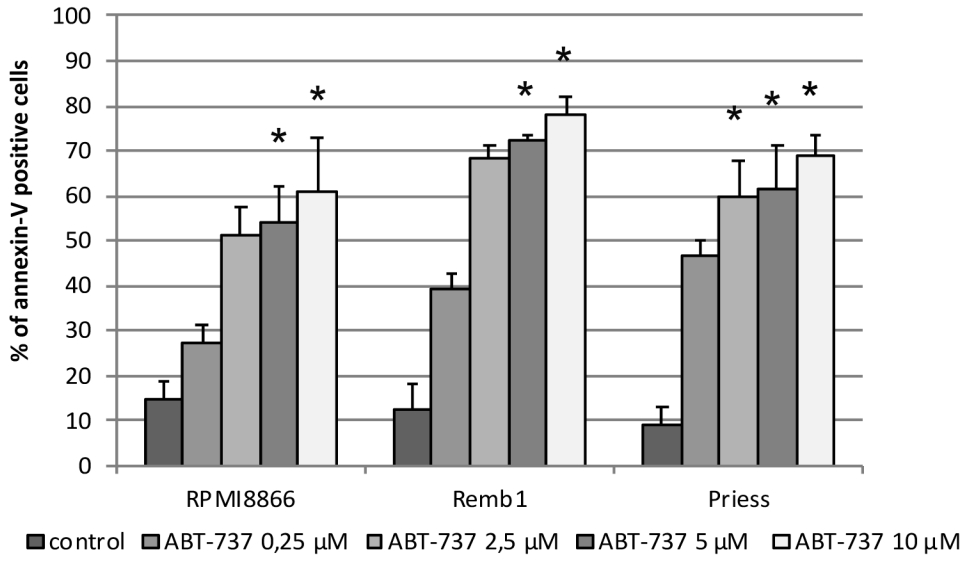
% of annexin-V positive cells
100
90
80
70
60
50
40
30
20
10
0
RPMI8866
Remb1
Priess
control
ABT-737 0,25 µM
ABT-737 2,5 µM
ABT-737 5 µM
ABT-737 10 µM

Figure 2

a

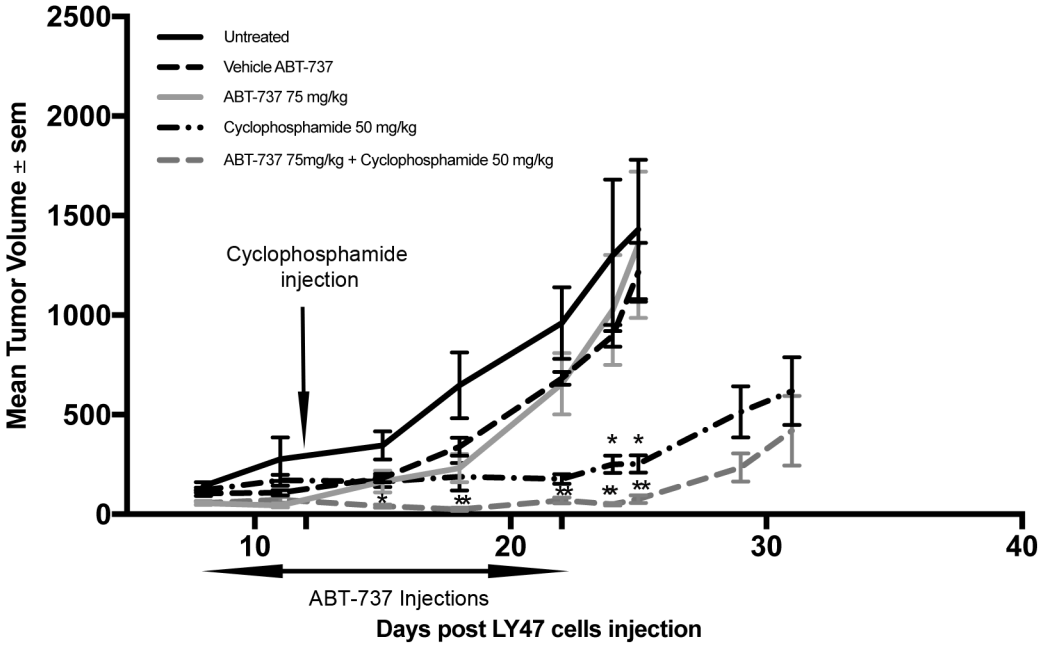

b

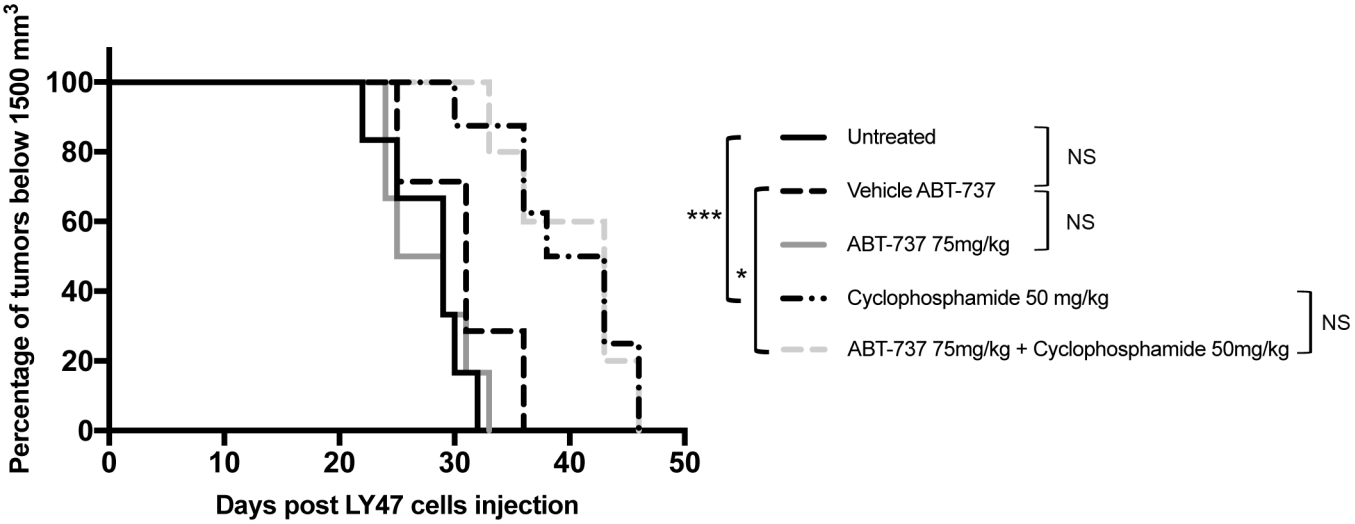

	Median survival
Untreated	29
Vehicle ABT-737	31
ABT-737 75 mg/kg	27
Cyclophosphamide 50 mg/kg	40, 5
ABT-737 75 mg/kg +Cyclophosphamide 50 mg/kg	43

Figure 3

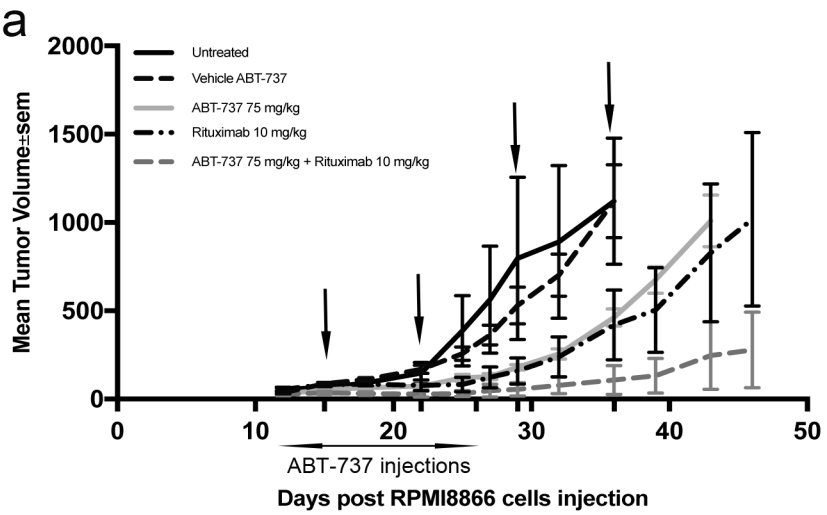

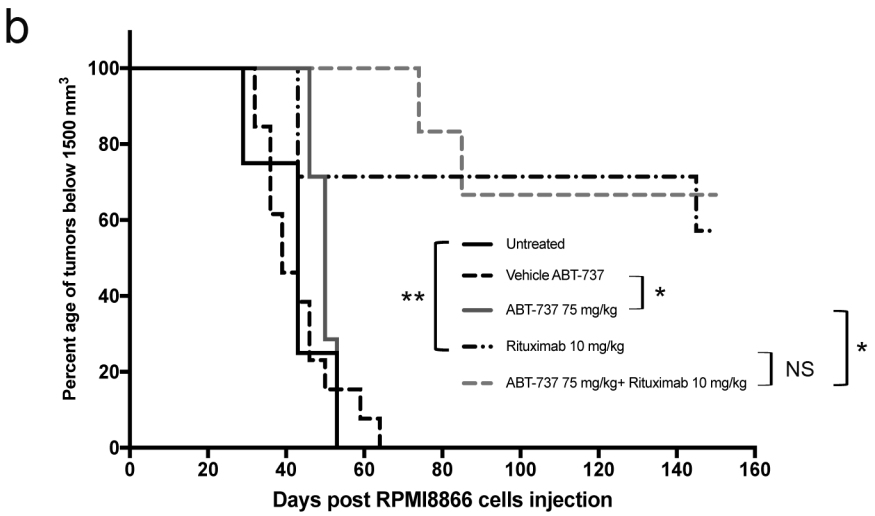

	Median Survival
Untreated	43
vehicle ABT-737	39
ABT-737 75 mg/kg	50
Rituximab 10 mg/kg	Undefined
ABT-737 75 mg/kg+ Rituximab 10 mg/kg	Undefined

Figure 4

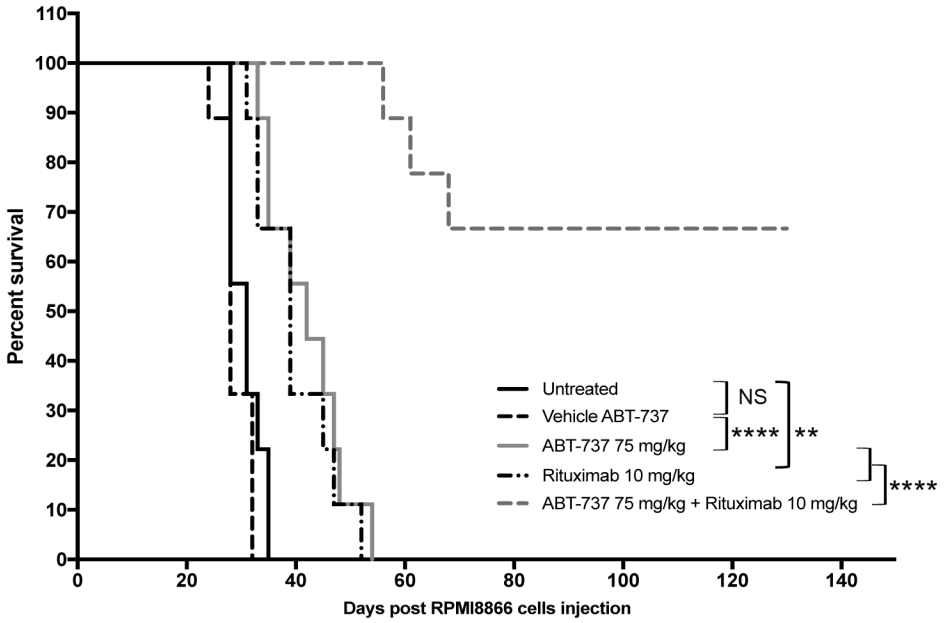

	Median Survival
Untreated	31
Vehicle ABT-737	28
ABT-737 75 mg/kg	42
Rituximab 10 mg/kg	39
ABT-737 75 mg/kg+ Rituximab 10 mg/kg	Undefined

Suplemental figure 1

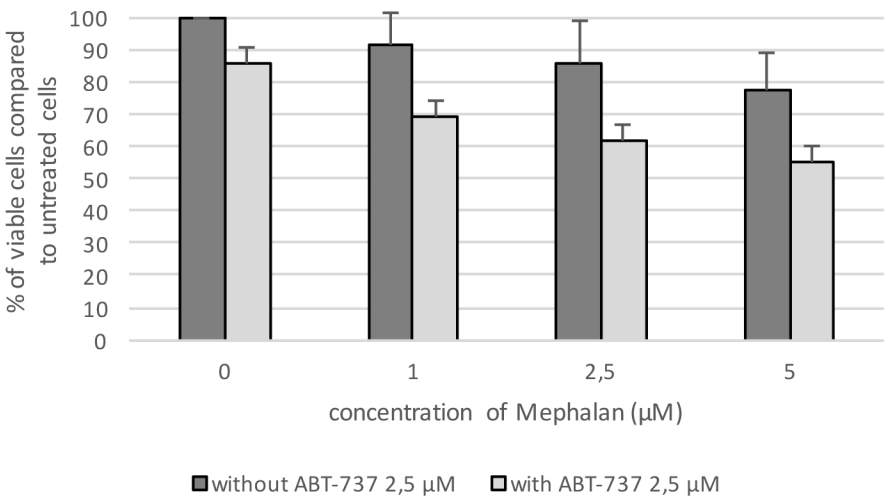

Résumé

L'altération des mécanismes d'apoptose joue un rôle central dans le développement des cancers et limite l'efficacité des thérapies conventionnelles. Les travaux que je mène ont une triple visée : 1) analyser les mécanismes d'apoptose induits par certains stimuli, 2) essayer de mieux comprendre comment les mécanismes de résistance à l'apoptose se mettent en place, 3) tenter de les contrecarrer et d'induire l'apoptose des cellules tumorales par d'autres voies. Nos modèles d'études sont différents lymphomes B notamment ceux associés au virus d'Epstein-Barr (EBV) comme le lymphome de Burkitt (LB), le syndrome lymphoprolifératif post-transplant (PTLD) et le lymphome diffus à grandes cellules B (DLBCL).

Dans ce cadre, je me suis intéressée au glycolipide Gb3/CD77, qui est fortement exprimé à la surface des cellules de certains lymphomes B comme le LB, et de certaines tumeurs solides résistantes aux chimiothérapies. Nous avons montré que l'induction de l'apoptose par une toxine bactérienne se fixant spécifiquement sur Gb3/CD77 implique plusieurs membres pro-apoptotiques de la famille BCL-2 dans. Par ailleurs, nous avons montré, dans un modèle de carcinome ovarien que l'expression de Gb3/CD77 est directement corrélée à la résistance des cellules aux drogues et à l'expression de MDR1 (Multidrug resistance-1), une protéine impliquée dans ce mécanisme grâce à ses propriétés de pompes membranaires d'efflux des substances cytotoxiques. Enfin, nos travaux récents ont mis en évidence que la fixation d'anticorps spécifiques de Gb3/CD77 à la surface des cellules cancéreuses exprimant ce glycolipide pouvait induire leur mort en utilisant le système de la cascade du complément. Ces résultats font de Gb3/CD77 une cible thérapeutique intéressante. La suite de ce projet consistera à explorer le potentiel thérapeutique d'un anticorps monoclonal dirigé contre l'Ag Gb3/CD77 dans le traitement du LB et de certaines tumeurs chimiorésistantes.

L'inactivation de p53 par la surexpression de protéines régulatrices est aussi un mécanisme permettant aux cellules tumorales d'échapper à l'apoptose. Des travaux précédents ont montré que de nombreuses lignées de LB exprimant une p53 sauvage présentent aussi une forte expression de MDM2. La réactivation de p53 par la nutline 3 (une petite molécule rompant l'interaction entre p53 et MDM2) dans les cellules de LB EBV- et EBV+ en latence I permet leur entrée massive en apoptose, cependant, elle ne suffit pas à induire la mort des cellules EBV+ en latence III. Cette résistance à l'apoptose p53 dépendante induite par EBV repose sur deux mécanismes complémentaires : une autophagie constitutive et la surexpression de la protéine anti-apoptotique BCL-2. Ainsi, nous avons montré qu'ABT-737, un inhibiteur de BCL-2 restaurait la sensibilité des cellules à l'apoptose induite par la nutline 3 *in vitro* et grâce à l'utilisation de modèles murins xénogreffés qu'il représentait une nouvelle approche thérapeutique intéressante dans le cadre du traitement des PTLD que ce soit seul ou en combinaison avec des traitements conventionnels. Néanmoins, l'utilisation d'inhibiteurs de BCL-2 peut induire une résistance des cellules cancéreuses en raison d'une surexpression des protéines non ciblées. Nous cherchons donc à développer en collaboration avec le laboratoire de F. Roussi à ICSN à Gif sur Yvette, d'autres inhibiteurs des membres de la famille BCL-2 pour contrecarrer ces résistances.